The University Of Sheffield.

Targeting the Fanconi anaemia pathway in neuroblastoma

By:

Leona Fields

A thesis submitted in partial fulfilment of the requirements for the degree of Doctor of Philosophy

The University of Sheffield
Faculty of Medicine, Dentistry and Health
Department of Oncology and Metabolism

September 2022

Acknowledgements

Firstly, I would like to thank my supervisor Dr. Helen Bryant for her support and guidance throughout the entire project. The pandemic created some challenging times during the past few years, and her mentorship and positive strategies made this project achievable. I would also like to thank Dr. Spencer Collis and Dr. Ruth Thompson for their insight on the FA pathway and DNA repair and for their advice and useful discussions during lab meetings. Thank you to Dr. David King for his expert advice on neuroblastoma and his help in the creation of this project. I would also like to express my gratitude to the Little Princess Trust and all of its donors for funding this research project.

Thank you to Dr. Anestis Tsakiridis, Dr. Luis Montano-Gutierrez and Dr. Manoj Valluru for helping undertake RNA-seq analyses. I would also like to thank Hannah Walsh for her help during the final six months of my PhD, her assistance with staining the never-ending IFs was invaluable. I would like to thank everyone in the Bryant, Collis, and Thompson lab groups, past and present, for their friendship and support. I am very grateful to have been in a helpful and supportive lab atmosphere throughout my PhD.

Finally, I would like to thank my parents, sisters and grandparents for their unconditional support, encouragement and understanding during my PhD. Thank you for reminding me that life goes on, even when western blots continue to fail, and for being a constant source of happiness throughout this project.

Abstract

Neuroblastoma is the most common extracranial solid tumour of childhood. Amplification of the *MYCN* oncogene is observed in 20% of neuroblastoma cases and is always associated with high-risk disease. The overall survival rate for high-risk disease remains below 50%, highlighting a need for novel therapeutics which can improve the efficacy of current treatment strategies. High *MYCN* expression induces greater levels of replication stress and DNA damage, and this sensitises cells to inhibition of DNA repair and replication stress limiting pathways. The Fanconi anaemia (FA) pathway functions to repair DNA inter-strand crosslinks and limit replication stress. We hypothesised the FA pathway is a potential therapeutic target in *MYCN*-amplified neuroblastoma.

We demonstrated *MYCN* overexpression and amplification induced transcriptional upregulation of FANC and HRR-associated FA pathway genes in neuroblastoma cell lines and tumours, and observed direct binding of MYCN at the promoter of most FA genes. Expression of *MYCN* also induced greater FA pathway activation. FA pathway inhibition by curcumin increased replication stress and R-loop accumulation in *MYCN*-expressing cells, indicating FANCD2 functions in the suppression of MYCN-induced R-loops. Curcumin was selectively more toxic in *MYCN*-expressing cells, suggesting increased FA pathway activation is required to limit MYCN-induced replication stress to tolerable levels. Curcumin also sensitised neuroblastoma cells to DNA crosslinking chemotherapeutics. Altogether our results indicate *MYCN* expression induces a greater FA pathway dependency which could be therapeutically exploited.

REDACTED

Overall, this thesis demonstrates the therapeutic potential of exploiting MYCN-induced replication stress to sensitise neuroblastoma cells to FA pathway inhibition, **REDACTED**.

Table of Contents

List of Figures

List of Tables

List of Accompanying Material

All appendix figures are in Chapter 7. Appendix.

All appendix tables are in Additional File 1 (Excel file).

The Covid impact form outlining the disruption to the project is also provided.

Abbreviations

ADRN	adrenergic
ANOVA	analysis of variance
APS	ammonium per sulphate
ASCT	autologous stem cell transplant
AURKA	Aurora kinase A
BET	bromodomain and extra-terminal domain
BP	biological process
BSA	bovine serum albumin
CC	cellular component
cDNA	complementary DNA
CFS	common fragile site
cispt	cisplatin
CldU	5-Chloro-2'-deoxyuridine
CNS	central nervous system
CRC	core regulatory circuitry
curc	curcumin
DAPI	4′,6-diamidino-2-phenylindole
ddH_2O	ultra-pure deionised water
DDR	DNA damage response
DMEM	Dulbecco's modified eagles medium
DMSO	dimethyl sulfoxide
DNA	deoxyribonucleic acid
Dox	Doxycycline
DSB	double strand break
ECM	extra-cellular matrix
EDTA	ethylenediaminetetraacetic acid
EMT	epithelial-to-mesenchymal transition
ESR1	oestrogen receptor-alpha
FA	Fanconi anaemia
FACS	fluorescence-activated cell sorting
FANC	Fanconi anaemia complementation group
FCS	fetal calf serum

FDA	Food and Drug Administration
FDR	false discovery rate
GBM	glioblastoma
hNET	human norepinephrine transporter
HRP	horse radish peroxidase
HRR	homologous recombination repair
HSPC	haematopoietic stem and progenitor cell
HU	hydroxyurea
ICL	inter-strand crosslink
IdU	5-Iodo-2'-deoxyuridine
IMS	industrial methylated spirit
INGRSS	International Neuroblastoma Risk Group Staging System
iPSC	induced pluripotent stem cell
IR	ionising radiation
KEGG	Kyoto Encyclopaedia of Genes and Genomes
LOH	loss of heterozygosity
MES	mesenchymal
MF	molecular function
MMC	mitomycin C
MMP	matrix metalloprotease
MNA	MYCN amplified
MRD	minimal residual disease
mRNA	messenger RNA
NB	neuroblastoma
NCC	neural crest cell
NER	nucleotide excision repair
nFAPi	novel FA pathway inhibitor
NHEJ	non-homologous end joining
Non-MNA	non-MYCN amplified
PBS	phosphate buffered saline
PCR	polymerase chain reaction
PI	propidium iodide
pRPA	phospho-RPA

RIPA	radioimmunoprecipitation assay buffer
rlog	regularised log
RNA	ribonucleic acid
ROS	reactive oxygen species
RPM	reads per million
RPMI	Roswell Park Memorial Institute medium
RT-qPCR	quantitative reverse transcription polymerase chain reaction
SAC	spindle assembly checkpoint
SEM	standard error of the mean
siRNA	small interfering RNA
SNV	single nucleotide variant
SSA	single strand annealing
ssDNA	single stranded DNA
Tet	tetracycline
TLS	translesion synthesis
TMZ	temozolomide
TSS	transcriptional start site
REDACTED	**REDACTED**
UV	ultra-violet

Declaration by Author

I, the author, confirm that the Thesis is my own work. I am aware of the University's Guidance on the Use of Unfair Means (www.sheffield.ac.uk/ssid/unfair-means). This work has not been previously been presented for an award at this, or any other, university.

Exception to declaration (collaborations):

In Chapter 3, RNA-Seq of SHEP-Tet21N MYCN ON and OFF cells was undertaken. I extracted the RNA from these cells, which was then sent for RNA-Seq analysis in collaboration with Dr. Anestis Tsakiridis' laboratory group at the University of Sheffield. Raw reads were analysed by Dr. Florian Halbritter and Dr. Luis Montano-Gutierrez at St. Anna Children's Cancer Research Institute (CCRI), to provide raw counts. I used these raw counts to analyse expression using DESeq2.

In Chapter 3, RNA-Seq analysis of FA pathway expression across 39 neuroblastoma cell lines was undertaken. Raw read data was downloaded from the GSE89413 RNA-Seq dataset and analysed by Dr. Manoj Valluru at the University of Sheffield, to provide expected counts. I used these expected counts to analyse expression using DESeq2.

In Chapter 4, Hannah Walsh helped me undertake the staining of H2AX, FANCD2/RPA, and R-loop immunofluorescence experiments (Figures 4.16-4.20) in the lab. I then imaged and analysed all slides.

In Chapter 5, **REDACTED**. Hannah Walsh helped undertake a repeat of this experiment.

Chapter 1. Introduction

1.1 Neuroblastoma

1.1.1 Survival statistics of neuroblastoma

Neuroblastoma is an embryonal neuroendocrine tumour arising from aberrant development of the peripheral sympathetic nervous system (Maris, 2010; Matthay et al., 2016; Ponzoni et al., 2022). Accounting for 6% of childhood cancer registrations in the UK, neuroblastoma is the most common extracranial solid tumour of childhood and is the most common malignancy diagnosed in the first year of life (Maris, 2010). The average age of diagnosis is 2 years old, with 90% of cases occurring in those less than 5 years old (Qiu and Matthay, 2022). Primary tumours can occur anywhere in the sympathetic nervous system such as the abdomen, thorax and neck, however over 50% of cases form in the medulla of the adrenal glands (Vo et al., 2014). The most common sites of metastases are the bone marrow, bone, lymph nodes, brain and liver (DuBois et al., 1999; Cohn et al., 2009). Although outcomes have improved, neuroblastoma accounts for 15% of all paediatric cancer mortality and the five-year survival of those with high-risk neuroblastoma remains at 50% (Gatta et al., 2002; Maris, 2010; Park et al., 2013; Irwin et al., 2021). This highlights the need for novel neuroblastoma therapeutics with greater efficacy.

1.1.2 Neuroblastoma risk group classification

Neuroblastoma risk-group assignment has been globally unified by the International Neuroblastoma Risk Group Staging System (INRGSS) (Cohn et al., 2009; Irwin et al., 2021). Patients are classified into very low, low, intermediate and high-risk groups (Table 1.1). The statistically significant prognostic features that define risk group classification are; tumour stage, an age threshold of 18 months, tumour histology, grade of tumour differentiation, *MYCN* amplification status, chromosome 11q aberrations and DNA ploidy (Brodeur et al., 1984; London et al., 2005; Cohn et al., 2009; Irwin et al., 2021). The INRGSS enables prognosis prediction and treatment stratification despite a broad heterogeneity of neuroblastoma clinical phenotypes (Cohn et al., 2009; Maris, 2010). Clinical

behaviour ranges from spontaneous regression without treatment to metastatic progression or relapse despite escalation in dose-intensive, multimodal treatment (Maris, 2010; Qiu and Matthay, 2022). Extensive diversity between risk groups is reflected in the reduction of five-year survival from 98% in low-risk cases to 50% in high-risk cases (Matthay et al., 1999; Perez et al., 2000; Cohn et al., 2009; Maris, 2010; Park et al., 2013; Irwin et al., 2021).

Table 1.1 International Neuroblastoma Risk Group (INRG) pre-treatment classification. Neuroblastoma cases are classified into very low, low, intermediate, and high-risk groups according to these prognostic features. INRG stages classified as: L1; tumour confined to organ of origin with no image-defined risk factors, L2; locoregional tumour with image-defined risk factors, M; distant metastases, MS; distant metastases limited to skin, liver and bone marrow in patients below 18 months. GN; ganglioneuroma, GNB; ganglioneuroblastoma. Blank field = 'any'. Table adapted from Cohn et al., (2009).

Pre-treatment risk group	INRG stage	Age (months)	Histologic category	Grade of tumour differentiation	MYCN amplification	11q aberration	Ploidy
Very low	L1		Any (except GN maturing; GNB intermixed)		No		
	L1/L2		GN maturing; GNB intermixed				
	L2		GN maturing; GNB intermixed				
	MS	< 18			No	No	
Low	L2	< 18	Any (except GN maturing; GNB intermixed)		No	No	
	L2	≥ 18	GNB nodular; neuroblastoma	Differentiating	No	No	
	M	< 18			No		Hyperdiploid
Intermediate	L2	< 18	Any (except GN maturing; GNB intermixed)		No	Yes	
	L2	≥ 18	GNB nodular; neuroblastoma	Differentiating	No	Yes	
	L2	≥ 18	GNB nodular; neuroblastoma	Poorly/Un- differentiated	No		
	M	< 12			No		Diploid
	M	12 to < 18			No		Diploid
High	L1		Any (except GN maturing; GNB intermixed)		Yes		
	L2				Yes		
	M	< 18			Yes		
	M	≥ 18					
	MS	< 18			No	Yes	
	MS	< 18			Yes		

1.1.3 Neuroblastoma treatment pipelines

1.1.3.1 Treatment of low- and intermediate-risk neuroblastoma

Development of risk-adapted treatment strategies has reduced treatment intensity for those with low- and intermediate-risk disease whilst maintaining a five-year survival rate of 98% and 96% respectively (Perez et al., 2000; Baker et al., 2010; Strother et al., 2012; Irwin et al., 2021). Most localised low-risk neuroblastoma

cases require surgery alone (Perez *et al.*, 2000; London *et al.*, 2005; Strother *et al.*, 2012; Park *et al.*, 2013). Low-risk cases, in particular those with stage MS disease, show frequent spontaneous regression meaning expectant observation is often considered safe primary therapy (Cole and Everson, 1956; Carlsen, 1990; Hero et al., 2008; Cohn et al., 2009; Nuchtern et al., 2012; Strother et al., 2012). Patients with metastatic or locally advanced disease of intermediate-risk undergo surgery and four to eight cycles of moderate-dose, multi-agent chemotherapy (Matthay et al., 1998; Baker et al., 2010; Rubie et al., 2011; Park et al., 2013). However, a phase III clinical trial is currently being undertaken to determine the outcome of observation alone in asymptomatic intermediate-risk cases with favourable disease biology (Qiu and Matthay, 2022). Low- and intermediate-risk treatment optimisation therefore aims to further reduce treatment intensity to minimise long term adverse effects such as hearing loss and secondary malignancies (Gurney et al., 2007; Laverdiére et al., 2009; Rubie et al., 2011; Cohen et al., 2014; Applebaum et al., 2015; Zheng et al., 2018; Geurten et al., 2019; Norsker et al., 2020).

1.1.3.2 Treatment of high-risk neuroblastoma

Half of all neuroblastoma cases are classified as high-risk at diagnosis. High-risk neuroblastoma is often characterised by unfavourable tumour histology, an age over 18 months, *MYCN* amplification, loss of heterozygosity at 1p or 11q loci, and disease metastasis (Huang and Weiss, 2013; Matthay et al., 2016; Qiu and Matthay, 2022). In contrast to low-risk therapy minimisation, high-risk neuroblastoma treatment is intensive and multimodal. The high-risk treatment strategy consists of multi-agent induction chemotherapy, surgical resection, high-dose myeloablative consolidation chemotherapy with autologous stem cell transplant (ASCT), radiotherapy, differentiating therapy and GD2-directed immunotherapy (Figure 1.1) (Matthay *et al.*, 1999; Simon *et al.*, 2004; Pritchard *et al.*, 2005; Park *et al.*, 2013; Smith and Foster, 2018; Qiu and Matthay, 2022).

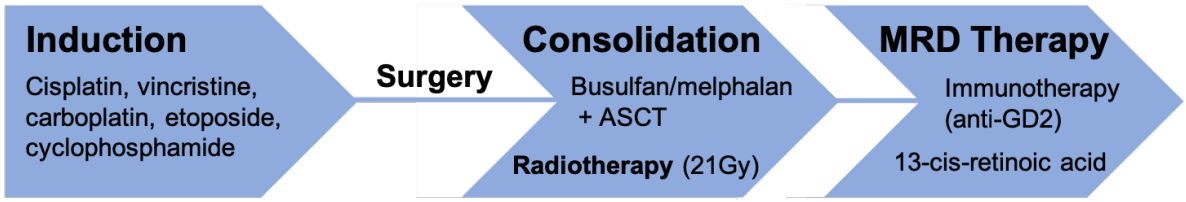

Figure 1.1. High-risk neuroblastoma treatment schema.
Induction chemotherapy delivered at 10-day intervals (eight cycles), surgical resection, myeloablative consolidation chemotherapy with autologous stem cell transplant (ASCT), radiotherapy and minimal residual disease (MRD) therapy. Drugs used in the UK for each stage are listed.

The SIOP European Neuroblastoma group employs rapid COJEC based induction chemotherapy in which the chemotherapeutics cisplatin, vincristine, carboplatin, etoposide and cyclophosphamide are given in eight treatment cycles delivered at 10 day intervals (Qiu and Matthay et al., 2022). Cisplatin, carboplatin and cyclophosphamide are DNA crosslinking agents which most commonly attack guanine bases on DNA to form intra- and inter-strand crosslinks (Eastman, 1986; Deans and West, 2011). Vincristine inhibits microtubule polymerisation and therefore disrupts spindle formation and mitosis (Skubnik et al., 2021). Etoposide inhibits topoisomerase II enzymes by binding to the enzyme-DNA complex and preventing re-ligation of the DSB generated by topoisomerase II (Montecucco et al., 2015). This results in higher levels of DNA damage and a reduction in the levels of topoisomerase II available to relieve DNA supercoiling (Montecucco et al., 2015). Induction chemotherapy response rates range from 71% to 85%, and patients which respond to induction chemotherapy have longer event-free survival (Ladenstein et al., 2017; Park et al., 2019; Pinto et al., 2019; Garaventa et al., 2021). Efforts have therefore been made to intensify induction therapy to improve response rates, however addition of further chemotherapy cycles did not significantly improve event-free survival (Ladenstein et al., 2017; Garaventa et al., 2021). Alternative strategies to improve the efficacy of induction chemotherapeutics are therefore required.

Following surgical resection, busulfan and melphalan are used in high-dose myeloablative consolidation chemotherapy followed by ASCT (Matthay et al., 1999; Berthold et al., 2005). Busulfan and melphalan are bifunctional alkylating agents which commonly induce formation of inter- and intra-strand crosslinks, particularly

between guanine bases (Osborne and Lawley 1993; Myers et al., 2017). Radiotherapy is then delivered at a dose of 21Gy to the primary tumour bed (Matthay et al., 1999; Haas-Kogan et al., 2003). This high-dose consolidation therapy has increased risks of acute and long-term organ toxicities and it is therefore desirable to minimise the need for these treatments through development of targeted therapeutics.

Maintenance therapy is then used to treat minimal residual disease and reduce relapse risk. This involves treatment with 13-*cis*-retinoic acid to differentiate residual tumour cells and immunotherapies such as anti-GD2 antibodies (Matthay et al., 2009; Yu et al., 2010; Ladenstein et al., 2018; Yu et a. 2021). GD2 is a disialoganglioside expressed on the surface of neuroectodermal tumours (Voeller and Sondel 2019). Anti-GD2 monoclonal antibodies induce death of neuroblastoma cells through antibody-dependent cell-mediated cytotoxicity and complement-dependent cytotoxity (Voeller and Sondel 2019). Development of immunotherapies to overcome the suppression of anti-tumour immunity induced by high-risk neuroblastomas is currently a large area of ongoing research (Bernards et al., 1986; Raffaghello et al., 2004; Wölfl et al., 2005; Asgharzadeh et al., 2012; Mina et al., 2015; Federico et al., 2017; Melaiu et al., 2017; Mody et al., 2017; Mody et al., 2020; Furman, 2021; Furman et al., 2022; Theruvath et al., 2022). Relapsed disease is treated with established salvage chemotherapy regimens including temozolomide with irinotecan or topotecan (Kushner et al., 2006; London et al., 2011; Bagatell et al., 2011; Di Giannatale et al., 2014).

Improvements in treatment efficacy over the past few decades have resulted in an increase in five-year survival from below 20% to approximately 50% (Qiu and Matthay, 2022). However, given the high toxicity and extensive late-onset adverse effects induced by current treatments, further progress in treatment efficacy is unlikely to be achieved through further escalation in treatment intensity (Matthay et al., 1999; Gurney et al., 2007; Laverdiére et al., 2009; Rubie et al., 2011; Bhatnagar and Sarin, 2012; Park *et al.*, 2013; Cohen et al., 2014; Applebaum et al., 2015; Zheng et al., 2018; Geurten et al., 2019; Norsker et al., 2020; Qiu and Matthay, 2022). Novel, targeted therapy is therefore required to reduce long-term side-effects and improve high-risk neuroblastoma survival (Qiu and Matthay, 2022). Correlating the genetic profiles of tumours with tumour-specific pathway dependencies enables identification of novel targets for personalised therapy. Recent clinical trials

demonstrate the potential direct translation of neuroblastoma molecular target identification into novel therapy, such as the development of ALK inhibitors which target neuroblastoma cells harbouring *ALK* gain of function aberrations (George et al., 2008; Infarinato et al., 2016; Mosse et al., 2017; Mossé et al., 2017; Schulte and Eggert 2021; Foster et al., 2021). However, development of novel neuroblastoma therapeutics is further complicated by inadequate agent formulation for administration to young children (Park *et al.*, 2013; Barone *et al.*, 2019).

1.1.4 Cellular origin of neuroblastoma

Neuroblastoma arises from cells of the developing sympathetic nervous system. During normal embryonic development, multipotent neural crest cells (NCCs) undergo an epithelial-to-mesenchymal transition (EMT) following closure of the central nervous system (CNS) neural tube (Kerosuo *et al.*, 2018; Leathers and Rogers, 2022). NCCs then migrate from the dorsal neural tube and differentiate to form the sympathetic chain, suprarenal sympathetic ganglion and adrenal medulla neuroendocrine cells (Dong et al., 2020; Jansky et al., 2021; Kameneva et al., 2021; Kildisiute et al., 2021). Early migrating NCCs primarily differentiate into sympathoadrenal progenitor cells and subsequently into sympathetic ganglion cells and a small population of adrenal chromaffin cells (Tsubota et al., 2017; Ponzoni et al., 2022). Late-migrating NCCs differentiate into Schwann cell precursors (SCPs) and subsequently into the majority of adrenal medulla chromaffin cells (Furlan *et al.*, 2017; Tsubota et al., 2017; Ponzoni et al., 2022). Neuroblastomas form in the adrenal gland or along the sympathetic chain and therefore likely originate from the malignant transformation of NCCs or their downstream SCPs (Qiu and Matthay, 2022). Differentiation along these lineages is tightly regulated by a network of transcription factors which drive changes in the epigenetic and transcriptional landscapes (Ponzoni et al., 2022). Whilst tumorigenesis results from disruption of this regulation, expression of neural crest markers and key temporally-regulated transcription factors are also observed in neuroblastoma cells (Gershon et al., 2005; Kerosuo *et al.*, 2018; Kildisiute et al., 2021). For example, expression of GD2 biosynthetic enzymes, *ALK*, human norepinephrine transporter (*hNET*), and *MYCN,* is often observed (Cheung et al., 1985; DuBois et al., 2012; Jansky et al., 2021; Dong et al., 2020; Kildisiute et al., 2021; Kameneva et al., 2021).

Correlating the development of neural crest lineages to the origin of different neuroblastoma stages is important in understanding the vast clinical heterogeneity observed. Recent single-cell transcriptomic analyses demonstrate that neuroblastoma cells transcriptionally resemble cells of different stages along the normal lineage of embryonic neural crest differentiation (Jansky et al., 2021; Kameneva et al., 2021). Neuroblastomas containing a greater proportion of cells with a mature, differentiated neuroblast phenotype have better prognoses than those with more early neuroblast-like cells (Jansky et al., 2021; Kameneva et al., 2021).

Resemblance of different neural crest lineage stages also partially accounts for intra-tumour heterogeneity. Both differentiated adrenergic (ADRN) and less-differentiated mesenchymal (MES) cell populations regulated by distinct super-enhancer landscapes are observed within singular neuroblastomas (Boeva et al., 2017; van Groningen et al., 2017; van Groningen et al., 2019). Super-enhancers are large clusters of enhancers with high levels of transcription factor binding. The super-enhancer landscape describes the position of such active enhancers within the genome, with different landscapes driving high expression of genes which typically define cell identity (Kai et al., 2021). This super-enhancer landscape and cell identity is often promoted and maintained in a positive feedback loop in which the transcription factors that bind to the super-enhancers are themselves regulated by super-enhancers. However, epigenetic modifications can drive evolution of super-enhancer landscapes throughout cellular differentiation, enabling differentiation of stem cells down different lineages (Kai et al., 2021).

Neuroblastoma cell lines comprise either a mixture of both cell types or a singular MES or ADRN cell type (Biedler et al., 1973; Boeva *et al.*, 2017). These two cell types are induced by establishment of two different core regulatory circuitries (CRCs) (Boeva *et al.*, 2017; van Groningen *et al.*, 2017; Zeid *et al.*, 2018). CRCs are a set of super-enhancer marked transcription factors which bind and define virtually all active enhancer and super-enhancer profiles to induce and maintain lineage specification in an auto-regulatory loop (van Groningen *et al.*, 2017; Durbin *et al.*, 2018). The MES-specific CRC consists of 20 transcription factors which induce an NCC-like state including TWIST1 and NOTCH2, whereas the ADRN-specific CRC includes 18 transcription factors involved in sympathoadrenal lineage specification including PHOX2B and HAND1 (van Groningen et al., 2017; van Groningen et al., 2019). MES cells display greater chemo-resistance and are enriched for in following

chemotherapy treatment (Boeva *et al.*, 2017; van Groningen *et al.*, 2017). Given these two cell states are interchangeable, this enrichment could be accounted for by both MES selection and ADRN to MES trans-differentiation (Boeva et al., 2017; van Groningen et al., 2017; van Groningen et al., 2019). For example, ADRN-to-MES transition conferred resistance to ALK inhibitors (Westerhout et al., 2022). These two cell states therefore contribute to the dynamic nature of intra-tumoral heterogeneity in neuroblastoma. Interestingly, distinct super-enhancer signatures were also observed between neuroblastoma risk subtypes, suggesting CRCs also contribute to inter-tumoral heterogeneity (Gartlgruber et al., 2021). The ability to target both ADRN and MES cell types despite their divergent gene expression profiles is important in the treatment of minimal residual disease to prevent relapse.

1.1.5 Genetic characteristics of neuroblastoma

1.1.5.1 Familial neuroblastoma: Germline aberrations in *PHOX2B* and *ALK*

A rare subgroup of neuroblastomas, accounting for 2-3% of cases, arise from autosomal dominant germline mutations (Knudson and Strong, 1972; Friedman *et al.*, 2005; Mossé *et al.*, 2008). The genetic aetiology of familial neuroblastoma is largely attributed to inherited inactivating aberrations in *PHOXB2* or activating aberrations in *ALK* (Amiel et al., 2003; Mosse et al., 2004; Trochet et al., 2004; Raabe et al., 2007; Mossé et al., 2008). *PHOX2B* encodes a transcription factor which is a master regulator of neural crest lineage specification, whilst *ALK* encodes a receptor tyrosine kinase expressed exclusively in the developing nervous system with a putative function in neuronal differentiation (Amiel et al., 2003; Mosse et al., 2004; Trochet et al., 2004; Raabe et al., 2007; Mossé et al., 2008). Both PHOX2B and ALK therefore function in sympathoadrenal development.

Activating *ALK* aberrations are observed in 80% of familial neuroblastomas, but also occur somatically in 3-14% of sporadic neuroblastomas (George et al., 2008; Mossé et al., 2008; Janoueix-Lerosey et al., 2009; De Brouwer et al., 2010; Schönherr et al., 2012; Hasan et al., 2013; Takagi et al., 2017). Expression of activating *ALK* mutations in the neural crest of transgenic mice induces neuroblastoma formation (Heukamp et al., 2012). A role in cell proliferation,

migration and invasion explains the tumorigenic potential of *ALK* activating mutations (Hasan et al., 2013). *ALK* mutation and amplification is associated with poor prognosis and frequently occurs in parallel with amplification of *MYCN* (De Brouwer et al., 2010; Jeison et al., 2010). In fact, *ALK* activating mutations and coincident *MYCN* mis-expression synergistically drive NCC transformation and neuroblastoma tumorigenesis (Berry et al., 2012; Heukamp et al., 2012; Schönherr et al., 2012; Zhu et al., 2012; Hasan et al., 2013; Schulte et al., 2013). This synergistic tumorigenic effect may occur via ALK-mediated upregulation and stabilisation of MYCN (Schönherr et al., 2012; Hasan et al., 2013). Similarly, MYCN directly upregulates *ALK* expression to establish a MYCN-inducing positive feedback loop, leading to rapid MYCN-induced malignant transformation (Berry et al., 2012; Schönherr et al., 2012; Hasan et al., 2013). ALK therefore also potentiates the oncogenic activity of MYCN and is therefore a promising therapeutic target (George et al., 2008; Park et al., 2013; Infarinato et al., 2016; Mosse et al., 2017; Schulte and Eggert, 2021; Foster et al., 2021).

1.1.5.2 Common somatic aberrations in neuroblastoma

Somatic genetic alterations primarily define neuroblastoma clinical behaviour (Park et al., 2013). Similar to other paediatric tumours, neuroblastoma rarely exhibits recurrent driver mutations yet displays a high frequency of characteristic chromosomal copy number changes (Pugh et al., 2012; Pugh et al., 2013; Janoueix-Lerosey et al., 2009; Tsubota and Kadomatsu, 2017). Genomic sequencing of 240 high-risk neuroblastomas showed most mutations, predominantly in neuritogenesis genes, occur at frequencies below 1% (Cheung et al., 2012; Molenaar et al., 2012; Kumps et al., 2013; Pugh et al., 2013). A recurrent *MYCN* point mutation, inducing 2-fold *MYCN* expression, was observed in 2% of cases (Pugh et al., 2013).

Chromosome copy number imbalances and segmental alterations therefore drive neuroblastoma progression (Attiyeh et al., 2005; Janoueix-Lerosey et al., 2009; Schleiermacher et al., 2010; Kumps et al., 2013). Gain or loss of whole chromosomes can result in hyperdiploidy, and this is associated with favourable prognosis in non-*MYCN* amplified (non-MNA) disease (George et al., 2005). In contrast, segmental chromosome alterations are associated with poor prognosis (Bown et al., 1999; Maris et al., 2000; Janoueix-Lerosey et al., 2009; Carén et al.,

2010; Matthay et al., 2016). Recurrent characteristic chromosomal aberrations include 17q gain and loss of heterozygosity (LOH) at 1p or 11q (Brown et al., 1999; Guo et al., 1999; Attiyeh et al., 2005; White et al., 2005; Sanmartín et al., 2017b). Less frequent alterations observed to correlate with poor prognosis include loss of 3p, 4p, 5p, 6q, 9p, or 18q (Depuydt et al., 2018; Qiu and Matthay, 2022). 17q gain is observed in 50% of neuroblastomas and is the most frequent alteration in high-risk cases (Bown et al., 1999). Given the proposed transcriptional addiction to the CRC in neuroblastoma cells, it has been suggested that 17q gain confers selective advantage through increased expression of the neuroblastoma CRC transcription factor TBX2 encoded at this locus (Decaesteker et al., 2018). LOH at 1p is observed in 23-35% of neuroblastoma cases and correlates with *MYCN* amplification (Maris et al., 2000; Attiyeh et al., 2005; White et al., 2005; Thompson et al., 2016). In contrast, LOH at 11q is observed in 11-48% of cases and is almost mutually exclusive with *MYCN* amplification (Guo et al., 1999; Luttikhuis et al., 2001; Maris et al., 2001; Plantaz et al., 2001; Spitz et al., 2003; Attiyeh et al., 2005; Carén et al., 2010). Both 11q and 1p deletions are associated with reduced event-free survival, likely due to the tumour suppressor genes encoded at 1p loci such as *CHD5*, *CAMTA1*, *ARID1A, AJAP1*, *KIF1B* and *CASZ1* (Maris et al., 2000; Fujita et al., 2008; Okawa et al., 2008; Henrich et al., 2012; Sausen et al., 2013; Shi et al., 2020), and at 11q loci such as *ATM, CHK1, MRE11A* and *H2AFX* (Luttikhuis et al., 2001; Mandriota et al., 2015; Sanmartin et al., 2017b; Mlakar et al., 2017; Carén et al., 2010; Takagi et al., 2017).

Several specific gene alterations are also frequently observed in neuroblastomas, such as amplification of *MYCN* and rearrangements at the *TERT* locus. Chromosomal rearrangements which position super-enhancers near the *TERT* locus are observed in 25% of high-risk neuroblastomas (Peifer et al., 2015; Valentijn et al., 2015; Ackermann et al., 2018; Roderwieser et al., 2019). This induces *TERT* overexpression and therefore upregulates telomerase activity to maintain telomere length. *MYCN* amplification is observed in approximately 20% of neuroblastomas, and is always associated with high risk disease due to its association with an aggressive clinical phenotype (Kohl et al., 1983; Schwab et al., 1983; Brodeur et al., 1984; Schwab, 1990; Moreau et al., 2006; Cohn et al., 2009). The role of MYCN in neuroblastoma is further discussed below in Chapter 1.1.6.

1.1.6 MYCN in neuroblastoma

1.1.6.1 MYCN in embryonic development

MYCN is a transcription factor that regulates a wide array of cellular processes including differentiation, proliferation, growth, metabolism, and apoptosis (Huang and Weiss, 2013). Whilst *MYCN* is not usually expressed in adult tissues, spatial and temporal regulation of *MYCN* expression is essential during embryogenesis (Zimmerman et al., 1986). Homozygous knockout of *MYCN* function is lethal in mouse embryos, with defects in cranial and spinal ganglia observed (Charron et al., 1992). MYCN is particularly crucial for brain development, with inactivation of MYCN specifically in neuronal progenitor cells resulting in ataxia and behavioural abnormalities (Jakobovits et al., 1985; Knoepfler et al., 2002; Hatton et al., 2006). Heterozygous germline loss-of-function alterations in *MYCN* results in Feingold syndrome, characterised by digital abnormalities, microcephaly, gastrointestinal atresia and variable learning disabilities (Cognet et al., 2011). This highlights the vital and pluripotent role of MYCN in human embryonic development.

Neuroblastomas arise from aberrant sympathoadrenal development (Figure 1.2). Temporal changes in *MYCN* expression are vital in normal sympathoadrenal development. Initially, *MYCN* is highly expressed in NCCs to promote expansion and ventral migration from the neural plate border (Wakamatsu et al., 1997; Ponzoni et al., 2022). However, *MYCN* is then downregulated to very low levels during NCC migration (Ponzoni et al., 2022). Subsequently *MYCN* is expression is re-induced in sympathoadrenal progenitors by Wnt signalling to promote neuronal fate commitment and cellular expansion of neural precursors before it is gradually downregulated to enable terminal differentiation into sympathetic neuronal or chromaffin cells (Zimmerman et al., 1986; Wakamatsu *et al.*, 1997; Knoepfler et al., 2002; Hansford et al., 2004; ten Berge et al., 2008; Kapeli and Hurlin, 2011; Alam et al., 2009; Ponzoni et al., 2022).

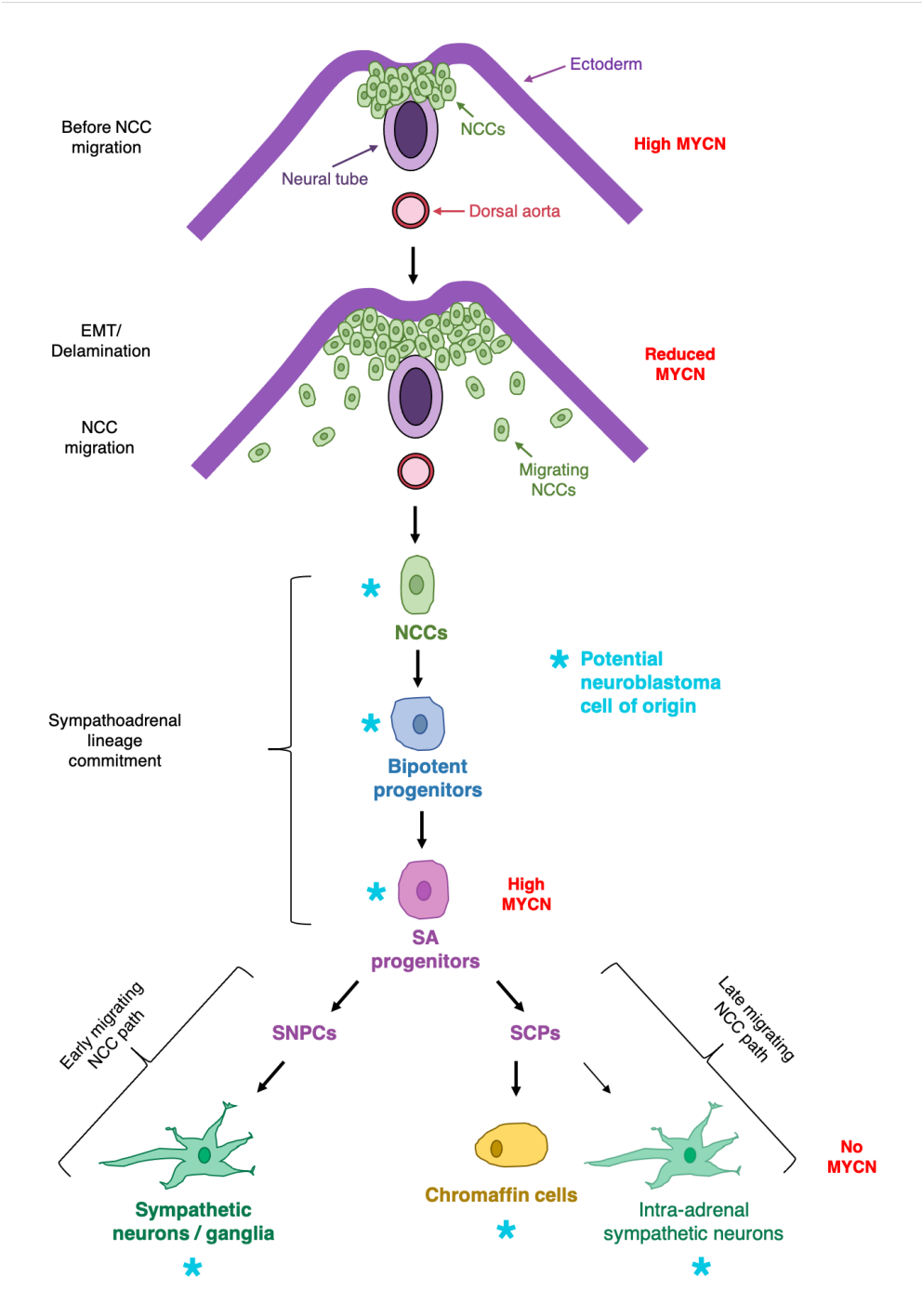

Figure 1.2. Neuroblastoma initiation during embryonic sympathoadrenal development.
During embryonic development, *MYCN* is downregulated in neural crest cells (NCCs) to promote NCC migration from the neural plate. NCCs differentiate into sympathoadrenal progenitors (SA progenitors) which upregulate *MYCN* expression to high levels to promote expansion and neural lineage commitment. Early migrating NCCs primarily differentiate into sympathetic neurons/ganglia via SNPCs (Sympathetic Neural Progenitor Cells). Late migrating NCCs primarily differentiate into adrenaline-producing chromaffin cells in the adrenal medulla, whilst some differentiate into intra-adrenal sympathetic neurons. *MYCN* is downregulated during this terminal differentiation. Aberrant differentiation at any stage along this pathway has the potential to induce neuroblastoma formation, with neuroblastoma cells often resembling NCCs. For example, aberrant high expression of MYCN in sympathetic neurons may promote neuroblastoma tumorigenesis.

1.1.6.2 *MYCN* amplification in high-risk neuroblastoma

Deregulation of the *MYCN* oncogene has been implicated in the pathogenesis of several childhood cancers including neuroblastoma, medulloblastoma, retinoblastoma and Wilm's tumour, as well as adult cancers such as non-small cell lung cancer, prostate cancer, basal cell carcinoma and breast cancer (Kohl et al., 1983; Armstrong and Krystal et al., 1992; Marshall et al., 2014; Rickman et al., 2018). *MYCN* amplification occurs in 20-25% of neuroblastomas, inducing a 20- to 140-fold amplification in expression (Kohl et al., 1983; Brodeur et al., 1984; Schwab et al., 1984; Moreau et al., 2006; Maris, 2010). *MYCN* amplified (MNA) disease is characterised by stroma-poor, undifferentiated tumours in patients over one year of age (Shimada et al., 1995; Moreau et al., 2006; Cohn et al., 2009). Clinically, *MYCN* amplification significantly correlates with rapid tumour progression, early chemo-resistance and reduced event-free survival, even in localised disease (Kohl et al., 1983; Brodeur et al., 1984; Seeger et al., 1985; Moreau et al., 2006; Canete *et al.*, 2009; Maris, 2010). MNA neuroblastomas are therefore always classified as high-risk, independent of tumour stage (Cohn et al., 2009; Irwin et al., 2021). As such, *MYCN* amplification has important clinical value as one of the most reliable, independent prognostic biomarkers for high-risk disease and advanced tumour stage, as indicated by an increase in *MYCN* amplification prevalence to 50% in stage 3 and 4 neuroblastomas alone (Seeger et al., 1985; Moreau et al., 2006; Thompson et al., 2016). However, activation of the MYCN pathway has been suggested to be more prognostically relevant than amplification of its genomic locus (Valentijn et al., 2012; Suenaga et al., 2014). MYC-signalling is hypothesised to be important for induction of an aggressive neuroblastoma phenotype as MYC overexpression is often observed in high-risk cases without *MYCN* amplification (Breit and Schwab, 1989). Despite improvements in the intensive multimodal treatment strategies, the five-year survival rate for MNA neuroblastoma remains below 50%. Even in high-risk cases with unfavourable histology, *MYCN* amplification further reduced progression-free survival from 29% to 13% (Shimada et al., 1995). This highlights a need for novel therapeutics which improve current treatment efficacy.

1.1.6.3 MYCN drives tumour progression

It is well established that aberrant oncogene expression drives malignant transformation and progression (Tonini et al., 1994; Schwab, 1999). Activation of proto-oncogenes can occur via; increased singular gene expression, activating mutations, genetic rearrangement, or DNA amplification (Kohl et al., 1983; Brodeur et al., 1984). Although the precise timing or mechanism of *MYCN* amplification in neuroblastoma is unknown, *MYCN* amplification is present at diagnosis and is never acquired during later tumour progression (Cohn et al., 2009). This suggests amplification or mis-expression of *MYCN* is an early driver event in neuroblastoma, in contrast to most other cancers in which gene amplifications are usually observed in late tumorigenesis (Matthay et al., 2016; Rickman et al., 2018).

Multiple studies have demonstrated that mis-expression of *MYCN* is sufficient for tumorigenesis (Tsubota et al., 2018; Otte et al., 2021). Initially, *MYCN* mis-expression was shown to induce the neoplastic transformation of cultured embryonic rat cells (Schwab et al., 1985). Similarly, *MYCN* mis-expression is sufficient to transform primary neural crest cells into neuroblastoma cells with tumorigenic potential (Olsen et al., 2017). Weiss et al., (1997) demonstrated that targeted *MYCN* overexpression in neuroectodermal cells is sufficient to induce neuroblastoma in TH-MYCN transgenic mice. During normal development, an excess of sympathoadrenal precursors are produced which undergo controlled apoptosis during final maturation stages following a reduction in neural growth factor signalling (Yuan and Yakner, 2000). As a master regulator of proliferation, differentiation and apoptosis, MYCN has been shown to induce neuroblastoma formation by promoting the proliferation and inhibiting the differentiation and apoptosis of neural progenitors (Rickman et al., 2018). For example, Hansford et al., (2004) showed that whilst normal mice developed neuroblast hyperplasia at birth which fully regressed by two weeks, targeted *MYCN* overexpression in TH-MYCN mice induced an increase in neuroblastoma hyperplasia formation and delayed hyperplasia regression leading to tumour formation six weeks after birth. This suggested *MYCN* mis-expression induced tumorigenesis by preventing the normal apoptosis of sympathoadrenal precursor cells (Hansford et al., 2004). Similarly, Alam et al., (2009) observed that MYCN drives formation of neuroblastoma in TH-MYCN mice by promoting the expansion and inhibiting the differentiation of PHOX2B-expressing neural

progenitors, leading to observation of hyperplastic lesions in the sympathetic ganglia in the first few weeks after birth. Also, Zhu et al., (2012) showed that mis-expression of *MYCN* in zebrafish sympathoadrenal progenitor cells induced neuroblastoma formation by aberrantly maintaining progenitor multipotency and blocking development of chromaffin cells.

1.2 Molecular functions of MYCN

1.2.1 MYCN in the MYC family of transcription factors

The human MYC family of helix-loop-helix/leucine zipper transcription factors comprises *MYC, MYCN* and *MYCL* genes encoding c-Myc, N-Myc and L-Myc proteins respectively (Kohl et al., 1983; Brodeur et al., 1984; Zeid et al., 2018). For clarity, these genes are referred to as *MYCC, MYCN* and *MYCL*, and their proteins are referred to as MYCC, MYCN and MYCL throughout this thesis. MYC transcription factors heterodimerize with Max at consensus E-box motifs to regulate a vast array of transcriptional targets and therefore regulate a wide variety of cellular processes including promotion of proliferation, growth, pluripotency and self-renewal and inhibition of cell cycle arrest and differentiation (Schwab et al., 1985; Yancopoulos et al., 1985; Cavalieri and Goldfarb, 1988; Alex *et al.*, 1992; Torres *et al.*, 1992; Huang and Weiss, 2013). As master regulators of many cancer hallmarks, MYC transcription factors are widely recognised as major drivers of tumorigenesis. This is evidenced by the high frequency of MYC gene alteration and deregulation observed across many malignancies, and the ability of MYC protein misexpression to promote tumorigenesis (Schwab et al., 1985; Weiss et al., 1997; Hansford et al., 2004; Alam et al., 2009; Zhu et al., 2012; Dang, 2012; Olsen et al., 2017; Rickman et al., 2018; Schaub et al., 2018). In particular, *MYCC* is deregulated in up to 70% of malignancies, and amplification of at least one MYC family member is observed in 28% of all cancers (Dang, 2012; Schaub et al., 2018).

The *MYCN* oncogene was initially identified in neuroblastoma cell lines as a region of amplified DNA with high homology to viral *MYCC* (Schwab et al., 1983). *MYCN* is localised on chromosome 2p23-24 however the *MYCN* amplification locus varies (Cox et al., 1965; Kohl et al., 1983; Schwab et al., 1983, Brodeur et al., 1984; Schwab et al., 1984). The three MYC isoforms are highly structurally and functionally

homologous, with highly conserved amino acid sequences termed ‘MYC boxes’ defining binding regions for DNA and key interacting proteins that are necessary for MYC function (Kohl et al., 1986; Baluapuri et al., 2020). Similar biological function and partial functional redundancy is demonstrated by the prevention of embryonic lethality and rescue of immune function in *MYCC*-knockout mice following knock-in of *MYCN* at the *MYCC* locus (Malynn et al., 2000). An example of shared functionality is the ability of both *MYCN* and *MYCC* to maintain stem cell pluripotency and self-renewal. Mis-expression of either isoform reverts fibroblasts to induced pluripotent stem cells (iPSCs) (Varlakhanova et al., 2010). This accounts for the reduced differentiation observed in MNA-neuroblastomas (Moreau *et al.*, 2006). Frequent *MYC* deregulation in high-risk cases without *MYCN* amplification suggests MYC-signalling may be vital for this aggressive phenotype (Breit and Schwab, 1989).

Despite these shared cellular functions and tumorigenic capabilities, it should be noted that each MYC paralogue also has unique properties as demonstrated by differences in the characteristics and dependencies of tumours with aberrant expression of different MYC proteins (Cole et al., 1986; Huang and Weiss, 2013; Baluapuri et al., 2020). Functional redundancy is also limited endogenously due to spatiotemporal differences in regulation during embryonic development and in adult tissues. Zimmerman et al., (1986) observed tissue-specific differences in the expression patterns of *MYCC* and *MYCN* in both new-born and adult mice. During embryonic development *MYCN* expression is predominantly observed in haematopoietic stem cells and neuronal precursors, with high expression observed in the brain and kidney of new-born mice (Zimmerman et al., 1986; Nagy et al., 1998; Knoepfler et al., 2002). In adult mice tissues, virtually no *MYCN* expression was observed, consistent with the lack of *MYCN* expression observed postnatally in human sympathetic ganglia (Zimmerman et al., 1986; Kerosuo et al., 2018). In contrast, *MYCC* was expressed more ubiquitously throughout many tissues in new-born mice, with highest expression observed in the thymus, spleen and liver (Zimmerman et al., 1986). *MYCC* expression was substantially reduced in most adult tissues, however low expression levels were observed in the thymus, spleen and intestine (Zimmerman et al., 1986). *MYCC* and *MYCN* therefore demonstrated higher expression in the developing tissues that give rise to their characteristic malignancies (Kohl et al., 1986; Zimmerman et al., 1986; Stanton et al., 1992). As such, endogenous *MYCC* expression is unable to compensate for *MYCN*-knockout

during mouse embryonic development leading to morphological central nervous system defects and embryonic lethality (Charron et al., 1992; Stanton et al., 1992; Sawai et al., 1993). Also, endogenous *MYCN* expression is unable to compensate for *MYCC*-knockout during embryonic development, resulting in early embryonic lethality (Davis et al., 1993). Similarly, whilst knockout of *MYCN* in neural stem and progenitor cells resulted in decreased proliferation of cerebellar granule neural precursors, knockout of *MYCC* had no effect (Kenney et al., 2003; Hatton et al., 2006). *MYCN* and *MYCC* also transcriptionally regulate each other, meaning expression of each isoform is often mutually exclusive (Breit and Schwab, 1989; Rosenbaum et al., 1989; Westermann et al., 2008).

1.2.2 Mechanisms of gene regulation employed by MYCN

As neuroblastoma is predominantly diagnosed in early childhood and rarely exhibits recurrent driver mutations, the ability of *MYCN* overexpression to drive neuroblastoma progression is unlikely due to mutations in MYCN target genes (Pugh et al., 2013). MYCN-induced differential expression therefore has a major role in driving the aggressive MNA phenotype. MYC proteins regulate the global transcriptional profile through multiple mechanisms (Baluapuri et al., 2020). Firstly, MYC transcription factors are observed to activate or repress a discrete set of target genes (Walz et al., 2014; Sabò et al., 2014; Zeid et al., 2018). MYC transcription factors predominantly induce upregulation of target genes transcribed by RNA Pol I and RNA Pol III but can either upregulate or downregulate target genes transcribed by RNA Pol II (Gomez-Roman et al., 2003; Grandori et al., 2005; Sabò et al., 2014). MYC and MYCN have been observed to regulate distinct sets of target genes which are often highly dependent on the cell type and experimental conditions (Baluapuri et al., 2020). In contrast, MYC proteins have also been shown to bind to all active promoters and enhancers to induce a global upregulation of all active genes and enhance the overall rate of transcription (Lin et al., 2012; Nie et al., 2012; Zeid et al., 2018).

These two seemingly conflicting observations can be accounted for by the gene-specific affinity model (Zeid et al., 2018; Baluapuri et al., 2020). Promoters and enhancers differ in their MYC binding affinity, and as such the level of MYC required for MYC-induced regulation differs (Zeid et al., 2018). Therefore MYC proteins can

regulate different sets of genes depending on its own expression level (Yustein et al., 2010; Zeid et al., 2018). At physiological levels, MYC transcription factors directly regulate target genes by high-affinity binding to consensus MYC E-box motifs within promoters and enhancers. In neuroblastoma, these high affinity targets comprise genes involved predominantly in growth and proliferation (Murphy et al., 2009; Valentijn et al., 2012; Zeid et al., 2018). At deregulated oncogenic levels, excess MYC can invade the active and accessible cis-regulatory landscape, binding to low-affinity non-canonical E-boxes which are prevalent within promoters and enhancers to induce further pleiotropic regulation and a weak upregulation of all active genes (Zeid et al., 2018; Baluapuri et al., 2020). This is highly dependent on the cell's pre-established chromatin landscape and explains the tissue and tumour-type specificity of global upregulation observed (Murphy et al., 2009; Valentijn et al., 2012; Zeid et al., 2018). Given the weaker MYC binding affinity, genes regulated by MYC proteins in a distal enhancer dominant manner display the greater transcriptional sensitivity to changes in MYC expression. In neuroblastoma, these low affinity targets comprise genes involved predominantly in de-differentiation (Zeid et al., 2018). For example, key neuroblastoma oncogenes and neural crest markers such as *HAND2* and *TH* are regulated by MYCN enhancer invasion and display the greatest transcriptional sensitivity to *MYCN* perturbation (Zeid et al., 2018).

The CRC and resulting active enhancer landscape therefore drives both lineage specification and tumour-type specific responses to changes in *MYCN* expression (Perini et al., 2005; Zeid et al., 2018). This could suggest *MYCN* amplification may therefore induce divergent phenotypes in MES and ADRN cell types which have differing CRCs. However, it has been observed that MYCN upregulates expression of ADRN CRC transcription factors such as PHOX2B, HAND2, GATA3 and ASCL1 through enhancer invasion to promote an ADRN phenotype (Zeid et al., 2018; Wang et al., 2019). Similarly, *MYCN* is expressed in sympathoadrenal progenitors during normal neural crest differentiation to promote neural fate commitment (Knoepfler et al., 2002; ten Berge et al., 2008; Kapeli and Hurlin, 2011). As such, the majority of *MYCN*-amplified neuroblastoma cell lines have an ADRN phenotype (Boeva et al., 2017; Durbin et al., 2018). Furthermore, Durbin et al., (2018) identified 147 potential gene dependencies specific to MNA neuroblastoma cells using an unbiased genome-scale CRISPR-Cas9 approach. Many ADRN CRC transcription factors were detected among these gene

dependencies, demonstrating that MNA neuroblastoma cells are addicted to the ADRN CRC. In support of this, MNA cells were shown to be dependent on the ADRN CRC to maintain high *MYCN* expression (Durbin et al., 2018), with another study observing that some *MYCN* amplicons are regulated by translocated ADRN CRC-driven super-enhancers (Helmsauer et al., 2020).

The affinity-based model of MYCN function is further complicated by the ability of MYCN to bind transcriptional targets via protein-protein interactions (Baluapuri et al., 2020). Similarly, interaction of MYCN with multiple epigenetic remodellers enables *MYCN* expression to redefine the global active cis-regulatory landscape that it regulates (Figure 1.3) (Baluapuri et al., 2020). For example, MYCN associates with EZH2; a methyltransferase in Polycomb Repressive Complex 2 (PRC2) that is responsible for H3K27 trimethylation (Figure 1.3A) (Corvetta et al., 2013). *MYCN* overexpression therefore downregulates PRC2 target genes (Tsubota et al., 2018). This is mechanism is important in NCC transformation, as evidenced by the reduction in tumour formation in TH-MYCN mice upon EZH2 knockdown (Tsubota et al., 2018). MYCN also interacts with DNA methyltransferases such as DNMT3A to methylate CpG islands at promoters and repress gene expression (Figure 1.3B) (Murphy et al., 2009). This mediates silencing of genes such as CDK inhibitor $p21^{CIP1}$, resulting in the inhibition of cell cycle arrest upon *MYCN* overexpression (Brenner et al., 2005). Finally, MYCN upregulates expression of histone deacetylases such as HDAC1, HDAC2 and SIRT1 in neuroblastoma (Figure 1.3C) (Knoepfler et al., 2006; Huang and Weiss, 2013; Zeid et al., 2018). SIRT1 stabilises MYCN to create a feed-forward loop (Marshall et al., 2011).

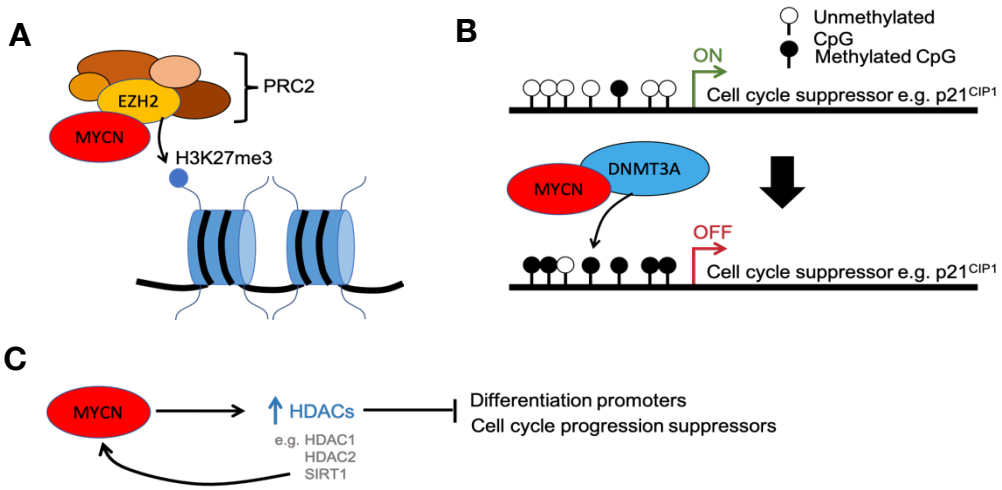

Figure 1.3. Mechanisms of epigenetic regulation by MYCN.
(A) MYCN associates with EZH2, a methyltransferase in Polycomb Repressive Complex 2 (PRC2) responsible for H3K27 trimethylation which marks regions of transcriptional silencing. **(B)** MYCN interacts with DNMT3A, a DNA methyltransferase which methylates CpG islands in gene promoters to repress gene expression. **(C)** MYCN upregulates histone deacetylases such as HDAC1, HDAC2 and SIRT1 in neuroblastoma. SIRT1 stabilises MYCN, creating a feed-forward loop.

Recent studies have demonstrated that MYCN also regulates global gene expression by regulating RNA Pol II transcription elongation. Zeid et al., (2018) demonstrated that depletion of MYCN from promoters resulted in loss of initiating and elongating RNA Pol II and subsequently a downregulation of global transcription. This suggested that, similarly to MYC, MYCN regulates Pol II binding to promoters and the release of Pol II from promoter-proximal pausing into productive transcription elongation. Subsequently it was demonstrated that MYCN associates with TFIIIC and RAD21 at active Pol II promoters to promote Pol II promoter escape and release of Pol II from promoter-proximal pausing (Büchel et al., 2019). Additionally, Baluapuri et al., (2019) demonstrated that MYCN promoted the processivity of transcription. This likely occurred through a similar mechanism to that employed by MYC. MYC binds SPT5, a subunit of the elongation factor DSIF, and it recruits to active promoters (Baluapuri et al., 2019). MYC then transfers SPT5 to Pol II in a CDK7-dependent manner, enabling Pol II to engage in productive transcription elongation (Baluapuri et al., 2019). High oncogenic levels of MYC sequester SPT5 into non-functional complexes, resulting in reduced expression of growth-suppressive genes

(Baluapuri et al., 2019). Regulation of gene expression by MYCN is therefore highly complex and includes both target gene-specific and broad global mechanisms.

1.2.3 Cellular impact of MYCN expression

Through target-gene specific and global mechanisms, MYCN regulates the expression of a vast array of genes involved in proliferation, survival, pluripotency, self-renewal, metastasis and angiogenesis (Figure 1.4) (Valentijn et al., 2012). As such, the impact of MYCN-induced differential expression on the cell is pleiotropic, and has a major role in driving the aggressive MNA neuroblastoma phenotype (Huang and Weiss, 2013).

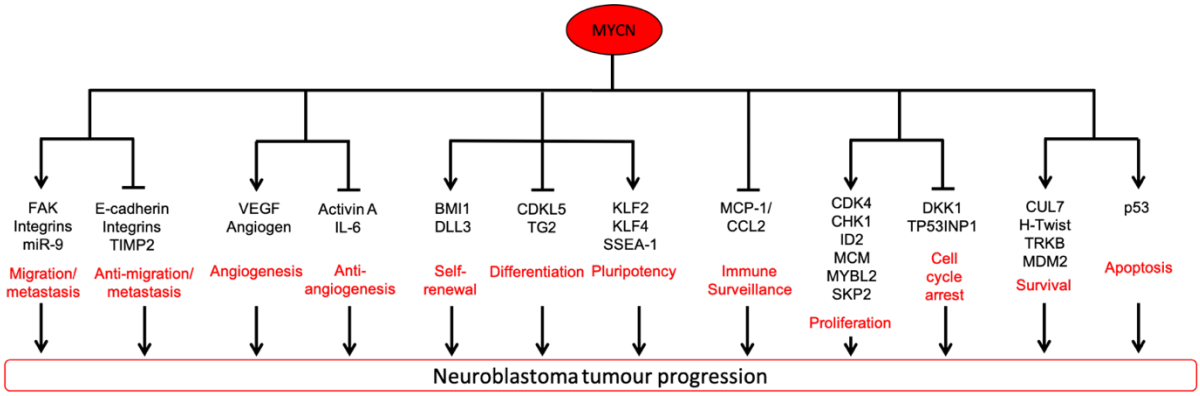

Figure 1.4. Summary of the cellular impact of MYCN expression in neuroblastoma progression.
The role of MYCN mis-expression or amplification in tumour progression is multifaceted, involving promotion of metastasis, angiogenesis, self-renewal, pluripotency, proliferation, survival and apoptosis, and downregulation of anti-metastasis, anti-angiogenesis, differentiation, cell cycle arrest, and immune surveillance proteins.

1.2.3.1 MYCN regulates cellular proliferation via cell cycle checkpoint inhibition

MYCN was first demonstrated to induce proliferation in quiescent fibroblasts (Cavalieri and Goldfarb, 1988). MYCN promotes proliferation and cell cycle progression by regulating expression of genes involved in the G1 to S-phase transition (Figure 1.5). As such, knockdown of MYCN in MNA neuroblastoma cells increases the population of cells in G1 (Bell et al., 2006). MYCN promotes

expression of cyclin D and CDK4 genes (Bouchard et al., 1999; Bouchard et al., 2001; Westermann et al., 2008). This promotes partial Rb phosphorylation by the cyclin D/CDK4 complex, enabling E2F-mediated transcription of cyclin E. Full Rb phosphorylation and inactivation by cyclin E/CDK2 enables E2F transcription factors to induce S-phase. MYCN also promotes S-phase entry by inducing expression of E2F transcription factors and upregulating ID2 which inhibits Rb tumour suppressor (Lasorella et al., 2000; Lasorella et al., 2002; Woo et al., 2008; Pickering et al., 2009). Additionally, MYCN promotes bypass of the G1 checkpoint by upregulating SKP2 and EZH2, resulting in reduced expression of the p21 CDK inhibitor (Bell et al., 2007; Kramer et al., 2016; Liu et al., 2017). Similarly, *MYCN* expression reduces protein levels of the CDK inhibitor p27, likely due to its sequestration in excess cyclin D/CDK4 complexes (Bouchard et al., 1999; Woo et al., 2008). As such, *MYCN* overexpression prevents arrest in G1 following DNA damage in MNA-neuroblastoma cell lines by attenuating $p21^{WAF1}$ induction (Bell et al., 2006; Gogolin et al., 2013). MYCN also regulates proliferation through direct transcriptional repression of antiproliferative proteins such as Dickkopf-1 and CDKL5, and upregulation of proliferation drivers such as BMI1, NLRR1 and MYBL2, and genes which function in DNA replication such as MCM genes (Koppen et al., 2007a; Koppen et al., 2007b; Hossain et al., 2008; Huang et al., 2011a; Valli et al., 2012).

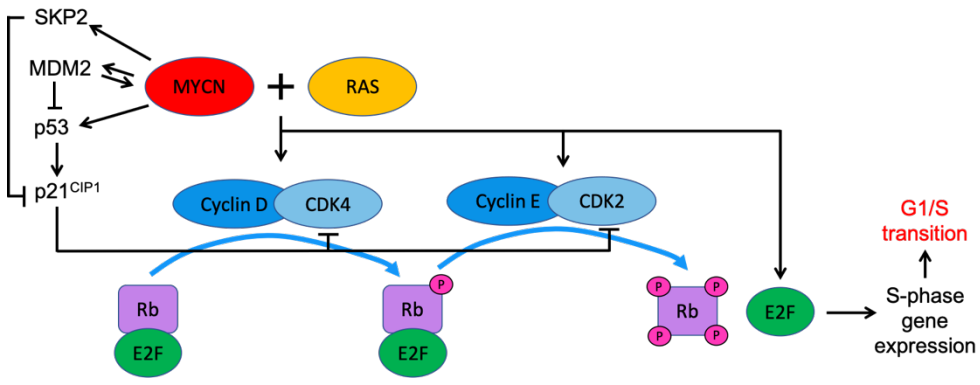

Figure 1.5. MYCN regulation of G1 to S-phase transition.
Summary of the mechanisms employed by MYCN to promote G1 to S-phase transition. MYCN promotes expression of cyclin D and CDK4 genes. This promotes partial Rb phosphorylation by the cyclin D/CDK4 complex, enabling E2F-mediated transcription of cyclin E. Full Rb phosphorylation and inactivation by cyclin E/CDK2 enables E2F transcription factors to induce S-phase. MYCN also promotes bypass of the G1 checkpoint by upregulating SKP2 and EZH2, resulting in reduced expression of the p21 CDK inhibitor.

1.2.3.2 MYCN inhibits differentiation and promotes self-renewal and pluripotency

MYCN expression promotes pluripotency and self-renewal and is therefore able to revert fibroblasts into induced pluripotent stem cells (iPSCs) (Alam et al., 2009; Varlakhanova et al., 2010; Izumi and Kaneko, 2012). MYCN promotes and maintains this stem-like phenotype through induction of self-renewal and pluripotency genes such as KLF2, ID2, KLF4, LIN28B, SSEA-1, BMI1 and DLL3 (Yaari et al., 2005; Cotterman and Knoepfler, 2009; Zhao et al., 2009; Ochiai et al., 2010; Izumi and Kaneko, 2012).

MYCN also inhibits differentiation, as indicated by the upregulation of late neuroblast-specific genes and neuronal differentiation markers such as NSE, TrkA and TrkC following depletion of *MYCN* in MNA neuroblastoma cells (Kang et al., 2006; Nara et al., 2007; Cotterman and Knoepfler, 2009; Varlakhanova et al., 2010; Gómez-Casares et al., 2013; Jansky et al., 2021). Additionally it has been observed that induction of differentiation in neuroblastoma cells by retinoic acid is associated with reduced *MYCN* expression, which precedes morphological differentiation (Thiele et al., 1985). MYCN has been shown to block induction of neuronal differentiation by nerve growth factor signalling by repressing oestrogen receptor-〈 (ESR1) (Loven et al., 2010; Dzieran et al., 2018). However, as previously noted in Chapter 1.1.6.1, the role of MYCN in embryonal neural crest differentiation is highly temporally dependent. Whilst *MYCN* is initially expressed in NCCs to promote pluripotency, expansion and migration, *MYCN* is subsequently re-expressed in sympathoadrenal progenitors to promote neuronal fate commitment (Wakamatsu et al., 1997; Knoepfler et al., 2002; Hansford et al., 2004; ten Berge et al., 2008; Alam et al., 2009; Kapeli and Hurlin, 2011; Ponzoni et al., 2022). Similarly, it has been demonstrated that *MYCN* expression is required for the induction of differentiation in neuroblastoma cells (Guglielmi et al., 2014). Overall, the ability of MYCN to promote pluripotency and inhibit differentiation accounts for the reduced differentiation observed in MNA neuroblastomas (Moreau et al., 2006).

1.2.3.3 MYCN promotes EMT, invasion, metastasis and angiogenesis

Wakamatsu et al., (1997) demonstrated that *MYCN* expression promoted migration of NCCs during chick embryo development. Similarly, *MYCN* amplification correlates with increased invasion and metastasis in neuroblastoma and is therefore associated with advanced stage disease (Zaizen et al., 1993). At the cellular level, MYCN promotes miR-9 microRNA to supress E-cadherin and promote EMT (Ma et al., 2010). Direct upregulation of ALK has also been observed to contribute to MYCN-induced migration (Hasan et al., 2013). MYCN-induced adhesion reduction is mediated through down-regulation of integrins α1 and β1 and upregulation of focal adhesion kinase to promote detachment from the extra-cellular matrix (ECM) (van Golen et al., 2003; Tanaka and Fukuzawa, 2008; Megison et al., 2013). MYCN promotes ECM degradation and invasion through suppression of TIMP-2; a matrix metalloprotease (MMP) antagonist (Noujaim et al., 2002). *MYCN* amplification also correlates with increased vascularity and dissemination (Meitar et al., 1996; Ribatti et al., 2002; Ozer et al., 2007). MYCN promotes angiogenesis by suppressing anti-angiogenic factors such as Activin A, LIF, and IL-6, and inducing pro-angiogenic factors such as angiogenin and VEGF (Hatzi et al., 2000; Hatzi et al., 2002a, Hatzi et al., 2002b; Kang et al., 2008; Dungwa et al., 2012).

1.2.3.4 MYCN regulates metabolic reprogramming

MYCN induces metabolic reprogramming via the Warburg effect to enable high tumour cell growth and proliferation rates (Naifeh and Varacallo, 2018; Wang et al., 2018). However, *MYCN* overexpression promotes mitochondrial metabolism, including oxidative phosphorylation and glutaminolysis (Wang et al., 2018; Oliynyk et al., 2019; Yoshida, 2020). In fact, *MYCN* amplification is associated with glutaminolysis addiction in neuroblastoma, leading to heightened reactive oxygen species (ROS) generation (Wang et al., 2018). Furthermore, MYCN promotes fatty acid uptake and upregulates enzymes associated with fatty acid β-oxidation and this is a critical metabolic dependency for MNA neuroblastomas (Yoshida 2020; Tao et al., 2022).

1.2.3.5 MYCN regulates p53-dependent apoptosis

Similarly to MYCC, MYCN paradoxically sensitises neuroblastoma cells to apoptosis simultaneously to promoting proliferation (Chen et al., 2010; Petroni et al., 2011; Huang and Weiss, 2013). p53 induces cell cycle arrest or apoptosis following detection of DNA damage or replication stress. MDM2 is an E3 ubiquitin-ligase which ubiquitinates p53 for degradation and therefore promotes survival (Slack et al., 2005). MDM2 is a target of p53-mediated transcription, enabling auto-regulation of p53 activation by p53 itself in a negative feedback loop (Slack et al., 2005). MYCN directly upregulates both *TP53* and its signalling suppressor MDM2, and therefore sensitises neuroblastoma cells to p53-dependent apoptosis induced by DNA-damaging chemotherapy (Figure 1.6A) (Slack et al., 2005; Chen et al., 2010; Petroni et al., 2011; Gu et al., 2012; Agarwal et al., 2018).

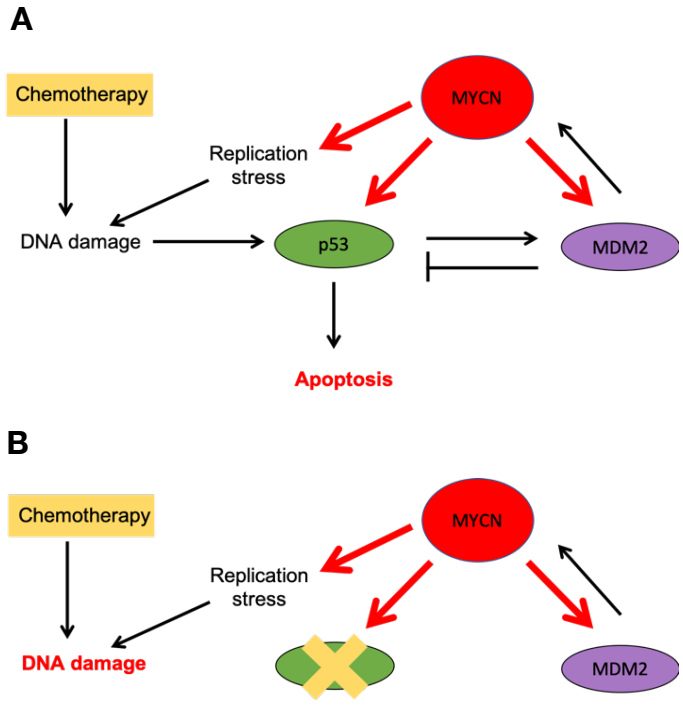

Figure 1.6. MYCN sensitises neuroblastoma cells to p53-mediated apoptosis. Following detection of DNA damage or replication stress, p53 induces cell cycle arrest or apoptosis. MDM2 ubiquitinates p53 for degradation, promoting survival. MDM2 is a target of p53-mediated transcription, enabling auto-regulation of p53 activation by p53 itself in a negative feedback loop. **(A)** MYCN directly upregulates p53 and MDM2 and therefore sensitises MNA tumour cells to p53-mediated apoptosis. **(B)** Following relapse, neuroblastoma tumours often harbour inactivating mutations in *TP53*. These tumours accumulate DNA damage without inducing p53-mediated apoptosis. A positive feedback loop between MYCN and MDM2 is established to promote survival and proliferation of these resistant cells.

Additionally, HIPK2 phosphorylates p53 at Ser46 in response to ATM activation following detection DNA damage (D'Orazi et al., 2001; Petroni et al., 2011). This results in p53-mediated induction of PTEN which restrains MDM2 expression and function, forming an apoptotic amplification cycle (Mayo et al., 2002; Chang et al., 2004). HMGA1 inhibits HIPK2 activity by promoting relocalisation of HIPK2 to the cytoplasm (Pierantoni et al., 2007). MYCN also further sensitises cells to p53-mediated apoptosis by upregulating both *HIPK2* and *HMGA1* (Petroni et al., 2011).

TP53 mutations are rare in primary neuroblastoma tumours at diagnosis (Komuro et al., 1993; Petroni et al., 2011, Petroni et al., 2012). Upregulation of p53-dependent apoptotic pathways therefore accounts for the high initial response rate of MNA neuroblastomas to chemotherapy (Qiu and Matthay, 2022). p53 must be functionally inactivated in these tumours to evade this apoptotic response, perhaps via MYCN-induced upregulation of p53 signalling suppressors such as MDM2, BMI1 and miRNA-380-5p (Slack et al., 2005; Swarbrick et al., 2010; Gu et al., 2012; Petroni et al., 2012). p53 is also frequently functionally inactivated in neuroblastoma cells by cytoplasmic sequestration (Davidoff et al., 1992; Moll et al., 1995; Isaacs et al., 1998). However, this functional inactivation is reversible (Goldman et al., 1996; Isaacs et al., 1998; McKenzie et al., 1999).

Following relapse, neuroblastoma tumours often harbour loss-of-function *TP53* mutations. These tumours accumulate DNA damage without inducing p53-mediated apoptosis. Additionally, Gu et al., (2012) showed that MDM2 upregulates *MYCN* expression by stabilising MYCN mRNA and inducing its translation. Genetic inactivation of p53 therefore results in the formation of a positive feedback loop between MYCN and MDM2 which further promotes the survival and proliferation of these chemotherapy-resistant cells, in mechanism independent of p53 function (Figure 1.6B) (He et al., 2011). This accounts for the frequent gain of therapeutic resistance upon relapse of MNA-neuroblastoma.

1.3 Targeting MYCN in neuroblastoma

1.3.1 Targeting MYCN directly is challenging

Targeting genetic driver events that initiate and maintain cancer cell proliferation and survival enables the development of tumour-targeted therapeutics. Constitutive oncogenic signalling often results in the over-reliance of cancer cells on a specific oncogene in a concept called oncogene addiction (Weinstein, 2002). Oncogene addiction was initially observed in *MYCC*-driven tumours in mice, where brief *MYCC* inactivation resulted in the sustained tumour regression (Jain et al., 2002). Similarly, multiple studies have demonstrated that MNA neuroblastoma cells are 'addicted' to MYCN. Depletion of MYCN using siRNA or antisense oligonucleotides inhibited proliferation and induced differentiation and apoptosis in MNA neuroblastoma cells and reduced tumour growth a transgenic MNA neuroblastoma mouse model (Negroni et al., 1991; Burkhart et al., 2003; Tonelli et al., 2005; Kang et al., 2006).

However, the pleiotropic roles of MYCN and the challenges in transcription factor targeting have led to difficulty in identifying direct MYCN inhibitors with therapeutic potential (Murphy et al., 2009; Park et al., 2013; Whitfield et al., 2017). Many studies therefore aim to target MYCN indirectly. Inhibitors of bromodomain and extra-terminal domain (BET) proteins have been shown to inhibit *MYCN* transcription and demonstrated efficacy in neuroblastoma cell lines and multiple MYCN-driven neuroblastoma mouse models (Puissant et al., 2013; Henssen et al., 2016). MYCN can also be indirectly targeted by blocking pathways which stabilise MYCN to promote MYCN degradation (Figure 1.7).

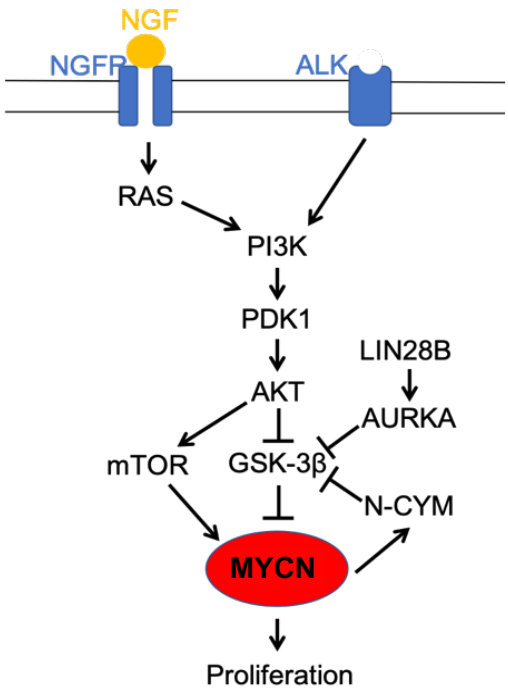

Figure 1.7. MYCN stabilisation pathways.
ALK and RAS signalling activates AKT via PI3K. AKT phosphorylates GSK-3β to prevent GSK3β-mediated promotion of MYCN degradation. PI3K/mTOR signalling also promotes MYCN stabilisation. LIN28B induces AURKA-mediated inhibition of GSK-3β. *NCYM* is a cis-antisense gene of *MYCN* which stabilises MYCN via GSK-3β inhibition. NGF; Nerve growth factor. NGFR; Nerve growth factor receptor.

For example, ALK and RAS signalling activates AKT which then phosphorylates GSK-3β (Huang and Weiss, 2013). This inactivates GSK-3β to prevent it promoting MYCN degradation. Inhibition of RAS or AKT inhibits the proliferation of MNA neuroblastoma cells (Yaari et al., 2005; Le Grand et al., 2020), whilst ALK inhibitors show high efficacy in inhibiting neuroblastoma growth and are currently in clinical trials for addition to high-risk treatment (George et al., 2008; Infarinato et al., 2016; Mosse *et al.*, 2017; Schulte and Eggert, 2021; Foster et al., 2021). Similarly, the PI3K/mTOR pathway stabilises MYCN and inhibitors of this pathway selectively killed *MYCN*-expressing neuroblastoma cells and induced apoptosis in TH-MYCN mouse neuroblastomas (Schramm *et al.*, 2013; Vaughan et al., 2016). LIN28B induces AURKA-mediated inhibition of GSK-3β to prevent MYCN degradation (Molenaar et al., 2012; Schnepp et al., 2015; Chen et al., 2020). AURKA inhibitors also induce regression of MYCN-driven neuroblastomas and are currently in clinical trials for relapsed neuroblastomas (Brockmann et al., 2013; Gustafson et

al., 2014; Büchel et al., 2017; DuBois et al., 2018; Du et al., 2019; DuBois et al., 2020). Additionally, *NCYM*, a cis-antisense gene of *MYCN* that is co-amplified and co-expressed with *MYCN*, stabilises MYCN via GSK-3β inhibition (Armstrong and Krystal, 1992; Suenaga et al., 2014).

1.3.2 Targeting MYCN downstream pathways

Given the difficulties in targeting MYCN, alternative therapeutic strategies which target the molecular mechanism of MYCN or the downstream cellular effects of *MYCN* overexpression are currently being investigated. For example, MYCN-driven neuroblastomas are dependent on MYCN-induced overexpression of CDKs to promote cell cycle progression, and inhibitors of CDKs selectively inhibit MYCN-driven proliferation of neuroblastoma cells and induce tumour regression in MYCN-driven mouse models (Molenaar et al., 2009; Chipumuro et al., 2014; Delehouzé et al., 2013; Gogolin et al., 2013; Rader et al., 2013). Efficacy of CDK4/6 inhibitors are currently in clinical trial (Geoerger et al., 2017). Additionally, MYCN-driven proliferation is dependent on the cell-cycle checkpoint kinase WEE1 and the WEE1 inhibitors Adavosertib is in early phase clinical trials (Cole et al., 2020). MYCN also upregulates the p53-dependent apoptotic pathway and its regulators, and this can also be therapeutically exploited. Inhibition of MDM2 by the small molecule Nutlin-3 stabilised p53, induced HIPK2, and promoted apoptosis preferentially in MNA neuroblastoma cells (Petroni et al., 2011; Veschi et al., 2012). Nutlin-3 also induced tumour regression and inhibited metastasis in neuroblastoma xenografts (Petroni et al., 2011). MYCN also upregulates MDM2 to promote neuroblastoma cell survival, and deficiency or inhibition of MDM2 suppresses MYCN-driven tumour growth (Barbieri et al., 2006; Chen et al., 2009; He et al., 2011; Wang et al., 2017; Van Goethem et al., 2017; Chen et al., 2019). MYCN-induced metabolic dependencies are also being investigated. For example, inhibitors of the serine-glycine-one-carbon pathway and fatty acid transport are selectively cytotoxic to MNA cells and tumours (Tao et al., 2022; Xia et al., 2019). Inhibitors of polyamine biosynthesis inhibit MYCN-driven proliferation and are currently in clinical trial in for treatment of high-risk neuroblastoma in combination with induction chemotherapeutics (Hogarty et al., 2008; Sholler et al., 2018).

Targeting the molecular mechanism of MYCN involves inhibiting its ability to induce global transcriptomic changes via direct DNA binding or epigenetic regulation. Heterodimerisation with Max is required for binding of MYCN to DNA. Development of inhibitors which block the interaction between MYC and Max proteins is a promising therapeutic strategy but is currently limited by lack of specificity and bioavailability (Berg et al., 2002; Fletcher and Prochownik, 2015). MYCN mediates repression of many differentiation-inducing or growth inhibiting genes through association with the methyltransferase EZH2 (Corvetta et al., 2013; Tsubota et al., 2018). This is important for MYCN-induced oncogenic transformation of NCCs (Tsubota et al., 2018). As such, depletion or inhibition of EZH2 induces cell death selectively in MNA neuroblastoma cells and inhibits tumorigenesis in TH-MYCN mice (Chen et al., 2018; Tsubota et al., 2018). Additionally, it was demonstrated that MNA neuroblastomas are dependent on the histone acetyltransferase EP300 to control the enhancer landscape and facilitate ADRN CRC-driven transcription, and were sensitised to its targeted degradation (Durbin et al., 2022).

Durbin et al., (2018) demonstrated that analysis of changes in the transcriptomic profile induced by *MYCN* amplification identifies gene dependencies specific to MNA-neuroblastoma, enabling identification of new therapeutic targets. A genome-wide CRISPR-Cas9 screen identified 147 MNA-neuroblastoma dependency genes whose expression was selectively essential for MNA-neuroblastoma cell growth and survival relative to 26 other tumour types (Durbin et al., 2018). In particular, ADRN CRC transcription factors were identified among the top gene dependencies in MNA neuroblastoma, with MNA cells reliant on the ADRN CRC to maintain high *MYCN* expression and a transformed phenotype (Durbin et al., 2018; Helmsauer et al., 2020). Dual inhibition of BRD4 and CDK4, encoded by ADRN CRC target genes, downregulated CRC transcription factor expression and induced cell death selectively in MNA cells (Durbin et al., 2018). This screen also identified that MNA neuroblastoma cells were highly dependent on DNA repair genes, likely due to the high levels of genomic instability induced by *MYCN* overexpression as discussed below (Durbin et al., 2018).

1.3.3 Oncogene-induced replication stress is therapeutically exploitable

Oncogene activation promotes cellular proliferation through the deregulation of many cellular processes. For example, oncogenes induce deregulation of DNA replication, known as replication stress (Kotsantis et al., 2018). Chronic replication stress manifests as increased replication fork stalling or collapse and ultimately results in replication-born DNA damage. Increased replication stress therefore results in higher genomic instability and is an important early driver of tumorigenesis (Bartkova et al., 2005; Gorgoulis et al., 2005; Bartkova et al., 2006;). Oncogene-induced replication stress is attributed to a range of factors, including aberrant origin firing, increased replication-transcription collisions, increased R-loop accumulation, induction of reactive oxygen species (ROS), and impaired nucleotide metabolism (Di Micco et al., 2006; Bester et al., 2011; Kotsantis et al., 2018).

However, oncogene-induced replication stress is also a tumour specific vulnerability that is therapeutically exploitable. Oncogene-driven cancer cells are more dependent on replication-stress limiting pathways to maintain endogenous replication stress at tolerable levels (Kotsantis et al., 2018; Nazareth et al., 2019). Oncogene-induced activation therefore sensitises cells to inhibition of DNA repair and replication-stress limiting pathways (Nazareth et al., 2019). For example, overexpression of MYCC sensitises tumour cells to inhibition of ATR or CHK1 DNA damage response (DDR) proteins (Schoppy et al., 2012; Murga et al., 2011).

The DDR is commonly activated by DNA damage sensors ATR and ATM in response to replication stress and DNA damage (Kastan and Bartek, 2004; Cimprich and Cortez, 2008; Maréchal and Zou, 2013). Activation of the DDR induces cellular senescence, apoptosis or a transient cell cycle block via checkpoint activation (Kastan and Bartek, 2004; Cimprich and Cortez, 2008; Maréchal and Zou, 2013). This enables DNA repair before mitosis, preventing inheritance of mutations into daughter cells (Kastan and Bartek, 2004; Cimprich and Cortez, 2008). DDR signalling also recruits DNA repair proteins to resolve the DNA damage or aberrant DNA replication intermediates. Whereas ATM is activated by double strand breaks (DSBs) alone, ATR is the primary responder to replication stress and is primarily activated by accumulation of single stranded DNA (ssDNA) at aberrant replicative structures and DSBs (Figure 1.8) (Cobb et al., 2005; Labib and Hodgson, 2007; Petermann and Helleday, 2010; Toledo et al., 2011; Maréchal and Zou, 2013;

Srinivasan et al., 2013). Persistent replicative stress within tumours therefore activates both ATM and ATR DDR pathways due to the formation of DSBs at collapsed replication forks (Shreeram et al., 2006; Murga et al., 2011). ATM phosphorylates CHK2 and activates p53 to induce cell cycle arrest at G1-S, intra-S or G2-M checkpoints, or to induce apoptosis. ATR phosphorylates CHK1 to induce cell cycle arrest at intra-S or G2-M checkpoints. CHK1 and CHK2 can phosphorylate Cdc25A and Cdc25C depending on the type of DNA damage. ATM and ATR therefore have overlapping but non-redundant DDR functions due to multiple points of pathway crosstalk (Cimprich and Cortez, 2008; Lempiäinen and Halazonetis, 2009; Maréchal and Zou, 2013).

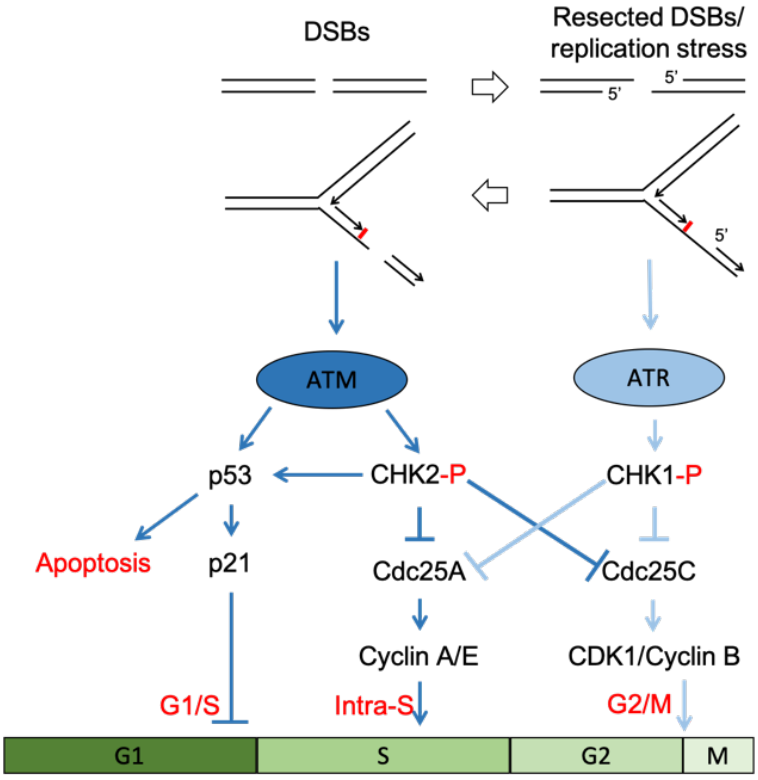

Figure 1.8. ATM and ATR link DNA damage and repair to cell cycle progression.
ATM and ATR DNA damage response (DDR) proteins mediate regulation of cell checkpoint activation and apoptosis following induction by DNA damage and replicative stress, with overlapping but non-redundant DDR functions due to multiple points of pathway crosstalk. ATM is activated by blunt DSBs whereas ATR is the primary activated by ssDNA accumulation at resected DSBs and aberrant S-phase replicative structures. ATM phosphorylates CHK2 and activates p53 to induce cell cycle arrest at G1/S, intra-S or G2/M checkpoints, or induce apoptosis. ATR phosphorylates CHK1 to induce cell cycle arrest at intra-S or G2/M checkpoints. DSBs; double strand breaks.

It should be noted that whilst oncogene-induced replication stress sensitises cancer cells to inhibition of the DDR, loss of DDR function promotes tumorigenesis. During tumorigenesis, oncogene-induced replication stress activates the DDR to induce apoptosis, senescence or cell cycle arrest to limit pre-neoplastic expansion (Di Micco et al., 2006). For example, *MYC*-induced replication stress reduced lymphoma tumorigenesis in transgenic E⌠-Myc mice by inducing apoptosis via ATM and p53 (Shreeram *et al.*, 2006; Reimann *et al.*, 2007; Murga *et al.*, 2011). DDR disruption is therefore necessary for tumorigenesis, with 48% of neuroblastomas harbouring ATM defects often via LOH at 11q (Kastan and Bartek, 2004; Bartkova et al., 2005; Gorgoulis et al., 2005; Takagi et al., 2013, Takagi et al., 2017; Mandriota et al., 2015). Therefore, more specifically, tumour cells displaying high oncogene-induced replicative stress therefore have a greater dependence on non-disrupted DDR and DNA repair pathways. This is indicated by the mutual exclusivity of neuroblastoma ATM single nucleotide variants (SNVs) with SNVs in other DDR-associated genes, such as *FANCM*, *FAN1*, *PALB2* and *MRE11A* (Molenaar et al., 2012; Pugh et al., 2013; Takagi et al., 2017).

1.3.4 High *MYCN* expression induces replication stress and DNA damage

Multiple studies have demonstrated that *MYCN* amplification or overexpression induces higher levels of replication stress and genomic instability. Gu et al (2015) observed that *MYCN* amplification increased ATR/Chk1 signalling and increased ©-H2AX levels. Similarly, King et al., observed that *MYCN* overexpression induced an increase in ©-H2AX, 53BP-1, phospho-RPA (pRPA) and RAD51 foci (King et al., 2020; King et al., 2021). In addition, *MYCN* overexpression reduced replication fork speed and increased replication fork stalling and new origin firing (King et al., 2020; King et al., 2021).

MYC proteins drive replication stress and genomic instability through multiple mechanisms, such as forced S-phase entry and promotion of DNA replication (Felsher and Bishop, 1999; Ray et al., 2006; Robinson et al., 2009). Both MYCN and MYCC accelerate progression through the G1-S phase checkpoint by modulating the expression of genes involved in cell cycle regulation such as cyclins D1 and D2,

CDK4, p21, ID2 and E2F transcription factors (Bouchard et al., 1999; Bouchard et al., 2001; Westermann et al., 2008; Pickering et al., 2009; Woo et al., 2008; Lasorella et al., 2000; Lasorella et al., 2002; Bell et al., 2007; Kramer et al., 2016; Liu et al., 2017). MYCN has also been shown to upregulate genes involved in DNA replication such as MCM genes (Koppen et al., 2007b), and MYCC has been shown to upregulate the DNA replication licensing factor CDT1 (Valovka et al., 2013).

MYCC also promotes DNA replication independently from its transcription factor function. MYCC interacts with the DNA pre-replicative complex to recruit Cdc45, thereby increasing the density of active replication origins and altering the spatiotemporal profile of replication initiation (Dominguez-Sola et al., 2007; Srinivasan et al., 2013). This increased origin firing overwhelms pathways that regulate fork restart, progression, and termination, meaning MYCC-driven replication forks are more prone to stall, collapse and generate DSBs (Srinivasan et al., 2013). Given the high functional homology between MYCC and MYCN, and the increased new origin firing observed upon *MYCN* overexpression, it is postulated that MYCN also promotes DNA replication through similar transcription-independent functions (King et al., 2021).

It is speculated that the ability of MYC proteins to globally amplify transcription initiation and elongation may also enhance replication stress levels, as this would increase the number of collisions between transcription and replication machinery. Transcription-replication conflicts also results in the formation of R-loops (Santos-Pereira and Aguilera, 2015; Alonso and Noordermeer, 2021). R-loops are three-stranded nucleic acid structures, composed of an RNA-DNA hybrid and displaced ssDNA which is vulnerable to damage (Santos-Pereira and Aguilera, 2015). As such, R-loops are both a source of, and a product of, replication stress and genomic instability (Santos-Pereira and Aguilera, 2015). Although R-loops are postulated to function in modulating gene expression, DNA repair and telomere lengthening, inhibition of R-loop accumulation is necessary to limit genomic instability (Santos-Pereira and Aguilera, 2015; Alonso and Noordermeer, 2021; Petermann et al., 2022).

Interestingly, MYCN has been shown to drive multiple mechanisms of R-loop resolution. It has been observed that MYCN promotes escape of RNAPII from transcriptional pause sites in promoters to limit promoter-proximal R-loop formation and enhance transcriptional activation (Herold et al., 2019; Zeid et al., 2018; Büchel

et al., 2017). However, Herold et al., (2019) observed that when RNAPII escape fails during high replication and transcription stress, MYCN recruits BRCA1 to promoter-proximal regions. BRCA1 stabilises mRNA de-capping complexes to resolve the MYCN-induced accumulation of promoter-proximal R-loops. Additionally Roeschert et al., (2021) observed that MYCN recruited AURKA during S-phase to promote incorporation of histone H3.3 into promoter regions and therefore prevent co-transcriptional R-loop formation. Recruitment of AURKA also stabilised MYCN at promoters blocking binding of the SCF^{FBXW7}-ligase and it was speculated that this promoted recruitment of BRCA1 (Otto et al., 2009; Roeschert et al., 2021). Similarly, Büchel et al., (2017) demonstrated that the recruitment of AURKA to MYCN during S-phase antagonised recruitment of TFIIIC and RAD21, and therefore blocked MYCN-dependent release of RNAPII from promoters. As such, MYCN employs multiple mechanisms to modulate its own ability to drive transcription, and MNA cells are dependent on these mechanisms to limit transcriptional and replication stress. The proteins involved in these mechanisms are therefore potential therapeutic targets specific to MNA cells. For example, *MYCN* amplification sensitises cells to AURKA inhibition (Brockmann et al., 2013; Gustafson et al., 2014; DuBois et al., 2018; Du et al., 2019; Büchel et al., 2017).

1.3.5 Targeting DNA repair pathways in MNA neuroblastoma

Determining pathway dependencies induced by *MYCN* amplification may exploit oncogene addiction in MNA neuroblastoma. Durbin et al., (2018) demonstrated that analysis of the effect of *MYCN* amplification on the transcriptional profile of neuroblastoma cells identifies gene dependencies and therefore potential therapeutic targets. Multiple studies have demonstrated that 'DNA repair' is among the most significantly upregulated gene ontology groups in neuroblastomas with high *MYCN* expression (Valentijn et al., 2012; Hallett et al., 2016; Durbin et al., 2018). Similarly, MYCN has been shown to transcriptionally upregulate many DDR and DNA repair genes in neuroblastoma including *CHK1, MRE11, PARP-1/2, BLM, BRCA1*, and components of alternative non-homologous end joining (alt-NHEJ) such as DNA Ligase I and DNA Ligase III (Cole et al., 2011; Valentijn et al., 2012; Chayka et al., 2015; Gu et al., 2015; Newman et al., 2015; Hallett et al., 2016; Petroni et al., 2016; Colicchia et al., 2017; Newman et al., 2017; Durbin et al., 2018; Petroni et al.,

2018; Zhang et al., 2018; Herold et al., 2019; King et al., 2020). Increased expression of *CHK1*, alt-NHEJ components, and *PARP-1/2* were observed to correlate with increased activity of the DNA repair pathways they function in (Gu et al., 2015; King et al., 2020; Newman et al., 2015). Furthermore, high expression of these DNA repair genes correlates with poor prognosis in neuroblastoma (Chayka et al., 2015; Hallett et al., 2016; Durbin et al., 2018; Petroni et al., 2018; Herold et al., 2019; King et al., 2020). This suggests MNA neuroblastoma has a therapeutically exploitable dependency on DDR and DNA repair pathways, which are required to limit MYCN-induced replication stress and DNA damage. Indeed, it has been observed that *MYCN* amplification or overexpression sensitises neuroblastoma cells to inhibition of ATR, CHK1, MRE11 and PARP (Cole et al., 2011; Murga *et al.*, 2011; Gu et al., 2015; Newman et al., 2015; Colicchia et al., 2017; Petroni et al., 2018; King et al., 2020; Southgate et al., 2020; King et al., 2021). This MYCN-induced sensitivity was often associated with an induction of intolerable levels of replication-stress dependent DNA damage (Colicchia et al., 2017; Petroni et al., 2018; King et al., 2020; Southgate et al., 2020; King et al., 2021). Similarly, blocking the binding site of PCNA, an essential protein for efficient DNA replication, with peptide R9-caPep interfered with DNA replication fork extension to exacerbate MYCN-induced replication stress, resulting in selective lethality in MNA-neuroblastoma cells (Gu et al., 2015).

MYCN amplification therefore sensitises neuroblastoma cells to inhibition of DNA repair pathways which exacerbates MYCN-dependent replication-stress and DNA damage to intolerable levels. Upregulation of other DNA repair pathways by MYCN may be indicative of a putative dependency specific to MNA tumour cells which could be exploited therapeutically. Hallett et al., (2016) identified a gene signature that is associated with poor prognosis in MNA neuroblastoma, and that therefore predicts dependencies and therapeutic targets in MNA tumours. Genes involved in the Fanconi Anaemia (FA) DNA repair pathway were enriched in this gene signature, suggesting a putative dependency of MNA cells on FA pathway function. However, the impact of *MYCN* amplification on FA pathway expression and sensitivity to FA pathway inhibition is unknown.

1.4 The FA pathway as a chemotherapeutic target

1.4.1 The FA pathway in DNA repair

In the context of neuroblastoma, a previously unstudied pathway involved in DNA repair and replication stress is the Fanconi anaemia (FA) pathway. The FA pathway is a DNA damage response network which co-ordinates proteins from multiple other DNA repair pathways such as nucleotide excision repair (NER), translesion synthesis (TLS) and homologous recombination repair (HRR) primarily to resolve DNA inter-strand crosslinks (ICLs) in a replication-dependent manner (Sasaki, 1975; Taniguchi et al., 2002a; Räschle et al., 2008; Moldovan and D'Andrea, 2009; Rodriguez and D'Andrea, 2017). ICLs represent a class of DNA lesions that covalently link both DNA strands together, preventing unwinding by DNA helicases and therefore blocking progression of replication and transcription machineries (Deans and West, 2011; Kim and D'Andrea, 2012; Kotteman and Smogorzewska 2013). Unrepaired ICLs are therefore highly cytotoxic. The FA pathway also contributes to the replication-dependent repair of a range of other DNA lesions, including those induced by UV and IR (Garcia-Higuera et al., 2001; Howlett et al., 2002; Taniguchi et al., 2002b; Dunn et al., 2006; Moldovan and D'Andrea, 2009). However, these lesions can be repaired by multiple alternative repair mechanisms (Garcia-Higuera et al., 2001; Taniguchi et al., 2002b; Houghtaling et al., 2003; Niedzwiedz et al., 2004; Bridge et al., 2005; Dunn et al., 2006). In contrast, the FA pathway is the primary mechanism for efficient and high-fidelity ICL repair (Sasaki et al., 1975; Akkari et al., 2000; Taniguchi et al., 2002a). Many FA pathway proteins also function to limit replication stress through several repair-independent mechanisms to prevent accumulation of replication stress-associated DNA damage (Sobeck et al., 2006; Schwab et al., 2010; Schlacher et al., 2012; Garcia-Rubio et al., 2015). Given the FA pathway acts to repair DNA in a replication-dependent manner, FA pathway activation is observed almost exclusively in S-phase (Akkari et al., 2000; Taniguchi et al., 2002a).

By combining all KEGG-defined FA pathway genes with four more recently identified FA pathway genes, we define the FA pathway as network of proteins encoded by 58 FA pathway-associated genes. Within this, 23 key FA complementation genes have so far been identified as being vital for FA pathway

function, and we refer to these as FANC genes (Velleuer and Carlberg, 2020). For clarity, these genes are listed in Table 1.2.

Table 1.2. 23 key FA complementation group (FANC) genes vital for FA pathway function.
Bi-allelic germline mutation of one of these genes causes Fanconi anaemia. References referring to their identification as FANC genes are provided.

FANC Gene	Alternative Gene Name	Reference
FANCA	-	(Lo Ten Foe et al., 1996)
FANCB	-	(Meetei et al., 2004)
FANCC	-	(Strathdee et al., 1992)
FANCD1	BRCA2	(Howlett et al., 2002)
FANCD2	-	(Timmers et al., 2001)
FANCE	-	(de Winter et al., 2000a)
FANCF	-	(de Winter et al., 2000b)
FANCG	-	(de Winter et al., 1998)
FANCI	-	(Dorsman et al., 2007; Sims et al., 2007; Smogorzewska et al., 2007)
FANCJ	BRIP1	(Levitus et al., 2005)
FANCL	-	(Meetei et al., 2003)
FANCM	-	(Meetei et al., 2005; Singh et al., 2009; Bogliolo et al., 2018; Catucci et al., 2018)
FANCN	PALB2	(Reid et al., 2007)
FANCO	RAD51C	(Vaz et al., 2010)
FANCP	SLX4	(Kim et al., 2011; Stoepker et al., 2011)
FANCQ	ERCC4	(Bogliolo et al., 2013)
FANCR	RAD51	(Ameziane et al., 2015; Wang et al., 2015)
FANCS	BRCA1	(Sawyer et al., 2015)
FANCT	UBE2T	(Hira et al., 2015; Rickman et al., 2015; Virts et al., 2015)
FANCU	XRCC2	(Park et al., 2016)
FANCV	REV7	(Bluteau et al., 2016)
FANCW	RFWD3	(Knies et al., 2017)
FANCY	FAAP100	(Ling et al., 2007; Amenábar et al., 2019)

1.4.1.1 The mechanism of ICL repair by the FA pathway

The FA pathway coordinates three classic repair pathways to mediate replication-dependent ICL repair; NER to promote incision at ICLs, TLS to bypass the resulting DNA adduct, and HRR to repair the subsequent DSB (Rodriguez and D'Andrea, 2017) (summarised in Figure 1.9).

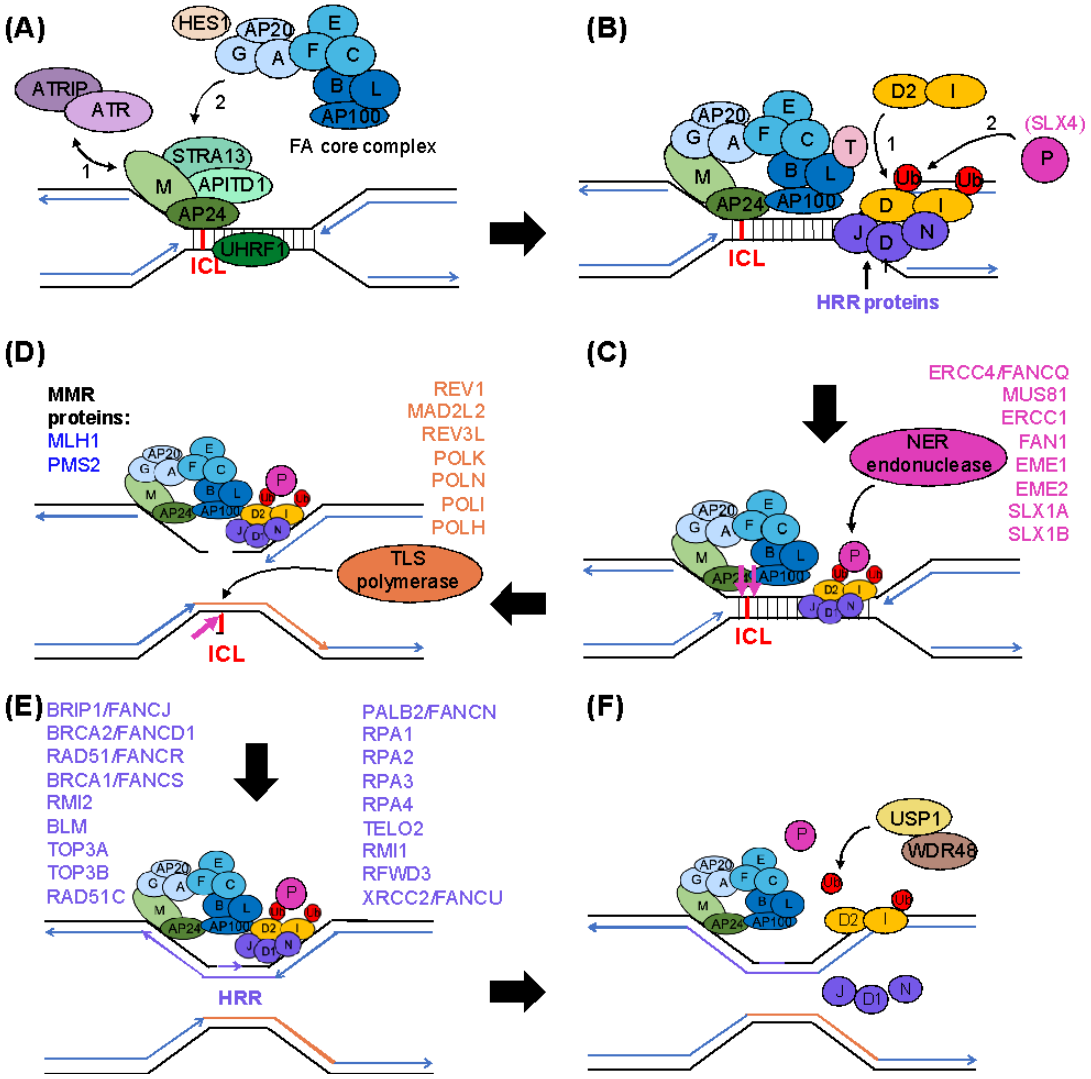

Figure 1.9. Mechanism of ICL repair by the Fanconi anaemia pathway. **(A)** The FANCM-FAAP24 heterodimer recognises the ICL, stabilises the stalled replication fork, recruits the FA core complex, and initiates the ATR DNA damage response. **(B)** FANCD2-FANCI complex is targeted to chromatin following ATR-mediated FANCI phosphorylation. In cooperation with the E2 conjugating enzyme FANCT, FANCL E3 ubiquitin ligase in the FA core complex monoubiquitylates FANCD2 and FANCI. This is a key regulatory step in FAP activation. Mono-ubiquitinated FANCD2-FANCI colocalises at DNA repair foci with HRR proteins. Mono-ubiquitinated FANCD2 recruits SLX4/FANCP to the stalled replication fork. **(C)** SLX4 acts as a scaffold protein for nucleotide excision repair (NER) endonucleases which unhook the crosslink to generate a DSB and DNA adduct. **(D)** The DNA adduct is bypassed by translation synthesis (TLS) to restore the nascent strand. **(E)** The DSB is preferentially repaired by high fidelity HRR. **(F)** The FA pathway is inactivated via de-ubiquitination of FANCD2-FANCI by USP1-WDR48/UAF1.

ICLs may originate endogenously, for example by liver metabolites such as reactive aldehydes which are produced during alcohol detoxification and lipid peroxidation, or exogenously, for example by DNA crosslinking chemotherapeutics such as cisplatin (Ridpath et al., 2007; Langevin et al., 2011; Rosado et al., 2011; Clauson et al., 2013; Garaycoechea and Patel, 2014). ICLs block DNA replication forks, converging from both directions, with forks stalling 20-40 nucleotides from the crosslink (Räschle et al., 2008). One replication fork then moves further, stopping one nucleotide before the crosslink (Räschle et al., 2008). Stalled replication forks activate ATR signalling which induces the phosphorylation and therefore activation of the DNA translocase FANCM at Ser1045 (Singh et al., 2013). This, along with interaction of FANCM with the Bloom syndrome complex (BLM-TOP3A-RMI1-RMI2), promotes recruitment of FANCM to the stalled fork in complex with FAAP24, MHF-1 and MHF-2, where FANCM recognises and binds to the ICL site (Meetei et al., 2003; Xue et al., 2008; Deans and West, 2009; Collis and Boulton, 2010; Ling et al., 2016). Similarly, FANCM can activate ATR signalling following detection of ICLs to induce cell cycle arrest and promote recruitment of proteins which stabilise stalled replication forks (Collis et al., 2008). FANCM translocase activity regresses replication forks, while FAAP24 binding stabilises ssDNA at the stalled fork (Xue et al., 2008; Deans and West, 2009; Moldovan and D'Andrea, 2009; Collis and Boulton, 2010). Furthermore, the FANCM-FAAP24-MHF complex recruits the FA core complex to the ICL site (Ciccia et al., 2007; Deans and West, 2009).

The FA core complex is a large asymmetric multi-protein complex which comprises three sub-complexes; FANCB-FANCL-FAAP100, FANCA-FANCG-FAAP20, and FANCC-FANCE-FANCF (Huang et al., 2014; Swuec et al., 2017; van Twest et al., 2017; Shakeel et al., 2019). The FANCA-FANCG-FAAP20 sub-complex promotes FA core complex nuclear localisation and chromatin association (Yuan et al., 2012; Huang et al., 2014). The FANCB-FANCL-FAAP100 sub-complex is the catalytic subcomplex with E3 ligase activity (Huang et al., 2014). The FANCC-FANCE-FANCF sub-complex mediates interaction of the FA core complex with its substrate FANCD2-FANCI complex, selectively in the DNA-bound form (Huang et al., 2014; Swuec et al., 2017; van Twest et al., 2017).

Structurally, two FANCB-FAAP100 heterodimers form a scaffold flanked by two FANCL E3 ligases which have different conformations, suggesting functional

asymmetry (Swuec et al., 2017; Shakeel et al., 2019). FANCL selectively binds to the E2 ubiquitin-conjugating enzyme UBE2T/FANCT to determine the high substrate specificity of the FA core complex ubiquitin ligase activity (Hodson et al., 2014). In co-operation with UBE2T, FANCL mono-ubiquitinates FANCD2 and FANCI at Lysine-561 and -523 respectively (Sims et al., 2007; Smogorzewska et al., 2007; Joo et al., 2011; Rajendra et al., 2014). The FANCD2-FANCI heterodimer is targeted to chromatin following ATR-mediated FANCI phosphorylation, which also promotes complex dissociation and interface exposure, enabling access to these lysine residues (Ishiai et al., 2008; Sareen et al., 2012; Alcón et al., 2020). This mono-ubiquitination of FANCD2 stabilises the FANCD2-FANCI complex on DNA in a closed clamp conformation (Alcón et al., 2020). Mono-ubiquitination of FANCD2 is a key regulatory step in FA pathway activation that is necessary for recruitment of proteins that function in downstream ICL resolution (Knipscheer et al., 2009).

Mono-ubiquitinated FANCD2 recruits SLX4/FANCP to the stalled replication fork (Yamamoto et al., 2011; Klein Douwel et al., 2014; Zhang and Walter, 2014; Zhang et al., 2019a). SLX4 acts as a scaffold protein for NER endonucleases such as MUS81-EME1, ERCC1-ERCC4/FANCQ, SLX1, and FAN1, which cleave either side of the crosslink on one parental DNA strand (De Silva et al., 2000; Kuraoka et al., 2000; Niedernhofer et al., 2004; Hanada et al., 2006; Bhagwat et al., 2009; Castella and Taniguchi, 2010; Kratz et al., 2010; Liu et al., 2010; MacKay et al., 2010; Smogorzewska er al. 2010; Yoshikiyo et al., 2010; Bogliolo et al., 2013; Kim et al., 2013; Benitez et al., 2014; Klein Douwel et al., 2014; Zhang and Walter, 2014). This effectively ‘unhooks’ the crosslink to generate a DSB on the cleaved parental DNA strand, and an ICL adduct on the opposite parental DNA strand (Molodovan and D’Andrea, 2009). It has been suggested that the primary endonuclease employed by the FA pathway is ERCC4-ERCC1, whose preferred substrate is the splayed arms DNA structure induced by ICLs, whilst other endonucleases act redundantly in ICL repair (Klein Douwel et al., 2014; Zhang and Walter, 2014; Zhang et al., 2019). However, whilst it has been observed that mono-ubiquitinated FANCD2 is responsible for SLX4 recruitment (Yamamoto et al., 2011; Klein Douwel et al., 2014), other studies have demonstrated that SLX4 can be recruited to ICLs in a FANCD2-independent manner (Sarkar et al., 2006; Lachaud et al., 2014).

The resulting DNA adduct is bypassed by TLS polymerases (Waters et al., 2009). The FA core complex and ubiquitinated PCNA recruits TLS polymerases such

as REV1, REV7/FANCV, REV3L, POLK, POLN and POLI to complete nascent DNA synthesis across the ICL adduct (Niedzwiedz et al., 2004; Nojima et al., 2005; Guo et al., 2006; Mirchandani et al., 2008; Moldovan and D'Andrea, 2009, Kim et al., 2012; Budzowska et al., 2015; Roy and Schärer, 2016). Given TLS is error-prone, mutations are introduced around the ICL site at a frequency of 1% (Budzowska et al., 2015). The NER machinery then removes the unhooked crosslink from the parental DNA strand. The resulting repaired duplex strand can be used in HRR-mediated repair of the DSB (Moldovan and D'Andrea, 2009).

The DSB is repaired by high fidelity HRR, which is promoted by recruitment of HRR proteins by mono-ubiquitinated FANCD2 (Perry and Evans, 1975; Niedzwiedz et al., 2004; Nakanishi et al., 2005; Niedernhofer et al., 2005; Yamamoto et al., 2005). Briefly, FANCD2 cooperates with BRCA1/FANCS to recruit DNA helicases and exonucleases BLM, CtIP, MRN and EXO1 to resect the parental DNA strand of the DSB and generate an RPA-coated 3' overhang (Molodovan and D'Andrea, 2009; Murina et al., 2014; Ceccaldi et al., 2016). The Rad51 recombinase, aided by BRCA2/FANCD1, PALB2/FANCN, RAD51C/FANCO, BRIP1/FANCJ, BRCA1/FANCS and XRCC2/FANCU, promotes RPA eviction and drives strand invasion of the 3' overhang into the repaired DNA duplex to form a D-loop (Johnson et al., 1999; Takata et al., 2001; Taniguchi et al., 2002a; Niedzwiedz et al., 2004; Somyajit et al., 2010; Long et al., 2011; Foo and Xia, 2022). The D-loop is extended and DNA synthesis occurs. This enables high-fidelity extension of the nascent DNA strand and second end capture to form a double Holliday junction resulting in full DSB resolution. It is worth noting that ICL-induced DSBs can also be repaired by two other pathways; single strand annealing (SSA) and non-homologous end joining (NHEJ) (Yuan et al., 2012; Ceccaldi et al., 2016; Benitez et al., 2018). However, given many FANC genes are well-established HRR factors, and the presence of a readily available HRR template following TLS, HRR is identified as the preferential pathway over error-prone NHEJ (Palovcak et al., 2017). These pathways require different levels of existing homology and DSB end resection Following completion of ICL repair, the FA pathway is inactivated by the USP1-UAF1-RAD51AP1 complex which de-ubiquitinates the FANCD2-FANCI complex, releasing it from the site of damage (Nijman et al., 2005; Cukras et al., 2016; Arkinson et al., 2018; Liang et al., 2019b).

It should be noted that a replication- and HRR- independent mechanism of ICL resolution has been observed outside of S-phase, in which the crosslink is recognised and unhooked by NER machinery and subsequently bypassed by multiple TLS polymerases (Schärer et al., 2005; Sarkar et al., 2006). However, it has also been observed that the majority of crosslinks are repaired during S-phase, and therefore FA pathway activation is the primary mechanism of ICL repair (Akkari et al., 2000; Taniguchi et al., 2002a).

1.4.1.2 FA pathway activation is integrated with DDR activity

The ATR pathway is initiated by, and can itself initiate, FA pathway activation (Collis et al., 2008; Singh et al., 2013) (Figure 1.10). Collis et al., (2008) observed that activation of FANCM-FAAP24 following detection of stalled replication forks is necessary for efficient ATR checkpoint signalling, which is activated to halt cell cycle progression upon detection of replication stress. Similarly, Schwab et al., (2010) observed impaired ATR pathway activation in FANCM-deficient cells. Singh et al., (2013) demonstrated that ATR signalling induces phosphorylation and therefore activation of FANCM at Ser1045, which promotes recruitment of FANCM to ICLs to initiate FA pathway activation. Similarly phosphorylation of multiple FANC proteins by ATR pathway kinases is necessary for efficient downstream FA pathway activation. ATR-mediated FANCG phosphorylation enables FA core complex assembly, while ATR-mediated FANCA phosphorylation enables FA core complex nuclear localisation (Qiao et al., 2004; Wilson et al., 2008; Collins et al., 2009). Chk1-mediated FANCE phosphorylation inhibits core complex E3 ligase activity (Wang et al., 2007). ATR phosphorylates FANCI to promote chromatin binding and interface exposure of the FANCD2-FANCI complex to enables its mono-ubiquitination (Ishiai et al., 2008; Sareen et al., 2012; Chen et al., 2015a; Alcón et al., 2020). ATR deficiency therefore impairs FA pathway activation (Andreassen et al., 2004).

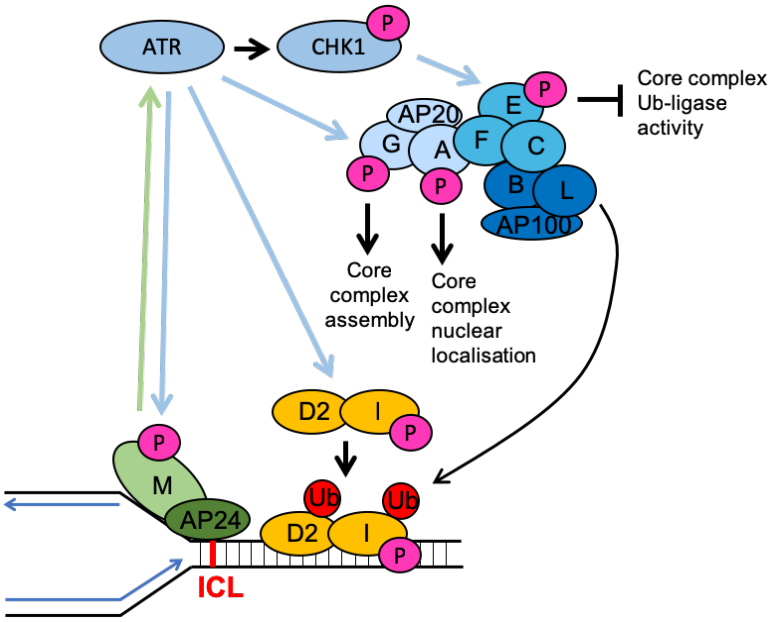

Figure 1.10. FA pathway activation is integrated with DDR activity.
Upon detection of stalled forks, the FANCM-FAAP24 complex activates ATR signalling to restrict cell cycle progression. FANCM-FAAP24 is also necessary for downstream ATR checkpoint signalling. ATR pathway kinases phosphorylate multiple FANC proteins to enable efficient FA pathway activation. ATR phosphorylates FANCM to promote its recruitment to ICLs. ATR also phosphorylates FANCI to promote recruitment of FANCD2-FANCI to chromatin and promote interface exposure for mono-ubiquitination. FANCG and FANCA are phosphorylated by ATR to promote core complex assembly and nuclear localisation respectively. Chk1 phosphorylates FANCDE to inhibit core complex E3 ligase activity.

1.4.2 The FA pathway in replication stress limitation

Increasing evidence demonstrates that many FANC proteins have alternative cellular functions independent from ICL repair (Sumpter and Levine, 2017), as summarised in Table 1.3. For example, many FANC proteins function to limit replication stress in a repair-independent manner by stabilising stalled replication forks, regulating replication fork dynamics, or promoting R-loop resolution (Fajardo et al., 2022). This prevents the accumulation of replication-associated DNA damage (Sobeck et al., 2006). However, many of these alternative FA pathway functions act independently of FANCD2 mono-ubiquitination.

Table 1.3. Alternative cellular functions of FANC proteins.
Summary of the alternative cellular functions of FANC proteins. ssDNA; single stranded DNA. DSB; double strand break. HR; homologous recombination. (Table continues overleaf).

Cellular Function	Known FANC proteins involved	Description	Reference
Stalled replication fork stabilisation	FANCD2 FANCI RAD51/FANCO BRCA1/FANCS BRCA2/FANCD1	Stabilises stalled replication forks by protecting ssDNA to prevent collapse and DSB generation.	(Howlett et al., 2005; Schwab et al., 2010; Schlacher et al., 2011; Schlacher et al., 2012)
Resolution of R-loops	FANCD2 FANCM BRCA1/FANCS BRCA2/FANCD1	Detects and resolves R-loops upon transcription-replication collisions to prevent DNA damage and further fork stalling.	(García-Rubio et al., 2015; Schwab et al., 2015; Okamoto et al., 2019; Herold et al., 2019; Liang et al., 2019a)
Regulation of replication fork dynamics	FANCA BRCA2/FANCD1 FANCD2 FANCI FANCJ	Regulates DNA replication initiation and restart of stalled replication forks.	(Chaudhury et al., 2013; Lossaint et al., 2013; Yeo et al., 2014; Raghunandan et al., 2015)
NHEJ suppression	BRCA1/FANCS	FA proteins prevent DSB access to NHEJ factors to channel DSB repair into HRR.	(Cao et al., 2009; Adamo et al., 2010; Bouwman et al., 2010; Bunting et al., 2010; Pace et al., 2010; Eccles et al., 2018)
ATR-dependent DNA damage checkpoint	FANCM	FANCM activates the ATR pathway to initiate DDR upon detection of DNA lesion.	(Collis et al., 2008)
ATM-dependent intra-S checkpoint	FANCD2	Upon DSB detection by MRN, ATM is activated and phosphorylates FANCD2 at Ser222 to enable activation of the intra-S checkpoint.	(Taniguchi et al., 2002b)
Alternative Lengthening of Telomeres (ALT)	FANCM BRCA1/FANCS FANCD2	Limits replication stress and R-loop formation during ALT in telomerase-null cells.	(Fan et al., 2009; Pan et al., 2017; Lu et al., 2019; Pan et al., 2019; Silva et al., 2019; Xu et al., 2019)
Ultrafine DNA bridge resolution	BRCA2/FANCD1 FANCD2 FANCI	Prevents appearance of DNA ultrafine bridges linking separating condensed chromosomes during mitosis.	(de Oca et al., 2005)
Suppression of sister chromatid exchange (SCE)	FANCM	FANCM dissociates RAD51-induced D-loops to suppress sister chromatid exchange.	(Sun et al., 2008; Prakash et al., 2009; Raya et al., 2009)

Table 1.3. Alternative cellular functions of FANC proteins (continued).
Table legend on previous page.

Cellular Function	Known FANC proteins involved	Description	Reference
Maintenance of G-rich DNA sequences	BRIP1/FANCJ	Unwinds G-quadraduplex secondary structures at sites of stalled replication forks.	(Bosch et al., 2014)
Handling ROS	FANCC FANCD2	FANCC interacts with GSTP1, and FANCD2 interacts with FOXO3a, to prevent ROS accumulation. FANC proteins also protect the promoters of antioxidant defence genes.	(Schindler et al., 1988; Cumming et al., 2001; Li et al., 2010; Du et al., 2012)
Modulation of mitochondrial stress response	FANCD2	FANCD2 limits activation of the mitochondrial stress response and prevents mitochondrial dysfunction.	(Fernandes et al., 2021)
Promotion of mitophagy	FANCA FANCF FANCC FANCL FANCD2 FANCS/BRCA1 FANCD1/BRCA2	Promote removal of damaged mitochondria.	(Sumpter and Levine, 2016)

1.4.2.1 FANC proteins stabilise stalled replication forks

Prolonged stalling of replication forks leads to replisome dissociation and fork collapse (Fajardo et al., 2022). The aberrant replicative intermediates resulting from fork collapse are highly recombinogenic and therefore increase genomic instability. Additionally, stalled forks themselves are vulnerable to exonuclease degradation. FA pathway proteins protect the fidelity of stalled replication forks, as evidenced by an increase in fork breakage and deletion mutations in FA pathway deficient cells (Howlett et al., 2005; Gari et al., 2008; Schwab et al., 2010; Schlacher et al., 2011; Schlacher et al., 2012; Yang et al., 2015; Madireddy et al., 2016). For example, several FANC proteins protect nascent DNA strands from exonuclease degradation. At stalled forks, mono-ubiquitinated FANCD2 connects BRCA1- and BRCA2-stabilised RAD51 to replisome components such as PCNA (Schlacher et al., 2011; Schlacher et al., 2012; Daza-Martin et al., 2019). This promotes RAD51 loading to

protect stalled forks from nucleolytic degradation and fork collapse. This mechanism of fork protection is dependent on FANCD2 mono-ubiquitination (Schlacher et al., 2012). FA machinery and BRCA proteins therefore display linked functionality in both ICL repair and protection of stalled replication forks. Additionally, FANCM promotes regression of stalled replication forks, which can aid in the repair of replication-blocking lesions and promote fork restart (Higgins et al., 1976; Postow et al., 2001; Gari et al., 2008; Schwab et al., 2010).

1.4.2.2 FANC proteins regulation DNA replication fork dynamics

FA pathway proteins also regulate replication fork dynamics by modulating new origin firing, fork restart and fork progression (Lossaint et al., 2013; Yeo et al., 2014; Raghunandan et al., 2015). This occurs independently from FANCD2 mono-ubiquitination (Lossaint et al., 2013; Yeo et al., 2014; Raghunandan et al., 2015). ATR signalling promotes the interaction of FANCD2 with the MCM helicase to restrain replication fork progression during high replication stress (Lossaint et al., 2013). It has also been observed that BRIP1, BRCA2, FANCD2 cooperate with BLM, ATRX and CtIP to promote restart of stalled replication forks and suppress new origin firing upon induction of replication stress (Chaudhury et al., 2013; Yeo et al., 2014; Raghunandan et al., 2015; Madireddy et al., 2016; Thompson et al., 2017; Raghunandan et al., 2020). Chen et al., (2015) observed that whilst ATR-mediated FANCI phosphorylation inhibited new origin firing and promoted restart of stalled forks, FANCI deficiency results in reduced new origin firing. FANCD2 and FANCI therefore have common as well as independent and potentially opposing roles in regulating replication fork dynamics (Chaudhury et al., 2013; Thompson et al., 2017).

1.4.2.3 FANC proteins regulate R-loop suppression

High levels of replication stress and DNA damage induce an increase in the number of transcription-replication collisions, leading to an increase in R-loop formation. R-loops are both a product of, and a source of, replication stress (Santos-Pereira and Aguilera, 2015). R-loop accumulation therefore further escalates replication stress levels (Allison and Wang, 2019). This occurs frequently at common fragile sites (CFSs); conserved genomic loci prone to replication-stress-induced

breakage and R-loop formation (Okamoto et al., 2018b; Pladevall-Morera et al., 2019). Multiple FA pathway proteins have been observed to function in the suppression of co-transcriptional R-loops, with FA-deficient cells displaying enhanced R-loop accumulation (Bhatia et al., 2014; Garcia-Rubio et al., 2015; Hatchi et al., 2015; Schwab et al., 2015; Matos et al., 2020).

It has been shown that both BRCA1 and BRCA2 function in R-loop resolution. Bhatia et al., (2014) initially demonstrated that BRCA2 contributes to the resolution of R-loops, likely through association with TREX-2 mRNA export factor PCID2. It has also been shown that BRCA2 recruits RNase H2 to modulate the levels of DSB-associated RNA-DNA hybrids (D'Alessandro et al., 2018). BRCA1 is recruited to R-loops at transcription termination sites, where it mediates the recruitment of senataxin to promote R-loop resolution (Hatchi et al., 2015). This is required to prevent formation of R-loop driven DNA damage at these transcriptional pause sites. Additionally, it was observed that loss of function of BRCA1 induced enrichment of R-loops at the 5' end of genes which display promoter-proximal pausing of RNAPII in breast cancer cells (Zhang et al., 2017). This suggested RNAPII pausing contributes BRCA1-associated R-loop accumulation (Zhang et al., 2017). Similarly, BRCA1 is specifically recruited by MYCN to resolve promoter-proximal R-loops in neuroblastoma cells, enabling MYCN to promote transcription elongation without exacerbating replication stress (Herold et al., 2019). BRCA1 mediates this resolution of MYCN-induced R-loops by recruiting mRNA de-capping complexes (Herold et al., 2019).

Garcia-Rubio et al., (2015) demonstrated that FANCD2 and FANCA are involved in R-loop resolution and that many DNA breaks that accumulate in FANCD2- and FANCA-deficient cells are R-loop dependent. Additionally, formation of FANCD2 foci was largely R-loop dependent, further suggesting FANCD2 functions at sites of R-loops. Schwab et al., (2015) demonstrated that R-loop accumulation activates the FA pathway, and that FANCD2 is required to prevent replication fork arrest and DNA damage resulting from co-transcriptional R-loops. Altogether this suggested FANCD2 mono-ubiquitination functions in the resolution of co-transcriptional R-loops and associated damage. In agreement with this, it was subsequently demonstrated that R-loop binding by FANCD2 induces its mono-ubiquitination (Liang et al., 2019a). It has also been shown that high replication stress induced accumulation of FANCD2 at R-loops in CFSs (Madireddy et al., 2016;

Okamoto et al., 2018b; Okamoto et al., 2019). It was further demonstrated that FANCD2 suppresses R-loop levels at CFSs through association with RNA processing factors such as hnRNP U and DDX47 which promote efficient processing of long RNA transcripts (Okamoto et al., 2018a; Okamoto et al., 2019). Additionally, FANCD2 was also observed to localise at CFSs with ATRX; a chromatin remodeller which limits genomic instability at CFSs (Pladevall-Morera et al., 2019). It is therefore suggested that FANCD2 mono-ubiquitination promotes R-loop resolution primarily through recruitment of R-loop processing factors such as hnRNP U, DDX47 and BRCA1-SETX and BRCA2-TREX complexes (Garcia-Rubio et al., 2015; Schwab et al., 2015; Liang et al., 2019; Okamoto et al., 2019; Pladevall-Morera et al., 2019). FANCM was also shown to directly promote R-loop resolution through its translocase activity which was observed to induce R-loop unwinding in vitro (Schwab et al., 2015). Telomeric R-loop formation during alternative lengthening of telomeres (ALT) is also disrupted by FANCM (Pan et al., 2017; Pan et al., 2019; Silva et al., 2019). Furthermore, it was demonstrated that the MRN complex promotes FANCD2- and FANCM-mediated suppression of transcription-associated R-loops (Chang et al., 2019b).

1.4.3 Loss of function of the FA pathway

1.4.3.1 Fanconi anaemia results from biallelic germline mutations in FANC genes

Bi-allelic germline alterations in any of the 23 key FANC genes causes Fanconi anaemia (FA) (Table 1.2) (Rosenberg et al., 2011; Nalepa and Clapp, 2018). Whilst 23 genetically distinct FA complementation groups have so far been identified, more FA pathway genes are continually being revealed as key FANC genes through genotypic analysis of FA patients. FA is inherited in an autosomal-recessive manner, with the exception of FA-B and FA-R complementation groups which are inherited in an X-linked and autosomal-dominant manner respectively (Meetei et al., 2004; Ameziane et al., 2015). The phenotypic severity of FA is dependent upon which FANC gene is disrupted and the extent of loss-of-function in the resulting protein (Nalepa and Clapp, 2018). Most FA patients harbour core

complex mutations, with ~90% encoding mutations in *FANCA*, *FANCC* or *FANCG* (Rodríguez and D'Andrea, 2017; Liu et al., 2020a).

FA is therefore both genetically and clinically heterogeneous, and is characterised by progressive bone marrow failure, anaemia, congenital abnormalities and cancer predisposition (Alter, 1996; Moldovan and D'Andrea, 2009; Steinberg-Shemer et al., 2020). Given FA results from impaired FA pathway activity, these symptoms are driven by genomic instability (Moldovan and D'Andrea, 2009). For example, bone marrow failure occurs in 80% of FA patients and results from the accumulation of endogenous DNA damage in haematopoietic stem and progenitor cells (HSPCs) (Pontel et al., 2015; Walter et al., 2015; Garaycoechea et al., 2018; Steinberg-Shemer et al., 2020; Rodriquez et al., 2021b). These high levels of DNA damage induce hyperactivation of p53 and TGF-β growth suppressive pathways which exacerbates HSPC exhaustion (Ceccaldi et al., 2012; Zhang et al., 2016; Rodriquez et al., 2021a; Rodriquez et al., 2021b). A recent survey of 111 FA patients demonstrated a cancer frequency of 30% (Steinberg-Shemer et al., 2020). FA patients are predominantly predisposed to acute myeloid leukaemia, head and neck squamous cell carcinomas and embryonal tumours (Garaycoechea and Patel, 2014; Wang and Smogorzewska, 2015). Mono-allelic germline FANC alterations commonly increases risk of breast, ovarian and pancreatic cancers, a widely known example being BRCA1/2-associated hereditary breast cancer (Merajver et al., 1995; Pejovic et al., 2006; Kuchenbaecker et al., 2017; Niraj et al., 2019). Loss of FA pathway function sensitises cells to DNA crosslinking and replication-stress inducing agents, and this is a clinical marker of Fanconi anaemia (Sasaki et al., 1975; Auerbach and Wolman, 1976; German et al., 1987; Auerbach, 1988; Taniguchi et al., 2002a; Houghtaling et al., 2003; Niedzwiedz et al., 2004; Bridge et al., 2005; Dai et al., 2015; Dai et al., 2017). As such, FA-associated cancers require lower chemotherapeutic doses which reduces cancer treatment efficacy (Zhang et al., 2008; Moldovan and D'Andrea, 2009; Compostella et al., 2010).

1.4.3.2 Somatic FA pathway mutations in cancer

Somatic FA pathway genomic aberrations also contribute to tumorigenesis and tumour progression in various primary sporadic cancers, with at least one FANC gene alteration (mutation, gain or loss) detected in 40-65% of cancers (Niraj et al.,

2019; Liu et al., 2020a; Zhao et al., 2010). Bladder, ovarian and breast cancers display the highest FANC gene alteration frequency (Niraj et al., 2019). Although FA patients most commonly harbour mutations in *FANCA*, *FANCC* or *FANCG*, the somatic mutation frequency in cancers is approximately even across all FANC genes, with the alterations occurring most frequently in HRR-related FANC genes such as *BRCA2/FANCD1* (Liu et al., 2020a; Niraj et al., 2019). This discrepancy in relative FANC gene mutation frequencies in FA and cancer suggests FANC genes have differing roles in the development of FA and cancer (Liu et al., 2020a). Interestingly, although both gain and loss of function alterations co-exist across cancer types for all FANC genes, there is a trend in the most frequent type of alteration observed for each FANC gene (Niraj et al., 2019; Liu et al., 2020a). Whilst 75% of alterations in HRR-related FANC genes are characterised by mutations and deletions, core complex FANC gene alterations are predominantly characterised by amplifications (Niraj et al., 2019). Similarly, the type of alteration differs across cancer types, with amplification predominantly observed in ovarian cancer but deletion predominantly observed in prostate cancer (Niraj et al., 2019). The presence of both gain and loss of function FANC gene alterations in cancer suggests both impairment and enhancement of FA pathway activity could be beneficial during tumour progression.

1.4.3.3 FA pathway mutations in neuroblastoma

Low frequency somatic alterations in FA pathway genes such as *FANCM*, *FAN1* and *PALB2* have been observed in neuroblastoma (Guerra et al., 2010; Hu et al., 2010; Molenaar et al., 2012; Pugh et al., 2013; Takagi et al., 2017). Also, development of neuroblastoma has been observed in several FA cases (Bissig et al., 2002; Compostella et al., 2010; Serra et al., 2012; Loizidou et al., 2016). Bi-allelic germline mutations in *PALB2/FANCN* and *BRCA2/FANCD1*, causing FA-N and severe FA-D1 subtypes respectively, confer high risk of embryonal tumours such as neuroblastoma and Wilms tumours (Reid et al., 2007; Mehmet et al., 2016). *PALB2* and *BRCA2* mutations may pre-dispose embryonal tumours by inducing severe genomic instability in shared embryonal progenitor cells, with *MYCN* expression exacerbating this effect in NCCs to induce neuroblastoma (Reid et al., 2007; Serra et al., 2012). The therapeutic potential of targeting the FA pathway in MNA

neuroblastoma would therefore be dependent upon the mutational profile of FA pathway genes, as loss-of-function alterations would prevent development of an FA pathway dependency.

1.4.3.4 FA pathway expression in cancer

Similarly to the observation of both gain- and loss-of-function mutations, upregulation and downregulation of FANC genes has been observed across cancer types. Liu et al., (2020) observed broad transcriptional upregulation of most FANC genes in multiple tumour types compared to normal tissue controls including breast, ovarian, colon, bladder, melanoma and lung cancers. *UBE2T/FANCT* was the most upregulated FANC gene in all tumour types, whilst *FANCC, FANCE, FANCL* and *FANCM* were downregulated in some cancer types. However, no change in FANC gene expression was observed in prostate cancer. Kao et al., (2011) observed that the extent of FANC gene overexpression in melanoma correlated with increased melanoma thickness. However, NER gene expression was downregulated or unchanged (Kao et al., 2011). High expression of FANC genes has frequently been associated with increased tumour aggressiveness, chemo-resistance and reduced event-free survival (Taniguchi et al., 2003; Swisher et al., 2009; Ozawa et al., 2010; Nakanishi et al., 2012; Swarts et al., 2013). In particular, the upregulation of *FANCD2* in ovarian, breast and uterine cancers correlates with HRR-deficiencies, increased tumour stage, and poor prognosis (Van Der Groep et al., 2008; Wysham et al., 2012; Kais et al., 2016; Feng and Jin, 2019).

In contrast, Zhang et al., (2010) observed that low *FANCD2* expression correlated with high tumour grade and metastasis in breast cancer. Furthermore, it has been observed that a greater proportion of breast cancers have no detectable FANCD2 expression compared to benign tissues (Van Der Groep et al., 2008; Rudland et al., 2010; Zhang et al., 2010; Feng and Jin 2019). However, this could be specific to nuclear FANCD2 (Rudland et al., 2010). In head and neck squamous cell carcinoma, downregulation of at least one FANC gene was observed in 66% of cases (Wreesmann et al., 2007). Therefore, whilst FANC gene inactivation promotes tumorigenesis through increased genomic instability, FA pathway upregulation is advantageous during later tumour progression to limit excess genomic instability and mediate chemotherapeutic resistance (Liu et al., 2020a).

1.4.4 Therapeutic potential of FA pathway inhibition

1.4.4.1 Loss of FA pathway function sensitises cells to DNA damaging chemotherapy and DNA repair inhibitors

The FA pathway is the major mechanism for efficient ICL repair (Sasaki et al., 1975; Akkari et al., 2000; Taniguchi et al., 2002a). Loss of FA pathway function therefore primarily sensitises cells to DNA crosslinking agents, and this is a clinical marker of Fanconi anaemia (Sasaki et al., 1975; Auerbach et al., 1976; German et al., 1987; Auerbach 1988; Taniguchi et al., 2002a; Houghtaling et al., 2003; Niedzwiedz et al., 2004; Bridge et al., 2005; Dai et al., 2015; Dai et al., 2017). FA pathway proteins also functions to limit replication stress through multiple mechanisms, and FA pathway deficiencies therefore also sensitise cells to replication-stress inducing agents (Howlett et al., 2005). Whilst the FA pathway contributes to the replication-dependent repair of UV- and IR-induced DNA lesions, these lesions have multiple alternative repair mechanisms, and therefore loss of FA pathway function induces limited sensitisation to UV and radiotherapy (Garcia-Higuera et al., 2001; Taniguchi et al., 2002a; Houghtaling et al., 2003; Niedzwiedz et al., 2004; Bridge et al., 2005; Dunn et al., 2006). Targeted inhibition of the FA pathway would therefore be beneficial in sensitising tumours to DNA crosslinking chemotherapeutics.

1.4.4.2 FA pathway inhibitors

There are currently no widely accepted small molecule FA pathway inhibitors that directly and selectively inhibit FA pathway activation (Liu et al., 2020a; Taylor et al., 2020; Sharp et al., 2021). However, high throughput biochemical screening methods have been optimised to aid future identification of specific FA pathway inhibitors, with promising development of FANCL and UBE2T inhibitors being undertaken (Morreale et al., 2017; Cornwell et al., 2019; Sharp et al., 2020; Sharp et al., 2021). Instead, many non-specific FA pathway inhibitors have been identified through cell-based or in vitro screening assays and, despite broad off-target effects, these are commonly used to study the potential effects of FA pathway inhibition

(Chirnomas et al., 2006; Landais et al., 2009a; Landais et al., 2009b; Jacquemont et al., 2012; Jun et al., 2013; Sharp et al., 2020). For example, Chirnomas et al., (2006) undertook a cell-based screen which identified the kinase inhibitors wortmannin and H-9, and the natural di-phenolic compound curcumin as effective FA pathway inhibitors, capable of inhibiting FANCD2 mono-ubiquitination and foci formation and of sensitising cancer cells to the crosslinking chemotherapeutic cisplatin. The FA pathway modulating target of curcumin is unknown but is hypothesised to be IKK, a component of the NF-┤ B pathway that interacts with the FA core complex (Otsuki et al., 2002; Kasinski et al., 2008; Landais et al., 2009a). Jun et al., (2013) used similar cell-based screening methods to identify ouabain, a cardiac glycoside, as an effective FA pathway inhibitor which downregulates FANCD2 expression and foci formation and sensitises cancer cells to the crosslinking agent mitomycin C (MMC). Ouabain inhibits FA pathway activation in a p38 MAPK-dependent manner (Jun et al., 2013).

Curcumin is a natural di-phenolic small molecule derived from the rhizome Curcuma longa that demonstrates treatment efficacy in a range of diseases including cancer, cystic fibrosis, and malaria and neurodegenerative diseases (Picone et al., 2014). In cancer, curcumin demonstrates anti-proliferative, pro-apoptotic, and anti-metastatic effects and sensitises tumours to DNA damaging or replication fork stalling chemotherapeutics including cisplatin and gemcitabine (Cheng et al., 2001; Chirnomas et al., 2006; Schlacher et al., 2012; Picone et al., 2014). However, it should be noted that although curcumin commonly is used to analyse the effect of FA pathway inhibition, many non-specific effects also contribute to the anti-tumorigenic effects of curcumin. For example in neuroblastoma cells, curcumin has been demonstrated to induce apoptosis through induction of mitochondrial dysfunction, an increase in ROS production, upregulation of pro-apoptotic genes such as Bax and p53, and inhibition of AKT and NF-kB (Liontas et al., 2004; Aravindan et al., 2008; Freudlsperger et al., 2008; Pisano et al., 2010; D'Aguanno et al., 2012; Picone et al., 2014; Kalashnikova et al., 2017; Sidhar and Giri, 2017). Additionally, curcumin has been shown to induce upregulation and activation of multiple DNA repair proteins such as ATM, ATR, DNA-PK, BRCA1, BRCA2, and MRE11 (Landais et al., 2009a; Shang et al., 2016; Chen et al., 2017; Wang et al., 2022a). Similarly, ouabain also induces cancer cell death through other off-target

effects such as induction of ROS and exacerbation of ER stress and DNA damage (Chang et al., 2019a; Du et al., 2018; Du et al., 2021; Yang et al., 2021;). In particular, ouabain induces DSB accumulation through inhibition of NHEJ (Du et al., 2018). Additionally, ouabain was shown to regulate expression of other DNA repair proteins. Chang et al., (2019a) observed that ouabain induced a downregulation of BRCA1 and DNA-PK, whilst Yang et al., (2021) observed that ouabain upregulated PARP and BRCA1 and downregulated DNA-PK.

1.4.4.3 FA pathway inhibition sensitises cancer cells to DNA damaging and replication-stress inducing chemotherapeutics

FA pathway inhibition has been demonstrated to sensitise a range of cancer cells to DNA crosslinking and alkylating chemotherapeutics. For example, FA pathway inhibition by curcumin significantly sensitised glioblastoma (GBM) cell lines to the mono-alkylating chemotherapeutic temozolomide (TMZ) (Patil et al., 2014; Chen et al., 2007). FA pathway inhibition by curcumin has also been shown to sensitise ovarian cancer, breast cancer, non-small cell lung cancer (NSCLC), retinoblastoma, and laryngeal carcinoma cells to the DNA crosslinking chemotherapeutics cisplatin and carboplatin (Chirnomas et al., 2006; Chen et al., 2015b; Yallapu et al., 2010; Chanvorachote et al., 2009; Sreenivasan et al., 2013; Zhang et al., 2013; Kang et al., 2015; Zou et al., 2018; Huang et al., 2022; Wang et al., 2022b). Curcumin has also been shown to sensitise the non-MNA neuroblastoma cell line SK-N-AS to cisplatin, however an association with FA pathway inhibition was not explored (Sukumari-Ramesh et al., 2011).

It has also been demonstrated that curcumin treatment sensitises cancer cells, including neuroblastoma cells, to replication-stress inducing chemotherapeutics such as gemcitabine and doxorubicin (Kunnumakkara et al., 2007; Sukumari-Ramesh et al., 2011; Yoshida et al., 2017; Namkaew et al., 2018; Fonseka et al., 2020; Liu et al., 2020b). However, it has also been suggested that FA pathway inhibition could enable faster crosslink resistance acquisition through increased mutation rates (Edwards et al., 2008; Sakai et al., 2008; Moldovan and D'Andrea, 2009). We therefore hypothesised that FA pathway inhibition would sensitise neuroblastoma cells to induction crosslinking chemotherapeutics used in current neuroblastoma treatment such as cisplatin, carboplatin and

cyclophosphamide (Deans and West, 2011; Di Giannatale et al., 2014; Mody et al., 2017; Mody et al., 2020). Additionally, the high replication stress induced by *MYCN* amplification may sensitise cells to FA pathway inhibition (Gu et al., 2015; King et al., 2020).

1.4.4.4 FA pathway inhibition re-sensitises cancer cells that are resistant to DNA crosslinking chemotherapy

Resistance to DNA crosslinking and alkylating agents via accelerated removal of DNA adducts is often acquired by upregulation or reactivation of FA genes and is selected for during chronic exposure to DNA crosslinking agents (Chen et al., 2005; van der Heijen et al., 2005; Chen et al., 2007; Chen et al., 2016). Hence tumour cells resistant to crosslinking chemotherapeutics are heavily reliant on the FA pathway for survival (Chen et al., 2007; Zhao et al., 2014; Bretz et al., 2016). Targeted inactivation of ICL repair via FA pathway inhibition has therefore been demonstrated to re-sensitise resistant GBM, breast cancer and lung cancer cells to temozolomide, MMC and cisplatin respectively (Chirnomas et al., 2006; Zhao et al., 2014; Dai et al., 2015). Similarly, ATR inhibition re-establishes crosslinking sensitivity due to its integral role in FAP activation (Dai et al., 2017).

1.5 REDACTED

1.5.1 REDACTED

REDACTED

1.5.2 REDACTED

REDACTED

1.5.3 REDACTED

REDACTED

1.5.4 REDACTED

REDACTED

1.6 Aims and Hypotheses

Approximately half of all neuroblastoma cases are high-risk at diagnosis, for which the five year overall survival rate remains below 50% despite escalation of treatment intensity. Development of novel therapeutics which improve treatment efficacy without increasing morbidity are therefore desperately required. *MYCN* amplification occurs in 20% of neuroblastomas and is always indicative of high-risk disease due to its significant association aggressive and refractory disease. *MYCN* expression promotes proliferation and pluripotency and therefore malignant progression, but also induces high levels of replication stress and DNA damage. MNA neuroblastomas are therefore sensitised to treatments which target the cell cycle and inhibitors of DNA repair and replication-stress limiting pathways. A MYCN-induced dependency on these DNA repair pathways is often indicated by their upregulation upon *MYCN* overexpression or amplification.

The FA pathway primarily functions in the repair of ICLs and limitation of replication stress. Upregulation of FA pathway expression is frequency observed across multiple cancer types and often correlates with poor prognosis. Additionally, inhibition of the FA pathway sensitises a broad range of cancer cell lines to DNA crosslinking and alkylating chemotherapeutics. However the therapeutic potential of FA pathway inhibition in neuroblastoma is unknown.

REDACTED

Given *MYCN* amplification induces high levels of replication stress and DNA damage, it was theorised that MNA neuroblastoma cells would have a greater dependency on the FA pathway to limit MYCN-induced replication stress. As such, we first hypothesised that MYCN would transcriptionally upregulate the FA pathway to prevent accumulation of replication stress-induced DNA damage. Secondly, we hypothesised that *MYCN* overexpression or amplification would sensitise cells to inhibition of the FA pathway, and that FA pathway inhibition would additionally sensitise neuroblastoma cells to clinically relevant DNA crosslinking chemotherapeutics. **REDACTED**

The aims of this project are to:

1. Examine the effect of *MYCN* overexpression and amplification on FA pathway expression in neuroblastoma cell lines and tumours.
2. Determine the efficacy of FA pathway inhibition in sensitising neuroblastoma cells to DNA crosslinking chemotherapeutics and to MYCN-induced replication stress.
3. **REDACTED**

1.7 Thesis overview

This thesis explores the therapeutic potential of targeting the FA pathway in MNA neuroblastoma. In Chapter 3, we demonstrate that *MYCN* overexpression or amplification induces an upregulation of FANC and HRR-associated FA pathway genes but does not impact the expression of TLS- or NER-associated FA pathway genes. Additionally, we show MYCN binds at the promoters of most FA pathway genes, suggesting potential direct regulation by MYCN. In Chapter 4, we observe *MYCN* overexpression induces higher FA pathway activation which can be inhibited by the non-specific FA pathway inhibitor curcumin. We also determine the efficacy of FA pathway inhibition as a monotherapy or in combination with DNA damaging chemotherapy. *MYCN* overexpression and amplification sensitised neuroblastoma cells to FA pathway inhibition by curcumin, and this was associated with an accumulation of R-loops specifically in cells with high *MYCN* expression, and with an increase in replication stress. Additionally, curcumin induced a small sensitisation of neuroblastoma cells to crosslinking chemotherapeutics. **REDACTED**

Chapter 2. Materials and Methods

2.1 Materials

2.1.1 Lab Equipment, Reagents and Solutions

Table 2.1. Laboratory Equipment

Item	Company
Balance	Fisher scientific
Benchtop centrifuge accuspin™ Micro	Fisher Scientific
Biological safety cabinet Class II	Walker
Bolt Mini Gel Tank	Invitrogen
BioRad Criterion Blotter	BioRad
Colony counter	Stuart Scientific
Confocal microscope	Nikon
Eppendorf min-spin centrifuge (4ºC)	Eppendorf
Film processor	Konica
GeneAmp PCR System 2700	Applied Biosystems
Haemocytometer	Neubauer
Heat block (Ori-Block)	Techne
Heraeus MegaFuge 16 Centrifuge	Thermo Scientific
Hoefer™ Mighty Small™ II Mini Vertical Electrophoresis System tank	Amersham Biosciences, Hoefer
Incubator	Sanyo
Light microscope Eclipse TS100	Nikon
Multiskan FC plate reader	Thermo Scientific
pH meter	Jenway
Pipettes	Gilson
Real-time qPCR machine 7900	Applied Biosystems
SpectraMax microplate reader	Molecular devices
Shaking platform	Stovall Life Science
Power pack	Bio0Rad
Vortexer	Labinco
Water Bath	Grant Instruments

Table 2.2. Glassware, plastics, disposables.

Item	Company
Tissue culture T75 and T25 flasks	Starstedt
Cryovials	Starstedt
15 ml Falcon tube	Starstedt
Cell scraper	Sarstedt
50 ml Falcon Tube	Fisherbrand
6-well Nunclon delta surface tissue culture plates	Thermo scientific
12-well Nunclon delta surface tissue culture plates	Thermo scientific
96 well tissue culture plates	Costar
Eppendorf	Sarstedt
Filter tips	Sarstedt
25G needles	Becton Dickinson
Millex-GP syringe filter (0.22 µm pore size)	Merck Millipore
5 ml, 10 ml, 25 ml plastic pipettes	Fisherbrand
Refill pipette tips	Sarstedt
Sterile syringes	Becton Dickinson
10 cm tissue culture dish	Greiner Bio-one Cellstar

Table 2.3. Laboratory Reagents.

Reagent	Company
30% acrylamide: 0.8% bis-acrylamide	National Diagnostics
Ammonium per sulphate (APS)	Fisher Scientific
Acetic Acid	Fisher Scientific
Amersham ECL Western blotting Detection Reagent	GE Healthcare
Bovine Serum Albumin (BSA)	Sigma-Aldrich
cOmplete™ Mini EDTA-free Protease Inhibitor Cocktail	Sigma, Roche
Dimethyl sulfoxide (DMSO)	Fisher Scientific
DAPI	ThermoFisher Scientific
Ethanol	Fisher Scientific
Ethylenediaminetetraacetic acid (EDTA)	Sigma-Aldrich
Glycine	Fisher Scientific
Hydrochloric Acid (HCl)	Fisher Scientific
HiMark™ Pre-stained Protein Standard	ThermoFisher Scientific
Hydrochloric acid	Sigma-Aldrich
Industrial methylated spirit (IMS)	Fisher Scientific
Methanol	Fisher Scientific
Methylene blue	Sigma-Aldrich
Sodium Hydroxide (NaOH)	Fisher Scientific
Normal saline	Sigma-Aldrich
NuPAGE™ LDS sample buffer	Invitrogen
20X NuPAGE™ Tris-Acetate SDS Running Buffer	Invitrogen
NP-40 Alternative	Sigma-Aldrich
4% Paraformaldehyde (PFA)	Santa Cruz
Precision Plus Protein™ Dual Colour Standards	Bio-Rad
PhosSTOP phosphatase inhibitor cocktail	Sigma, Roche
Phenylmethylsulfonyl fluoride (PMSF)	ThermoFisher Scientific
Protein Assay Dye Reagent Concentrate	Bio-Rad
Resazurin	Sigma-Aldrich
Spectra Multicolour Broad Range Protein Ladder	ThermoFisher Scientific
Sodium chloride (NaCl)	Fisher Scientific
Sodium dodecyl sulfate (SDS)	Sigma-Aldrich
Sodium hydroxide (NaOH)	Fisher Scientific
Tetramethylethylenediamine (TEMED)	VWR
Tris-Base	Fisher Scientific
Tween	Acros Organics
Milk powder	Marvel
Oxoid PBS tablet	Thermo Scientific
ECL	Amersham
Universal developer	Champion Protochemistry
Universal fixer	Champion Protochemistry

2.1.1.1 Sterilisation

Glassware was washed with RBS detergent, rinsed in cold water and subsequently rinsed in distilled water. Glassware was then dried at 80 ºC before being sterilised by autoclaving using a MP24 Rodwell autoclaver. Autoclaving was undertaken for 15 min at 120 ºC and 15 pounds per square inch (psi). Buffers and solutions such as PBS were sterilised as necessary by autoclaving. Drug solutions used in cell culture were sterilised using a syringe and Millex GP syringe filter unit (0.22 µm pore size).

2.1.1.2 Purified water

Ultra-pure deionised water (ddH_2O) was produced using the Triple Red System, with a resistivity of 18.0 MOhm cm.

Table 2.4. Buffers and solutions.
Unless otherwise stated, contents refer to those used for 1X concentration.

Solution	Content
0.5M EDTA, pH 8.0	93 g EDTA disodium salt in 700 ml ddH_2O, adjusted to pH 8.0 with NaOH, made up to 500 ml with ddH_2O
PBS	1 Oxoid PBS tablet dissolved in 100 ml ddH_2O and autoclaved.
1M Tris-HCl, pH 6.8 and 8	121.1 g Tris base in 800 ml ddH_2O, adjusted to pH 6.8 or 8.0 with HCl and made up to 1 L with ddH_2O
1.5M Tris-HCl, pH 8.8	181.7 g Tris base in 800 ml ddH_2O, adjusted to pH 8.8 with HCl and made up to 1 L with ddH_2O
5X RIPA buffer	25 ml Tris-HCl (pH 8.0), 75 ml 1M NaCl, 0.5% (w/v) SDS, 5.0% (v/v) NP-40, 2.5% (w/v) sodium deoxycholate
1X RIPA buffer	0.2 ml 5X RIPA (50 mM Tris pH 8.0, 150 mM NaCl, 0.1% SDS, 1% NP-40, 0.5% sodium deoxycholate), 10 µl 1 mM PMSF, 10 µl 100X cOmplete™ Mini EDTA-free Protease Inhibitor Cocktail (Sigma, Roche), 10 µl 100X PhosSTOP phosphatase inhibitor cocktail (Sigma, Roche), made up to 1 ml with ddH_2O.
SDS running buffer	3.03 g Tris base, 14.3 g glycine, 5 g SDS, made up to 1 L with ddH_2O.
SSC buffer	8.7 g NaCl, 4.4 g sodium citrate dissolved in ddH_2O, adjusted to pH 7.0 with HCl, made up to 1 L with ddH_2O.
TAE Buffer	4.8 g Tris base, 2 ml 0.5M EDTA (pH 8.0), 1.14 ml acetic acid, made up to 1 L with ddH_2O.
Towbin transfer buffer	3.03 g Tris base, 14.3 g glycine, 200 ml methanol, made up to 1 L with ddH_2O.
TBS	2.4 g Tris base, 8.2 g NaCl dissolved in 800 ml ddH_2O, adjusted to pH 7.6 with HCl and made up to 1 L in ddH_2O.
TBST	2.4 g Tris base, 8.2 g NaCl dissolved in 800 ml ddH_2O, adjusted to pH 7.6 with HCl and made up to 1 L in ddH_2O with 0.1% (v/v) Tween-20.
FACS block buffer	PBS with 0.5% BSA 0.25% Triton-X-100
Resazurin solution	30 mg Resazurin in 100 ml TBS, sterile filtered (0.22 µm).

Table 2.5. Primary antibodies used in experiments.
IF; Immunofluorescence. ChIP; Chromatin Immunoprecipitation. FACS; Fluorescence-activated cell sorting.

Primary Antibody	Species raised in	Isotype	Clonality	Company	Working Dilution					Incubation Time, Temp (°C)
					Western blot	*IF*	*DNA Fibre*	*ChIP*	*FACS*	
BrdU	mouse	IgG_1	Mono-clonal	Becton Dickinson (347580)			1:1000			1hr, RT
BrdU	rat	IgG_{2a}	Mono-clonal	Abcam (ab6326)			1:750			1hr, RT
DNA-RNA Hybrid (S9.6)	mouse	IgG_{2aK}	Mono-clonal	Merck (MABE1095)		1:200				1hr, RT
FANCD2	mouse	IgG_1	Mono-clonal	Santa Cruz (sc-20022)	1:1000	1:200				Overnight, 4ºC
GAPDH	mouse	IgG_{2b}	Mono-clonal	Protein tech (60004)	1:20000					Overnight, 4ºC
γ-H2AX (pSer139)	rabbit	IgG	Poly-clonal	Cell Signalling (2577)		1:250				Overnight, 4ºC
N-Myc	mouse	IgG_{2a}	Mono-clonal	Santa Cruz (sc-53993)	1:250					Overnight, 4ºC
N-Myc	mouse	IgG_1	Mono-clonal	Abcam (ab16898)				2 µg		Overnight, 4ºC
Nucleolin	rabbit	IgG	Poly-clonal	Abcam (ab50279)		1:150				1hr, RT
ß-tubulin	mouse	IgG_1	Mono-clonal	Sigma (T8328)	1:5000					Overnight, 4ºC
pSer4/8 RPA32/RPA2	rabbit	IgG	Mono-clonal	Abcam (ab243866)		1:250				Overnight, 4ºC
Histone H3	rabbit	IgG	Mono-clonal	Cell Signalling (4620)				1:50		Overnight, 4ºC
pSer10 Histone H3	rabbit	IgG	Poly-clonal	Abcam (ab47297)					1:500	1hr, RT

Table 2.6. Secondary antibodies used in experiments.
IF; Immunofluorescence. FACS; Fluorescence-activated cell sorting.

Secondary Antibody	Conjugate	Species raised in	Clonality	Company	Working Dilution				Incubation Time, Temp (°C)
					Western blot	*IF*	*DNA Fibres*	*FACS*	
Anti-mouse	HRP	Horse	Poly-clonal	Cell signalling (7076)	1:1000				1 hr, RT
Anti-mouse	Alexa-Fluor488	Goat	Poly-clonal	Life Technologies (A11017)		1:500			1hr, RT
Anti-rabbit	Alexa-Fluor594	Goat	Poly-clonal	Life Technologies (A11012)		1:500			1hr, RT
Anti-rabbit	Alexa-Fluor488	Mouse	Poly-clonal	Life Technologies (A11008)				1:200	1.5hr, RT
Anti-rat	Alexa-Fluor555	Goat	Poly-clonal	Life Technologies **(**A21434)			1:500		1.5hr, RT

Table 2.7. Profile of human neuroblastoma cell lines used in experiments.

Cell Line	Cell Line Origin	MYCN status	ALK mutation	p53 mutation	Reference
IMR-32	Human neuroblastoma	Amplified	WT	WT	(Tumilowicz et al., 1970)
Kelly	Human neuroblastoma	Amplified	F1174L	P177T	(Schwab et al., 1983)
SK-N-SH	Human neuroblastoma	Non-amplified	F1174L	WT	(Biedler et al., 1973)
SH-SY5Y	Neuroblast-like subclone of SK-N-SH	Non-amplified	F1174L	WT	(Biedler et al., 1973)
SHEP-1	Epithelial-like subclone of SK-N-SH	Non-amplified	F1174L	WT	(Biedler et al., 1973)
SHEP-Tet21N	Derived from SHEP-1	Tetracycline-regulated MYCN expression system (Tet-OFF)	F1174L	WT	(Lutz et al., 1996)
SHEP-PLXI-MYCN	Derived from SHEP-1	Doxycycline-regulated MYCN expression system (Tet-ON)	F1174L	WT	(Zeid et al., 2018)

Table 2.8. Tissue culture specific reagents, solutions and media.

Reagent	Company
1X Trypsin-EDTA Solution	Sigma
Roswell Park Memorial Institute medium (RPMI) with L-glutamine	Sigma
Dulbecco's modified eagles medium (DMEM) with 4.5g/L glucose and L-glutamine	Sigma
Hams F12 medium	Gibco
Heat-inactivated FBS	Thermo Fisher Scientific (10500064)
Tetracycline-free FCS	Biosera
FCS	LSP
Non-essential amino acids	Sigma
Glucose solution (200g/L)	Sigma
Doxycycline hyclate	Sigma
Trypan blue stain (0.4%)	Gibco
Resazurin	Sigma-Aldrich
Dimethyl sulfoxide (DMSO)	Fisher Scientific
Presept tablets	Johnson and Johnson Medical ltd
Tetracycline hydrochloride	Sigma

Table 2.9. Drugs used in tissue culture

Drug	Company	Solvent	Stock solution concentration (mM)	Mechanism of action
Curcumin	Acros Organics	DMSO	50	Small molecule inhibitor of the FA pathway
Ouabain	Sigma	DMSO	100	Small molecule inhibitor of the FA pathway
Cisplatin	Sigma	Normal saline	4	DNA crosslinking/alkylating agent
Temozolomide	Tocris Bioscience	DMSO	50	DNA alkylating agent
5-Chloro-2'-deoxyuridine (CldU)	Sigma-Aldrich	DMEM	2.5	Thymidine analogue
5-Iodo-2'-deoxyuridine (IdU)	Sigma-Aldrich	DMEM	2.5	Thymidine analogue
Hydroxyurea (HU)	Sigma-Aldrich	DMEM	2	Ribonucleotide reductase inhibitor
LY3295668	MedChemExpress	DMSO	5	AURKA inhibitor
nFAPi	- (Provided by S. Collis, TUoS)	DMSO	0.1	Inhibitor of the FA Pathway
VE-821	Sigma-Aldrich	DMSO	10	Inhibitor of ATR
Carboplatin	Sigma-Aldrich	ddH_2O	20	DNA crosslinking/alkylating agent

2.2 Methods

2.2.1 Bioinformatic analyses

2.2.1.1 Analysis of FA pathway gene expression in neuroblastoma tumours

The mRNA expression of 58 FA pathway associated genes and 13 DNA damage repair (DDR) or key neuroblastoma-associated (NB) genes including *MYCN* was analysed in 498 human neuroblastoma samples from the GSE62564 RNA-Seq dataset using the R2: Genomics Analysis and Visualisation Platform (http://r2.amc.nl). Five samples without *MYCN* amplification status classification were excluded from analysis (n = 493). The list of FA pathway-associated genes analysed was a product of all 54 KEGG-defined FA pathway genes with the addition of the four more recently discovered FA pathway associated genes; *FAAP20*, *MAD2L2* (*REV7*), *RFWD3* and *UHRF1* (Ali et al., 2012; Liang et al., 2015; Bluteau et al., 2016; Knies et al., 2017). When downloading gene expression data from R2:Genomics, HugoOnce mode was used to ensure a single probe represented each gene. The log2(RPM+1) transformed expression data in all 493 tumours was downloaded for each gene of interest and plotted in R-studio: Integrated Development for R (R Studio, Inc., Boston, MA, http://www.rstudio.com/). The $\log_2$(fold-change) in expression of each gene between MNA and non-MNA tumours was calculated. The statistical significance of differential expression between MNA and non-MNA tumours was determined for each gene by a Student's t-test using false discovery rate (FDR) to correct for multiple testing. A Volcano plot of the $\log_2$(fold-change) in expression and $-\log_{10}$(p-value) was plotted for all FA pathway genes. Genes were considered to be significantly differentially expressed between MNA and non-MNA tumours when $\log_2$(fold-change) > 0.5, and p-value < 0.05. The $\log_2$(RPM+1) count data of each FA pathway gene was correlated with that of *MYCN* across all 493 tumours. Statistical significance of this correlation was analysed by determination of the Pearson's correlation co-efficient.

Log_2(RPM+1) count data was used to calculate Z-scores independently for each gene across all tumours. The Z-score represents the number of standard deviations away from the mean each expression value is, and was calculated using the following formula:

$$\text{Z-score} = \frac{\text{Observed expression for gene 1 in sample 1} - \text{Mean expression for gene 1 across all samples}}{\text{Standard deviation of expression of gene 1 across all samples}}$$

Z-scores were calculated for each gene in each sample and plotted in a heatmap using the 'ComplexHeatmap' package in R Studio alongside patient metadata downloaded from R2:Genomics. The average Z-score in MNA and non-MNA tumour subgroups was also presented in a heatmap created using ComplexHeatmap.

Kaplan-Meier curves displaying overall survival probability with respect to expression of each FA pathway gene were plotted. With a minimum group size of 8, scan modus was used to determine the optimum high/low expression cut-off for best p-values in a log-rank test. Bonferroni correction was used to account for multiple testing. Significance was considered achieved at $p < 0.05$. Overall survival analysis was undertaken for the cohort as a whole as well as for each MNA subgroup individually.

2.2.1.2 FA Pathway and global gene expression analysis in SHEP-Tet21N MYCN ON and OFF cells

2.2.1.2.1 RNA extraction for RNA-Seq analysis

SHEP-Tet21N MYCN ON cells were treated with 1 µg/ml tetracycline for 48 hours in a T75 flask to induce a MYCN OFF state. SHEP-Tet21N MYCN ON and MYCN OFF cells were detached from the flask surface by incubation with 1X trypsin-EDTA at 37 °C. Trypsin activity was inhibited by addition of media and cells were pelleted by centrifugation at 1200 rpm for 3 min. As described in Chapter 2.2.5.1, total RNA was extracted using the GenElute Mammalian Total RNA Miniprep Kit (Sigma, RTN350) according to supplied protocols and the RNA concentration and purity determined using a Nanodrop. Three biological replicates of each MYCN ON and OFF sample was obtained. RNA was stored at -80°C until it was sent for RNA-Seq processing in collaboration with Dr. Anestis Tsakiridis' laboratory group at the University of Sheffield. Dr. Anestis Tsakiridis collaborated with Dr. Florian Halbritter and Dr. Luis Montano-Gutierrez at St. Anna Children's Cancer Research Institute (CCRI) to undertake whole

cell RNA-sequencing and raw read analysis to produce raw count data. We then used this raw RNA-seq count data in the gene expression analyses described below.

2.2.1.2.2 DESeq2 gene expression analysis

A standard DESeq2 (v. 1.36.0) workflow was used to compare global gene expression in MYCN ON and OFF cells (Love et al., 2014). Using DESeq2, raw read counts were normalised and minimal pre-filtering was performed to remove genes with no or very low expression from analysis. More strict independent filtering which is normally automatically applied by DESeq2 analysis was turned off to prevent removal of genes of interest. Genes that were significantly differentially expressed in MYCN ON cells compared to MYCN OFF cells were identified using a generalised linear model in DESeq2 with a significance threshold of $p < 0.05$.

Normalised count data was log-transformed to enable plotting. A regularised log (rlog) transformation was applied to the normalised count data, as opposed to a shifted or variance stabilised log transformation, as this transformed dataset had the most equal standard deviation across the whole expression range.

2.2.1.2.3 FA pathway gene expression analysis in MYCN ON and OFF cells

The rlog-transformed count data of 55 FA pathway-associated genes and 12 DNA damage repair (DDR) or key neuroblastoma-associated genes in MYCN ON compared to MYCN OFF cells was plotted in R studio. The statistical significance of differential expression between MYCN ON and OFF cells was determined for each gene by a t-test. A Student's t-test was used for normally distributed data whilst a Mann Whitney U test was used for data that was not normally distributed. A Volcano plot of the $\log_2$(fold-change) in expression and $-\log_{10}$(p-value) was plotted for all FA pathway genes. Genes were considered to be significantly differentially expressed between MYCN ON and OFF cells when $\log_2$(fold-change) > 0.5, and p-value < 0.05.

The rlog-transformed count data of each FA pathway gene was correlated with that of *MYCN* across all biological replicates. Statistical significance of this correlation was analysed by determination of the Pearson's correlation co-efficient.

rlog-transformed normalised count data was used to calculate Z-scores independently for each gene across all MYCN ON and OFF samples, and this was

plotted in a heatmap generated by the 'ComplexHeatmap' R package. Z-scores were calculated as described in chapter 2.2.1.1. The average Z-score in MYCN ON and MYCN OFF cells was also plotted in a heatmap. Genes were clustered according to k-means analysis.

2.2.1.2.4 Global gene expression analysis in MYCN ON and OFF cells

A volcano plot of the $\log_2$(fold-change) in expression and $-\log_{10}$(p-value) of all significantly differentially expressed genes, as calculated by DESeq2, was plotted. All significantly differentially expressed genes were ranked according to $\log_2$(fold-change) and the top 30 most upregulated and downregulated genes were selected. The rlog-transformed normalised count data of these genes was used to calculate Z-scores independently for each gene. Z-scores were calculated as described in chapter 2.2.1.1. The average Z-score in MYCN ON and MYCN OFF cells was presented in a heatmap with genes clustered by k-means analysis.

To determine whether the FA pathway was observed as one of the most differentially expressed pathways upon high *MYCN* expression, the top 10 most enriched gene ontology terms and KEGG pathways in the set of all significantly upregulated and downregulated genes was determined using the gseGO and gseKEGG functions in the 'Clusterprofiler' R package. This calculated enrichment based on the gene ratio of each ontology term and KEGG pathway. The gene ratio represents the fraction of genes within each ontology term or KEGG pathway that was significantly differentially expressed. Significance of enrichment was also determined and was adjusted for multiple comparisons by Benjamini-Hochberg correction, with p-value threshold of $p < 0.05$. Only significantly enriched terms and pathways were presented. The minimum and maximum group size was set to 3 and 800 respectively. For gene ontology analysis, the top 10 most enriched biological process (BP), molecular function (MF) and cellular component (CC) gene ontologies were presented.

2.2.1.3 FA Pathway and global gene expression analysis across 39 neuroblastoma cell lines

2.2.1.3.1 DESeq2 gene expression analysis

The mRNA expression of 58 FA pathway-associated genes and 13 DNA damage repair (DDR) or key neuroblastoma-associated genes was analysed across 39 neuroblastoma cell lines using the GSE89413 RNA-Seq dataset (Harenza et al., 2017). Raw reads were downloaded and analysed by Dr. Manoj Valluru at the University of Sheffield to generate global estimated counts across all 39 cell lines.

Cell lines were grouped in turn according to *MYCN* amplification status and presence or absence of ALK mutations, 17q gain, aberration at 1p, aberration at 3p or aberration at 11q. The expected counts generated for each gene in each cell line were used to analyse global differential expression between each pairwise grouping using the DESeq2 standard workflow (Love et al., 2014) as described above in Chapter 2.2.1.2.2. A list of significantly differentially expressed genes between each pairwise grouping was therefore produced, including between MNA and non-MNA cell lines. A regularised log (rlog) transformation was applied to the normalised count data to enable plotting in R Studio.

2.2.1.3.2 FA pathway gene expression analysis in MNA and non-MNA cell lines

The rlog-transformed count data of 58 FA pathway-associated genes and 13 DNA damage repair (DDR) or key neuroblastoma-associated genes in MNA compared to non-MNA cell lines was plotted in R studio. The statistical significance of differential expression between MNA and non-MNA cells was determined for each gene by a t-test. A Student's t-test, Welch t-test and Mann Whitney U test was used for data that was normally distributed with equal variance, normally distributed with unequal variance, and not normally distributed respectively. A Volcano plot of the $\log_2$(fold-change) in expression in MNA compared to non-MNA cell lines, and $-\log_{10}$(p-value) was plotted for all FA pathway genes. Genes were considered to be significantly differentially expressed between MNA and non-MNA cell lines when $\log_2$(fold-change) > 0.5, and p-value < 0.05.

rlog-transformed count data of each FA pathway gene was correlated with that of *MYCN* across all 39 cell lines. Statistical significance of this correlation was analysed by Pearson's correlation.

rlog-transformed count data was used to calculate Z-scores independently for each gene across all cell lines, and this was plotted in a heatmap generated by the 'ComplexHeatmap' R package alongside cell line metadata provided by Harenza et al., (2017). Z-scores were calculated as described in chapter 2.2.1.1. The average Z-score of each gene in MNA and non-MNA cell lines was also plotted in a heatmap. Genes were clustered according to k-means analysis.

2.2.1.3.3 Global gene expression analysis in MNA and non-MNA neuroblastoma cell lines

Similarly to as described above for MYCN ON and OFF cells in Chapter 2.2.1.2.3, analysis of differences in global gene expression patterns between MNA and non-MNA neuroblastoma cell lines was analysed. A volcano plot of all significantly differentially expressed genes, as calculated by DESeq2, was plotted. All significantly differentially expressed genes were ranked according to $\log_2$(fold-change) and the top 30 most upregulated and downregulated genes were selected. The rlog-transformed normalised count data of these genes was used to calculate Z-scores across all 39 cell lines independently for each gene and this was presented in a heatmap with genes clustered by k-means analysis. Z-scores were calculated as described in chapter 2.2.1.1.

The top 10 most enriched gene ontology terms and KEGG pathways in the set significantly upregulated and downregulated genes was determined using the gseGO and gseKEGG functions in the 'Clusterprofiler' R package. Significance of enrichment was also determined and was adjusted for multiple comparisons by Benjamini-Hochberg correction, with p-value threshold of $p < 0.05$. Only significantly enriched terms and pathways were presented, such that less than 10 enriched terms and pathways were observed. The minimum and maximum group size was set to 3 and 800 respectively. For gene ontology analysis, the most enriched biological process (BP), molecular function (MF) and cellular component (CC) gene ontologies were presented.

2.2.1.4 MYCN ChIP-Seq analysis across FA pathway genes

2.2.1.4.1 MYCN ChIP-Seq read and count processing at FA pathway gene promoters

Using ChIP-Seq data provided by Zeid et al., (2018) (GSE80151 dataset), MYCN binding was analysed at the promoters of 58 FA pathway-associated genes, 13 DDR or neuroblastoma-associated genes and three control genes in MYCN-inducible SHEP-PLXI-MYCN tet-ON and SHEP-Tet21N tet-OFF cell lines and MYCN amplified cell lines SK-N-BE(2)-C, NGP and KELLY. The control genes analysed were *APEX1*, *NDUFA3* and *RPL30*. These are a MYCN target positive control gene, a house-keeping gene, and a MYCN target negative control gene respectively (Barrilleaux et al., 2013). For each cell line, raw MYCN ChIP-seq reads and input control reads were downloaded from the GSE80151 dataset and quality checked with FastQC (v. 0.11.7) using default parameters. Cutadapt (v. 1.15) was used with default parameters to trim Illumina TruSeq adapters from reads and remove reads with less than 10 bp. Trimmed reads were then mapped to the hg19 human genome using bowtie2 (v. 2.4.4) with default parameters. Samtools (v. 1.7) was used to convert the resulting SAM files to sorted BAM files and to produce BAM index files. Peak calling with MACS2 (v.2.2.6) was used to evaluate the significance of enriched MYCN ChIP regions in comparison to the input control using default MACS2 parameters including a q-value cut-off of $q < 0.01$. q-values are calculated from p-values using a Benjamini-Hochberg correction. A narrowPeak BED file was therefore produced for each cell line containing the significant MYCN ChIP peak locations, input-normalised peak signal value (signalValue), p-value and q-value.

The ‘ChIPpeakAnno’ R package was used to find which significant MYCN peaks overlap across all MYCN ON and MNA cell lines examined. ChIPpeakAnno and the organism annotation package ‘org.Hs.eg.db’ was also used to annotate MYCN peaks which overlapped with gene promoters using the following parameters: output = overlapping, PeakLocForDistance = middle. Gene promoters were defined as regions 5000 bp upstream and 500 bp downstream from all transcriptional start sites (TSS). MYCN peaks at the promoters of FA pathway, DDR and neuroblastoma-associated genes were analysed. For each gene, the signal values of all MYCN peaks at the promoter were summed. The total promoter MYCN signal value for each gene was plotted in a heatmap for all cell lines analysed using ComplexHeatmap.

2.2.1.4.2 Global MYCN ChIP-seq analysis

The top 10 most enriched gene ontology terms and KEGG pathways in all MYCN promoter-bound genes was analysed for each cell line using the getEnrichedGO and getEnrichedPATH functions in the 'ChIPpeakAnno' R package. GO and KEGG pathway enrichment was also analysed for the set of genes where MYCN promoter binding was observed in all cell lines. The 'org.Hs.eg.db' organism annotation package was used for these analyses. For KEGG pathway analysis, the pathway annotation package 'KEGG.db' was used. For gene ontology analysis, the minGOterm was set to 3 and the top 10 most enriched biological process (BP), molecular function (MF) and cellular component (CC) gene ontologies were presented. Significance of enrichment was determined and was adjusted for multiple comparisons by Benjamini-Hochberg correction, with p-value threshold of $p < 0.05$.

2.2.2 Mammalian tissue culture

2.2.2.1 Passaging Cells

All cell lines were cultured in a 37 °C humidified incubator at 5% CO_2. Routine passaging of cells was undertaken in standard tissue-culture T25 or T75 flasks. For all adherent cell lines (SHEP-1, SHEP-Tet21N, SHEP-PLXI-MYCN, IMR32, Kelly), cells were washed in PBS (137 mM NaCl, 3 mM KCl, 8 mM Na_2HPO_4, 1.5 mM KH_2PO_4, pH 7.3) and incubated with 1 ml 1X trypsin-EDTA (Sigma) at 37 °C to remove cells from the flask surface. Trypsin activity was stopped by diluting in 9 ml of relevant media. This cell suspension was used to seed new flasks in the relevant ratio as stated for each cell line below. Experiments were undertaken when cells were at 60-80% confluency to ensure cells were in logarithmic growth phase.

2.2.2.1.1 SHEP-1

SHEP-1 cells were cultured in DMEM supplemented with 5% (v/v) 100X non-essential amino acids and 10% FCS. Cells were typically passaged twice a week, when at 70-90% confluency, in a ratio of 1:5.

2.2.2.1.2 SHEP-Tet21N

SHEP-Tet21N cells were derived via introduction of a tetracycline-regulated (tet-off) conditional *MYCN* expression system in the non-MNA SHEP-1 cell line (Figure 2.1) (Gossen and Bujard, 1992; Lutz et al., 1996). This enables study of differential *MYCN* expression in an isogenic cell model. SHEP-Tet21N cells were cultured in RPMI supplemented with 10% heat-inactivated FBS or 10% tetracycline-free FCS, in a MYCN ON state. *MYCN* expression was suppressed to induce a MYCN OFF state by treatment with 1 µg/ml tetracycline at least 48 hours prior to experiments. Cells were typically passaged twice a week, when at 70-90% confluency, in a ratio of 1:8.

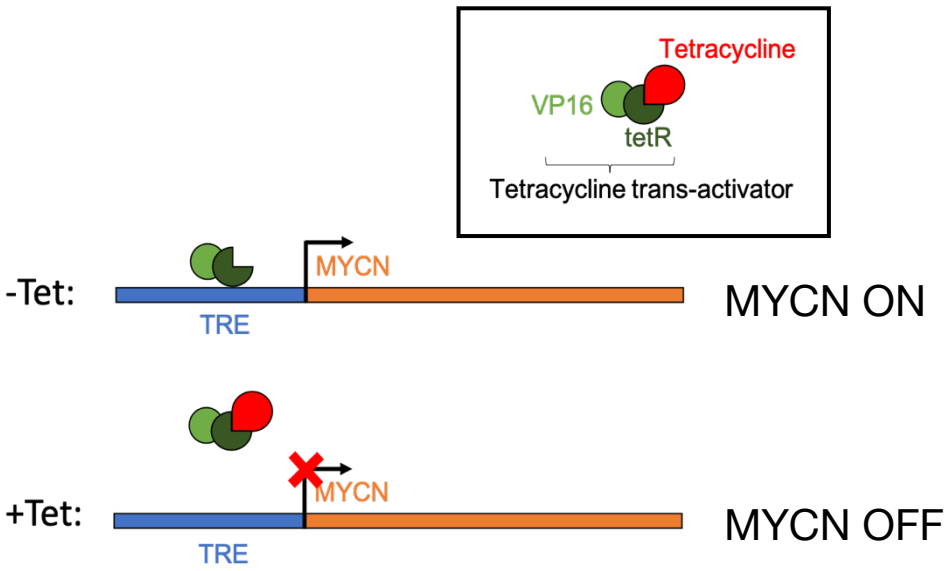

Figure 2.1. SHEP-Tet21N tet-OFF conditional MYCN expression system. SHEP-Tet21N cells were derived via establishment of a MYCN tet-off system in the MYCN non-amplified SHEP-1 cell line (Lutz et al., 1996). This involved introduction of a construct encoding a tetracycline trans-activator (tTA) and a tTA-dependent promoter that controls expression of downstream MYCN cDNA (Lutz et al., 1996). The tTA-dependent promoter encodes the tetracycline response element (TRE) which contains tetracycline operator (tetO) repeats (Gossen and Bujard, 1992). tetO is recognised by the tet repressor (tetR) of the *Escherichia coli* Tn10 tetracycline-resistance operon (Gossen and Bujard, 1992). tetR is fused to the carboxy-terminal transcriptional activation domain of VP16, a herpes simplex virus protein, to form the tTA fusion protein (Gossen and Bujard, 1992). In the absence of tetracycline, the tTA is able to bind the TRE, enabling the VP16 activation domain to promote MYCN expression and induce a MYCN ON state. Tetracycline binds tetR to inhibit binding of the tTA to the TRE. This prevents tTA-dependent transcriptional activation of MYCN to induce a MYCN OFF state.

2.2.2.1.3 SHEP-PLXI-MYCN

Similar to SHEP-Tet21N cells, SHEP-PLXI-MYCN cells were derived via introduction of a tetracycline-regulated conditional *MYCN* expression system in the SHEP-1 cell line (Zeid et al., 2018). However, SHEP-PLXI-MYCN cells were generated via lentiviral transduction of a vector encoding a MYCN tet-on system (Figure 2.2) (Gossen et al., 1995; Zhou et al., 2006; Zeid et al., 2018).

SHEP-PLXI-MYCN cells were gifted from Charles Lin (Baylor College of Medicine, Department of Molecular and Human Genetics, Houston, TX) and cultured in RPMI supplemented with 10% tetracycline-free FCS, in a MYCN OFF state. MYCN expression was promoted to induce a MYCN ON state by treatment with 0.5 µg/ml doxycycline (a second-generation tetracycline) at least 48 hours prior to experiments, with doxycycline-RPMI changed every 24 hours. Cells were typically passaged twice a week, when at 70-90% confluency, in a ratio of 1:5.

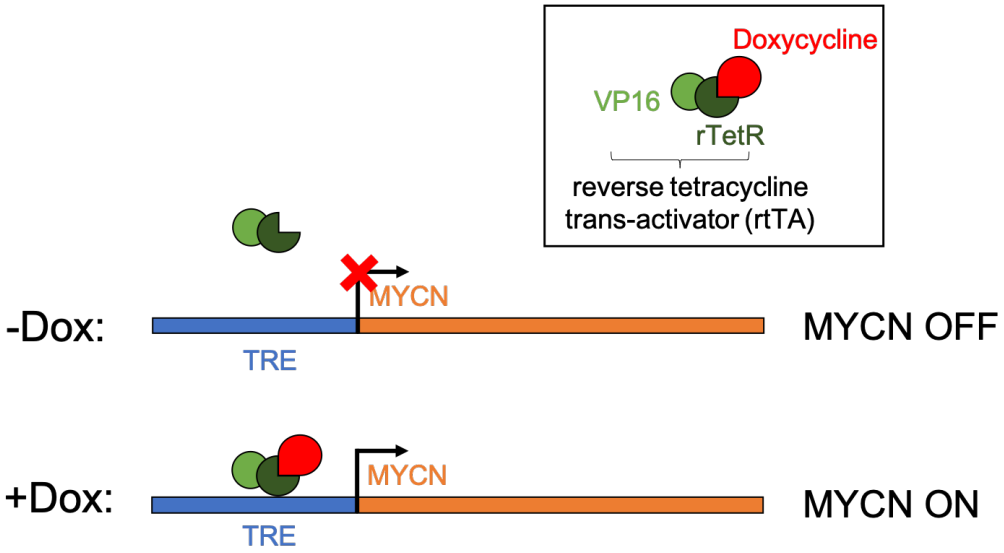

Figure 2.2. SHEP-PLXI tet-ON conditional MYCN expression system.
The tet-on conditional expression system was derived through modification of the tet-off system (Gossen et al., 1995; Zhou et al., 2006). Mutation of residues in the tet repressor (tetR) of the *Escherichia coli* Tn10 operon generated a reverse tet repressor (rTetR) which requires binding of tetracycline derivatives to enable interaction with the tetracycline operator (tetO) in the TRE promoter element (Gossen et al., 1995). This is in contrast to tetR in the tet-off system which is inhibited from TRE interaction by tetracycline binding. rTetR is fused to the transcriptional activation domain of VP16 to generate the reverse tetracycline-controlled transactivator (rtTA) (Gossen et al., 1995). SHEP-PLXI-MYCN cells were generated via lentiviral transduction of a MYCN-encoding Tet-On pLIX401 vector (Zeid et al., 2018). This vector encodes the rtTA and an rtTA-dependent promoter that controls expression of a downstream MYCN cDNA. In the absence of doxycycline, a second-generation tetracycline, the rtTA cannot bind the TRE in the rtTA-dependent promoter, preventing transcriptional activation of MYCN to induce a MYCN OFF state. Addition of doxycycline enables binding of rtTA to the TRE to induce MYCN expression and a MYCN ON state.

2.2.2.1.4 IMR32

IMR32 cells were cultured in DMEM:RPMI (50:50) supplemented with 10% FCS. Cells were typically passaged twice a week, when at 70-90% confluency, in a ratio of 1:5.

2.2.2.1.5 Kelly

Kelly cells were cultured in RPMI supplemented with 10% FCS. Cells were typically passaged twice a week, when at 70-90% confluency, in a ratio of 1:5.

2.2.2.1.6 SH-SY5Y

SH-SY5Y cells are semi-adherent and were cultured in DMEM : Hams F12 medium (50:50) supplemented with 10% FCS. Medium containing suspension cells was removed, centrifuged at 1200 rpm for 3 min to pellet cells and the resulting media supernatant discarded. Adherent cells were PBS washed and incubated with 1 ml 1X trypsin-EDTA at 37 °C to remove cells from the flask surface. Trypsin activity was stopped by diluting in 9 ml of relevant media. The pellet of suspension cells was resuspended in the media containing adherent cells. This final cell suspension was used to seed new flasks in a ratio of 1:5. Cells were passaged twice a week, when at 70-90% confluency.

2.2.2.1.7 SK-N-SH

SK-N-SH cells were cultured in DMEM supplemented with 5% (v/v) 100X non-essential amino acids and 10% FCS. Cells were typically passaged twice a week, when at 70-90% confluency, in a ratio of 1:5.

2.2.2.2 Cell Line Cryopreservation

Cells were PBS washed and removed from flask surfaces via incubation with 1 ml 1X trypsin-EDTA at 37 °C. Trypsin activity was stopped by diluting in 9 ml of relevant media. This cell suspension was centrifuged at 1200 rpm for 3 min and the media supernatant discarded. T75 flask cell pellets were resuspended in 2 ml freezing medium (90% relevant media, 10% DMSO), aliquoted into 1 ml per cryovial and stored at -80 °C.

2.2.2.3 Thawing cell lines

Cells stored at -80 ºC in cryovials were thawed rapidly in a 37 °C water bath, transferred to a falcon tube and slowly diluted in 9 ml media. This cell suspension was centrifuged at 1200 rpm for 3 min and the resultant media supernatant discarded. The cell pellet was resuspended in 5 ml media and transferred to a T25 standard tissue-culture flask.

2.2.2.4 Cell line validation

SHEPTet21N cells, SHEP-1 and IMR-32 cells were STR tested by Culture Collections, Public Health England, Porton Down, UK. SK-N-SH cells were gifted from Louis Chesler's laboratory in London and further STR testing was not undertaken. SHEP-PLXI-MYCN cells were gifted from Charles Lin's laboratory in Dana-Farber Cancer Institute, Boston, MA, USA and further STR testing was not undertaken.

2.2.2.5 Mycoplasma detection

PCR-based mycoplasma testing (Geneflow EZ-PCR Mycoplasma Test Kit) was carried out monthly, before cryopreservation and after thawing as per supplied protocols on all cell lines.

2.2.3 Protein analysis by western blot

2.2.3.1 Cell lysate preparation

Unless stated otherwise, cells were plated at a density of 1 x 10^6 cells per 10 cm dish (Greiner Bio-one Cellstar) or 2 x 10^5 cells per well in a 6-well plate (Thermo Scientific Nunc™ Cell-Culture Treated) for 6-24 hours before treatment was applied for the desired time. Following two washes in ice-cold PBS, cells were scraped directly into ice-cold 1X RIPA buffer (200 µl 5X RIPA (50 mM Tris pH 8.0, 150 mM NaCl, 0.1% SDS, 1% NP-40, 0.5% sodium deoxycholate), 10 µl 100 mM PMSF, 10 µl 100X cOmplete™ Mini EDTA-free Protease Inhibitor Cocktail (Sigma, Roche), 10 µl 100X PhosSTOP phosphatase inhibitor cocktail (Sigma, Roche), made up to 1 ml with ddH_2O). This enabled optimum retention of protein modifications such as mono-ubiquitination and phosphorylation. 100 µl 1X RIPA buffer was used for approximately

every 1 x 10^6 cells plated. This cell suspension was vortexed immediately after collection and subsequently vortexed every 10 min during a 30 min incubation on ice. This was then passed through a 25G needle ten times to shred the DNA, and centrifuged at 13400 rpm, 4°C for 10 min to pellet cell debris. The cell lysate supernatant was stored at -20°C before quantification, SDS-PAGE and western blotting.

2.2.3.2 Bradford protein quantification assay

Total cell lysate protein concentration was quantified using the Bradford assay to enable calculation of gel loading volume for each sample prior to SDS-PAGE (Bradford, 1976). When bound to protein, the absorbance maximum of the acidic Coomassie blue dye solution shifts from 465 nm to 595 nm, enabling colorimetric protein quantification. Six 800 µl bovine serum albumin (BSA) (Sigma-Aldrich) protein standards at 0-20 µg/µl were made. 2 µl of the cell lysate sample was added to 800 µl ddH_2O. 200 µl Bio-Rad protein assay dye reagent concentrate was added to each 800 µl standard and sample which were then briefly vortexed. The absorbance at 595 nm (A_{595}) was then measured using the Thermo Scientific Multiskan FC. A_{595} values of protein standards were plotted against BSA concentration to formulate a standard curve, from which the sample protein concentration and gel loading volume was calculated.

2.2.3.3 SDS-PAGE Western blot

Western blotting of cell lysate samples is undertaken to enable semi-quantitative estimation of the level of protein of interest within a sample (Towbin et al., 1979; Burnette, 1981). Following denaturation in SDS buffer, protein samples are separated according to molecular weight via gel electrophoresis. Proteins are then transferred from the gel onto a nitrocellulose membrane and non-specific binding sites are blocked with a dilute protein solution. The membrane is incubated with a primary antibody specific to the protein of interest, followed by incubation with a species-specific secondary antibody conjugated to the horse radish peroxidase (HRP) enzyme. Application of a chemiluminescent substrate leads to HRP-catalysed light emission which is visualised by exposure of the membrane to an x-ray film. This allows identification of the protein and relative quantification by band intensity analysis. Table 2.10 displays the molecular weight of all key proteins analysed by western blot in this thesis.

Table 2.10. Molecular weight of key proteins analysed by western blot.

Protein	Molecular Weight (kDa)
FANCD2	166
MYCN	67
MYCC	62
ß-tubulin	50
GAPDH	36

2.2.3.3.1 Cell lysate preparation for SDS-PAGE

4X NuPAGE™ LDS sample buffer (ThermoFisher Scientific) containing 50 mM DTT was diluted 1:4 into cell lysate protein samples which were subsequently heated at 95°C for 10 min to denature proteins.

2.2.3.3.2 SDS-polyacrylamide gel electrophoresis

10-12% (w/v) SDS-polyacrylamide gels (0.75 mm) were made as detailed in Table 2.11, with lower percentage gels used for detection of proteins with higher molecular weight. 20µg of denatured cell lysate protein sample was loaded into each well. 5 µl Precision Plus Protein™ Dual Colour Standards (BioRad), or Spectra Multicolour Broad Range Protein Ladder (ThermoFisher Scientific) was loaded for molecular weight determination of protein bands. Gels were run in Hoefer™ Mighty Small™ II Mini Vertical Electrophoresis System tanks in 1X SDS running buffer (25 mM Tris Base, 190 mM glycine, 0.1% SDS) at 140V for 1.5 hours to separate proteins by molecular weight.

Table 2.11. Reagent volumes required to make 10% and 12% resolving gels and 5% stacking gel for one 0.75 mm SDS-polyacrylamide gel.

	Volume (ml)		
Gel reagents	**10% Resolving gel**	**12% Resolving gel**	**5% Stacking gel**
ddH_2O	4.0	3.3	3.4
30% acrylamide: 0.8% bis-acrylamide (National Diagnostics)	3.3	4.0	0.83
1.5M Tris, pH 8.8	2.5	2.5	0
1.0M Tris, pH 6.8	0	0	0.63
10% SDS	0.1	0.1	0.05
10% (w/v) Ammonium Persulfate	0.1	0.1	0.05
TEMED	0.004	0.004	0.005

2.2.3.3.3 Gradient (3-8%) tris-acetate gel electrophoresis

Cell lysates were run on a gradient gel to enable greater separation of mono-ubiquitinated and un-ubiquitinated FANCD2 protein bands. This allowed the extent of FA pathway activation (measured by the ratio of mono-ubiquitinated FANCD2:un-ubiquitinated FANCD2 band intensity) to be determined, as well as total FANCD2 protein levels. 15µg of denatured cell lysate protein sample was loaded into each well of a NuPAGE™ 1.0 mm, 3-8% Tris-Acetate Protein Gel (Invitrogen). 10 µl HiMark™ Pre-stained Protein Standard (ThermoFisher Scientific) was loaded for molecular weight determination of protein bands. Gels were run in a Novex™ Bolt™ Mini Gel Tank (Invitrogen) in 1X NuPAGE™ Tris-Acetate Running Buffer (Invitrogen) at 120V for 1.5 hours to separate proteins by molecular weight.

2.2.3.3.4 Western blot

Proteins in SDS-polyacrylamide or NuPAGE™ 3-8% tris-acetate gels were transferred immediately onto a 0.2 µM-pore nitrocellulose membrane (BioRad) in a BioRad Criterion Blotter at 100V for 2 hours in 1X Towbin transfer buffer (25 mM Tris Base, 190 mM glycine, 20% (v/v) methanol), cooled with ice. Membranes were with blocked in 5% Marvel-TBST (5% (w/v) Marvel in 1X TBST (0.1% (v/v) Tween-20, 20 mM Tris Base, 140 mM NaCl, pH 7.6)) for 1 hour at RT on a shaker to prevent non-specific binding during immunodetection. Primary antibodies (Table 2.5) diluted in 5% Marvel-TBST were applied to the membrane overnight at 4°C on a shaker. Membranes

underwent three, 10 min TBST washes before application of the relevant HRP-labelled secondary antibody (Table 2.6), diluted in 5% milk-TBST, for 1 hour at RT on a shaker. Following three further 10 min TBST washes, membranes were coated with 1 ml of Amersham ECL Western blotting Detection Reagent (GE Healthcare) and exposed to Fuji Medical X-ray film (Fujifilm). X-ray film was fixed and developed using a Konica SRX 101A Processor.

2.2.3.3.5 Western blot band intensity quantification

X-ray films were scanned and band intensity was quantified using FIJI (Schindelin et al., 2012; Rueden et al., 2017). FANCD2 western blot doublet bands depicting mono-ubiquitinated (L) and un-ubiquitinated (S) FANCD2 were often close together on the blot. The traces for the two bands therefore often overlapped slightly during quantification. To quantify these two FANCD2 bands separately, a straight line was drawn at the base of the two peaks to ensure these traces were split consistently for all FANCD2 bands. An example of this is shown in Figure 2.3. It should be noted that there is a non-linear relationship between band intensity and protein concentration when western blots are developed using ECL and X-ray film, particularly for over-exposed bands. This may therefore introduce quantification errors for over-exposed bands.

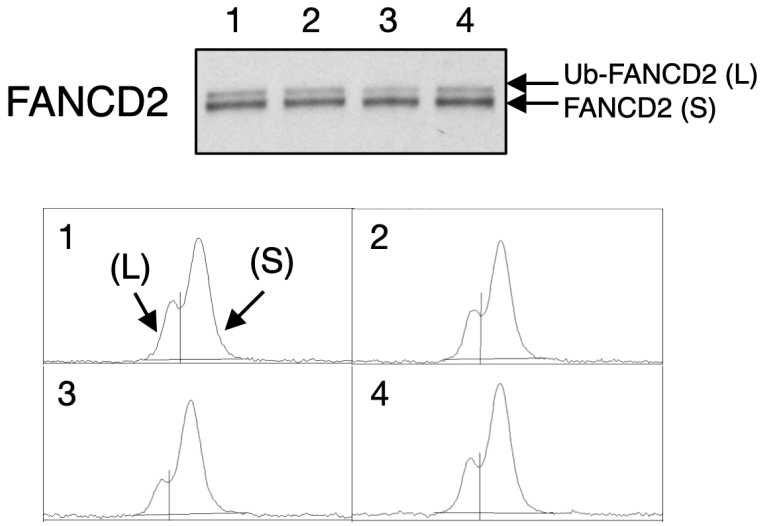

Figure 2.3. Example of FANCD2 western blot band quantification using FIJI.
To quantify mono-ubiquitinated (L) and un-ubiquitinated (S) FANCD2 western blot doublet bands, both bands were quantified in a single trace. For each FANCD2 doublet band, a line was drawn at the lowest point between the two FANCD2 band peaks to separate the trace and enable quantification of the two bands separately. An example of four FANCD2 western blot bands and their respective quantification traces are shown.

2.2.4 siRNA transfection

2.2.4.1 Depletion of MYCN in IMR32 cells using an siRNA pool

Lipofectamine RNAiMAX transfection reagent (Invitrogen) was used to transfect IMR-32 cells with a pool of 30 siRNAs targeting the human MYCN (siTOOLs Biotech) and a pool of 30 scrambled negative control siRNAs (siTOOLs Biotech). siRNA pools are provided at a stock concentration of 50 µM in 10mM Tris solution and stored at -20 °C. siRNA pools were diluted in RNase-free water (siTOOLs Biotech) to 150 nM working stocks.

IMR-32 cells were plated at a density of 2 x 10^5 cells per well in 2 ml media in 6-well plates, 24 hours prior to transfection for approximately 60% confluency at the time of transfection. Two wells were plated for each siRNA condition to allow cell lysates to be taken at two timepoints following transfection. Cells were transfected with the MYCN siRNA pool (siTOOLs Biotech) or the scrambled negative control siRNA pool (siTOOLs Biotech) to a final concentration of 3 nM using 0.2% Lipofectamine RNAiMAX per well

(Invitrogen, Life Technologies). Per well, 40 µl of 150 nM siRNA pool was diluted with 210 µl FCS-free DMEM. 4 µl Lipofectamine RNAiMAX was diluted with 246 µl FCS-free DMEM and pipette mixed. These siRNA pool and Lipofectamine RNAiMAX dilutions were incubated for 5 min at RT before being combined in a 1:1 ratio. This combined transfection mix was incubated for 15 min at RT. During this incubation, the media on the plated cells was replaced with 1.5 ml normal FCS-containing media in each well. The 500 µl transfection mix was added dropwise to cells to a final volume of 2 ml per well. Non-transfected controls were achieved by adding 500 µl FCS-free DMEM to cells in place of the transfection mix. Lipofectamine RNAiMAX vehicle controls were achieved by diluting 4 µl Lipofectamine RNAiMAX in 496 µl FCS-free DMEM, incubating for 25 min and adding dropwise to cells as above. Cells were doubly transfected by repeating the above transfection 24 hours after initial transfection. Cell lysates were collected 24 and 48 hours after the second transfection. MYCN depletion and FANCD2 protein levels in all cell lysates were analysed by western blot, with band intensity quantified relative to scrambled negative control siRNA transfected cells.

2.2.4.2 Singular siRNA-mediated FANCD2 depletion in SHEP-Tet21N cells

Dharmafect-1 transfection reagent (Horizon Discovery) was used to transfect SHEP-Tet21N MYCN ON and OFF cells with one of three ON-TARGETplus siRNAs targeting the human FANCD2 gene (Horizon Discovery) (Table 2.12) or a scrambled negative control ON-TARGETplus siRNA (Horizon Discovery, D00181001). siRNAs were resuspended in 1x siRNA Buffer (Horizon Discovery) at a stock concentration of 100 µM and stored at -20 °C. siRNAs were diluted in RNase-free water to 5 µM working stocks. Cells were transfected with an ON-TARGETplus siRNA to a final concentration of 25 nM using 0.15% Dharmafect-1 per well (Invitrogen, Life Technologies).

Table 2.12. Human FANCD2 gene target sequences of ON-TARGETplus siRNA (Horizon Discovery).

siRNA	Target sequence (5'-3')
FANCD2 siRNA-1	UGGAUAAGUUGUCGUCUAU
FANCD2 siRNA-2	CAACAUACCUCGACUCAUU
FANCD2 siRNA-3	GGAUUUACCUGUGAUAAUA

2.2.4.2.1 Singular FANCD2 siRNA transfection for western blot analysis

SHEP-Tet21N MYCN ON and OFF cells were plated at a density of 2 x 10^5 cells per well in 2 ml media in 6-well plates, 24 hours prior to transfection for approximately 70% confluency at the time of transfection. Per well, 10 µl of 5 µM ON-TARGETplus siRNA was diluted with 190 µl FCS-free RPMI-1640. 3 µl Dharmafect-1 was diluted with 197 µl FCS-free RPMI-1640 and pipette mixed. These siRNA and Dharmafect-1 dilutions were incubated for 5 min at RT before being combined in a 1:1 ratio. This combined transfection mix was incubated for 15 min at RT. During this incubation, the media on the plated cells was replaced with 1.6 ml normal FCS-containing media in each well. The 400 µl transfection mix was added dropwise to cells to a final volume of 2 ml per well. Non-transfected controls were achieved by adding 400 µl FCS-free RPMI-1640 to cells in place of the transfection mix. Dharmafect-1 vehicle controls were achieved by diluting 3 µl Dharmafect-1 in 397 µl FCS-free DMEM, incubating for 25 min at RT and adding dropwise to cells as above. Cell lysates were collected 48 hours after transfection, and FANCD2 depletion was analysed by western blotting.

2.2.4.2.2 Singular FANCD2 siRNA transfection for viability analysis by Alamar blue

SHEP-Tet21N MYCN ON and OFF cells were plated at a density of 4 x 10^4 cells per well in 1 ml media in 12-well plates, 24 hours prior to transfection for approximately 60% confluency at the time of transfection. Per well, 5 µl of 5 µM ON-TARGETplus siRNA was diluted with 95 µl FCS-free RPMI-1640. 1.5 µl Dharmafect-1 was diluted with 98.5 µl FCS-free RPMI-1640 and pipette mixed. These siRNA and Dharmafect-1 dilutions were incubated for 5 min at RT before being combined in a 1:1 ratio. This combined transfection mix was incubated for 15 min at RT. During this incubation, the media on the plated cells was replaced with 800 µl normal FCS-containing media in each well. The 200 µl transfection mix was added dropwise to cells to a final volume of 1 ml per well. Non-transfected controls were achieved by adding 200 µl FCS-free RPMI-1640 to cells in place of the transfection mix. Dharmafect-1 vehicle controls were achieved by diluting 1.5 µl Dharmafect-1 in 198.5 µl FCS-free DMEM, incubating for 25 min at RT and adding dropwise to cells as above. 24 hours after transfection, cells were treated with 5 µM curcumin, 100 nM ouabain or left un-treated for 40 hours before cell viability was analysed using Alamar blue. Viability of FANCD2 siRNA transfected cells

was determined relative to scrambled siRNA transfected and un-treated cells independently for MYCN ON and OFF cells. This enabled comparison of the effect of FANCD2 depletion on viability of MYCN ON compared to MYCN OFF cells. Viability of curcumin- or ouabain-treated cells was determined relative to un-treated cells for each siRNA and MYCN condition. This enabled comparison of the effect of FANCD2 depletion on curcumin and ouabain sensitivity.

2.2.4.3 Depletion of FANCD2 in SHEP-Tet21N cells using an siRNA pool

Dharmafect-1 transfection reagent (Horizon Discovery) was used to transfect SHEP-Tet21N MYCN ON and OFF cells with a pool of 30 siRNAs targeting the human FANCD2 gene (siTOOLs Biotech) and a pool of 30 scrambled negative control siRNAs (siTOOLs Biotech). siRNA pools are provided at a stock concentration of 50 µM in 10mM Tris solution and stored at -20 °C. siRNA pools were diluted in RNase-free water (siTOOLs Biotech) to 150 nM working stocks. Cells were transfected with the FANCD2 siRNA pool (siTOOLs Biotech) or the scrambled negative control siRNA pool (siTOOLs Biotech) to a final concentration of 3 nM using 0.15% Dharmafect-1 per well (Invitrogen, Life Technologies).

2.2.4.3.1 FANCD2 siRNA pool transfection for western blot analysis

SHEP-Tet21N MYCN ON and OFF cells were plated at a density of 2 x 10^5 cells per well in 2 ml media in 6-well plates, 24 hours prior to transfection for approximately 70% confluency at the time of transfection. Per well, 40 µl of 150 nM siRNA pool was diluted with 210 µl FCS-free RPMI-1640. 3 µl Dharmafect-1 was diluted with 246 µl FCS-free RPMI-1640 and pipette mixed. These siRNA pool and Dharmafect-1 dilutions were incubated for 5 min at RT before being combined in a 1:1 ratio. This combined transfection mix was incubated for 15 min at RT. During this incubation, the media on the plated cells was replaced with 1.5 ml normal FCS-containing media in each well. The 500 µl transfection mix was added dropwise to cells to a final volume of 2 ml per well. Non-transfected controls were achieved by adding 500 µl FCS-free RPMI-1640 to cells in place of the transfection mix. Dharmafect-1 vehicle controls were achieved by diluting 3 µl Dharmafect-1 in 496 µl FCS-free DMEM, incubating for 25 min at RT and adding dropwise to cells as above. Cell lysates were collected 48 hours after

transfection, and FANCD2 depletion was analysed by western blotting, with band intensity quantified relative to scrambled negative control siRNA transfected cells.

2.2.4.3.2 FANCD2 siRNA pool transfection for viability analysis by Alamar blue

SHEP-Tet21N MYCN ON and OFF cells were plated at a density of 4 x 10^4 cells per well in 1 ml media in 12-well plates, 24 hours prior to transfection for approximately 50% confluency at the time of transfection. Per well, 20 µl of 150 nM siRNA pool was diluted with 105 µl FCS-free RPMI-1640. 1.5 µl Dharmafect-1 was diluted with 123.5 µl FCS-free RPMI-1640 and pipette mixed. These siRNA pool and Dharmafect-1 dilutions were incubated for 5 min at RT before being combined in a 1:1 ratio. This combined transfection mix was incubated for 15 min at RT. During this incubation, the media on the plated cells was replaced with 0.75 ml normal FCS-containing media in each well. The 250 µl transfection mix was added dropwise to cells to a final volume of 1 ml per well. Non-transfected controls were achieved by adding 250 µl FCS-free RPMI-1640 to cells in place of the transfection mix. Dharmafect-1 vehicle controls were achieved by diluting 1.5 µl Dharmafect-1 in 248.5 µl FCS-free DMEM, incubating for 25 min at RT and adding dropwise to cells as above. 24 hours after transfection, cells were treated with 5 µM curcumin, 100 nM ouabain or left un-treated for 40 hours before cell viability was analysed using Alamar blue. Viability of FANCD2 siRNA transfected cells was determined relative to scrambled siRNA transfected and un-treated cells independently for MYCN ON and OFF cells. This enabled comparison of the effect of FANCD2 depletion on viability of MYCN ON compared to MYCN OFF cells. Viability of curcumin- or ouabain-treated cells was determined relative to un-treated cells for each siRNA and MYCN condition. This enabled comparison of the effect of FANCD2 depletion on curcumin and ouabain sensitivity.

2.2.4.2 Singular siRNA-mediated BRCA1 depletion in SHEP-Tet21N cells for IF analysis

Dharmafect-1 transfection reagent (Horizon Discovery) was used to transfect SHEP-Tet21N MYCN ON and OFF cells with an ON-TARGETplus siRNA targeting the human BRCA1 gene (Horizon Discovery) or a scrambled negative control ON-TARGETplus siRNA (Horizon Discovery, D00181001) (Table 2.13). siRNAs were resuspended in 1x siRNA Buffer (Horizon Discovery) at a stock concentration of 100 µM

and stored at -20 °C. siRNAs were diluted in RNase-free water to 5 μM working stocks. Cells were transfected with an ON-TARGETplus siRNA to a final concentration of 25 nM using 0.15% Dharmafect-1 per well (Invitrogen, Life Technologies).

Table 2.13. Human BRCA1 gene target sequences of ON-TARGETplus siRNA (Horizon Discovery).

siRNA	Target sequence (5'-3')
BRCA1 siRNA-1	CAACAUGCCCACAGAUCAA

SHEP-Tet21N MYCN ON and OFF cells were plated at a density of 3 x 10^4 cells per well in 0.5 ml media in 24-well plates, 24 hours prior to transfection for approximately 60% confluency at the time of transfection. Per well, 2.5 μl of 5 μM ON-TARGETplus siRNA was diluted with 95 μl FCS-free RPMI-1640. 0.75 μl Dharmafect-1 was diluted with 49.25 μl FCS-free RPMI-1640 and pipette mixed. These siRNA and Dharmafect-1 dilutions were incubated for 5 min at RT before being combined in a 1:1 ratio. This combined transfection mix was incubated for 15 min at RT. During this incubation, the media on the plated cells was replaced with 400 μl normal FCS-containing media in each well. The 100 μl transfection mix was added dropwise to cells to a final volume of 0.5 ml per well. Non-transfected controls were achieved by adding 100 μl FCS-free RPMI-1640 to cells in place of the transfection mix. Dharmafect-1 vehicle controls were achieved by diluting 0.75 μl Dharmafect-1 in 99.25 μl FCS-free DMEM, incubating for 25 min at RT and adding dropwise to cells as above. 48 hours after transfection, cells were fixed with 4% PFA for 15 min and subsequently stained for immunofluorescence analysis.

2.2.5 TaqMan RT-qPCR

TaqMan-based reverse-transcription quantitative polymerase chain reaction (RT-qPCR) enables quantification of mRNA expression levels of a gene of interest (Mullis and Faloona, 1987; Holland et al., 1991). Total RNA is extracted from cells and reverse transcribed into cDNA by reverse transcriptase. Quantitative detection of the target gene within the cDNA sample relative to an internal control house-keeping gene such as GAPDH is determined using TaqMan Gene Expression Assays (ThermoFisher Scientific). TaqMan assays utilise a fluorogenic probe and the 5' exonuclease activity of

Taq polymerase to enable measurement of accumulation of the cDNA target region throughout PCR cycles via a fluorescent signal. The threshold cycle (Ct) at which the fluorescence intensity reaches a defined fluorescence threshold is determined for each sample. Fold-change in gene expression relative to the control sample is calculated using the $2^{-\Delta\Delta Ct}$ relative quantification method (Winer et al., 1999; Schmittgen et al., 2000; Livak and Schmittgen, 2001).

2.2.5.1 Total RNA extraction

The mRNA expression level of a panel of 25 FA pathway-associated genes was analysed by RT-qPCR in SHEP-Tet21N cells, over a 7 day MYCN ON to OFF time course, and in a panel of NB cell lines. SHEP-Tet21N MYCN ON cells were plated at a density of 1 x 10^5 – 6 x 10^5 cells per 10 cm dish and left to adhere for 16 hours. Subsequently, MYCN ON cells were treated with 100 μM temozolomide for 16 hours (as a positive control sample for FA pathway activation) or were treated with 1μg/ml tetracycline to induce a MYCN OFF state. At timepoints between 0-168 hours after addition of tetracycline, media was removed and cells were PBS washed and incubated with 1X trypsin-EDTA at 37°C to remove from the dish surface. Trypsin was stopped by diluting in 9 ml media and cells were pelleted by centrifugation at 1200 rpm for 3 min. This cell pellet was resuspended in 1 ml PBS, transferred to a 1.5 ml eppendorf, and re-pelleted by centrifugation at 1200 rpm for 3 min. PBS supernatant was removed and cell pellets were stored at -80°C.

SHEP-1, SH-SY5Y, IMR32 and Kelly cell lines were plated at a density of 1 x 10^6 cells per 10 cm dish and left to adhere for 24 hours. Cells were subsequently trypsinised, pelleted and stored at -80°C as for SHEP-Tet21N above.

Total RNA was extracted from cell pellets using a GenElute Mammalian Total RNA Miniprep Kit (Sigma, RTN350) according to supplied protocols, with a final elusion into 50 μl elution buffer per sample. RNA concentration was determined using the Nanodrop (ThermoFisher) as per recommended protocol. RNA sample quality was determined by an A_{260}/A_{230} ratio of 2.0-2.2 to determine nucleic acid purity, and an A_{260}/A_{280} ratio of approximately 2.0 to determine RNA purity. RNA was reverse transcribed into cDNA immediately after extraction and excess RNA stored at -80°C.

2.2.5.2 Reverse transcription: cDNA synthesis from total RNA

Total RNA was reversed transcribed into cDNA using the Applied Biosystems High Capacity cDNA Reverse Transcription Kit (ThermoFisher Scientific, 4368814) according to the manufacturer's protocol. Briefly, for each 20 µl reaction, 2 µg of total RNA was added to 10 µl master mix and subsequently made up to 20 µl with nuclease-free H_2O as in Table 2.14. All PCR reaction tubes were pipette mixed three times and briefly centrifuged. Reverse transcription was undertaken using recommended thermal cycling conditions in the PCR thermocycler (Table 2.15). 100 µl cDNA was produced for each sample, with output cDNA concentration assumed to be equal to that of the starting RNA concentration in the reverse transcription reaction mixture at 0.1 µg/µl. cDNA was stored at -20°C.

Table 2.14. Composition of 20 µl reverse transcription reaction mixture, using the Applied Biosystems High Capacity cDNA Reverse Transcription Kit recommended conditions.

Reagent	Concentration in reaction mixture	Volume of reagent per 20µl reaction (µl)
10X RT Buffer	1X	2.0
25X dNTP Mix (100 mM)	4 mM	0.8
10X RT Random Primers	1X	2.0
MultiScribe™ Reverse Transcriptase (50 U/µl)	50U	1.0
Nuclease-free H2O	-	4.2
0.2 µg/µl total RNA	0.1 µg/µl	10

Table 2.15. Recommended thermal cycling conditions for reverse transcription reactions using the Applied Biosystems High Capacity cDNA Reverse Transcription Kit.

Temp (°C)	Time (min)	Cycles
25	10	1
37	120	1
85	5	1
4	∞	1

2.2.5.3 TaqMan qPCR

TaqMan Gene Expression Assays specific to a panel of 25 FA pathway associated genes categorised with DNA repair ontology were procured from Applied Biosystems (Table 2.16). The panel of FA pathway associated genes analysed covered a range of FA pathway roles. A GAPDH-specific TaqMan Gene Expression Assay (Table 2.16) was used to determine the expression level of GAPDH in each cDNA sample on every PCR reaction plate for use as an endogenous normalisation control gene. This enabled inter-sample comparisons.

Gene expression was analysed in three biological replicates of each condition. Real-time qPCR reactions were carried out in triplicate for each biological replicate with each TaqMan Gene Expression Assay probe (Table 2.16). Triplicate 'no template control' reactions in which no cDNA is added to the qPCR reaction mixture were carried out in parallel for each TaqMan Gene Expression Assay probe to assess DNA contamination.

Table 2.16. Applied Biosystems 20X TaqMan Gene Expression Assays used in the analysis of FA pathway and GAPDH mRNA expression. Assays include unlabelled primers and a TaqMan probe labelled with a 5' FAM™ fluorescent reporter dye and a 3'end MGB-NFQ (minor groove binder and non-fluorescent quencher). Detection; inter-strand crosslink detection, Core; FA core complex, NER; nucleotide excision repair, TLS; translation synthesis, MMR; mis-match repair, HRR; homologous recombination repair.

FA Pathway Role	Gene	Assay ID
Detection	FANCM	Hs00913609_m1
Core	FANCA	Hs01116668_m1
Core	FANCB	Hs00537483_m1
Core	FANCC	Hs00984545_m1
Core	FANCE	Hs00272482_m1
Core	FANCL	Hs01017205_m1
D2-I	FANCD2	Hs00276992_m1
D2-I	FANCI	Hs00383049_m1
NER	ERCC1	Hs01012158_m1
NER	ERCC4	Hs01063530_m1
NER	MUS81	Hs00228383_m1
TLS	MAD2L2	Hs01057448_m1
TLS	REV1	Hs01019768_m1
TLS	REV3L	Hs00161301_m1
TLS	POLI	Hs00969214_m1
TLS	POLK	Hs00211965_m1
TLS	POLN	Hs00394916_m1
HRR	RPA1	Hs00161419_m1
HRR	BLM	Hs00172060_m1
HRR	BRCA1	Hs01556193_m1
HRR	BRCA2	Hs00609073_m1
HRR	BRIP1	Hs00908143_m1
HRR	PALB2	Hs00954121_m1
MMR	PMS2	Hs00241053_m1
HRR	RAD51	Hs00947967_m1
Endogenous control	GAPDH	Hs03929097_m1

A TaqMan qPCR master mix comprising TaqMan Universal PCR Master Mix (no AmpErase™ UNG) (Applied Biosystems), the relevant TaqMan Gene Expression Assay probe (Applied Biosystems) and nuclease-free H_2O was prepared on ice for each gene as per Applied Biosystems protocols. The TaqMan Universal PCR Master Mix utilises AmpliTaq Gold DNA polymerase and includes a ROX-based passive internal reference dye. For each reaction, 9 µl of the relevant TaqMan qPCR master mix was aliquoted into one well of a MicroAmp™ optical 384-well reaction plate (Applied Biosystems) before addition of 1 µl of 0.1 µg/µl cDNA (100ng cDNA per reaction) to a final reaction volume of 10 µl (Table 2.17). Plates were sealed with MicroAmp™ optical adhesive film (ThermoFisher) and centrifuged at 1000 rpm for 1 min. Real-time qPCR reactions were

undertaken in an Applied Biosystems 7900 Real-Time PCR machine using recommended thermal cycling conditions (Table 2.18). PCR product accumulation was measured by fluorescence intensity over 40 amplification cycles.

Table 2.17. Composition of 10 µl TaqMan qPCR reaction mixtures per well, using Applied Biosystems recommended conditions.

Reagent	Concentration in reaction mixture	Volume of reagent per 10µl reaction (µl)
2X TaqMan Universal PCR Master Mix (Applied Biosystems, 4324018)	1X	5.0
20X TaqMan Gene Expression Assay (Applied Biosystems)	1X	0.5
Nuclease-free H_2O	-	3.5
0.1 µg/µl cDNA	10 ng/µl	1

Table 2.18. TaqMan qPCR recommended thermal cycling conditions using Applied Biosystems 7900 Real-Time PCR machine.

Temp (°C)	Time (min)	Cycles
95	10.00	1
95	0.25	40
60	1.00	

The $2^{-\Delta\Delta Ct}$ relative quantification method was used to calculate the fold-change in expression of each gene relative to the reference sample (Winer et al., 1999; Schmittgen et al., 2000; Livak and Schmittgen, 2001). Using the Applied Biosystems 7900 SDS 2.4 software, ΔRn was calculated as below and amplification plots of log(ΔRn) versus PCR cycle number were generated.

$$Rn = \left(\frac{TaqMan\ probe\ reporter\ dye\ fluorescence}{ROX\ based\ passive\ reference\ dye\ fluorescence}\right)$$

$$\Delta Rn = Rn - baseline\ Rn$$

A ΔRn fluorescence threshold of 0.2 was defined by the Applied Biosystems 7900 SDS 2.4 software and used to determine the Ct value (PCR cycle number at which the defined fluorescence threshold is reached) of each reaction. This fluorescence threshold consistently occurred within the log phase increase in fluorescence for every reaction.

For each target FA pathway-associated gene:

- Triplicate Ct values in each sample were analysed to ensure precision and the average Ct value for each sample calculated.
- ΔCt was calculated for each sample: Difference in the average Ct value of the target gene and the average Ct value of the GAPDH endogenous control gene in the same sample.

$$\Delta Ct = Average\ Ct\ value\ of\ target\ gene - Average\ Ct\ value\ of\ GAPDH$$

- ΔΔCt was calculated for each treated sample: Difference in the ΔCt value of the target gene within each treated sample and the ΔCt value of the target gene within the reference sample. For SHEP-Tet21N MYCN ON to OFF time-course, the 0hr (-Tet, MYCN ON) sample was used as the reference. For NB cell lines, the SHEP-1 cell line was used as the reference sample.

$$\Delta\Delta Ct = \Delta Ct\ in\ treated\ sample - \Delta Ct\ in\ control\ sample$$

- Fold-change in expression of the target gene was calculated for each treated sample relative to the reference sample.

$$Fold\ Change = 2^{-\Delta\Delta Ct}$$

A $\log_2$ transformation was applied to the fold change expression data. Average $\log_2$(fold-change) (n=3) was calculated for each condition and plotted using the R-studio ComplexHeatmap package.

2.2.6 MYCN ChIP-PCR at the FANCD2 Promoter MYCN E-box

Chromatin immunoprecipitation (ChIP) -PCR is undertaken to determine whether a protein of interest binds to a genomic region of interest. Cells are incubated with formaldehyde to covalently crosslink proteins bound onto DNA. Cells are scraped into ice-cold PBS containing protease inhibitors, and the nuclei extracted. Chromatin is digested to 150-900bp fragments by incubation with Micrococcal nuclease and nuclear membranes are lysed by sonication. The sheared chromatin is incubated with a primary antibody against the protein of interest overnight at 4°C with rotation. Protein G magnetic beads are added to the chromatin, incubated for 2 hours at 4°C with rotation, and subsequently pelleted using a magnetic separation rack. The protein G magnetic beads, now bound to the primary antibody and therefore the protein of interest and its

DNA binding sites, are washed with low to high salt washes. Chromatin bound to the protein of interest is eluted from the antibody-protein G magnetic beads by incubation at 65°C for 30 min with gentle vortexing, and the magnetic beads are pelleted and removed. Crosslinks between the protein of interest and chromatin are reversed by incubation with proteinase K and 5M NaCl for 2 hours at 65°C. Resulting DNA fragments are purified using spin columns and the presence of a genomic region of interest assayed by PCR and agarose gel electrophoresis.

Chromatin immunoprecipitation (ChIP) was performed using the SimpleChIP® Enzymatic Chromatin IP Kit (Magnetic Beads) (Cell Signalling) as per supplied protocols. SHEP-Tet21N MYCN ON and OFF cells were plated at a density of 4 x 10^6 cells per 15 cm dish and cultured at 37°C for 24 hours. An extra dish of cells were plated each for MYCN ON and OFF cells to enable determination of cell number per dish before crosslinking. Cells from this dish were trypsinised, resuspended in 20 ml media and counted using a haemocytometer. 4 x 10^6 cells were used for each immunoprecipitation (IP) per condition (approximately half a 15 cm dish of cells at 80% confluency). Cells were crosslinked with 1% formaldehyde, scraped into ice-cold PBS containing 1X protease inhibitor cocktail, and nuclei prepared as per supplied protocols. Chromatin was digested and nuclear membranes lysed as per supplied protocols with minor changes. An optimised volume of 0.5 µl Micrococcal nuclease per 4 x 10^6 cells was used to enable optimal DNA digestion to a length of 150-900 bp. Resulting lysates were subsequently sonicated on ice to lyse nuclear membranes using a 2 mm sonicator probe for 3 x 20 s pulses with 30 s incubations on ice in between pulses. Chromatin digestion and concentration was analysed to ensure optimal digestion in both MYCN ON and OFF cells as per supplied protocols. Chromatin IP was undertaken using 5 µg of digested cross-linked chromatin per IP with 10 µl anti-histone H3 (1:50) (positive control), 2 µl anti-IgG (1:250) (negative control) or 2 µg anti-N-Myc (ab16898) (Table 2.5) with protein G magnetic beads as in supplied protocols. Chromatin was eluted from the magnetic beads and crosslinks reversed before DNA was purified using spin columns according to the provided protocols.

To determine whether *FANCD2* is a direct MYCN target gene, the presence of the *FANCD2* promoter in the pool of MYCN target DNA fragments was determined by PCR. Primers were designed to enable amplification of a canonical MYCN E-box within the *FANCD2* promoter (Table 2.19). A primer set targeting *APEX1* which has been previously validated as a MYCN/MYCC target in SHEP-Tet21N MYCN ON and OFF cells was used as a positive control for presence of an MYCN target gene (Table 2.19)

(Barrilleaux et al., 2013). Primers provided with the SimpleChIP® Enzymatic Chromatin IP Kit targeting exon 3 of *RPL30* were used as a positive control in the histone H3 positive control ChIP sample. Presence or absence of these three genes was tested by PCR amplification of the 2% input sample, the positive control histone H3 sample, the negative control normal IgG sample and the MYCN IP sample alongside a no template control for DNA contamination for both MYCN ON and OFF conditions.

Table 2.19. PCR primers used in MYCN ChIP-PCR.

Primer	Target sequence (5'-3')	Gene Target Site	Tm (°C)	Company
FANCD2 For	CCACAGGTACCTTTCTGCGT	FANCD2 promoter	60.0	Sigma-Aldrich
FANCD2 Rev	AAGTCTTGTCAGCACGTCCG	FANCD2 promoter	60.6	Sigma-Aldrich
APEX1 For	GGCGGGACCTGGTGCGGGGA	APEX1	81.3	Sigma-Aldrich
APEX1 Rev	ACCGCGTCACCCACCGAAGCA	APEX1	78.0	Sigma-Aldrich

PCR reaction mixtures for *FANCD2*, *APEX1* and *RPL30* were prepared on ice as in Table 2.20 and reactions were undertaken in a PCR machine using thermal cycling conditions as in Table 2.21. To assess accumulation of PCR product, 2µl of 6X loading dye (NEB) was mixed with 10 µl PCR product from each ChIP sample and loaded onto a 1% (w/v) TAE-agarose gel containing 1X GelGreen nucleic acid stain (Biotium). 4 µl 1kb Plus DNA ladder (NEB) was loaded for PCR product size determination. The agarose gel was run in 1X TAE buffer (40 mM Tris, 20 mM acetic acid, 1 mM EDTA) at 70V for 1.5 hours. Gels were visualised using a BioRad gel imaging system.

Table 2.20. Composition of PCR reaction mixtures for the amplification of *FANCD2* promoter, *APEX1*, or *RPL30* exon 3.

Reagent	Concentration in reaction mixture			Volume of reagent per 20 µl reaction (µl)		
	APEX1	FANCD2	RPL30	APEX1	FANCD2	RPL30
5X GoTaq Flexi Buffer (Promega)	1X	1X	1X	4	4	4
$MgCl_2$ (25 mM stock, Promega)	1.8 mM	2 mM	2 mM	1.5	1.6	1.6
dNTP Mix (10 mM each, Thermo Scientific)	0.2 mM	0.2 mM	0.2 mM	0.4	0.4	0.4
APEX1 For Primer (10 µM)	0.75uM	-	-	1.5	-	-
APEX1 Rev Primer (10 µM)	0.75uM	-	-	1.5	-	-
FANCD2 For Primer (10 µM)	-	0.5uM	-	-	1	-
FANCD2 Rev Primer (10 µM)	-	0.5uM	-	-	1	-
RPL30 Primer Mix (5 µM)	-	-	0.5uM	-	-	2
GoTaq G2 Flexi DNA Polymerase (5 U/µl, Promega)	0.5U	0.5U	0.5U	0.1	0.1	0.1
Template DNA (40 ng/µl)	4 ng/µl	4 ng/µl	4 ng/µl	2	2	2
Nuclease-free H_2O	-	-	-	9	9.9	9.9

Table 2.21. Thermal cycling conditions for the amplification of *FANCD2* promoter, *APEX1*, or *RPL30* exon 3.

Temp (°C)			Time (min)	Cycles
APEX1	FANCD2	RPL30		
95	95	95	2.00	1
95	95	95	0.5	35
60	58	62	0.5	
72	72	72	0.5	
72	72	72	5	1
4	4	4	Hold	

2.2.7 Immunofluorescence (IF)

Immunocytochemistry can be used to quantify expression, localisation and co-localisation of proteins within a cell. Cells are plated on coverslips and treated as appropriate before being fixed and permeabilised. Coverslips are then blocked with a dilute protein solution to prevent non-specific binding during subsequent immunodetection steps. Coverslips are then incubated with primary antibody(s) specific to the protein(s) of interest, followed by incubation with species-specific secondary antibody(s) conjugated to Alexa Fluor dyes. Incubation with DAPI (4′,6-diamidino-2-phenylindole) is used to stain the nucleus. Visualisation of the fluorophore-labelled antibodies and therefore the location of the protein(s) of interest within a cell is undertaken using a confocal fluorescence microscope.

2.2.7.1 γ-H2AX foci immunofluorescence

SHEP-Tet21N MYCN ON and OFF cells were plated on sterilised coverslips at a density of 3 x 10^4 - 4.5 x 10^4 cells per well in a 24-well plate and left to adhere for 24 hours. Cells were treated as indicated. Media was removed and cells were fixed in 4% paraformaldehyde (PFA) in PBS for 20 min at room temperature, then washed for 3 x 5 min in PBS. Cells were permeabilised by incubation in 0.3% (v/v) Triton-X-100 in PBS for 10 min at room temperature, then washed in wash buffer (0.1% (v/v) NP-40 (Sigma) in PBS) for 3 x 5 min. Coverslips were blocked by incubation in blocking buffer (1% goat serum, 0.1% NP-40 in PBS) for 1 hour at room temperature and subsequently washed for a further 3 x 5 min in wash buffer. The anti-γ-H2AX-Ser139 primary antibody was diluted in antibody buffer (3% goat serum, 0.1% NP-40 in PBS) at a dilution of 1:250 (Table 2.5). Diluted primary antibodies were applied to the coverslips overnight in a humidified chamber at 4°C. Coverslips were washed 3 x 10 min in wash buffer followed by incubation with DAPI (ThermoFisher Scientific) and the Alexa-fluor 594 goat anti-rabbit IgG (ThermoFisher Scientific) secondary antibody (Table 2.6) diluted 1:1000 in antibody buffer, for 1 hour at room temperature in the dark. Coverslips were washed 3 x 5 min in wash buffer and mounted onto microscope slides using Shandon™ ImmuMount™ (Thermo Scientific). Specificity of the Alexa-fluor 594 goat anti-rabbit IgG secondary antibody was demonstrated by use of a no primary antibody control (Appendix Figure A1A).

2.2.7.1 FANCD2/phospho-RPA foci co-immunofluorescence

SHEP-Tet21N MYCN ON and OFF cells were plated on sterilised coverslips at a density of 3 x 10^4 - 4.5 x 10^4 cells per well in a 24-well plate and left to adhere for 24 hours. Cells were treated as indicated. Media was removed and cells were fixed in 4% paraformaldehyde (PFA) in PBS for 20 min at room temperature, then washed for 3 x 5 min in PBS. Cells were permeabilised by incubation in 0.3% (v/v) Triton-X-100 in PBS for 10 min at room temperature, then washed in wash buffer (0.1% (v/v) NP-40 (Sigma) in PBS) for 3 x 5 min. Coverslips were blocked by incubation in blocking buffer (1% goat serum, 0.1% NP-40 in PBS) for 1 hour at room temperature and subsequently washed for a further 3 x 5 min in wash buffer. Anti-FANCD2 and anti-pSer4/8 RPA32/RPA2 primary antibodies were diluted in antibody buffer (3% goat serum, 0.1% NP-40 in PBS) at a dilution of 1:200 and 1:250 respectively (Table 2.5). Diluted primary antibodies were applied to the coverslips overnight in a humidified chamber at 4°C. Coverslips were washed 3 x 10 min in wash buffer followed by incubation with DAPI (ThermoFisher Scientific) and secondary antibodies Alexa-fluor 594 goat anti-rabbit IgG (ThermoFisher Scientific) and Alexa-fluor 488 goat anti-mouse IgG (ThermoFisher Scientific) (Table 2.6), all diluted 1:1000 in antibody buffer, for 1 hour at room temperature in the dark. Coverslips were washed 3 x 5 min in wash buffer and mounted onto microscope slides using Shandon™ ImmuMount™ (Thermo Scientific).

The specificity of the Alexa-fluor 594 goat anti-rabbit IgG and Alexa-fluor 488 goat anti-mouse IgG secondary antibodies was demonstrated by use of a no primary antibody control (Appendix Figure A1B). The lack of non-specific cross-binding between these secondary antibodies was also demonstrated by staining with the anti-FANCD2 primary antibody alone, or with the anti-pSer4/8 RPA32/RPA2 primary antibody alone, followed by staining with both secondary antibodies (Appendix Figure A1B).

2.2.7.2 R-loop immunofluorescence

SHEP-Tet21N MYCN ON and OFF cells were plated on sterilised coverslips at a density of 4.5 x 10^4 cells per well in a 24-well plate and left to adhere for 24 hours. Cells were treated as indicated. Media was removed and coverslips were washed once with PBS before cells were fixed and permeabilised by incubation with ice-cold methanol:acetone (1:1) for 10 min at -20°C. Following 3 x 5 min washes in ice-cold

PBS, coverslips were treated with 150 U/ml RNase H in 1X RNase H Reaction Buffer (NEB, M0297) or 1X RNase H Reaction Buffer alone for 24 hours at 37°C in a humidified chamber. Following a further 3 x 5 min washes in PBS, coverslips were blocked in block buffer (3% (w/v) BSA, 0.1% Tween-20, 4X SSC buffer (600 mM NaCl, 60 mM sodium citrate, pH 7.0) in PBS) for 30 min at room temperature. Anti-DNA-RNA hybrid, S9.6 and anti-nucleolin primary antibodies were diluted in block buffer at a dilution of 1:200 and 1:150 respectively (Table 2.5). Coverslips were incubated with diluted primary antibodies for 1 hour at room temperature and were subsequently washed in block buffer for 3 x 5 min. DAPI (ThermoFisher Scientific) was diluted 1:1000 in block buffer and secondary antibodies Alexa-fluor 594 goat anti-rabbit IgG (ThermoFisher Scientific) and Alexa-fluor 488 goat anti-mouse IgG (ThermoFisher Scientific) were diluted 1:500 in block buffer (Table 2.6). Cells were incubated with diluted DAPI and secondary antibodies for 1 hour at room temperature in the dark and were subsequently washed in block buffer for 3 x 5 min. Coverslips were further washed in PBS for 5 min and then mounted onto microscope slides using ImmuMount™ (Thermo Scientific).

The specificity of the Alexa-fluor 594 goat anti-rabbit IgG and Alexa-fluor 488 goat anti-mouse IgG secondary antibodies was demonstrated by use of a no primary antibody control (Appendix Figure A1C). The lack of non-specific cross-binding between these secondary antibodies was also demonstrated by staining with the anti-DNA-RNA hybrid, S9.6 primary antibody alone, or with the anti-nucleolin primary antibody alone, followed by staining with both secondary antibodies (Appendix Figure A1C).

2.2.7.3 Immunofluorescence microscopy and image analysis

A Nikon Eclipse T200 inverted microscope (Melville, USA) was used for fluorescence microscopy with a 60X objective lens. Images were taken using NIS-Elements Imaging Software (Nikon). Images were processed and quantified using FIJI (Schindelin et al., 2012; Rueden et al., 2017). At least 100 cells were analysed per condition in each individual biological replicate. Where over 100 cells were analysed, data for 100 cells per condition was randomly selected to avoid image bias.

The number of foci per cell was measured using a foci counting macro. This macro defined the area of nuclei using the DAPI image, then counted the number of foci in each nucleus based on a chosen foci intensity threshold which was used across all images. Examples of the use of this macro in the analysis of γ-H2AX foci and

FANCD2/phospho-RPA co-immunofluorescence foci are shown in Figure 2.4 and Figure 2.5 respectively.

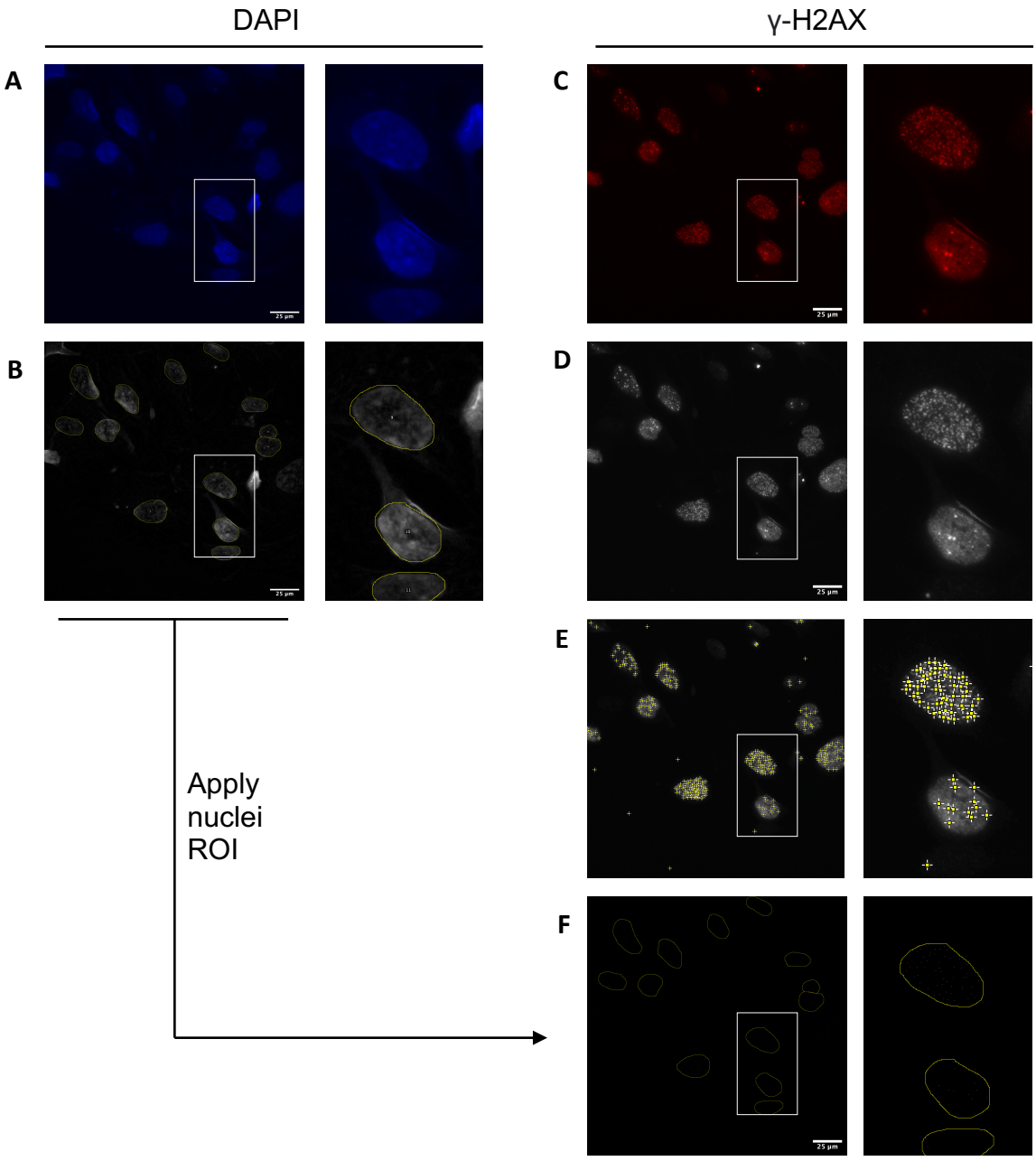

Figure 2.4. Analysis of γ-H2AX foci in FIJI.
Foci were counted in γ-H2AX immunofluorescence images using a macro in FIJI. An example of the image processing steps is shown. The DAPI image **(A)** is converted to 16-bit, the background subtracted (rolling=200) and a gaussian blur (sigma=2) applied. A threshold applied is then applied alongside an adjustable watershed (tolerance=2) to define the nucleus region of interest (ROI) **(B)**. The γ-H2AX image **(C)** is converted to 16-bit **(D)** and the foci defined using the 'Find Maxima' function, with the noise threshold kept consistent for each experiment **(E)**. An output of 'single points' is generated showing a white dot for each foci. The nuclei ROIs are applied to this single points image **(F)**, and the number of foci within each nucleus ROI is counted by the macro.

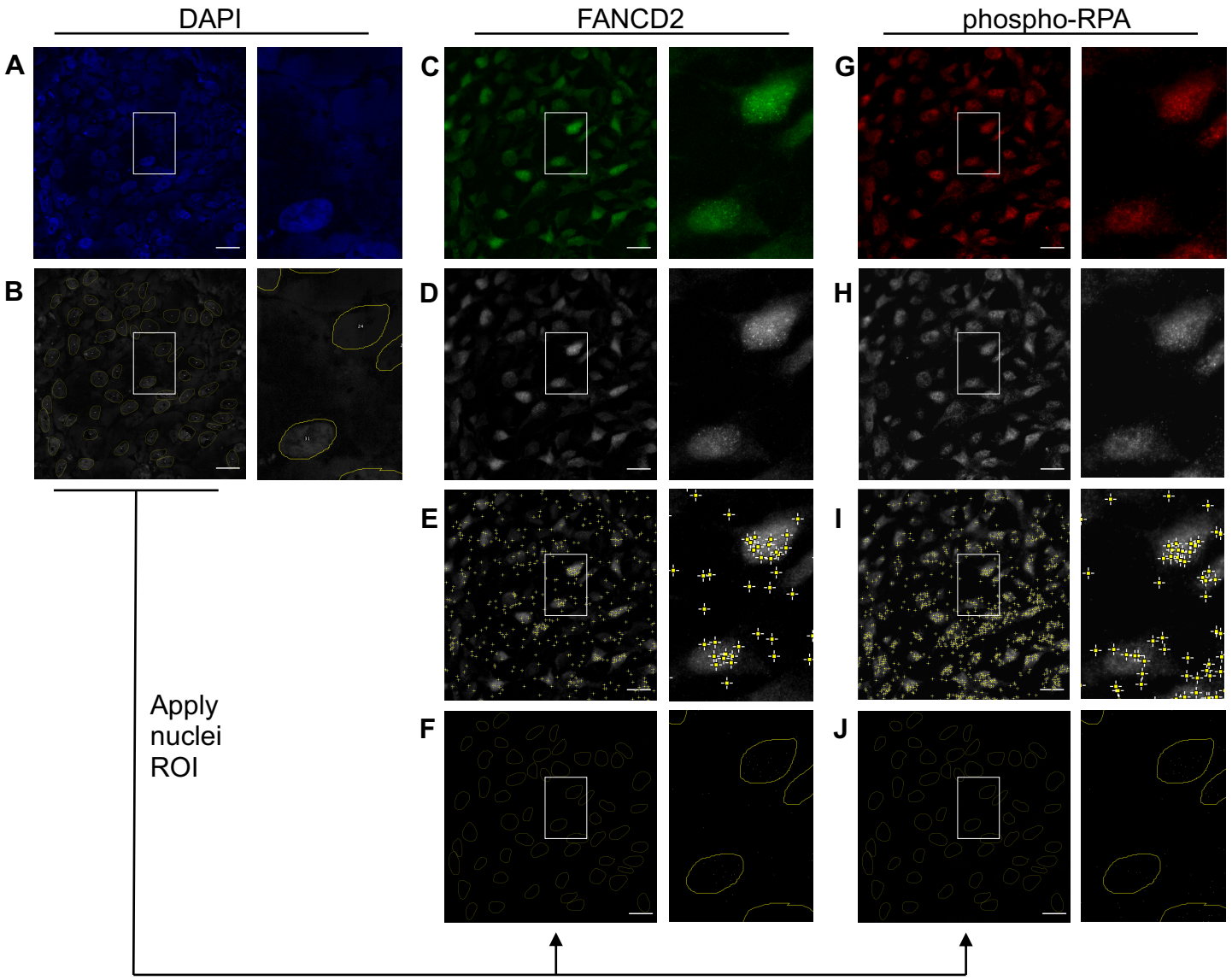

Figure 2.5. Analysis of FANCD2 and phospho-RPA foci in FIJI. (Legend overleaf).

Figure 2.5. Analysis of FANCD2 and phospho-RPA foci in FIJI.
Foci were counted in FANCD2/phospho-RPA co-immunofluorescence images using a macro in FIJI. An example of the image processing steps is shown. The DAPI image **(A)** is converted to 16-bit, the background subtracted (rolling=200) and a gaussian blur (sigma=2) applied. A threshold applied is then applied alongside an adjustable watershed (tolerance=2) to define the nucleus region of interest (ROI) **(B)**. The FANCD2 image **(C)** or phosho-RPA image **(G)** is converted to 16-bit **(D/H)** and the foci defined using the 'Find Maxima' function, with the noise threshold kept consistent for each experiment **(E/I)**. An output of 'single points' is generated showing a white dot for each foci. The nuclei ROIs are applied to this single points image **(F/J)**, and the number of foci within each nucleus ROI is counted by the macro.

The R-loop corrected total cell fluorescence (CTCF) was measured for each nucleus and nucleolus using a R-loop intensity measuring macro. This macro defined the area of the nucleus using the DAPI image, and the area of the nucleoli using the nucleolin stained image. It then created an index of which nucleoli were within each nucleus and determined the R-loop intensity (IntDen) of all nuclei and nucleoli. The average background intensity of the R-loop image was also determined. An example of the R-loop image analysis process by this macro is shown in Figure 2.6. The resulting nuclei and nucleoli intensity data, alongside the nucleus-nucleolus index, was then imported into R Studio which was used to calculate the R-loop CTCF of each nucleus excluding nucleoli intensity. To calculate the CTCF the intensity of the nucleoli was excluded as this is the site of ribosome biogenesis and therefore represents non-specific binding of the anti-RNA-DNA hybrid (S9.6) antibody. The R-loop CTCF was calculated for each nucleus in R Studio using the following equation:

$$CTCF = (Rloop\ intensity\ of\ nucleus - Rloop\ intensity\ of\ relevant\ nucleoli) - (average\ background\ intensity * (area\ of\ nucleus - area\ of\ relevant\ nucleoli))$$

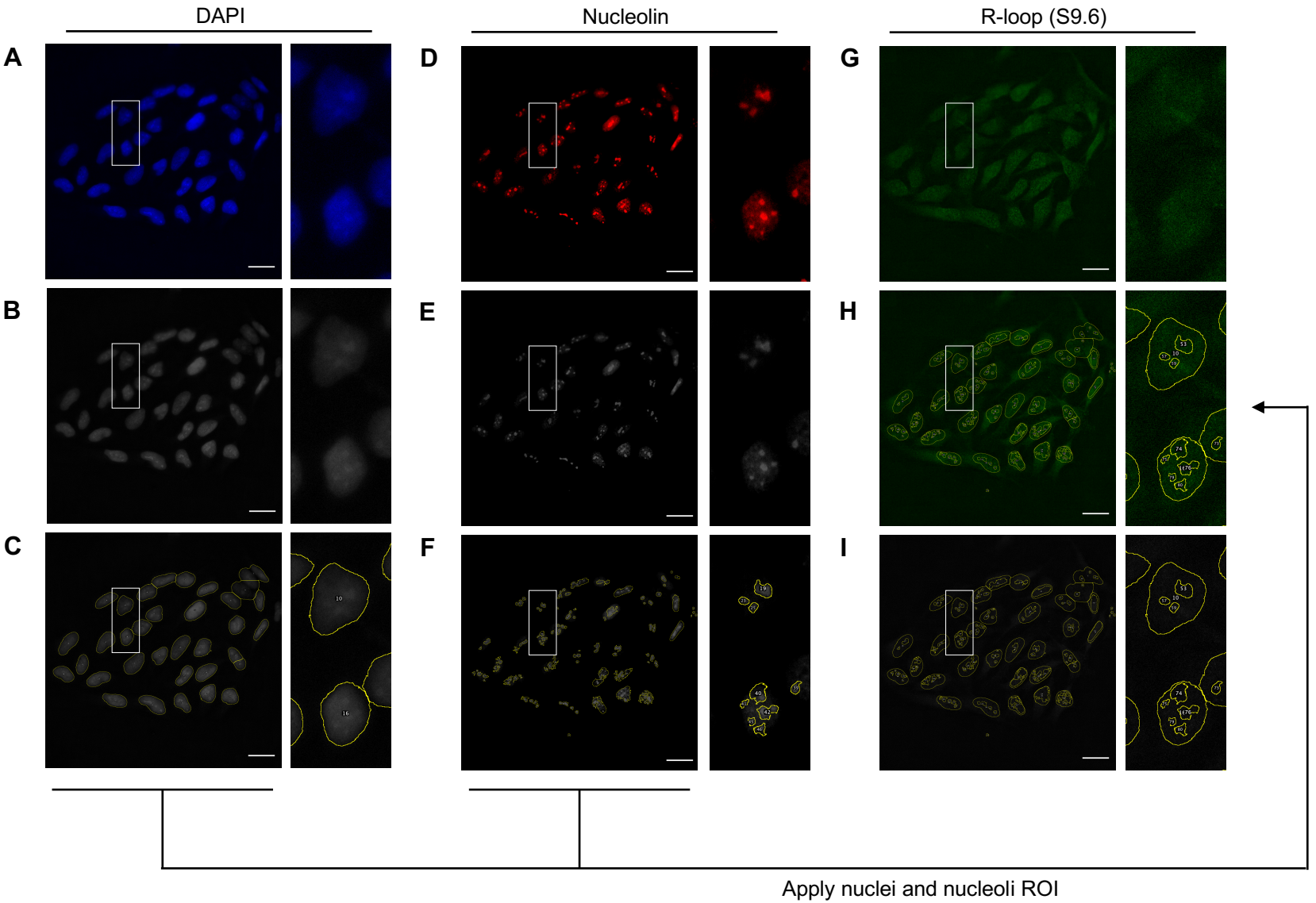

Figure 2.6. Analysis of R-loop nucleus intensity in FIJI. (Legend overleaf).

Figure 2.6. Analysis of R-loop nucleus intensity in FIJI.
R-loop staining intensity was analysed in R-loop (S9.6)/nucleolin co-immunofluorescence images using a macro in FIJI. An example of the image processing steps is shown. The DAPI image **(A)** is converted to 16-bit, the background subtracted (rolling=200) and a gaussian blur (sigma=2) applied **(B)**. A threshold is then applied alongside an adjustable watershed (tolerance=2) to define the nucleus region of interest (ROI) **(C)**. The nucleolin image **(D)** is converted to 16-bit, the background subtracted (rolling=30) and a gaussian blur (sigma=2) applied **(E)**. A threshold applied is then applied to define the nucleolus region of interest (ROI) **(F)**. The R-loop (S9.6) image **(G)** is overlayed with the nuclei and nucleoli ROIs **(H)** and converted to 16-bit **(I)**. The R-loop intensity (IntDen) of each nucleus and nucleolus ROI is measured. The intensity of three random background points in the R-loop 16-bit image is also measured and the average background intensity calculated for each image. An index of which nucleoli are within each nucleus is created. This, alongside the intensity data, is used to calculate corrected total cell fluorescence of each nucleus.

2.2.8.1 DNA fibre staining

DNA fibre analysis enables visualisation of DNA replication dynamics, providing insight into the extent of replication stress within a population of cells. Ongoing DNA replication is labelled with thymidine analogues by incubation of cells with CldU and subsequently IdU. Cells are spotted on a microscope slide and lysed before the slide is tilted to spread the DNA fibres down the slide. The fibres are fixed to the slide and the dsDNA strands are denatured by incubation with HCl. Non-specific binding sites are blocked with a dilute protein solution. Slides are incubated with anti-BrdU antibodies produced in rat (anti-CldU) and mouse (anti-IdU) (Table 2.5), fixed, and washed in blocking buffer. Anti-rat and anti-mouse secondary antibodies labelled with different fluorophores are applied to the slide. Slides are then washed and mounted before the CldU and IdU labelled fibres are visualised by fluorescence microscopy. Analysis of the length and patterns of CldU and IdU tracks enables quantification of replication dynamics.

SHEP-Tet21N MYCN ON and OFF cells were plated at a density of 2 x 10^5 cells per well in a 6-well plate and treated as appropriate. 2.5 mM CldU was added to wells at a final concentration of 25 µM, and plates incubated at 37°C for 20 min. 2.5 mM IdU was then added to wells at a final concentration of 250 µM before cells were incubated for a further 20 min at 37°C. Cells were washed twice with ice-cold PBS and subsequently scraped into 0.2 ml ice-cold PBS. This cell suspension was counted using a haemocytometer and diluted with ice-cold PBS to 4 x 10^5 cells/ml. For each sample, 2

µl of cells was pipetted on each of 3 microscope slides and left to dry for approximately 5-7 min until sticky. 7 µl of spreading buffer (200 mM Tris-HCl pH 7.4, 50 mM EDTA, 0.5% SDS) was added to the cells, mixed by stirring with a pipette tip, and incubated for 2 min. Slides were tilted to slowly spread the DNA fibres down the slide for 3-5 min. Once air-dried, fibres were fixed by incubation in methanol:acetic acid (3:1) for 10 min at room temperature. Slides were air-dried again and stored at 4°C overnight.

Slides were washed in ddH_2O for 2 x 5 min, rinsed once in 2.5M HCl and then incubated in 2.5M HCl for 1 hour at room temperature to denature DNA strands. Slides were then rinsed twice in PBS, washed for 2 x 5 min in blocking solution (1% (w/v) BSA, 0.1 % Tween-20 in PBS), then all non-specific binding sites blocked for 1 hour in blocking solution at room temperature. Rat anti-BrdU (Table 2.5) was diluted 1:1000 and mouse anti-BrdU (Table 2.5) was diluted 1:750 in blocking buffer. Diluted primary antibodies were applied to slides for 1 hour at room temperature. Slides were rinsed three times in PBS and subsequently fixed in 4% paraformaldehyde in PBS. Following three further rinses in PBS, slides were washed for 3 x 5 min in blocking solution. Alexa-fluor 555 goat anti-rat IgG and Alexa-fluor 488 goat anti-mouse IgG secondary antibodies (Table 2.6) were both diluted 1:500 in blocking solution and applied to slides for 1.5 hours at room temperature. Slides were rinsed twice in PBS, washed for 3 x 5 min in blocking solution, further rinsed twice in PBS and then mounted using ImmuMount™ (Thermo Scientific). Slides were stored at -20°C until fibres were imaged.

2.2.8.2 DNA fibre imaging and analysis

DNA fibres were visualised using an Olympus FV1000 confocal microscope with 60X oil objective lens. AlexaFluor 488 and AlexaFluor 555 secondary antibodies were visualised using lasers of wavelength 488 nm and 542 nm respectively. At least 100 fibres were analysed per treatment condition per biological replicate. DNA replication fork status was quantified by counting the number of fibres with each type of CldU and IdU track pattern. New origin; IdU (green) only labelled tracts. Progressing forks; CldU-IdU (red-green) labelled tracks. Bidirectional forks; IdU-CldU-IdU (green-red-green) labelled tracks. Fork collisions; CldU-IdU-CldU (red-green-red) labelled tracks. Stalled forks; CldU (red) only labelled tracks. Example images of these tracts are displayed in Chapter 3, Figure 3.3. One biological replicate was undertaken.

2.2.9 Cell Viability and Survival Assays

2.2.9.1 Trypan blue exclusion assay of cell viability

Trypan blue is a negatively charged dye used as a cell stain in the dye exclusion test of cell viability (Strober, 2001). The permeability of dead cells with compromised cell membranes, but not viable cells with intact cell membranes, to impermeable charged dyes enables exclusive staining of dead cells alone. Hence, an accurate viable cell count can be determined.

2.2.9.1.1 Assessment of MYCN ON and OFF proliferation rate

SHEP-Tet21N MYCN ON and MYCN OFF cells were plated at a density of 2 x 10^5 cells per well in a 6-well plate. Tetracycline was added to MYCN OFF cells at a final concentration of 1 µg/ml to maintain MYCN suppression. MYCN ON and OFF cells were counted at 24, 48 and 72 hours after plating. Cells were PBS washed and incubated with 0.5 ml 1X trypsin-EDTA per well at 37°C. Trypsin activity was stopped by adding 2 ml media per well. Resulting cell suspensions were diluted 1:1 with 0.4% trypan blue (ThermoFisher Scientific) to enable exclusion of stained dead cells. Non-stained cells were counted using a haemocytometer. Five technical replicates of viable cell counts were obtained from each well. Average total cell number per well was calculated for each biological replicate (n=3), and the average and SEM of these biological repeats was then calculated. Welch's T-test was used to determine the statistical significance of differences between MYCN ON and OFF viable cell number as each time point.

2.2.9.1.1 REDACTED

REDACTED

2.2.9.2 Alamar Blue cell viability assay

The Alamar Blue assay is a colorimetric and fluorometric assay used to measure cellular metabolic activity. The alamarBlue reagent contains the blue, weakly fluorescent REDOX indicator dye resazurin (7-Hydroxy-3H-phenoxazin-3-one 10-oxide). Viable cells with active metabolism reduce resazurin to the pink, highly fluorescent resorufin via aerobic respiration.

SHEP-1 and SHEP-Tet21N MYCN ON and OFF cells were plated at a density of 4×10^4 cells per well in 12-well plates. IMR32, Kelly and SH-SY5Y cells were plated at a density of 8×10^4 cells per well in 12-well plates. Six hours following plating, cells were treated as indicated. 0.3 mg/ml resazurin in PBS was diluted 1:10 into the relevant media. Upon completion of the treatment time-course, media was removed from wells and replaced with 1 ml resazurin/media. Tetracycline was re-added to SHEP-Tet21N MYCN OFF cells at a final concentration of 1 µg/ml. Cells were incubated with resazurin in the dark for 4 hours at 37°C, after which fluorescence in each well was measured using the SpectraMax plate reader with excitation and emission wavelengths at 560 nm and 590 nm respectively. The fluorescence intensity is proportional to the number of aerobically respiring viable cells. Fluorescence intensity measured for each treatment condition was normalised to the background intensity of resazurin/media alone. Relative cell viability was calculated for each treatment condition compared to vehicle alone for each biological replicate. The average and SEM of relative cell viability across at least three biological repeats was then calculated. The statistical significance of differences in the viability between SHEP-Tet21N MYCN ON and OFF cells at each concentration or treatment condition was determined by Student's t-test. The statistical significance between viability following scrambled siRNA transfection compared to FANCD2 siRNA

transfection was determined by a one-way ANOVA for each MYCN ON and OFF condition.

2.2.9.3 Clonogenic cell survival assay

SHEP-1, IMR32, Kelly and SHEP-Tet21N MYCN ON and OFF cells were plated at a density of 500-4000 cells per well in a 6-well plate. Cells were left to adhere for 6 hours before adding drugs. Cells were treated with 0-25 μM curcumin alone for 40 hours, 0-100 nM ouabain alone for 40 hours, or with 0-5 μM curcumin alone for 16 hours before adding 0-20 μM cisplatin, 0-20 μM carboplatin or 0-100 μM TMZ for the subsequent 24 hours before media was replaced. Alternatively, cells were treated with 0-100 nM nFAPi alone and media was not replaced. Plates were incubated at 37°C for 10 days (SHEP-1, IMR32, SHEP-Tet21N) or 21 days (Kelly) before the media was removed and colonies were fixed and stained with 0.4% methylene-blue (0.4% (w/v) methylene blue (Fisher Scientific) in 70% methanol). The Stuart Scientific colony counter was used to count colonies and the relative survival was calculated as the percentage colony forming efficiency was relative to vehicle control. At least three biological replicates of each assay was undertaken, and the average and SEM of these three biological replicates was calculated. Statistical significance between relative survival of MYCN ON and OFF cells, or between curcumin-treated and curcumin un-treated cells, was determined by a Student's t-test. IC_{50} (half maximal inhibitory concentration) of each treatment was determined for each cell line by using the dose response curve graph to read the drug concentration at 50% survival.

2.2.10 FACS

2.2.10.1 FACS cell harvesting and fixing

SHEP-Tet21N MYCN ON and OFF cells were plated at a density of 5 x 10^5 cells per 10 cm dish and treated as appropriate. **REDACTED**. Media was removed and cells were PBS washed. Media and PBS wash-offs were collected. Cells were then detached from the dish/coverslip by incubation with 1 ml 1X trypsin-EDTA at 37°C. Trypsin was stopped by addition of media and detached cells were combined with the relevant collected media and PBS wash-offs. Cells were then pelleted by centrifugation at 1200 rpm for 5 min, washed twice in ice-cold PBS and resuspended in 1 ml ice-cold 100%

methanol to fix. Cells were stored in methanol at -20°C for minimum of 1 hour and a maximum of 2 weeks.

2.2.10.2 Propidium iodide staining

Propidium iodide staining was used to determine DNA content and therefore the cell cycle phase of each cell. Methanol was poured off cells, which were then PBS washed twice. Cells were subsequently resuspended in 200 µl PI/RNAse A solution (18 µg/ml PI, 8 µg/ml RNAse A in PBS) and then incubated at 4 °C for a minimum of 1.5 hours before cells were analysed with a BD Biosciences FACSCalibur.

2.2.10.3 Propidium iodide (PI) and phospho(Ser10) Histone H3 co-staining

Ser10 phospho-Histone H3 staining enables the fraction of mitotic cells to be separated from the G2M fraction of cells determined by propidium iodide staining. Methanol was poured off cells, which were then PBS washed twice. Cells were subsequently resuspended in FACS block buffer (PBS with 0.5% BSA 0.25% Triton-X-100 (Sigma-Aldrich)) and incubated on ice for 15 min to block non-specific sites. Cells were then pelleted by centrifugation at 1200 rpm for 5 min, the supernatant was removed and cells were resuspended in FACS block buffer containing 1:500 dilution of phospho(Ser10)-Histone H3 primary antibody and incubated for 1 hour at RT. Cells were then washed twice with PBS containing 0.25% Triton-X-100 and resuspended in 100 µl PBS containing 1% BSA and a 1:200 dilution of anti-rabbit Alexa-488 secondary antibody. Cells were incubated with the secondary antibody for 30 min in the dark at RT. Cells were then washed once with PBS, resuspended in 200 µl PI/RNAse A solution (18 µg/ml PI, 8 µg/ml RNAse A in PBS) and then incubated at 4 °C for a minimum of 1.5 hours before cells were analysed with a BD Biosciences FACSCalibur.

2.2.10.4 FACS Analysis

FL3 (PI)-Area was plotted against FL3-Width and cells with low FL3-Width were gated to exclude cell doublets from FACS analysis. At least 8000 events were collected in this gating region per sample. **REDACTED**. Cell cycle analysis was undertaken on this single cell population. An FL3-Height histogram was produced of all gated events,

representing a histogram of PI intensity per event (an example of this plot is shown in Chapter 3, Figure 3.2A). This FL3-Height histogram was gated to quantify the proportion of cells in each stage of the cell cycle. Gating across the base of the first peak (at approximately 200 FL3-H) in the FL3-Height plot defined the G1 proportion of cells. Gating across the base of the second peak (at approximately 400 FL3-H) defined the G2M proportion of cells. The S phase population was defined as the total signal between these two peaks, and the sub-G1 population was defined as the total signal to the left of the first peak. If cells were also stained for Ser10 phospho-Histone H3, the mitotic population was discriminated from the G2M population by further analysis. The FL3-Height (an indicator of PI intensity) was plotted against the FL1-Height (an indicator of the intensity of Ser10 phospho-Histone H3 staining). Gating around the population of cells within the G2M FL3-H (PI) peak, but with a FL1-H peak at least 0.5 logs greater than other G2M cells enabled discrimination between the mitotic and G2 proportion of cells.

2.2.11 REDACTED

REDACTED

Figure 2.7. REDACTED

2.2.11.1 REDACTED

REDACTED

Table 2.22. REDACTED

REDACTED

Table 2.23. REDACTED

REDACTED

2.2.11.2 REDACTED

REDACTED

2.2.12 Statistics

Statistical analyses were performed using R2 genomics, Excel or R-Studio: Integrated Development for R (v.3.4.4) (R Studio, Inc., Boston, MA, http://www.rstudio.com/). Normal distribution and homogeneity of variance were confirmed by Shapiro-Wilk and the Levene's tests respectively. Data were presented as

means ± SEM (standard error of the mean). If data were normally distributed with equal variances, statistically significant differences were analysed using an independent Student's t-test, or a one-way or two-way ANOVA with Tukey's HSD post hoc test (unless stated otherwise). If data were not equally distributed, statistically significant differences were analysed by Welch's t-test. If data were not normally distributed, statistically significant differences were analysed by Mann-Whitney U test. Unless otherwise stated, significance was considered achieved at $p < 0.05$.

Chapter 3. MYCN induces differential FA pathway expression

3.1 Introduction

Amplification of the *MYCN* oncogene occurs in 20% of neuroblastoma cases and is always associated with high-risk disease, independent of tumour stage (Moreau et al., 2006; Cohn et al., 2009; Maris, 2010). Significant correlation of *MYCN* amplification with rapid tumour progression and reduced event-free survival, despite high intensity treatment (Brodeur et al., 1984; Seeger et al., 1985), highlights a need for novel therapeutics with greater efficacy and reduced off-target toxicity. Analysis of the pathways through which *MYCN* exerts its oncogenic effects is necessary to identify therapeutic targets for *MYCN* amplified neuroblastoma (MNA-neuroblastoma). MYCN is a paralogue of MYCC and functions primarily as a transcription factor (Schwab et al., 1983; Meyer and Penn 2008). As neuroblastoma is predominantly diagnosed in early childhood and rarely exhibits recurrent driver mutations (Pugh et al., 2013), the ability of *MYCN* overexpression to drive neuroblastoma progression is unlikely due to mutations in MYCN target genes. MYCN-induced differential gene expression therefore likely has a major role in driving the aggressive MNA phenotype.

The mechanism through which MYCN regulates the global transcriptional profile is highly complex. MYCN binds cis-regulatory elements in an affinity-dependent manner, resulting in identification of different sets of target genes depending on the MYCN expression level (Zeid et al., 2018; Baluapuri et al., 2020). At physiological levels during development, MYCN binds high-affinity canonical MYCN E-boxes in promoters and enhancers to directly regulate a set of target genes. At oncogenic levels, excess MYCN invades the active and accessible cis-regulatory landscape, binding to prevalent low-affinity non-canonical E-boxes, to induce a global upregulation of all active genes. This is highly dependent on the cell's pre-established chromatin landscape and accounts for the tumour-type specificity of global upregulation observed (Murphy et al., 2009; Valentijn et al., 2012; Zeid et al., 2018). However, this affinity-based model is further complicated by the ability of MYCN to bind transcriptional targets via protein-protein interactions, and the ability of MYCN to interact with multiple epigenetic remodellers to redefine the active cis-regulatory landscape which it upregulates (Brenner et al., 2005; Corvetta et al., 2013; Tsubota et al., 2018; Zeid et al., 2018; Baluapuri et al., 2020).

Overexpression of *MYCN* has been shown to induce higher levels of chronic replication stress and DNA damage (Gu et al., 2015; King et al., 2020). MNA tumour cells therefore have a greater dependency on DNA damage repair and replication stress limiting pathways and are sensitised to their inhibition. For example, it has been previously demonstrated that MNA neuroblastoma cells show enhanced sensitivity to inhibition of ATR, CHK1, MRE11 and PARP (Cole et al., 2011; Colicchia et al., 2017; Petroni et al., 2018; King et al., 2020; King et al., 2021; Southgate et al., 2020). This increased dependency on CHK1, MRE11 and PARP correlated with a MYCN-dependent upregulation in expression (Cole et al., 2011; Gu et al., 2015; Petroni et al., 2016; Colicchia et al., 2017; Petroni et al., 2018; King et al., 2020). High *MYCN* expression has also been shown to transcriptionally upregulate many other DNA repair genes in neuroblastoma such as *BLM*, *BRCA1*, and components of the DDR and alternative NHEJ (Valentijn et al., 2012; Chayka et al., 2015; Hallett et al., 2016; Newman et al., 2015; Durbin et al., 2018; Herold et al., 2019). This upregulation of DNA repair genes frequently correlates with poor prognosis in neuroblastoma (Chayka et al., 2015; Hallett et al., 2016; Durbin et al., 2018; Petroni et al., 2018; Herold et al., 2019; King et al., 2020). Upregulation of other DNA repair pathways may be indicative of a putative dependency, specifically in MNA tumour cells, which could be exploited therapeutically.

The FA pathway is composed of 23 FANC proteins and many FA associated proteins, and primarily functions to repair DNA inter-strand crosslinks through co-ordination of multiple other DNA repair pathways such as HRR, NER and TLS (Kim and D'Andrea, 2012; Ceccaldi et al., 2016). However, many FA pathway proteins also have roles in limiting replication stress (Schlacher et al., 2011; Schlacher et al., 2012; Lossaint et al., 2013; Garcia-Rubio et al., 2015; Schwab et al., 2015; Zhang et al., 2017; Daza-Martin et al., 2019; Herold et al., 2019; Liang et al., 2019a; Okamoto et al., 2019). For example, whilst FANCD2 mono-ubiquitination is a key step for FA pathway activation, FANCD2 also functions in the protection of stalled replication forks, resolution of R-loops and facilitation of replication restart following DNA repair (Schlacher et al., 2011; Schlacher et al., 2012; Chaudhury et al., 2013; Lossaint et al., 2013; Schwab et al., 2015; Lachaud et al., 2016). Increased expression of FANC genes, including *FANCD2*, has been observed in melanoma, bladder, colon, ovarian, breast, uterine and lung cancers (Kais et al., 2016; Kao et al., 2011; Liu et al., 2020a). The extent of FANC gene upregulation often correlates with increased tumour aggressiveness and progression (Kais et al., 2016; Kao et al., 2011; Wysham et al.,

2012; Van Der Groep et al., 2008; Feng and Jin 2019). Upregulation of FA pathway genes has also been linked to evolution of resistance to DNA crosslinking chemotherapy (Taniguchi et al., 2003; Chen et al., 2005; van der Heijden et al., 2005; Swisher et al., 2009; Chen et al., 2016; Nagel et al., 2017).

The impact of *MYCN* amplification on FA pathway expression in neuroblastoma is unknown. Upregulation of FA pathway genes could indicate a therapeutically exploitable increased dependency on FA pathway function. Hallett et al., (2016) identified a gene signature that is associated with poor prognosis in MNA neuroblastoma, and that therefore predicts dependencies and therapeutic targets in MNA tumours. FA pathway genes were enriched among the DNA repair genes in this gene signature, suggesting a putative dependency of MNA cells on FA pathway function. We hypothesised that MYCN transcriptionally upregulates the FA pathway to prevent accumulation of replication stress-induced DNA damage. The aim of this chapter is to determine the effect of *MYCN* overexpression and amplification on FA pathway expression in neuroblastoma cell lines and tumours.

3.2 Results

3.2.1 FA pathway expression correlates with the *MYCN* expression level in *MYCN*-inducible neuroblastoma cells

First, the *MYCN*-inducible SHEP-Tet21N and SHEP-PLXI-MYCN cell lines were used to study the effects of differential *MYCN* expression in two separate isogenic systems.

3.2.1.1 Characterisation of the SHEP-Tet21N tet-OFF MYCN expression system

SHEP-Tet21N cells contain a tetracycline-regulated (tet-OFF) conditional *MYCN* expression system, as previously described in the materials and methods (Chapter 2.2.2.1.2) (Gossen and Bujard, 1992; Lutz et al., 1996). *MYCN* expression has previously been successfully inhibited in SHEP-Tet21N cells within 4-8 hours of treatment with 1 ⌈g/ml tetracycline (King et al., 2020, King et al., 2021). To confirm the length of tetracycline treatment necessary to induce inhibition of *MYCN* expression, SHEP-Tet21N cells were treated with 1 ⌈g/ml tetracycline for timepoints up to 72 hours, and MYCN protein expression was determined by western blot (Figure 3.1A). MYCN

expression was inhibited by 4 hours post tetracycline treatment and remained downregulated throughout the 72 hour time-course (Figure 3.1A-B). Subsequently, SHEP-Tet21N cells were routinely cultured without tetracycline treatment in a 'MYCN ON' state, and a 'MYCN OFF' state was induced by treatment with 1 ⌈g/ml tetracycline for at least 48 hours prior to the start of experiments.

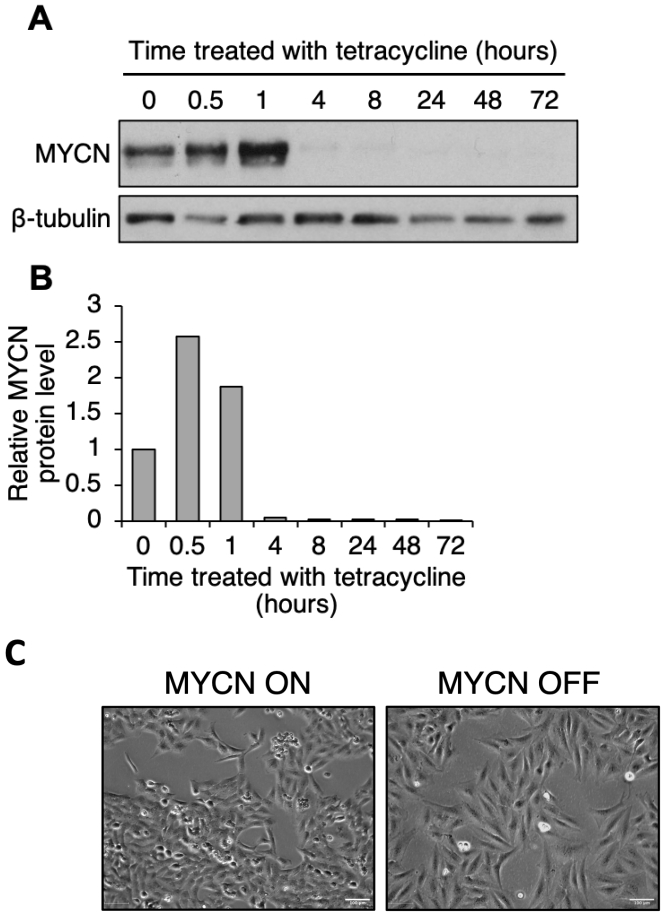

Figure 3.1. A MYCN OFF state is induced in the SHEP-Tet21N conditional MYCN expression system 4 hours after tetracycline treatment.
SHEP-Tet21N cells, containing a tet-OFF MYCN expression system, were treated with 1μg/ml tetracycline to repress MYCN expression (MYCN OFF) or left untreated (MYCN ON). **(A)** MYCN protein levels in cell lysates harvested at timepoints 0-72 hours post tetracycline treatment were determined by western blotting (n=1). **(B)** MYCN band intensity was quantified relative to 0 hour tetracycline treatment and normalised to ß-tubulin band intensity. **(C)** Brightfield images of MYCN ON cells and MYCN OFF cells (48 hours after tetracycline treatment), taken at 10X magnification using a Nikon confocal microscope (n=1). Scale bar indicates 100μm.

Effective inhibition of *MYCN* expression following 48 hour tetracycline treatment was also validated phenotypically. The global effects of *MYCN* inhibition were observed by morphological changes in SHEP-Tet21N cells (Figure 3.1C). MYCN ON cells were

smaller, rounder and had a more epithelial-type morphology, whereas MYCN OFF cells were larger with a more neuronal-type morphology. In addition, it has been extensively demonstrated that *MYCN* expression increases proliferation rate in various systems by promoting a G1 to S-phase transition (Cavalieri and Goldfarb, 1988; Lasorella et al., 2002; Bell et al., 2007; Woo et al., 2008; Huang et al., 2011; Molenaar et al., 2012; Gogolin et al., 2013; Kramer et al., 2016; Liu et al., 2017; Chen and Guan 2022). *MYCN* expression in SHEP-Tet21N cells did not induce significant changes in the cell cycle profile, however an increase in the proportion of cells in S and G2M phases and a reduction in the proportion of cells in G1 was observed in two of three repeats (Figure 3.2A-B). Induction of a MYCN OFF state also led to a significant reduction in the viable cell count observed 24, 48 and 72 hours following plating (Student's t-test, $p < 0.05$) (Figure 3.2C). Through DNA fibre analysis, which enables study of the progression of individual replication forks, high *MYCN* expression has also been shown to increase levels of replication stress (Gu et al., 2015; King et al., 2020; King et al., 2021). Similarly, we found MYCN ON cells had a greater proportion of fork collisions, stalled forks and new fork origins, and a reduced proportion of progressing forks (Figure 3.3A-B). This indicates expression of *MYCN* in the SHEP-Tet21N system promotes faster proliferation and increased replication stress. These data together are consistent with the findings of previous studies and therefore validate the SHEP-Tet21N system in my hands.

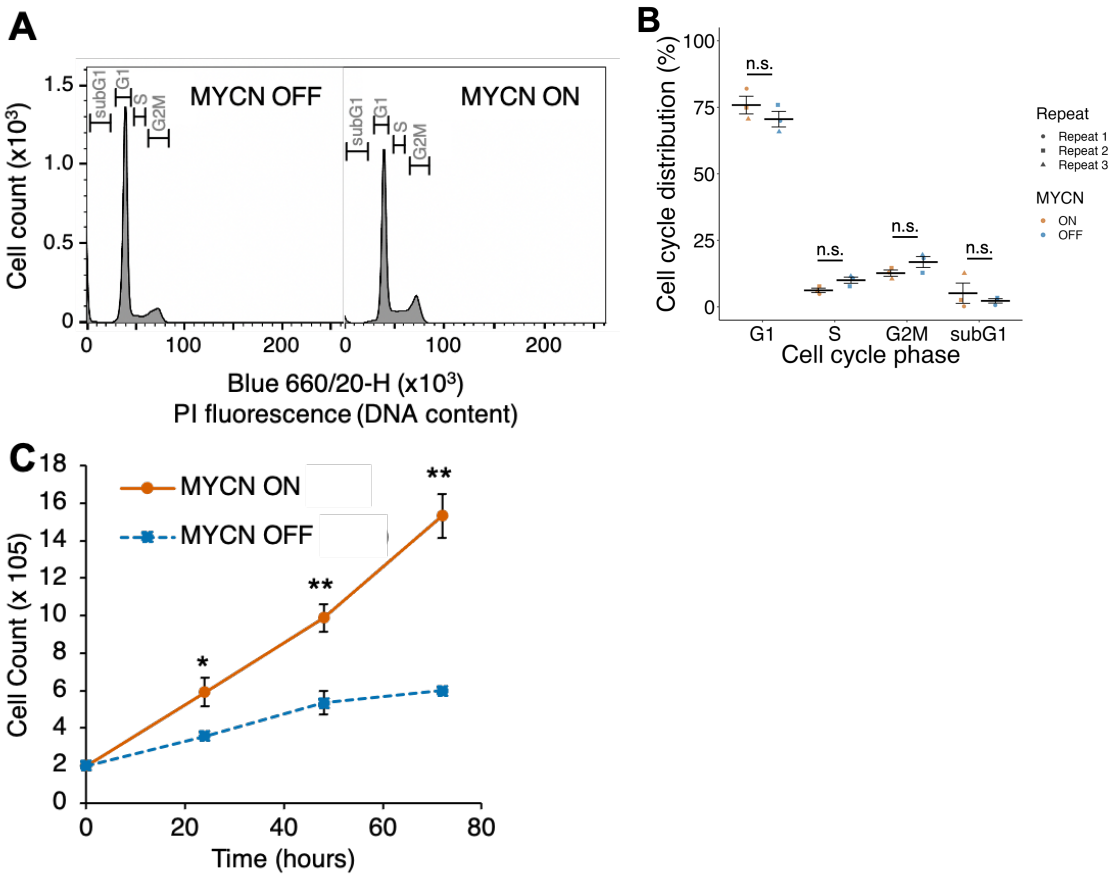

Figure 3.2. MYCN expression affects the proliferation rate in neuroblastoma cells.
SHEP-Tet21N cells were treated with 1µg/ml tetracycline to repress MYCN expression (MYCN OFF) or left untreated (MYCN ON). **(A)** Representative FACS cell cycle profiles for SHEP-Tet21N MYCN OFF and MYCN ON cells, with DNA content determined by propidium iodide staining. **(B)** Percentage of cells in each cell cycle phase for MYCN ON and MYCN OFF cell populations. Data are presented as means ±SEM (n=3). Statistical significance between MYCN ON and OFF at each cell cycle phase was determined by a two-way ANOVA and Tukey HSD post-hoc test where n.s. = not significant, *p<0.05, **p<0.01, ***p<0.001. **(C)** Viable cell count of MYCN ON and OFF cells was quantified at 24, 48 and 72 hours after plating using trypan blue exclusion. A MYCN OFF state was induced by treatment with 1µg/ml tetracycline for 48 hours prior to plating. Data are presented as means ±SEM (n=3). Statistical significance between MYCN ON and OFF at each timepoint was determined by Student's t-test where n.s.=non-significant, *p<0.05, **p<0.01, ***p<0.001.

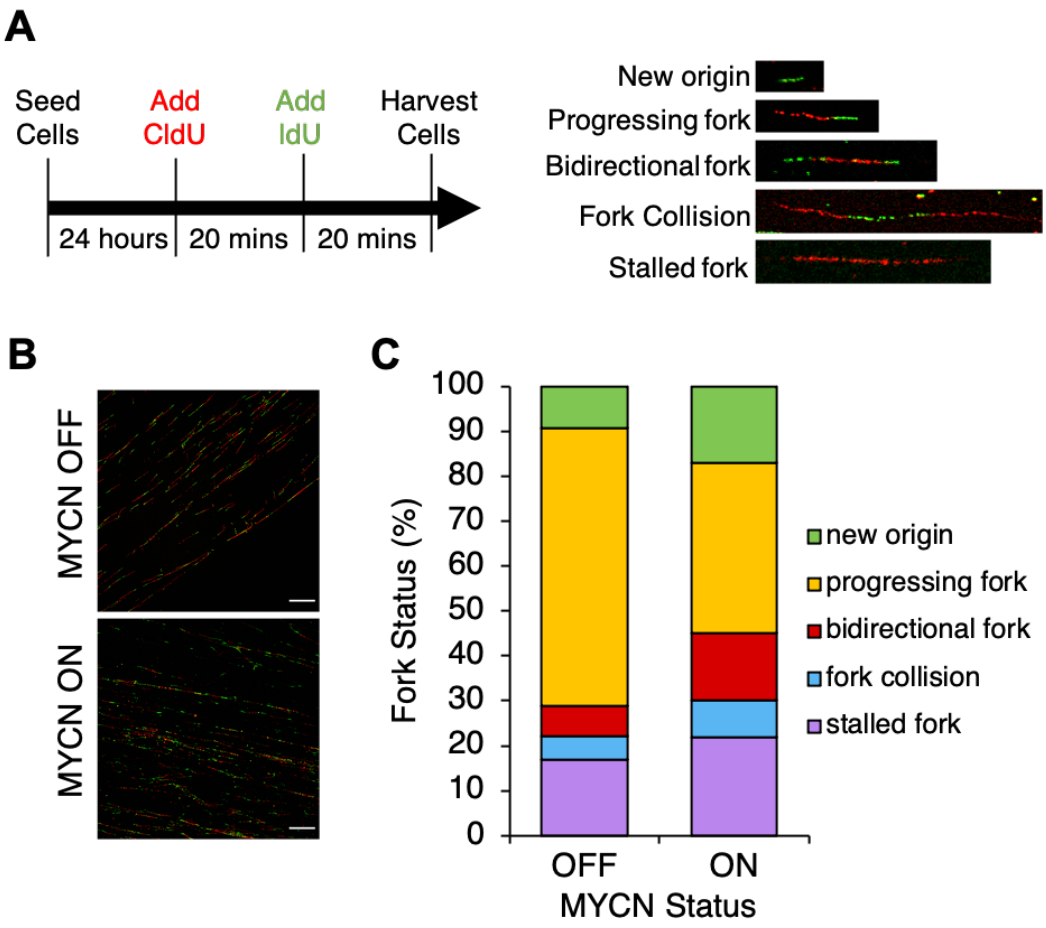

Figure 3.3. Differences in DNA replication fork dynamics observed in MYCN ON compared to MYCN OFF cells.
DNA replication fork progression in SHEP-Tet21N MYCN ON and MYCN OFF cells was examined by DNA fibre analysis. **(A)** Cells were pulse labelled with CldU and subsequently IdU for 20 min each before lysing. DNA fibres were spread, denatured and incubated with anti-BrdU antibodies to enable visualisation of CldU (red) and IdU (green) fibre tracks using an Olympus FV1000 confocal microscope. DNA replication fork status was quantified by analysis of CldU and IdU track patterns in each fibre. New origin; IdU (green) only labelled tracts. Progressing fork; CldU-IdU (red-green) labelled tracks. Bidirectional fork; IdU-CldU-IdU (green-red-green) labelled tracks. Fork collision; CldU-IdU-CldU (red-green-red) labelled tracks. Stalled fork; CldU (red) only labelled tracks. **(B)** Representative images of MYCN ON and OFF DNA fibre tracks. Scale bar = 25 μm. **(C)** Proportion of each DNA replication fork status in MYCN ON and OFF cells. At least 100 fibres were analysed per MYCN ON/OFF (n=1).

3.2.1.2 Inhibition of MYCN expression downregulates FANCD2 protein expression in SHEP-Tet21N

FANCD2 is a key protein in FA pathway-mediated DNA repair and also functions to minimise replication stress through protection of stalled replication forks and R-loop resolution (Schlacher et al., 2011; Schlacher et al., 2012; Chaudhury et al., 2013; Lossaint et al., 2013; Schwab et al., 2015; Lachaud et al., 2016). Therefore, the effect of *MYCN* expression on FANCD2 protein expression in SHEP-Tet21N cells was analysed by western blot (Figure 3.4A). SHEP-Tet21N cells were treated with tetracycline to inhibit *MYCN* expression over a seven day time-course. A MYCN ON to OFF transition occurred within 4 hours, and FANCD2 protein levels were significantly downregulated by approximately 50% in 24 hours ($F(12,26) = 12.84$, $p = 0.041$) (Figure 3.4A-B). This significant downregulation was maintained throughout all subsequent MYCN OFF timepoints ($p < 0.001$). In addition to total FANCD2 levels, the extent of FA pathway activation was also determined by measuring the ratio of mono-ubiquitinated FANCD2 (L) to non-ubiquitinated FANCD2 (S). Addition of temozolomide (TMZ) served as a positive control for activation. Initially the level of FA pathway activation was highly variable but by 72 hours the level became more consistent, such that a non-significant reduction in FA pathway activation was observed in MYCN OFF compared to MYCN ON cells ($F(12,26) = 3.34$, $p > 0.05$) (Figure 3.4A,C). This data suggests that, like other DDR genes, FANCD2 expression and activation levels are higher when *MYCN* is expressed.

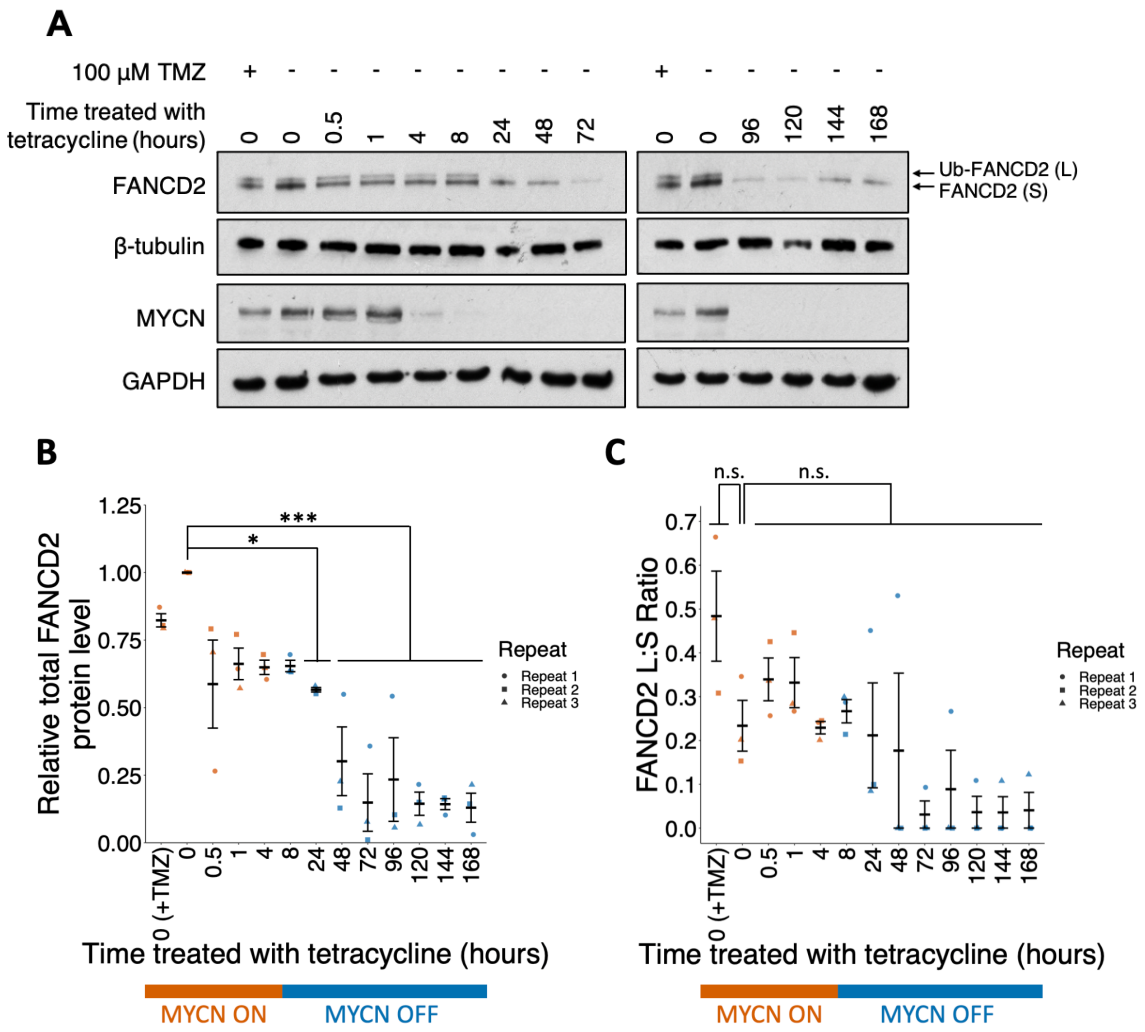

Figure 3.4. FANCD2 protein levels are downregulated by inhibition of MYCN expression in SHEP-Tet21N cells.
SHEP-Tet21N MYCN ON cells were treated with 1 μg/ml tetracycline for 0-168 hours to induce a MYCN OFF state. MYCN ON cells were treated with 100 μM temozolomide (TMZ) for 16 hours as a positive control for FA pathway activation. **(A)** MYCN and FANCD2 protein levels in cell lysates harvested at each indicated timepoint were determined by western blotting. **(B)** Total FANCD2 band intensity (sum of L and S band intensities) was quantified relative to 0 hour tetracycline treatment (-TMZ) and normalised to ß-tubulin band intensity. Means ±SEM are shown (n=3). **(C)** FA pathway activation was quantified by the extent of FANCD2 mono-ubiquitination. The band intensity ratio of mono-ubiquitinated FANCD2 (L, upper band) to non-ubiquitinated FANCD2 (S, lower band) was calculated for each condition. Means ±SEM are shown (n=3). Statistical significance in (B and C) between 0 hour tetracycline treatment (-TMZ) and all other treatments was determined by a one-way ANOVA and Tukey HSD post-hoc test where *p<0.05, **p<0.01, ***p<0.001.

3.2.1.3 Optimisation of the SHEP-PLXI-MYCN tet-ON expression system

The SHEP-Tet21N tet-OFF system enables study of the effect of *MYCN* expression inhibition. In contrast, SHEP-PLXI-MYCN cells contain a tet-ON conditional *MYCN* expression system and can be used to examine the effect of induction of *MYCN* expression (Chapter 2.2.2.1.3) (Gossen et al., 1995; Zeid et al., 2018). Optimisation of the treatment conditions required for induction and maintenance of *MYCN* expression was undertaken. Treatment of SHEP-PLXI-MYCN cells with up to 1.5 ⌠g/ml tetracycline for 24 hours (Figure 3.5A), or with 1 ⌠g/ml tetracycline for up to 72 hours (Figure 3.5B), did not effectively induce *MYCN* expression. The low efficacy of rtTA (tet-ON) system induction by tetracycline has been previously demonstrated in HeLa cells (Krueger et al., 2004; Zhou et al., 2006). Doxycycline, a second-generation tetracycline with higher stability, has been evidenced as a potent alternative rtTA effector (Krueger et al., 2004; Zhou et al., 2006). Treatment of SHEP-PLXI-MYCN with a range of doxycycline doses for 24 hours induced *MYCN* expression (Figure 3.6).

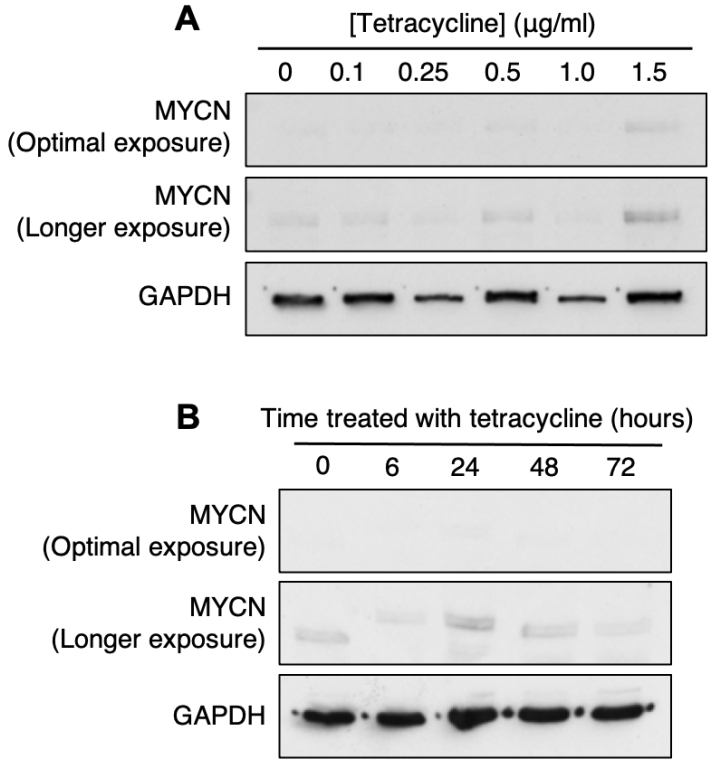

Figure 3.5. Tetracycline treatment does not induce MYCN expression in SHEP-PLXI-MYCN cells.
(A) SHEP-PLXI-MYCN cells, containing a MYCN tet-on system, were treated with 0-1.5 µg/ml tetracycline for 24 h before cell lysates were harvested and MYCN protein levels determined by western blotting (n=1). **(B)** SHEP-PLXI-MYCN cells were treated with 1 µg/ml tetracycline for 0-72 hours. MYCN protein levels in cell lysates harvested at each timepoint were determined by western blotting (n=1). In (A and B) longer exposures are displayed to enable visualisation of background MYCN levels present in the MYCN OFF state.

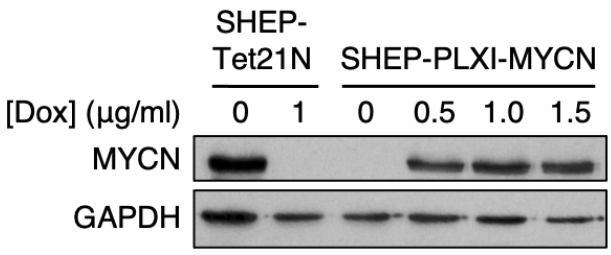

Figure 3.6. Doxycycline treatment induces MYCN expression in SHEP-PLXI-MYCN cells.
SHEP-PLXI-MYCN cells, containing a MYCN tet-on system, were treated with 0-1.5 µg/ml doxycycline (Dox) for 24 hours before cell lysates were harvested and MYCN protein levels determined by western blotting (n=1). SHEP-Tet21N cells, containing a MYCN tet-off system, were treated with 1 µg/ml doxycycline for 24 hours as a positive control for MYCN differential expression in a tetracycline-regulated MYCN expression system.

To determine the time-course of *MYCN* expression induction, SHEP-PLXI-MYCN cells were treated with 0.5 ⌈g/ml doxycycline and the MYCN protein level was determined at time-points up to 72 hours by western blotting (Figure 3.7A). *MYCN* expression was induced six hours following doxycycline treatment, however this expression reduced 6-fold in the following 72 hours (Figure 3.7B). Replacing the media containing 0.5 ⌈g/ml doxycycline at 24 hour intervals enabled maintenance of high *MYCN* expression over the 72 hour time-course (Figure 3.8A-B). Subsequently SHEP-PLXI-MYCN cells were routinely passaged without doxycycline treatment in a 'MYCN OFF' state. A 'MYCN ON' state was induced by treatment with 0.5 ⌈g/ml doxycycline every 24 hours for at least 48 hours prior to, and during, experiments.

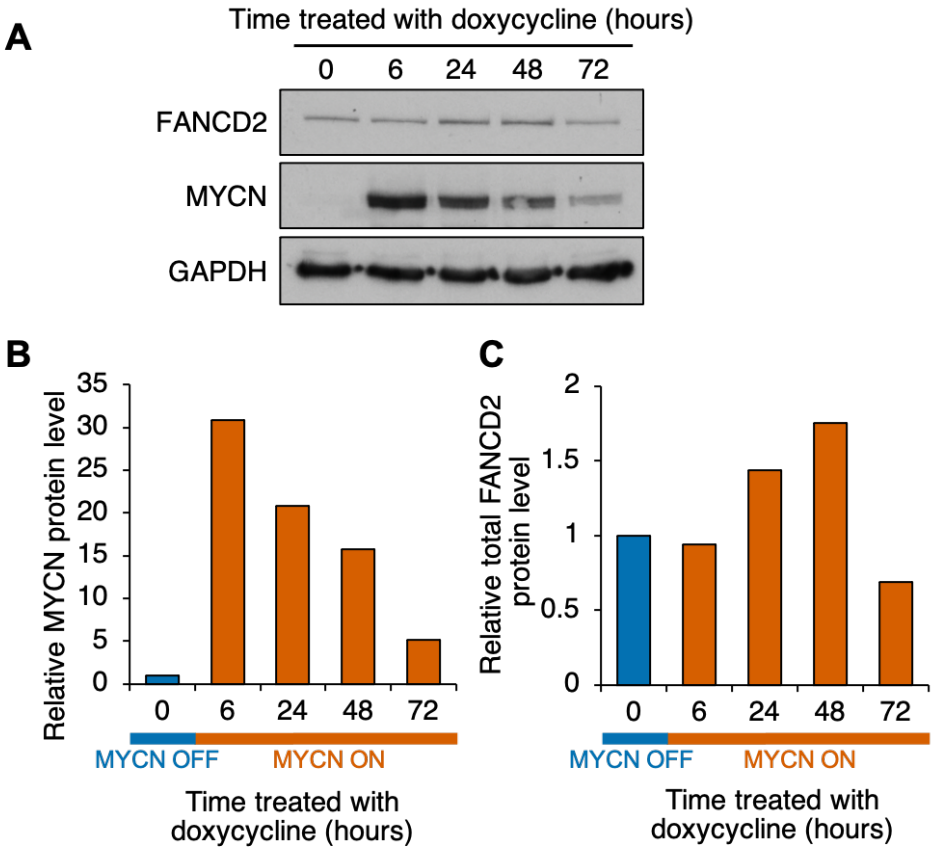

Figure 3.7. Differential MYCN expression in SHEP-PLXI-MYCN cells induces differential FANCD2 expression.
SHEP-PLXI-MYCN cells were treated with 0.5 µg/ml doxycycline for 0-72 hours. **(A)** MYCN and total FANCD2 protein levels in cell lysates harvested at each timepoint were determined by western blotting (n=1). **(B)** MYCN and **(C)** total FANCD2 band intensities were quantified relative to 0 hour doxycycline treatment, and normalised to GAPDH band intensity.

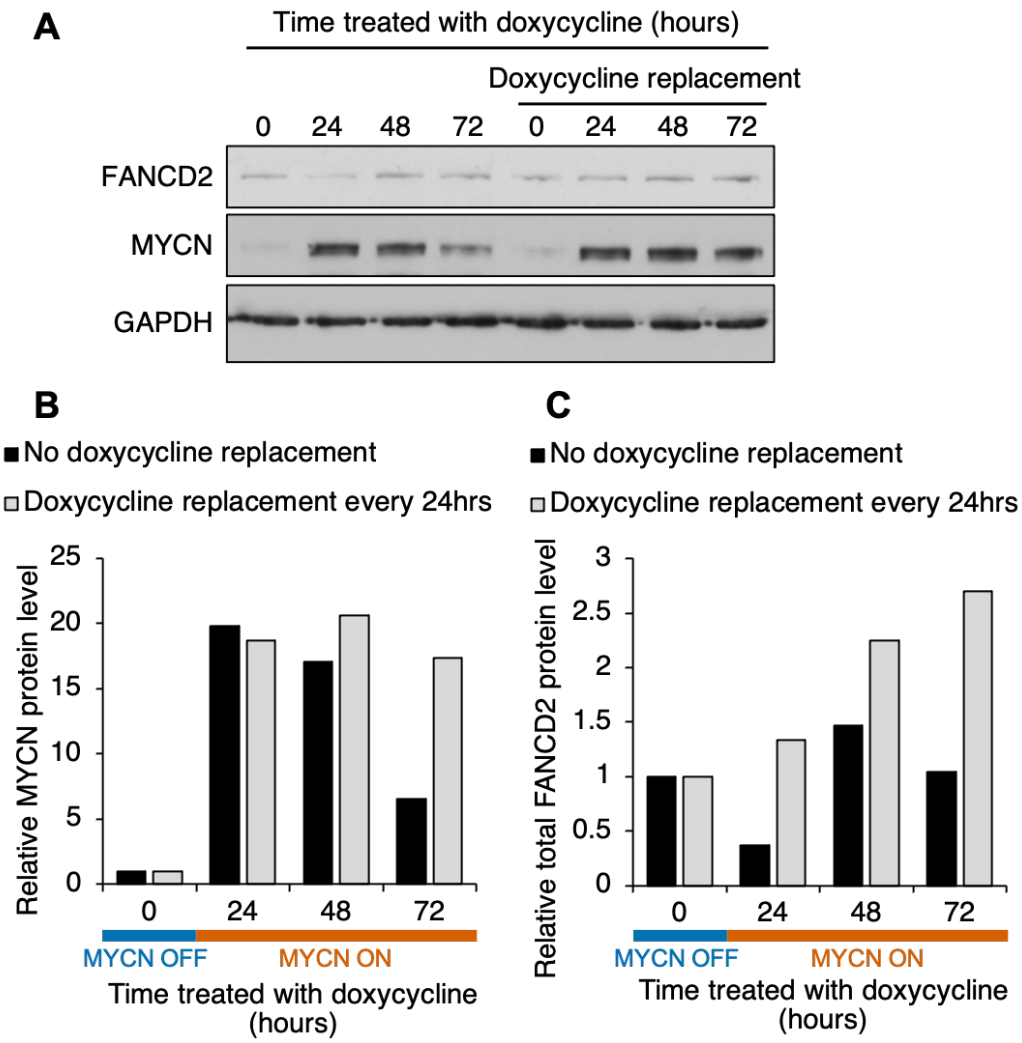

Figure 3.8. Repeated treatment with doxycycline is required to maintain a MYCN ON state in SHEP-PLXI-MYCN cells.
SHEP-PLXI-MYCN cells were treated with 0.5 µg/ml doxycycline for 0-72 h. Cells were dosed either once at 0 hours (No doxycycline replacement), or every 24 hours (Doxycycline replacement). **(A)** MYCN and total FANCD2 protein levels in cell lysates harvested at each timepoint were determined by western blotting (n=1). **(B)** MYCN and **(C)** total FANCD2 band intensities were quantified relative to 0 hour doxycycline treatment in each doxycycline dosage course, and normalised to GAPDH band intensity.

3.2.1.4 Induction of MYCN expression upregulates FANCD2 protein expression in SHEP-PLXI-MYCN cells

The effect of induction of *MYCN* expression on FANCD2 protein levels in SHEP-PLXI-MYCN cells was determined by western blot in conjunction with optimisation of the doxycycline treatment schedule. SHEP-PLXI-MYCN cells were treated with a single dose of doxycycline to induce *MYCN* expression over a 72 hour time-course (Figure

3.7A). A MYCN OFF to ON transition occurred within six hours (Figure 3.7B), and subsequently FANCD2 protein levels were upregulated by approximately 50% in 24 hours (Figure 3.7C). This is consistent with the extent and timing of FANCD2 downregulation observed following a MYCN ON to OFF transition in SHEP-Tet21N cells (Figure 3.4B). However, a gradual reduction in *MYCN* expression in the SHEP-PLXI-MYCN cells resulted in a return to base level FANCD2 expression at 72 hours (Figure 3.7C, 3.8C). Maintenance of the MYCN ON state in SHEP-PLXI-MYCN cells over the 72 hour time-course by repeated doxycycline treatment resulted in consistent FANCD2 upregulation, with a 2.7-fold upregulation observed at 72 hours (Figure 3.8C). This data is in agreement with the SHEP-Tet21N cell data and adds further evidence to support the hypothesis that *MYCN* expression is associated with higher expression of *FANCD2*.

3.2.1.5 MYCN-induced FANCD2 upregulation is reversible in SHEP-PLXI-MYCN cells

The downregulation of FANCD2 following a reduction in *MYCN* expression in SHEP-PLXI-MYCN cells indicated that the MYCN-induced upregulation of FANCD2 was reversible (Figure 3.7). To confirm this reversibility in regulation, SHEP-PLXI-MYCN cells were treated with doxycycline to induce a MYCN ON state for 72 hours before the doxycycline was removed to re-induce a MYCN OFF state for a further 72 hours (Figure 3.9A). Consistent FANCD2 upregulation was again observed during the 72 hour MYCN ON state (Figure 3.9A-B). Removal of doxycycline induced a MYCN ON to OFF transition within 24 hours. However, FANCD2 upregulation continued for a further 48 hours in the MYCN OFF state before FANCD2 expression reduced back to initial baseline levels by 72 hours. This confirms that the MYCN-dependent upregulation of FANCD2 is reversable but suggests a delayed reversibility occurs, perhaps reflective of protein turnover time.

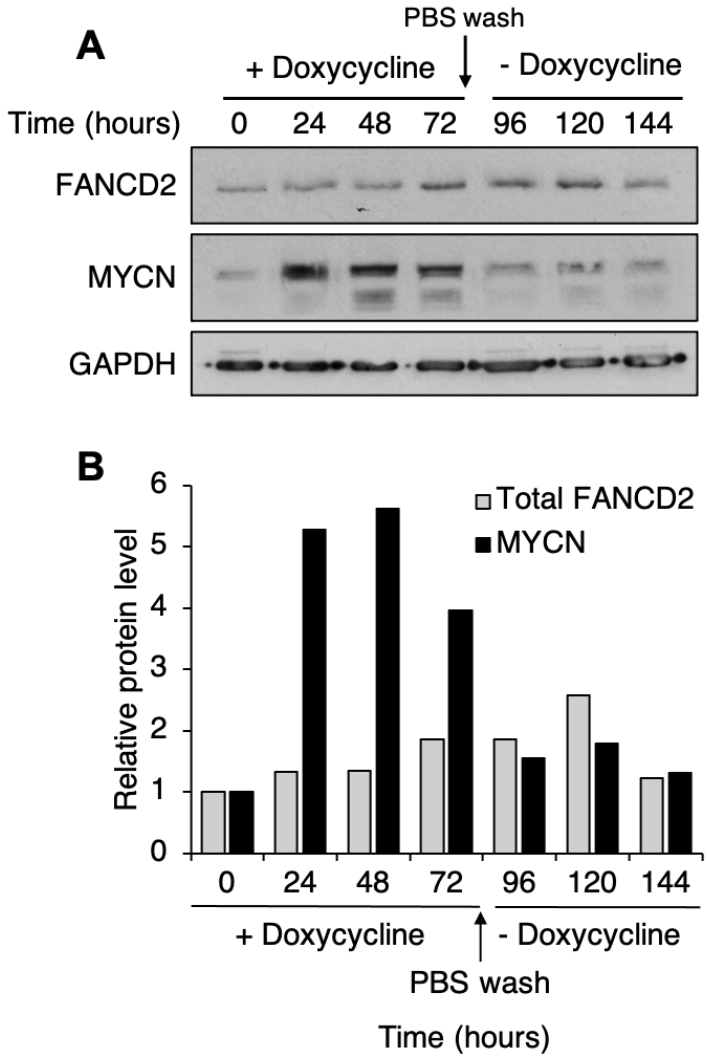

Figure 3.9. MYCN-induced upregulation of FANCD2 protein levels is reversible in SHEP-PLXI-MYCN cells.
SHEP-PLXI-MYCN cells were treated with 0.5 µg/ml doxycycline every 24 hours for 72 hours to induce a MYCN ON state, then PBS washed to remove doxycycline and induce a MYCN OFF state for a further 72 hours. **(A)** MYCN and total FANCD2 protein levels in cell lysates harvested at each timepoint were determined by western blotting (n=1). **(B)** MYCN and total FANCD2 band intensities were quantified relative to 0 hour doxycycline treatment, and normalised to GAPDH band intensity.

The reversibility of MYCN-induced FANCD2 differential expression was further analysed in SHEP-Tet21N cells by reversal of the tet-OFF system. SHEP-Tet21N cells were pre-treated with tetracycline for 48 hours to inhibit *MYCN* expression, and were then washed and released into tet-free media for up to 7 days in order to restore MYCN levels. In contrast to previous studies which have demonstrated reversibility of the SHEP-Tet21N system (Boon et al., 2001; Raetz et al., 2003), western blot analysis of MYCN and FANCD2 expression showed 48 hours pre-treatment with tetracycline

induced an irreversible MYCN OFF state (Figure 3.10A). Small fluctuations in background MYCN expression following tetracycline removal did not correlate with FANCD2 expression (Figure 3.10B) ($r_s(10) = 0.126$, $p = 0.700$) or FA pathway activation ($r_s(10) = -0.067$, $p = 0.837$) (Figure 3.10C), and it should be considered that MYCN levels were determined from blots where exposure times were very long and expression levels very low, making them unreliable.

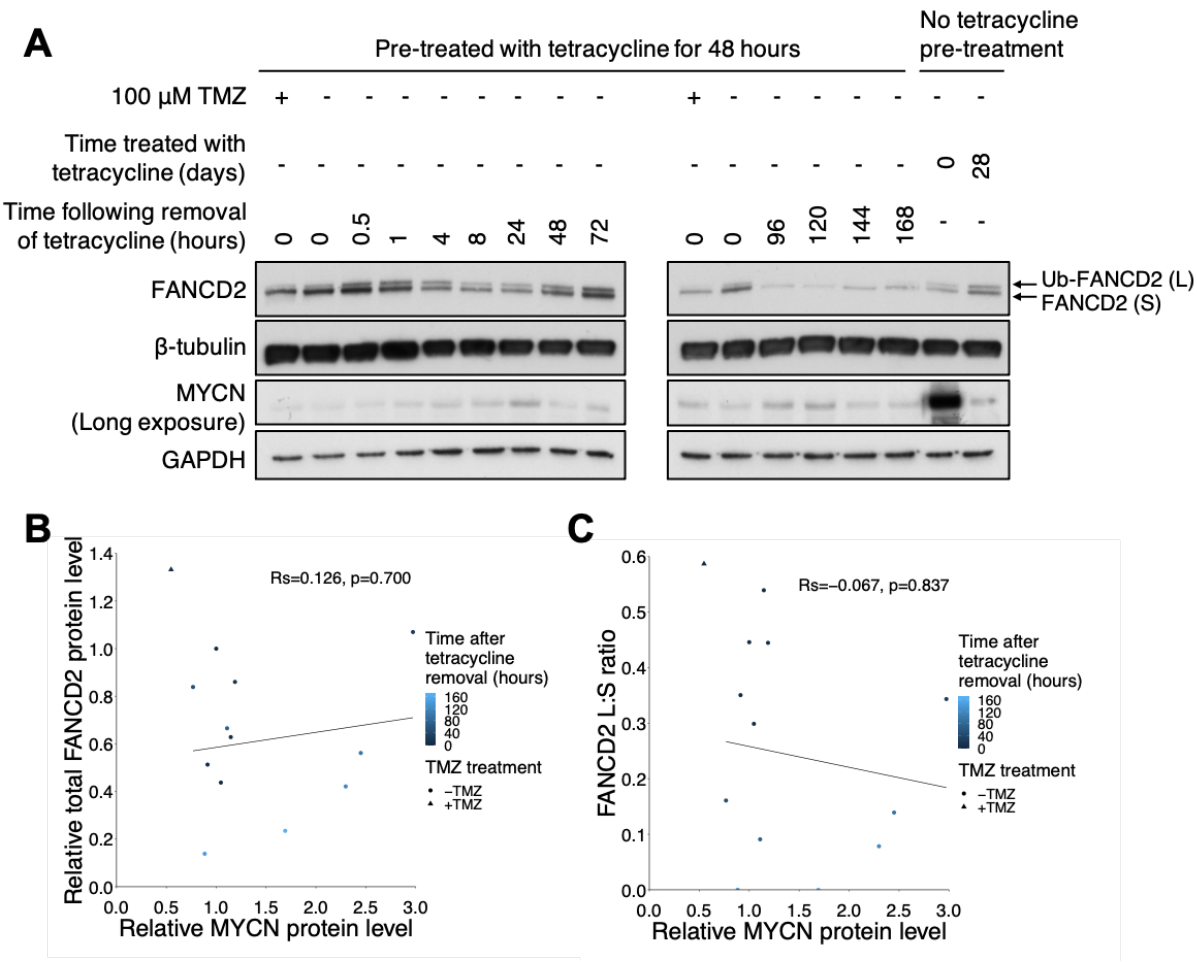

Figure 3.10. Treatment of SHEP-Tet21N cells with tetracycline for 48 hours induces an irreversible MYCN OFF state.
SHEP-Tet21N MYCN ON cells were cultured in 1 µg/ml tetracycline to induce a MYCN OFF state for 48 hours. Cells were then PBS washed and cultured without tetracycline for 0-168 hours in an attempt to re-induce a MYCN ON state. SHEP-Tet21N cells with 28 days or no tetracycline pre-treatment were included for comparison. Cells were treated with 100 µM temozolomide (TMZ) for 16 hours as a positive control for FA pathway activation. **(A)** MYCN and FANCD2 protein levels in cell lysates harvested at each timepoint were determined by western blotting (n=1). **(B)** Total FANCD2 (sum of L and S) and MYCN band intensities were quantified relative to 0 hour tetracycline removal (-TMZ) and normalised to ß-tubulin and GAPDH band intensities respectively. Relative total FANCD2 and MYCN protein level in all 48 hour tetracycline pre-treated samples are plotted. **(C)** For all 48 hour tetracycline pre-treated samples, FANCD2 L:S band intensity ratios were calculated and plotted against relative MYCN protein level. In (B and C) statistical significance of correlation between samples without TMZ treatment was determined by Spearman's correlation. Rs = Spearman's rank correlation coefficient, p = p-value.

In order to investigate this further, SHEP-Tet21N MYCN ON cells were pre-treated with tetracycline to induce a MYCN OFF state for 28 days before tetracycline was removed for timepoints up to 7 days in an attempt to re-induce a MYCN ON state. MYCN and FANCD2 protein levels were analysed by western blot (Figure 3.11A). Again, *MYCN* repression could not be reversed and therefore the reversibility of FANCD2 downregulation in SHEP-Tet21N cells could not be determined. However, with the same caveat previously mentioned about reduced reliability of long exposure and low level blots, a significant correlation was observed between FANCD2 expression and fluctuations in low background *MYCN* expression in the MYCN OFF state ($r(10) = 0.618$, $p = 0.032$) (Figure 3.11B). No correlation was observed between background MYCN levels and FA pathway activation in MYCN OFF cells ($r(10) = 0.057$, $p = 0.861$) (Figure 3.11C). It should be noted that after 28 days in a MYCN OFF state, the SHEP-Tet21N cells were still cycling but at a much slower rate. This data suggests that transient upregulation of *MYCN* leads to a reversible upregulation of FANCD2 protein levels.

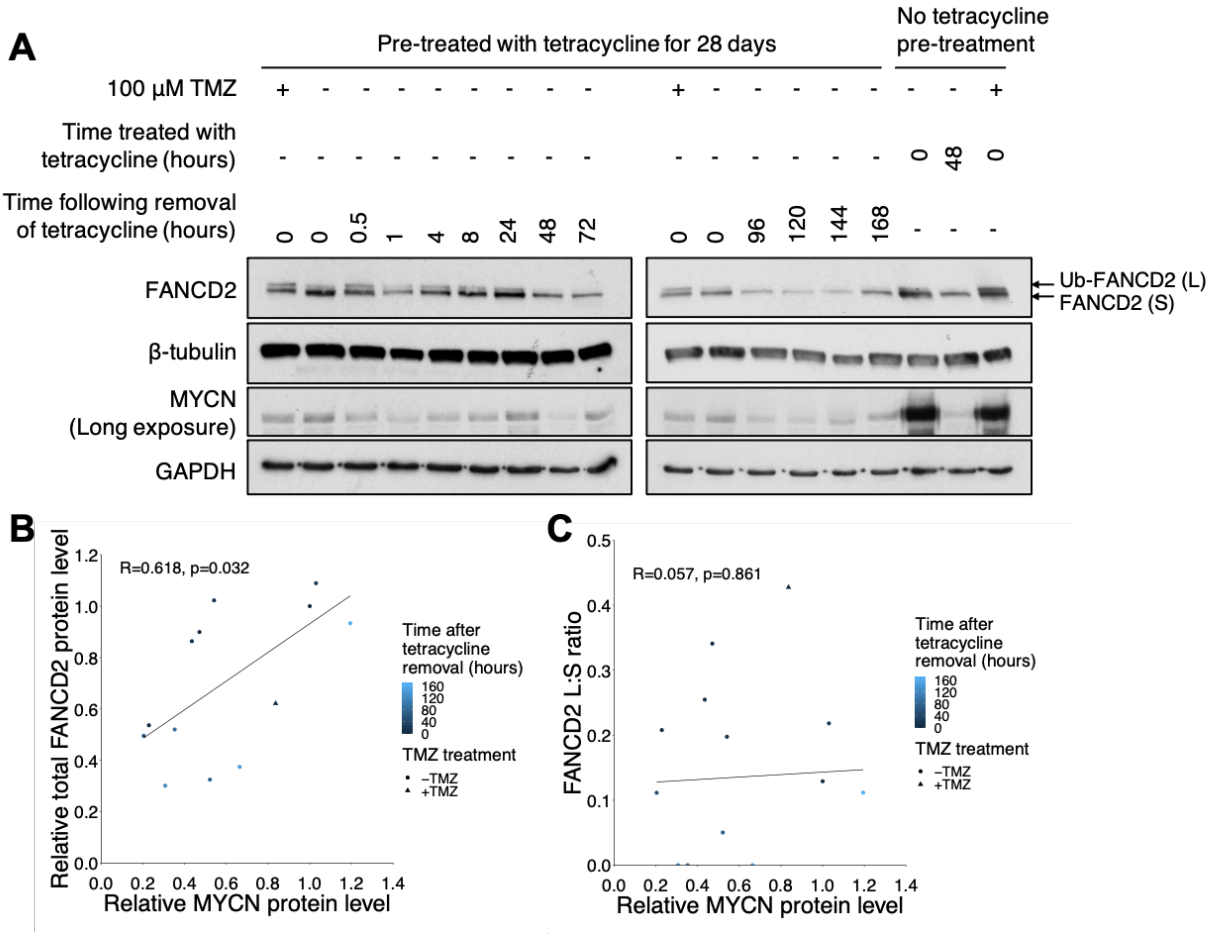

Figure 3.11. Treatment of SHEP-Tet21N cells with tetracycline for 28 days induces an irreversible MYCN OFF state.
SHEP-Tet21N MYCN ON cells were cultured in 1 µg/ml tetracycline to induce a MYCN OFF state for 28 days. Cells were then PBS washed and cultured without tetracycline for 0-168 hours in an attempt to re-induce a MYCN ON state. SHEP-Tet21N cells without tetracycline pre-treatment were treated with 1 µg/ml tetracycline for 0 and 48 hours and included for comparison of routinely used MYCN ON and OFF states respectively. Cells were treated with 100 µM temozolomide (TMZ) for 16 hours as a positive control for FA pathway activation. **(A)** MYCN and FANCD2 protein levels in cell lysates harvested at each timepoint were determined by western blotting (n=1). **(B)** Total FANCD2 (sum of L and S) and MYCN band intensities were quantified relative to 0 hour tetracycline removal (-TMZ) and normalised to ß-tubulin and GAPDH band intensities respectively. Relative total FANCD2 and MYCN protein level in all tetracycline pre-treated samples are plotted. **(C)** For all tetracycline pre-treated samples, FANCD2 L:S band intensity ratios were calculated and plotted against relative MYCN protein level. In (B and C) statistical significance of correlation between samples without TMZ treatment was determined by Pearson's correlation. R = Pearson's correlation coefficient, p = p-value.

3.2.1.6 Tetracycline treatment does not induce changes in FANCD2 protein levels

SHEP-1 is the parental cell line of both SHEP-Tet21N and SHEP-PLXI-MYCN cell lines and does not contain a tetracycline-regulated *MYCN* expression system. To confirm differential FANCD2 expression observed in SHEP-Tet21N and SHEP-PLXI-MYCN was due to the changes in *MYCN* expression, rather than the effect of tetracycline treatment itself, FANCD2 expression and mono-ubiquitination was analysed in SHEP-1 cells treated with 1 ⌠g/ml tetracycline for up to 7 days by western blotting (Figure 3.12A). Although fluctuations in FANCD2 expression are observed, tetracycline treatment did not result in maintained changes in FANCD2 expression (Figure 3.12B). Similarly, only a small reduction in FANCD2 mono-ubiquitination was observed following 48 to 168 hours tetracycline treatment in SHEP-1 cells in comparison to the undetectable levels of FA pathway activation observed following inhibition of *MYCN* expression in SHEP-Tet21N cells (Figure 3.12C). This data confirms that any regulation of FANCD2 was due to changes in *MYCN* expression, rather than tetracycline treatment.

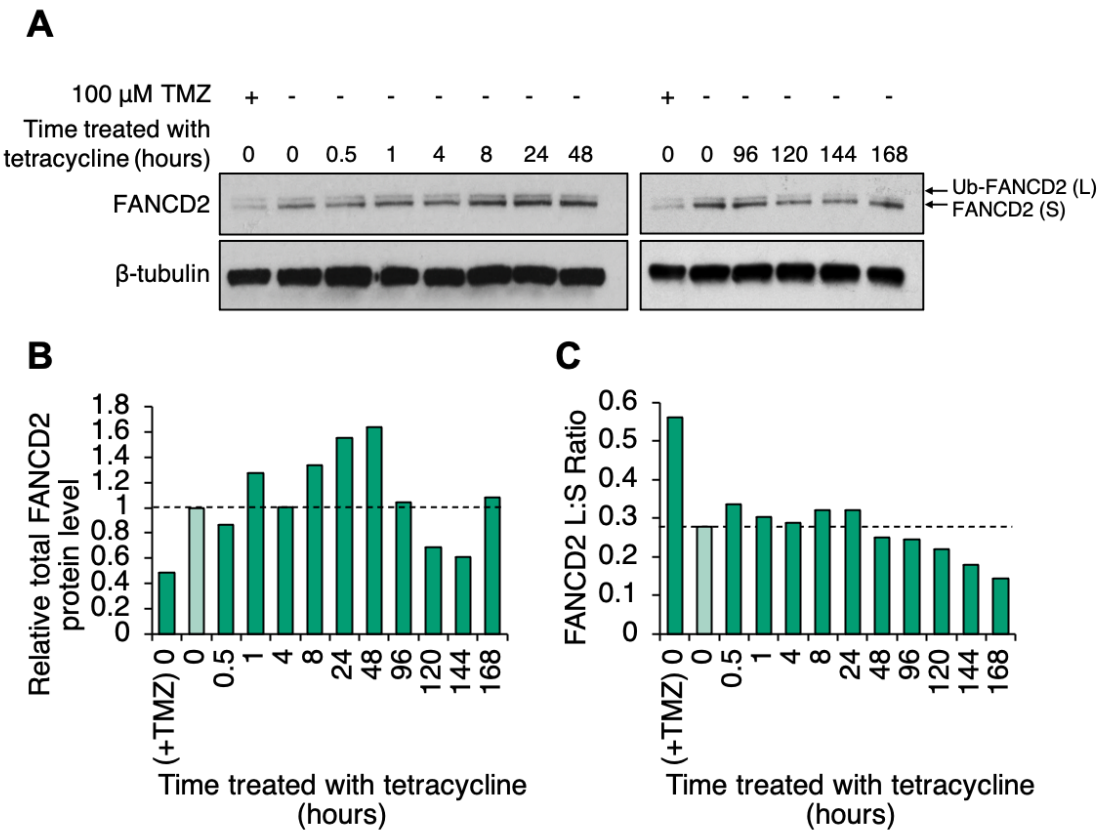

Figure 3.12. Tetracycline treatment does not induce a maintained downregulation of FANCD2 protein levels in MYCN non-amplified SHEP-1 cells.
SHEP-1 cells were treated with 1 µg/ml tetracycline for 0-168 hours. Cells were treated with 100 µM temozolomide (TMZ) for 16 hours as a positive control for FA pathway activation. **(A)** FANCD2 protein level at each indicated timepoint was determined by western blotting (n=1). **(B)** Total FANCD2 (sum of L and S) band intensity was quantified relative to 0 hour tetracycline treatment (-TMZ) and normalised to ß-tubulin band intensity. **(C)** FANCD2 L:S ratios were calculated relative to 0 hour tetracycline treatment (-TMZ).

3.2.1.7 Inhibition of MYCN expression in SHEP-Tet21N cells induces significant differential expression of FA pathway genes at the transcriptional level

To determine whether the MYCN-induced FANCD2 upregulation was occurring at a transcriptional level, and to expand analysis of the impact of *MYCN* overexpression on FA pathway expression to a greater number of genes, the mRNA expression of a panel of 25 FA pathway genes was analysed in SHEP-Tet21N cells by RT-qPCR. In parallel to the harvesting of cell lysates for FANCD2 and MYCN protein analysis (Figure 3.4), RNA samples were taken from SHEP-Tet21N cells following tetracycline treatment, over a seven day MYCN ON to OFF time-course. Following the MYCN ON to

OFF transition between 4-8 hours, 15 genes were downregulated and two genes were upregulated with a maintained $\log_2$(fold-change) greater than 0.5 (Figure 3.13; Appendix Table A1). Six of these genes showed significant downregulation at any point across the seven days: *FANCD2*, *FANCE*, *BRCA2*, *BRCA1*, *FANCI*, *BLM* (ANOVA, $p < 0.05$) (Appendix Table A2). *POLN* was the only gene significantly upregulated across the time-course ($F(12,26) = 9.09$, $p < 0.001$). Differential expression of FA pathway genes clustered according to FA pathway role. Downregulation is observed for all genes involved in HRR, ICL detection, the FA core complex and the FANCD2-FANCI complex, whilst most TLS and NER genes were upregulated or showed no substantial differential expression.

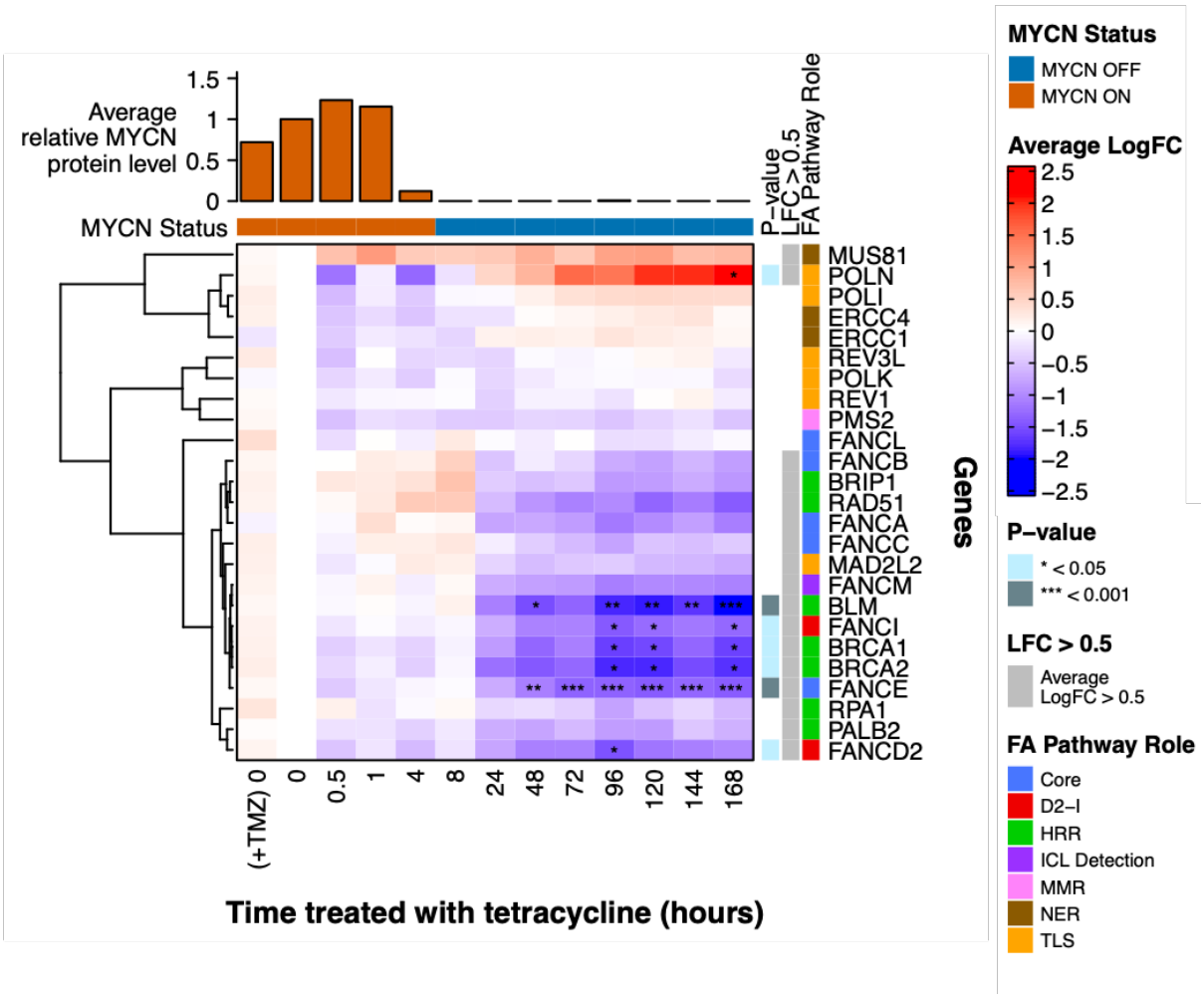

Figure 3.13. FA pathway associated genes are differentially expressed over a seven day MYCN ON to OFF time-course in SHEP-Tet21N cells.
SHEP-Tet21N MYCN ON cells were treated with 1 µg/ml tetracycline for 0-168 hours to induce a MYCN OFF state. MYCN ON cells were treated with 100 µM temozolomide (TMZ) for 16 hours as a positive control for FA pathway activation. Total RNA was extracted from cells at indicated timepoints and reverse transcribed into cDNA. The mRNA expression level of 25 FA pathway associated genes was analysed by qPCR using TaqMan probes. The $\log_2$(fold-change) in expression of each gene was calculated at each timepoint relative to 0 hour tetracycline treatment (-TMZ) using the $2^{-\Delta\Delta CT}$ method. Average $\log_2$(fold-change) (Average LogFC) is presented (n=3). Statistical significance between 0 hour tetracycline treatment (-TMZ) and all other treatments was determined for each gene by a one-way ANOVA and Tukey HSD post-hoc test using dCt values, where *p < 0.05, **p < 0.01, ***p < 0.001. 'P-value' annotation displays the highest significance level observed across all timepoints for each gene. 'LFC > 0.5' annotation identifies genes with an average $\log_2$(fold-change) consistently greater than 0.5. Genes are clustered by Pearson correlation analysis. Genes are annotated by 'FA Pathway Role'; Core; FA core complex, D2-I; FANCD2-FANCI complex, HRR; homologous recombination repair, ICL detection; inter-strand crosslink detection, MMR; mis-match repair, NER; nucleotide excision repair, TLS; translesion synthesis. 'MYCN Status' at each timepoint was determined by average MYCN protein level (n=3), analysed by western blotting of cell lysates prepared in parallel to RNA extraction and quantified relative to 0 hour tetracycline treatment (-TMZ); representative western blot images are shown in Figure 3.5.

In parallel with this RT-qPCR analysis, and in collaboration with Dr Anestis Tsakiridis' laboratory group at the University of Sheffield and Dr. Florian Halbritter's laboratory group at St. Anna Children's Cancer Research Institute (CCRI), whole cell RNA-seq analysis was undertaken for SHEP-Tet21N MYCN ON and OFF cells. Raw read analysis was undertaken by Dr Luis Montano-Gutierrez at St. Anna CCRI to produce raw count data. We then used DESeq2 to study the effect of *MYCN* overexpression on the expression of all 23 FANC genes and the 32 remaining KEGG-defined FA pathway genes. Parallel analysis of 12 DNA damage repair and neuroblastoma-associated genes, for many of which MYCN-induced differential expression has been previously observed, were used as controls for expected expression changes (Breit and Schwab, 1989; Slack et al., 2005; Otto et al., 2009; Chen et al., 2010; Cole et al., 2011; Gu et al., 2015; Ke et al., 2015; Petroni et al., 2016; Petroni et al., 2018; Yin et al., 2019; King et al., 2020). 19 FA pathway genes were significantly upregulated and one FA pathway gene was significantly downregulated in MYCN ON compared to OFF cells (Student's t-test, $p < 0.05$; $\log_2$(fold-change) > 0.5) (Figure 3.14A; Appendix Table A3).

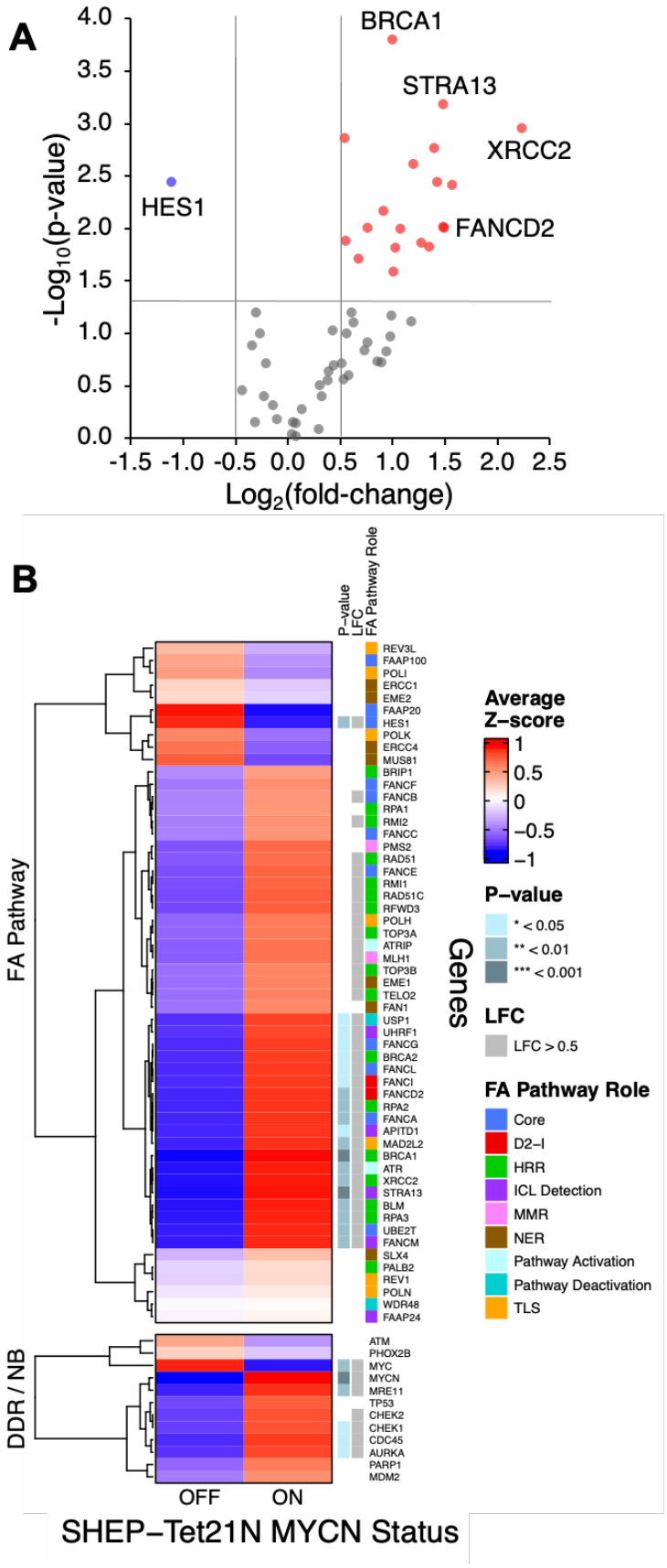

Figure 3.14. FA pathway associated genes are significantly differentially expressed between MYCN ON and MYCN OFF states in SHEP-Tet21N cells. (Legend overleaf).

Figure 3.14. FA pathway associated genes are significantly differentially expressed between MYCN ON and MYCN OFF states in SHEP-Tet21N cells. SHEP-Tet21N MYCN ON cells were treated with 1 µg/ml tetracycline for 48 hours to induce a MYCN OFF state. mRNA expression of 55 FA pathway associated genes and 12 DNA damage repair (DDR) or key neuroblastoma-associated (NB) genes were analysed in SHEP-Tet21N MYCN ON and MYCN OFF cells (n=3) by RNA-Seq. Differential expression analysis was undertaken using DESeq2. A regularised log2 (rlog) transformation was applied to the normalised count data, from which statistical significance of differential expression was determined for each gene by a Student's t-test or Mann Whitney U test, depending on data distribution. **(A)** Volcano plot of FA pathway associated genes. Each dot represents one gene. Grey dots represent genes with no significant differential expression or $\log_2$(fold-change)<0.5. Red and blue dots represent significantly upregulated and downregulated genes respectively with a $\log_2$(fold-change)>0.5. **(B)** rlog-transformed normalised count data was used to calculate Z-scores independently for each gene in all samples (n=3). The average Z-score in MYCN ON and MYCN OFF cells is presented. Genes are clustered by k-means analysis. 'P-value' annotation displays statistical significance of differential expression. 'LFC' indicates which genes show a $\log_2$(fold-change)>0.5. Genes are annotated by 'FA Pathway Role'; Core; FA core complex, D2-I; FANCD2-FANCI complex, HRR; homologous recombination repair, ICL detection; inter-strand crosslink detection, MMR; mis-match repair, NER; nucleotide excision repair, TLS; translesion synthesis.

As observed by RT-qPCR (Figure 3.13), differential expression of FA pathway genes clustered according to their FA pathway role. Predominantly, downregulation or no change in expression was observed for TLS and NER genes, whereas genes in all other FA pathway roles were primarily upregulated following *MYCN* expression (Figure 3.14B; Appendix Figure A2; Appendix Tables A4-A5). For example, similarly to that observed by RT-qPCR, *FANCD2* was significantly upregulated in MYCN ON cells, by a $\log_2$(fold-change) of 1.5 ($t(4) = -4.6$, $p = 0.010$) (Figure 3.15A). *FANCD2* expression was also significantly correlated with *MYCN* expression in SHEP-Tet21N cells ($r(4) = 0.925$, $p = 0.008$) (Figure 3.15C). The TLS gene *REV3L* showed no significant differential expression between MYCN ON and OFF states ($p > 0.05$) (Figure 3.15B) and no significant correlation with *MYCN* expression levels ($p > 0.05$) (Figure 3.15D). In general, most FA pathway genes were transcriptionally upregulated when *MYCN* was expressed, which is consistent with the FANCD2 protein expression changes seen above. This is summarised in Figure 3.16.

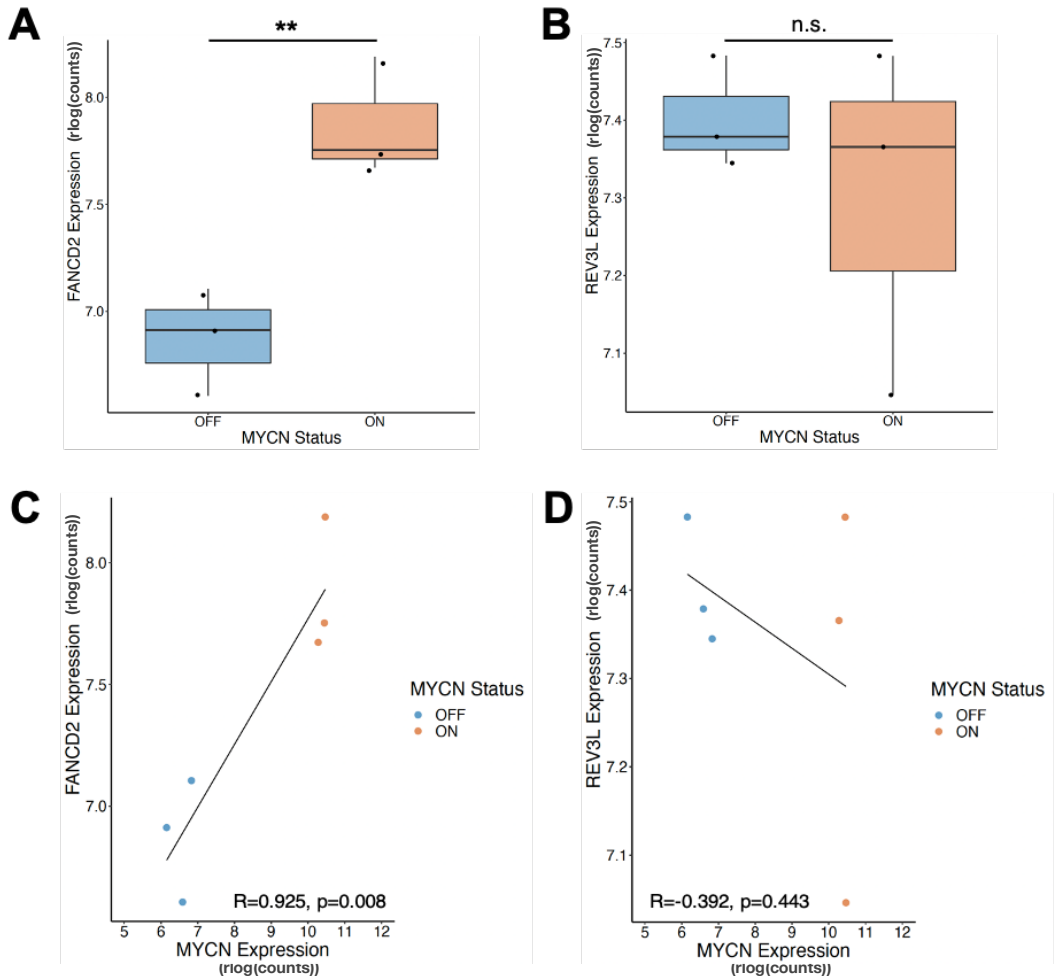

Figure 3.15. RNA-Seq shows FANCD2 is significantly upregulated and REV3L is not differentially expressed in MYCN ON compared to MYCN OFF SHEP-Tet21N cells.
SHEP-Tet21N MYCN ON cells were treated with 1 µg/ml tetracycline for 48 hours to induce a MYCN OFF state. mRNA expression of FANCD2 and REV3L was analysed in SHEP-Tet21N MYCN ON and MYCN OFF cells using RNA-Seq and DESeq2 (n=3). Boxplots display regularised log2 (rlog) transformed normalised count data of **(A)** FANCD2 and **(B)** REV3L in MYCN ON and OFF states. Statistical significance in (A) and (B) was determined by Student's t-test where n.s. = non-significant, *p<0.05, **p<0.01, ***p<0.001. rlog-transformed normalised count data of MYCN was plotted against that of **(C)** FANCD2 and **(D)** REV3L for each repeat. Points are coloured according to MYCN status. Statistical significance in (C) and (D) was determined by Pearson's correlation; R = Pearson's correlation coefficient, p = p-value.

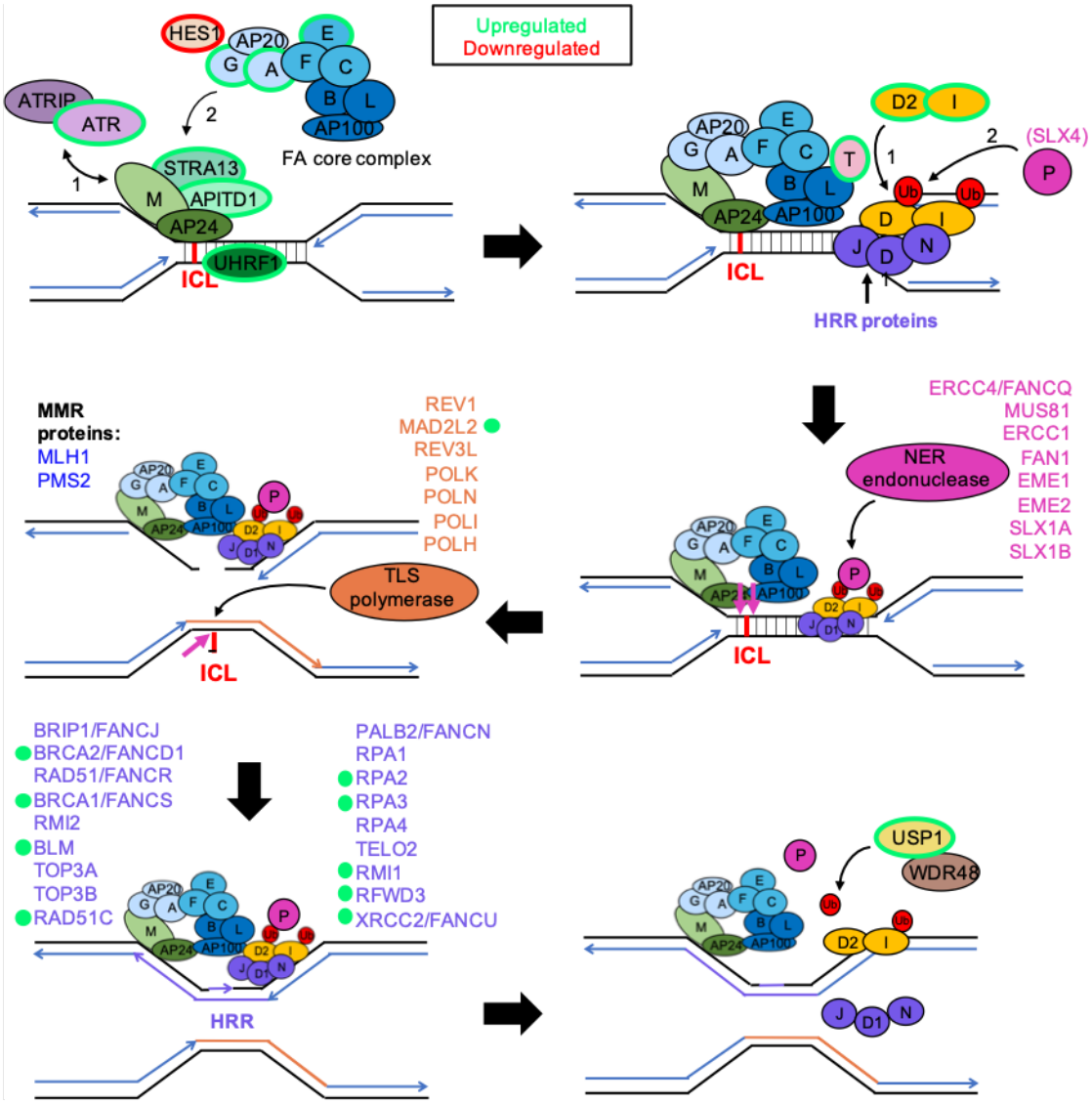

Figure 3.16. MYCN-induced differential expression of FA pathway genes clusters according to FA pathway role.
Summary of the differential expression of all 58 FA pathway genes observed in MYCN ON compared to MYCN OFF SHEP-Tet21N cells by RNA-seq, as displayed in Figure 3.14. Green outline/dot represents genes that are significantly upregulated ($p < 0.05$) in MYCN ON compared to OFF cells with a $\log_2$(fold-change) > 0.5. Red outline/dot represents genes that are significantly downregulated ($p < 0.05$) in MYCN ON compared to OFF cells with a $\log_2$(fold-change) < -0.5. Differential expression analysis was undertaken using DESeq2. Statistical significance of differential expression was determined for each gene by a Student's t-test or Mann Whitney U test, depending on data distribution.

As well as looking specifically at FA pathways genes, the whole RNA-seq data set was analysed. Genes with the greatest differential expression between MYCN ON and OFF cells were identified (Appendix Figure A3; Appendix Tables A6-A7), and the

top 10 most enriched gene ontologies and KEGG pathways in the set of significantly upregulated and downregulated genes were determined. Although DNA repair was not one of the top 10 significantly enriched gene ontologies (Appendix Figure A4; Appendix Table A8), KEGG pathway enrichment analysis identified the FA pathway to be the eighth most enriched pathway in the set of significantly upregulated genes in MYCN ON cells (Figure 3.17; Appendix Table A9).

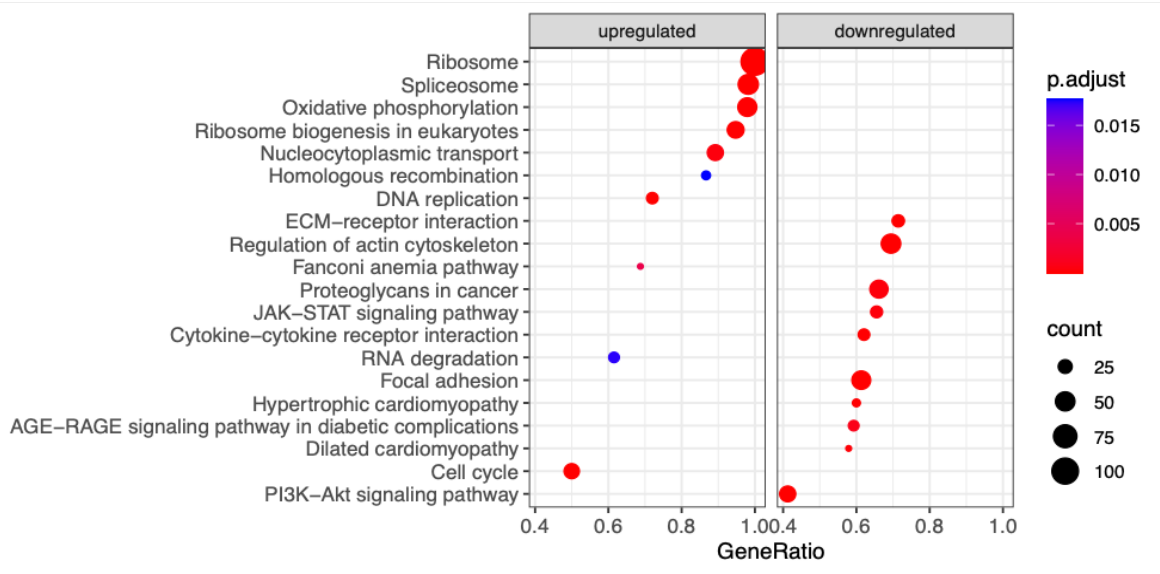

Figure 3.17. The FA pathway is one of the top 10 most enriched KEGG pathways in all significantly upregulated genes in MYCN ON compared to MYCN OFF SHEP-Tet21N cells.
SHEP-Tet21N MYCN ON cells were treated with 1 µg/ml tetracycline for 48 hours to induce a MYCN OFF state. Global mRNA expression was analysed in SHEP-Tet21N MYCN ON and MYCN OFF cells by RNA-Seq (n=3). Log_2(fold-change) and significance of differential expression between MYCN ON and MYCN OFF cells was analysed using DESeq2. Significantly enriched KEGG pathways in the set of significantly upregulated ($p < 0.05$, log_2(fold-change) > 0.5) and downregulated ($p < 0.05$, log_2(fold-change) < -0.5) genes was determined. Top 10 most enriched KEGG pathways in upregulated and downregulated genes are presented. Gene ratio represents the fraction of genes within each KEGG pathway that is significantly differentially expressed. Points coloured by significance of enrichment (p.adjust) and sized according to number of genes significantly differentially expressed (count).

3.2.2 FA pathway expression inconsistently correlates with *MYCN* expression and amplification status across neuroblastoma cell lines

3.2.2.1 FANCD2 protein expression correlates with MYCN protein expression across neuroblastoma cell lines

It has been previously demonstrated that *MYCN* amplification status does not always correlate with *MYCN* expression (Bordow et al., 1998). To determine whether the MYCN-induced *FANCD2* upregulation observed in isogenic tet-regulated models is representative of the effects of *MYCN* amplification, protein expression of FANCD2, MYCN and MYCC was analysed across a panel of neuroblastoma cell lines by western blot (Figure 3.18A). Total FANCD2 expression significantly correlated with MYCN expression across MNA (IMR32, Kelly), non-MNA (SHEP-1), and MYCN-inducible (SHEP-Tet21N, SHEP-PLXI-MYCN) cell lines (excluding SH-SY5Y as an outlier) ($r_s(5) = 0.955$, $p < 0.001$) (Figure 3.18B). MYCN expression also non-significantly correlated with FA pathway activation (again, excluding SH-SY5Y as an outlier) ($r_s(5) = 0.613$, $p > 0.05$) (Figure 3.18C). Higher *MYCC* expression is often observed in non-MNA neuroblastoma cell lines and tumours (Breit and Schwab, 1989; Westermann et al., 2008). Similarly, we observed higher MYCC protein levels in non-MNA and MYCN OFF cells (Figure 3.18A). SH-SY5Y displayed high FANCD2 expression and FA pathway activation, despite its lack of MYCN expression (Figure 3.18B-C). This could be partially accounted for by its relatively high MYCC expression.

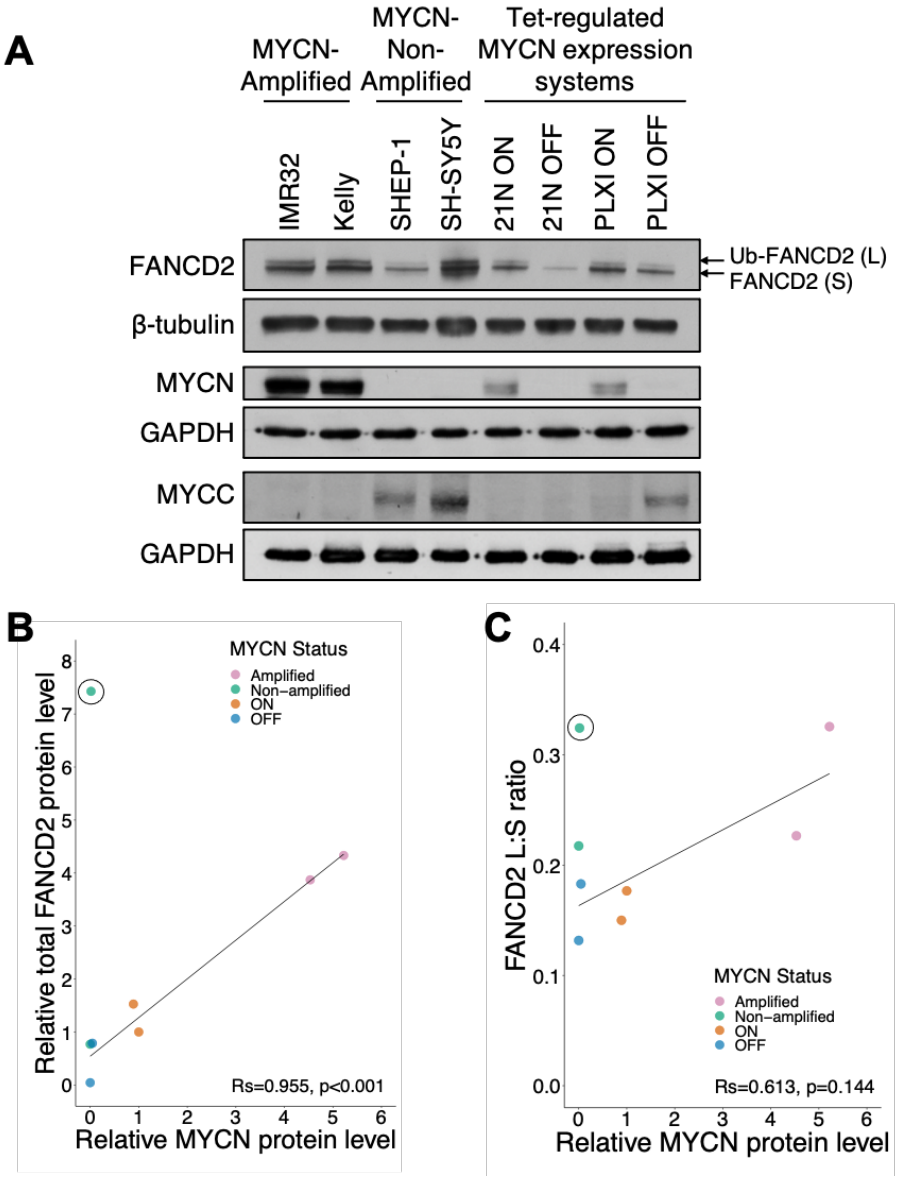

Figure 3.18. FANCD2 expression correlates with MYCN expression across neuroblastoma cell lines.
Cell lysates were harvested from a panel of MYCN amplified (IMR32, Kelly), MYCN non-amplified (SHEP-1, SH-SY5Y) and MYCN inducible (SHEP-Tet21N, SHEP-PLXI-MYCN) neuroblastoma cell lines. A MYCN OFF state was induced in SHEP-Tet21N cells by 48 hours treatment with 1 µg/ml tetracycline. A MYCN ON state was induced in SHEP-PLXI-MYCN cells by 48 hours treatment with 0.5 µg/ml doxycycline. **(A)** FANCD2, MYCN and MYCC protein levels were determined by western blotting (n=1). **(B)** Total FANCD2 (sum of L and S) and MYCN band intensities were quantified relative to SHEP-Tet21N MYCN ON and normalised to ß-tubulin and GAPDH band intensities respectively. **(C)** FANCD2 L:S ratios were calculated relative to SHEP-Tet21N MYCN ON and plotted against MYCN protein level. For (B) and (C), cell lines are coloured according to MYCN status. Statistical significance of correlation (excluding SH-SY5Y as an outlier as circled in plot) was determined by Spearman's correlation. Rs = Spearman's rank correlation coefficient, p = p-value.

To validate the correlation in expression between MYCN and FANCD2, FANCD2 expression was analysed in MNA IMR32 cells by western blotting following siRNA-mediated MYCN depletion (Figure 3.19A). 24 and 48 hours following double transfection with a pool of MYCN-targeted siRNAs, the average MYCN protein level was significantly reduced to 35% ($t(4) = 7.25$, $p = 0.002$) and 41% ($t(4) = 3.17$, $p = 0.034$) of that in the scrambled siRNA control respectively (Figure 3.19B). However, there were no significant changes in the FANCD2 protein level or FA pathway activation level following MYCN depletion (Student's t-test, $p > 0.05$) (Figure 3.19B-C). This could be because there was residual MYCN expression after depletion, and therefore the depletion was unable to reduce MYCN levels to below the threshold required to induce changes in FANCD2 expression.

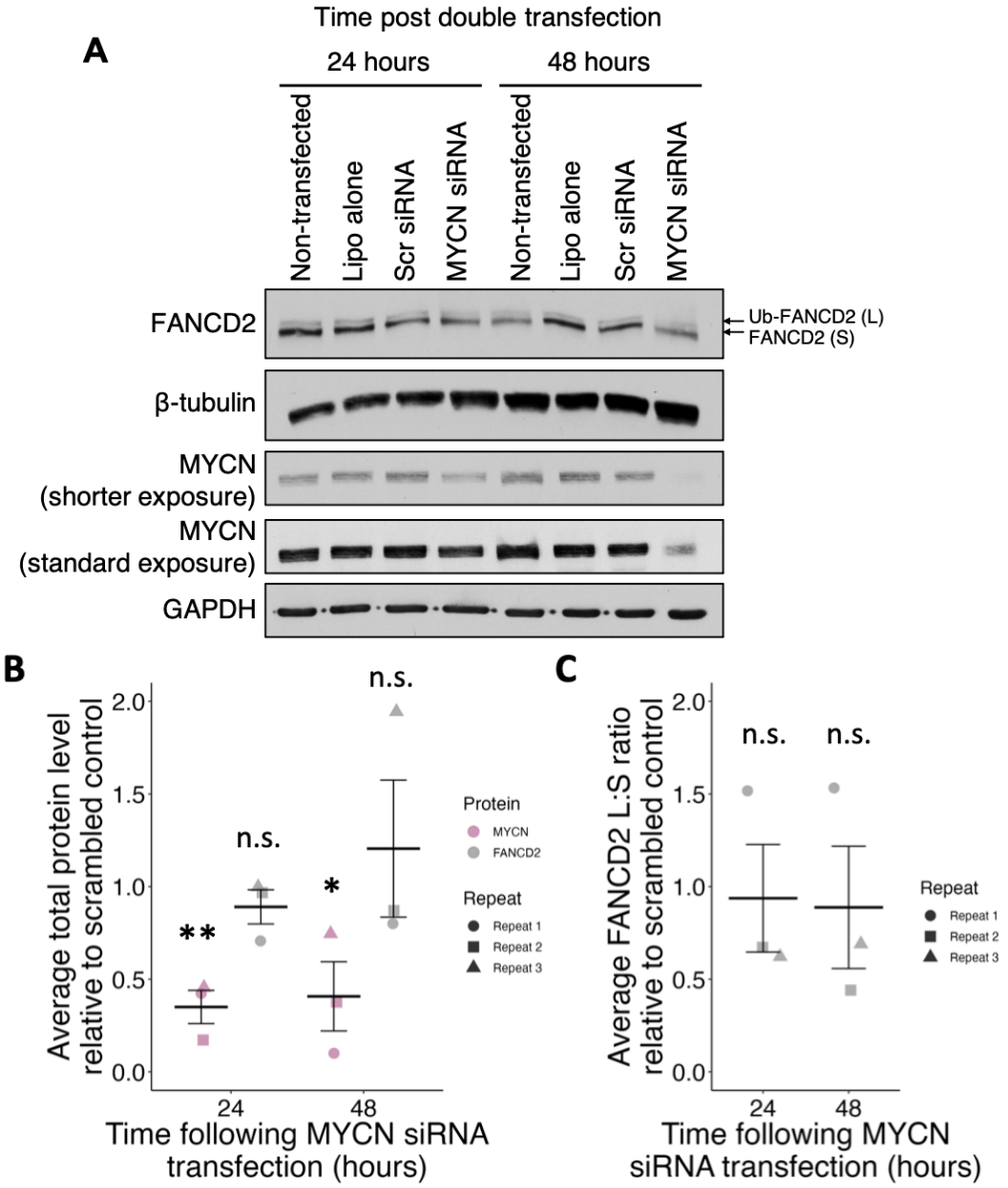

Figure 3.19. MYCN depletion by siRNA in IMR32 cells does not affect FANCD2 expression or FA pathway activation.
MYCN amplified IMR32 cells were non-transfected or doubly transfected with lipofectamine alone, a pool of scrambled siRNAs, or a pool of MYCN siRNAs. **(A)** Cell lysates were harvested 24 and 48 hours following the second transfection and FANCD2 and MYCN protein levels were determined by western blotting (n=3). A shorter exposure of MYCN is shown to better represent MYCN depletion. **(B)** Total FANCD2 (sum of L and S) and MYCN band intensities in the MYCN siRNA transfected sample were quantified relative to that in the scrambled siRNA transfected sample. Total FANCD2 and MYCN band intensities were normalised to ß-tubulin and GAPDH band intensities respectively. **(C)** FANCD2 L:S ratios in the MYCN siRNA transfected sample were calculated relative to that in the scrambled siRNA transfected sample. For (B) and (C), statistical significance of the difference in protein level in MYCN siRNA transfected samples compared to scrambled siRNA transfected samples was determined by Student's t-test at each timepoint where n.s. = non-significant, *p<0.05, **p<0.01, ***p<0.001.

3.2.2.2 FA pathway differential expression between MYCN-amplified and MYCN non-amplified neuroblastoma cell lines is not consistently observed at an mRNA level

The impact of *MYCN* amplification on the expression of a wider array of FA pathway associated genes was determined by RT-qPCR and RNA-Seq. Using RT-qPCR, the mRNA expression of a panel of 25 FA pathway genes, previously analysed in SHEP-Tet21N cells, was analysed in two MNA (IMR32, Kelly) and two non-MNA (SHEP-1, SH-SY5Y) cell lines (Figure 3.20; Appendix Table A10). In comparison to non-MNA SHEP-1 cells, 13 FA pathway genes were upregulated with a $\log_2$(fold-change) greater than 0.5 in both Kelly and IMR32 MNA cell lines. Of these, 12 genes showed significant upregulation in both cell lines: *FANCM, RPA1, PALB2, FANCD2, FANCL, FANCA, BLM, BRCA1, RAD51, FANCB, FANCC, FANCI* (ANOVA, $p < 0.05$) (Appendix Table A11). Significant *FANCD2* upregulation in MNA cells was therefore confirmed at the transcriptional level, with a $\log_2$(fold-change) of 1.5 in both MNA cell lines ($F(3,8) = 102.64$, $p < 0.001$). Seven genes showed downregulation or no substantial change in expression in both MNA cell lines. Of these, only one gene was significantly downregulated with a $\log_2$(fold-change) greater than 0.5 in both cell lines: *MUS81* ($F(3,8) = 77.77$, $p < 0.001$).

As seen previously with *MYCN* overexpression in SHEP-Tet21N cells (Figures 3.13, 3.14), *MYCN* amplification-associated changes in FA pathway expression clustered according to FA pathway roles. All genes upregulated in both MNA cell lines are involved in the FA core complex, FANCD2-FANCI complex, HRR or ICL detection (Figure 3.20). All genes which were downregulated or showed no substantial change in expression in both MNA cells lines are involved in TLS and NER. Similarly to both MNA cell lines, 18 FA pathway genes were significantly upregulated in non-MNA SH-SY5Y cells compared to SHEP-1 cells (ANOVA, $p < 0.05$; $\log_2$(fold-change) > 0.5) and 7 genes showed no significant change in expression, all of which have roles in TLS and NER. However, no substantial downregulation of TLS or NER genes was observed as in the MNA cell lines.

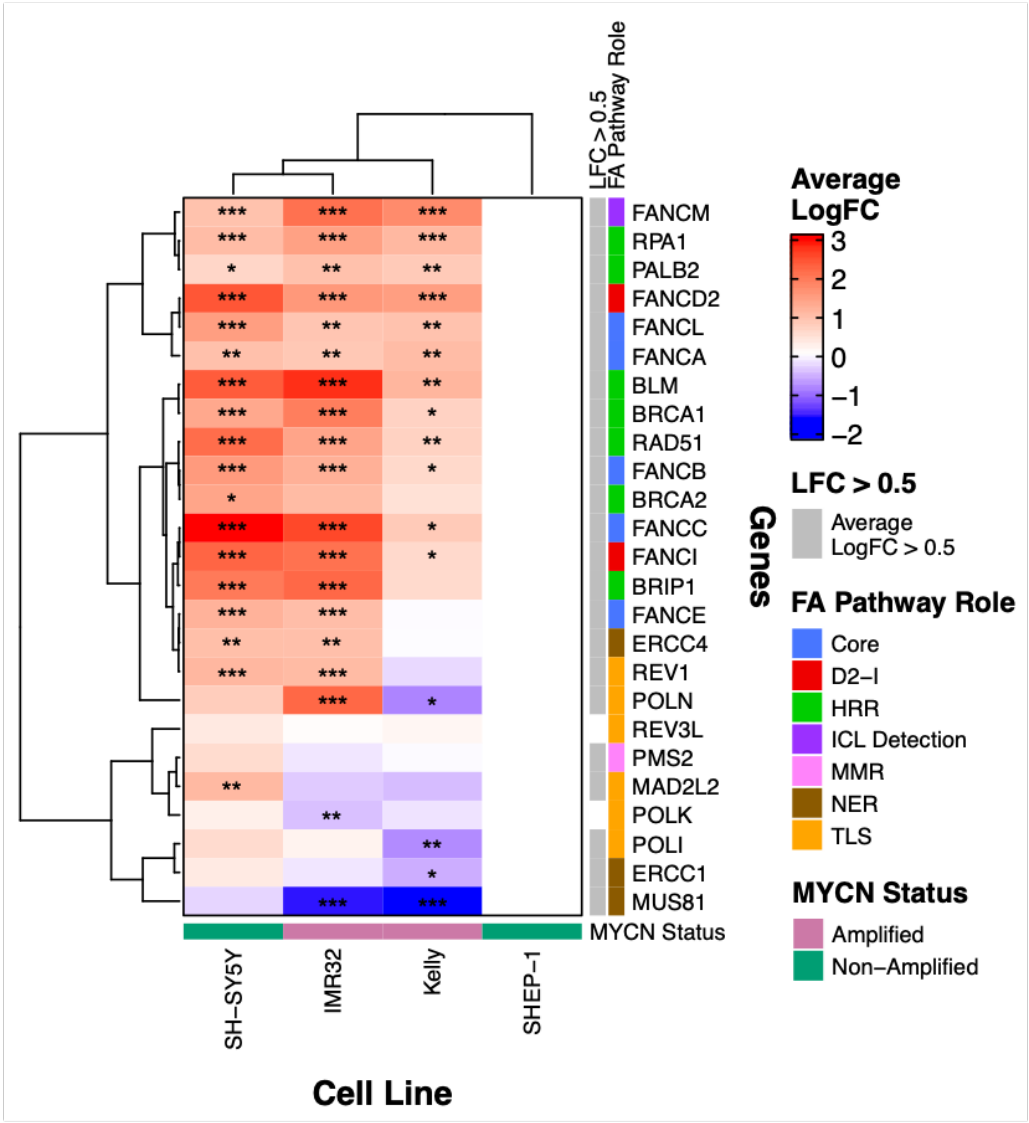

Figure 3.20. FA pathway associated genes are differentially expressed across MYCN amplified and MYCN non-amplified neuroblastoma cell lines.
Total RNA was extracted from MYCN amplified (Kelly, IMR32) and MYCN non-amplified (SHEP-1, SH-SY5Y) neuroblastoma cell lines and reverse transcribed into cDNA. The mRNA expression level of 25 FA pathway associated genes was analysed in each cell line by qPCR using TaqMan probes. The $\log_2$(fold-change) in expression of each gene was calculated for each cell line using the $2^{-\Delta\Delta CT}$ method relative to average SHEP-1 dCt values. Average $\log_2$(fold-change) in expression in SH-SY5Y, IMR32 and Kelly relative to SHEP-1 is presented (n=3). Statistical significance of expression differences between SHEP-1 and all other cell lines was determined for each gene by a one-way ANOVA and Tukey HSD post-hoc test using dCt values, where *p < 0.05, **p < 0.01, ***p < 0.001. 'LFC > 0.5' annotation identifies genes with an average $\log_2$(fold-change) greater than 0.5 in at least one cell line. Cell lines are annotated by MYCN amplification status. Genes and cell lines are clustered by Pearson correlation analysis. Genes are annotated by 'FA Pathway Role'; Core; FA core complex, D2-I; FANCD2-FANCI complex, HRR; homologous recombination repair, ICL detection; inter-strand crosslink detection, MMR; mis-match repair, NER; nucleotide excision repair, TLS; translesion synthesis.

Using the GSE89413 RNA-Seq dataset and DESeq2, the effect of *MYCN* amplification on the mRNA expression of all 58 FA pathway associated genes and 13 key DDR and neuroblastoma-associated genes was analysed across 39 neuroblastoma cell lines. Only three FA pathway genes were significantly upregulated with a $\log_2$(fold-change) greater than 0.5 in MNA compared to non-MNA cell lines; *XRCC2* ($t(37) = 3.37$, $p = 0.002$), *BRCA1* ($W = 260$, $p = 0.002$) and *FANCA* ($t(37) = 2.24$, $p = 0.031$) (Figure 3.21A; Appendix Table A12). *SLX1B* was the only FA pathway gene significantly downregulated in MNA cell lines ($t(37) = -2.52$, $p = 0.016$; $\log_2$(fold-change) > 0.5). Differential expression of FA pathway genes did not cluster according to FA pathway role as previously observed (Figure 3.21B; Appendix Table A13). In contrast to previous results, expression of both *FANCD2* and *REV3L* was not significantly different between *MYCN* amplification subgroups (Student's t-test, $p > 0.05$; $\log_2$(fold-change) < 0.5) (Figure 3.22A-B) and did not significantly correlate with *MYCN* expression across cell lines (Pearson's correlation, $p > 0.05$) (Figure 3.22C-D). DESeq2 was also used to analyse the effect of other common neuroblastoma aberrations, such as 1p36 deletion, 3p26 deletion, 11q23 deletion, 17q gain and *ALK* mutation, on FA pathway expression across the 39 neuroblastoma cell lines. No significant differential FA pathway expression was observed between cell lines with and without these aberrations (Appendix Table A14-A15; Appendix Figure A5).

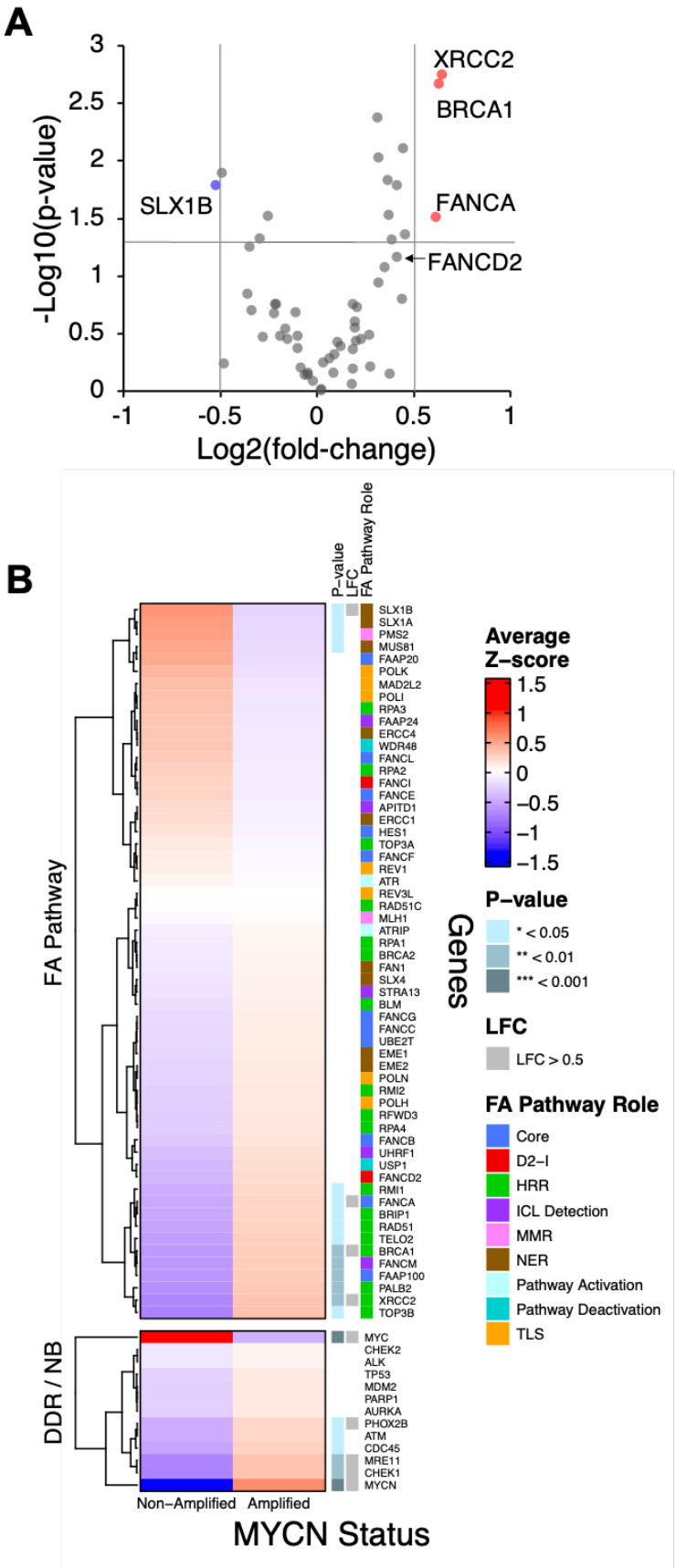

Figure 3.21. FA pathway genes show limited differential expression between neuroblastoma cell lines with different MYCN amplification statuses.
(Legend overleaf).

Figure 3.21. FA pathway genes show limited differential expression between neuroblastoma cell lines with different MYCN amplification statuses.
mRNA expression of 58 FA pathway associated genes and 13 DNA damage repair (DDR) or key neuroblastoma-associated (NB) genes was analysed in 39 neuroblastoma cell lines using the GSE89413 RNA-Seq dataset (n=1). Differential expression between MYCN amplified and MYCN non-amplified cell lines was analysed using DESeq2. A regularised log2 (rlog) transformation was applied to the normalised count data, from which statistical significance of differential expression was determined for each gene by a Student's t-test, Welch t-test or Mann Whitney U test, depending on data distribution. **(A)** Volcano plot of FA pathway associated genes. Each dot represents one gene. Grey dots represent genes with no significant differential expression or log_2(fold-change)<0.5. Red and blue dots represent significantly upregulated and downregulated genes respectively with a log_2(fold-change)>0.5. (B) rlog-transformed normalised count data was used to calculate Z-scores independently for each gene across all 39 cell lines. The average Z-score in MYCN amplified and MYCN non-amplified subgroups is presented. Genes are clustered by k-means analysis. 'P-value' annotation displays the statistical significance of differential expression. 'LFC' indicates which genes show a log_2(fold-change)>0.5. Genes are annotated by 'FA pathway role': Core; FA core complex, D2-I; FANCD2-FANCI complex, HRR; homologous recombination repair, ICL detection; inter-strand crosslink detection, MMR; mis-match repair, NER; nucleotide excision repair, TLS; translesion synthesis.

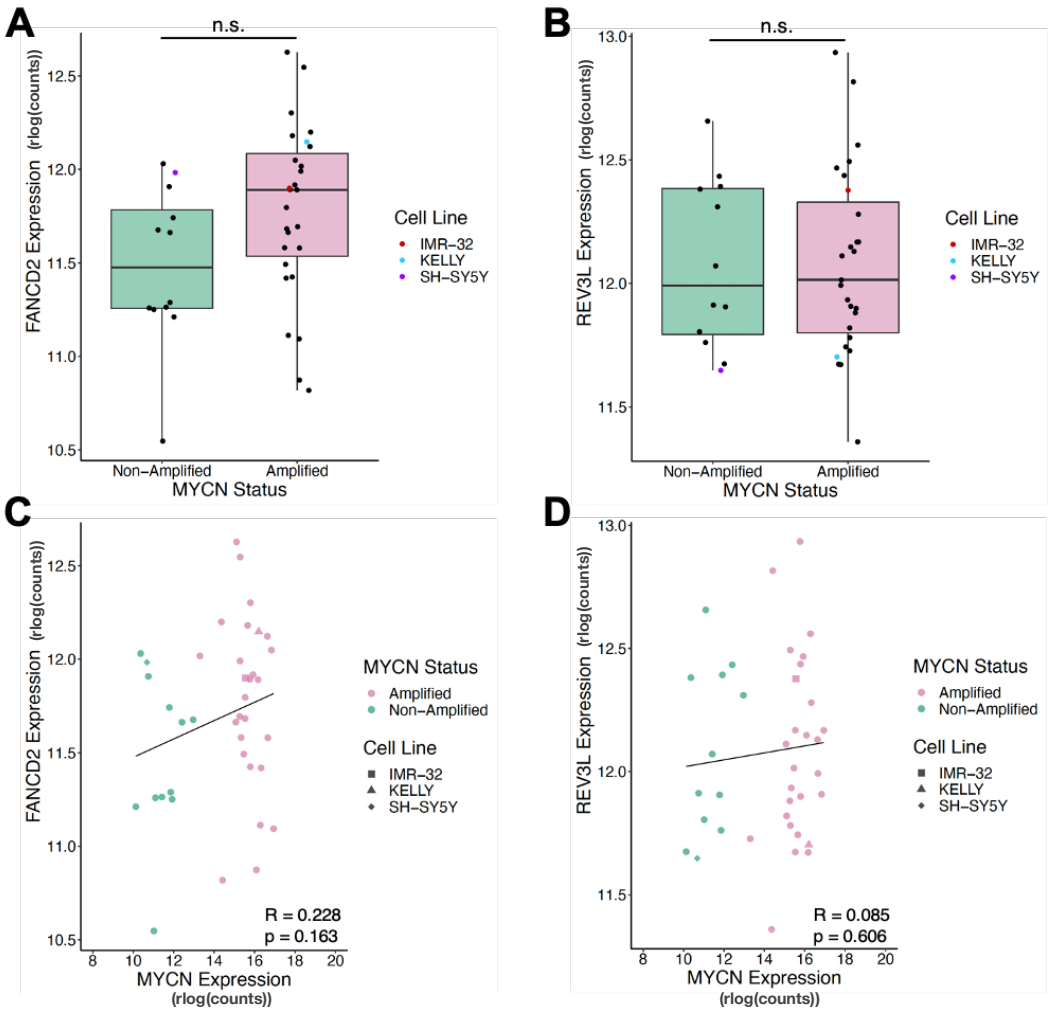

Figure 3.22. RNA-Seq shows FANCD2 and REV3L are not significantly differentially expressed between MYCN amplified and MYCN non-amplified neuroblastoma cell lines.
mRNA expression of FANCD2 and REV3L was analysed in 39 neuroblastoma cell lines using the GSE89413 RNA-Seq dataset (n=1) and DESeq2. Boxplots display regularised log2 (rlog) transformed normalised count data of **(A)** FANCD2 and **(B)** REV3L in MYCN amplified and MYCN non-amplified cell lines. Statistical significance in (A) and (B) was determined by Student's t-test where n.s. = non-significant, *p<0.05, **p<0.01, ***p<0.001. Cell lines used previously in RT-qPCR analysis of FA pathway gene expression (Figure 3.19) are indicated by colour. rlog-transformed normalised count data of MYCN was plotted against that of **(C)** FANCD2 and **(D)** REV3L for each cell line. Points are coloured by MYCN status. Statistical significance in (C) and (D) was determined by Pearson's correlation; R = Pearson's correlation coefficient, p = p-value. Cell lines used previously in RT-qPCR analysis of FA pathway gene expression (Figure 3.19) are indicated by point shape.

Global analysis of top differentially expressed genes between MNA and non-MNA cells was undertaken (Appendix Figure A6; Appendix Tables A16-A17), and the top 10 enriched gene ontology terms and KEGG pathways in the set of significantly differentially expressed genes was determined. DNA repair was not within the top 10 enriched ontology terms, however multiple RNAPII regulatory DNA binding ontologies were within the top 10 upregulated terms (Appendix Figure A7; Appendix Table A18), highlighting the previously observed transcriptional addiction in MNA cells (Bradner et al., 2017; Decaesteker et al., 2018; Durbin et al., 2018). The only KEGG pathway term significantly enriched in the upregulated genes was 'Ribosome' (Appendix Figure A8; Appendix Table A19).

This expression data across the 39 neuroblastoma cell lines does not support the findings of differential expression at the transcriptional and protein level observed in *MYCN*-inducible cell lines and across a smaller panel of neuroblastoma cell lines.

3.2.3 FA pathway associated genes are predominantly upregulated in *MYCN*-amplified compared to *MYCN* non-amplified neuroblastoma tumours

In comparison to *MYCN*-inducible cell lines, there was a lack of significant differential expression of FA pathway genes upon *MYCN* amplification across a broad panel of neuroblastoma cell lines. Previous studies have suggested the detrimental effects of *MYCN* amplification are better correlated with the extent of MYCN protein overexpression (Valentijn et al., 2012). In addition, the impact of *MYCN* amplification may be masked by the effect of other genetic differences between cell lines. To determine the effect of *MYCN* amplification on FA pathway expression in neuroblastoma tumours, the mRNA expression of 58 FA pathway associated genes and 13 key DDR and neuroblastoma-associated genes was analysed across 493 neuroblastoma tumours using the GSE62564 RNA-Seq data set and the R2: Genomics Analysis and Visualisation Platform (http://r2.amc.nl). 37 FA pathway genes were significantly upregulated in MNA compared to non-MNA tumours (Student's t-test, $p < 0.05$), of which 16 genes had a $\log_2$(fold-change) greater than 0.5 (Figure 3.23A; Appendix Table A20). 14 FA pathway genes were significantly downregulated in MNA neuroblastoma (Student's t-test, $p < 0.05$), of which four were downregulated by a $\log_2$(fold-change) greater than 0.5. Notably, seven of these 14 genes were TLS or NER genes (Figure 3.23B; Appendix Table A21). MNA-associated FA pathway differential expression in tumours therefore correlated with FA pathway role, with predominant

upregulation of FA pathway activation, FA core complex, FANCD2-FANCI complex, HRR and ICL detection genes, but downregulation of most TLS genes observed. For example, whilst *FANCD2* was significantly upregulated by a $\log_2$(fold-change) of 0.97 in MNA tumours ($t(491) = 10.19$, $p < 0.001$) (Figure 3.24A), the TLS gene *REV3L* was significantly downregulated by a $\log_2$(fold-change) of -0.63 ($t(491) = -11.51$, $p < 0.001$) (Figure 3.24B).

To validate that the differential expression observed between *MYCN* amplification status subgroups was due to differences in *MYCN* expression, the correlation between expression of each FA pathway gene and *MYCN* was determined. Expression of all genes that were significantly upregulated or downregulated in MNA tumours (LFC>0.5, p<0.05), also significantly correlated with expression of *MYCN* across all tumours ($p < 0.05$) (Appendix Table A20). For example, expression of *FANCD2* ($r(491) = 0.448$, $p < 0.001$) (Figure 3.24C) and *REV3L* ($r(491) = -0.355$, $p < 0.001$) (Figure 3.24D) was significantly positively and negatively correlated with *MYCN* expression respectively.

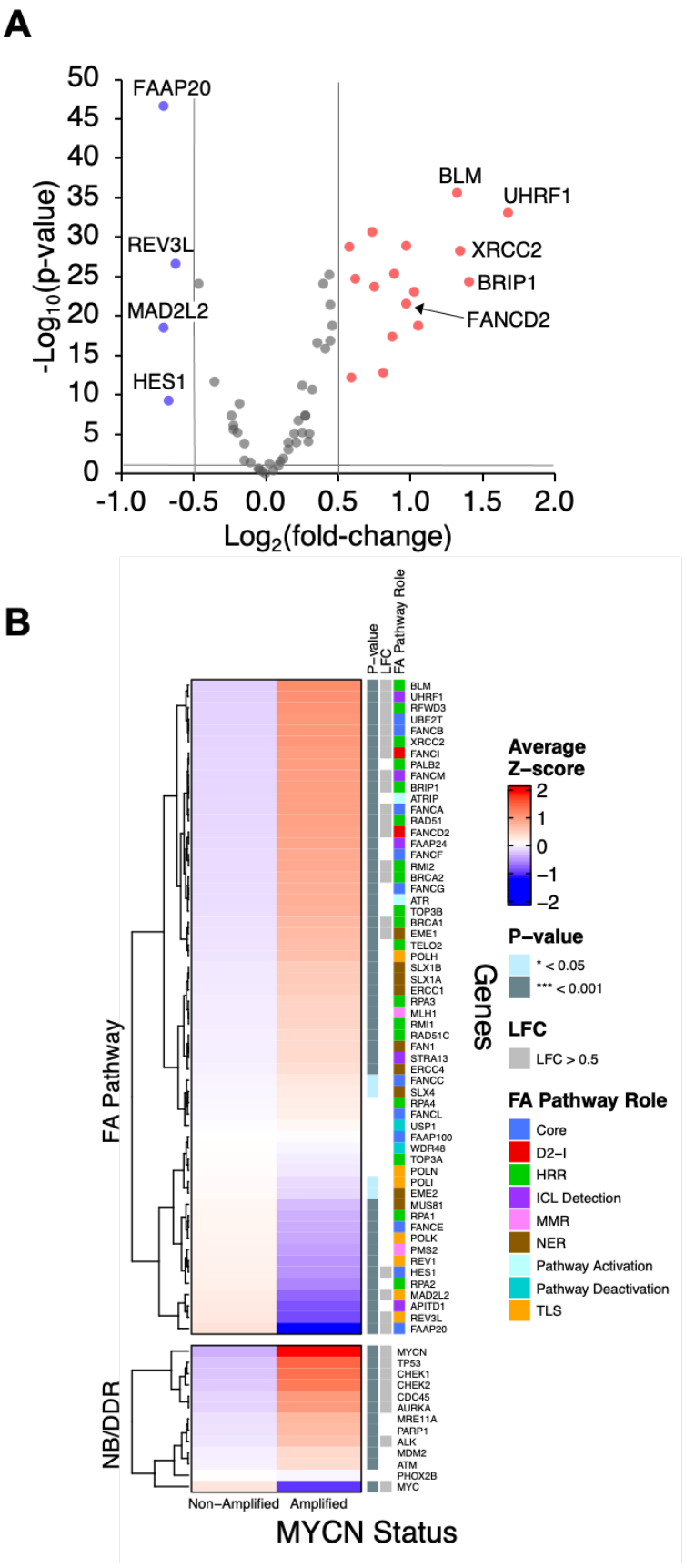

Figure 3.23. FA pathway associated genes are significantly differentially expressed between MYCN amplified and MYCN non-amplified neuroblastoma tumours. (Legend overleaf).

Figure 3.23. FA pathway associated genes are significantly differentially expressed between MYCN amplified and MYCN non-amplified neuroblastoma tumours.
mRNA expression of 58 FA pathway associated genes and 13 DNA damage repair (DDR) or key neuroblastoma-associated (NB) genes was analysed in 493 neuroblastoma tumours using the GSE62564 RNA-Seq data set and the R2: Genomics Analysis and Visualisation Platform. The log_2(fold-change) in expression between MYCN amplified and MYCN non-amplified tumours was calculated using log_2(RPM+1) expression data. Statistical significance of differential expression was determined for each gene by a Student's t-test. **(A)** Volcano plot of FA pathway associated genes. Each dot represents one gene. Grey dots represent genes with no significant differential expression or log_2(fold-change)<0.5. Red and blue dots represent significantly upregulated and downregulated genes respectively with a log_2(fold-change)>0.5. **(B)** Log_2(RPM+1) expression data was used to calculate Z-scores independently for each gene in all tumours. The average Z-score in MYCN amplified and MYCN non-amplified subgroups is presented. 'P-value' annotation displays the statistical significance of differential expression. 'LFC' indicates which genes show a log_2(fold-change)>0.5. Genes are annotated by 'FA pathway role': Core; FA core complex, D2-I; FANCD2-FANCI complex, HRR; homologous recombination repair, ICL detection; inter-strand crosslink detection, MMR; mis-match repair, NER; nucleotide excision repair, TLS; translesion synthesis.

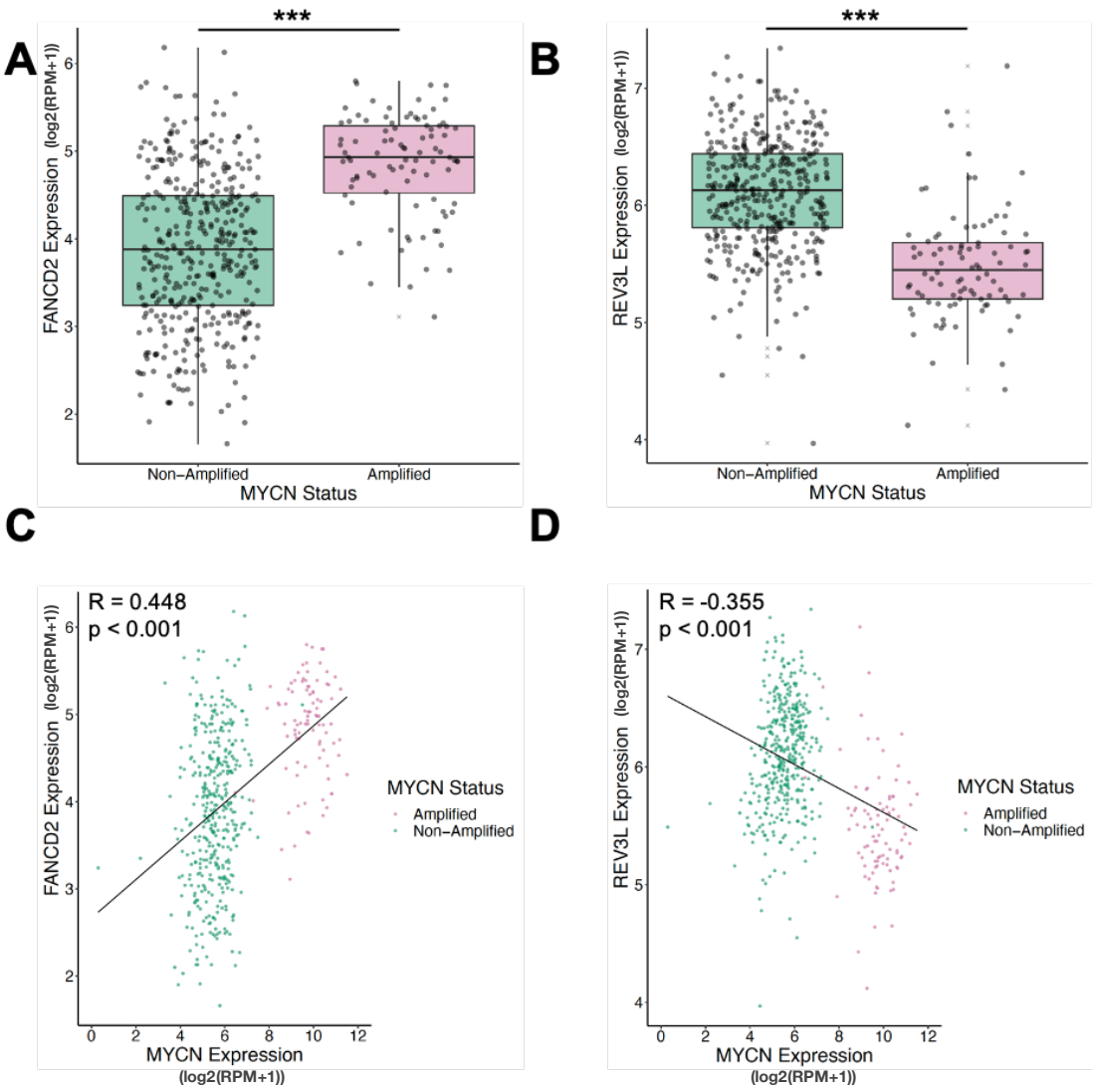

Figure 3.24. RNA-Seq shows FANCD2 is significantly upregulated, and REV3L is significantly downregulated, in MYCN amplified compared to MYCN non-amplified neuroblastoma tumours.
mRNA expression of FANCD2 and REV3L was analysed in 493 neuroblastoma tumours using the GSE62564 RNA-Seq data set and the R2: Genomics Analysis and Visualisation Platform. Boxplots display log_2(RPM+1) count data of **(A)** FANCD2 and **(B)** REV3L in MYCN amplified and MYCN non-amplified tumours. Statistical significance in (A) and (B) was determined by Student's t-test where *p<0.05, **p<0.01, ***p<0.001. Log_2(RPM+1) count data of MYCN was plotted against that of **(C)** FANCD2 and **(D)** REV3L for each tumour. Points are coloured by MYCN status. Statistical significance in (C) and (D) was determined by Pearson's correlation; R = Pearson's correlation coefficient, p = p-value.

In agreement with findings from Durbin et al., (2018) which suggest the MNA-induced gene signature is better correlated with high risk than MNA itself, presence of the MNA-associated FA pathway gene signature in non-MNA tumours is frequently associated with high risk, advanced stage and disease progression (Appendix Figure A9; Appendix Table A22). Similarly, expression levels of 14 of the 20 significantly

differentially expressed FA pathway genes ($p < 0.05$, $\log_2$(fold-change) > 0.5) can significantly stratify neuroblastoma overall survival in the non-MNA patient subgroup specifically (Appendix Figure A10). Expression levels of 19 of the 20 significantly differentially expressed FA pathway genes can significantly stratify neuroblastoma overall survival across all patients (Appendix Figure A11). High expression of genes which were significantly upregulated in MNA tumours such as *FANCD2* (Figure 3.25A-B), and low expression of genes which were significantly downregulated in MNA tumours such as *REV3L* (Figure 3.25D-E), was associated with a significant reduction in overall survival ($p < 0.05$). However, these significant associations between FA pathway gene expression and survival were not observed within the MNA subgroup of patients alone (Figure 3.25C,F).

Therefore, in contrast to the expression data across the large panel of 39 neuroblastoma cell lines, expression data from neuroblastoma tumours does correlate with the findings from *MYCN*-inducible cell lines and supports the idea that *MYCN* and *FANCD2* expression is correlated in neuroblastoma.

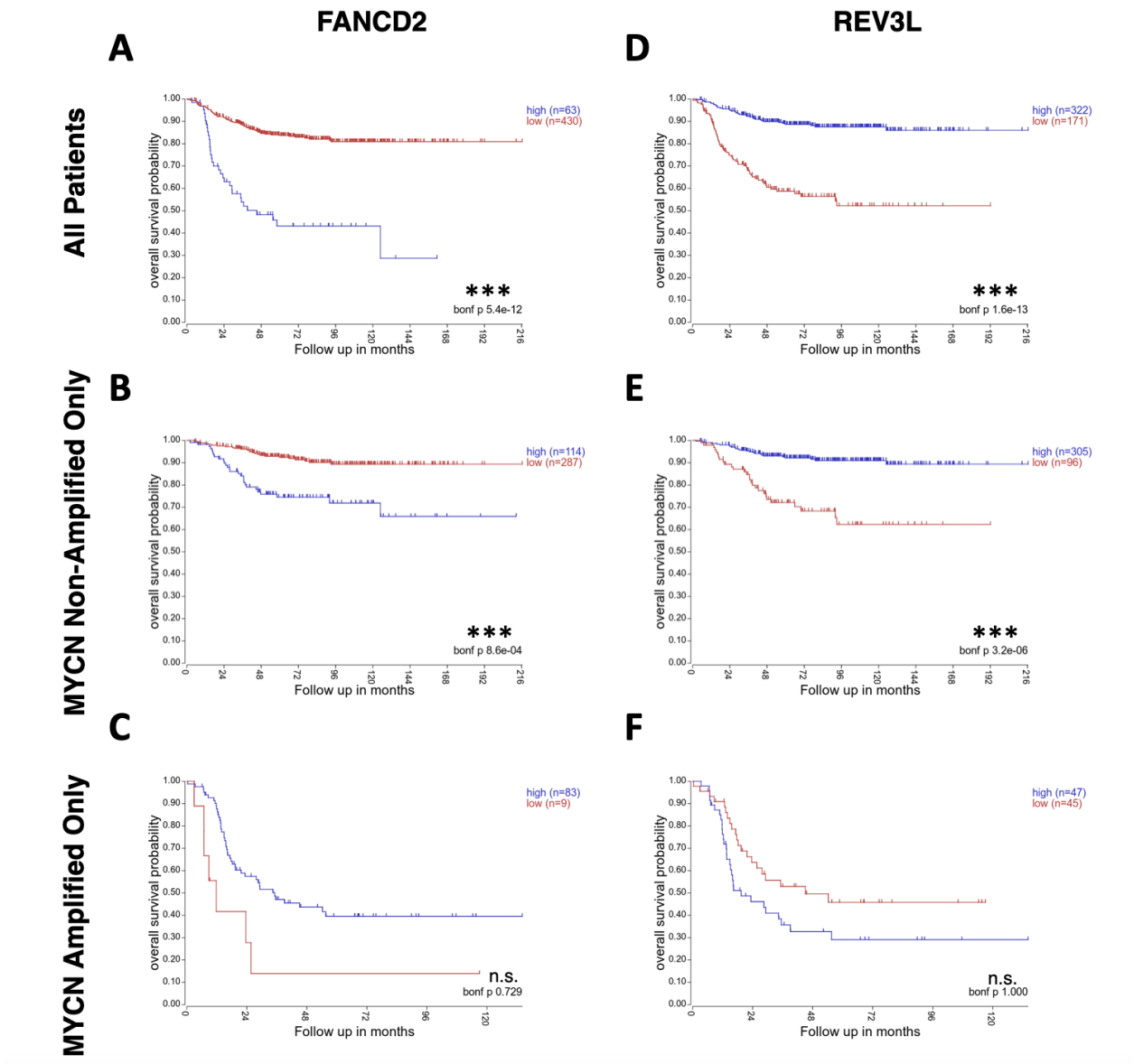

Figure 3.25. High FANCD2 expression and low REV3L expression is associated with a significant reduction in overall survival.
mRNA expression of FANCD2 and REV3L in neuroblastoma tumours and overall survival was analysed in 493 patients using the GSE62564 RNA-Seq data set and the R2: Genomics Analysis and Visualisation Platform. Patients were grouped according to tumour MYCN amplification status. Kaplan-Meier curves are presented demonstrating overall survival for patients with high or low expression of **(A-C)** FANCD2 or **(D-F)** REV3L. High and low expression threshold of each gene was determined by 'scan modus' in R2: Genomics. Statistical significance of difference in overall survival determined by a log-rank test and Bonferroni correction; p-value annotated by 'bonf p', where n.s. = no significance, *p<0.05, **p<0.01, ***p<0.001.

3.2.4 Most FA pathway genes are direct transcriptional targets of MYCN.

MYCN may regulate FA pathway expression directly, through promoter binding, or indirectly through enhancer binding, activation of intermediate genes, or by promoting chromatin remodelling. To determine whether FA pathway genes are direct transcriptional targets of MYCN, MYCN binding at FA pathway gene promoters was analysed by ChIP techniques. Following identification of a canonical MYCN E-box within the *FANCD2* promoter, ChIP-PCR was used initially to determine whether *FANCD2* was a direct transcriptional target of MYCN in SHEP-Tet21N MYCN ON and MYCN OFF cells and MNA IMR32 cells. PCR amplification of the MYCN E-box within the *FANCD2* promoter, as well as the positive control MYCN target gene *APEX1* and house-keeping gene *RPL30*, was undertaken using DNA fragments that were immunoprecipitated by anti-MYCN, anti-IgG (negative control IP) and anti-H3 (positive control IP) antibodies (Figure 3.26A). Relative to the IgG negative control, MYCN binding at the *FANCD2* E-box is enriched by approximately 2.5-fold in SHEP-Tet21N MYCN ON cells and 1.5-fold in IMR32 MNA cells but is not enriched in SHEP-Tet21N MYCN OFF cells (Figure 3.26B). A similar trend of MYCN binding is observed at the *APEX1* positive control MYCN binding site. Analysis of the *RPL30* house-keeping gene acted as a positive control gene for the anti-H3 positive control IP, as it is known histone H3 is bound at this *RPL30* locus.

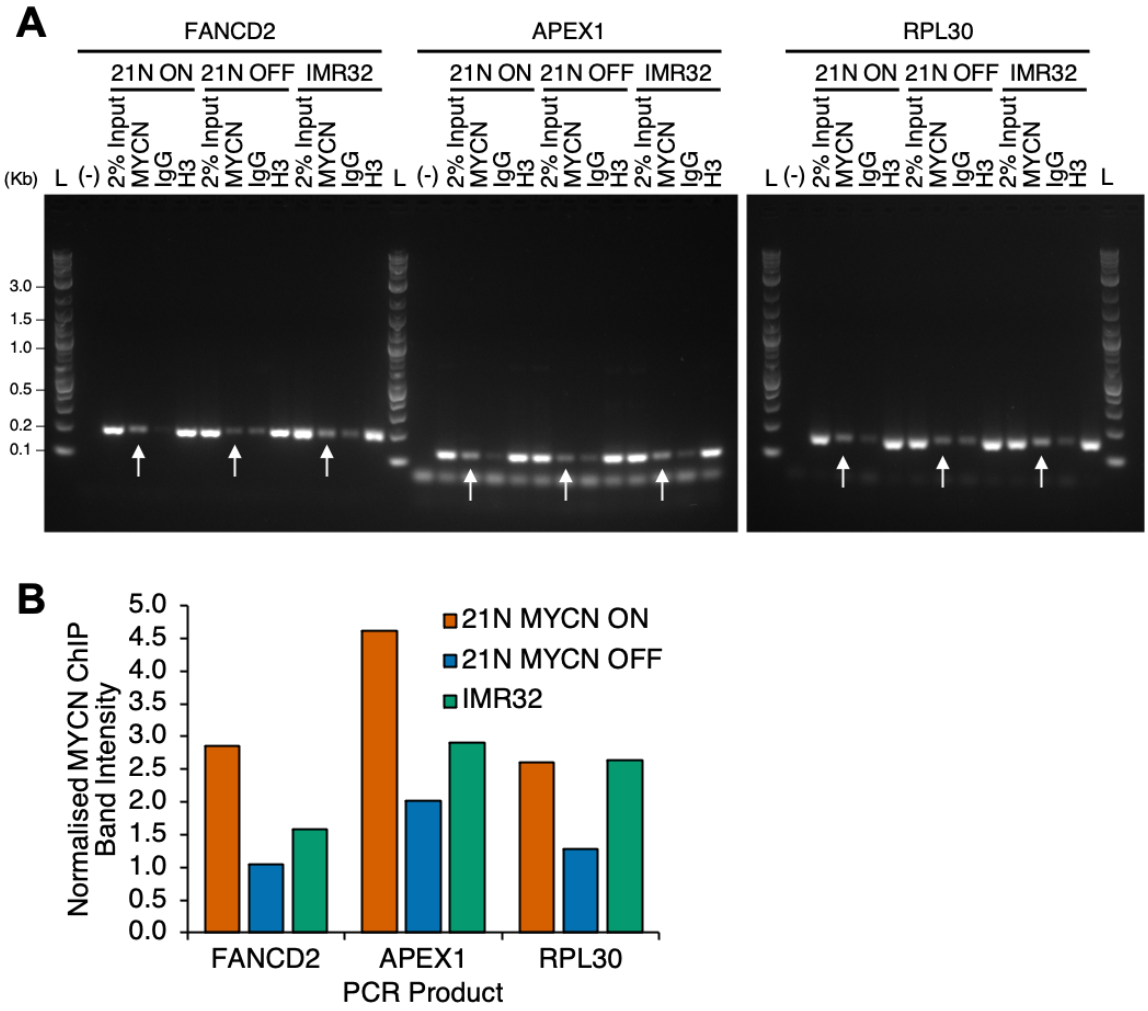

Figure 3.26. MYCN binds at canonical MYCN E-box in FANCD2 promoter in IMR32 and SHEP-Tet21N MYCN ON cells.
(A) ChIP-PCR detection of canonical MYCN E-box in FANCD2 promoter, APEX1 MYCN binding site (MYCN target positive control) and RPL30 (house keeping gene, H3 ChIP positive control). PCR amplification was undertaken with DNA fragments from SHEP-Tet21N MYCN ON, SHEP-Tet21N MYCN OFF and IMR32 cells, that were immunoprecipitated by anti-MYCN (IP), anti-IgG (mock IP), anti-H3 (positive control IP) antibodies or with diluted total DNA fragments (2% Input). MYCN bands are indicated by white arrows. 'L' indicates 2-Log Ladder (NEB). (-) indicates no template DNA negative PCR control. (n=1) **(B)** PCR product band intensity following MYCN ChIP was determined and normalised to IgG ChIP band intensity for each cell line (n=1).

Using the GSE80151 ChIP-Seq dataset (Zeid et al., 2018), MYCN binding was analysed at the promoters of all 58 FA pathway genes, 13 key DDR and neuroblastoma-associated genes and 3 control genes in *MYCN*-inducible SHEP-PLXI-MYCN and SHEP-Tet21N cell lines and MNA cell lines SK-N-BE(2)-C, NGP and KELLY (Figure 3.27; Appendix Table A23). Across all cell lines, MYCN was bound at the

promoter of 51 of 58 FA pathway genes, suggesting direct regulation either through DNA binding or protein-protein interactions within a complex.

Zeid et al., (2018) found MYCN binds promoters and enhancers in an affinity dependent manner. High affinity binding sites at the promoters of MYCN target genes are bound at physiological MYCN levels, whilst low affinity MYCN binding sites in promoters and enhancers are flooded at oncogenic MYCN levels to induce global upregulation of all active genes (Zeid et al., 2018). Whilst most FA pathway genes are directly regulated at oncogenic levels, the MYCN affinity of FA gene promoters vary, as indicated by variation in the number of MYCN-bound FA gene promoters between cell lines with different *MYCN* expression levels. High MYCN affinity is indicated by MYCN binding at low *MYCN* expression levels, suggesting *HES1, RMI1, PMS2, REV3L SLX1A, SLX1B, EME1, FANCC* and *RPA3* promoters have the highest affinity for MYCN binding. On average across all cell lines, the *HES1* promoter had the greatest MYCN binding affinity. This is in agreement with SHEP-Tet21N and tumour RNA-Seq data which indicated *HES1* was consistently one of the most significantly downregulated FA pathway genes (Figures 3.14A, 3.22A). Zeid et al., (2018) found genes which are regulated predominantly by low-affinity MYCN binding were the most sensitive to perturbations in *MYCN* expression. This suggests genes such as *MAD2L2, BRCA1, FANCB, FANCM, BRIP1, UBE2T* and *FANCD2*, which are only bound during higher *MYCN* expression, would be most sensitive to changes in *MYCN* expression (Figure 3.27). This is supported by the high fold change in expression often observed for these genes between high and low MYCN levels (Figures 3.14A, 3.22A).

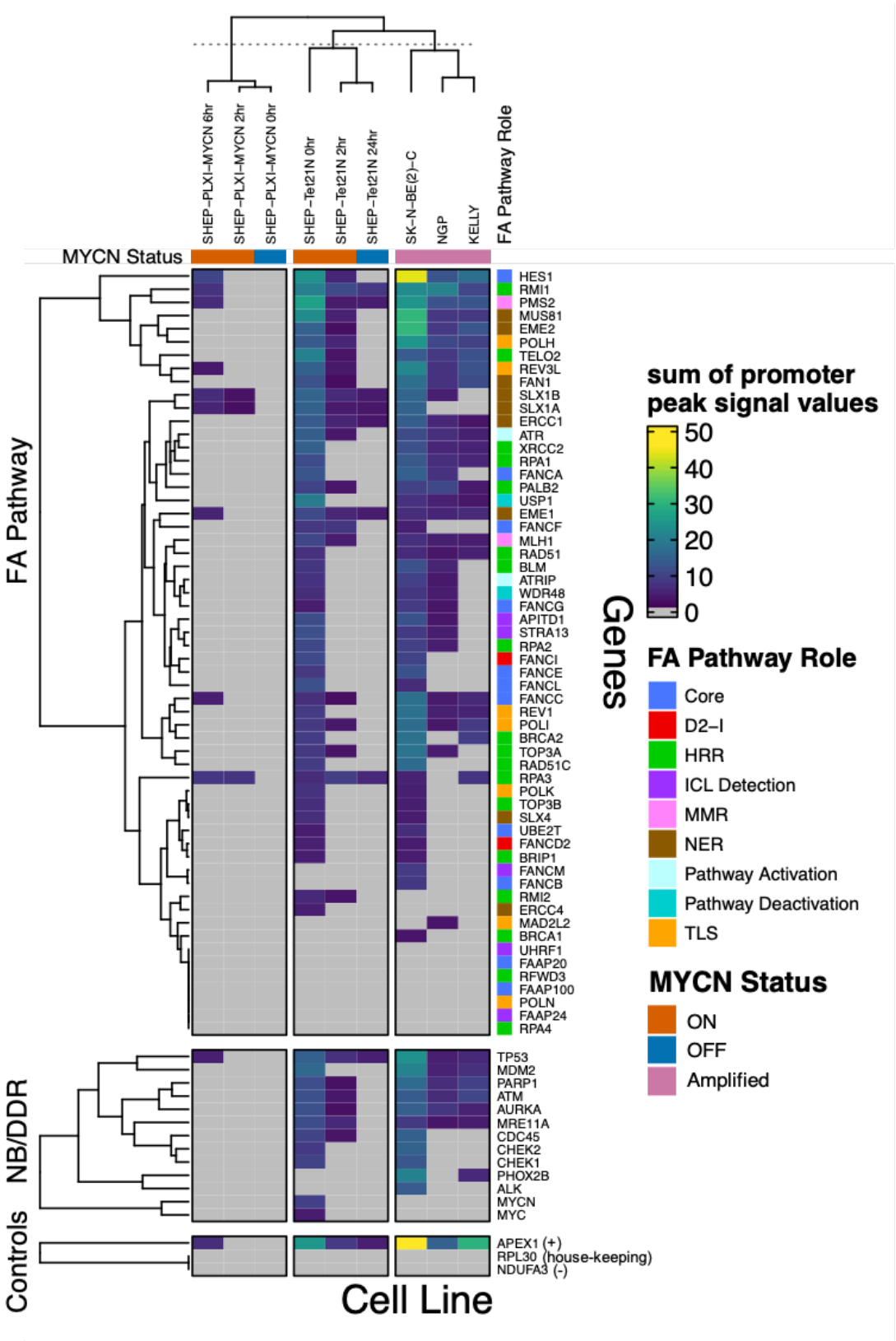

Figure 3.27. MYCN binds at multiple FA pathway gene promoters in neuroblastoma cells. (Legend overleaf).

Figure 3.27. MYCN binds at multiple FA pathway gene promoters in neuroblastoma cells.
Using the GSE80151 ChIP-Seq dataset, MYCN binding at the promoters of 58 FA pathway associated genes, 13 DNA damage repair (DDR) or key neuroblastoma-associated (NB) genes and 3 control genes was analysed in MYCN-inducible SHEP-PLXI-MYCN tet-ON and SHEP-Tet21N tet-OFF cell lines and MYCN amplified cell lines SK-N-BE(2)-C, NGP and KELLY. SHEP-PLXI-MYCN and SHEP-Tet21N cells were treated with doxycycline for indicated timepoints to induce induction and inhibition of MYCN expression respectively. MYCN status of cells is indicated. The sum of the input-normalised signal values of all promoter MYCN peaks was calculated for each gene. APEX1; MYCN target positive control, RPL30; house keeping gene; NDUFA3; MYCN target negative control. Genes are annotated by 'FA pathway role': Core; FA core complex, D2-I; FANCD2-FANCI complex, HRR; homologous recombination repair, ICL detection; inter-strand crosslink detection, MMR; mis-match repair, NER; nucleotide excision repair, TLS; translesion synthesis.

In both *MYCN*-inducible cell lines, the number of MYCN-bound FA pathway genes is reduced with decreasing levels of MYCN. However, the timing of MYCN binding is also indicative of MYCN affinity. In SHEP-Tet21N cells with constitutive MYCN expression, 47 FA gene promoters are bound by MYCN. After induction of *MYCN* expression for 6 hours in SHEP-PLXI-MYCN cells, MYCN is bound to only 9 FA gene promoters which have similar high MYCN affinity to the positive control gene *APEX1*.

Overall analysis of promoter binding by MYCN supports direct transcriptional regulation of *FANCD2* and other FA genes consistent with previous findings of correlated expression. However, direct MYCN promoter binding does not occur at all genes which are significantly differentially expressed between *MYCN* high and low expression states such as *FAAP20, RFWD3* and *UHRF1* (Figure 3.23A), suggesting other indirect mechanisms also regulate FA gene expression.

Gene ontology and KEGG pathway enrichment analysis was also undertaken for all genes with MYCN-bound promoters. In SHEP-Tet21N MYCN ON cells, 'cellular response to DNA damage stimulus' was within the top 10 enriched GO terms (Figure 3.28; Appendix Figure A12; Appendix Table A24). In all three MNA cell lines, 'DNA replication' was within the top 10 enriched KEGG pathways (Figure 3.29; Appendix Table A25). Analysis of genes which were bound by MYCN in all MYCN ON and MNA cell lines showed 'Base excision repair' was one of the top 10 enriched KEGG pathways (Figure 3.29; Appendix Table A25).

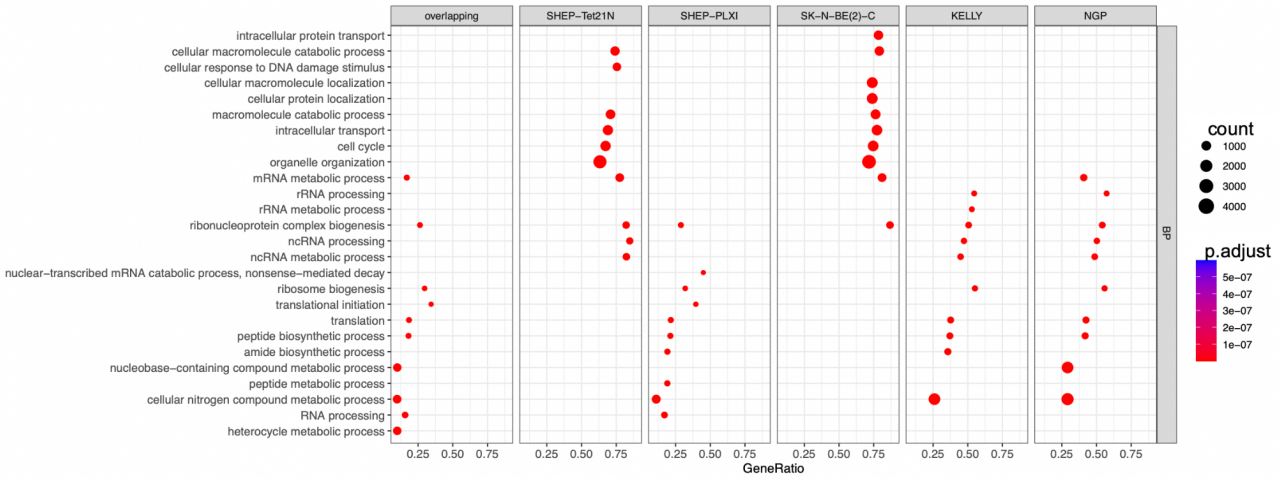

Figure 3.28. 'Cellular response to DNA repair' is one of the top 10 enriched gene ontology terms for MYCN-bound genes in SHEP-Tet21N MYCN ON cells.

MYCN ChIP-Seq read data was downloaded from the GSE80151 dataset, and peaks were mapped and quantified using bowtie2 and MACS2. Peaks within gene promoters were annotated, and significantly enriched gene ontologies in the set of MYCN-bound genes was determined by ChIPpeakAnno. MYCN binding in SHEP-Tet21N MYCN ON, SHEP-PLXI-MYCN ON, SK-N-BE(2)-C, KELLY and NGP neuroblastoma cell lines was analysed. Gene ontology enrichment was similarly analysed for genes which were bound by MYCN in all MYCN ON and MYCN amplified cell lines analysed (overlapping). Top 10 most enriched biological process (BP) gene ontologies in the set of MYCN-bound genes in each cell line are presented. Gene ratio represents the fraction of genes within each ontology that is bound by MYCN. Points coloured by significance of enrichment (p.adjust) and sized according to number of genes bound by MYCN (count).

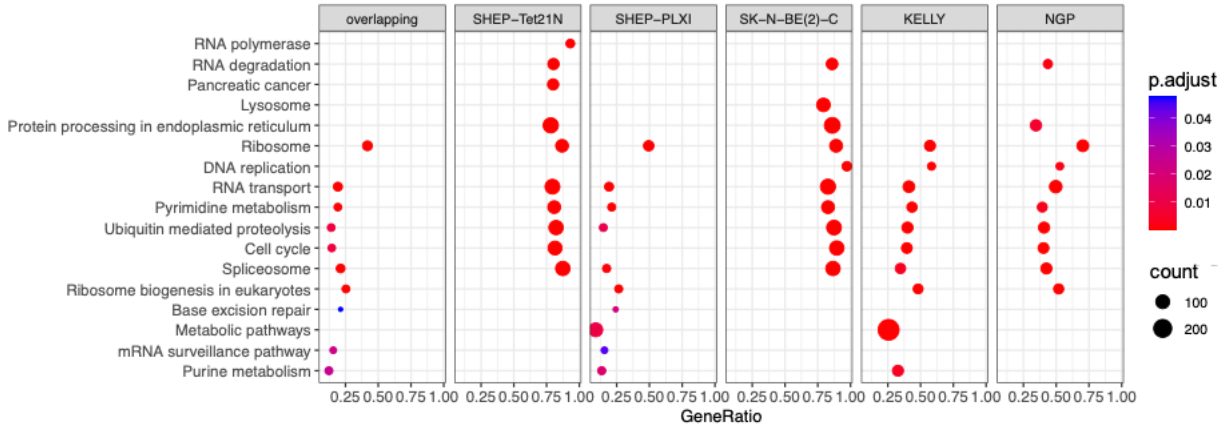

Figure 3.29. 'Base excision repair' is one of the top 10 enriched KEGG pathways in MYCN-bound genes across a panel of neuroblastoma cell lines.
MYCN ChIP-Seq read data was downloaded from the GSE80151 dataset, and peaks were mapped and quantified using bowtie2 and MACS2. Peaks within gene promoters were annotated, and significantly enriched KEGG pathways in the set of MYCN-bound genes was determined by ChIPpeakAnno. MYCN binding in SHEP-Tet21N MYCN ON, SHEP-PLXI-MYCN ON, SK-N-BE(2)-C, KELLY and NGP neuroblastoma cell lines was analysed. KEGG pathway enrichment was similarly analysed for genes which were bound by MYCN in all MYCN ON and MYCN amplified cell lines analysed (overlapping). Top 10 most enriched KEGG pathways in the set of MYCN-bound genes in each cell line are presented. Gene ratio represents the fraction of genes within each KEGG pathway that is bound by MYCN. Points coloured by significance of enrichment (p.adjust) and sized according to number of genes bound by MYCN (count).

3.3 Discussion:

MYCN overexpression induces higher levels of DNA damage and replication stress, resulting in a therapeutically exploitable dependence on DNA repair and replication stress limiting pathways (Cole et al., 2011; Gu et al., 2014; Gu et al., 2015; Colicchia et al., 2017; Petroni et al., 2018; King et al., 2020; King et al., 2021; Southgate et al., 2020). This increased dependence is often indicated by a MYCN-induced transcriptional upregulation of DNA repair genes (Cole et al., 2011; Valentijn et al., 2012; Chayka et al., 2015; Gu et al., 2015; Newman et al., 2015; Hallett et al., 2016; Petroni et al., 2016; Colicchia et al., 2017; Durbin et al., 2018; Petroni et al., 2018; Herold et al., 2019; King et al., 2020). The FA pathway has a vital role in maintaining genome stability through DNA damage repair, stalled replication fork protection, and R-loop resolution (Schlacher et al., 2011; Kim and D'Andrea, 2012; Schlacher et al., 2012; Chaudhury et al., 2013; Lossaint et al., 2013; Garcia-Rubio et al., 2015; Schwab et al., 2015; Ceccaldi et al., 2016; Lachaud et al., 2016; Zhang et al., 2017; Daza-Martin et al., 2019; Herold et al., 2019; Liang et al., 2019a; Okamoto et al., 2019). Upregulation of FA pathway expression has been observed in multiple other cancer types and frequently correlates with increased tumour aggressiveness (Van Der Groep et al., 2008; Kao et al., 2011; Wysham et al., 2012; Kais et al., 2016; Feng and Jin 2019; Liu et al., 2020a). The effect of *MYCN* overexpression on FA pathway expression is unknown.

Here, we analysed the effect of *MYCN* overexpression and amplification on the expression of FA pathway associated genes in neuroblastoma at the transcriptional and protein level by RT-qPCR, RNA-Seq and western blotting. The mechanism of FA pathway expression regulation by MYCN was analysed by ChIP-PCR and ChIP-Seq. Across isogenic tet-regulated *MYCN* expression systems, a small group of neuroblastoma cell lines, and in neuroblastoma tumours, *MYCN* overexpression or amplification induced differential expression of FA pathway genes which clustered according to FA pathway role. Whilst FANC and HRR genes were predominantly transcriptionally upregulated, TLS and NER genes were inconsistently downregulated or showed no substantial change in expression. Similarly, a correlation between MYCN expression and FA pathway activation is observed across neuroblastoma cell lines. However, when expanded to a broader panel of 39 neuroblastoma cell lines, very limited significant differential FA pathway expression is observed between *MYCN* status subgroups, suggesting observation of this MYCN-induced regulation is dependent on

the wider genomic context. ChIP analysis suggests MYCN directly regulates expression of many FA pathway genes through promoter binding.

3.3.1 Upregulation of FANC and HRR genes suggests an increased reliance on HRR and FA pathway function in *MYCN*-amplified neuroblastoma

Study of FA pathway expression in tetracycline-regulated *MYCN* expression systems by western blot, RT-qPCR and RNA-Seq (Figures 3.4, 3.8, 3.13, 3.14), in a small panel of neuroblastoma cell lines by RT-qPCR (Figures 3.17, 3.19), and in neuroblastoma tumours by RNA-Seq (Figure 3.23), showed *MYCN* overexpression or amplification was associated with significant transcriptional upregulation of most FANC and HRR genes. This implies MNA neuroblastoma has an increased dependency on these FA pathway proteins which could be therapeutically exploitable. Notably, FA genes with a role in HRR such as *XRCC2, BRCA1, BLM* and *BRIP1* most consistently showed the greatest upregulation across all RNA-Seq datasets (Figures 3.14, 3.20, 3.22). This is consistent with previous observations of HRR gene upregulation in MNA neuroblastoma (Valentijn et al., 2012; Chayka et al., 2015; Petroni et al., 2016; Petroni et al., 2018; Herold et al., 2019; King et al., 2020). Elevated *XRCC2* expression has been previously observed across a wide variety of cancer types (Chen et al., 2018) but has not yet been demonstrated in neuroblastoma. All FA pathway genes with evidenced roles in replication stress limitation also consistently cluster as some of the most upregulated FA genes, including *FANCD2, BRCA1, BRCA2, RAD51, FANCM, BRIP1* and *BLM* (Davies et al. 2007; Garcia-Rubio et al., 2015; Schwab et al., 2015; Pan et al., 2017; Zhang et al., 2017; Herold et al., 2019; Liang et al., 2019a; Lu et al., 2019; Okamoto et al., 2019; Pladevall-Morera et al., 2019; Silva et al., 2019). This could suggest MNA neuroblastoma is primarily dependent on HRR and the replication stress limiting functions of the FA pathway.

Previous studies have also observed upregulation of some of the FA pathway genes we analysed in MNA compared to non-MNA neuroblastoma, such as *ATR, BLM, BRCA1,* and *RAD51*, and this validates our findings (Valentijn et al., 2012; Chayka et al., 2015; Herold et al., 2019; King et al., 2020). Similarly, known differential expression of other key DNA repair and neuroblastoma-associated genes in MNA neuroblastoma, such as upregulation of *ALK, AURKA, CHEK1, CHEK2, TP53, MDM2, PARP, MRE11,* and reduced *MYCC* expression, was also observed in our SHEP-Tet21N and neuroblastoma tumour RNA-Seq analyses (Figure 3.14, 3.22) (Slack et al., 2005;

Shang et al., 2009; Chen et al., 2010; Cole at al. 2011; Hasan et al., 2013; Gu et al., 2015; Petroni et al., 2016; Colicchia et al., 2017; King et al., 2020). However, expression of *PHOX2B*, a master regulator of neural crest lineage specification, was not significantly correlated with *MYCN* expression as previously described (Ke et al., 2015). Expression of all FA pathway genes which were significantly differentially expressed between *MYCN* amplification subgroups, was also significantly correlated with *MYCN* expression (Appendix Tables A12, A20). This validates that the differential expression observed is primarily due to *MYCN* expression itself, rather than other genetic features commonly associated with *MYCN* amplification such as *ALK* amplification or chromosome 1p deletions (Luttikhuis et al., 2001; De Brouwer et al., 2010). However, this also means induction of *MYCN* expression in an isogenic system does not fully recapitulate the effect of *MYCN* amplification and may account for the differences observed between the neuroblastoma models and tumours analysed, such as the less frequent significant downregulation of TLS genes in SHEP-Tet21N MYCN ON cells compared to in MNA tumours.

Differential expression of the 23 FANC genes has also been observed in other cancer types. Liu et al., (2020a) observed prevalent transcriptional upregulation of most FANC genes in a variety of cancer types compared to normal tissue controls, including melanoma, breast, ovarian, colon, bladder, and lung cancers. However, no substantial changes in FANC gene expression were observed in prostate cancer, despite a *MYCN* amplification frequency of 45% (Liu et al., 2020a; Liu et al., 2021). The effect of *MYCN* amplification on FA pathway expression may therefore be tumour-type dependent, as suggested by the tumour-type specific profile of global active gene upregulation induced by *MYCN* overexpression (Zeid et al., 2018). Kao et al., (2011) observed transcriptional upregulation of nine FANC genes in melanoma, with the extent of overexpression correlating with melanoma thickness. This upregulation of FANC genes in melanoma may also be associated with oncogene activation as it was observed that activation or amplification of the oncogenic microphthalmia-associated transcription factor (*MiTF*), observed in a subset of melanoma cases, induces upregulation of FANC genes (Bourseguin et al., 2016). This MiTF-induced FANC upregulation promotes proliferation and migration and inhibits senescence in malignant melanoma (Bourseguin et al., 2016).

Many other studies have also shown high expression of FANC genes in tumours correlates with increased tumour aggressiveness, chemo-resistance and reduced event-free survival (Taniguchi et al., 2003; Swisher et al., 2009; Ozawa et al., 2010;

Nakanishi et al., 2012; Swarts et al., 2013). For example, the extent of *FANCD2* overexpression in ovarian, breast, uterine and hepatocellular carcinomas correlates with increased tumour grade and stage, and increased risk of recurrence (Van Der Groep et al., 2008; Kais et al., 2016; Wysham et al., 2012; Komatsu et al., 2017; Feng and Jin 2019). Furthermore, Kais et al., (2016) found *FANCD2* is upregulated in BRCA-mutated and HRR-deficient subgroups of these cancers relative to HRR-proficient subgroups. FANC genes are therefore frequently transcriptionally upregulated across a broad range of cancer types, and this commonly is associated with increased tumour aggressiveness and poor prognosis. Given the association of *MYCN* amplification with rapid tumour progression and reduced event free survival (Brodeur et al., 1984; Seeger et al., 1985), our results similarly indicate a link between FA pathway upregulation and increased tumour aggressiveness.

However, FANC gene downregulation or inactivation has also been observed in tumours. In breast carcinomas and head and neck squamous cell carcinomas, methylation or deletion of *FANCC* was associated with poor survival (Sinha et al., 2008; Ghosh et al., 2013). In fact, downregulation of at least one FANC gene was observed in 66% of head and neck squamous cell carcinomas (Wreesmann et al., 2007). Also, although many studies have shown *FANCD2* overexpression in breast cancer is associated with poor prognosis (Kais et al., 2016; Wysham et al., 2012; Van Der Groep et al., 2008; Kais et al., 2016; Feng and Jin 2019; Liu et al., 2020a), Zhang et al., (2010) found *FANCD2* expression was inversely correlated with breast cancer tumour grade and metastasis. Furthermore, it is often observed that a greater proportion of breast carcinomas have no detectable *FANCD2* expression compared to benign tissues, with 10-65% of malignant breast cancers displaying no *FANCD2* expression (Van Der Groep et al., 2008; Rudland et al., 2010; Zhang et al., 2010; Feng and Jin 2019). However, Rudland et al., (2010) showed this may be specific to nuclear FANCD2. Both transcriptional upregulation and inactivation of *FANCD2* is therefore observed within breast cancer. Similarly, whilst FANC gene upregulation is commonly observed in tumours, germline and somatic FANC gene inactivation often confer increased risk of cancer, with FANC gene alterations detected in 40% of all cancers (Merajver et al., 1995; Pejovic et al., 2006; Garaycoechea and Patel, 2014; Wang and Smogorzewska, 2015; Kuchenbaecker et al., 2017; Niraj et al., 2019; Liu et al., 2020a). HRR-related FANC genes are the most commonly altered, however 75% of these alterations are characterised by mutations and deletions, whilst core complex FANC gene alterations are predominantly amplifications (Niraj et al., 2019). In contrast, we find HRR-related

FANC genes are often the most upregulated by *MYCN* overexpression in neuroblastoma (Figures 3.14, 3.20, 3.22).

Altogether this suggests a biphasic FA pathway dependency during tumour progression, in which FA pathway deficiencies may promote carcinogenesis through induction of high genomic instability, whilst FA pathway upregulation is advantageous during later tumour progression by limiting excess genomic instability and mediating chemotherapeutic resistance. This may account for the stage-specificity of FA pathway expression changes often observed. Our data suggests this biphasic FA pathway dependency is also observed in neuroblastoma, as although bi-allelic germline mutations in *PALB2* (*FANCN*) and *BRCA2* (*FANCD1*) predisposes FA patients to neuroblastoma (Reid et al., 2007; Loizidou et al., 2016), and somatic defects in *FANCM, FAN1* and *PALB2* have been observed in neuroblastoma (Pugh et al., 2013), we demonstrate MYCN-driven neuroblastoma upregulates FA pathway function. Although FA genes are not enriched for somatic mutations in high-risk neuroblastoma (Pugh et al., 2013), the efficacy of FA pathway inhibition in MNA neuroblastoma would be dependent on the mutational profile of FA pathway genes.

3.3.2 FA pathway activation increases in parallel with FANC and HRR gene upregulation in *MYCN*-amplified neuroblastoma

Although multiple previous studies have demonstrated FA pathway activity and DNA damage sensitivity can be controlled through transcriptional regulation of FA pathway genes (Vaughn et al., 1996; Pejovic et al., 2006; Chen et al., 2007; Hoskins et al., 2008; Kais et al., 2016; Feng and Jin 2019), MYCN-induced FA pathway upregulation is not necessarily directly indicative of an increase in FA pathway activation. We therefore assessed FANCD2 mono-ubiquitination, an established hallmark of FA pathway activation (Garcia-Higuera et al., 2001; Taniguchi et al., 2002a; Liang et al., 2016; Van Twest et al., 2017). In SHEP-Tet21N cells, a MYCN ON to OFF transition consistently resulted in reduced FA pathway activation in parallel with FANCD2 downregulation (Figure 3.4A). Similarly, increased FA pathway activation non-significantly correlated with higher MYCN expression levels across a panel of MNA, non-MNA and MYCN-inducible cell lines (Figure 3.18B). *MYCN* overexpression may induce FA pathway activation due to increased replication stress and an increased capacity for FANCD2 mono-ubiquitination through upregulation of many FA core complex components. However, it must be noted that changes in *FANCD2* expression

may have affected L:S ratio analyses, as the mono-ubiquitinated FANCD2 western blot band is more difficult to detect at lower expression levels.

3.3.3 Increased FA pathway activation and FANC gene upregulation suggests the FA pathway is a potential tumour-specific therapeutic target in MNA neuroblastoma

MYCN overexpression induces high levels of DNA damage and replication stress (Gu et al., 2015; King et al., 2020). As such, inhibition of key DNA repair and DDR pathways has been demonstrated to induce intolerable levels of replication stress and DNA damage selectively in MNA cells (Cole et al., 2011; Gu et al., 2014; Gu et al., 2015; Colicchia et al., 2017; Petroni et al., 2018; King et al., 2020; King et al., 2021; Southgate et al., 2020). These pathways are therefore potential novel targets for MNA neuroblastoma. The increased reliance of MYCN-driven proliferation on these DNA repair pathways was indicated by upregulation of DNA repair genes such as *BRCA1, PARP, MRE11, BLM, ATR, CHK1* and *CHK2* in MNA neuroblastoma (Zhang et al., 2009; Cole et al., 2011; Petroni et al., 2018; Herold et al., 2019; King et al., 2021). The FA pathway is the eighth most enriched KEGG pathway among genes upregulated by *MYCN* overexpression in SHEP-Tet21N cells (Figure 3.17). Increased FA pathway activation across MNA neuroblastoma cell lines (Figure 3.18B) and predominant upregulation of FANC and HRR genes by MYCN in *MYCN*-inducible cell lines (Figures 3.4, 3.8, 3.13, 3.14), and neuroblastoma tumours (Figure 3.23), suggests MNA neuroblastoma has an increased dependency on the FA pathway and HRR. FA pathway inhibition may therefore exploit this increased dependency to selectively target MNA tumour cells. This specificity is desirable in identification of novel therapeutics with reduced off target toxicity.

3.3.4 High FANC and HRR gene expression may be a prognostic biomarker in neuroblastoma

Although high FANC gene expression is commonly associated with poor prognosis across many cancer types (Van Der Groep et al., 2008; Zhang et al., 2009; Wysham et al., 2012; Fagerholm et al., 2013; Kais et al., 2016; Bravo-Navas et al., 2019; Feng and Jin 2019; Liu et al., 2020a), this is not always consistent (Rudland et al., 2010; Zhang et al., 2010). Similarly, despite aiding chemo-resistance, higher FA pathway activation is not always associated with reduced event-free survival (Feng and

Jin 2019). In neuroblastoma, upregulation of DNA repair and response genes such as *BRCA1, PARP, BLM, MRE11, CHEK1* and *CHEK2*, has previously been shown to correlate with poor prognosis (Chayka et al., 2015; Hallett et al., 2016; Durbin et al., 2018; Petroni et al., 2018; Herold et al., 2019; King et al., 2020). Similarly, we find the expression levels of most FA genes that are significantly differentially expressed between *MYCN* status subgroups are able to significantly stratify overall survival across all neuroblastoma cases, and across non-MNA cases specifically (Figure 3.25A-B; Appendix Figure A10-A12). This indicates the increased DNA repair capacity induced by higher expression of FANC and HRR genes is also advantageous in neuroblastoma tumours without *MYCN* amplification, which still harbour greater replication stress than non-cancerous cells (Bartkova et al., 2005; Gorgoulis et al., 2005). High FANC and HRR gene expression may therefore be a potential marker of poor prognosis in non-MNA neuroblastoma. However, expression of each FA gene is unable to significantly stratify overall survival between MNA cases specifically (Figure 3.25C), perhaps due to all cases exhibiting relatively high FANC and HRR gene expression. This is in contrast to the findings of Hallett et al (2016), in which FA pathway genes were enriched in a gene signature capable of predicting poor prognosis in MNA neuroblastoma cases alone. MNA neuroblastoma prognosis may therefore be better stratified by a gene signature encompassing differential expression of all FA pathway genes, rather than by expression of each gene individually.

3.3.5 Inconsistent downregulation of NER and TLS genes suggests not all FA pathway functions are upregulated in MNA neuroblastoma

Liu et al., (2020a) examined the dependency of cancer cells on expression of each FANC gene across a panel of 600 cell lines. Although low or modest dependency was observed for each gene, dependency scores of *FANCD2, FANCI* and core complex FANC genes were highly correlated, whilst downstream FANC genes involved in HRR, TLS and NER had divergent dependency scores. This reflects the complexity of the roles of these downstream FANC genes in non-FA pathways. Similarly, *MYCN* overexpression or amplification did not induce a cohesive change in expression of all FA pathway genes in neuroblastoma. Whilst upstream FANC and HRR-related FA pathway genes were predominantly upregulated in MNA cases, expression of TLS and NER FA pathway genes was often downregulated or unchanged (Figures 3.13, 3.14, 3.19, 3.22).

The extent of TLS and NER gene downregulation is inconsistent across neuroblastoma models. *MYCN* overexpression in SHEP-Tet21N only induces significant downregulation of one TLS gene *POLN* (Figure 3.13), although other TLS and NER genes are non-significantly downregulated (Figure 3.14). In MNA tumours, five of seven TLS genes are significantly downregulated including *REV3L*, but NER genes are instead predominantly upregulated (Figure 3.23). Significant TLS downregulation is therefore primarily associated with *MYCN* amplification rather than overexpression, and therefore may instead be induced by other genetic factors that correlate with *MYCN* amplification, rather than high *MYCN* expression itself. Alternatively, TLS gene inactivation could be more frequent during malignant transformation of MNA tumours. Differences in the length of time *MYCN* is overexpressed in tumour cells compared to tet-regulated cells could also account for this variation in TLS and NER expression changes.

Downregulation of NER genes, in parallel with upregulation of FANC genes, has also been observed previously in melanoma and breast cancer (Kao et al., 2011; Fagerholm et al., 2013). The extent of NER downregulation correlated with melanoma thickness (Kao et al., 2011). This pattern of differential expression across FA pathway roles is therefore associated with increased tumour aggressiveness. Although TLS genes are commonly upregulated among various cancers (Zafar and Eoff, 2017), *POLK* was observed to be downregulated in colorectal tumours, loss of *POLH* pre-disposes to skin cancer, and *REV3L* is downregulated in lung, stomach and colorectal cancers (Masutani et al., 1999; Lemée et al., 2006; Pan et al., 2005). Divergent regulation of TLS and NER gene expression from other FA pathway roles may suggest MNA neuroblastoma primarily has greater dependence on the replication-stress limiting and HRR-related FA pathway functions, rather than ICL repair. However, TLS also acts to reduce replication stress by enabling bypass of DNA replication blocks (Zafar and Eoff, 2017). Whilst most downstream FA pathway steps are dependent on FANCD2 mono-ubiquitination, the TLS step is regulated by the FA core complex and does not require FANCD2 mono-ubiquitination (Kim et al., 2012). At sites of DNA damage, the FA core complex is therefore able to promote both rapid error-prone TLS repair, as well as a more accurate, FANCD2 mono-ubiquitination dependent HRR mechanism (Howlett et al., 2009). Upregulation of FANC and HRR genes, and downregulation of TLS and NER genes, may enable MYCN to promote this more accurate mechanism of FA pathway-mediated repair.

3.3.6 MYCN-induced FA pathway differential expression is not always conserved across neuroblastoma cell lines

MYCN-induced FA pathway differential expression is not always observed across all neuroblastoma cell lines. Firstly, siRNA-mediated depletion of MYCN in MNA IMR32 cells did not induce downregulation of FANCD2 (Figure 3.19). However, this may reflect an inability to deplete *MYCN* expression to below the threshold at which it induces *FANCD2* upregulation. Also, prolonged high *MYCN* expression in MNA cell lines may induce epigenetic changes which result in the upregulation of FANCD2 being irreversible.

Secondly, extending analysis to a wider panel of 39 cell lines reduced the size and significance of changes in FA pathway gene expression (Figure 3.21). For example, whilst *FANCD2* was consistently observed to be significantly upregulated in many of the MYCN ON and MNA conditions analysed (Figure 3.13, 3.14A, 3.19, 3.22A), a non-significant $\log_2$(fold-change) of only 0.4 was observed in MNA cells in the 39 cell line RNA-Seq dataset (Figure 3.21A), with MNA cell lines exhibiting a wide distribution of *FANCD2* expression (Figure 3.22A). Also, the direction of change in expression was not conserved for many genes, such as *FANCI* and multiple core complex genes. Other genetic differences which impact FA pathway expression may be masking the effect of *MYCN* amplification, however other common genetic aberrations in neuroblastoma were also not associated with FA pathway differential expression in this dataset (Appendix Table A14). In contrast, the impact of *MYCN* amplification on FA pathway expression in tumours strongly resembles that of *MYCN* overexpression in tet-regulated cell lines.

Lastly, FA pathway expression and activation in the non-MNA cell line SH-SY5Y showed greater similarity to MNA cell lines than the non-MNA cell line SHEP-1 (Figures 3.17, 3.19). Similar to MNA cells, SH-SY5Y cells upregulated upstream FANC and HRR FA genes (Figure 3.20). However, in contrast to MNA cells, SH-SY5Y cells also upregulated TLS and NER genes. This may be accounted for by high *MYCC* expression in SH-SY5Y cells (Figure 3.18A), suggesting induction of FA pathway differential expression is not exclusive to MYCN in the MYC family of transcription factors. Given high *MYCC* expression is often observed in high-risk non-MNA cases (Breit and Schwab, 1989), high *MYCC* expression may also account for the lack of FA pathway differential expression between *MYCN* amplification subgroups in the 39 neuroblastoma cell line RNA-Seq dataset (Figure 3.21B). In agreement, Fredlund et al., (2008) found

that neuroblastoma prognosis correlated with the combined activity of all MYC family proteins, suggesting MYC-signalling rather than MNA status is important for defining risk. Further study of the effect of MYCC on FA pathway expression would be necessary to determine whether our results may also be applicable in *MYCC*-deregulated cancers.

3.3.7 Multiple mechanisms of regulation may determine changes in FA pathway gene expression induced by *MYCN* overexpression

The numerous cellular functions of MYCN complicates the elucidation of the mechanism by which it regulates FA pathway genes. Given the large number of FA genes and the complexity of their roles in multiple DNA repair pathways, there may not be one cohesive regulatory mechanism. MYCN can transcriptionally regulate a vast array of direct target genes by high-affinity binding to E-boxes in promoters (Zeid et al., 2018). We observed MYCN binding at a canonical MYCN E-box within the *FANCD2* promoter by ChIP-PCR in SHEP-Tet21N MYCN ON cells and MNA IMR32 cells (Figure 3.26). ChIP-Seq analysis revealed MYCN binds to 51 of 58 FA gene promoters in neuroblastoma cells with high *MYCN* expression (Figure 3.27). This suggests most FA genes are directly regulated by MYCN, however analysis of reporter gene expression regulated by upstream FA gene promoters would be necessary to confirm this. The number of FA pathway gene promoters MYCN was bound to was reduced with decreasing levels of MYCN. Promoters at which MYCN is bound to during low *MYCN* expression have the highest affinity for MYCN binding, such as *HES1, RMI1, PMS2, REV3L, SLX1A, SLX1B, EME1, FANCC* and *RPA3*. Zeid et al., (2018) found genes regulated by low-affinity MYCN binding showed the greatest changes in expression upon perturbation of *MYCN* expression. FA genes with promoters which have weaker MYCN affinity, such as *MAD2L2, BRCA1, FANCB, FANCM, BRIP1, UBE2T* and *FANCD2* would therefore be most sensitive to changes in *MYCN* expression. In agreement, these genes were often among the most upregulated FA pathway genes in MNA and MYCN ON cells (Figure 3.13, 3.14, 3.19, 3.22). However, MYCN does not bind at the promoters of all genes which are significantly differentially expressed between *MYCN* status subgroups, such as *FAAP20, RFWD3* and *UHRF1* (Figures 3.14, 3.22). This suggests *MYCN* overexpression also regulates FA gene expression through other indirect mechanisms.

At physiological levels, MYCN directly regulates target genes by binding to high-affinity E-boxes in cis-regulatory elements (Zeid et al., 2018). However, at oncogenic levels, *MYCN* overexpression induces global upregulation of all active genes through invasion of excess MYCN at clustered, low-affinity E-boxes in promoters and enhancers of active genes. Zeid et al., (2018) observed that the timing of differential expression upon *MYCN* deregulation is important for elucidating the MYCN regulatory mechanism. In the following 2 to 24 hours after inhibition of *MYCN* expression in SHEP-Tet21N cells, MYCN is preferentially depleted from weaker binding sites in enhancers, inducing a global reduction in mRNA fold change (Zeid et al., 2018). Global loss of active chromatin marks was not observed until after 24 hours (Zeid et al., 2018). Conversely, high-affinity promoter E-boxes are preferentially bound following induction of *MYCN* expression in SHEP-PLXI-MYCN cells (Zeid et al., 2018). The few FA genes with higher MYCN promoter affinity such as *HES1, RMI1, PMS2, REV3L, SLX1A, SLX1B, EME1, FANCC* and *RPA3* were bound within 6 hours of *MYCN* induction in SHEP-PLXI-MYCN and retained MYCN binding even at very low *MYCN* expression levels in SHEP-Tet21N cells (Figure 3.27). However, most FA genes lost MYCN binding within 2 hours of *MYCN* shutdown in SHEP-Tet21N cells and were not bound by MYCN within 6 hours of *MYCN* induction in SHEP-PLXI-MYCN. Also, the most substantial change in expression for many FA pathway genes occurred between 8 and 24 hours following *MYCN* shutdown in SHEP-Tet21N cells (Figures 3.13, 3.4). The kinetics of FA pathway differential expression therefore suggests enhancer binding and other indirect mechanisms also contribute to FA pathway regulation by MYCN.

MYCN may also induce FA pathway differential expression epigenetically through regulation of, or association with, chromatin remodellers (Brenner et al., 2005; Corvetta et al., 2013; Tsubota et al., 2018; Zeid et al., 2018; Baluapuri et al., 2020). For example, *BRCA1* was shown to be significantly hypomethylated in high-risk neuroblastoma patients, suggesting a selective pressure for high *BRCA1* expression in MNA neuroblastoma (Herold et al., 2019). This may account for the high upregulation of *BRCA1* observed in SHEP-Tet21N MYCN ON cells (Figures 3.13, 3,14), despite lack of MYCN binding at the *BRCA1* promoter (Figure 3.27).

MYCN may also regulate FA pathway expression through other downstream effectors. It has been previously shown that E2F transcription factors have a vital role in coordinated regulation of FA gene expression throughout the cell cycle (Vaughn et al, 1996; Hoskins et al, 2008; Mitxelena et al, 2018; Liu et al., 2019). Jaber et al., (2016) showed p21/E2F4 downregulates nine FANC genes following induction of p53. It was

further elucidated that 19 FA genes are targets of the p53-DREAM pathway, which downregulates target genes during G0 and G1 when E2F4/5 associates with the DREAM complex (Engeland, 2018). Decaesteker et al., (2018) demonstrated that MYCN, in conjunction with TBX2, drives proliferation through activation of these p21-DREAM repressed targets.

E2F proteins can also induce expression of genes during S-phase (Hoskins et al., 2008; Engeland, 2018). E2F1/2 binds at FANC gene promoters to induce upregulation upon increased proliferation (Hoskins et al., 2008). The ability of MYCN to accelerate proliferation may therefore also contribute to FANC gene upregulation. However, although most studies observe a correlation between *FANCD2* expression and proliferation in both tumour cells and normal tissues (Hölzel et al., 2003; Van Der Groep et al., 2008; Rudland et al., 2010; Kais et al., 2016; Feng and Jin et al., 2019), this is not always consistent (Rudland et al., 2010; Kao et al., 2011). Also, the expression of *FANCD2* has been observed to be consistent throughout the cell cycle (Taniguchi et al., 2002a; Cantres-Velez et al., 2021), and therefore the impact of MYCN on cell cycle progression should not affect the FA pathway expression profile. Instead, aberrant regulation of other FA-regulating transcription factors such as NF-kB and p53 may contribute to cell-cycle independent FANC gene upregulation (Yarde et al., 2009; Liebetrau et al., 1997). Also, differentiation of leukaemia cells into macrophages induced downregulation of *FANCD2* and many FA core complex genes (Lu et al., 2011). Induction of a more stem-like state upon *MYCN* overexpression (Kerosuo et al., 2018), may therefore also contribute to the induction of FANC gene upregulation in a similar manner. Regardless of the mechanism of MYCN-induced FA pathway regulation, upregulation of FANC and HRR pathway genes suggests a greater reliance on FA pathway function in MNA neuroblastoma and supports the investigation of the FA pathway as a novel MNA-neuroblastoma target.

3.3.8 Limitations

Whilst the *MYCN*-inducible cell lines SHEP-Tet21N and SHEP-PLXI-MYCN enabled study of the effect of *MYCN* overexpression in an isogenic system, these models do not fully recapitulate a *MYCN* amplified environment, which often has higher *MYCN* expression (Figure 3.18A) and is frequently associated with other genetic aberrations such as *ALK* amplification or chromosome 1p deletions (Luttikhuis et al., 2001; De Brouwer et al., 2010). Furthermore, although *MYCN* amplification is

associated with high-risk, the clinical significance of high *MYCN* expression in neuroblastoma is controversial, and *MYCN* amplification status does not always correlate with *MYCN* expression (Chan et al., 1997, Bordow et al., 1998). In addition, the relevance of short term *MYCN* overexpression compared to the effects of constitutive high *MYCN* expression in MNA cells is uncertain. Tetracycline treatment, required to induce or inhibit *MYCN* expression, has been shown to impact gene expression patterns, resulting in metabolic and proliferation rate changes (Hackl et al., 2010; Ahler et al., 2013). The impact tetracycline-induced gene expression changes on our data was mitigated by demonstrating tetracycline treatment does not induce changes in FANCD2 expression in parental SHEP-1 cells with no tet-regulated *MYCN* expression system (Figure 3.12).

mRNA expression levels are frequently used to estimate functional differences at the protein level, however mRNA levels do not always strongly correlate with protein levels (Vogel and Marcotte, 2012). Further investigation could be carried out to determine protein expression levels of more FANC genes across a larger panel of cell lines and primary samples. The RNA-Seq dataset used to analyse FA pathway expression across 39 neuroblastoma cell lines only contained one replicate per cell line. Cell lines were therefore clustered by *MYCN* amplification status to determine statistical significance of average expression changes. Similarly, the statistical significance of differences in MYCN promoter binding between cell lines could not be determined as the ChIP-Seq dataset only contained one repeat per cell line. Also, only MYCN promoter binding was analysed using the ChIP-Seq dataset, which could be further explored to analyse MYCN binding at FA gene enhancers.

The FANCD2 L:S ratios used to determine FA pathway activation could be affected by *FANCD2* expression level, as the mono-ubiquitinated FANCD2 western blot band is often more difficult to detect at lower expression levels. Also, not all FA pathway functions are dependent on FANCD2 mono-ubiquitination, such as recruitment of TLS polymerases or regulation of DNA replication dynamics (Kim et al., 2012; Lossaint et al., 2013). Therefore, FANCD2 L:S ratios may not measure the full extent of FA pathway function.

FA pathway expression in neuroblastoma cells relative to non-cancerous cells was not determined. Given neuroblastoma is an embryonal cancer, and can occur within multiple tissues, it is difficult to establish an accurate normal cell line control. However, FA pathway expression could be further analysed in the hTERT-immortalized

retinal epithelial cell line RPE-1, which has been used as a normal cell control in previous neuroblastoma studies (Harenza et al., 2017).

3.3.9 Summary

In this chapter, we met the criteria of the first thesis aim by demonstrating that MYCN overexpression or amplification induced differential expression of FA pathway genes which clustered according to FA pathway role. In isogenic MYCN expression systems, across a small panel of neuroblastoma cell lines, and in neuroblastoma tumours, upstream FANC genes and HRR genes were predominantly transcriptionally upregulated, whilst TLS and NER genes were inconsistently downregulated or showed no substantial change in expression. ChIP analysis suggested MYCN may directly regulate expression of FA pathway genes through promoter binding. This upregulation of FANC genes is indicative of an increased dependence on FA pathway function in neuroblastoma cells with high MYCN expression, and therefore validates the FA pathway as a putative therapeutic target. In Chapter 4 we therefore determine the effect of MYCN overexpression and amplification on the efficacy of FA pathway inhibition in neuroblastoma cells, and explore the molecular mechanism behind this.

Chapter 4. FA pathway inhibition has therapeutic potential in neuroblastoma

4.1 Introduction

The FA pathway is a DNA damage response network which co-ordinates proteins from multiple other DNA repair pathways such as NER, TLS and HRR to remove DNA inter-strand crosslinks (ICLs) in a replication-dependent manner. (Sasaki et al., 1975; Taniguchi et al., 2002a; Moldovan and D'Andrea, 2009; Rodriguez and D'Andrea, 2017). The FA pathway also functions to limit replication stress through several repair-independent mechanisms to prevent replication-associated DNA damage (Sobeck et al., 2006).

Firstly, multiple FA pathway proteins protect the fidelity of stalled replication forks (Howlett et al., 2005; Gari et al., 2008; Schwab et al., 2010; Schlacher et al., 2011; Schlacher et al., 2012; Yang et al., 2015; Daza-Martin et al., 2019; Madireddy et al., 2016). For example, mono-ubiquitination of FANCD2 promotes loading of BRCA1/2-stabilised RAD51 at stalled forks to protect from nucleolytic degradation (Schlacher et al., 2012). Secondly, FA pathway proteins regulate replication fork restart and progression, independently from FANCD2 mono-ubiquitination (Lossaint et al., 2013; Yeo et al., 2014; Raghunandan et al., 2015). For example, FANCD2, BRCA1 and BRCA2 regulate the BLM helicase to promote restart of stalled replication forks whilst restraining new origin firing (Chaudhury et al., 2013; Yeo et al., 2014; Raghunandan et al., 2015; Thompson et al., 2017). Thirdly, the FANCM-FAAP24 FA pathway complex is vital for efficient ATR checkpoint signalling (Collis et al., 2008). Similarly, ATR DDR activity is necessary for efficient FA pathway activation (Andreassen et al., 2004; Qiao et al., 2004; Collis et al., 2008; Wilson et al., 2008; Collins et al., 2009; Singh et al., 2013; Chen et al., 2015; Wang et al., 2007). Lastly, FA pathway proteins function in the resolution of R-loops (Garcia-Rubio et al., 2015; Schwab et al., 2015; Madireddy et al., 2016; Barroso et al., 2019; Pan et al., 2019; Silva et al., 2019). R-loops are often formed as a consequence of transcription-replication conflicts and are therefore both a source of, and a product of, replication stress and genomic instability (Santos-Pereira and Aguilera, 2015; Allison and Wang, 2019). FANCD2, BRCA1, BRCA2 and ATR function in R-loop resolution, often by recruiting RNA processing enzymes (Bhatia et al., 2014; Garcia-Rubio et al., 2015; Hatchi et al., 2015; Schwab et al., 2015; Madireddy et al., 2016; Zhang et al., 2017; D'Alessandro et al., 2018; Okamoto et al., 2018a;

Okamoto et al., 2018b; Okamoto et al., 2019; Chang et al., 2019b; Herold et al., 2019; Pladevall-Morera et al., 2019; Matos et al., 2020). R-loop binding by FANCD2 induces its mono-ubiquitination (Liang et al., 2019a).

Altogether, FA pathway function is primarily vital for ICL repair and mitigation of replication stress. Loss of FA pathway function therefore primarily sensitises cells to DNA crosslinking and replication-stress inducing agents (Sasaki et al., 1975; Taniguchi et al., 2002a; Houghtaling et al., 2003; Niedzwiedz et al., 2004; Bridge et al., 2005; Dai et al., 2015; Dai et al., 2017). As such, targeted FA pathway inhibition would be beneficial in enhancing the efficacy of DNA crosslinking chemotherapeutics. However, despite promising ongoing developments (Voter et al., 2016; Cornwell et al., 2019; Morreale et al., 2017; Sharp et al., 2020), there are currently no widely accepted specific FA pathway inhibitors (Liu et al., 2020a; Taylor et al., 2020). Instead, many non-specific FA pathway inhibitors have been identified through cell-based or in vitro screening assays and, despite broad off-target effects, these are commonly used to study the potential effects of FA pathway inhibition (Chirnomas et al., 2006; Landais et al., 2009a; Landais et al., 2009b; Jacquemont et al., 2012; Jun et al., 2013; Sharp et al., 2020). For example, curcumin and ouabain were identified as indirect, non-specific inhibitors of FANCD2 mono-ubiquitination (Chirnomas et al., 2006; Jun et al., 2013), which sensitise a broad range of cancer cell lines to DNA crosslinking, DNA alkylating or replication stress-inducing chemotherapeutics (Chrinomas et al., 2006; Chen et al., 2007; Jun et al., 2013; Patil et al., 2014; Chen et al., 2015b; Kunnumakkara et al., 2007; Sukumari-Ramesh et al., 2011; Namkaew et al., 2018; Fonseka et al., 2020; Yoshida et al., 2017). Treatment with ouabain or curcumin alone exacerbates endogenous DNA damage in cancer cells (Rak et al., 2013; Chen et al., 2015b; Shang et al., 2016; Chang et al., 2019a; Yang et al., 2021; Du et al., 2021; Wang et al., 2022a) but have been observed to induce apoptosis through a wide array of mechanisms (Zhai et al., 2020).

Amplification of the *MYCN* oncogene occurs in 20% of neuroblastoma cases and is always associated with high-risk disease due to its significant association with aggressive, refractory and resistant disease (Brodeur et al., 1984; Seeger et al., 1985; Moreau et al., 2006; Cohn et al., 2009; Maris, 2010). The five-year survival rate for high-risk neuroblastoma remains at 50%, despite improvements to the intensive multimodal treatment strategies (Qiu and Matthay, 2022). This highlights a need for novel therapeutics which improve the efficacy of current treatments. Overexpression of *MYCN* has been shown to induce greater levels of replication stress and DNA damage (Gu et al., 2015; King et al., 2020), and this sensitises cells to inhibition of DNA repair and

replication stress limiting pathways (Cole et al., 2011; Colicchia et al., 2017; Petroni et al., 2018; King et al., 2020; King et al., 2021; Southgate et al., 2020). A greater reliance on these pathways in MNA cells was indicated by a MYCN-induced upregulation in their expression (Cole et al., 2011; Gu et al., 2015; Petroni et al., 2016; Colicchia et al., 2017; Petroni et al., 2018; King et al., 2020). In Chapter 3, we demonstrated MYCN induces an upregulation of FANC and HRR-associated FA pathway genes in neuroblastoma cell lines and tumours. However, the efficacy of FA pathway inhibition in neuroblastoma treatment has not yet been determined and the functional consequence of FA pathway upregulation and inhibition in the context of MYCN is unknown.

It was therefore hypothesised that inhibition of the FA pathway would sensitise neuroblastoma cells to (i) clinically relevant DNA crosslinking and alkylating chemotherapeutics, and (ii) MYCN-induced replication stress and DNA damage. This chapter aimed to: (a) Determine the efficacy of curcumin in inhibiting MYCN- and chemotherapy-induced FA pathway activation. (b) Examine the efficacy of curcumin in sensitising neuroblastoma cells to crosslinking chemotherapeutics and high *MYCN* expression. (c) Explore the molecular mechanism behind the MYCN-induced sensitivity to curcumin observed in neuroblastoma cells.

4.2 Results

4.2.1 Curcumin effectively inhibits endogenous and chemotherapy-induced FANCD2 mono-ubiquitination across a range of neuroblastoma cell lines

4.2.1.1 High MYCN expression induces FA pathway activation in neuroblastoma cells

The mono-ubiquitination of FANCD2 is required for many FA pathway functions and is therefore used as a marker of FA pathway activation (Moldovan and D'Andrea 2009; Schlacher et al., 2012; Liang et al., 2019a). In Chapter 3, it was observed that higher FANCD2 mono-ubiquitination was associated with higher *MYCN* expression across a panel of eight neuroblastoma cell lines, including SHEP-Tet21N MYCN ON and OFF cells (Figure 3.16C). To confirm this trend was based on *MYCN* expression, rather than other factors associated with *MYCN* amplification, we analysed the impact of *MYCN* expression on FA pathway activation in *MYCN*-inducible SHEP-Tet21N cells (Figure 4.1). The extent of FA pathway activation was measured by calculating the ratio of mono-ubiquitinated FANCD2 (L) to non-ubiquitinated FANCD2 (S) observed by

western blot (Figure 4.1A). Across multiple repeats, the extent of endogenous FANCD2 mono-ubiquitination was significantly higher in MYCN ON cells compared to MYCN OFF cells (Figure 4.1B). This data suggests high *MYCN* expression induces FANCD2 mono-ubiquitination in neuroblastoma cells.

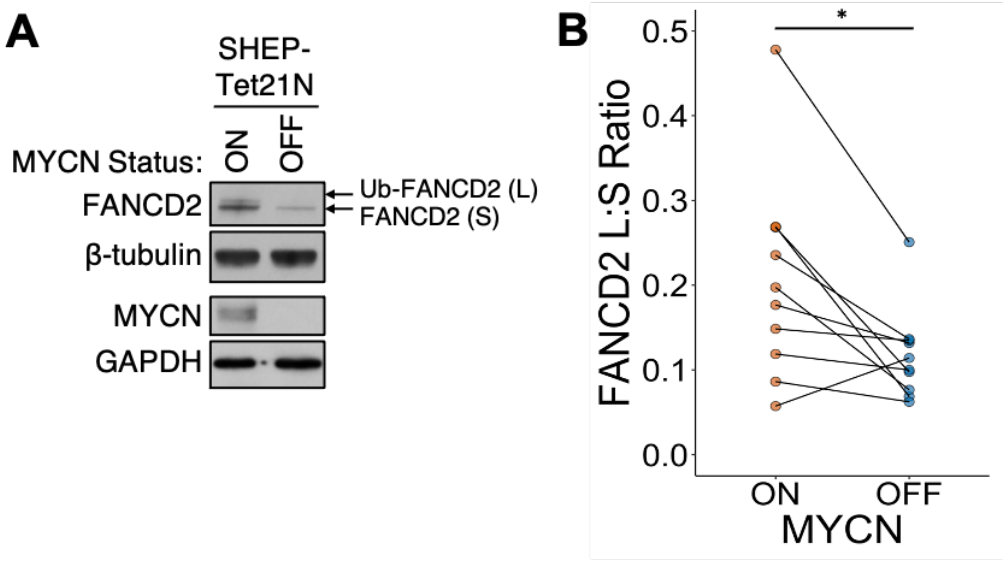

Figure 4.1. High MYCN expression significantly induces FA pathway activation in SHEP-Tet21N neuroblastoma cells.
Endogenous levels of FANCD2 mono-ubiquitination was quantified in SHEP-Tet21N MYCN ON and OFF cells across multiple experiments. This data is summarised here. **(A)** For clarity, part of Figure 3.16 is re-presented as an example of the FANCD2 protein bands compared in each experiment. MYCN and FANCD2 protein levels in untreated SHEP-Tet21N MYCN ON and OFF cells were determined by western blotting. **(B)** FANCD2 L:S ratios of un-treated SHEP-Tet21N MYCN ON and OFF cells were calculated for all repeats across six experiments (n=10). Western blots used for analysis are presented in Figures 3.16, 4.2, 4.4-4.7. Data are paired by repeat. Statistical significance between L:S ratios in MYCN ON and OFF cells was determined by a paired Student's t-test where n.s. = non-significant, *p<0.05, **p<0.01, ***p<0.001.

4.2.1.2 Temozolomide and cisplatin induce FA pathway activation in neuroblastoma cell lines

The DNA alkylating agent temozolomide (TMZ), and DNA crosslinking agent cisplatin, have been previously shown to induce FANCD2 mono-ubiquitination and therefore FA pathway activation across a range of cancer cell lines (Chirnomas et al., 2006; Chen et al., 2007; Jun et al., 2013; Patil et al., 2014; Chen et al., 2015b).

To determine the optimal dose of temozolomide required to induce FA pathway activation in neuroblastoma cells, SHEP-Tet21N MYCN ON and OFF cells were treated with 5 μM to 100 μM TMZ for 16 hours before FANCD2 protein expression was

analysed by western blot (Figure 4.2A). All TMZ doses induced an upregulation in total FANCD2 protein levels by over 50% in MYCN ON cells (Figure 4.2B). In both MYCN ON and OFF cells, all doses of temozolomide induced more than a 4-fold increase in the average FANCD2 L:S ratio (Figure 4.2C). To confirm that these doses of TMZ also effectively induced FA pathway activation across other neuroblastoma cell lines, MNA IMR32 cells and non-MNA SHEP-1 cells were treated with 50 μM or 100 μM TMZ for 24 hours before FANCD2 protein expression was analysed by western blot (Figure 4.3A). In both IMR32 and SHEP-1 cells, all TMZ doses increased total FANCD2 protein expression by over 50% (Figure 4.3B). TMZ treatment induced at least a two-fold increase in the FANCD2 L:S ratio in both IMR32 and SHEP-1 cells (Figure 4.3C).

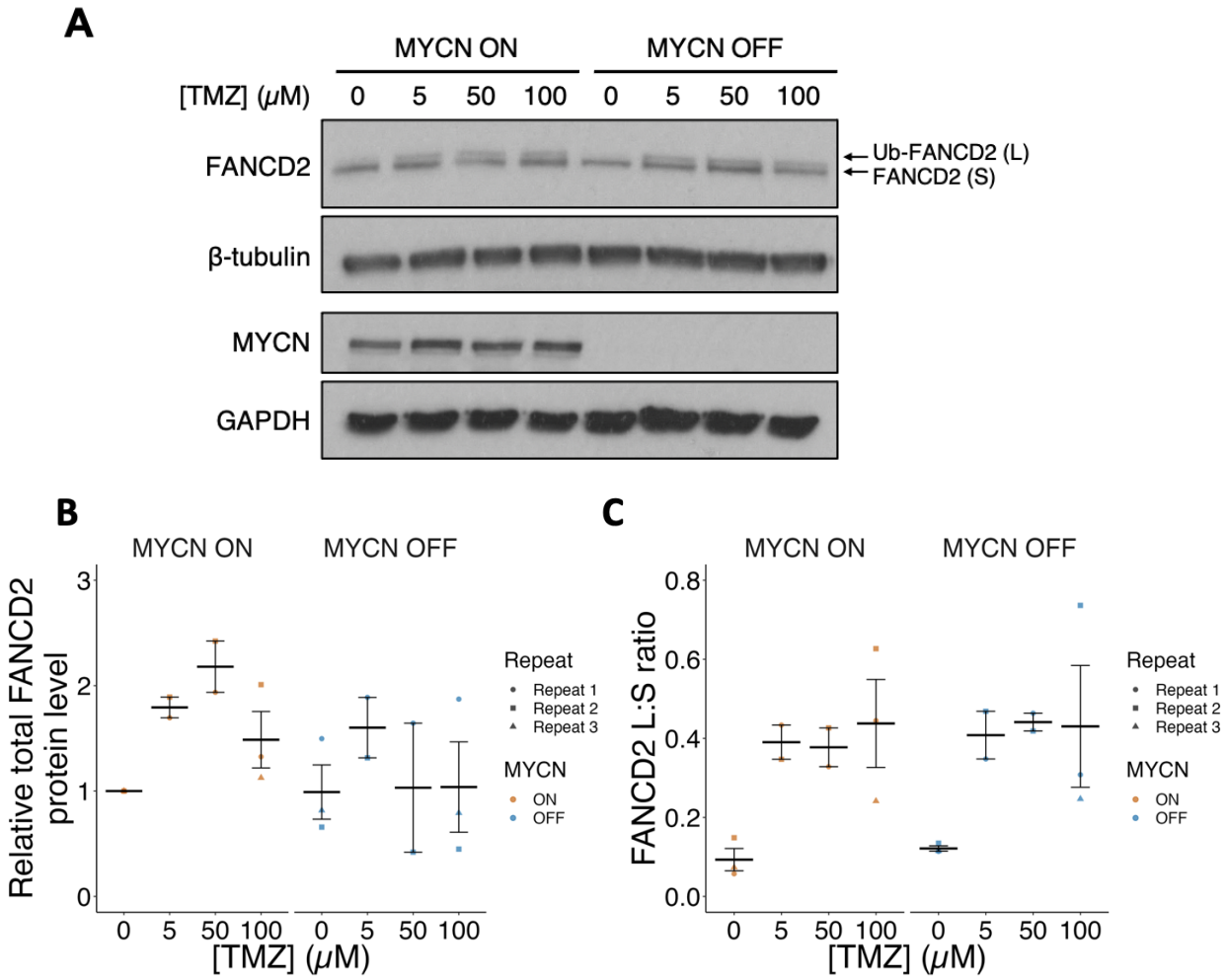

Figure 4.2. Temozolomide induces FA pathway activation in SHEP-Tet21N neuroblastoma cells.
SHEP-Tet21N MYCN ON and OFF cells were treated with 0-100 μM temozolomide (TMZ) for 16 hours. **(A)** MYCN and FANCD2 protein levels were determined by western blotting. **(B)** Total FANCD2 band intensity (sum of L and S band intensities) was quantified relative to MYCN ON 0 μM TMZ treatment and normalised to ß-tubulin band intensity. **(C)** FANCD2 L:S ratios were calculated for each condition. For (B) and (C), means ±SEM are shown (n ≥ 2).

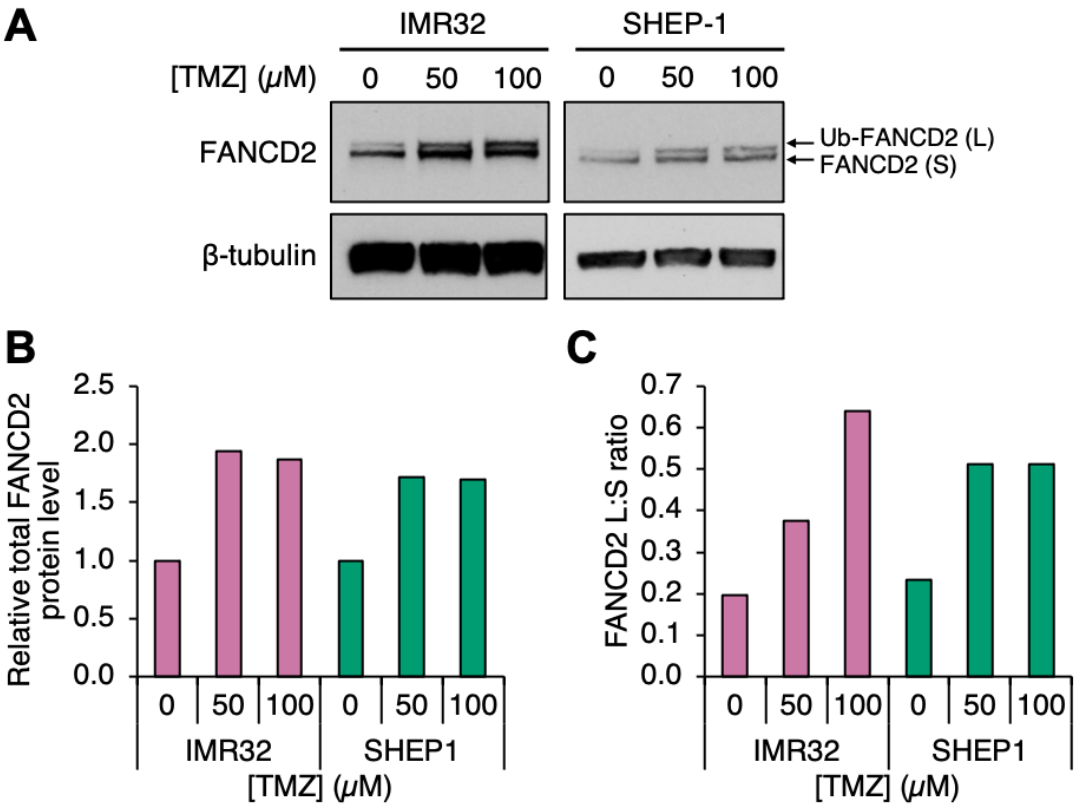

Figure 4.3. Temozolomide induces FA pathway activation in SHEP-1 and IMR32 cells.
SHEP-1 (MYCN non-amplified) and IMR32 (MYCN amplified) cells were treated with 0-100 μM temozolomide (TMZ) for 24 hours. **(A)** FANCD2 protein levels were determined by western blotting (n=1). **(B)** Total FANCD2 band intensity (sum of L and S band intensities) was quantified relative to 0 μM TMZ treatment for each cell line and normalised to ß-tubulin band intensity. **(C)** FANCD2 L:S

To determine the optimal dose of cisplatin necessary to induce FA pathway activation in neuroblastoma cells, SHEP-Tet21N MYCN ON and OFF cells were treated with 0.5 μM to 5 μM cisplatin for 24 hours before FANCD2 protein expression was analysed by western blot (Figure 4.4A). Increasing doses of cisplatin induced an increasing downregulation of total FANCD2 protein levels in MYCN OFF cells but did not effect FANCD2 protein levels in MYCN ON cells (Figure 4.4B). Cisplatin induced FANCD2 mono-ubiquitination in a dose-dependent manner in both MYCN ON and OFF cells, with the biggest induction observed in MYCN OFF cells (Figure 4.4C).

This data demonstrates 50 μM TMZ and 5 μM cisplatin effectively induce high levels of FA pathway activation in neuroblastoma cells regardless of *MYCN* status.

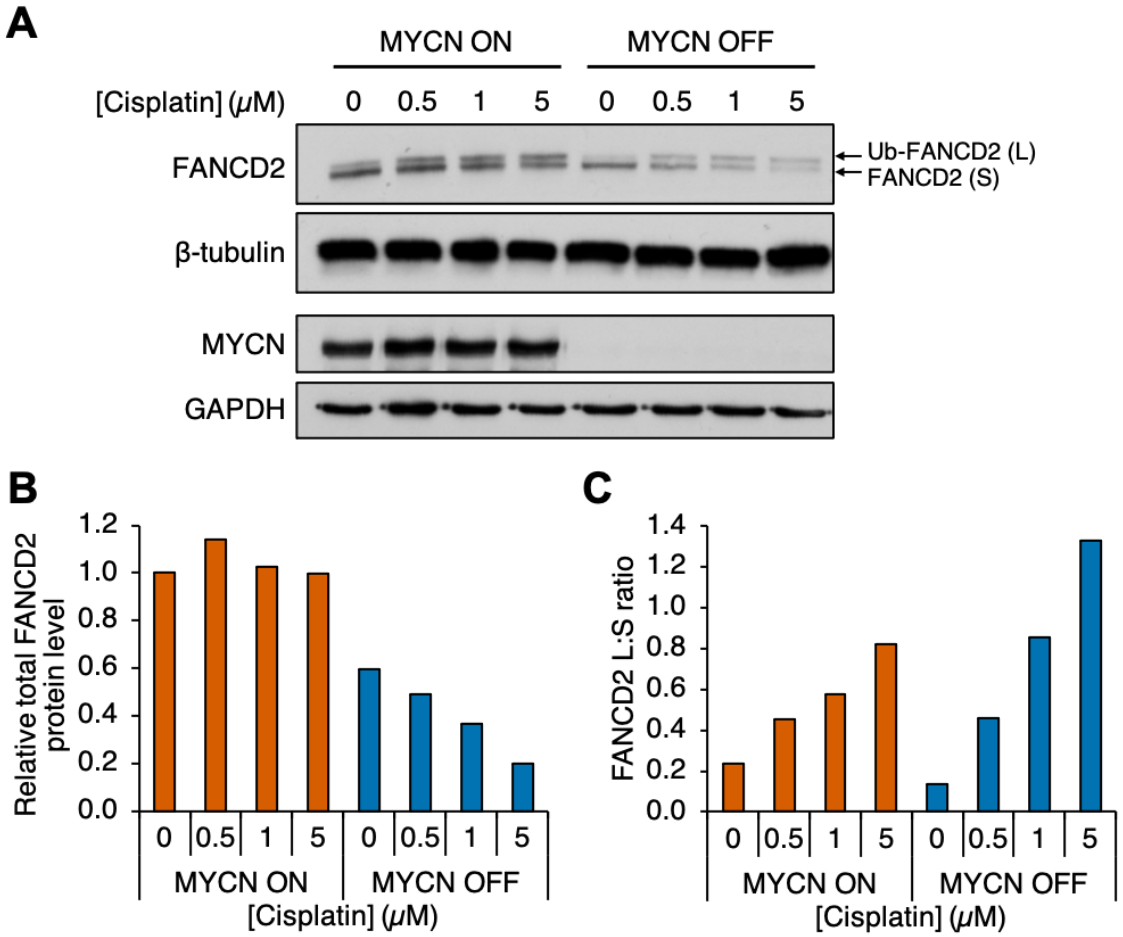

Figure 4.4. Cisplatin induces FA pathway activation in SHEP-Tet21N neuroblastoma cells.
SHEP-Tet21N MYCN ON and OFF cells were treated with 0-5 μM cisplatin for 24 hours. **(A)** MYCN and FANCD2 protein levels were determined by western blotting (n=1). **(B)** Total FANCD2 band intensity (sum of L and S band intensities) was quantified relative to MYCN ON 0 μM cisplatin treatment and normalised to

4.2.1.3 Curcumin inhibits endogenous and cisplatin-induced FA pathway activation

Curcumin, a natural polyphenolic compound, was identified as an inhibitor of FANCD2 mono-ubiquitination by Chirnomas et al., (2006) and has since been demonstrated to effectively inhibit chemotherapy-induced FA pathway activation in a range of cancer cell lines (Chirnomas et al., 2006; Patil et al., 2014; Chen et al., 2015b). However, curcumin also induces a wide range of off-target effects and is therefore a non-specific FA pathway inhibitor (Zhai et al., 2020). To determine whether curcumin effectively inhibits FA pathway activation in neuroblastoma cells, SHEP-Tet21N MYCN ON and OFF cells were pre-treated with 0 μM or 10 μM curcumin for 16 hours before

addition of 0 μM to 10 μM cisplatin for 24 hours. FANCD2 protein levels were then determined by western blot (Figure 4.5A). Increasing doses of cisplatin did not alter total FANCD2 expression in either MYCN ON or OFF cells (Figure 4.5B). However, curcumin treatment induced a downregulation of total FANCD2 expression consistently across all cisplatin doses in MYCN OFF cells. Cisplatin induced FANCD2 mono-ubiquitination in both MYCN ON and OFF cells, with the greatest increase in activation again observed in MYCN OFF cells (Figure 4.5C). 10 μM curcumin treatment effectively inhibited both endogenous and cisplatin-induced FANCD2 mono-ubiquitination in MYCN ON and OFF cells.

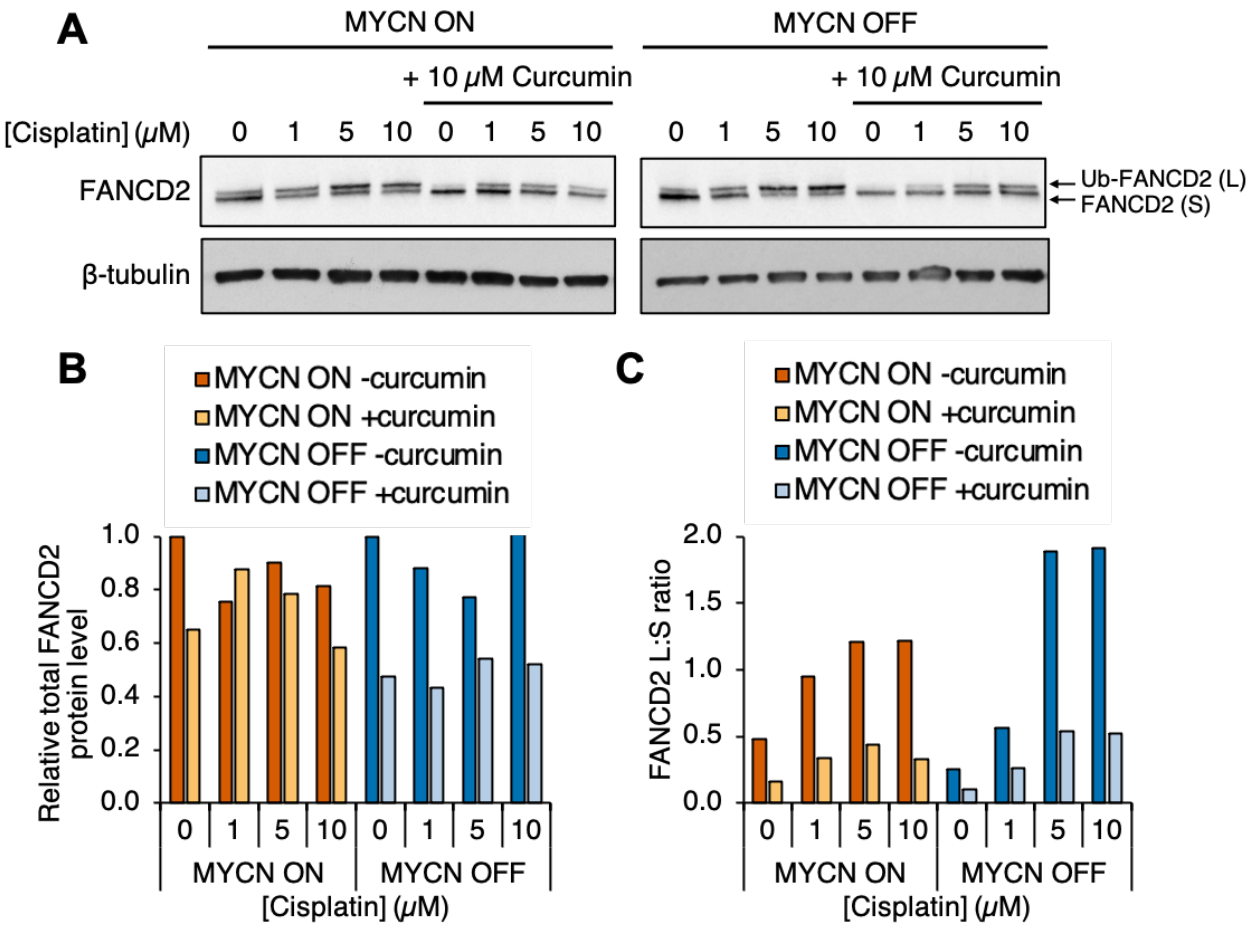

Figure 4.5. Curcumin inhibits endogenous and cisplatin-induced FA pathway activation in SHEP-Tet21N neuroblastoma cells.
SHEP-Tet21N MYCN ON and OFF cells were pre-treated with 0 μM or 10 μM curcumin for 16 hours before addition of 0-10 μM cisplatin for 24 hours. **(A)** FANCD2 protein levels were determined by western blotting (n=1). **(B)** Total FANCD2 band intensity (sum of L and S band intensities) was quantified relative to 0 μM curcumin with 0 μM cisplatin treatment, independent and normalised to ß-tubulin band intensity. **(C)** FANCD2 L:S ratios were calculated for each condition.

To determine the optimal curcumin dose for inhibition of endogenous and cisplatin-induced FA pathway activation, SHEP-Tet21N MYCN ON and OFF cells were pre-treated with 5 to 15 μM curcumin for 16 hours before addition of 0 μM or 0.5 μM cisplatin for 24 hours. FANCD2 protein expression and mono-ubiquitination was then analysed by western blot (Figure 4.6A). With no curcumin pre-treatment, cisplatin induced a non-significant increase in total FANCD2 protein levels in both MYCN ON and OFF cells ($F(3) = 0.109$, $p > 0.05$). (Figure 4.6B). Treatment with 15 μM curcumin induced a non-significant downregulation in total FANCD2 levels in MYCN ON cells ($F(3) = 0.109$, $p > 0.05$). Curcumin also inhibited endogenous and cisplatin-induced FANCD2 mono-ubiquitination in MYCN ON cells in a dose-dependent manner (Figure

4.6C), however this inhibition was not statistically significant ($F(3) = 0.233$, $p > 0.05$), perhaps because of the highly variable level of FA pathway induction achieved by cisplatin. In MYCN OFF cells, treatment with 10 μM curcumin inhibited cisplatin-induced but not endogenous FA pathway activation. Treatment with 15 μM curcumin induced an induction in FANCD2 mono-ubiquitination in MYCN OFF cells. It was observed by eye that 15 μM curcumin induced greater cell death and therefore this increased FA pathway activation could be indicative of increased toxicity by pleiotropic effects.

This data therefore indicates that treatment with 5 μM curcumin consistently inhibits cisplatin-induced and endogenous FA pathway activation in MYCN ON cells across all three replicates, however it must be noted that this is not statistically significant. In contrast, 5 μM curcumin does not inhibit endogenous FA pathway activation in MYCN OFF cells. This suggests curcumin inhibits MYCN-induced FA pathway activation. Given the lower endogenous level of FANCD2 expression and mono-ubiquitination, inhibition of endogenous FA pathway activation in MYCN OFF cells may be difficult to observe. Additionally, treatment with 15 μM curcumin induces FA pathway activation in MYCN OFF cells.

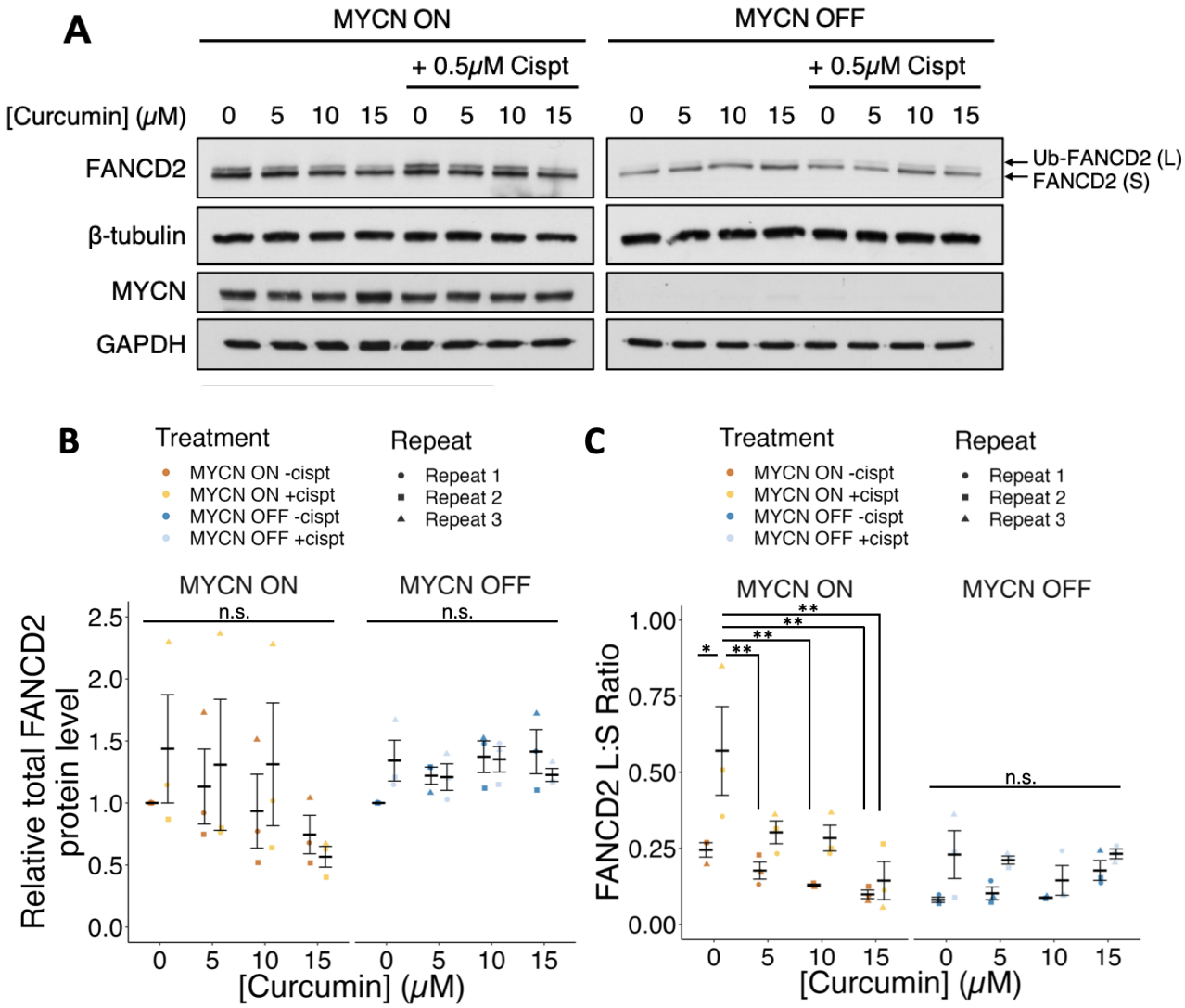

Figure 4.6. 5 μM curcumin inhibits endogenous and cisplatin-induced FA pathway activation in SHEP-Tet21N cells.
SHEP-Tet21N MYCN ON and OFF cells were pre-treated with 0-15 μM curcumin for 16 hours before addition of 0 μM or 0.5 μM cisplatin for 24 hours. **(A)** MYCN and FANCD2 protein levels were determined by western blotting. **(B)** Total FANCD2 band intensity (sum of L and S band intensities) was quantified relative to 0 μM curcumin with 0 μM cisplatin treatment and normalised to ß-tubulin band intensity. **(C)** FANCD2 L:S ratios were calculated for each condition. In (B) and (C), means ±SEM are shown (n=3). Statistical significance between different treatment conditions was determined by a two-way ANOVA for each MYCN ON and OFF group where n.s. = non-significant, *p<0.05, **p<0.01, ***p<0.001.

4.2.1.4 Optimised cisplatin and curcumin doses effectively induce and inhibit FA pathway activation across a panel of neuroblastoma cell lines

In Figures 4.4-4.6, it was observed that 5 μM cisplatin and 5 μM curcumin effectively induced and inhibited FA pathway activation respectively in SHEP-Tet21N MYCN ON cells. To enable direct comparison of the levels of FA pathway activation in MYCN ON and OFF cells at these optimised doses, SHEP-Tet21N MYCN ON and OFF cells were pre-treated with 0 μM or 5 μM curcumin for 16 hours before addition of 0 μM or 5 μM cisplatin for 24 hours. FANCD2 protein levels were determined by western blot (Figure 4.7A). FANCD2 expression levels were not affected by curcumin or cisplatin treatment in MYCN ON cells, however both treatments induced a small reduction in total FANCD2 levels in MYCN OFF cells (Figure 4.7B). At these optimised doses, curcumin inhibited cisplatin-induced FANCD2 mono-ubiquitination in both MYCN ON and OFF cells and a small reduction in endogenous FANCD2 mono-ubiquitination was observed in one of two repeats (Figure 4.5C).

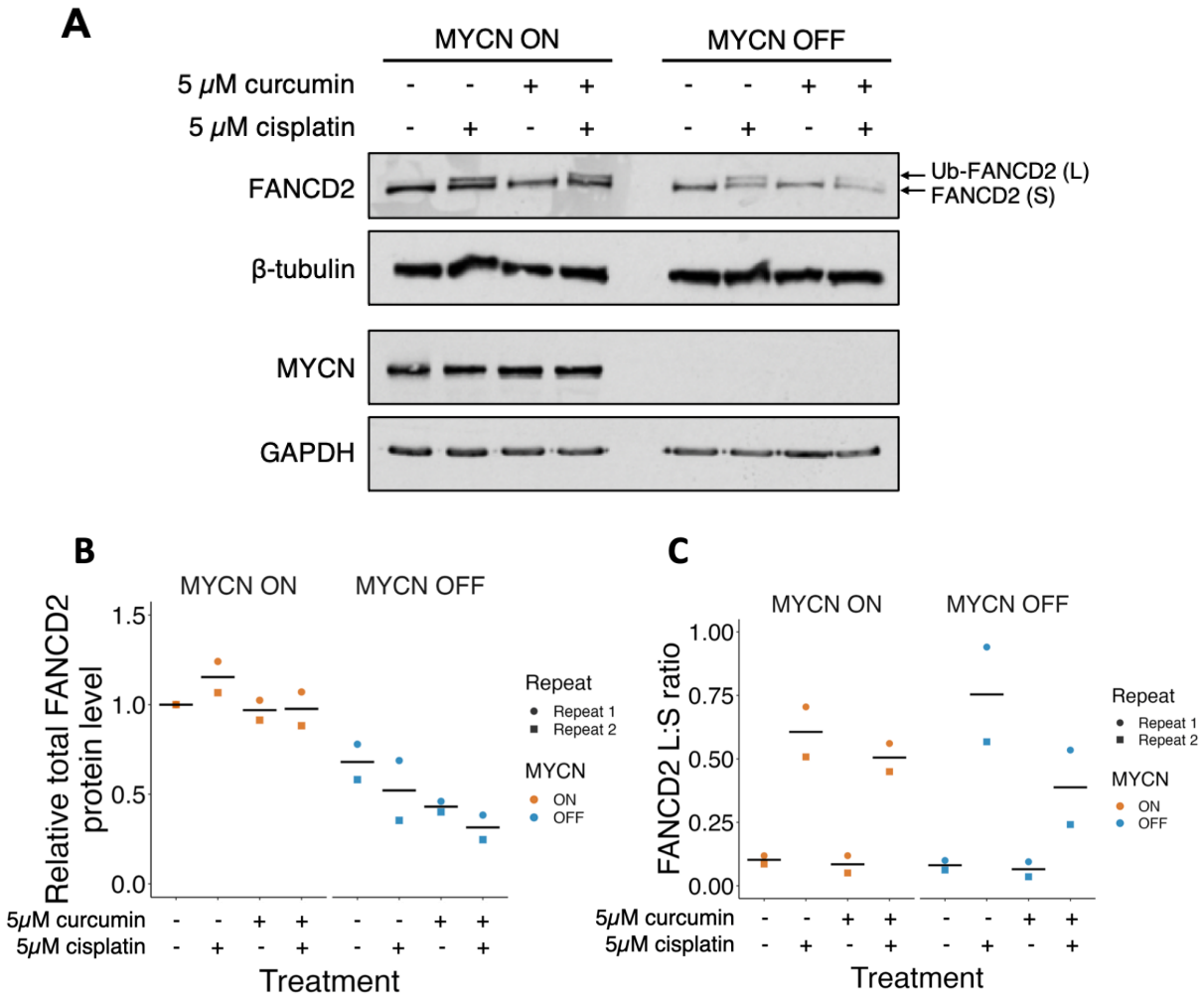

Figure 4.7. Optimised curcumin and cisplatin doses effectively induce and inhibit FA pathway activation in SHEP-Tet21N MYCN ON and OFF cells. SHEP-Tet21N MYCN ON and OFF cells were pre-treated with 0 μM or 5 μM curcumin for 16 hours before addition of 0 μM or 5 μM cisplatin for 24 hours. **(A)** MYCN and FANCD2 protein levels were determined by western blotting (n=2). **(B)** Total FANCD2 band intensity (sum of L and S band intensities) was quantified relative to 0 μM curcumin with 0 μM cisplatin treatment in MYCN ON cells and normalised to ß-tubulin band intensity. **(C)** FANCD2 L:S ratios were calculated for each condition. In (B) and (C), black bar displays means (n=2).

To determine whether these optimised curcumin and cisplatin doses were also effective in MNA and non-MNA neuroblastoma cell lines, MNA cell lines IMR32 and Kelly, and non-MNA cell lines SHEP-1 and SH-SY5Y, were pre-treated with 0 μM or 5 μM curcumin for 16 hours before addition of 0 μM or 5 μM cisplatin for 24 hours. FANCD2 protein expression in IMR32 and SHEP-1 cells was analysed in parallel by western blot (Figure 4.8A). Similarly to SHEP-Tet21N MYCN OFF cells, total FANCD2 expression in SHEP-1 cells was slightly reduced by curcumin and cisplatin treatment (Figure 4.8B). In IMR32 cells, cisplatin treatment induced higher FANCD2 expression and curcumin treatment downregulated FANCD2 expression. Treatment with 5 μM cisplatin induced FA pathway activation in both IMR32 and SHEP-1 cells (Figure 4.8C). Treatment with 5 μM curcumin inhibited both endogenous and cisplatin-induced FANCD2 mono-ubiquitination in IMR32 cells, but only inhibited cisplatin-induced FANCD2 mono-ubiquitination in SHEP-1 cells. FANCD2 protein expression in Kelly and SH-SY5Y cells was also analysed in parallel by western blot (Figure 4.9A). Cisplatin treatment induced an increase in total FANCD2 levels in Kelly cells, and curcumin treatment induced a downregulation in FANCD2 levels in both Kelly and SH-SY5Y cells (Figure 4.9B). Treatment with 5 μM cisplatin induced FA pathway activation in both Kelly and SH-SY5Y cells (Figure 4.9C). Unlike in MYCN OFF and non-MNA SHEP-1 cells, treatment with 5 μM curcumin inhibited both endogenous and cisplatin-induced FANCD2 mono-ubiquitination in SH-SY5Y cells. The observation of reduced endogenous FA pathway activation may be due to high *MYCC* expression in SH-SY5Y cells (Figure 3.16). In Kelly cells, 5 μM curcumin induced FANCD2 mono-ubiquitination. This could be indicative of a greater curcumin cytotoxicity in Kelly cells. Given curcumin treatment reduced FANCD2 expression in Kelly cells, this observation of FA pathway induction by curcumin may also be attributed to the reduced reliability of measuring FANCD2 L:S ratios by western blot when total FANCD2 expression is low.

This data indicates 5 μM cisplatin effectively induces FA pathway activation across a panel of *MYCN*-inducible, MNA and non-MNA neuroblastoma cells. Pre-treatment with 5 μM curcumin inhibits cisplatin-induced FA pathway activation across most cell lines, but only inhibits endogenous FA pathway activation in neuroblastoma cells with high *MYCN* or *MYCC* expression. In Kelly cells, 5 μM curcumin treatment induces FANCD2 mono-ubiquitination. This may be indicative of greater toxicity. Whilst the effect of cisplatin treatment on total FANCD2 levels varies across cell lines, curcumin consistently induces downregulation of FANCD2 expression across all cell lines with the exception of SHEP-Tet21N MYCN ON cells.

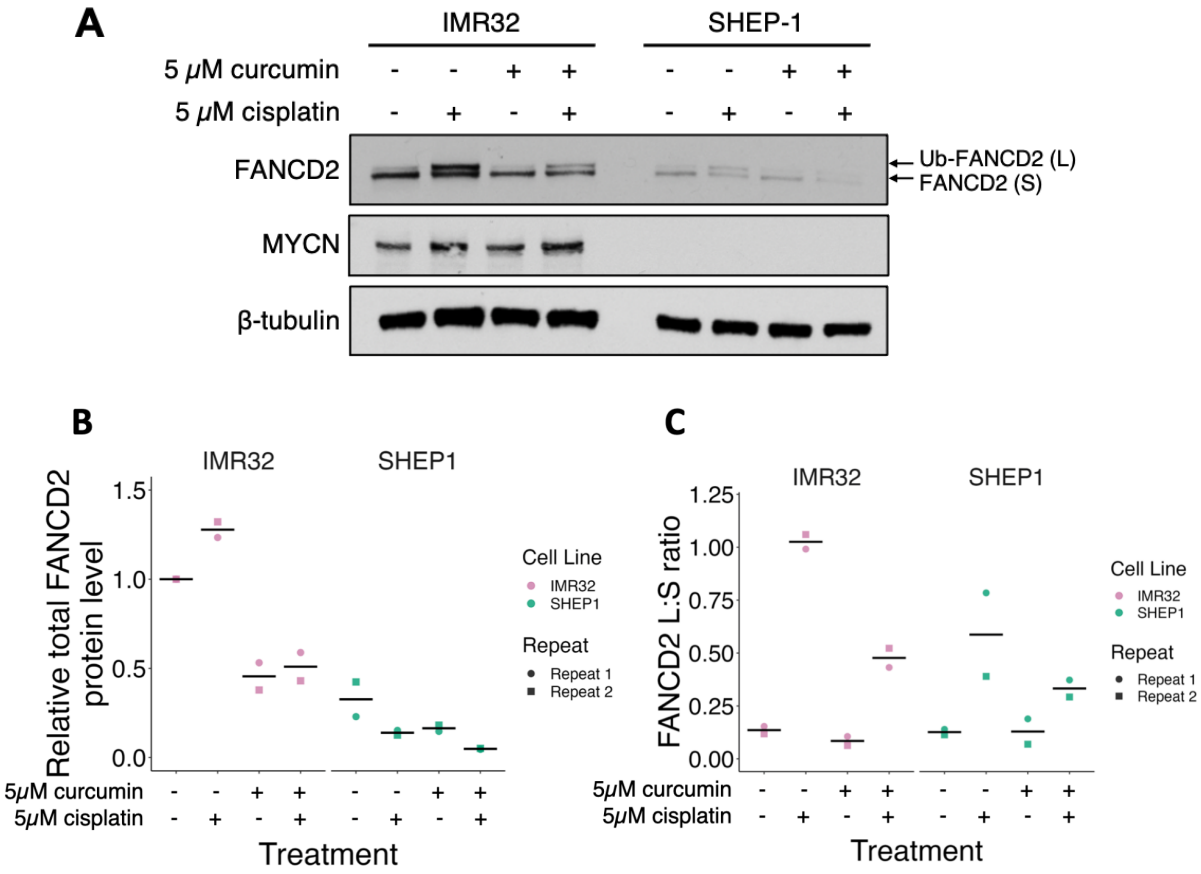

Figure 4.8. Optimised curcumin and cisplatin doses effectively induce and inhibit FA pathway activation in IMR32 and SHEP-1 cells.
IMR32 (MYCN amplified) and SHEP-1 (MYCN non-amplified) cells were pre-treated with 0 μM or 5 μM curcumin for 16 hours before addition of 0 μM or 5 μM cisplatin for 24 hours. **(A)** MYCN and FANCD2 protein levels were determined by western blotting (n=2). **(B)** Total FANCD2 band intensity (sum of L and S band intensities) was quantified relative to 0 μM curcumin with 0 μM cisplatin treatment in IMR32 cells and normalised to ß-tubulin band intensity. **(C)** FANCD2 L:S ratios were calculated for each condition. In (B) and (C), black bar indicates means (n=2).

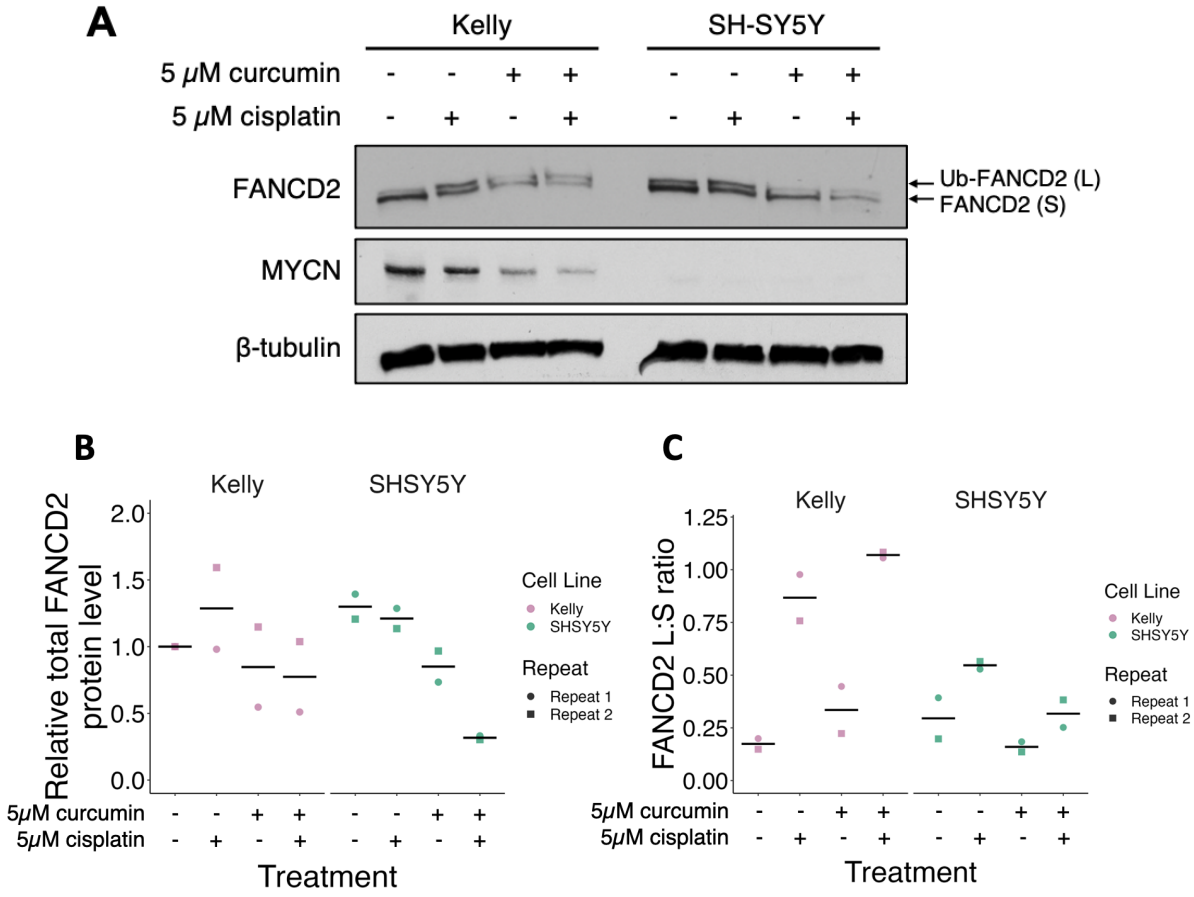

Figure 4.9. Optimised curcumin and cisplatin doses effectively induce and inhibit FA pathway activation in SH-SY5Y cells but not in Kelly cells.
Kelly (MYCN amplified) and SH-SY5Y (MYCN non-amplified) cells were pre-treated with 0 μM or 5 μM curcumin for 16 hours before addition of 0 μM or 5 μM cisplatin for 24 hours. **(A)** MYCN and FANCD2 protein levels were determined by western blotting (n=2). **(B)** Total FANCD2 band intensity (sum of L and S band intensities) was quantified relative to 0 μM curcumin with 0 μM cisplatin treatment in Kelly cells and normalised to ß-tubulin band intensity. **(C)** FANCD2 L:S ratios were calculated for each condition. In (B) and (C), black bar indicates means (n=2).

4.2.2 Curcumin sensitises neuroblastoma cells to high *MYCN* expression and crosslinking chemotherapeutics

4.2.2.1 Curcumin sensitises neuroblastoma cells to crosslinking chemotherapeutics.

Previous studies have shown high *MYCN* expression sensitises neuroblastoma cells and tumours to cisplatin treatment (Lu et al., 2005; Peirce and Findley, 2009; Boeva et al., 2017; van Groningen et al., 2017). To test this in our hands, SHEP-Tet21N MYCN ON and OFF cells were treated with 0 μM to 20 μM cisplatin for 24 hours before cell viability was determined by Alamar blue assays. In agreement with previous studies, *MYCN* expression significantly sensitised SHEP-Tet21N cells to cisplatin (Student's t-test, $p < 0.05$), with an average IC50 of 2 μM observed in MYCN ON cells and 12 μM observed in MYCN OFF cells (Figure 4.10A).

Previous studies have also shown curcumin treatment sensitises cancer cells to DNA crosslinking and alkylating agents by inhibiting FANCD2 mono-ubiquitination and therefore limiting DNA crosslink repair (Chirnomas et al., 2006; Chen et al., 2007; Patil et al., 2014; Chen et al., 2015b). Given curcumin inhibited cisplatin-induced FA pathway activation in neuroblastoma cells, it was hypothesised that curcumin could sensitise neuroblastoma cells to chemotherapeutics currently used in high-risk neuroblastoma treatment such as cisplatin, carboplatin and TMZ. Clonogenic survival of SHEP-Tet21N MYCN ON and OFF cells was analysed following pre-treatment with 0 μM or 5 μM curcumin for 16 hours before addition of increasing doses of cisplatin, carboplatin or TMZ for 24 hours. Curcumin treatment induced a slight sensitisation to cisplatin in both MYCN ON and OFF cells, however this was not significant (Student's t-test, $p > 0.05$) (Figure 4.10B). The ability of curcumin to sensitise non-MNA SHEP-1 and MNA IMR32 cells to increasing doses of cisplatin was also analysed. In these cells, treatment with 5 μM curcumin was too toxic and therefore IMR32 and SHEP-1 cells were instead pre-treated with 2.5 μM curcumin for all clonogenic survival assays. Curcumin treatment induced a small sensitization of SHEP-1 cells to cisplatin, however this was not statistically significant (Student's t-test, $p > 0.05$) (Figure 4.10C). Curcumin did not sensitise IMR32 cells to cisplatin.

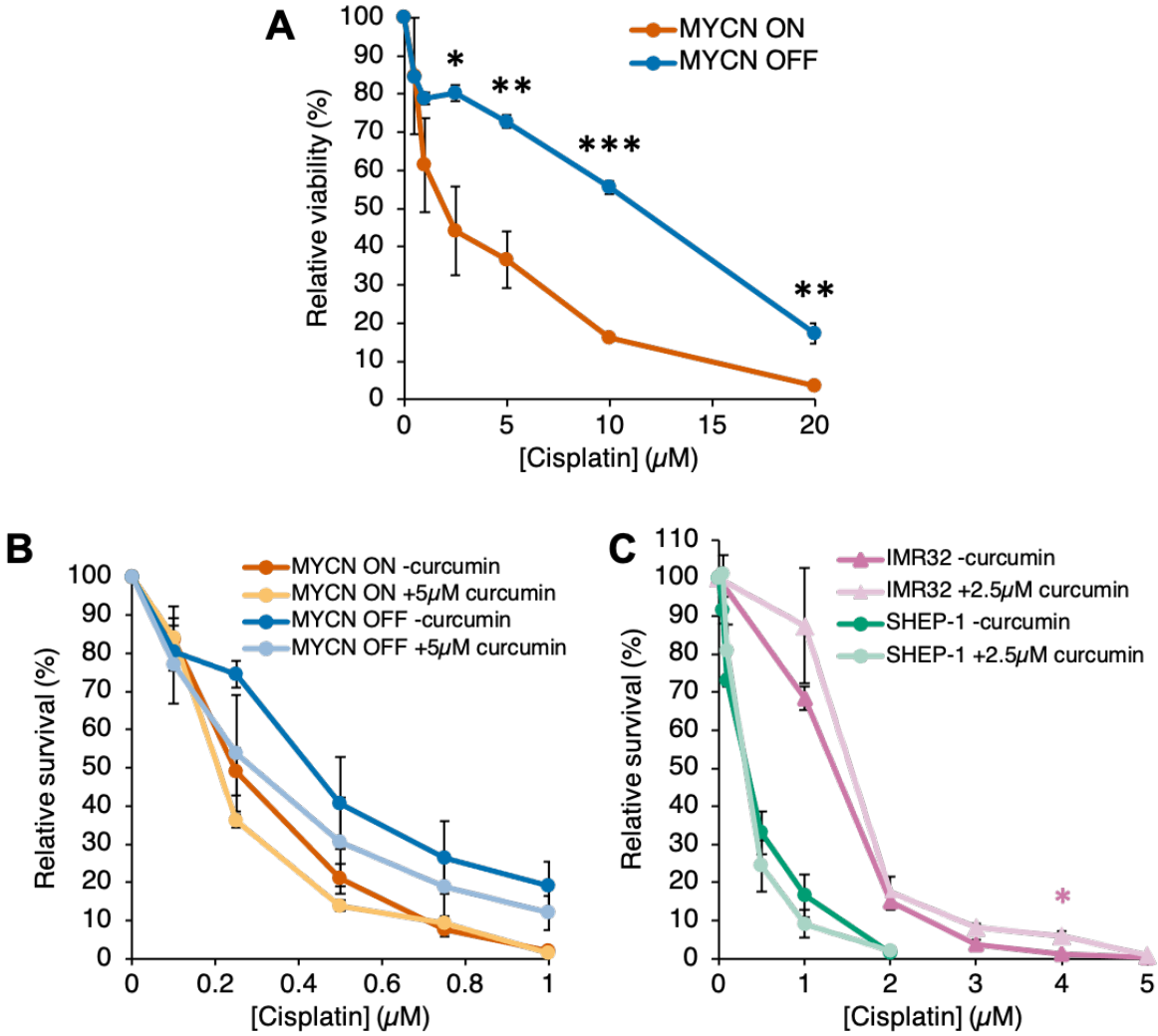

Figure 4.10. High MYCN expression sensitises SHEP-Tet21N neuroblastoma cells to cisplatin but curcumin induces only a small non-significant sensitisation.
(A) Relative cell viability of SHEP-Tet21N MYCN ON and OFF cells following treatment with 0-20 μM cisplatin for 24 hours. Percentage viability was determined by Alamar Blue assays 72 hours following addition of cisplatin and calculated relative to 0 μM cisplatin treatment. Data are presented as means ±SEM (n=3). Statistical significance between MYCN ON and OFF was determined at each concentration by a Student's t-test where *p<0.05, **p<0.01, ***p<0.001. **(B)** Relative survival of SHEP-Tet21N MYCN ON and OFF cells following pre-treatment with 0 μM or 5 μM curcumin for 16 hours, before addition of 0-1 μM cisplatin for 24 hours. **(C)** Relative survival of IMR32 and SHEP-1 cells following pre-treatment with 0 μM or 2.5 μM curcumin for 16 hours, before addition of 0-5 μM cisplatin for 24 hours. In (B) and (C) percentage survival was determined by clonogenic survival assays and calculated relative to 0 μM cisplatin with 0 μM curcumin treatment for each cell line. Data are presented as means ±SEM (n≥3). Statistical significance between survival with and without curcumin pre-treatment was determined at each cisplatin concentration by a Student's t-test where *p<0.05, **p<0.01, ***p<0.001. Cell lines are coloured according to MYCN status; orange = ON, blue = OFF, pink = amplified, green = non-amplified.

Similarly, curcumin treatment induced a small sensitisation to carboplatin in SHEP-Tet21N MYCN ON and OFF cells (Figure 4.11A) and SHEP-1 cells (Figure 4.11B), however this was not statistically significant (Student's t-test, $p > 0.05$). Curcumin treatment did not sensitise IMR32 cells to carboplatin (Figure 4.11B). Curcumin treatment also did not sensitise SHEP-Tet21N MYCN ON and OFF cells (Figure 4.12A), SHEP-1 cells (Figure 4.12B), or IMR32 cells (Figure 4.12B) to TMZ treatment. This could be because TMZ is a monofunctional alkylating agent, as opposed to a DNA crosslinking agent like cisplatin and carboplatin, and therefore induces DNA lesions which are repairable by other DNA repair pathways such as BER.

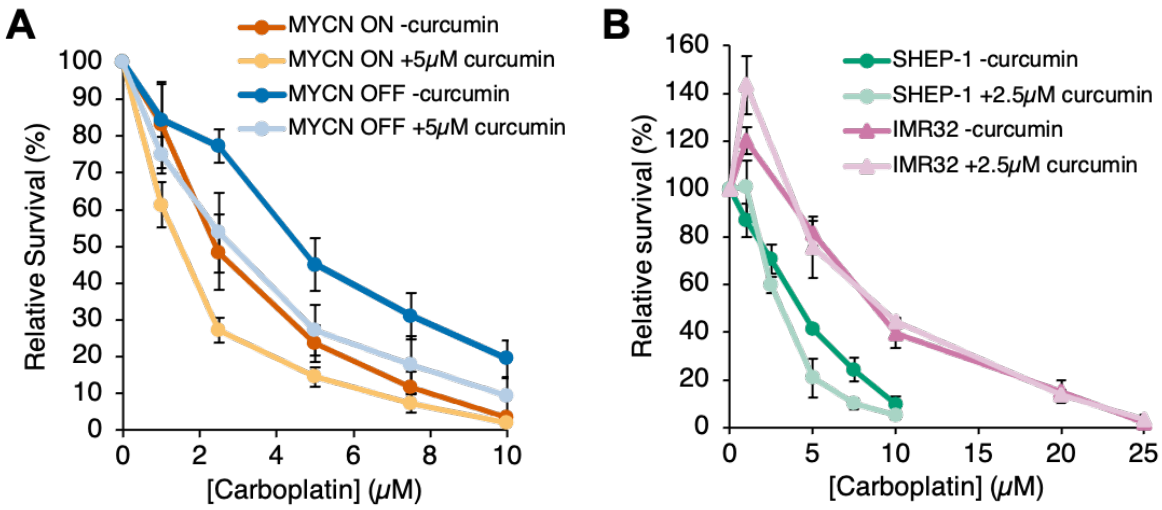

Figure 4.11. High MYCN expression sensitises SHEP-Tet21N neuroblastoma cells to carboplatin but curcumin induces only a small non-significant sensitisation.
(A) Relative survival of SHEP-Tet21N MYCN ON and OFF cells following pre-treatment with 0 μM or 5 μM curcumin for 16 hours, before addition of 0-10 μM carboplatin for 24 hours (n=3). **(B)** Relative survival of IMR32 cells (n≥3) and SHEP-1 cells (n≥2) following pre-treatment with 0 μM or 2.5 μM curcumin for 16 hours, before addition of 0-25 μM carboplatin for 24 hours. In (A) and (B), percentage survival was determined by clonogenic survival assays and calculated relative to 0 μM carboplatin with 0 μM curcumin treatment for each cell line. Data are presented as means ±SEM. Statistical significance between survival with and without curcumin pre-treatment was determined at each carboplatin concentration by a Student's t-test where *p<0.05, **p<0.01, ***p<0.001. Cell lines are coloured according to MYCN status; orange = ON, blue = OFF, pink = amplified, green = non-amplified.

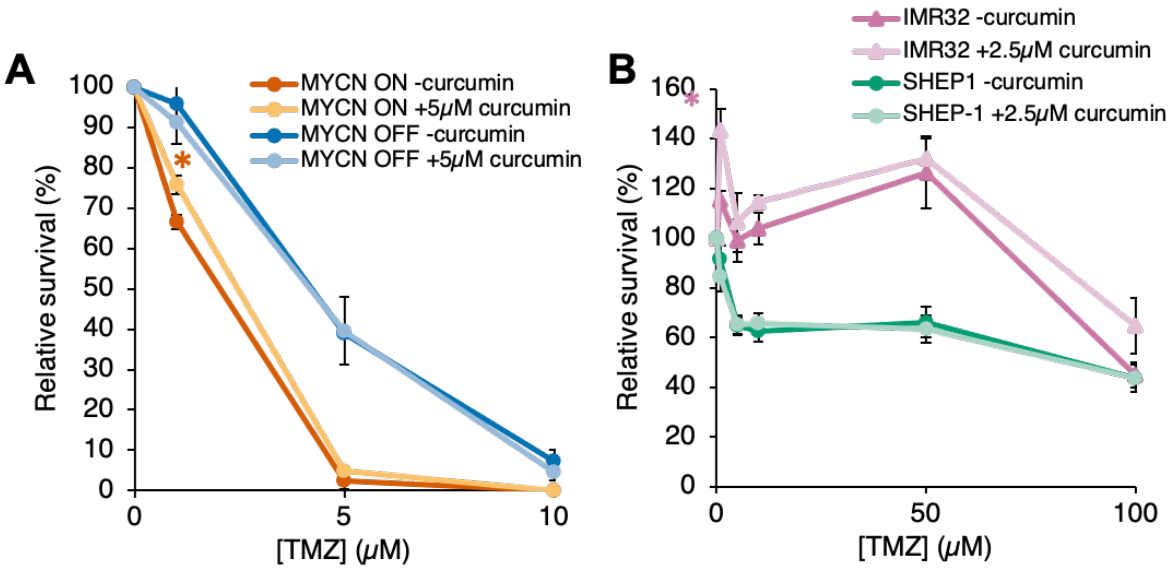

Figure 4.12. High MYCN expression and curcumin do not sensitise neuroblastoma cells to temozolomide.
(A) Relative survival of SHEP-Tet21N MYCN ON and OFF cells following pre-treatment with 0 μM or 5 μM curcumin for 16 hours, before addition of 0-10 μM temozolomide (TMZ) for 24 hours. **(B)** Relative survival of IMR32 and SHEP-1 cells following pre-treatment with 0 μM or 2.5 μM curcumin for 16 hours, before addition of 0-100 μM TMZ for 24 hours. In (A) and (B), percentage survival was determined by clonogenic survival assays and calculated relative to 0 μM TMZ with 0 μM curcumin treatment for each cell line. Data are presented as means ±SEM (n≥3). Statistical significance between survival with and without curcumin pre-treatment was determined at each TMZ concentration by a Student's t-test where *p<0.05, **p<0.01, ***p<0.001. Cell lines are coloured according to MYCN status; orange = ON, blue = OFF, pink = amplified, green = non-amplified.

The inability of curcumin to substantially sensitise SHEP-1 and IMR32 cells to cisplatin and carboplatin may be due to the lower dose of curcumin used. To determine whether 2.5 μM curcumin treatment is able to inhibit endogenous and chemotherapy-induced FANCD2 mono-ubiquitination as effectively as 5 μM curcumin treatment, SHEP-1 and IMR32 cells were pre-treated with 0 μM, 2.5 μM, or 5 μM curcumin for 16 hours before addition of 0 μM or 5 μM cisplatin for 24 hours. FANCD2 protein levels were analysed by western blot (Figure 4.13A). In IMR32 cells, 2.5 μM curcumin induced a smaller downregulation of total FANCD2 expression (Figure 4.13B) but was equally as effective at inhibiting cisplatin-induced FANCD2 mono-ubiquitination as 5 μM curcumin treatment (Figure 4.13D). In SHEP-1 cells, 2.5 μM curcumin treatment induced a smaller upregulation of FANCD2 expression (Figure 4.13C) but was not as effective at inhibiting cisplatin-induced FANCD2 mono-ubiquitination as 5 μM curcumin treatment (Figure 4.13E). Therefore the reduced downregulation of total FANCD2 in IMR32 cells, and the reduced inhibition of FANCD2 mono-ubiquitination in SHEP-1 cells

demonstrates 2.5 μM curcumin is not as effective at inhibiting FA pathway activation compared to 5 μM curcumin.

This data indicates inhibition of FANCD2 mono-ubiquitination by curcumin has the potential to sensitise neuroblastoma cells to DNA crosslinking chemotherapies such as carboplatin and cisplatin, but not TMZ which is a DNA alkylating agent. However, the high clonogenic toxicity of curcumin in some neuroblastoma cell lines such as IMR32 and SHEP-1 prevents study of optimally effective doses of curcumin.

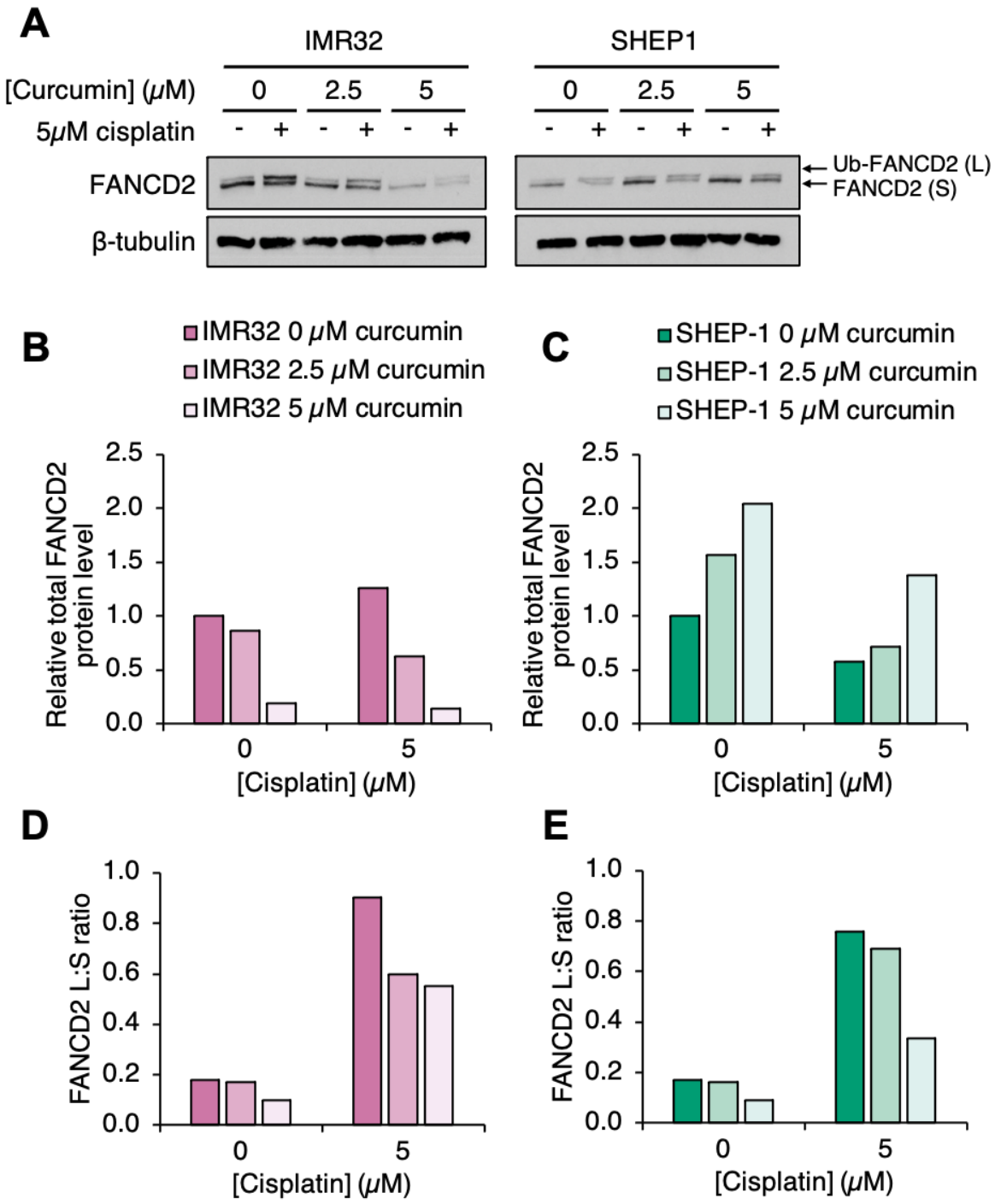

Figure 4.13. FA pathway inhibition by curcumin in IMR32 and SHEP-1 cells is dose-dependent.
IMR32 (MYCN amplified) and SHEP-1 (MYCN non-amplified) cells were pre-treated with 0 μM, 2.5 μM, or 5 μM curcumin for 16 hours before addition of 0 μM or 5 μM cisplatin for 24 hours. **(A)** FANCD2 protein levels were determined by western blotting (n=1). **(B-C)** Total FANCD2 band intensity (sum of L and S band intensities) was quantified relative to 0 μM curcumin with 0 μM cisplatin treatment and normalised to ß-tubulin band intensity. **(D-E)** FANCD2 L:S ratios were calculated for each condition.

4.2.2.2 High MYCN expression sensitises neuroblastoma cells to curcumin treatment alone

High *MYCN* expression has been shown to sensitise neuroblastoma cells to treatments which inhibit DNA damage repair and replication-stress limiting pathways (Cole et al., 2011; Colicchia et al., 2017; Petroni et al., 2018; King et al., 2020; King et al., 2021; Southgate et al., 2020). Additionally, we observed that curcumin inhibits MYCN-induced FA pathway activation (Figure 4.6). Given the FA pathway has a role in limiting replication stress, we next examined whether high *MYCN* expression would sensitise neuroblastoma cells to FA pathway inhibition by curcumin. To determine the effect of high *MYCN* expression on the sensitivity of neuroblastoma cells to curcumin alone, cell viability was analysed by Alamar blue assays in SHEP-Tet21N MYCN ON and OFF cells following treatment with up to 50 μM curcumin for 40 hours. SHEP-Tet21N MYCN ON cells were significantly more sensitive to 15 μM ($t(4) = 4.85$, $p = 0.008$) and 25 μM ($t(4) = 4.54$, $p = 0.011$) curcumin treatment than MYCN OFF cells (Figure 4.14A). MYCN ON and OFF cells had an average IC50 of 14 μM and 20 μM respectively.

To examine whether *MYCN* amplification also sensitised neuroblastoma cells to curcumin, MNA IMR32 and Kelly cell lines and non-MNA SHEP-1 and SH-SY5Y cell lines were treated with up to 25 μM curcumin for 40 hours before cell viability was assessed by Alamar blue assays. MNA cell lines were more sensitive to curcumin treatment than non-MNA cell lines (Figure 4.14B). IMR32 and Kelly cells had an average IC50 of 4 μM and 6 μM respectively, whilst SHEP-1 and SH-SY5Y cells had an average IC50 of 10 μM and 17 μM respectively.

The effect of high *MYCN* expression on clonogenic survival following treatment with increasing doses of curcumin alone was also analysed. Induction of high MYCN expression significantly sensitised SHEP-Tet21N cells to curcumin treatment (Figure 4.14C). However, whilst Kelly cells had a greater sensitivity to curcumin treatment than SHEP-1 cells, IMR32 cells had a similar curcumin sensitivity to SHEP-1 cells (Figure 4.14D). This may be due to the higher colony forming efficiency of IMR32 cells compared to SHEP-1 cells (Figure 4.14E). However it also suggests other genetic factors may impact clonogenic sensitivity to curcumin.

This data shows *MYCN* overexpression and amplification sensitises neuroblastoma cells to treatment with the FA pathway inhibitor curcumin as a monotherapy.

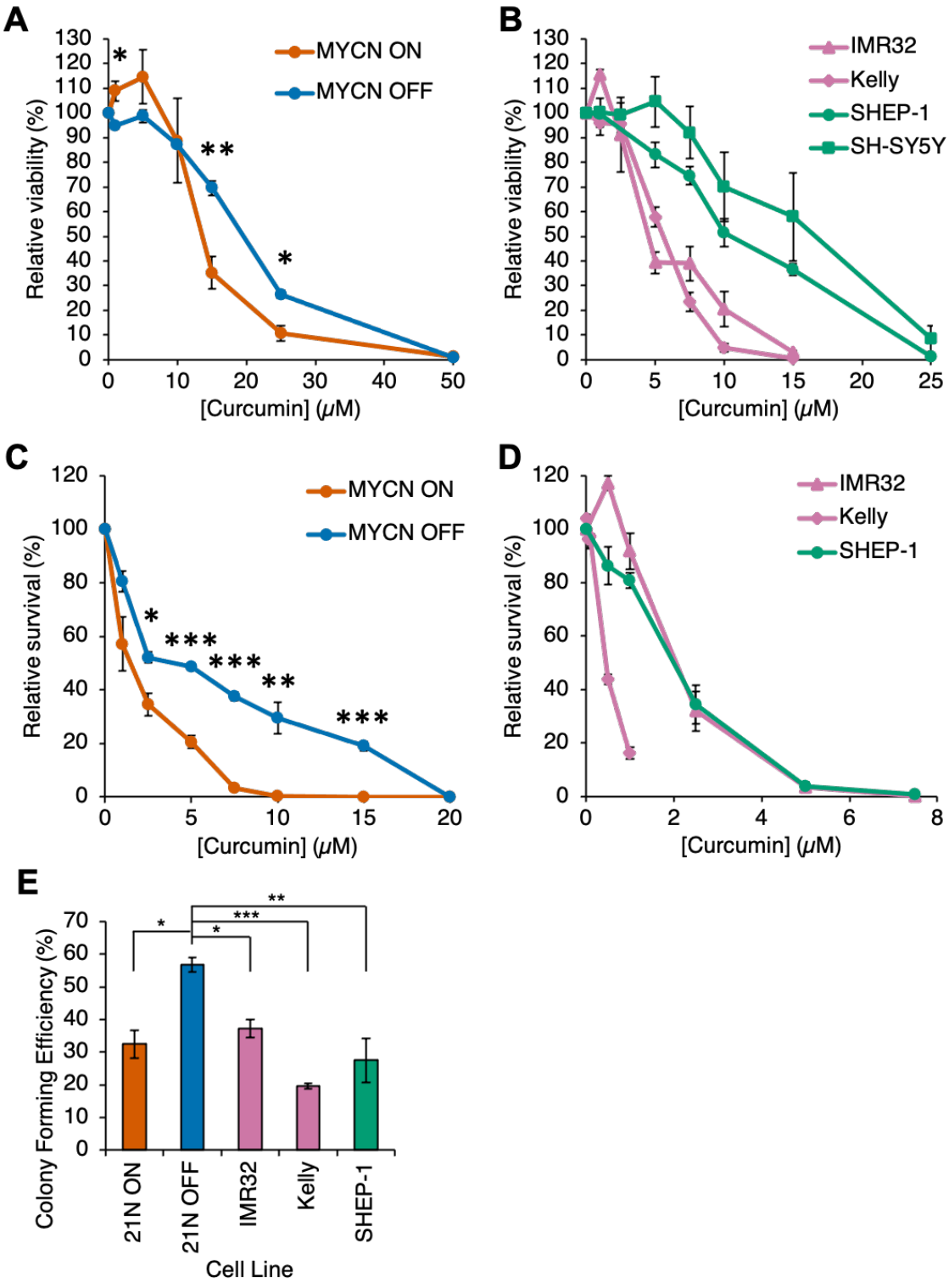

Figure 4.14. Neuroblastoma cell lines with high *MYCN* expression have greater sensitivity to curcumin. (Legend overleaf).

Figure 4.14. Neuroblastoma cell lines with high *MYCN* expression have greater sensitivity to curcumin.
Relative cell viability of **(A)** SHEP-Tet21N MYCN ON and OFF cells and **(B)** IMR32, Kelly, SHEP-1, and SH-SY5Y cell lines following treatment with indicated curcumin doses for 40 hours. Cell viability was determined 72 hours following addition of curcumin by Alamar Blue assays. Percentage viability was calculated relative to 0 μM curcumin treatment for each cell line. Data are presented as means ±SEM (n=3). Relative survival of **(C)** SHEP-Tet21N MYCN ON and OFF cells and **(D)** IMR32, Kelly and SHEP-1 cell lines following treatment with indicated curcumin doses for 40 hours. Percentage survival was determined by clonogenic survival assays and calculated relative to 0 μM curcumin treatment for each cell line. Data are presented as means ±SEM (n=3). In (A) and (C), statistical significance between MYCN ON and OFF at each curcumin concentration was determined by a Student's t-test where *p<0.05, **p<0.01, ***p<0.001. Cell lines are coloured according to MYCN status; orange = ON, blue = OFF, pink = amplified, green = non-amplified. **(E)** Colony forming efficiency of untreated SHEP-Tet21N MCYN ON and OFF cells, IMR32 cells, Kelly cells and SHEP-1 cells. Data are presented as means ±SEM (n ≥ 3). Statistical significance between cell lines was determined by a one-way ANOVA where n.s. = non-significant, *p<0.05, **p<0.01, ***p<0.001.

4.2.3 Curcumin treatment induces higher levels of replication stress in neuroblastoma cells

4.2.3.1 Curcumin enhances S-phase accumulation in MYCN ON cells

To begin to determine the molecular mechanism behind the MYCN-induced sensitisation to curcumin, the effect of curcumin on the cell cycle profile of SHEP-Tet21N MYCN ON and OFF cells was analysed. Cells were pre-treated with 0 μM or 5 μM curcumin for 16 hours before addition of 0 μM or 5 μM cisplatin for 24 hours. Cell cycle profiles were then determined by FACS following DNA staining with propidium iodide. Cisplatin induced an accumulation of both MYCN ON and OFF cells in G2/M, and this increase was statistically significant in MYCN OFF cells ($F(3,8) = 11.75$, $p = 0.034$) (Figure 4.15, Appendix Figure A13). Curcumin pre-treatment induced a slight reduction in this G2/M accumulation. MYCN OFF cells were also observed to accumulate in S phase following cisplatin treatment, and this accumulation was significant when combined with curcumin treatment ($F(3,8) = 9.16$, $p = 0.019$). However, no cisplatin-dependent S-phase accumulation was observed in MYCN ON cells. Curcumin treatment alone did not affect the cell cycle profile of MYCN OFF cells. In MYCN ON cells, curcumin treatment alone induced a small 3% increase in S-phase and

sub-G1 accumulation. This increase in sub-G1 accumulation is indicative of increased apoptotic death.

This data indicates curcumin treatment does not significantly mitigate or exacerbate cisplatin-induced G2/M and S-phase arrest. Whilst curcumin treatment alone does not impact the cell cycle profile of MYCN OFF cells, it does slightly enhance the S-phase accumulation in MYCN ON cells.

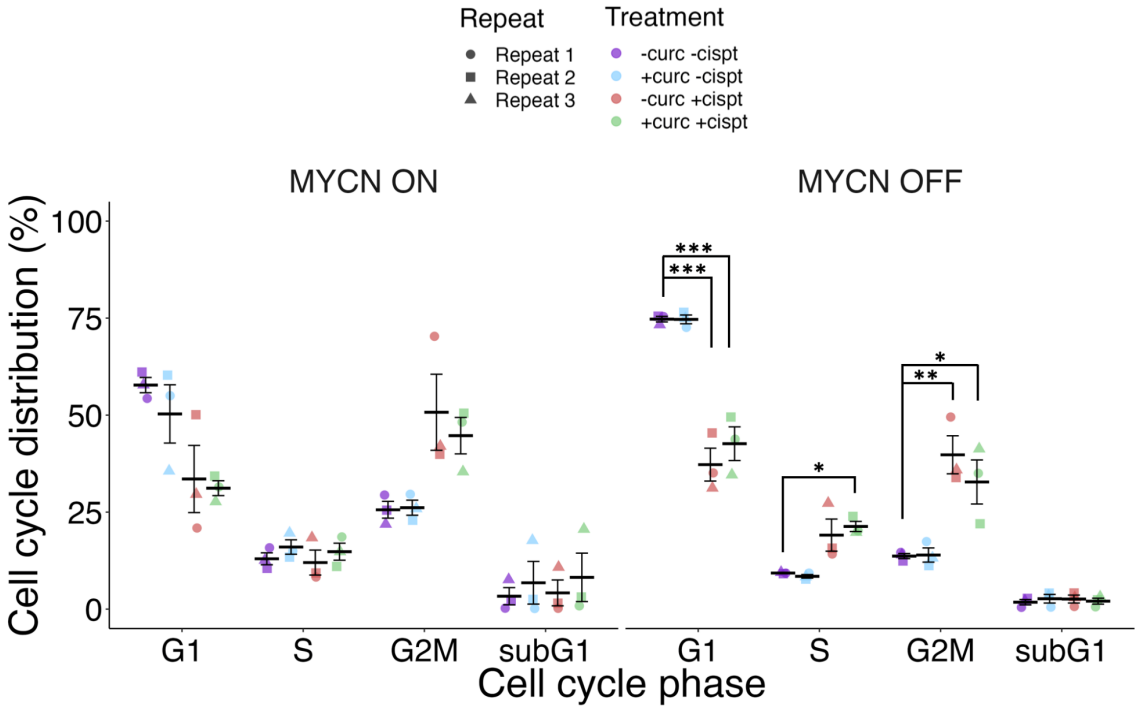

Figure 4.15. Curcumin has no substantial effect on the cell cycle distribution of SHEP-Tet21N MYCN ON and OFF cells but cisplatin induces G2M arrest.
SHEP-Tet21N MYCN ON and OFF cells were pre-treated with 0 μM or 5 μM curcumin for 16 hours before addition of 0 μM or 5 μM cisplatin for 24 hours. FACS cell cycle profiles were then determined with DNA content determined by propidium iodide staining. Percentage of cells in each cell cycle phase is displayed. Data are presented as means ±SEM (n=3). Statistical significance of cell cycle distribution differences between treatments was determined by a one-way ANOVA for each cell cycle phase and MYCN status where *p<0.05, **p<0.01, ***p<0.001.

4.2.3.2 Curcumin induces replication stress and exacerbates chemotherapy-induced DNA damage

FANCD2 has been demonstrated to limit replication stress by protecting stalled replication forks and aiding R-loop resolution (Schwab et al., 2010; Schlacher et al., 2011; Schlacher et al., 2012; Garcia-Rubio et al., 2015; Schwab et al., 2015; Okamoto et al., 2019). It was hypothesised that neuroblastoma cells with high *MYCN* expression had a higher sensitivity to curcumin because inhibition of the FA pathway exacerbated the high endogenous replication stress and DNA damage to intolerable levels. To test this, SHEP-Tet21N MYCN ON and OFF cells were treated with 0 μM or 5 μM curcumin for 16 hours before addition of 0 μM or 5 μM cisplatin for 24 hours. The effect of curcumin on the levels of replication stress and DNA damage in SHEP-Tet21N MYCN ON and OFF cells was determined by immunofluorescence analysis of FANCD2 foci (Figure 4.16A), pRPA foci (Figure 4.16A), γ-H2AX foci (Figure 4.16D) and R-loop intensity (Figure 4.17).

FANCD2 mono-ubiquitination is required for stable FANCD2 foci formation (Taniguchi et al., 2002a). The number of FANCD2 foci per cell is therefore another measure of FANCD2 mono-ubiquitination and FA pathway activation. The number of endogenous FANCD2 foci was higher in MYCN ON compared to MYCN OFF cells (Figure 4.16A-B). This suggests there is a higher level of FANCD2 mono-ubiquitination in MYCN ON cells as observed in Figure 4.1. Curcumin treatment alone inhibited formation of FANCD2 foci in MYCN ON cells, but not in MYCN OFF cells (Figure 4.16B, Appendix Figure A14A). Again, this is consistent with the effect of curcumin on endogenous FANCD2 L:S ratios observed in Figure 4.6. Cisplatin treatment increased the number of FANCD2 foci in both MYCN ON and OFF cells, with a higher number of cisplatin-induced FANCD2 foci observed in MYCN OFF cells (Figure 4.16B). This is also consistent with the level of FANCD2 mono-ubiquitination observed for these conditions by western blot (Figure 4.3C, 4.4C). This cisplatin-induced increase in FANCD2 foci is inhibited by curcumin treatment in both MYCN ON and OFF cells (Figure 4.16B), as observed previously for FANCD2 mono-ubiquitination (Figure 4.7C).

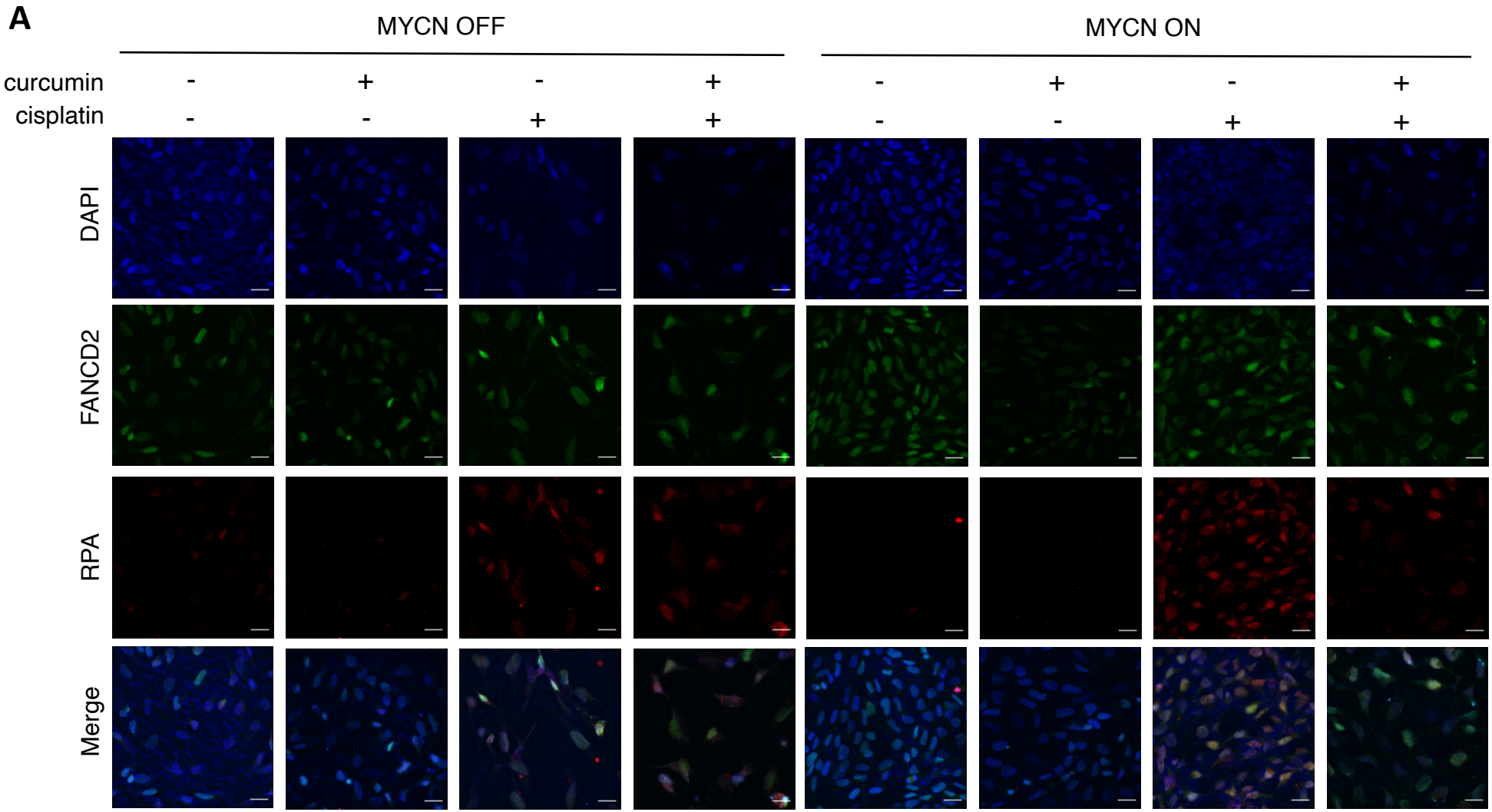

Figure 4.16. Curcumin inhibits FANCD2 foci formation, induces replication stress and exacerbates cisplatin-induced DNA damage in SHEP-Tet21N neuroblastoma cells. (Legend overleaf).

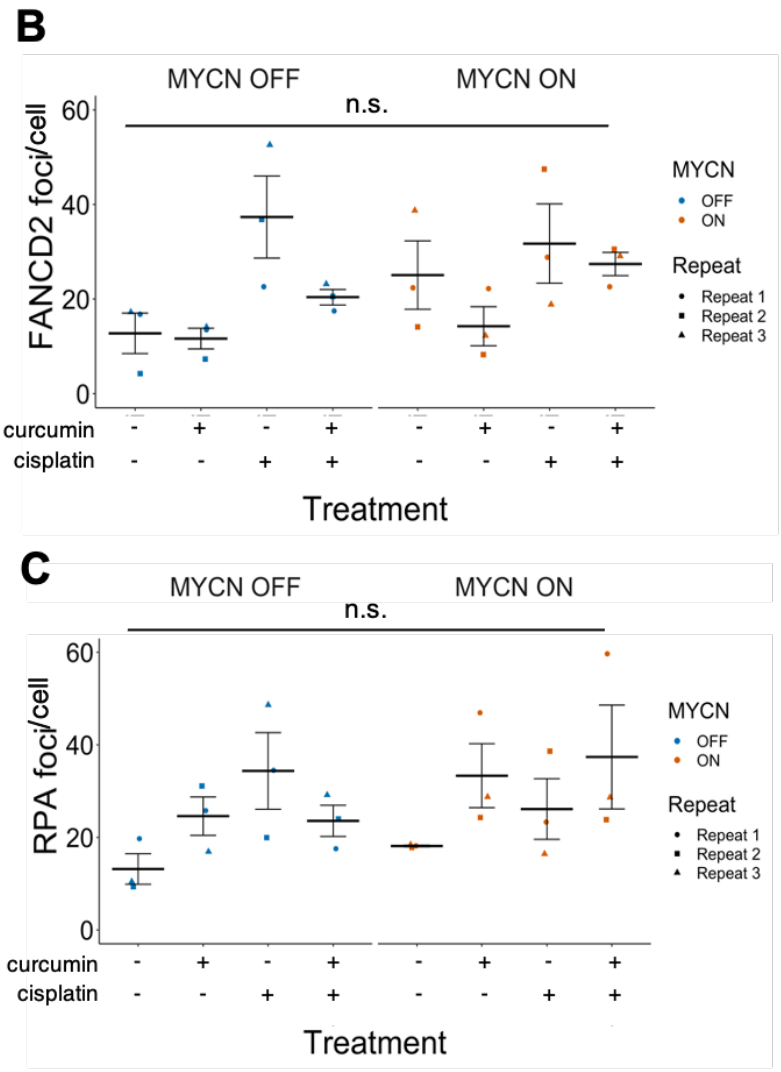

Figure 4.16. Curcumin inhibits FANCD2 foci formation, induces replication stress and exacerbates cisplatin-induced DNA damage in SHEP-Tet21N neuroblastoma cells. (Legend overleaf).

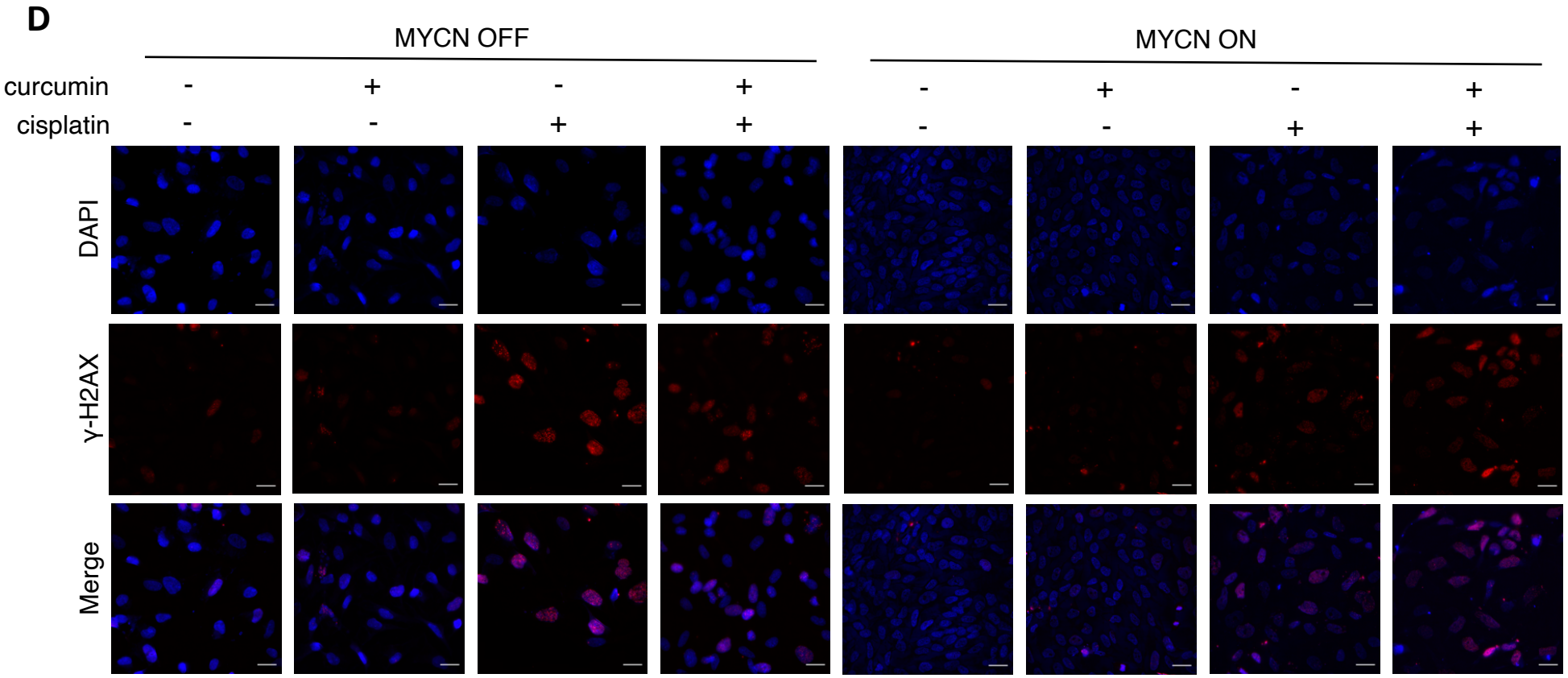

Figure 4.16. Curcumin inhibits FANCD2 foci formation, induces replication stress and exacerbates cisplatin-induced DNA damage in SHEP-Tet21N neuroblastoma cells. (Legend overleaf).

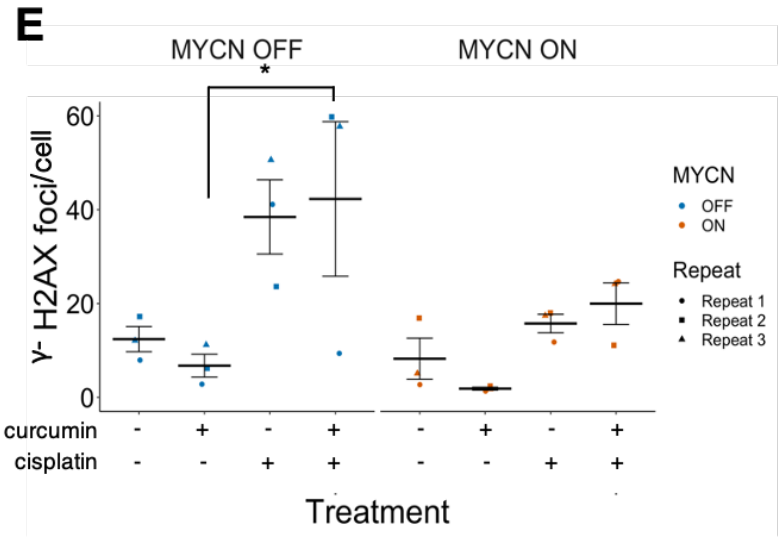

Figure 4.16. Curcumin inhibits FANCD2 foci formation, induces replication stress and exacerbates cisplatin-induced DNA damage in SHEP-Tet21N neuroblastoma cells.
SHEP-Tet21N MYCN ON and OFF cells were pre-treated with 0 μM or 5 μM curcumin for 16 hours before addition of 0 μM or 5 μM cisplatin for 24 hours. Cells were fixed for immunofluorescence analysis. Hannah Walsh helped with this Immunofluorescence staining. **(A)** Representative images of cells stained for FANCD2 and pRPA32/RPA2 are shown. Scale bar = 25 μm. Number of **(B)** FANCD2 foci per cell and **(C)** pRPA foci per cell was quantified for each treatment condition. **(D)** Representative images of cells stained for γ-H2AX are shown. Scale bar = 25 μm. **(E)** Number γ-H2AX foci per cell was quantified for each treatment condition. In (B), (C) and (E), 100 cells per repeat per treatment condition were quantified. Mean foci per cell is presented for each repeat, with black lines indicating overall mean ±SEM (n=3). Statistical significance between treatments was determined by a two-way ANOVA where n.s. = not significant, *p<0.05, **p<0.01, ***p<0.001.

Checkpoint kinases including ATM, ATR and DNA-PK phosphorylate RPA upon detection of DNA damage and replication stress to enable protection of ssDNA and recruitment of DNA repair proteins (Binz et al., 2004; Nuss et al., 2005; Wu et al., 2005; Vassin et al., 2009; Murphy et al., 2014; Maréchal and Zou, 2015). The number of pRPA foci per cell is therefore a measure of replication stress and DNA damage. MYCN ON cells had a higher endogenous level of pRPA foci per cell than MYCN OFF cells (Figure 4.16A,C). This suggests MYCN ON cells have a greater level of replication stress, as previously observed by King et al., 2020. Treatment with curcumin alone induced an increase in the number of pRPA foci in both MYCN ON and OFF cells (Figure 4.16C, Appendix Figure A14B). The number of pRPA foci in curcumin-treated MYCN ON cells was greater than or equivalent to that induced by cisplatin in both

MYCN ON and OFF cells. γ-H2AX foci are often used as a marker of DNA damage (Pilch et al., 2003; Mah et al., 2010). Additionally, γ-H2AX is also required for the recruitment of FANCD2 to stalled replication forks (Bogliolo et al., 2007). MYCN ON and OFF cells had a similar number of endogenous γ-H2AX foci per cell (Figure 4.16D-E, Appendix Figure A14C). Although curcumin treatment alone did not induce an increase in the number of γ-H2AX foci, curcumin exacerbated the increase in γ-H2AX foci induced by cisplatin in both MYCN ON and OFF cells.

R-loops are formed at transcription-replication conflicts and therefore accumulate at regions of high replication stress (Santos-Pereira and Aguilera, 2015). As such, R-loops are both a source of, and a product of, replication stress and genomic instability. It has been demonstrated that neuroblastoma cells with high *MYCN* expression are dependent on MYCN-driven mechanisms of R-loop resolution to limit MYCN-induced replication and transcription stress (Herold et al., 2019). Given FANCD2 has a role in the resolution of R-loops and this is dependent on FANCD2 mono-ubiquitination (Garcia-Rubio et al., 2015; Schwab et al., 2015; Liang et al., 2019a), we next examined the effect of curcumin on R-loop accumulation in SHEP-Tet21N MYCN ON and OFF cells. Analysis of R-loop immunofluorescence intensity demonstrated that MYCN ON cells had a lower endogenous level of R-loop accumulation than MYCN OFF cells (Figure 4.17, Appendix Figure A14D). However, inhibition of FANCD2 mono-ubiquitination by curcumin exacerbated endogenous and cisplatin-induced R-loop accumulation in MYCN ON cells only. This suggests there is a FANCD2 mono-ubiquitination-dependent mechanism of R-loop resolution that contributes to the limitation of MYCN-induced R-loops. A reduction in R-loop intensity following RNase H treatment confirmed specificity of the anti-RNA-DNA-hybrid antibody for R-loops.

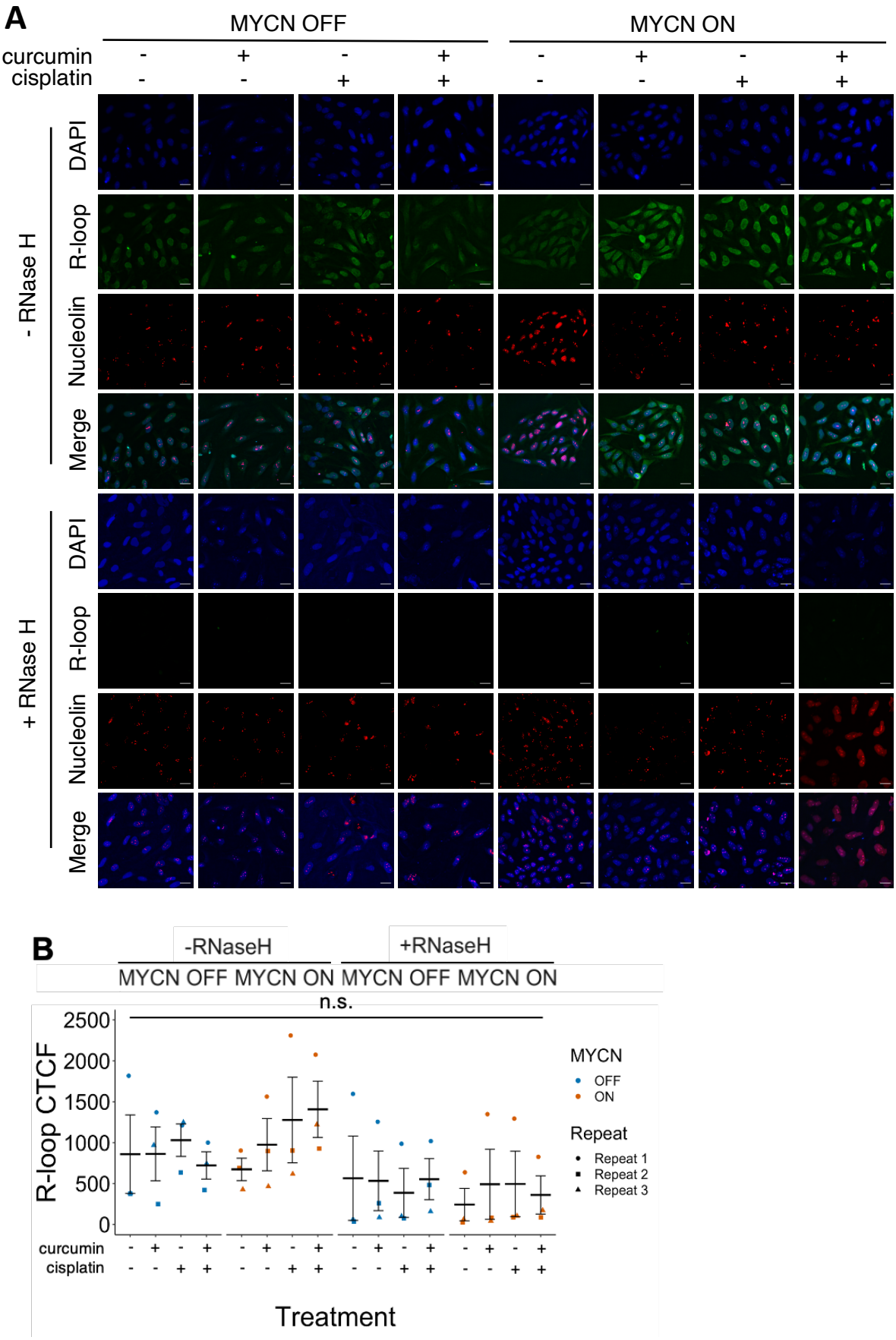

Figure 4.17. Curcumin induces R-loop accumulation selectively in MYCN ON cells. (Legend overleaf).

Figure 4.17. Curcumin induces R-loop accumulation selectively in MYCN ON cells.
SHEP-Tet21N MYCN ON and OFF cells were pre-treated with 0 μM or 5 μM curcumin for 16 hours before addition of 0 μM or 5 μM cisplatin for 24 hours. Cells were stained for R-loops and nucleolin and analysed by immunofluoresence. Cells were incubated with RNase H for 24 hours before staining to digest R-loops as a negative control. Hannah Walsh helped with this Immunofluorescence staining. **(A)** Representative images of R-loop and nucleolin staining are depicted. Scale bar = 25 μm. **(B)** R-loop corrected total cell fluorescence (CTCF) was quantified for 100 cells per repeat per treatment condition. To calculate R-loop CTCF, the R-loop intensity within each nucleus was quantified, the nucleoli R-loop intensity was deducted, and the nuclear R-loop intensity was normalised to the background intensity. Mean CTCF is presented for each repeat, with black lines indicating overall mean ±SEM (n=3). Statistical significance between treatments was determined by a two-way ANOVA where n.s. = not significant, *p<0.05, **p<0.01, ***p<0.001.

This data therefore indicates that cisplatin-induced activation and curcumin-induced inhibition of the FA pathway can also be observed by quantification of FANCD2 foci. In agreement with previous studies (Gu et al., 2015; King et al., 2020), analysis of pRPA foci indicated MYCN ON cells had a higher endogenous level of replication stress than MYCN OFF cells. Inhibition of FANCD2 foci formation by curcumin enhanced endogenous replication stress and cisplatin-induced DNA damage in both MYCN ON and OFF cells. Inhibition of FANCD2 mono-ubiquitination by curcumin also exacerbated endogenous and cisplatin-induced R-loop accumulation specifically in cells with high *MYCN* expression. This suggests FANCD2 functions in a pathway that resolves MYCN-induced R-loops.

4.2.3.3 FANCD2-dependent resolution of MYCN-induced R-loops is not dependent on BRCA1, AURKA or ATR

Two MYCN-driven pathways of R-loop resolution have been observed. Herold et. al (2019) demonstrated promoter-bound MYCN recruits BRCA1 and mRNA de-capping enzymes via USP11 during high transcription and replication stress to enable promoter-proximal R-loop resolution. Roeschert et al., (2021) demonstrated that MYCN recruits AURKA during S-phase to phosphorylate the histone residue H3Ser10. This promotes incorporation of histone H3.3 into promoters to suppress co-transcriptional R-loop formation. It was also suggested that recruitment of AURKA also stabilises MYCN at

promoters which enables it to recruit BRCA1 and USP11. It was hypothesised FANCD2 may have a role in these MYCN-dependent pathways of R-loop resolution.

It has been previously shown that BRCA1 regulates recruitment of FANCD2 to stalled replication forks (Yeo et al., 2014). To determine whether FANCD2 acts downstream of BRCA1 in the MYCN-BRCA1 R-loop resolution pathway described by Herold et al., (2019), the effect of siRNA-mediated BRCA1 depletion on R-loop intensity, FANCD2 foci formation and pRPA foci formation was analysed in SHEP-Tet21N MYCN ON and OFF cells. In agreement with previous studies (Herold et al., 2019), BRCA1 depletion induced a greater increase in R-loop intensity in MYCN ON cells compared to MYCN OFF cells in two out of three repeats (Figure 4.18A-B, Appendix Figure A15A), although this increase was not significant on average ($F(1) = 0.32$, $p > 0.05$). No significant change in the number of FANCD2 foci (Figure 4.18C-D, Appendix Figure A15B) or pRPA foci (Figure 4.18C, 4.19E, Appendix Figure A15C) was observed in MYCN ON or OFF cells following depletion of BRCA1. This suggests FANCD2 does not act downstream of BRCA1 in these R-loop resolution pathways.

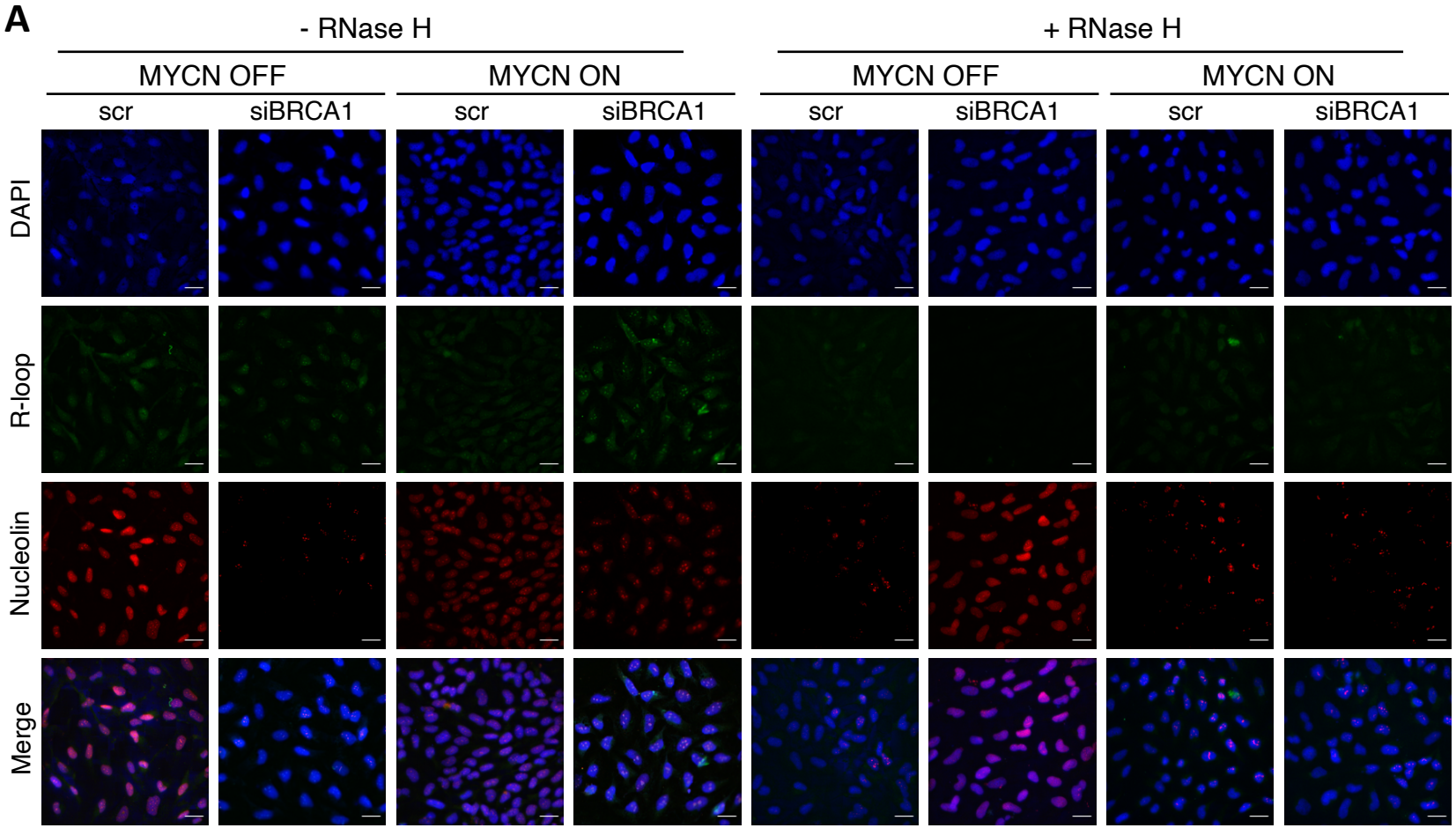

Figure 4.18. Depletion of BRCA1 induces R-loop accumulation in MYCN ON cells but does not alter FANCD2 or RPA foci formation. (Legend overleaf).

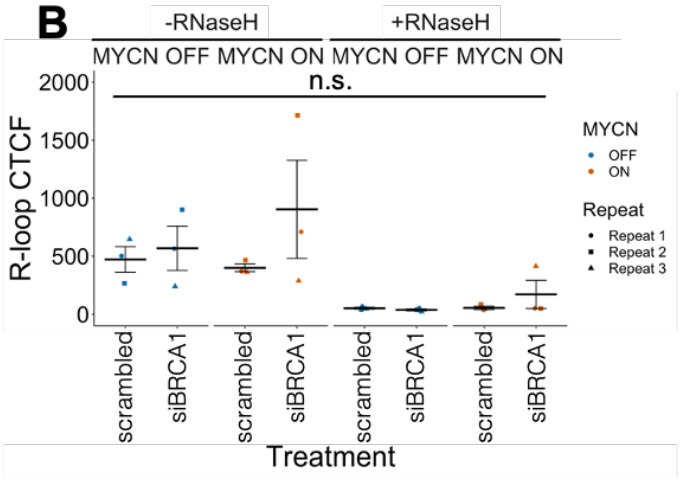

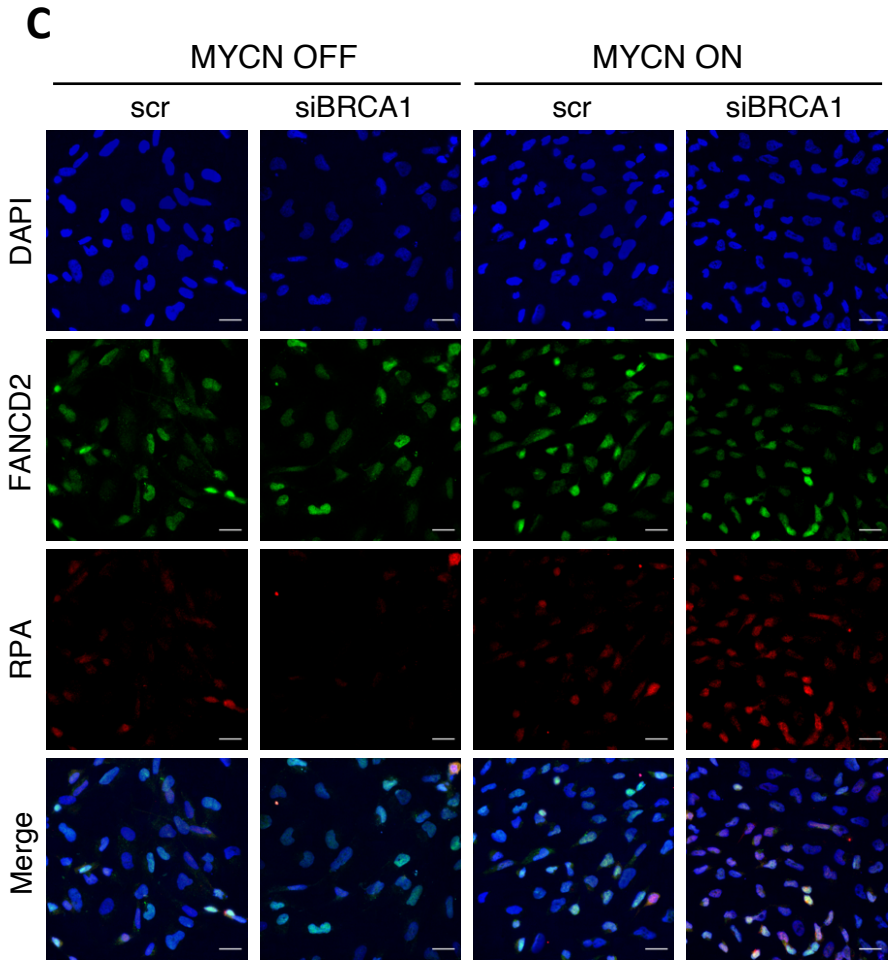

Figure 4.18. Depletion of BRCA1 induces R-loop accumulation in MYCN ON cells but does not alter FANCD2 or RPA foci formation. (Legend overleaf).

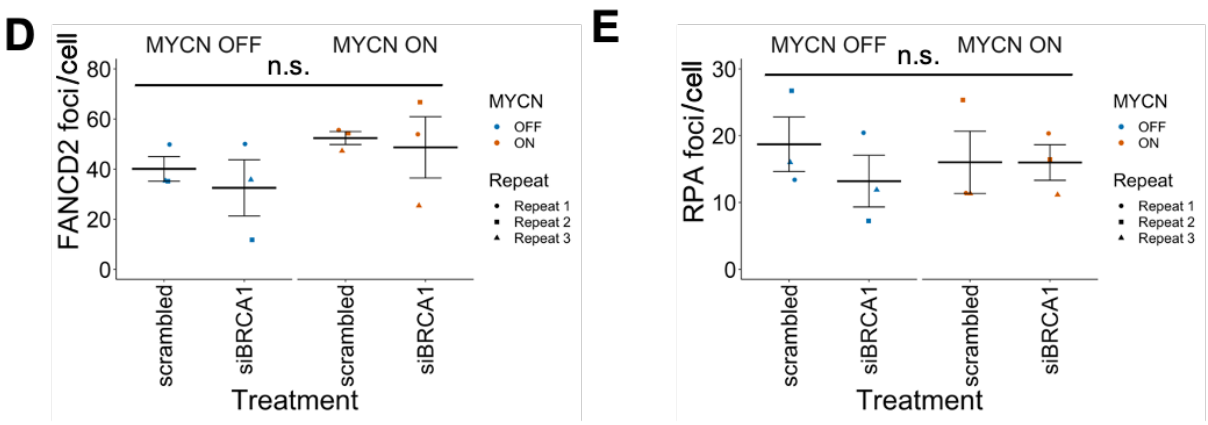

Figure 4.18. Depletion of BRCA1 induces R-loop accumulation in MYCN ON cells but does not alter FANCD2 or RPA foci formation.
SHEP-Tet21N MYCN ON and OFF cells were transfected with scrambled siRNA or BRCA1 siRNA using dharmafect-1 for 48 hours before cells were fixed, permeabilised and analysed by immunofluorescence. **(A)** Cells were stained for R-loops and nucleolin. Cells were incubated with RNase H for 24 hours before staining to digest R-loops as a negative control. Hannah Walsh helped with this Immunofluorescence staining. **(A)** Representative images of R-loop and nucleolin staining are depicted. Scale bar = 25 μm. **(B)** R-loop corrected total cell fluorescence (CTCF) was quantified for 100 cells per repeat per treatment condition. Mean CTCF is presented for each repeat, with black lines indicating overall mean ±SEM (n=3). **(C)** Representative images of cells stained for FANCD2 and pRPA32/RPA2 are shown. Scale bar = 25 μm. Number of **(D)** FANCD2 foci per cell and **(E)** pRPA foci per cell was quantified for each treatment condition. In (D) and (E), 100 cells per repeat per treatment condition were quantified. Mean foci per cell is presented for each repeat, with black lines indicating overall mean ±SEM (n=3). Statistical significance between treatments was determined by a two-way ANOVA where n.s. = not significant, *p<0.05, **p<0.01, ***p<0.001.

To determine whether FANCD2 acts within the MYCN-AURKA dependent R-loop resolution pathway described by Roeschert et al., (2021), the effect of AURKA inhibition on R-loop intensity, FANCD2 foci formation and pRPA foci formation was analysed in SHEP-Tet21N MYCN ON and OFF cells. Only small increases in the average R-loop intensity were observed in both MYCN ON and OFF cells following inhibition of AURKA, and wide variation was observed between replicates (Figure 4.19A-B, Appendix Figure A16A). Besides one replicate in which the number of FANCD2 foci increased in MYCN OFF cells, inhibition of AURKA did not affect FANCD2 foci formation in MYCN ON or OFF cells (Figure 4.19C-D, Appendix Figure A16B). The average number of pRPA foci per nuclei did not change in MYCN OFF cells but did increase slightly in MYCN ON cells following AURKA inhibition (Figure 4.19C, 4.20E, Appendix Figure A16B). The lack of R-loop accumulation upon AURKA inhibition is in contrast to the results observed by

Roeschert et al., (2021). Confirmation of the efficacy of LY3295668-mediated AURKA inhibition by western blot would be necessary to conclude whether FANCD2 acts within the MYCN-AURKA dependent R-loop resolution pathway.

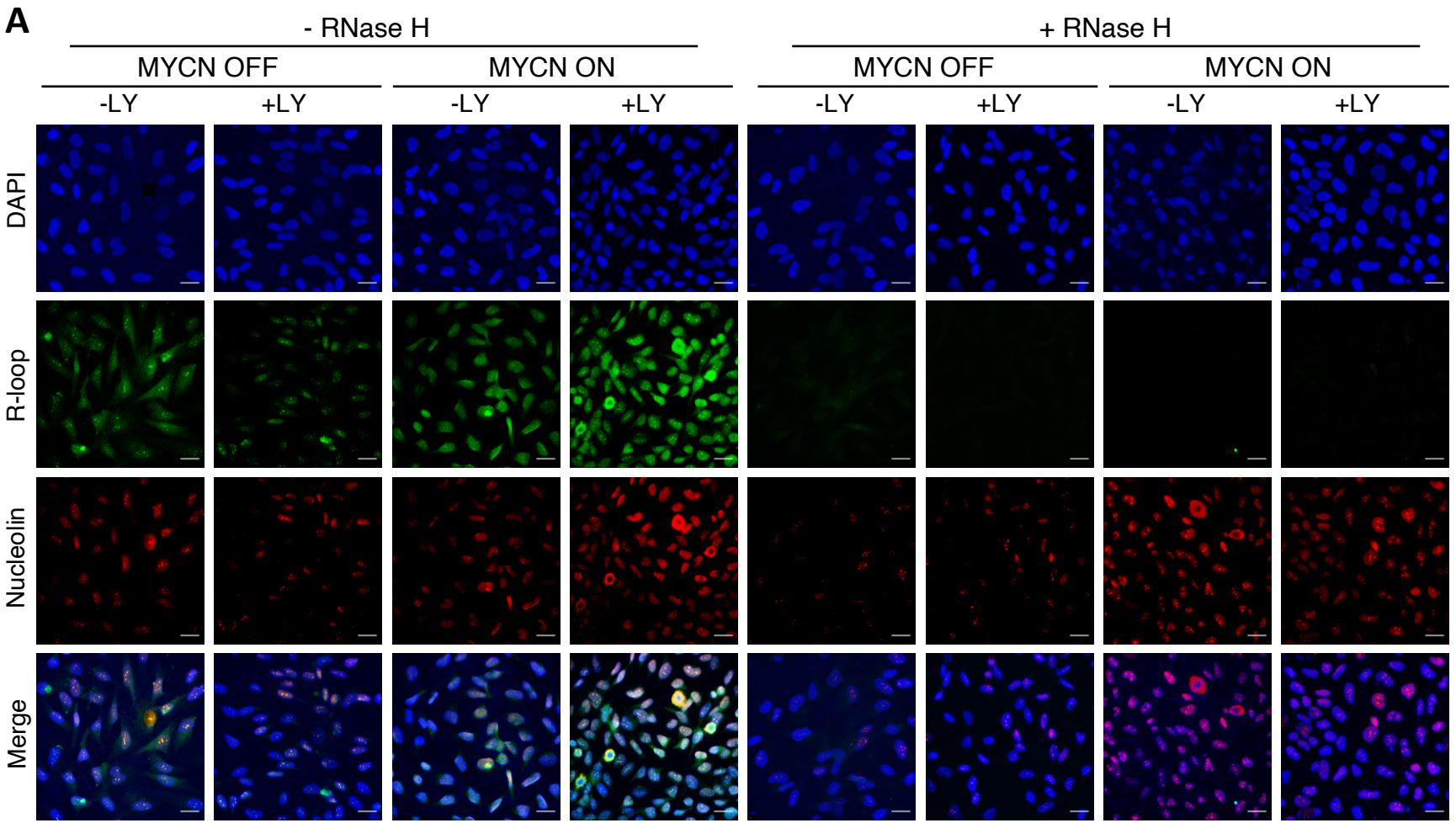

Figure 4.19. Treatment with AURKA inhibitor LY3295668 does not induce accumulation of R-loops, FANCD2 foci or RPA foci in SHEP-Tet21N MYCN ON and OFF cells. (Legend overleaf).

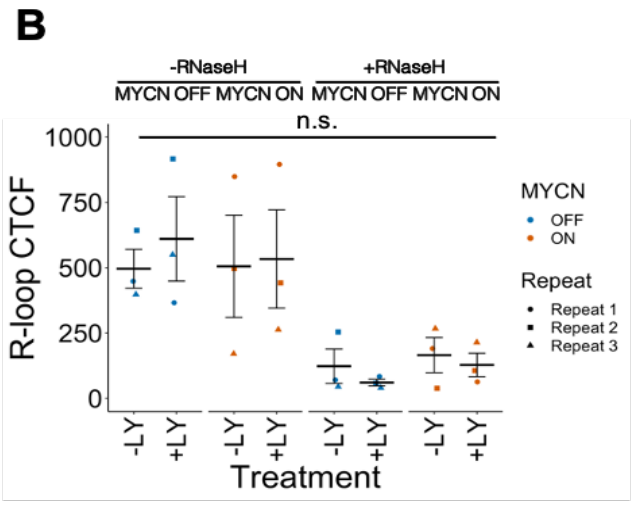

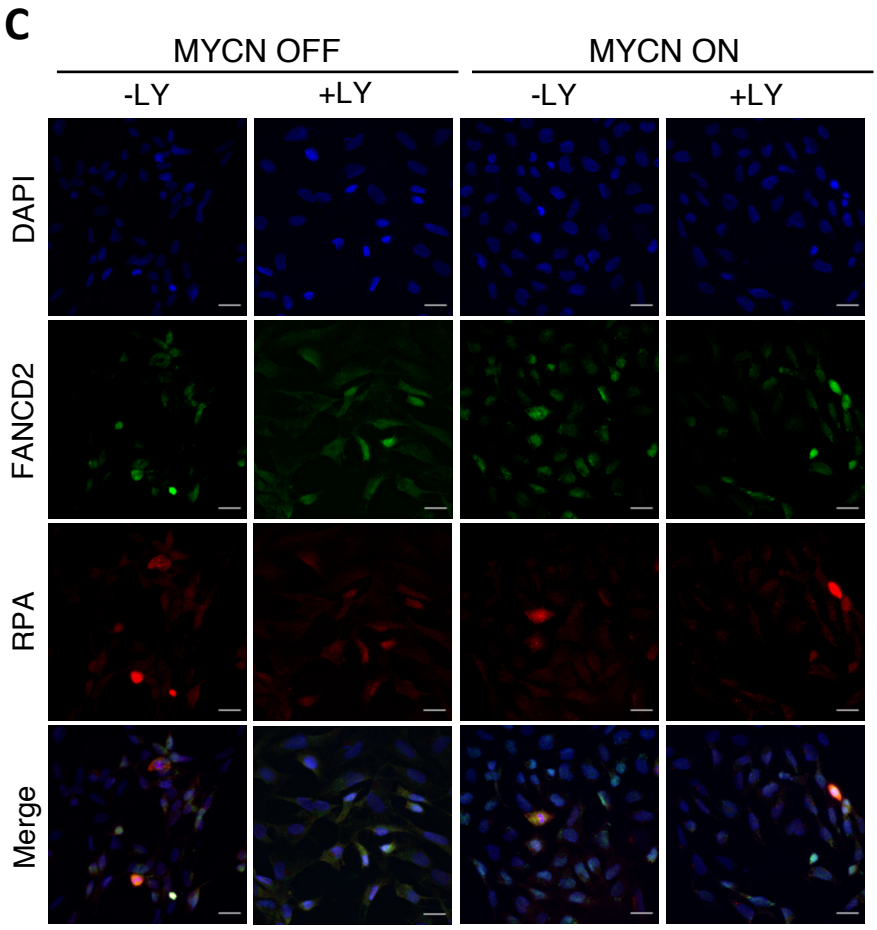

Figure 4.19. Treatment with AURKA inhibitor LY3295668 does not induce accumulation of R-loops, FANCD2 foci or RPA foci in SHEP-Tet21N MYCN ON and OFF cells. (Legend overleaf).

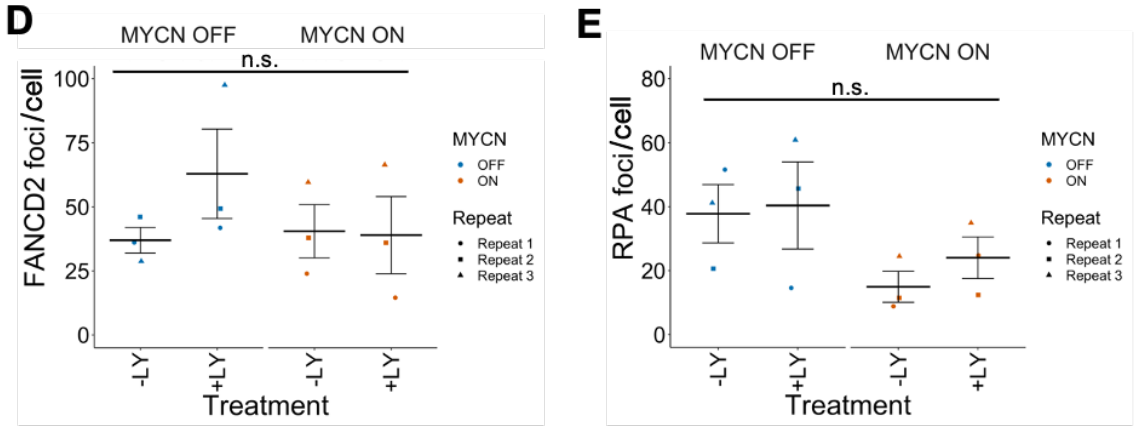

Figure 4.19. Treatment with AURKA inhibitor LY3295668 does not induce accumulation of R-loops, FANCD2 foci or RPA foci in SHEP-Tet21N MYCN ON and OFF cells.
SHEP-Tet21N MYCN ON and OFF cells were treated with 0 nM (-LY) or 50 nM (+LY) LY3295668, an AURKA inhibitor, for 2 hours. Cells were then fixed for immunofluorescence analysis. **(A)** Cells were stained for R-loops and nucleolin. Cells were incubated with RNase H for 24 hours before staining to digest R-loops as a negative control. Hannah Walsh helped with this Immunofluorescence staining. **(A)** Representative images of R-loop and nucleolin staining are depicted. Scale bar = 25 μm. **(B)** R-loop corrected total cell fluorescence (CTCF) was quantified for 100 cells per repeat per treatment condition. Mean CTCF is presented for each repeat, with black lines indicating overall mean ±SEM (n=3). **(C)** Representative images of cells stained for FANCD2 and pRPA32/RPA2 are shown. Scale bar = 25 μm. Number of **(D)** FANCD2 foci per cell and **(E)** pRPA foci per cell was quantified for each treatment condition. In (D) and (E), 100 cells per repeat per treatment condition were quantified. Mean foci per cell is presented for each repeat, with black lines indicating overall mean ±SEM (n=3). Statistical significance between treatments was determined by a two-way ANOVA where n.s. = not significant, *p<0.05, **p<0.01, ***p<0.001.

Previous studies have demonstrated a role for both ATR and FA pathway proteins in the resolution of R-loops (Garcia-Rubio et al., 2015; Schwab et al., 2015; Madireddy et al., 2016; Hamperl et al., 2017; Barroso et al., 2019; Okamoto et al., 2019; Liang et al., 2019a; Matos et al., 2020). Given FANCD2-mediated R-loop resolution is associated FANCD2 mono-ubiquitination (Liang et al., 2019a), and ATR activity is necessary for efficient FA pathway activation (Andreassen et al., 2004), it was hypothesised that FANCD2-dependent R-loop resolution would require ATR activity. To determine whether ATR inhibition disrupts the FANCD2-mediated resolution of MYCN-induced R-loops, SHEP-Tet21N MYCN ON and OFF cells were treated with 1 μM VE-821 for 24 hours. R-loop intensity, FANCD2 foci and pRPA foci were subsequently analysed by immunofluorescence. Inhibition of ATR induced a significant increase in R-loop intensity in MYCN OFF cells ($F(1) = 24.29$, $p < 0.001$), but a non-significant

reduction in R-loop intensity in MYCN ON cells ($F(1) = 24.29$, $p > 0.05$) (Figure 4.20A-B, Appendix Figure A17A). A small but non-significant increase in the number of FANCD2 foci per cell was observed following ATR inhibition in both MYCN ON and OFF cells ($F(1) = 1.62$, $p > 0.05$) (Figure 4.20C-D, Appendix Figure A17B). Consistent with the increase in R-loop accumulation selectively in MYCN OFF cells, ATR inhibition also resulted in an increase in pRPA foci in two out of three replicates selectively in MYCN OFF cells, however this increase was not significant ($F(1) = 0.64$, $p > 0.05$) (Figure 4.20C, 4.21E, Appendix Figure A17C).

This data suggests FANCD2 is not involved in the currently known MYCN-dependent pathways of R-loop resolution. However, analysis of the efficacy of BRCA1 depletion, AURKA inhibition and ATR inhibition in SHEP-Tet21N cells should be undertaken to confirm these findings. Interestingly, ATR inhibition induces R-loop accumulation specifically in MYCN OFF cells.

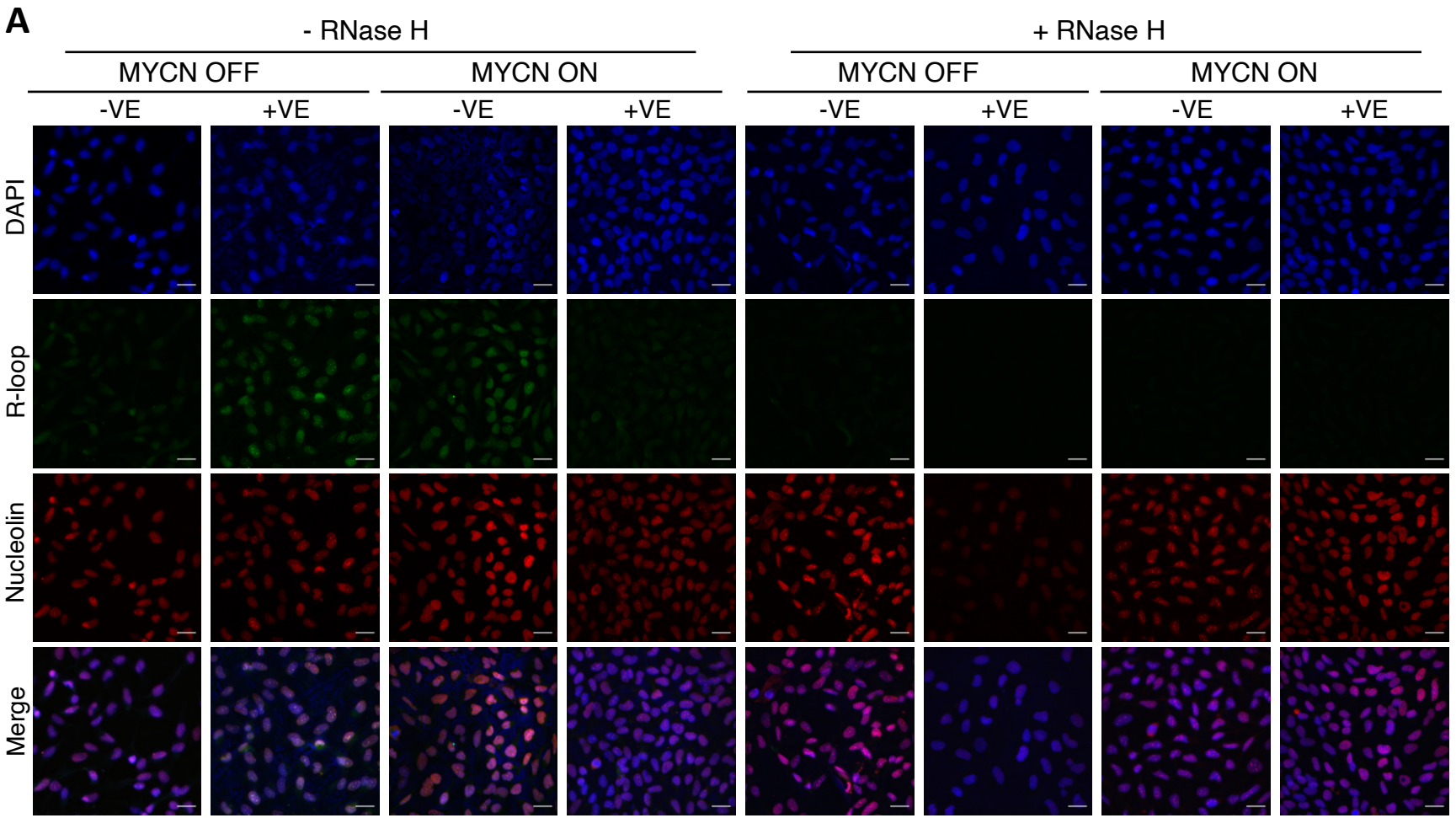

Figure 4.20. Treatment with ATR inhibitor VE-821 induces R-loop accumulation selectively in MYCN OFF cells but does not induce accumulation FANCD2 foci or RPA foci. (Legend overleaf).

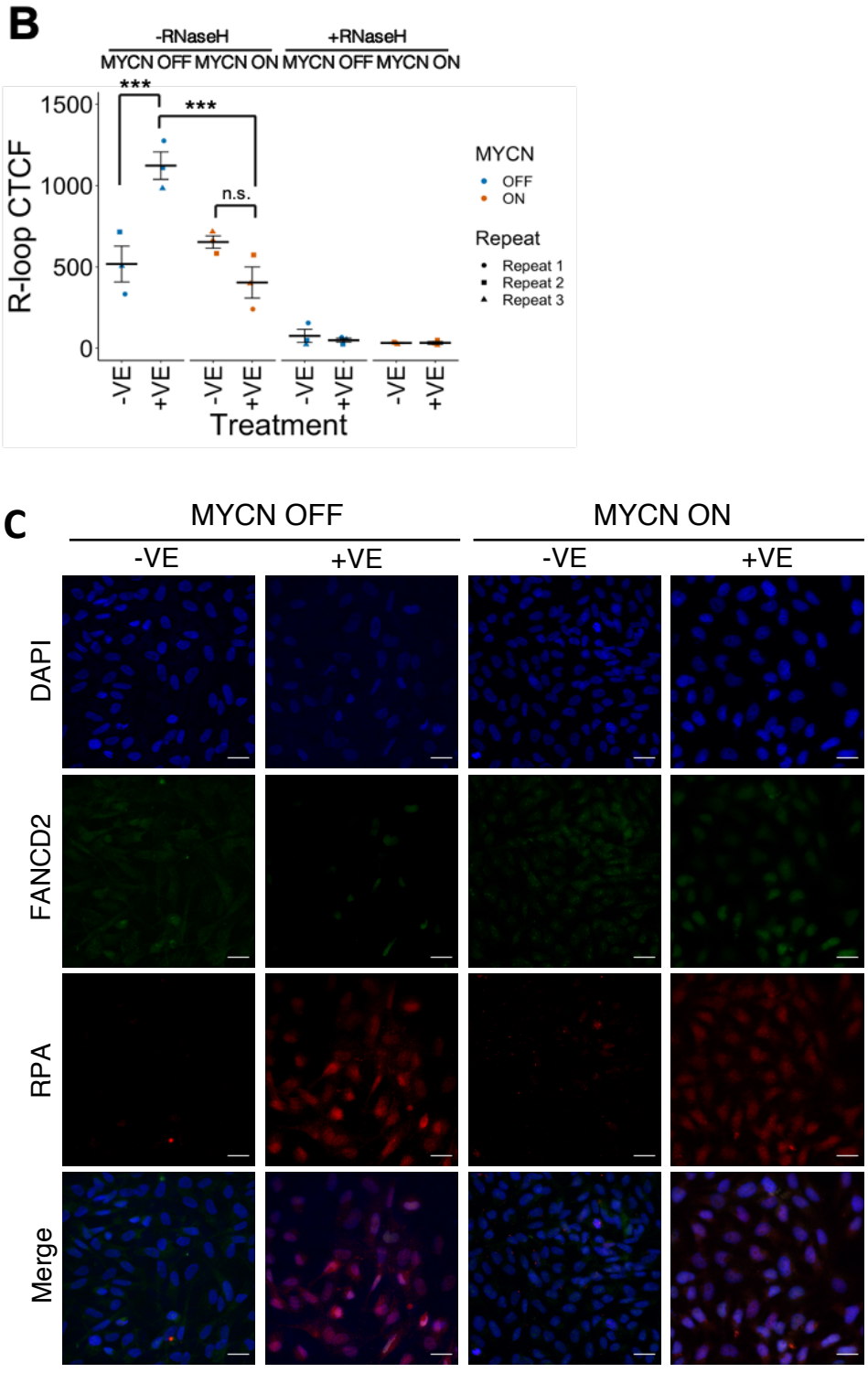

Figure 4.20. Treatment with ATR inhibitor VE-821 induces R-loop accumulation selectively in MYCN OFF cells but does not induce accumulation FANCD2 foci or RPA foci. (Legend overleaf).

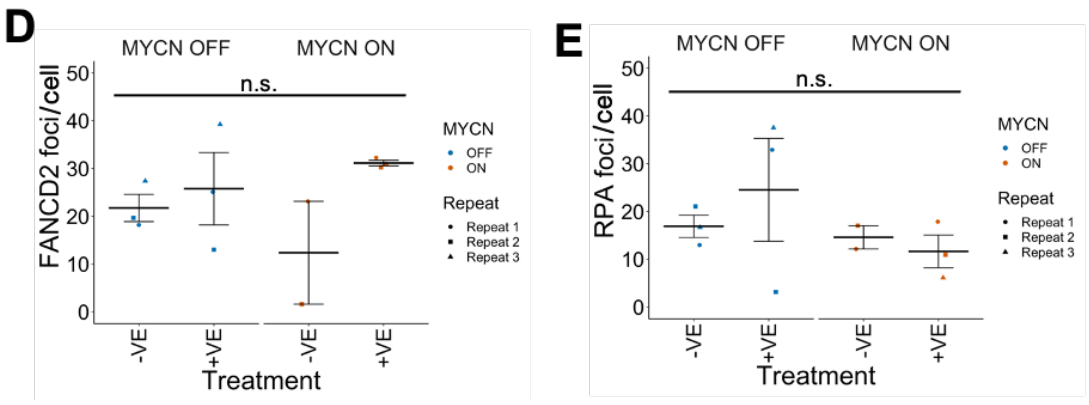

Figure 4.20. Treatment with ATR inhibitor VE-821 induces R-loop accumulation selectively in MYCN OFF cells but does not induce accumulation FANCD2 foci or RPA foci.
SHEP-Tet21N MYCN ON and OFF cells were treated with 0 μM (-VE) or 1 μM (+VE) VE-821 for 24 hours. Cells were then fixed for immunofluorescence analysis and stained for R-loops and nucleolin. Cells were incubated with RNase H for 24 hours before staining to digest R-loops as a negative control. Hannah Walsh helped with this Immunofluorescence staining. **(A)** Representative images of R-loop and nucleolin staining are shown. Scale bar = 25 μm. **(B)** R-loop corrected total cell fluorescence (CTCF) was quantified for 100 cells per repeat per treatment condition. Mean CTCF is presented for each repeat, with black lines indicating overall mean ±SEM (n=3). **(C)** Representative images of cells stained for FANCD2 and pRPA32/RPA2 are shown. Scale bar = 25 μm. Number of **(D)** FANCD2 foci per cell and **(E)** pRPA foci per cell was quantified for each treatment condition. In (D) and (E), 100 cells per repeat per treatment condition were quantified. Mean foci per cell is presented for each repeat, with black lines indicating overall mean ±SEM (n=3). Statistical significance between treatments was determined by a two-way ANOVA where n.s. = not significant, *p<0.05, **p<0.01, ***p<0.001.

4.2.4 Off-target effects of curcumin contribute to curcumin-induced toxicity in neuroblastoma cells

4.2.4.1 Inhibition of FANCD2 mono-ubiquitination only partially accounts for curcumin-induced toxicity

Curcumin is a non-specific FA pathway inhibitor and has therefore been demonstrated to induce a wide array of other off-target effects. For example, in neuroblastoma cells, curcumin promotes apoptosis and cell cycle arrest through upregulation of p53 and caspase signalling and suppression of AKT and NF-κB (Zhai et al., 2020). Therefore, we next examined whether the curcumin-induced toxicity observed in this chapter was due to on-target inhibition of FANCD2 mono-ubiquitination or off-target effects. Given SHEP-Tet21N MYCN ON cells have a greater sensitivity to curcumin treatment than MYCN OFF cells (Figure 4.10A,C), it was hypothesised that if curcumin was acting on-target, MYCN ON cells would also have a greater sensitivity to FANCD2 depletion. The efficacy of FANCD2 depletion by a range of single FANCD2 siRNAs and a pool of FANCD2 siRNAs relative to the appropriate scrambled siRNA control was confirmed in both MYCN ON and OFF cells by western blotting (Figure 4.21A). SHEP-Tet21N MYCN ON and OFF cells were transfected with FANCD2-targeted or scrambled siRNA for 64 hours before cell viability was determined by Alamar blue assays. Relative to the scrambled siRNA control, depletion of FANCD2 had a limited effect on survival in both MYCN ON and OFF cells (Figure 4.21B).

It was next hypothesised that if the toxicity of curcumin was only due to its ability to inhibit FANCD2 mono-ubiquitination, depletion of FANCD2 should abrogate the toxicity of curcumin. SHEP-Tet21N MYCN ON and OFF cells were transfected with scrambled or FANCD2 siRNA for 24 hours before addition of 0 μM or 5 μM curcumin for 40 hours. Cell viability was then analysed by Alamar blue assays. For each siRNA condition, percentage viability after curcumin treatment was calculated. Compared to the scrambled siRNA control, depletion of FANCD2 caused a small increase in viability following curcumin treatment (Figure 4.21C).

Given FANCD2 depletion only partially abrogates the sensitivity of MYCN ON and OFF cells to curcumin, and MYCN ON cells are not significantly more sensitive to FANCD2 depletion than MYCN OFF cells, this data suggests FA pathway inhibition only partially accounts for the cytotoxicity of curcumin in neuroblastoma cells. However, it is possible that FA pathway inhibition has a dominant negative effect on FANCD2 function

that depletion does not induce. As such, inhibition of the residual FANCD2 after depletion may be sufficient to cause the toxicity seen.

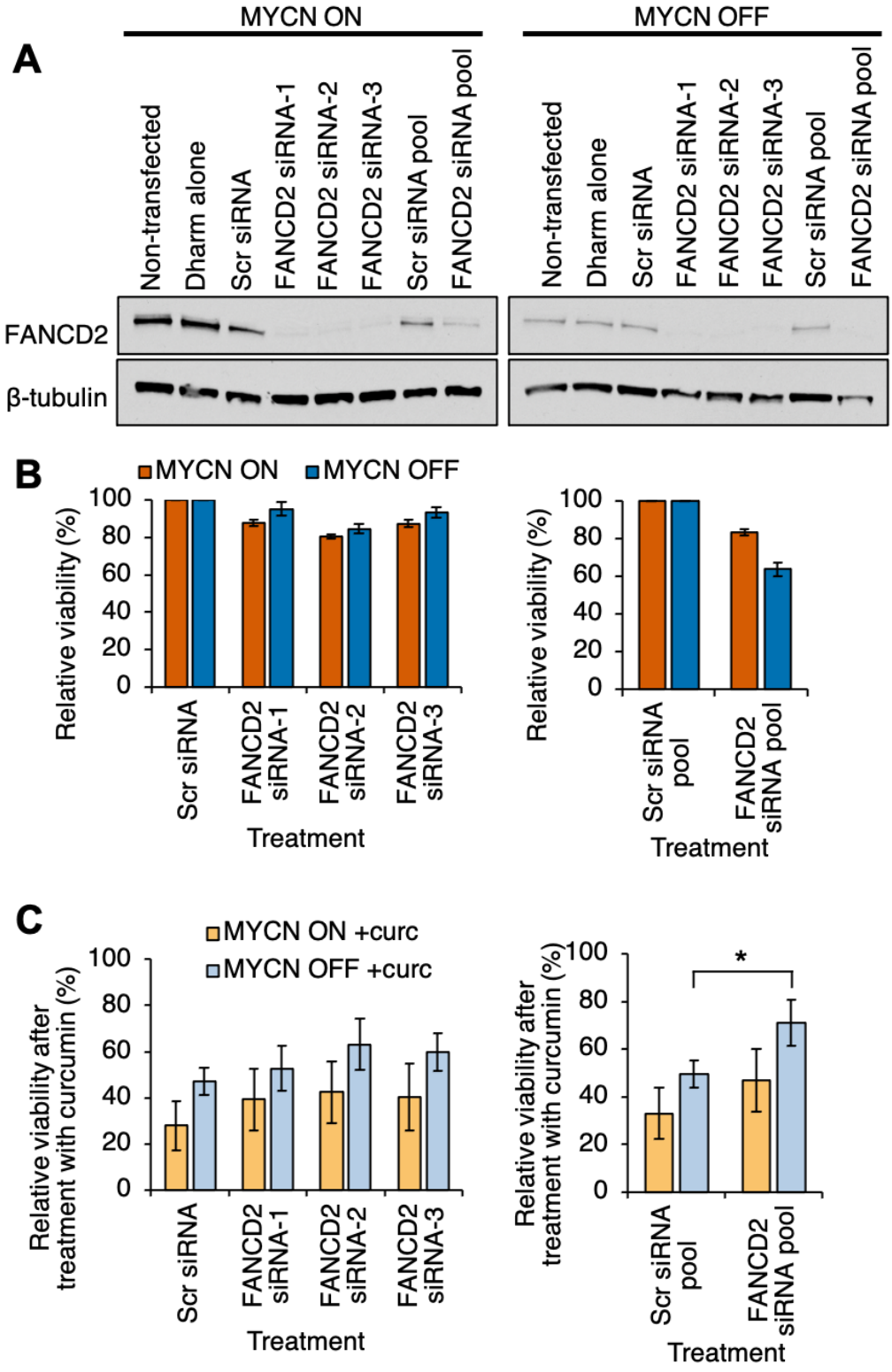

Figure 4.21. Inhibition of FANCD2 mono-ubiquitination partially accounts for the sensitivity of SHEP-Tet21N neuroblastoma cells to curcumin. (Legend overleaf).

Figure 4.21. Inhibition of FANCD2 mono-ubiquitination partially accounts for the sensitivity of SHEP-Tet21N neuroblastoma cells to curcumin. SHEP-Tet21N MYCN ON and OFF cells were non-transfected, or transfected with dharmafect-1 alone, scrambled siRNA, one of three FANCD2 siRNAs, a pool of scrambled siRNAs, or a pool of FANCD2 siRNAs. **(A)** Cell lysates were harvested 48 hours after transfection and FANCD2 protein levels determined by western blotting. **(B)** Cell viability was analysed 64 hours after transfection by Alamar blue assays. Percentage viability was determined for FANCD2 siRNA transfected cells relative to the corresponding scrambled siRNA transfected cells. Data are presented as means ±SEM (n=3). Statistical significance of viability for FANCD2 siRNA transfected cells compared to scrambled siRNA transfected cells was determined by Student's t-test where *p<0.05, **p<0.01, ***p<0.001. **(C)** 24 hours after transfection, cells were treated with 0 μM or 5 μM curcumin for 40 hours before cell viability was analysed by Alamar blue assays. Percentage viability of cells after curcumin treatment compared to those without curcumin treatment was determined for each siRNA-transfected condition. Data are presented as means ±SEM (n=3). Statistical significance of viability for FANCD2 siRNA transfected cells compared to scrambled siRNA transfected cells was determined by one-way ANOVA where *p<0.05, **p<0.01, ***p<0.001.

4.2.4.2 High MYCN expression sensitises neuroblastoma cells to other FA pathway inhibitors

In the absence of a specific FA pathway inhibitor, we attempted to validate the MYCN-induced sensitivity to FA pathway inhibition observed by analysing the toxicity of a different non-specific FA pathway inhibitor with different off-target effects. Ouabain is a cardiac glycoside which was identified as a non-specific inhibitor of FANCD2 mono-ubiquitination by Jun et al., (2013). The optimal dose of ouabain necessary for effective inhibition of endogenous and cisplatin-induced FA pathway activation was determined. SHEP-Tet21N MYCN ON and OFF cells were pre-treated with 50 nM to 200 nM ouabain for 16 hours before addition of 0 μM or 5 μM cisplatin for 24 hours. FANCD2 protein levels and mono-ubiquitination was determined by western blotting (Figure 4.22A). Ouabain induced a reduction in total FANCD2 protein levels in a dose-dependent manner in both MYCN ON and OFF cells (Figure 4.22B). Treatment with 100 nM ouabain effectively inhibited cisplatin-induced FA pathway activation in both MYCN ON and OFF cells (Figure 4.22C). Treatment with 50nM ouabain alone induced an increase in FANCD2 mono-ubiquitination in both MYCN ON and OFF cells. However, this was inhibited in a dose-dependent manner by 100 nM and 200 nM ouabain treatment in MYCN ON cells.

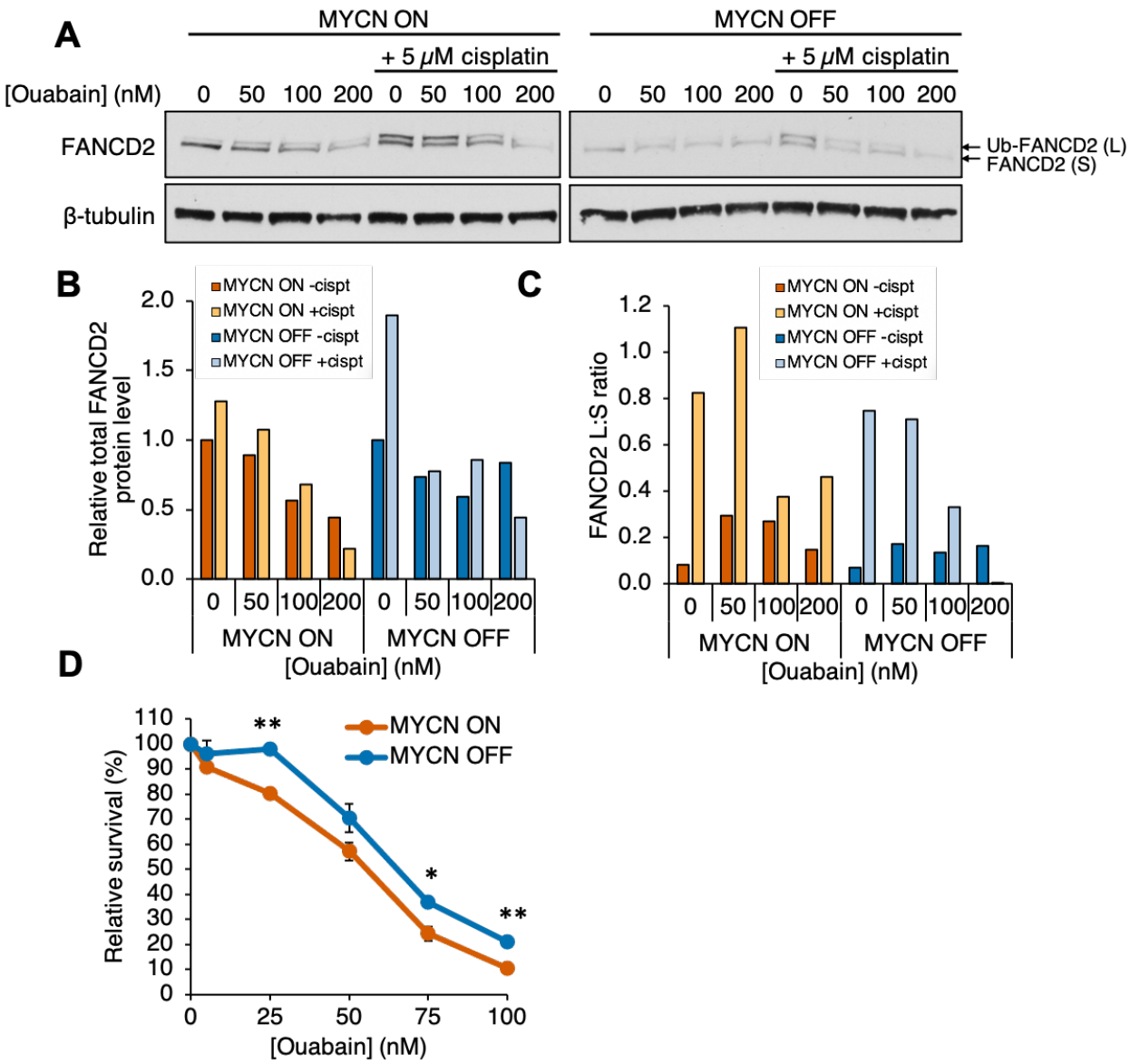

Figure 4.22. Ouabain inhibits endogenous and cisplatin-induced FA pathway activation in SHEP-Tet21N neuroblastoma cells.
SHEP-Tet21N MYCN ON and OFF cells were pre-treated with 0-200 nM ouabain for 16 hours before addition of 0 μM or 5 μM cisplatin for 24 hours. **(A)** FANCD2 protein levels were determined by western blotting. **(B)** Total FANCD2 band intensity (sum of L and S band intensities) was quantified relative to 0 μM ouabain with 0 μM cisplatin treatment and normalised to ß-tubulin band intensity. **(C)** FANCD2 L:S ratios were calculated relative to 0 μM ouabain with 0 μM cisplatin treatment. **(D)** Relative survival of SHEP-Tet21N MYCN ON and OFF cells following treatment with 0-100 nM ouabain for 40 hours. Percentage survival was determined by clonogenic survival assays and calculated relative to 0 μM ouabain treatment. Data are presented as means ±SEM (n=3). Statistical significance between MYCN ON and OFF was determined at each concentration by a Student's t-test where *p<0.05, **p<0.01, ***p<0.001.

To determine whether high *MYCN* expression also sensitises neuroblastoma cells to ouabain, clonogenic survival of SHEP-Tet21N MYCN ON and OFF cells was analysed following treatment with increasing doses of ouabain for 40 hours. MYCN ON cells were significantly more sensitive to ouabain than MYCN OFF cells (Student's t-test, $p < 0.05$) (Figure 4.22D). Given ouabain also has many off-target effects including inhibition of NHEJ (Du et al., 2018), the extent of toxicity induced by on-target inhibition of FANCD2 mono-ubiquitination was analysed. It was hypothesised that if the toxicity of ouabain was mediated purely by its ability to inhibit FA pathway activation, depletion of FANCD2 would abrogate all ouabain toxicity. SHEP-Tet21N MYCN ON and OFF cells were transfected with scrambled or FANCD2-targeted siRNA for 24 hours before addition of 0 nM or 100 nM ouabain for 40 hours. Cell viability was then analysed by Alamar blue assays. For each siRNA condition, percentage viability after ouabain treatment was calculated (Figure 4.23). Depletion of FANCD2 did not abrogate ouabain toxicity in comparison to the scrambled siRNA control. This could suggest minimal ouabain toxicity was attributed to the on-target inhibitory effects on the FA pathway. However, depletion of FANCD2 could have different effects to inhibition of FANCD2 mono-ubiquitination, and this could account for the lack of abrogation observed.

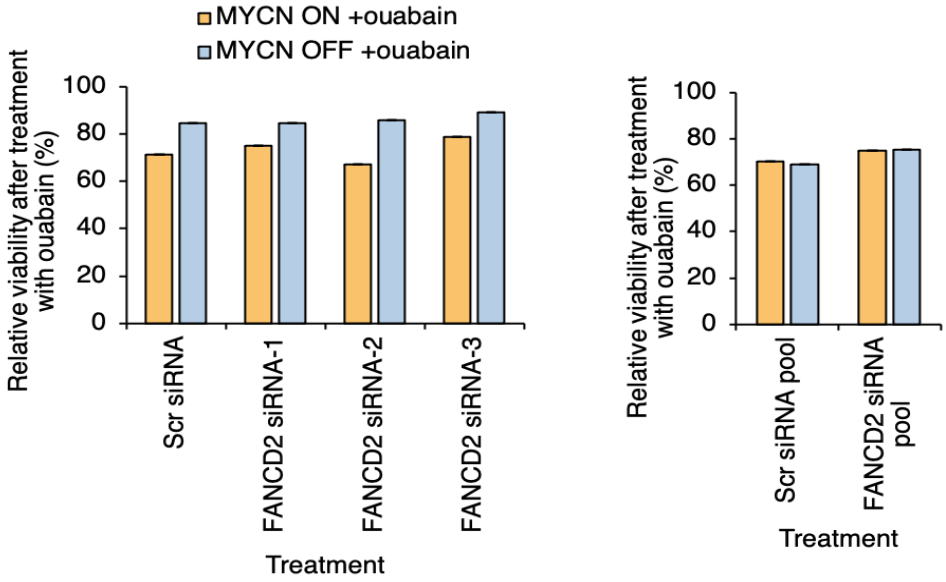

Figure 4.23. Off-target effects may largely account for toxicity of ouabain in SHEP-Tet21N neuroblastoma cells.
SHEP-Tet21N MYCN ON and OFF cells were transfected with scrambled siRNA, one of three FANCD2 siRNAs, a pool of scrambled siRNAs, or a pool of FANCD2 siRNAs. 24 hours after transfection, cells were treated with 0 nM or 100nM ouabain for 40 hours before cell viability was analysed by Alamar blue assays. Percentage viability of cells following ouabain treatment, relative to viability of cells without curcumin treatment, was determined for each siRNA-transfected condition (n=1).

In collaboration with Dr. Spencer Collis' laboratory group, the effect of high *MYCN* expression on the sensitivity of SHEP-Tet21N cells to a novel specific FA pathway inhibitor nFAPi was determined. Clonogenic survival of SHEP-Tet21N MYCN ON and OFF cells was analysed following treatment with 0 nM to 100 nM nFAPi. Although limited toxicity was observed overall, MYCN ON cells were significantly more sensitive to treatment with 100 nM nFAPi than MYCN OFF cells ($t(4) = -4.18$, $p = 0.014$) (Figure 4.24). The effective dose range of nFAPi in SHEP-Tet21N cells could be further optimised to clarify these results.

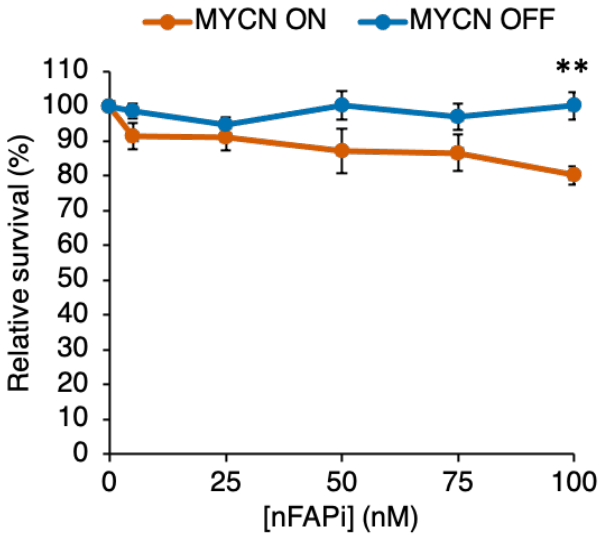

Figure 4.24. High MYCN expression may sensitise SHEP-Tet21N cells to higher doses of nFAPi, a specific FA pathway inhibitor.
Relative survival of SHEP-Tet21N MYCN ON and OFF cells following treatment with 0-100 nM nFAPi, a novel specific FA pathway inhibitor (Dr. S. Collis, University of Sheffield). Percentage survival was determined by clonogenic survival assays and calculated relative to 0 μM nFAPi treatment. Data are presented as means ±SEM (n=3). Statistical significance between MYCN ON and OFF was determined at each concentration by a Student's t-test where *p<0.05, **p<0.01, ***p<0.001.

This data validates the findings that high *MYCN* expression sensitises cells to FA pathway inhibition by demonstrating that SHEP-Tet21N MYCN ON cells were significantly more sensitive to treatment with ouabain; a different non-specific FA pathway inhibitor, and nFAPi; a novel specific FA pathway inhibitor. However, depletion of FANCD2 indicated non-specific effects contribute to the cytotoxicity of curcumin and ouabain in neuroblastoma cells.

4.3 Discussion

The FA pathway is a DNA damage repair network which functions in the replication-dependent repair of ICLs (Moldovan and D'Andrea, 2009; Rodriguez and D'Andrea, 2017). The FA pathway also functions to limit replication stress, for example by protecting stalled replication forks and resolving R-loops (Sobeck et al., 2006; Collis et al., 2008; Schlacher et al., 2012; Chaudhury et al., 2013; Lossaint et al., 2013; Garcia-Rubio et al., 2015; Schwab et al., 2015; Madireddy et al., 2016; Herold et al., 2019). Although there are no widely recognised specific FA pathway inhibitors, it has been shown that non-specific FA pathway inhibitors, such as curcumin, sensitise cancer cells to crosslinking, alkylating and replication stress-inducing chemotherapeutics (Chrinomas et al., 2006; Kunnumakkara et al., 2007; Patil et al., 2014). In Chapter 3, it was observed that high *MYCN* expression induced an upregulation of FANC and HRR-associated FA pathway genes in neuroblastoma cell lines and tumours. Also, higher endogenous FA pathway activation was associated with greater *MYCN* expression. This suggested high *MYCN* expression led to an increased reliance on the FA pathway. We therefore hypothesised that FA pathway inhibition would sensitise neuroblastoma cells to crosslinking chemotherapeutics and MYCN-induced replication stress and DNA damage.

Here, we analyse the impact of *MYCN* expression on FA pathway activation and examine whether inhibition of the FA pathway has therapeutic potential in MNA neuroblastoma. By quantifying FANCD2 mono-ubiquitination and foci formation, it was demonstrated that *MYCN* expression induces significantly higher levels of FA pathway activation in SHEP-Tet21N cells. Curcumin inhibited cisplatin-induced FA pathway activation in most cell lines but only inhibited endogenous FA pathway activation in cells with high *MYCN* or *MYCC* expression. Neuroblastoma cell viability was analysed by Alamar blue and clonogenic survival assays. Curcumin treatment sensitised SHEP-Tet21N MYCN ON and OFF cells to crosslinking chemotherapeutics cisplatin and carboplatin, but not the alkylating agent TMZ. High *MYCN* expression sensitised cells to curcumin treatment alone. Furthermore, we explored the molecular mechanism behind this MYCN-induced curcumin sensitivity. Curcumin treatment did not affect the cell cycle distribution of MYCN OFF cells but induced a small S-phase and sub-G1 accumulation in MYCN ON cells. In MYCN ON and OFF cells, curcumin exacerbated endogenous replication stress and cisplatin-induced DNA damage. Curcumin also induced R-loop accumulation specifically in MYCN ON cells. Depletion of FANCD2 by siRNA did not

fully abrogate the toxicity of curcumin treatment in MYCN ON and OFF cells, suggesting pleiotropic effects other than FA pathway inhibition may contribute to curcumin toxicity. However, high *MYCN* expression also sensitised cells to the non-specific FA pathway inhibitor ouabain and the specific FA pathway inhibitor nFAPi, and this validated the FA pathway as a potential target in MNA neuroblastoma.

4.3.1 High *MYCN* expression induces replication stress and FA pathway activation which is required for survival.

Here, we demonstrated in an isogenic system that expression of *MYCN* leads to increased endogenous FANCD2 mono-ubiquitination and formation of FANCD2 foci (Figure 4.1B, 4.17B). Together, these results indicate high *MYCN* expression induces FA pathway activation. Endogenously, many FA pathway proteins function to limit replication stress through protection of stalled replication forks and suppression of R-loops, often in a manner dependent on FANCD2 mono-ubiquitination (Schlacher et al., 2012; Liang et al., 2019a). Consistent with others (Gu et al., 2015; King et al., 2020), we observed *MYCN* expression increased replication stress as indicated by an increase in pRPA foci (Figure 4.16C) and an increase in S-phase accumulation (Figure 4.15). Inhibition of FANCD2 mono-ubiquitination by curcumin exacerbated both the increase in pRPA foci (Figure 4.16C) and the increase in S-phase accumulation (Figure 4.15). Thus we consider that higher levels of replication stress in MYCN ON cells likely activate FANCD2 in order to limit oncogene-induced replication stress.

Analysis of endogenous FA pathway activation levels across a panel of neuroblastoma cell lines demonstrates that presence of *MYCN* amplification does not correlate as clearly with higher FANCD2 mono-ubiquitination levels compared to *MYCN* overexpression in an isogenic system. Non-MNA SH-SY5Y cells were observed to have the highest FANCD2 L:S ratio of 0.30 (Figure 4.9C), followed by MNA Kelly cells at 0.17 (Figure 4.9C), MNA IMR32 cells at 0.14 (Figure 4.8C) and non-MNA SHEP-1 cells at 0.13 (Figure 4.8C). This highlights the impact of other genetic factors on endogenous FA pathway activation. In the case of SH-SY5Y, high *MYCC* expression may contribute to FA pathway activation (Figure 3.16). As such, wide variation in endogenous FA pathway activation levels is also observed across cancer types. For example, the endogenous FANCD2 L:S ratio is 0.6 in MCF-7 breast cancer cells and 0.3 in HeLa cervical cancer cells (Chirnomas et al., 2006). Additionally, we observed large variation in the endogenous FANCD2 L:S ratio MYCN ON cells between experiment replicates,

from 0.05 to 0.5. Similarly, Jun et al., (2013) observed that the endogenous FANCD2 L:S ratio in U2OS osteosarcoma cells ranged from 0.01 to 0.28. This highlights the impact of environmental factors on FA pathway activation.

Previously, FA pathway activation has been frequently observed in response to replication-stress inducing agents (Taniguchi et al., 2002a; Schlacher et al., 2012; Schwab et al., 2015; Yang et al., 2015; Okamoto et al., 2018b; Liang et al., 2019a). However, there is limited observation of oncogene-induced FA pathway activation, thus our data are important in highlighting this function of FANCD2 in a cancer setting. Helbling-Leclerc et al., (2019) observed that chronic expression of oncogenes *RAS* or *RAF1* in non-cancerous cells induced a transitory increase in *FANCD2* expression and mono-ubiquitination before increased replication stress induced oncogene-induced senescence, leading to FANCD2 depletion. Overexpression of *FANCD2* delayed oncogene-induced senescence (Helbling-Leclerc et al., 2019), suggesting the effects of FA pathway inhibition on cellular senescence in MNA neuroblastoma cells could be further explored. In support of this, silencing of *FANCD2* overexpression in melanoma cells harbouring activation or amplification of the *MiTF* oncogene rapidly induced cellular senescence (Bourseguin et al., 2016). Constitutive expression of the HPV oncogenes *E6* or *E7* has also been observed to induce an increase in FANCD2 mono-ubiquitination and foci formation (Khanal and Galloway, 2019).

The necessity of FA pathway activity in limiting oncogene-induced replication stress is highlighted in the mechanism of bone marrow failure in patients with Fanconi anaemia. In this, FA-deficient haematopoietic stem and progenitor cells (HSPCs) accumulate high levels of DNA damage, leading to hyperactivation of p53 and TGF-β growth suppressive pathways (Ceccaldi et al., 2012; Pontel et al., 2015; Walter et al., 2015; Zhang et al., 2016; Garaycoechea et al., 2018). To promote survival and proliferation under these conditions, FA-deficient HSPCs upregulate *MYCC*, or occasionally *MYCN* (Rodriguez et al., 2021). However, overexpression of MYC oncogenes exacerbates the chronic replication stress and DNA damage in FA-deficient cells to intolerable levels, leading to further HSPC death and bone marrow failure (Rodriguez et al., 2021). This supports our hypothesis that FA pathway activity is necessary to mitigate the replication stress and DNA damage induced by MYC oncogenes.

We therefore subsequently tested whether the increased FA pathway activation observed in *MYCN* expressing cells was required for survival. To do this, we first demonstrated the ability of curcumin to inhibit endogenous FA pathway activation in

MYCN expressing cells. It was observed that curcumin inhibited endogenous FA pathway activation consistently in MYCN ON SHEP-Tet21N cells, but not in MYCN OFF cells (Figure 4.6). Similarly, curcumin inhibited endogenous FANCD2 foci formation in MYCN ON cells but not MYCN OFF cells (Figure 4.16B). This suggests curcumin inhibited MYCN-induced FA pathway activation. Expanding analysis to more neuroblastoma cell lines, it was observed that curcumin was able to inhibit endogenous FANCD2 mono-ubiquitination in MNA IMR32 cells, and SH-SY5Y cells which have high *MYCC* expression (Figure 4.8C, 4.10C). However, endogenous FANCD2 mono-ubiquitination was not inhibited in non-MNA SHEP-1 cells, or in Kelly cells in which curcumin induced FA pathway activation likely through increased toxicity. Curcumin was also observed to reduce the total FANCD2 protein expression levels across all neuroblastoma cell lines analysed except SHEP-Tet21N MYCN ON cells (Figures 4.7A, 4.9A, 4.10A). However this downregulation is only significant in IMR32 cells (Figure 4.8A). Downregulation of FANCD2 expression may be another mechanism through which curcumin inhibits FA pathway activation.

Consistent with the increased FA pathway activation observed in neuroblastoma cells with high *MYCN* expression, expression of *MYCN* sensitised neuroblastoma cells to the FA pathway inhibitor curcumin (Figure 4.14A,C). Additionally, MNA neuroblastoma cell lines were more sensitive to curcumin than non-MNA cell lines (Figure 4.14B). This suggests *MYCN* expressing cells are dependent on the increased FA pathway activation for survival.

Overall, we observed that *MYCN* overexpression induced an increase in FA pathway activation, and this was inhibited by curcumin treatment. The increased FA pathway activation observed upon *MYCN* overexpression was shown to aid the limitation of MYCN-induced replication stress. This was demonstrated by the observation that curcumin exacerbated high replication stress levels in *MYCN* expressing cells. Additionally, curcumin was selectively more toxic in *MYCN* expressing cells, suggesting that MYCN-induced FA pathway activation is required for survival of these cells. In parallel with the increased FA pathway expression observed in Chapter 3, this indicates *MYCN* expression induces a greater dependency on the FA pathway which could be therapeutically exploited. It is tempting to speculate that FA pathway inhibitors could be used as single agents in the treatment of MNA neuroblastoma, however in reality combination therapies are more likely.

4.3.2 DNA crosslinking and alkylating chemotherapeutics activate the FA pathway in neuroblastoma cell lines

As expected, in addition to endogenous activation, we observed that TMZ or cisplatin treatment induced FANCD2 mono-ubiquitination in all neuroblastoma cell lines (Figures 4.2, 4.3, 4.7, 4.9, 4.10). Interestingly, cisplatin increased FANCD2 mono-ubiquitination to a greater extent in MYCN OFF cells compared to MYCN ON cells (Figure 4.4, 4.5, 4.7). This consistent with the fact that cisplatin induces S-phase arrest in MYCN OFF cells but not MYCN ON cells (Figure 4.15) and also induces a greater level of DNA damage in MYCN OFF compared to MYCN ON cells (Figure 4.16E). However, this greater cisplatin-induced FA pathway activation in MYCN OFF cells is not observed by FANCD2 foci levels, where cisplatin induces a greater number of FANCD2 foci in MYCN ON cells than MYCN OFF cells in two of three replicates (Figure 4.16B). Also, cisplatin induced greater FA pathway activation in MNA cell lines compared to non-MNA cell lines (Figures 4.9C, 4.10C).

Cisplatin was observed to induce a dose-dependent downregulation in total FANCD2 protein expression selectively in MYCN OFF cells (Figures 4.4B, 4.7B), however this observation was not always consistent (Figures 4.5B, 4.6B). Cisplatin also induced a small FANCD2 downregulation in non-MNA cells, but not MNA cells (Figures 4.9B, 4.10B). Cisplatin treatment therefore activates the FA pathway but reduces FANCD2 expression in non-MNA neuroblastoma cells. This cisplatin-induced FANCD2 downregulation was not observed in other cancer types (Chirnomas et al., 2006, Jun et al., 2013). Cisplatin-induced *FANCD2* downregulation may occur through activation of p53 by DNA damage, leading to assembly of the DREAM complex which associates with E2F4/5 in G0/G1 to repress target genes, including FA pathway genes such as *FANCD2* (Jaber et al., 2016; Engeland et al., 2018). This effect is perhaps mitigated in MYCN ON and MNA cells by the MYCN-induced upregulation of *FANCD2* observed in Chapter 3. TMZ had no consistent effect on total FANCD2 levels (Figure 4.2).

4.3.3 Curcumin inhibits chemotherapy-induced FA pathway activation and sensitises neuroblastoma cells to DNA crosslinking chemotherapeutics.

Previous studies have demonstrated that curcumin effectively inhibits chemotherapy-induced FA pathway activation in glioblastoma cells and ovarian, breast and cervical cancer cells (Chirnomas et al., 2006; Patil et al., 2014; Chen et al., 2015b). Similarly, we demonstrated that curcumin could inhibit cisplatin-induced activation of

FANCD2 in all NB cell lines tested (Figure 4.6, 4.7, 4.9, 4.10, 4.17B). Before examining whether curcumin could sensitise neuroblastoma cells to chemotherapy, we looked at the effect of *MYCN* overexpression on chemotherapy sensitivity. Expression of *MYCN* sensitised neuroblastoma cells to treatment with cisplatin (Figure 4.10A,B), carboplatin (Figure 4.11B) and TMZ (Figure 4.12B), despite cisplatin often inducing greater FA pathway activation (Figure 4.3C, 4.5C, 4.7C) and DNA damage (Figure 4.16E) in MYCN OFF cells. This is perhaps due to the faster proliferation rate and higher endogenous levels of replication stress and DNA damage in MYCN ON cells (Figures 3.2C, 4.17C) (Gu et al., 2015; King et al., 2020). Previous studies have also demonstrated that high *MYCN* expression or *MYCN* amplification in neuroblastoma cells and tumours induces greater initial sensitivity to cisplatin (Lu et al., 2005; Peirce and Findley, 2009; Boeva et al., 2017; van Groningen et al., 2017). MYCN may sensitise neuroblastoma cells to cisplatin-induced apoptosis through upregulation of the MDM2-p53 pathway (Fulda et al., 1999; Chen et al., 2010; Slack et al., 2005; Petroni et al., 2012; Veschi et al., 2012). The higher sensitivity of MYCN ON cells to the DNA crosslinking agents cisplatin and carboplatin suggests that the increase in FANC and HRR gene expression observed in Chapter 3 does not necessarily increase the efficacy of ICL repair in MYCN ON cells, perhaps due to the lack of upregulation of TLS and NER genes (Figure 3.14). This supports the hypothesis that FANC gene upregulation is instead primarily necessary to limit MYCN-induced replication stress. Similarly to *MYCN*, expression of the HPV oncogene *E6* also induces higher FA pathway expression and activation whilst simultaneously sensitising cells to crosslinking agents (Khanal and Galloway, 2019).

Regardless of the MYCN-induced differences in sensitivity, curcumin treatment sensitised both MYCN ON and OFF cells to cisplatin and carboplatin (Figure 4.10B, 4.12A). In agreement with our results, Sukumari-Ramesh et al., (2011) observed that curcumin sensitised the non-MNA neuroblastoma cell line SK-N-AS to cisplatin. However the mechanism by which curcumin induced this sensitivity was not determined. FA pathway inhibition by curcumin has also been shown to sensitise cell lines of different cancer types to cisplatin, such as ovarian, breast and lung cancer cell lines (Chirnomas et al., 2006; Chen et al., 2015b). Other studies also demonstrated the ability of curcumin to sensitise NSCLC, ovarian cancer, breast cancer and laryngeal carcinoma cells to cisplatin or carboplatin, however curcumin was shown to sensitise these cells through alternative mechanisms such as promotion of apoptosis, ROS production, suppression of NF-┤ B pathway activation, inhibition of β-catenin expression, and downregulation of genes which mediate cisplatin-resistance such as *FEN1* or *BCL-*

2 (Yallapu et al., 2010; Chanvorachote et al., 2009; Sreenivasan et al., 2013; Zhang et al., 2013; Kang et al., 2015; Zou et al., 2018; Wang et al., 2022a; Wang et al., 2022b).

In contrast, curcumin did not sensitise neuroblastoma cells to TMZ (Figure 4.12), However, previous studies have shown that FA pathway inhibition by curcumin significantly sensitised GBM cell lines to TMZ (Patil et al., 2014; Chen et al., 2007). This discrepancy may be observed because TMZ is a monofunctional alkylating agent and therefore primarily induces DNA methylation, which is repaired by BER, MMR or the DNA methyltransferase MGMT (Caporali et al., 2004; Trivedi et al., 2005; Liu and Gerson, 2006; Wang et al., 2006; Kondo et al., 2010; Fu et al., 2012). Therefore, whilst the FA pathway may contribute to the replication-associated repair of TMZ-induced DNA damage (Chen et al., 2007), its inhibition does not always sensitise cells to TMZ as the TMZ-induced lesions have multiple alternative repair mechanisms. GBM cells are more often defective in DNA repair processes such as MMR or dependent on the FA pathway for TMZ resistance and therefore may be more reliant on the FA pathway for repair of TMZ-induced damage (Friedman et al., 1997; Chen et al., 2007; Sarkaria et al., 2008).

Overall, these results indicate FA pathway inhibition could sensitise both MNA and non-MNA neuroblastoma cells to crosslinking chemotherapeutics used in the treatment of high-risk neuroblastoma. Use of FA pathway inhibitors in combination with induction chemotherapeutics could increase the efficacy of induction chemotherapy or enable use of lower doses to limit side-effects, and these are two major aims in neuroblastoma treatment development (Qiu and Matthay, 2022). FA pathway inhibition has also been previously shown to re-sensitise cancer cells which have acquired resistance to crosslinking or alkylating agents through FA pathway upregulation (Chirnomas et al., 2006; Chen et al., 2007; Zhao et al., 2014; Dai et al., 2015; Bretz et al., 2016; Dai et al., 2017). Given MNA neuroblastomas upregulate FA pathway expression, the potential of FA pathway inhibition in re-sensitising resistant neuroblastoma cells could be further explored.

4.3.4 MYCN-induced curcumin sensitivity is associated with increased replication stress

In agreement with findings from Gu et al., (2015) and King et al., (2020), we observed that high *MYCN* expression induces an increase in replication stress. This was demonstrated by an increase in pRPA foci (Figure 4.16C), which are formed when

RPA proteins are phosphorylated by checkpoint kinases ATM, ATR and DNA-PK upon detection of replication stress or DNA damage (Binz et al., 2004; Nuss et al., 2005; Wu et al., 2005; Vassin et al., 2009; Maréchal and Zou, 2015; Murphy et al., 2014). Previous studies demonstrated that this increased replication stress sensitised *MYCN* expressing neuroblastoma cells to inhibition of DNA repair and replication stress limiting pathways (Cole et al., 2011; Colicchia et al., 2017; Petroni et al., 2018; King et al., 2020; King et al., 2021; Southgate et al., 2020). As described in Chapter 4.3.1, we similarly observed that the MYCN-induced sensitivity to FA pathway inhibition by curcumin was associated with increased replication stress, as demonstrated by exacerbation of MYCN-induced S-phase accumulation and pRPA foci formation.

More specifically, curcumin induced a 3% increase in S-phase accumulation selectively in *MYCN* expressing cells (Figure 4.15), suggesting curcumin treatment results in greater activation of the S-phase checkpoint when *MYCN* is overexpressed. Curcumin also induced an increase in sub-G1 accumulation selectively in MYCN ON cells and this provides further indication that curcumin induces greater cell death upon *MYCN* overexpression. As observed in MYCN OFF cells, curcumin treatment had no effect on the cell cycle profile of basal cell carcinoma and cervical cancer cells (Chirnomas et al., 2006; Ghasemi et al., 2019). However, as observed in MYCN ON cells, curcumin treatment induced a 3% increase in the proportion of U2OS cells in S-phase (Jun et al., 2013). Curcumin has also been observed to induce G2/M-phase arrest in a wide variety of cancer types, including other neuroblastoma cell lines such as NUB-7 and LAN5, and this is indicative of the presence of damaged or incompletely replicated DNA (Liontas et al., 2004; Weir et al., 2007; Hu et al., 2017; Martinez-Castillo et al., 2018; Mo et al., 2021; Ye et al., 2021).

Although the impact of curcumin on cell cycle progression was specific to *MYCN* expressing cells, curcumin exacerbated pRPA foci levels in both MYCN ON and OFF cells (Figure 4.16C). However, given the higher endogenous replication stress level in MYCN ON cells, curcumin-treated MYCN ON cells had a greater level of replication stress than curcumin-treated MYCN OFF cells. As such, curcumin could exacerbate replication stress to intolerable levels specifically in MYCN ON cells. However the ability of curcumin to induce replication stress in MYCN OFF cells without effectively inhibiting endogenous FA pathway activation in these cells suggests curcumin may also induce replication stress through other mechanisms. For example, curcumin has been previously shown to downregulate RAD51 and this could contribute to the increased

replication stress observed (Zellweger et al., 2015; Mason et al., 2019; Wang et al., 2022a).

Despite this increase in replication stress, curcumin treatment alone was not observed to increase DNA damage levels, as demonstrated by analysis of γ-H2AX foci (Figure 4.16E). However, curcumin did exacerbate the number of cisplatin-induced γ-H2AX foci. In contrast, previous studies have demonstrated that FANCD2 depletion increases γ-H2AX foci formation (Garcia-Rubio et al., 2015; Schwab et al., 2015). Perhaps the expected impact of higher replication stress on DNA damage is mitigated by the curcumin-induced upregulation of *PARP, BRCA1, BRCA2, ERCC1* and *DNA-PK* (Shang et al., 2016; Chen et al., 2017). However, Wang et al., (2022a) demonstrated that curcumin induces γ-H2AX foci formation in triple-negative breast cancer cells, and other studies observed that curcumin enhances DNA fragmentation in laryngeal, cervical and breast cancer cells (Rak et al., 2013; Shang et al., 2016; Wang et al., 2022a).

4.3.5 The FA pathway contributes to the resolution of MYCN-induced R-loops

Given the FA pathway maintains genome integrity through the regulation of multiple DNA repair and replication stress-limiting pathways, its inhibition is likely multifaceted. FANCD2 mono-ubiquitination dependent mechanisms of replication stress limitation includes protection of stalled replication forks and resolution of R-loops (Taniguchi et al., 2002a; Sobeck et al., 2006; Collis et al., 2008; Schlacher et al., 2012; Garcia-Rubio et al., 2015; Schwab et al., 2015; Madireddy et al., 2016; Herold et al., 2019; Liang et al., 2019a). To further examine the role of the FA pathway in limiting MYCN-induced replication stress, the effect of curcumin on R-loop accumulation was examined in SHEP-Tet21N MYCN ON and OFF cells. Endogenously MYCN ON cells had a lower average level of R-loop accumulation than MYCN OFF cells (Figure 4.17B). This is likely due to the multiple mechanisms of MYCN-driven R-loop resolution which are employed by MYCN to limit replication and transcription stress (Herold et al., 2019; Roeschert et al., 2021). Treatment with curcumin exacerbated endogenous R-loop accumulation selectively in MYCN ON cells. This suggested the FA pathway was involved in the resolution of MYCN-induced R-loops in a manner dependent on FANCD2 mono-ubiquitination. Similarly, Liang et al., (2019a) demonstrated that binding of the FANCD2-FANCI complex to R-loops stimulates FANCD2 mono-ubiquitination.

Similarly to the curcumin-induced S-phase accumulation, curcumin treatment induced R-loop accumulation specifically in *MYCN* expressing cells. Given curcumin also inhibits endogenous FANCD2 mono-ubiquitination selectively in MYCN ON cells, this could suggest the higher FANCD2 mono-ubiquitination and foci formation observed in MYCN ON compared to MYCN OFF cells is driven primarily by an increase in FANCD2-mediated R-loop repair. However, analysis of FANCD2 foci formation in MYCN ON and OFF cells, in the presence and absence of R-loops, would be necessary to determine this.

Since inhibition of FANCD2 mono-ubiquitination increased R-loop accumulation selectively in MYCN ON cells, we next explored whether FANCD2 was involved in either of the two previously observed MYCN-dependent mechanisms of R-loop suppression. Herold et al., (2019) observed that MYCN promotes escape of RNAPII from transcriptional pause sites in promoters to enhance transcriptional activation. However, when RNAPII escape fails during high replication and transcription stress, MYCN recruits BRCA1 to promoter-proximal regions via USP11, which binds to MYCN when residue Thr58 is dephosphorylated. BRCA1 stabilises mRNA de-capping complexes to enable resolution of MYCN-induced promoter-proximal R-loops. BRCA1 also promotes R-loop resolution at transcription end sites in a MYCN-independent mechanism involving recruitment of DNA/RNA helicases such as senataxin (Hatchi et al., 2015). Similarly, FANCD2 has been observed to resolve R-loops through recruitment of RNA processing enzymes (Garcia-Rubio et al. 2015; Schwab et al. 2015; Okamoto et al., 2018a; Okamoto et al., 2018b; Okamoto et al., 2019). Although BRCA1 is not essential for FANCD2 foci formation (Garcia-Higuera et al., 2001), it has been shown that BRCA1 contributes to the recruitment of and activation of FANCD2 in the repair of DNA damage (Garcia-Higuera et al., 2001; Bunting et al., 2012; Duquette et al., 2012; Long et al., 2014). We therefore examined whether FANCD2 is also involved in this MYCN-BRCA1 dependent mechanism of promoter-proximal R-loop resolution. In agreement with Herold et al., (2019), depletion of BRCA1 induced a greater increase in R-loop accumulation in MYCN ON cells in two out of three repeats (Figure 4.18B). However, depletion of BRCA1 did not reduce FANCD2 foci formation (Figure 4.18D) or increase pRPA foci formation (Figure 4.18E) in MYCN ON or OFF cells, suggesting FANCD2 does not act downstream of BRCA1 in this R-loop resolution pathway.

Another MYCN-dependent R-loop resolution pathway was observed by Roeschert et al., (2021). MYCN was shown to recruit AURKA during S-phase, leading to phosphorylation at histone H3Ser10. This promoted incorporation of histone H3.3 into

promoter regions to prevent co-transcriptional R-loop formation. Recruitment of AURKA also stabilised MYCN by blocking binding of the SCF^{FBXW7}-ligase to pThr58 in MYCN (Otto et al., 2009; Roeschert et al., 2021). It is hypothesised that this would promote the dephosphorylation of this residue by the DNA damage-regulated EYA1 phosphatase to enable recruitment of USP11 and therefore BRCA1 (Roeschert et al., 2021). Recruitment of AURKA may therefore also promote the MYCN-BRCA1 dependent R-loop resolution mechanism described above. We therefore next examined whether FANCD2 is involved in this MYCN-AURKA dependent mechanism of R-loop suppression. However, in contrast to the observation of Roeschert et al., (2021), the AURKA inhibitor LY3295668 (LY) did not induce R-loop accumulation (Figure 4.19B) or FANCD2 foci formation (Figures 4.20D), and only a small increase in pRPA foci was observed in MYCN ON cells (Figure 4.19E). Given this discrepancy in observations, the efficacy of 50 nM LY treatment in inhibiting AURKA should be determined and the dosage further optimised. It therefore cannot be concluded whether FANCD2 has a role in this MYCN-AURKA R-loop resolution pathway.

FA pathway-mediated R-loop resolution requires FANCD2 mono-ubiquitination (Liang et al., 2019a) and therefore it was hypothesised that it also requires activation of the ATR DDR for efficient FA pathway activation. Both ATR and FA pathway proteins are involved in the resolution of R-loops (Garcia-Rubio et al., 2015; Schwab et al., 2015; Madireddy et al., 2016; Hamperl et al., 2017; Okamoto et al., 2019; Barroso et al., 2019; Liang et al., 2019a; Matos et al., 2020). For example, MUS81 endonuclease activity at R-loops recruits and activates ATR to prevent DSB formation (Matos et al., 2020). This MUS81 recruitment to R-loops could be driven by FANCD2, which has been shown to recruit MUS81 to telomeres during high ALT-associated replication stress (Xu et al., 2019). It was therefore next determined whether ATR was also necessary for resolution of MYCN-induced R-loops. Interestingly, the ATR inhibitor VE-821 significantly induced R-loop accumulation selectively in MYCN OFF cells (Figure 4.20D). In parallel with this increased R-loop accumulation, ATR inhibition also frequently resulted in an increase in pRPA foci specifically in MYCN OFF cells (Figure 4.20E). This is perhaps because the MYCN-dependent mechanisms of R-loop resolution are ATR-independent, and therefore *MYCN* expressing cells have a larger repertoire of pathways which can resolve R-loops in the absence of ATR signalling. In agreement with this, MYCN-dependent recruitment of BRCA1 to R-loops was shown to be ATR-independent, and AURKA inhibition activates the ATR pathway suggesting this mechanism is also ATR-independent (Herold et al., 2019; Roeschert et al., 2021).

Overall these results suggest the higher FA pathway activation observed in MYCN ON cells may be driven by a higher dependency on FANCD2 to resolve MYCN-induced R-loops. However, it is unknown whether MYCN ON cells are reliant on the known FANCD2-dependent mechanism of R-loop resolution (Garcia-Rubio et al., 2015; Schwab et al., 2015; Okamoto et al., 2019; Liang et al., 2019a) or whether, similarly to BRCA1, FANCD2 also functions in a separate MYCN-dependent mechanism of R-loop repair. It was observed that FANCD2 is unlikely to act downstream of BRCA1 in the MYCN-BRCA1 R-loop resolution pathway.

4.3.6 The effect of curcumin may be due to many pleiotropic effects

Whilst previous studies have demonstrated that the toxicity of curcumin in ovarian, cervical, and lung cancer cells is mediated at least in part by FA pathway inhibition or accumulation of DNA damage (Chirnomas et al., 2006; Landais et al., 2009b; Chen et al., 2015b; Shang et al., 2016), curcumin is a non-specific FA pathway inhibitor and therefore is known to induce a wide array of pleiotropic effects. For example, curcumin has been shown to induce apoptosis in neuroblastoma cells through induction of mitochondrial dysfunction, an increase in ROS production, upregulation of pro-apoptotic genes such as *BAX* and *TP53*, and inhibition of AKT and NF-κB (Liontas et al., 2004; Aravindan et al., 2008; Freudlsperger et al., 2008; Pisano et al., 2010; D'Aguanno et al., 2012; Picone et al., 2014; Kalashnikova et al., 2017; Sidhar et al., 2017; Bavisotto et al., 2020; Zhai et al., 2020). However, it has been hypothesised that curcumin indirectly inhibits FA pathway activation via inhibition of the NF-┤B pathway (Otsuki et al., 2002; Kasinski et al., 2008; Landais et al., 2009b). Similarly, this observed mitochondrial dysfunction and increase in ROS may be a result of FA pathway inhibition, as these effects are also observed in FA deficient cells (Kumari et al., 2013). Curcumin has also been observed to regulate the expression or activation of other DNA repair associated proteins, with upregulation or activation of ATM, ATR, MRE11, PARP, BRCA1, BRCA2, ERCC1 and DNA-PK and downregulation of RAD51 previously observed (Landais et al., 2009a; Shang et al., 2016; Chen et al., 2017; Wang et al., 2022a). This suggests curcumin may modulate DNA repair through multiple mechanisms.

Patil et al., (2014) validated that curcumin sensitised glioblastoma cell lines to TMZ through on target FA pathway inhibition by demonstrating that depletion of FANCD2 abrogated the curcumin-induced sensitisation. We therefore used siRNA-

mediated depletion of FANCD2 to determine whether the MYCN-induced sensitivity to curcumin was due to FA pathway inhibition, rather than other pleiotropic effects. In contrast to treatment with curcumin, depletion of FANCD2 induced limited cell death in SHEP-Tet21N MYCN ON and OFF cells (Figure 4.21B). MYCN ON and OFF cells showed approximately equal sensitivity to depletion of FANCD2. Also, the reduction in cell viability induced by curcumin was only slighted abrogated by depletion of FANCD2 (Figure 4.21C). This data suggests broad spectrum effects contribute to the overall curcumin-induced toxicity and the MYCN-induced sensitivity to curcumin. However, differences in the effects of FANCD2 inhibition compared to depletion could affect the ability of siRNA-mediated FANCD2 depletion to abrogate the toxicity of curcumin. The effects of curcumin on replication stress could also be validated by comparing with the effect of FANCD2 depletion on replication stress in MYCN ON and OFF cells.

To further validate the FA pathway as a potential target in MNA neuroblastoma, we analysed the sensitivity of SHEP-Tet21N MYCN ON and OFF cells to a different non-specific FA pathway inhibitor; ouabain. Treatment with ouabain induced a dose-dependent reduction in total FANCD2 levels in both MYCN ON and OFF cells (Figure 4.22A,B). Treatment with 100 nM ouabain effectively inhibited cisplatin-induced FANCD2 mono-ubiquitination in both MYCN ON and OFF cells (Figure 4.22C). Following an initial increase in FANCD2 mono-ubiquitination at 50 nM, ouabain also induced a dose-dependent reduction in the endogenous FANCD2 L:S ratio selectively in MYCN ON cells. Similarly, Jun et al., (2013) observed that 200 nM ouabain induced complete inhibition of cisplatin-induced FANCD2 mono-ubiquitination in osteosarcoma, cervical cancer and prostate cancer cell lines. Consistent with our observation that *MYCN* expression sensitises cells to curcumin, ouabain induced a significantly greater reduction in the cell viability of MYCN ON cells compared to MYCN OFF cells (Figure 4.22D).

Ouabain is a cardiac glycoside and therefore also has many other off-target effects such as induction of ROS generation and ER stress (Kulikov et al., 2007; Hiyoshi et al., 2012; Chang et al., 2019a). However, it is frequently observed that ouabain induces cancer cell death by exacerbating DNA damage, particularly DSBs (Chang et al., 2019a; Du et al., 2018; Du et al., 2021; Yang et al., 2021). Whilst it can be assumed FA pathway inhibition contributes to ouabain-induced DNA damage, it should also be noted that ouabain has been observed to inhibit NHEJ activity (Du et al., 2018). Additionally, ouabain was observed to downregulate BRCA1 and DNA-PK and upregulate PARP (Chang et al., 2019a; Yang et al., 2021). Although ouabain also has

numerous off-target effects, many of these are different to the off-target effects of curcumin. Therefore, the higher sensitivity of MYCN ON cells to two non-specific FA pathway inhibitors with different off-target effects further validates the FA pathway as a potential target in MNA neuroblastoma. However, FANCD2 depletion did not mitigate the effects of ouabain toxicity (Figure 4.23) suggesting non-specific effects may account for a large proportion of ouabain-induced toxicity and therefore these results should be interpreted cautiously.

The indirect and undefined mechanism of these non-specific inhibitors makes it difficult to distinguish the true effect of *MYCN* expression on the sensitivity of neuroblastoma cells to FA pathway inhibition. To further validate the FA pathway as a target in MNA neuroblastoma, the effect of high *MYCN* expression on the sensitivity of neuroblastoma cells to a novel specific FA pathway inhibitor (nFAPi) was determined. nFAPi was developed by Dr. Spencer Collis' laboratory group at the University of Sheffield. Although nFAPi had limited cytotoxic effects in both MYCN ON and OFF cells, MYCN ON cells were significantly more sensitive than MYCN OFF cells at 100 nM (Figure 4.24). Re-testing the sensitivity of SHEP-Tet21N cells to a new resuspension of nFAPi at higher doses may further elucidate the effect of *MYCN* expression on the sensitivity of neuroblastoma cells to specific FA pathway inhibitors. Our results therefore suggest FA pathway inhibitors have therapeutic potential neuroblastoma, both in sensitising cells to crosslinking chemotherapeutics and in sensitising cells to MYCN-induced replication stress. These results therefore provide further rationale for the development of specific FA pathway inhibitors for use in cancer treatment.

4.3.7 Limitations

We primarily examine the effect of FA pathway inhibition using non-specific FA pathway inhibitors. Depletion of FANCD2 in combination with curcumin or ouabain highlighted that the broad spectrum effects of these compounds contributed to their observed effects on cell viability, and these results should therefore be analysed with this in mind. We analysed cell viability using Alamar blue assays. Given the Alamar blue assay monitors metabolic activity, observed changes in cell viability may actually be reflective of changes in the proliferation rate, the metabolic rate, the type of cellular respiration or the cell area. This limitation was mitigated by analysing clonogenic survival in parallel to Alamar blue viability assays. Also, Rak et al., (2013) showed that the sensitivity of laryngeal cancer cells to curcumin correlated with the extent of

intracellular curcumin accumulation, and the effect of *MYCN* expression on cellular curcumin accumulation has not been determined.

We predominantly analysed FA pathway activation and inhibition by quantification of FANCD2 mono-ubiquitination in L:S ratios. However, not all FA pathway functions are dependent on FANCD2 mono-ubiquitination, such as the regulation of replication fork restart and new origin firing (Lossaint et al., 2013; Yeo et al., 2014; Chen et al., 2015a; Raghunandan et al., 2015). The full extent of FA pathway activity therefore may not be fully represented by measuring FANCD2 mono-ubiquitination. This limitation was mitigated by additionally analysing FANCD2 foci formation. Similarly, given curcumin inhibits the FA pathway by inhibiting FANCD2 mono-ubiquitination (Chirnomas et al., 2006), it may not be effective in inhibiting all the replication-stress limiting functions of the FA pathway. Furthermore, whilst we explored the effect of FA pathway inhibition on R-loop accumulation in MYCN ON and OFF cells, we did not explore the effect of FA pathway inhibition on other mechanisms of replication stress limitation that are dependent on FANCD2 mono-ubiquitination such as protection of stalled replication forks. This could therefore be explored in future work to further understand the increased dependency of *MYCN* expressing cells on FA pathway function.

We examined the DNA damage accumulation by measuring the number of γ-H2AX foci per cell. However, it should be noted that whilst γ-H2AX foci are often used primarily as a marker of DNA damage (Pilch et al., 2003; Mah et al., 2010), these foci are also markers of other factors such as cellular senescence and neural stem cell development (Turinetto and Giachino, 2015). In examining the potential role of FANCD2 in MYCN-induced R-loop resolution, the efficacy of siRNA-mediated BRCA1 depletion and the efficacy of AURKA and ATR inhibition was not confirmed by western blot. Also, only one BRCA1-targeted siRNA was used to demonstrate the effects of BRCA1 depletion. Analysis of the effect of multiple BRCA1-targeted siRNAs would confirm the observed results were not caused by off-target effects. Finally, this chapter only analysed the potential effect of *MYCN* overexpression and amplification on the sensitivity of neuroblastoma cells to FA pathway inhibition. Future work could study the effect of other common neuroblastoma-associated aberrations on FA pathway inhibitor sensitivity. For example, given FA pathway inhibition is synthetic lethal with ATM pathway deficiencies (Ceccaldi et al., 2016; Rodriguez and D'Andrea, 2017; Cai et al., 2020), 11q deletion may also sensitise neuroblastoma cells to FA pathway inhibition.

4.3.8 Summary

We addressed the first aim of this chapter through analysis of FANCD2 mono-ubiquitination and FANCD2 foci formation in SHEP-Tet21N cells and observed that curcumin inhibited cisplatin-induced and MYCN-induced FA pathway activation. Whilst treatment with curcumin induced a small sensitisation to crosslinking chemotherapeutics that was not statistically significant, cells with high MYCN expression were significantly sensitised to curcumin treatment alone. This observation addressed the second aim of this chapter however the lack of specific FA pathway inhibitors prevents determination of clear conclusions about the efficacy of FA pathway inhibition. The third aim of this chapter was to explore the molecular mechanism behind this putative MYCN-induced sensitivity to FA pathway inhibition. We observed that FA pathway inhibition by curcumin was accompanied by an increase in replication stress. Curcumin also increased R-loop accumulation specifically in neuroblastoma cells with high MYCN expression, suggesting the FA pathway may contribute to MYCN-mediated R-loop suppression necessary to limit replication stress to tolerable levels. **REDACTED**.

Chapter 5. REDACTED

5.1 REDACTED

5.2 REDACTED

5.2.1 REDACTED

Figure 5.1. REDACTED

Figure 5.2. REDACTED

5.2.2 REDACTED

Figure 5.3. REDACTED

5.2.3 REDACTED

Figure 5.4. REDACTED

5.2.4 REDACTED

Figure 5.5. REDACTED

5.3 REDACTED

5.3.1 REDACTED

5.3.2 REDACTED

5.3.3 REDACTED

5.3.4 REDACTED

5.3.5 REDACTED

5.3.6 REDACTED

Chapter 6. Discussion

6.1 High *MYCN* expression induces an increase in replication stress and FA pathway expression and activation

In this thesis, we examined the therapeutic potential of FA pathway inhibition in neuroblastoma and explored the effect of *MYCN* overexpression and amplification on this. High *MYCN* expression has been shown to induce high levels of replication stress and DNA damage (Gu et al., 2015; King et al., 2020), and we confirmed this through observation of increased pRPA foci. To cope with this increased genomic instability, MYCN has been shown to transcriptionally upregulate DNA repair genes such as *PARP, MRE11, BLM, BRCA1, CHK1,* and components of alternative NHEJ (Cole et al., 2011; Valentijn et al., 2012; Chayka et al., 2015; Gu et al., 2015; Hallett et al., 2016; Petroni et al., 2016; Colicchia et al., 2017; Newman et al., 2015; Durbin et al., 2018; Petroni et al., 2018; Herold et al., 2019; King et al., 2020). This upregulation of DNA repair genes frequently correlates with poor prognosis in neuroblastoma (Chayka et al., 2015; Hallett et al., 2016; Durbin et al., 2018; Petroni et al., 2018; Herold et al., 2019; King et al., 2020). MYCN-induced replication stress therefore results in a therapeutically exploitable dependence on DNA repair and replication-stress limiting pathways. For example, high *MYCN* expression sensitises neuroblastoma cells to inhibition of ATR, CHK1, MRE11 and PARP (Cole et al., 2011; Colicchia et al., 2017; Petroni et al., 2018; King et al., 2020; Southgate et al., 2020; King et al., 2021).

To begin to determine whether the FA pathway is a potential therapeutic target in MNA neuroblastoma, we first aimed to examine the effect of *MYCN* overexpression and amplification on FA pathway expression in neuroblastoma cell lines and tumours. We hypothesised that MYCN would transcriptionally upregulate the FA pathway to limit accumulation of replication stress-induced DNA damage. As with the expression of many other DDR genes, we found that overexpression of *MYCN* in *MYCN*-inducible cell lines resulted in a reversible upregulation of FANCD2 protein expression. Furthermore, FANCD2 protein expression significantly correlated with that of MYCN across a panel of eight MNA, non-MNA and MYCN-inducible cell lines. qRT-PCR and RNA-seq analyses confirmed this MYCN-induced upregulation of *FANCD2* at the transcriptional level and enabled wider analysis of all FA pathway associated genes. In *MYCN*-inducible SHEP-Tet21N cells, a small panel of four neuroblastoma cell lines, and in neuroblastoma tumours, *MYCN* overexpression or amplification induced differential expression of FA

pathway genes which clustered according to their FA pathway role. Whilst FANC and HRR genes were predominantly transcriptionally upregulated by *MYCN* overexpression or amplification, TLS and NER genes were predominantly downregulated or showed no substantial change in expression, as summarised in Figure 6.1. Additionally, the FA pathway was the eighth most upregulated KEGG pathway induced by *MYCN* overexpression in SHEP-Tet21N cells, confirming the first hypothesis of this thesis. FA pathway genes which have been shown to have a repair-independent role in limiting replication stress, such as *FANCD2, BRCA1* and *BLM*, were consistently among the most upregulated FA genes (Garcia-Rubio et al., 2015; Schwab et al., 2015; Pan et al., 2017; Herold et al., 2019; Liang et al., 2019a; Okamoto et al., 2019). We therefore speculate that MYCN induces this pattern of expression to promote the limitation of MYCN-induced replication stress and promote high fidelity HRR to limit genomic instability. However, when analysis was expanded to a wider panel of 39 neuroblastoma cell lines, very limited differential FA pathway expression was observed between *MYCN* status subgroups. This suggested the *MYCN*-induced modulation of FA pathway expression is dependent on the wider genomic context. Nevertheless, we observed that other common neuroblastoma aberrations, such as 11q deletion, were also not associated with significant changes in FA pathway expression in this panel of cell lines.

We observed that high expression of FA pathway genes that were upregulated in MNA neuroblastomas was significantly associated with reduced survival. Given *MYCN* amplification is associated with increased tumour aggressiveness and treatment resistance, our results are in agreement with previous studies which demonstrated that the extent of FA pathway upregulation correlated with increased tumour aggressiveness and progression in other cancer types such as melanoma and breast cancer (Van Der Groep et al., 2008; Kao et al., 2011; Wysham et al., 2012; Kais et al., 2016; Feng and Jin 2019). Interestingly, the pattern of FA pathway differential expression we observed in MNA compared to non-MNA neuroblastoma was similarly observed by Kao et al., (2011) in melanomas compared to normal tissue. FANC genes were predominantly upregulated but NER genes were downregulated or were not differentially expressed (Kao et al., 2011). This was proposed to be associated with the high incidence of melanoma in xeroderma pigmentosum patients who harbour germline defects in the NER pathway, suggesting impairment of the NER pathway is a frequent event in melanoma tumorigenesis.

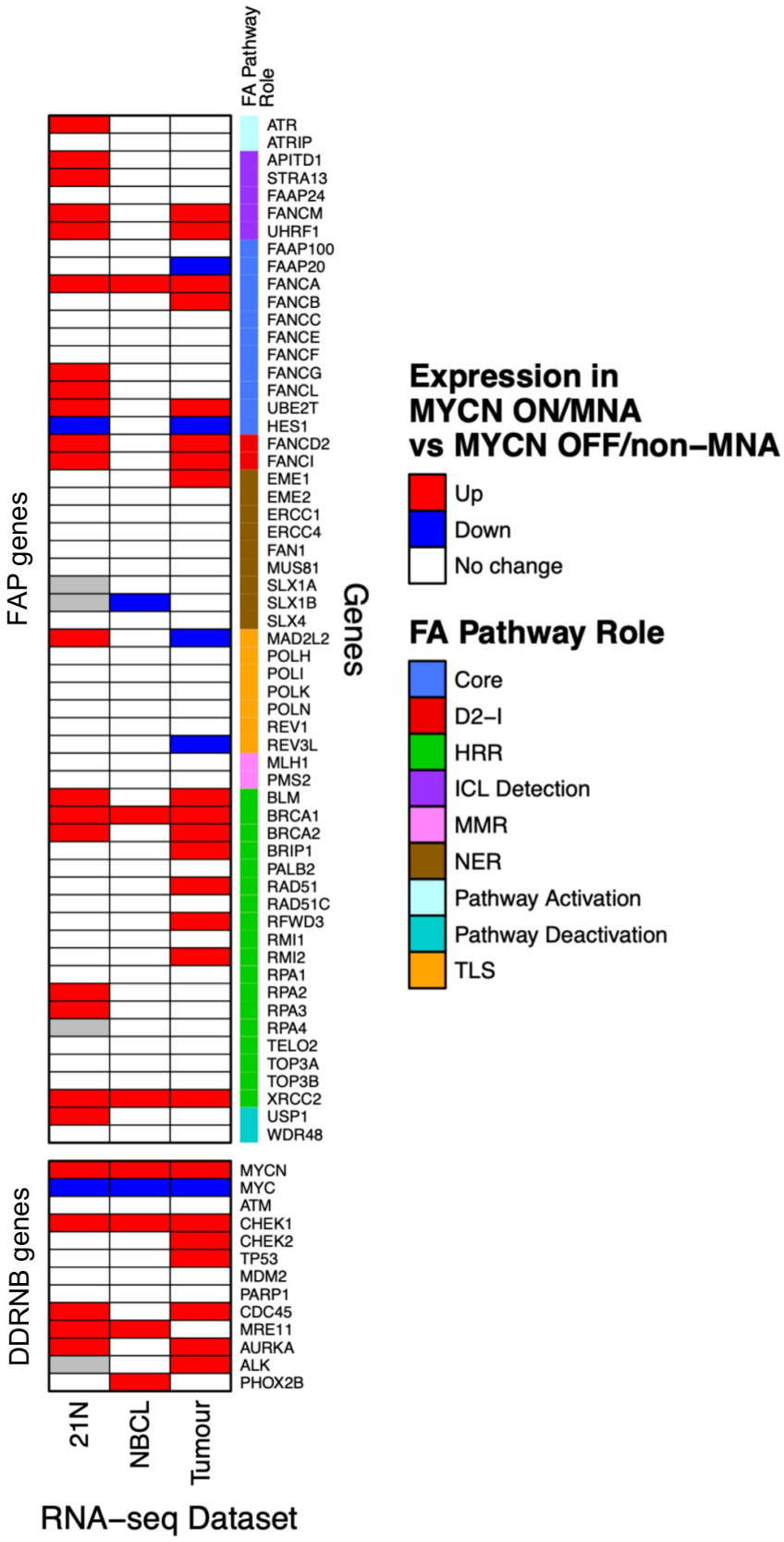

Figure 6.1. Summary of significant FA pathway differential expression in MYCN ON/MNA compared to MYCN OFF/non-MNA neuroblastoma cells across all RNA-seq dataset analyses. (Legend overleaf).

Figure 6.1. Summary of significant FA pathway differential expression in MYCN ON/MNA compared to MYCN OFF/non-MNA neuroblastoma cells across all RNA-seq dataset analyses.
mRNA expression of 58 FA pathway associated genes and 13 DNA damage repair (DDR) or key neuroblastoma-associated (NB) genes was analysed across three RNA-seq data sets in Chapter 3; (i) in SHEP-Tet21N cells (MYCN ON vs OFF) (21N), (ii) in 39 neuroblastoma cell lines (MNA vs non-MNA) using the GSE89413 data set (NB CL), (iii) in 493 neuroblastoma tumours (MNA vs non-MNA) using the GSE62564 data set (Tumour). Heatmap summarises significant differential expression ($p<0.05$, $\log_2$(fold-change)>0.5) of FA pathway genes observed in MYCN ON/MNA cells compared to MYCN OFF/non-MNA cells. Grey; genes filtered for low expression in all samples. Genes are ordered and annotated by 'FA pathway role': Core; FA core complex, D2-I; FANCD2-FANCI complex, HRR; homologous recombination repair, ICL detection; inter-strand crosslink detection, MMR; mis-match repair, NER; nucleotide excision repair, TLS; translesion synthesis.

At physiological levels of expression, MYCN regulates target genes by direct binding at high-affinity MYCN E-boxes (Zeid et al., 2018; Baluapuri et al., 2020). At oncogenic levels of expression, excess MYCN invades the active cis-regulatory landscape to induce a weak global upregulation of all active genes (Murphy et al., 2009; Valentijn et al., 2012; Zeid et al., 2018). MYCN can also regulate genes through protein-protein interactions and interaction with epigenetic remodellers (Brenner et al., 2005; Corvetta et al., 2013; Tsubota et al., 2018; Baluapuri et al., 2020). Through ChIP analyses, we determined that MYCN directly binds at the promoters of 51 of 58 FA pathway associated genes, including all FANC genes except *FANCW*. This suggests the MYCN-induced differential expression observed is regulated by direct promoter binding for most FA genes. However, the MYCN-affinity of FA gene promoters varied and analysis of the kinetics of MYCN binding and FA pathway differential expression suggested that MYCN enhancer binding likely contributed to regulation of FA gene expression. Also, MYCN did not bind at the promoters of *FAAP20, FANCW* or *UHRF1*, which were significantly differentially expressed upon *MYCN* overexpression or amplification. This suggests MYCN likely regulates expression of FA pathway associated genes through both direct promoter binding and indirect mechanisms such as enhancer binding or secondary effects. Future work could confirm the ability of MYCN to directly regulate FA pathway gene expression using FA promoter-regulated reporter genes.

We also demonstrated that high *MYCN* expression induces higher FA pathway activation in neuroblastoma cells. A trend between high *MYCN* expression and high

FANCD2 mono-ubiquitination was observed across a panel of eight MNA, non-MNA and MYCN-inducible cell lines. Further analysis demonstrated that induction of high *MYCN* expression in SHEP-Tet21N cells consistently induced greater FANCD2 mono-ubiquitination and foci formation. High *MYCN* expression is therefore associated with an upregulation of FA pathway expression and activation. This suggests MNA neuroblastoma cells are more reliant on the FA pathway. Altogether, these results suggest the FA pathway is a potential tumour-specific therapeutic target in MNA neuroblastoma. Interestingly, we also observed relatively high FA pathway expression and activation in SH-SY5Y cells, which do not harbour amplification of *MYCN* but overexpress *MYCC*. This suggests the FA pathway may also be a potential target in MYCC-driven tumours, however further analysis would be required to examine this. The potential mechanistic role of FANCD2 downstream of MYCN is discussed more comprehensively at the end of Chapter 4 and below.

6.2 MYCN-induced replication stress may sensitise neuroblastoma cells to FA pathway inhibition as a monotherapy

Given high MYCN expression was associated with increased FA pathway expression and activation, we secondly hypothesised that *MYCN* overexpression or amplification would sensitise cells to inhibition of the FA pathway due to an increased dependence on the FA pathway to limit replication stress. We therefore aimed to determine the efficacy of FA pathway inhibition in sensitising neuroblastoma cells to MYCN-induced replication stress. We demonstrated that neuroblastoma cells with high *MYCN* expression have a greater sensitivity to FA pathway inhibitors, which induced an increase in replication stress and MYCN-dependent R-loop accumulation.

We observed that *MYCN* overexpression or amplification sensitised cells to two non-specific FA pathway inhibitors; curcumin and ouabain, and a novel specific FA pathway inhibitor; nFAPi. Although the ability of curcumin and ouabain to induce neuroblastoma cell death has been previously reported, the impact of *MYCN* expression on this sensitivity has not been previously identified (Liontas et al., 2004; Aravindan et al., 2008; Freudlsperger et al., 2008; Pisano et al., 2010; D'Aguanno et al., 2012; Picone et al., 2014; Kalashnikova et al., 2017; Sidhar et al., 2017). We further analysed the mechanism of this MYCN-induced curcumin sensitivity in *MYCN*-inducible SHEP-Tet21N cells. It was observed that curcumin and ouabain inhibited endogenous FANCD2 mono-ubiquitination and foci formation specifically in cells with high *MYCN*

expression, and therefore inhibited MYCN-induced FA pathway activation. Curcumin treatment did not induce significant changes in the cell cycle profile of MYCN ON or OFF cells, however a slight increase in S-phase and sub-G1 accumulation was observed specifically in MYCN ON cells. Given one of the major functions of FANCD2 in the absence of exogenous DNA damage is to project from replication stress, and given MYCN is known to increase replication stress (Gu et al., 2015; King et al., 2020), we hypothesised that the ability of curcumin to inhibit MYCN-induced FA pathway activation resulted in greater levels of replication stress in MYCN ON cells. This was supported by our observation of increased pRPA foci. Whilst curcumin treatment exacerbated endogenous replication stress in both MYCN ON and OFF cells, the extent of curcumin-induced replication stress was highest MYCN ON cells. It is therefore likely that in MYCN ON cells, curcumin treatment increased replication stress to a level where cell death was induced. However, curcumin treatment alone did not increase γ-H2AX foci accumulation in MYCN ON or OFF cells. γ-H2AX foci are a marker of DNA damage and therefore this result is in contrast to other studies which have demonstrated that curcumin and ouabain induce DNA damage (Hiyoshi et al., 2012; Rak et al., 2013; Shang et al., 2016; Chang et al., 2019a; Du et al., 2018; Du et al., 2021; Yang et al., 2021; Wang et al., 2022a). FANCD2 has been shown previously to limit replication stress induced by other oncogenes (Helbling-Leclerc et al., 2019; Khanal and Galloway, 2019), and thus our data add to this concept through expanding the number of documented oncogenes.

There are multiple mechanisms of FA pathway-mediated replication stress limitation that are dependent on FANCD2 mono-ubiquitination, such as protection of stalled replication forks and resolution of R-loops (Schlacher et al., 2012; Liang et al., 2019a). We therefore analysed the effect of curcumin treatment on R-loop accumulation in MYCN ON and OFF cells. We found that MYCN ON cells had a lower endogenous level of R-loops than MYCN OFF cells and reasoned this was likely due to MYCN-induced mechanisms of R-loop resolution (Herold et al., 2019; Roeschert et al., 2021). Similarly, Herold et al., (2019) demonstrated that activation of *MYCN* suppressed formation of promoter-proximal R-loops. In contrast, expression of *RAS* and *Cyclin E* oncogenes was shown to promote R-loop formation (Jones et al., 2012; Kotsantis et al., 2016). Curcumin treatment exacerbated R-loop accumulation selectively in MYCN ON cells, suggesting FANCD2 functions in the resolution of MYCN-induced R-loops. This also indicated MYCN-induced R-loops contribute to the increased FA pathway activation observed in MYCN ON cells.

We next examined whether FANCD2 functions in the known MYCN-dependent mechanisms of R-loop resolution. Herold et al., (2019) observed that promoter-bound MYCN recruits BRCA1 during high replication stress to resolve promoter-proximal R-loops. In agreement, we observed that depletion of BRCA1 induced R-loop accumulation specifically in MYCN ON cells on two independent occasions. However, depletion of BRCA1 had no effect on FANCD2 foci formation. Roeschert et al., (2021) observed that MYCN interacts with AURKA to promote incorporation of histone H3.3 into MYCN-regulated promoters to prevent R-loop accumulation. Inhibition of AURKA did not induce R-loop accumulation and had no effect on FANCD2 foci formation, however validation of the efficacy of the AURKA inhibitor at the dosage used has not yet been undertaken. Given ATR is required for efficient FA pathway activation, and FA pathway-mediated R-loop resolution is associated with FANCD2 mono-ubiquitination, we hypothesised ATR activity would also be required for FA pathway-mediated R-loop resolution (Andreassen et al., 2004; Qiao et al., 2004; Wang et al., 2007; Collis et al., 2008; Wilson et al., 2008; Collins et al., 2009; Singh et al., 2013; Chen et al., 2015a; Liang et al., 2019a). Interestingly, ATR inhibition significantly increased R-loop resolution specifically in MYCN OFF cells. We speculate this could be because MYCN ON cells have more alternative ATR-independent mechanisms of R-loop resolution than MYCN OFF cells.

Future studies could further elucidate the dependence of MYCN-driven cells on FANCD2-mediated R-loop resolution by analysing the effect of RNase H1 expression on FANCD2 foci in MYCN ON and OFF cells. Furthermore, immunoprecipitation of MYCN in the presence and absence of R-loops could determine whether FANCD2 associates in a complex with MYCN in an R-loop dependent manner. Additionally, whilst we explored the effect of FA pathway inhibition on MYCN-dependent R-loop accumulation, we did not explore the effect of FA pathway inhibition on other replication stress-induced lesions. MYCN may upregulate the FA pathway to minimise multiple mechanisms through which it induces replication stress. For example, FANCD2 mono-ubiquitination also functions in the protection of stalled replication forks (Schlacher et al., 2012), and this may also be a mechanism that MYCN upregulates to limit replication stress. Similarly, FANCD2 also acts to restrain replication fork progression, promote restart of stalled replication forks, and suppress new origin firing during high replication stress (Chaudhury et al., 2013; Lossaint et al., 2013; Yeo et al., 2014; Raghunandan et al., 2015; Madireddy et al., 2016; Raghunandan et al., 2020). Although this regulation of replication fork dynamics is not dependent on FANCD2 mono-ubiquitination, MYCN

may upregulate *FANCD2* expression due to its dependency on these functions. Consistent with this, it has been shown that MYCN also induces replication stress through increased origin firing (King et al., 2021). The impact of FANCD2 inhibition or depletion on replication fork dynamics in *MYCN*-inducible cells could therefore be explored through DNA fibre assays. Furthermore, future work could examine whether other frequent neuroblastoma aberrations sensitise neuroblastoma cells to FA pathway inhibition. For example, ATM inhibition is synthetic lethal with FA pathway deficiencies (Cai et al., 2020), and therefore 11q deletion may also sensitise cells to FA pathway inhibition.

Overall, these results suggest that the upregulation of FA pathway expression and activation by MYCN is necessary to limit MYCN-induced R-loop accumulation and suppress intolerable levels of replication stress and DNA damage, as summarised in Figure 6.2. MYCN binds the active cis-regulatory network to globally promote transcription initiation and elongation through transcription-dependent and -independent mechanisms (Baluapuri et al., 2020). Transcriptional upregulation of *FANCD2* to limit R-loop accumulation may be an additional mechanism through which MYCN promotes transcription elongation to provide the increased levels of transcription required in neuroblastoma cells without suffering the consequence of paused replication. Alternatively, upregulation of *FANCD2* expression may be a mechanism employed by MYCN to overcome increased transcription stalling which may result from the increased replication origin firing induced by MYCN (King et al., 2021). Furthermore, our results suggest this increased FA pathway dependency induced by MYCN can be therapeutically exploited to selectively target MNA neuroblastoma cells. In a wider context, we demonstrate the potential of targeting the FA pathway to selectively kill tumour cells harbouring oncogene-induced replication stress. However, it is unlikely FA pathway inhibitors would be used as a monotherapy in high-risk neuroblastoma treatment. Instead, it would likely be used in combination with DNA damaging chemotherapeutics.

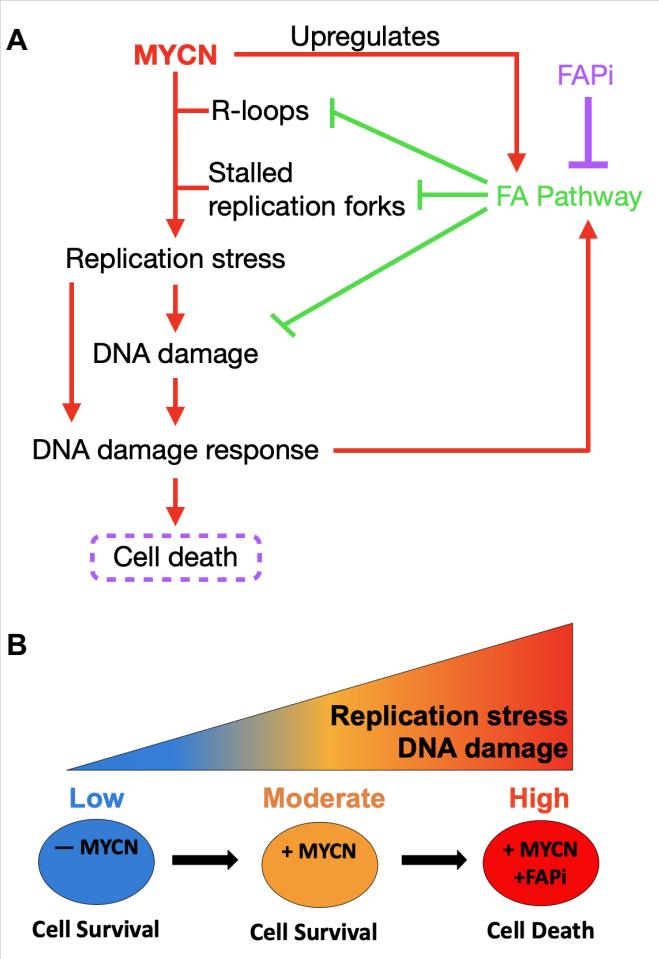

Figure 6.2. Model of proposed mechanism of action of FA pathway inhibition in MYCN amplified neuroblastoma cells.
Expression of MYCN increases replication stress and DNA damage. The FA pathway suppresses R-loop accumulation, protects stalled forks and contributes to DNA repair to limit MYCN-induced replication stress and DNA damage to tolerable levels. Inhibition of the FA pathway (FAPi) results in intolerable levels of MYCN-induced replications stress and DNA damage leading to cell death.

6.3 FA pathway inhibition may improve the efficacy of crosslinking induction chemotherapeutics

The FA pathway is the major mechanism for efficient ICL repair (Sasaki et al., 1975; Taniguchi et al., 2002a). Loss of FA pathway function therefore primarily sensitises cells to DNA crosslinking agents, and this is a clinical marker of Fanconi anaemia (Sasaki et al., 1975; Auerbach and Wolman, 1976; German et al., 1987; Auerbach 1988; Taniguchi et al., 2002a; Houghtaling et al., 2003; Niedzwiedz et al., 2004; Bridge et al., 2005; Dai et al., 2015; Dai et al., 2017). FA pathway inhibition therefore sensitises a broad range of cancer cell lines to DNA crosslinking and

alkylating chemotherapeutics. For example, curcumin has been shown to sensitise glioblastoma, breast cancer, ovarian cancer, NSCLC, retinoblastoma and neuroblastoma cells to crosslinking chemotherapeutics cisplatin or carboplatin or the alkylating agent TMZ (Chirnomas et al., 2006; Chanvorachote et al., 2009; Yallapu et al., 2010; Sukumari-Ramesh et al., 2011; Sreenivasan et al., 2013; Chen et al., 2015b; Kang et al., 2015; Zou et al., 2018; Huang et al., 2022; Wang et al., 2022a; Wang et al., 2022b).

We therefore hypothesised that FA pathway inhibition by curcumin would sensitise neuroblastoma cells to clinically relevant DNA crosslinking chemotherapeutics. We found that curcumin treatment induced a small, but statistically insignificant, sensitisation to cisplatin and carboplatin in SHEP-Tet21N MYCN ON and OFF cells and SHEP-1 cells. However, we failed to detect sensitisation to TMZ. Analysis of sensitisation in SHEP-1 and IMR32 cells was limited by the high curcumin toxicity in these cell lines. However, our results suggest curcumin may sensitise neuroblastoma cells to clinically relevant crosslinking chemotherapeutics, regardless of *MYCN* expression level. As such, addition of FA pathway inhibitors in combination with induction chemotherapy may increase treatment efficacy and enable use of lower doses. This is particularly important in the development of high-risk neuroblastoma treatment which aims to minimise treatment morbidity. However it has been suggested that integrating FA pathway inhibitors as a combination therapy alongside DNA crosslinkers may result in adverse events due to intolerable toxicity in all rapidly dividing cells, particularly in the bone marrow (Garaycoechea et al., 2012; Domenech et al., 2018; Sharp et al., 2021). Additionally, Sharp et al., (2021) argued that use of FA pathway inhibitors in the treatment of paediatric patients would entail greater risks of side-effects due to the importance of the FA pathway in embryonic development (Fiesco-Roa et al., 2019).

FA pathway inhibition has also been shown to re-sensitise resistant cancer cells to DNA crosslinking chemotherapeutics (Chirnomas et al., 2006; Chen et al., 2007; Lyakhovich and Surralles, 2007; Zhao et al., 2014; Dai et al., 2015; Bretz et al., 2016; Dai et al., 2017). Many cancer cells acquire resistance to crosslinking and alkylating chemotherapy through upregulation of FA pathway expression and activation (Taniguchi et al., 2003; Chen et al., 2005; van der Heijden et al., 2005; Pejovic et al., 2006; Chen et al., 2007; Swisher et al., 2009; Wysham et al., 2012; Chen et al., 2016; Nagel et al., 2017). Given MNA neuroblastoma is associated with increased frequency of relapse and resistance (Brodeur et al., 1984; Seeger et al., 1985; Ponzoni et al.,

2022) and increased FA pathway expression and activation, the efficacy of FA pathway inhibition in re-sensitising resistant MNA neuroblastoma could be further explored.

6.4 Development of specific FA pathway inhibitors would validate the observed MYCN-induced sensitivity to FA pathway inhibition

We observed that off-target effects contribute to the cell death induced by the non-specific FA pathway inhibitors curcumin and ouabain. Similarly, other studies have demonstrated that curcumin induces apoptosis in neuroblastoma cells through many pleiotropic effects such as induction of mitochondrial dysfunction, ROS production, upregulation of pro-apoptotic genes, and inhibition of AKT and NF-┤B (Liontas et al., 2004; Aravindan et al., 2008; Freudlsperger et al., 2008; Pisano et al., 2010; D'Aguanno et al., 2012; Picone et al., 2014; Kalashnikova et al., 2017; Sidhar et al., 2017). However, curcumin may inhibit FANCD2 mono-ubiquitination indirectly through inhibition of the NF-┤B pathway (Otsuki et al., 2002; Kasinski et al., 2008; Landais et al., 2009a) and lack of FA pathway function could be responsible for the observed mitochondrial dysfunction and ROS production (Kumari et al., 2013). Ouabain has been shown to induce ROS production, activate pro-apoptotic pathways, and activate DDR checkpoint-induced quiescence in neuroblastoma cells (Kulikov et al., 2007; Hiyoshi et al., 2012). Importantly, curcumin and ouabain have been observed to modulate expression and activation of other DNA repair pathways. Curcumin upregulates *PARP, BRCA1, BRCA2, ERCC1* and DNA-PK and downregulates of *RAD51* (Shang et al., 2016; Chen et al., 2017; Wang et al., 2022a). Ouabain was shown to inhibit NHEJ activity, downregulate DNA-PK and upregulate *PARP* and *BRCA1* (Du et al., 2018; Chang et al., 2019a; Yang et al., 2021). Given curcumin may modulate DNA repair through multiple mechanisms, future work could validate the observed impact of FA pathway inhibition on replication stress and DNA damage by comparing the effects of curcumin to that of FANCD2 depletion.

Whilst we validated the effect of *MYCN* overexpression on FA pathway inhibitor sensitivity through use of an unpublished specific FA pathway inhibitor (Dr. S. Collis, University of Sheffield), development of more specific FA pathway inhibitors would enable better study of its potential as a chemotherapeutic in neuroblastoma. Currently there are no widely accepted small molecule FA pathway inhibitors that directly and selectively inhibit FA pathway activation (Liu et al., 2020a; Taylor et al., 2020; Sharp et al., 2021). Most selective FA pathway inhibitors that have been identified target

downstream FA proteins involved in NER, TLS or HRR and therefore are not FA pathway specific and have broader effects on DNA repair (Huang et al., 2011b; Takaku et al., 2011; Budke et al., 2012; Zhu et al., 2013; Chapman et al., 2015; McNeil et al., 2015; Actis et al., 2016; Liu et al., 2020a). Voter et al., (2016) identified the small molecule PIP-199 which targets the upstream FANCM-RMI interaction to inhibit FA core complex recruitment and therefore FA pathway activation. However the efficacy of PIP-199 has not yet been demonstrated in a cellular context. Also, FANCM has DNA repair functions outside its role in the FA pathway, and therefore similarly may have broader effects on DNA repair (Xue et al., 2015; Pan et al., 2017; Pan et al., 2019; Silva et al., 2019).

High throughput biochemical screening methods have been optimised to aid future identification of specific FA pathway inhibitors (Sharp et al., 2020). One such screen identified the small molecule inhibitor CU2, which inhibits UBE2T/FANCL-mediated ubiquitination of FANCD2 and was demonstrated to inhibit FANCD2 foci formation in U2OS cells (Cornwell et al., 2019). Similarly, Morreale et al., (2017) used biophysical screening methods to identify fragments which bound to a previously unknown allosteric pocket on the UBE2T E2 ligase and inhibited FANCD2 mono-ubiquitination in vitro. Inhibition of the FANCL E3 ligase in the FA core complex relies on targeting protein-protein interactions and is therefore challenging (Surade and Blundell, 2012). However, advances in E3 ligase inhibition has been demonstrated, with inhibitors designed to block interactions between E3 and E2 ligases (Brenke et al., 2018), E3 ligases and substrate adaptors (Zeng et al., 2010; Chan et al., 2013), or E3 ligases and substrates (Sackton et al., 2014; Tisato et al., 2017) demonstrating efficacy. Targeting the E3 ligase activity of the FA core complex is therefore a promising strategy that would be advantageous as FANCD2 and FANCI are its only known substrates (Renaudin et al., 2014), and this inhibition would therefore be highly selective. Multiple FA core complex proteins are required for its efficient E3 ligase activity (van Twest et al., 2017), and any one of these proteins could therefore be targeted. However the clinical severity of FA is heterogeneous, with the loss of function of some FA proteins, such as FANCD2 and FANCB, inducing a more severe phenotype, and this should be considered (Fiesco-Roa et al., 2019; Jung et al., 2020). Given the structure of many FA core complex proteins has been elucidated (Shakeel et al., 2019; Farrell et al., 2020; Wang et al., 2020; Wang et al., 2021), structure-based drug design and in silico screening are also promising methods of FA core complex inhibitor development (Hodson et al., 2014).

6.5 REDACTED

6.6 Conclusion:

Overall, this thesis demonstrates the therapeutic potential of FA pathway inhibition **REDACTED** in the treatment of neuroblastoma. In particular, we speculate MYCN-induced replication stress and FA pathway dependency may sensitise MNA neuroblastoma to these treatments. Our results therefore provide further rationale for the development and use of specific FA pathway inhibitors in cancer treatment, **REDACTED**. In a broader context, our results demonstrate the potential of exploiting oncogene-induced replication stress to selectively sensitise cancer cells to treatments which inhibit DNA repair.

Chapter 7. Appendix

7.1 Chapter 2 Appendix

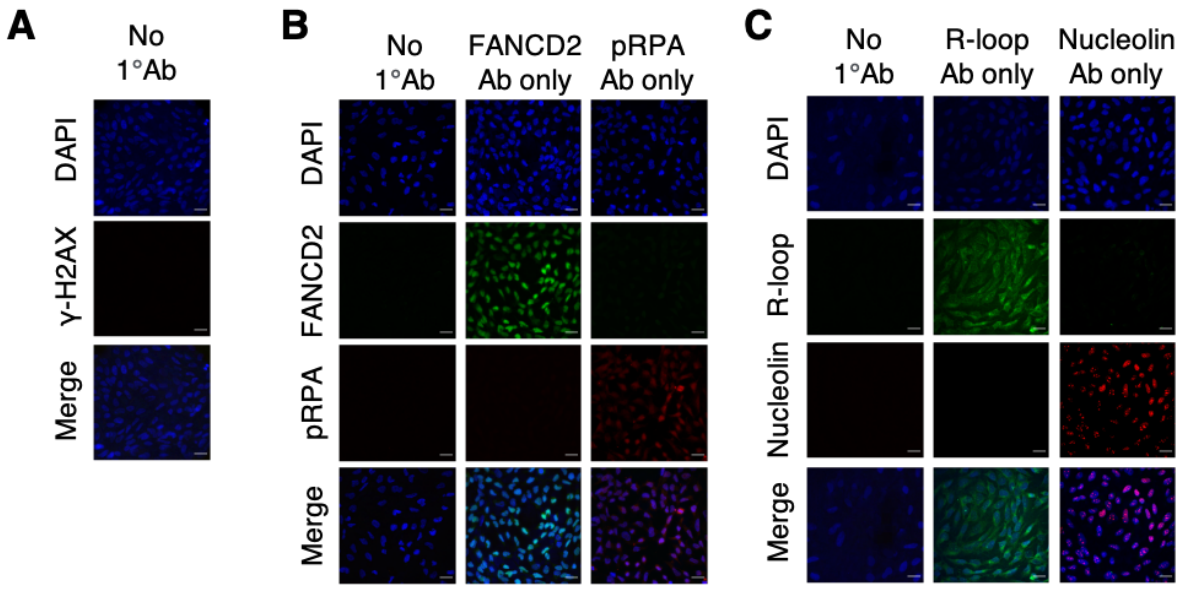

Figure 2.A1. Representative images of antibody control conditions for immunofluorescence experiments.
Alongside experimental conditions, un-treated SHEP-Tet21N MYCN ON cells were fixed, permeabilised and analysed by immunofluorescence for non-specific antibody interactions. These antibody control conditions were undertaken for each experiment. Representative images are displayed. **(A)** For γ-H2AX immunofluorescence experiments, cells were stained with no primary antibody before staining with the secondary antibody to verify there was no non-specific binding of the secondary antibodies. **(B)** For FANCD2/pRPA co-immunofluorescence experiments, cells were stained with no primary antibody before staining with the secondary antibody to verify there was no non-specific binding of the secondary antibodies. Additionally, cells were stained with only the FANCD2 or pRPA antibody alone before staining with the secondary antibody. This verified there no non-specific cross-binding between antibodies. **(C)** For R-loop (S9.6 antibody)/nucleolin co-immunofluorescence experiments, cells were stained with no primary antibody before staining with the secondary antibody to verify there was no non-specific binding of the secondary antibodies. Additionally, cells were stained with only the R-loop (S9.6) or nucleolin antibody alone before staining with

7.2 Chapter 3 Appendix

All Chapter 3 appendix tables are provided in **Additional File 1**.

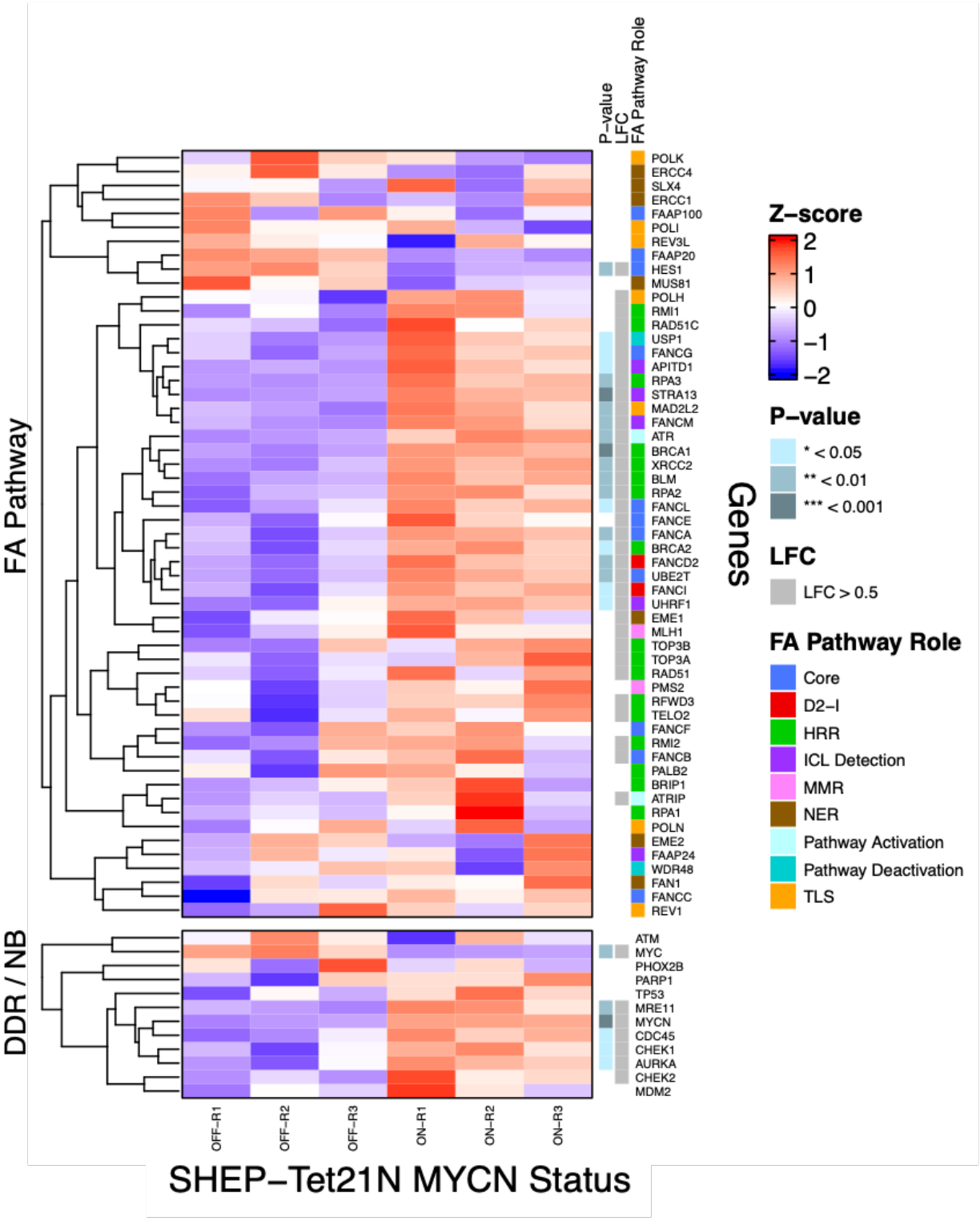

Figure A2. Differential expression of FA pathway associated genes across three biological replicates of SHEP-Tet21N MYCN ON and MYCN OFF cells. (Legend overleaf).

Figure A2. Differential expression of FA pathway associated genes across three biological replicates of SHEP-Tet21N MYCN ON and MYCN OFF cells. SHEP-Tet21N MYCN ON cells were treated with 1 µg/ml tetracycline for 48 hours to induce a MYCN OFF state. mRNA expression of 55 FA pathway associated genes and 12 DNA damage repair (DDR) or key neuroblastoma-associated (NB) genes were analysed in SHEP-Tet21N MYCN ON and MYCN OFF cells (n=3) by RNA-Seq. Differential expression between MYCN ON and MYCN OFF cells was analysed using DESeq2. 'LFC' indicates which genes show a $\log_2$(fold-change)>0.5. A regularised log2 (rlog) transformation was applied to the normalised count data, from which statistical significance of differential expression (annotated by 'P-value') was determined for each gene by a Student's t-test, Welch t-test or Mann Whitney U t-test, depending on data distribution. Z-scores calculated independently for each gene in all sample replicates using rlog-transformed normalised count data is presented. Genes are clustered according to k-means analysis and are annotated by 'FA pathway role': Core; FA core complex, D2-I; FANCD2-FANCI complex, HRR; homologous recombination repair, ICL detection; inter-strand crosslink detection, MMR; mis-match repair, NER; nucleotide excision repair, TLS; translesion synthesis.

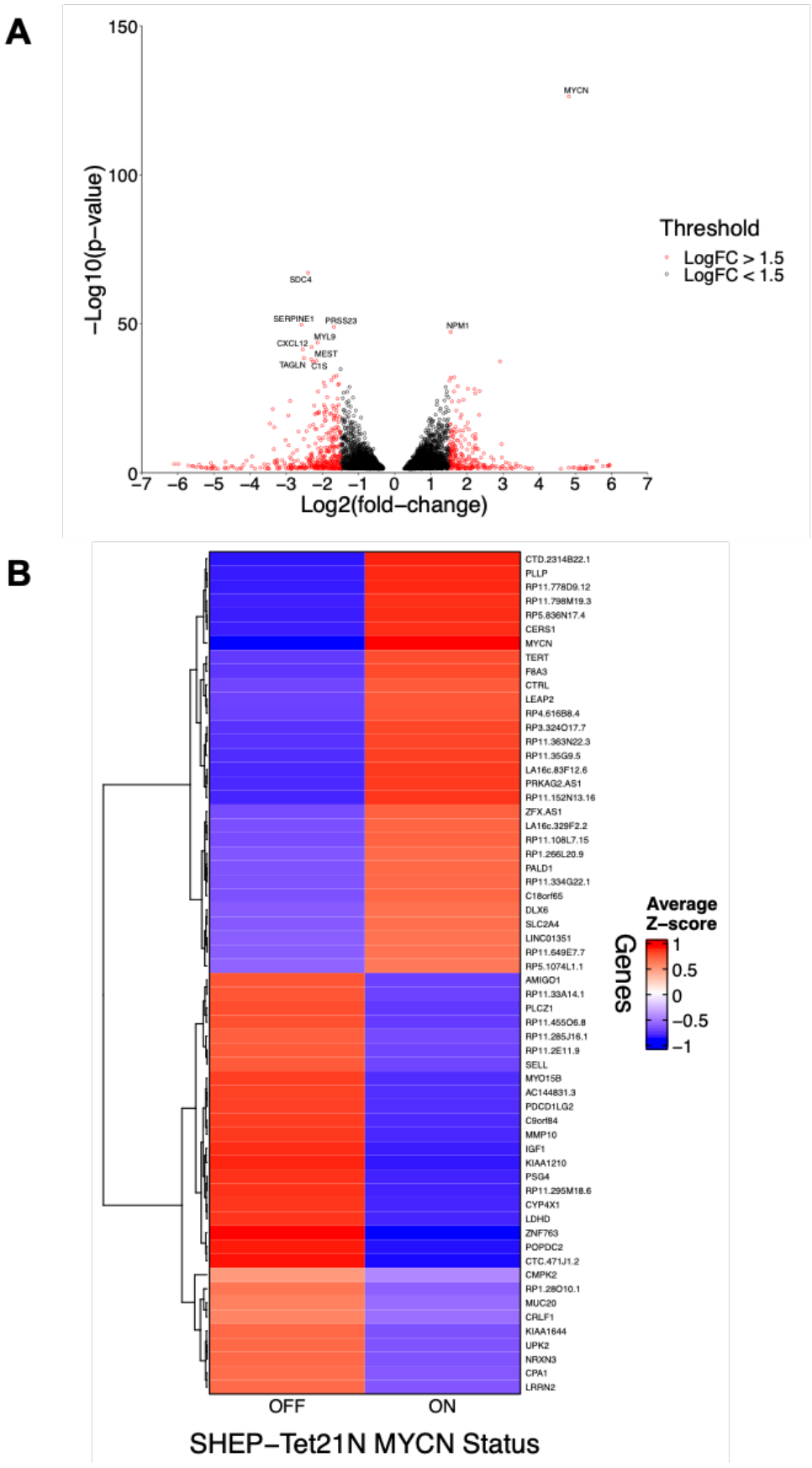

Figure A3. Global differential expression in SHEP-Tet21N MYCN ON and MYCN OFF cells. (Legend overleaf).

Figure A3. Global differential expression in SHEP-Tet21N MYCN ON and MYCN OFF cells.
SHEP-Tet21N MYCN ON cells were treated with 1 µg/ml tetracycline for 48 hours to induce a MYCN OFF state. Global mRNA expression was analysed in SHEP-Tet21N MYCN ON and MYCN OFF cells by RNA-Seq (n=3). Log_2(fold-change) and significance of differential expression between MYCN ON and MYCN OFF cells was analysed using DESeq2. **(A)** Volcano plot of all significantly differentially expressed genes ($p<0.05$). Red circles indicate genes with a log_2(fold-change)>0.5. Top 10 most significantly differentially expressed genes are annotated. **(B)** A regularised log2 (rlog) transformation was applied to the normalised count data. rlog-transformed normalised count data was used to calculate Z-scores independently for each of the top 30 most upregulated and downregulated genes in MYCN ON cells. The average Z-score in MYCN ON and MYCN OFF cells is presented. Genes are clustered by k-means analysis.

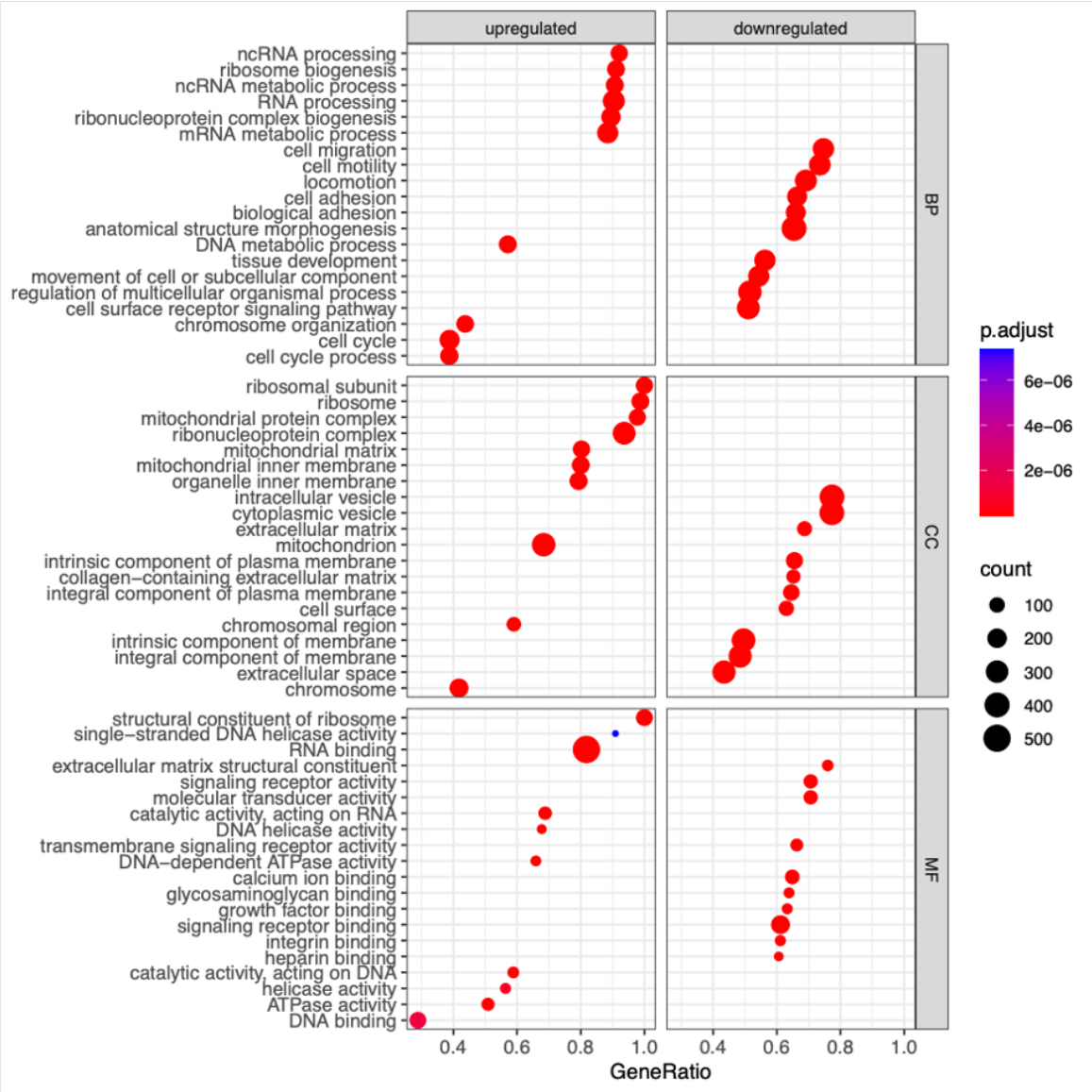

Figure A4. Top 10 gene ontologies enriched in all significantly upregulated and downregulated genes in MYCN ON compared to MYCN OFF SHEP-Tet21N cells.

SHEP-Tet21N MYCN ON cells were treated with 1 µg/ml tetracycline for 48 hours to induce a MYCN OFF state. Global mRNA expression was analysed in SHEP-Tet21N MYCN ON and MYCN OFF cells by RNA-Seq (n=3). Log_2(fold-change) and significance of differential expression between MYCN ON and MYCN OFF cells was analysed using DESeq2. Significantly enriched gene ontologies in the set of significantly upregulated ($p < 0.05$, log_2(fold-change) > 0.5) and downregulated ($p < 0.05$, log_2(fold-change) < -0.5) genes was determined. Top 10 most enriched biological process (BP), molecular function (MF) and cellular component (CC) gene ontologies in upregulated and downregulated genes are presented. Gene ratio represents the fraction of genes within each ontology that is significantly differentially expressed. Points coloured by significance of enrichment (p.adjust) and sized according to number of genes significantly

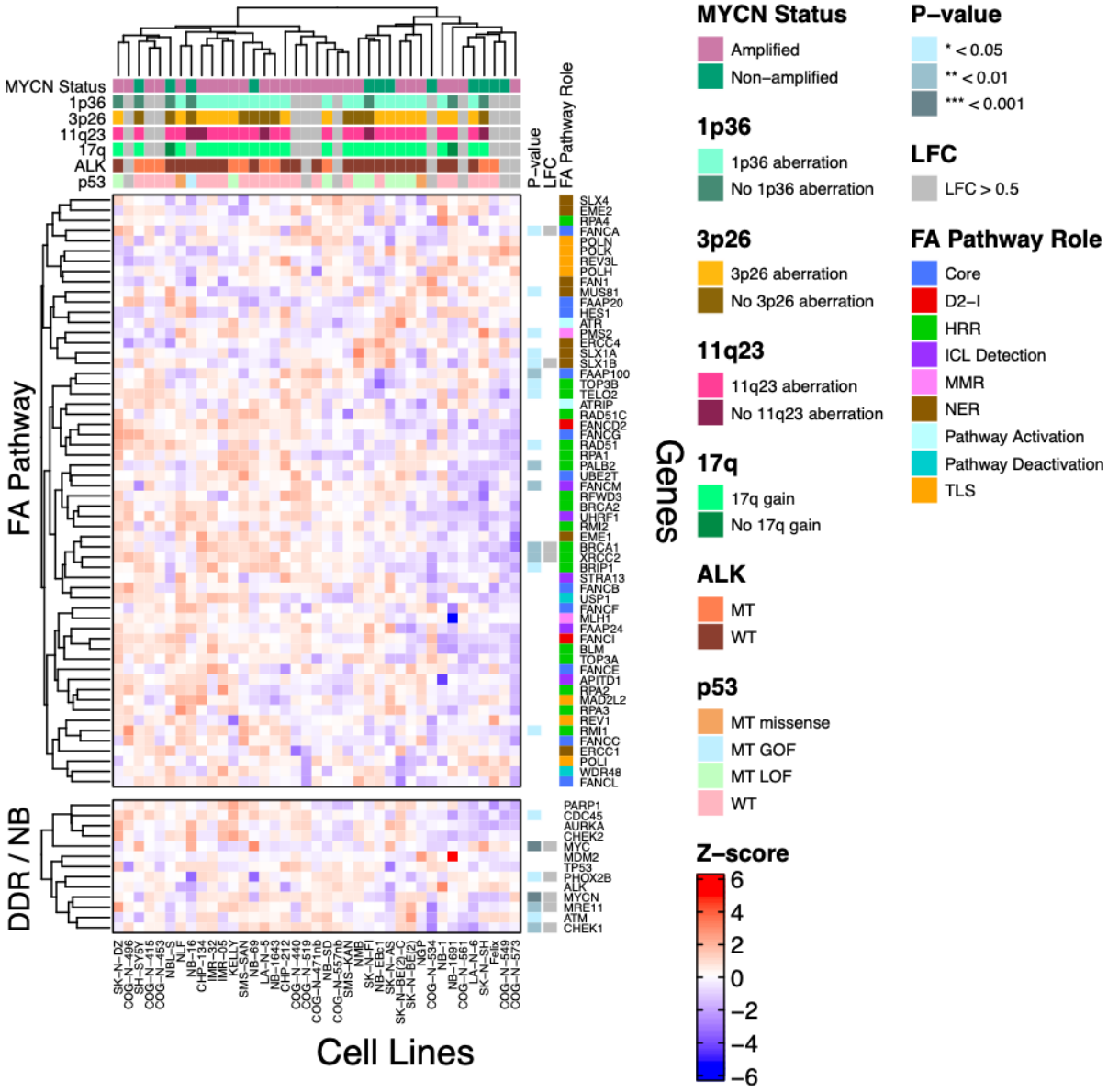

Figure A5. Differential expression of FA pathway genes across 39 neuroblastoma cell lines.
mRNA expression of 58 FA pathway associated genes and 13 DNA damage repair (DDR) or key neuroblastoma-associated (NB) genes was analysed across 39 neuroblastoma cell lines using the GSE89413 RNA-Seq dataset (n=1) Differential expression between MYCN amplified and MYCN non-amplified cell lines was analysed using DESeq2. 'LFC' indicates which genes show a $\log_2$(fold-change)>0.5. A regularised log2 (rlog) transformation was applied to the normalised count data, from which statistical significance of differential expression (annotated by 'P-value') was determined for each gene by a Student's t-test, Welch t-test or Mann Whitney U t-test, depending on data distribution. Z-scores calculated independently for each gene across all 39 cell lines using rlog-transformed normalised count data are presented. Genes and cell lines are clustered according to k-means analysis, with cell line clustering based on expression of FA pathway associated genes only. (Figure legend continues overleaf).

Figure A5. Differential expression of FA pathway genes across 39 neuroblastoma cell lines (continued).
Genes are annotated by 'FA pathway role': Core; FA core complex, D2-I; FANCD2-FANCI complex, HRR; homologous recombination repair, ICL detection; inter-strand crosslink detection, MMR; mis-match repair, NER; nucleotide excision repair, TLS; translesion synthesis. Cell lines annotated by amplification of MYCN, presence of aberration in 1p36, 3p26 and 11q23 loci, gain of 17q locus, and mutation of *ALK* and *TP53* genes.

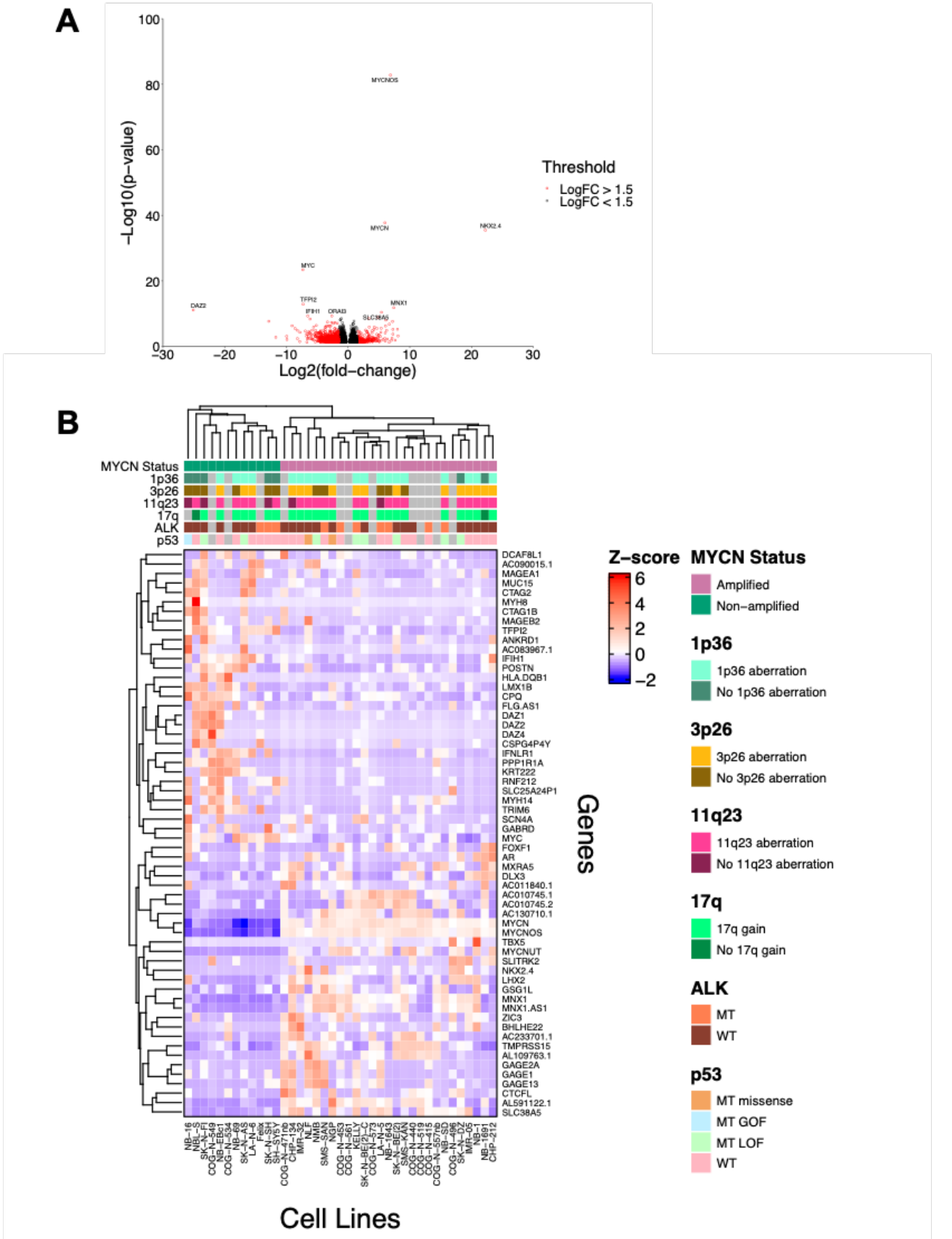

Figure A6. Global differential expression across 39 neuroblastoma cell lines. (Legend overleaf).

Figure A6. Global differential expression across 39 neuroblastoma cell lines.
Global mRNA expression was analysed across 39 neuroblastoma cell lines using the GSE89413 RNA-Seq dataset (n=1) Log_2(fold-change) and significance of differential expression between MYCN amplified and MYCN non-amplified cell lines was analysed using DESeq2. **(A)** Volcano plot of all significantly differentially expressed genes ($p<0.05$). Red circles indicate genes with a log_2(fold-change)>0.5. Top 10 most significantly differentially expressed genes are annotated. **(B)** A regularised log2 (rlog) transformation was applied to the normalised count data. rlog-transformed normalised count data was used to calculate Z-scores independently for each of the top 30 most upregulated and downregulated genes in MYCN amplified compared to MYCN non-amplified cell lines. The average Z-score in MYCN amplified and MYCN non-amplified cells is presented. Genes and cell lines are clustered by k-means analysis. Cell lines are annotated by MYCN amplification status, presence of deletion at 1p36, 3p26 and 11q23 loci, 17q gain, and mutation of *ALK* and *TP53* genes.

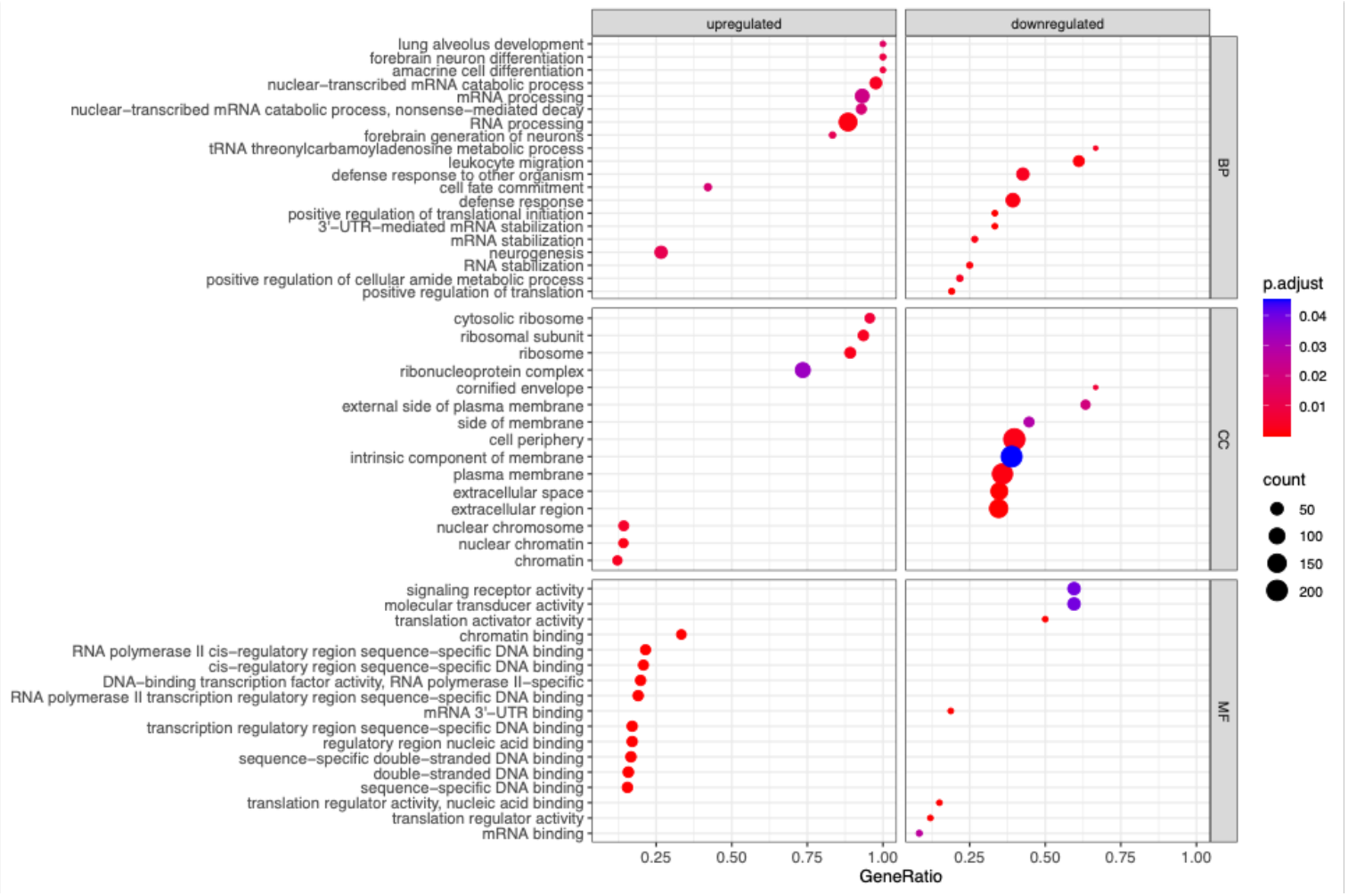

Figure A7. Top 10 gene ontologies enriched in all significantly upregulated and downregulated genes in MYCN amplified compared to MYCN non-amplified neuroblastoma cell lines. (Legend overleaf).

Figure A7. Top 10 gene ontologies enriched in all significantly upregulated and downregulated genes in MYCN amplified compared to MYCN non-amplified neuroblastoma cell lines.
Global mRNA expression was analysed across 39 neuroblastoma cell lines using the GSE89413 RNA-Seq dataset (n=1) Log_2(fold-change) and significance of differential expression of all genes in MYCN amplified compared to MYCN non-amplified cell lines was analysed using DESeq2. Significantly enriched gene ontologies in the set of significantly upregulated ($p < 0.05$, log_2(fold-change) > 0.5) and downregulated ($p < 0.05$, log_2(fold-change) < -0.5) genes was determined. Top 10 most enriched biological process (BP), molecular function (MF) and cellular component (CC) gene ontologies in upregulated and downregulated genes are presented. Gene ratio represents the fraction of genes within each ontology that is significantly differentially expressed. Points coloured by significance of enrichment (p.adjust) and sized according to number of genes significantly differentially expressed (count).

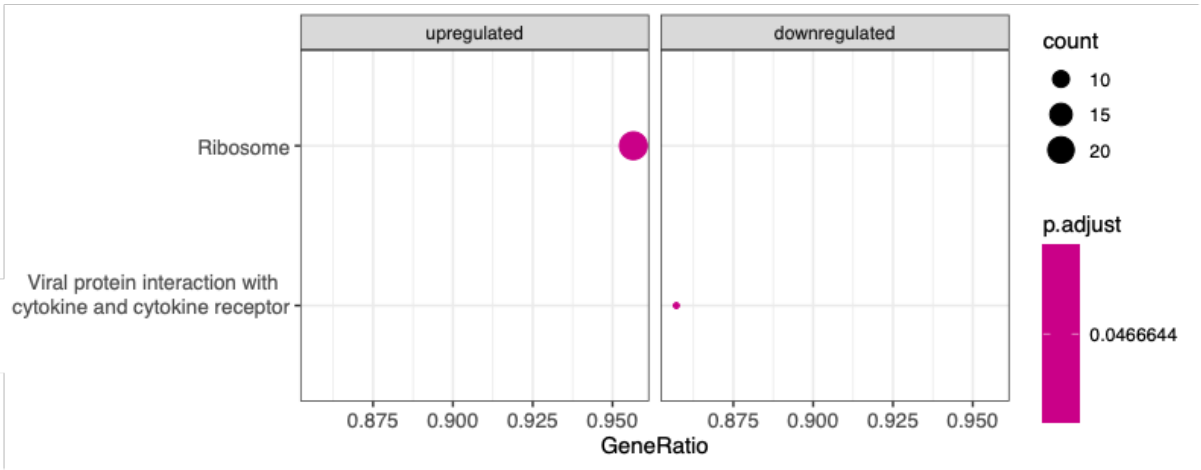

Figure A8. Top 10 KEGG pathways enriched in all significantly upregulated and downregulated genes in MYCN amplified compared to MYCN non-amplified neuroblastoma cell lines.
Global mRNA expression was analysed across 39 neuroblastoma cell lines using the GSE89413 RNA-Seq dataset (n=1) Log_2(fold-change) and significance of differential expression of all genes in MYCN amplified compared to MYCN non-amplified cell lines was analysed using DESeq2. Significantly enriched KEGG pathways in the set of significantly upregulated ($p < 0.05$, log_2(fold-change) > 0.5) and downregulated ($p < 0.05$, log_2(fold-change) < -0.5) genes was determined. Top 10 most enriched KEGG pathways in upregulated and downregulated genes are presented. Gene ratio represents the fraction of genes within each KEGG pathway that is significantly differentially expressed. Points coloured by significance of enrichment (p.adjust) and sized according to number of genes significantly differentially expressed (count).

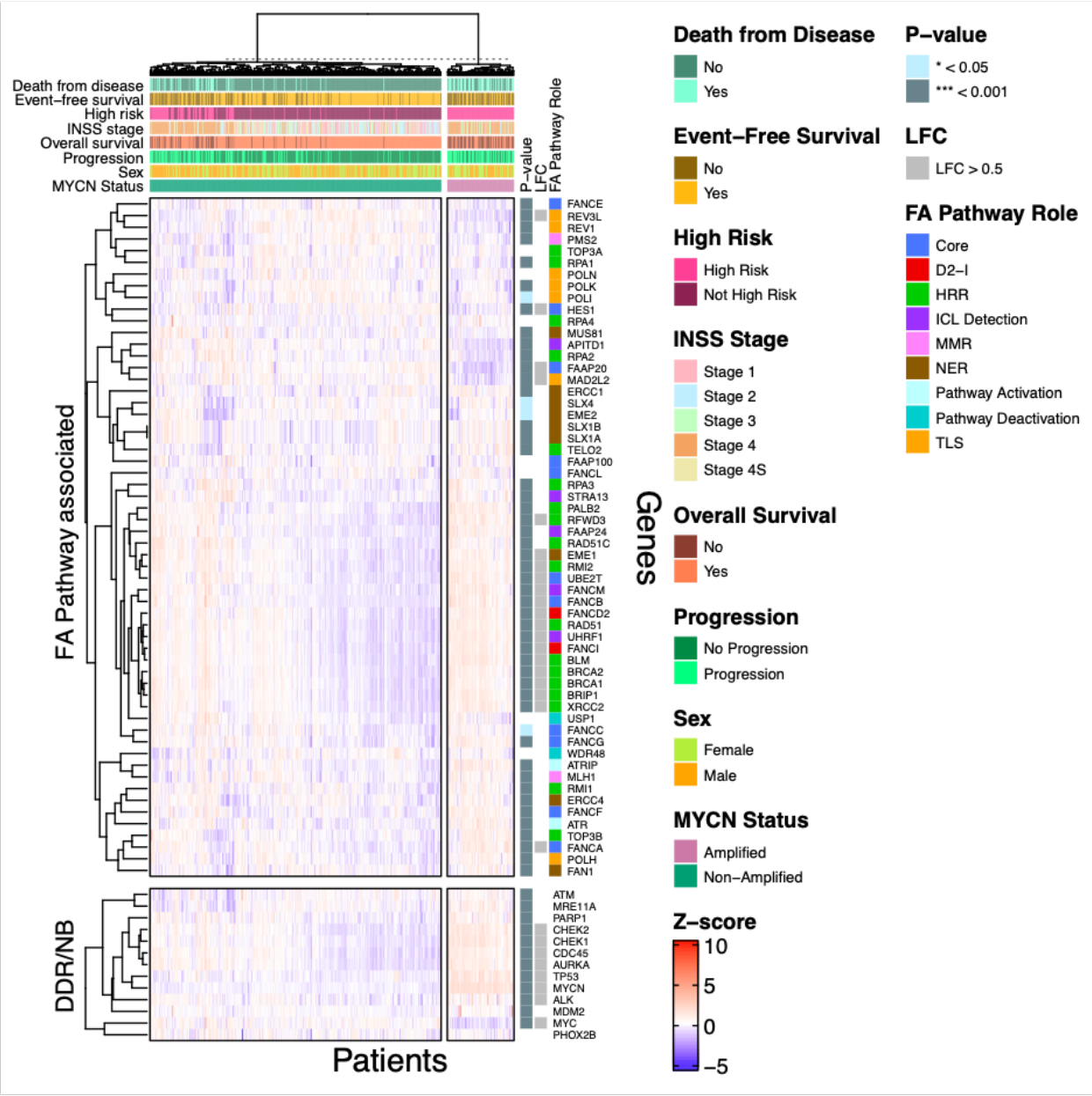

Figure A9. FA pathway associated genes are differentially expressed across 493 neuroblastoma tumours.

mRNA expression of 58 FA pathway associated genes and 13 DNA damage repair (DDR) or key neuroblastoma-associated (NB) genes was analysed in 493 neuroblastoma tumours using the GSE62564 RNA-Seq data set and the R2: Genomics Analysis and Visualisation Platform. Z-scores calculated for each gene independently using $\log_2$(RPM+1) expression values across all 493 tumours are presented. Genes and patients are clustered according to Pearson analysis, with patient clustering split by MYCN status and clustered based on expression of FA pathway associated genes only. 'LFC' indicates which genes show a $\log_2$(fold-change) in expression between MYCN amplified and MYCN non-amplified tumours greater than 0.5. Statistical significance of this differential expression (annotated by 'P-value') was determined for each gene by Student's t-test. Genes are annotated by 'FA pathway role': Core; FA core complex, D2-I; FANCD2-FANCI complex, HRR; homologous recombination repair, ICL detection; inter-strand crosslink detection, MMR; mis-match repair, NER; nucleotide excision repair, TLS; translesion synthesis. Patients annotated by MYCN amplification status, sex, disease progression, overall survival, INSS stage at diagnosis, high risk status at diagnosis, event-free survival, death from disease.

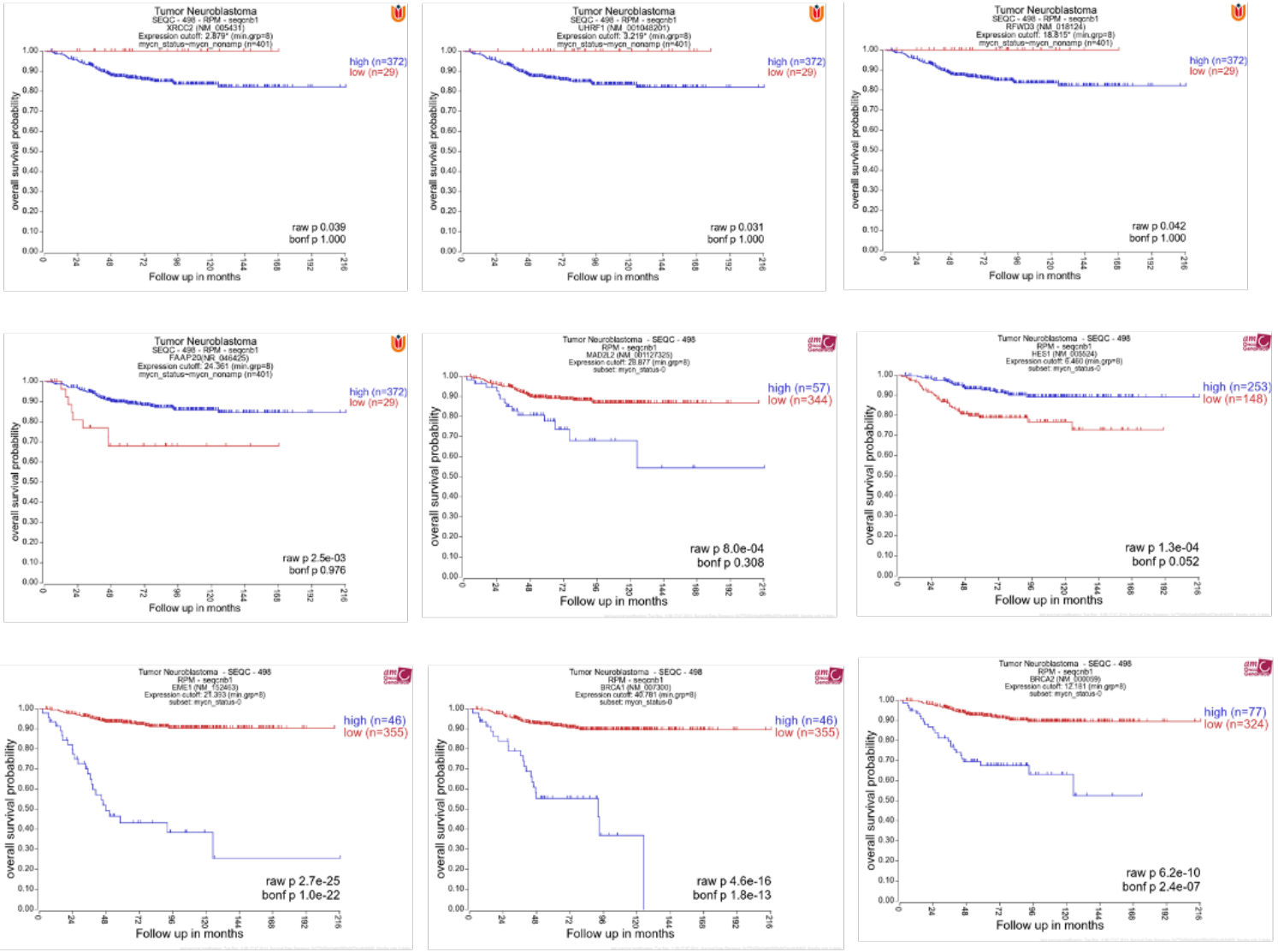

Figure A10. Overall survival stratification of non-MYCN amplified neuroblastoma cases can be significantly stratified by expression of most FA pathway genes that are significantly differentially expressed between MYCN amplified and MYCN non-amplified neuroblastomas. (Legend overleaf).

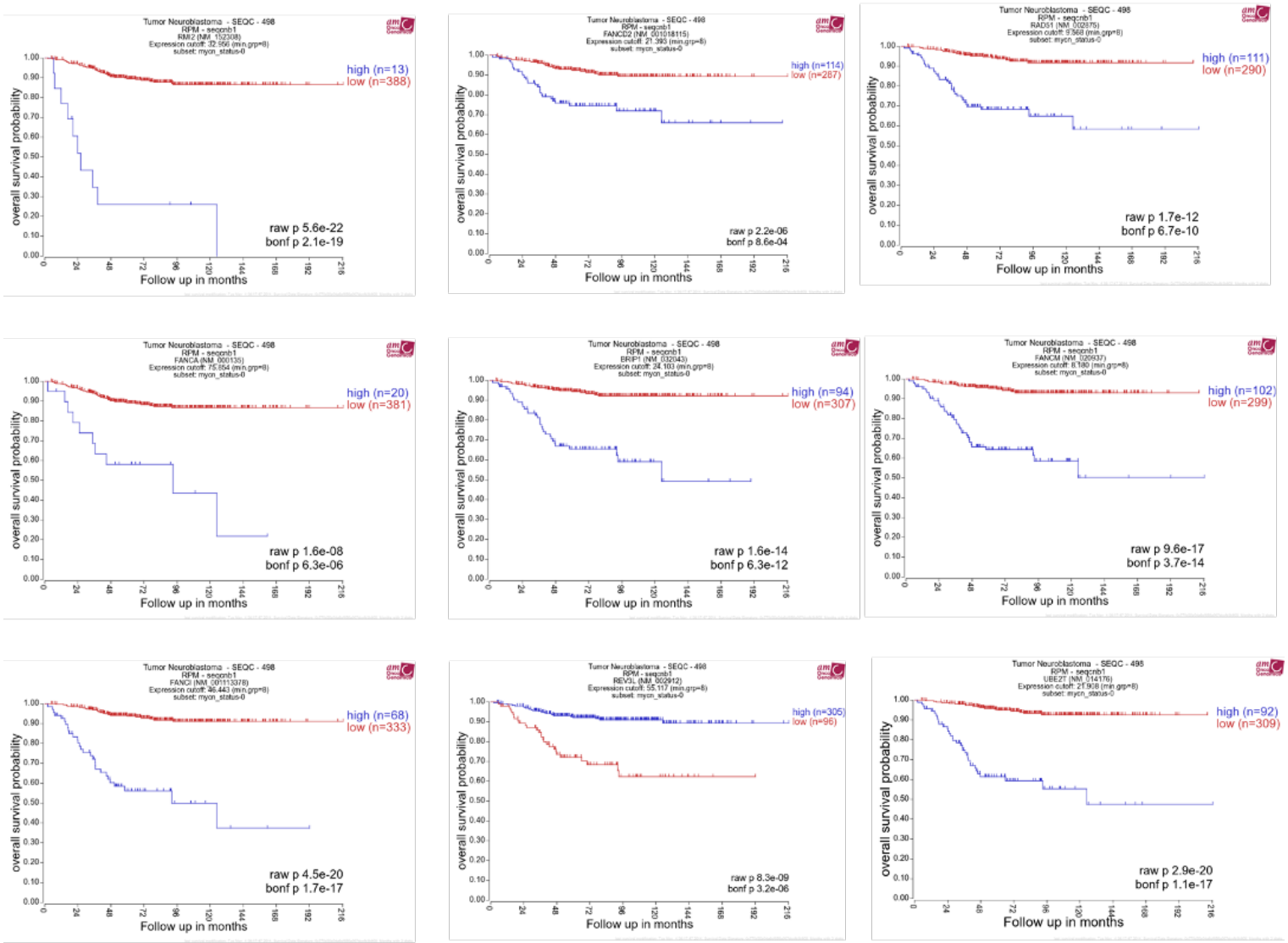

Figure A10. Overall survival stratification of non-MYCN amplified neuroblastoma cases can be significantly stratified by expression of most FA pathway genes that are significantly differentially expressed between MYCN amplified and MYCN non-amplified neuroblastomas. (Legend overleaf).

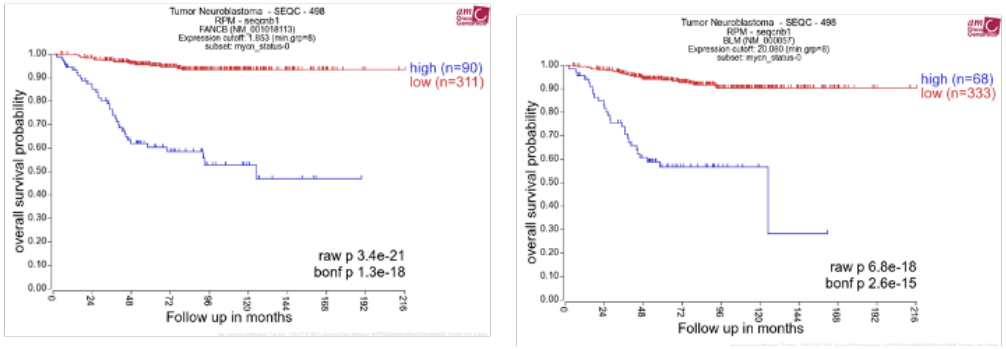

Figure A10. Overall survival stratification of non-MYCN amplified neuroblastoma cases can be significantly stratified by expression of most FA pathway genes that are significantly differentially expressed between MYCN amplified and MYCN non-amplified neuroblastomas.

FA pathway gene mRNA expression and overall survival was analysed across 493 neuroblastoma tumours using the GSE62564 RNA-Seq data set and the R2: Genomics Analysis and Visualisation Platform. Kaplan Meier curves are presented showing overall survival across 401 MYCN non-amplified neuroblastoma cases, with cases split according to expression level of each FA pathway gene that was significantly differentially expressed between MYCN amplified and MYCN non-amplified neuroblastoma tumours. High (blue line) and low (red line) expression threshold determined by scan modus. Significance determined by log-rank test (raw p). The P-value is adjusted for multiple testing by Bonferroni correction (bonf p).

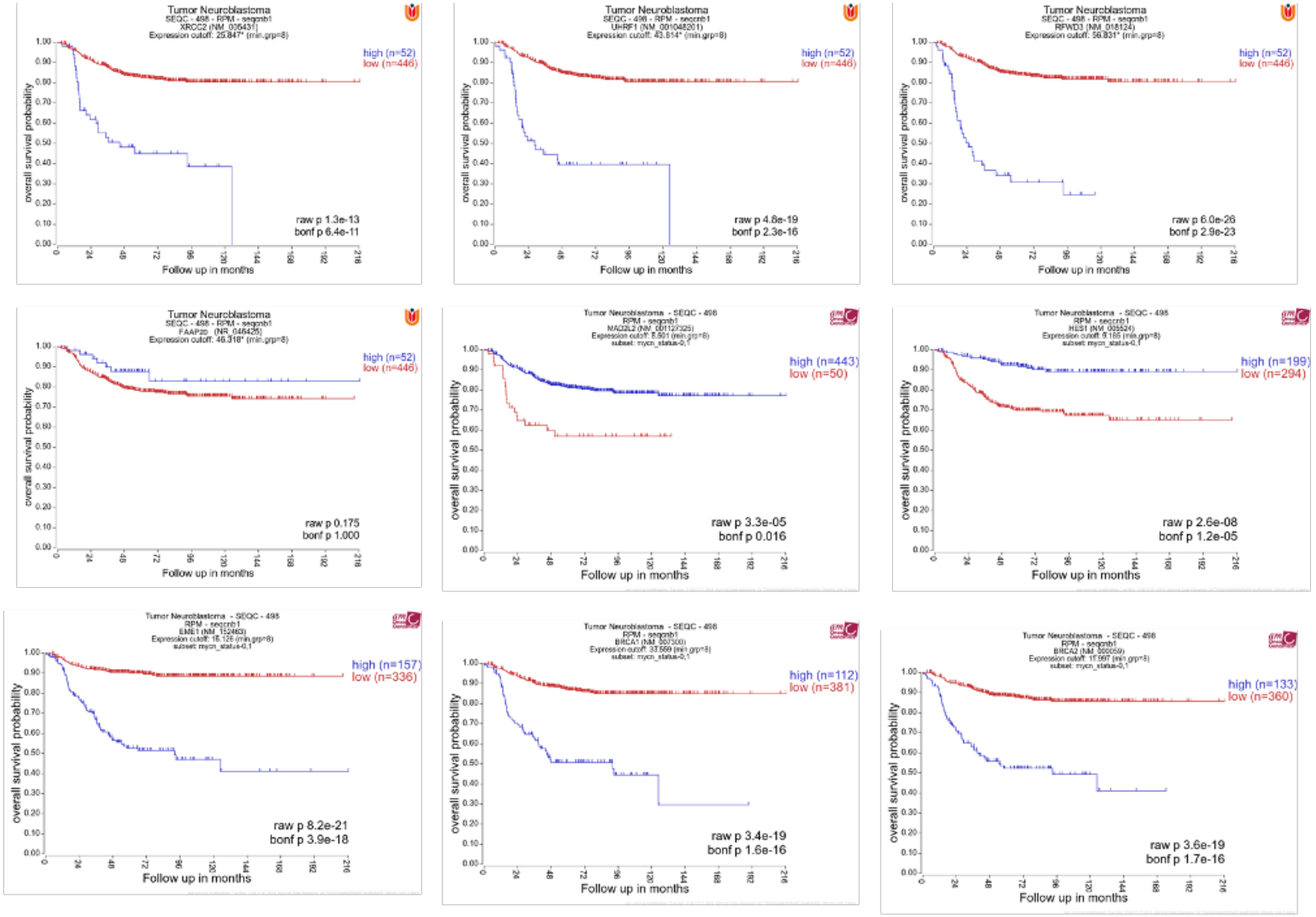

Figure A11. Overall survival stratification of all neuroblastoma cases can be significantly stratified by expression of most FA pathway genes that are significantly differentially expressed between MYCN amplified and MYCN non-amplified neuroblastomas. (Legend overleaf).

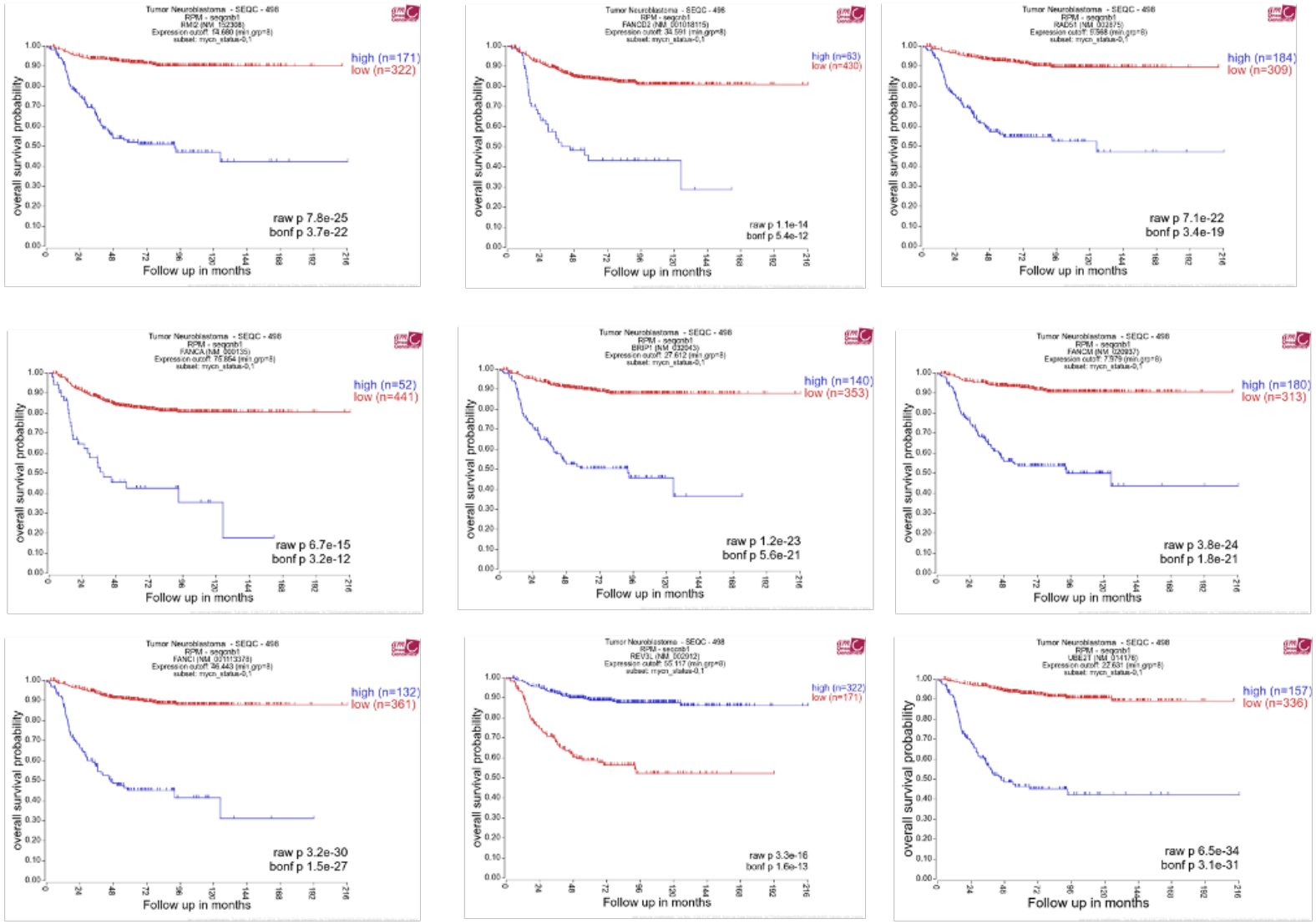

Figure A11. Overall survival stratification of all neuroblastoma cases can be significantly stratified by expression of most FA pathway genes that are significantly differentially expressed between MYCN amplified and MYCN non-amplified neuroblastomas. (Legend overleaf).

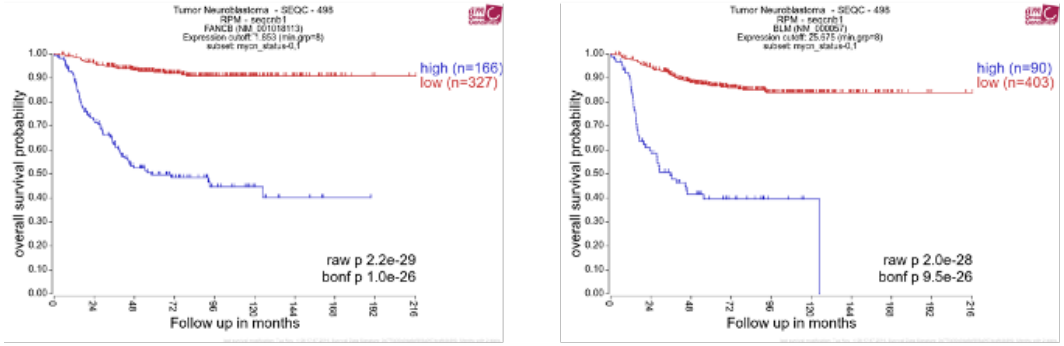

Figure A11. Overall survival stratification of all neuroblastoma cases can be significantly stratified by expression of most FA pathway genes that are significantly differentially expressed between MYCN amplified and MYCN non-amplified neuroblastomas.

FA pathway gene mRNA expression and overall survival was analysed across 493 neuroblastoma tumours using the GSE62564 RNA-Seq data set and the R2: Genomics Analysis and Visualisation Platform. Kaplan Meier curves are presented showing overall survival across all 493 neuroblastoma cases, with cases split according to expression level of each FA pathway gene that was significantly differentially expressed between MYCN amplified and MYCN non-amplified neuroblastoma tumours. High (blue line) and low (red line) expression threshold determined by scan modus. Significance determined by log-rank test (raw p). The P-value is adjusted for multiple testing by Bonferroni correction (bonf p).

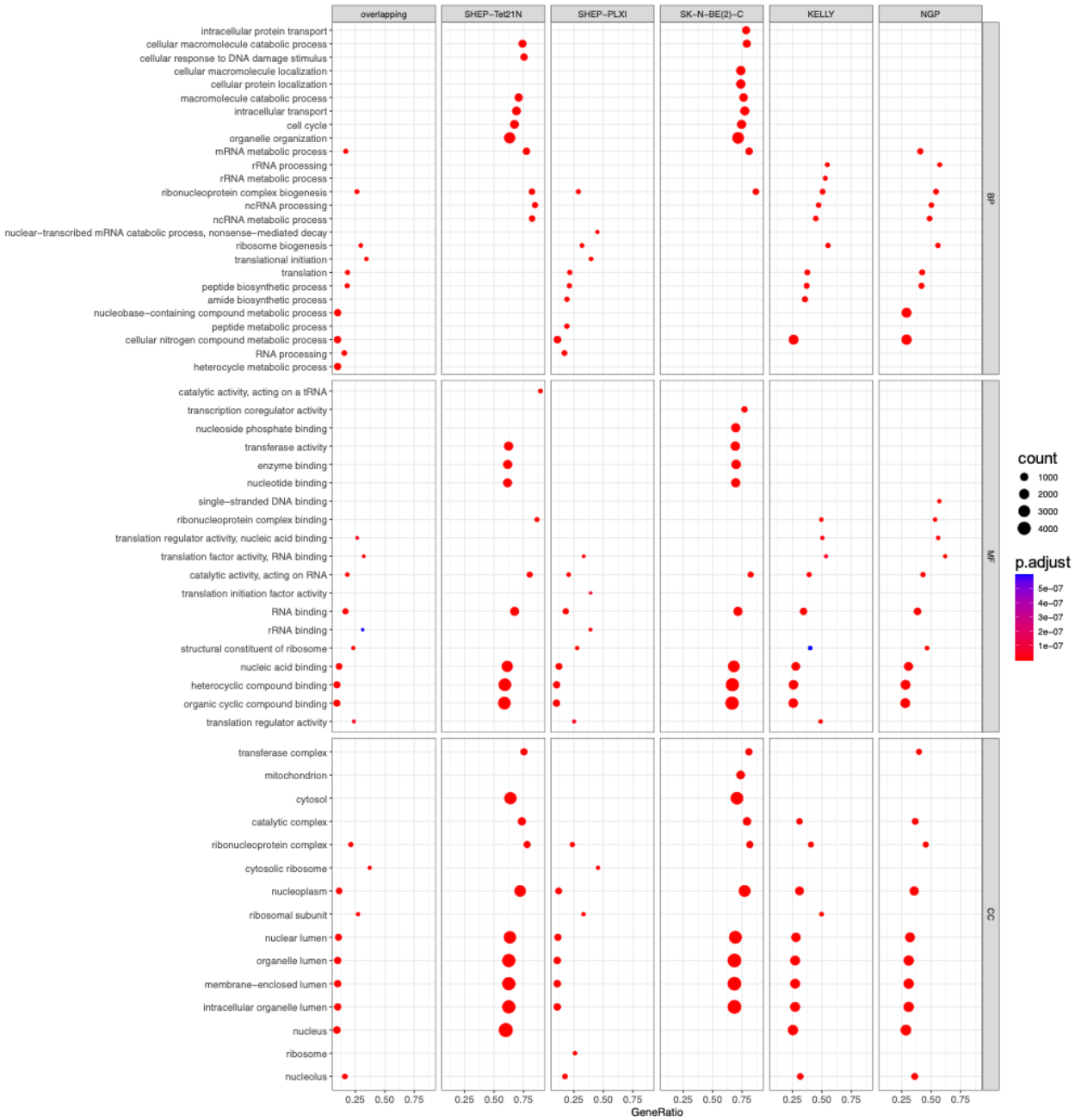

Figure A12. Top 10 gene ontologies enriched in MYCN-bound genes in neuroblastoma cells.
MYCN ChIP-Seq read data was downloaded from the GSE80151 dataset, and peaks were mapped and quantified using bowtie2 and MACS2. Peaks within gene promoters were annotated, and significantly enriched gene ontologies in the set of MYCN-bound genes was determined by ChIPpeakAnno. MYCN binding in SHEP-Tet21N MYCN ON, SHEP-PLXI-MYCN ON, SK-N-BE(2)-C, KELLY and NGP neuroblastoma cell lines was analysed. Gene ontology enrichment was similarly analysed for genes which were bound by MYCN in all MYCN ON and MYCN amplified cell lines analysed (overlapping). Top 10 most enriched biological process (BP), molecular function (MF) and cellular component (CC) gene ontologies in the set of MYCN-bound genes in each cell line are presented. Gene ratio represents the fraction of genes within each ontology that is bound by MYCN. Points coloured by significance of enrichment (p.adjust) and sized according to number of genes bound by MYCN (count).

7.3 Chapter 4 Appendix

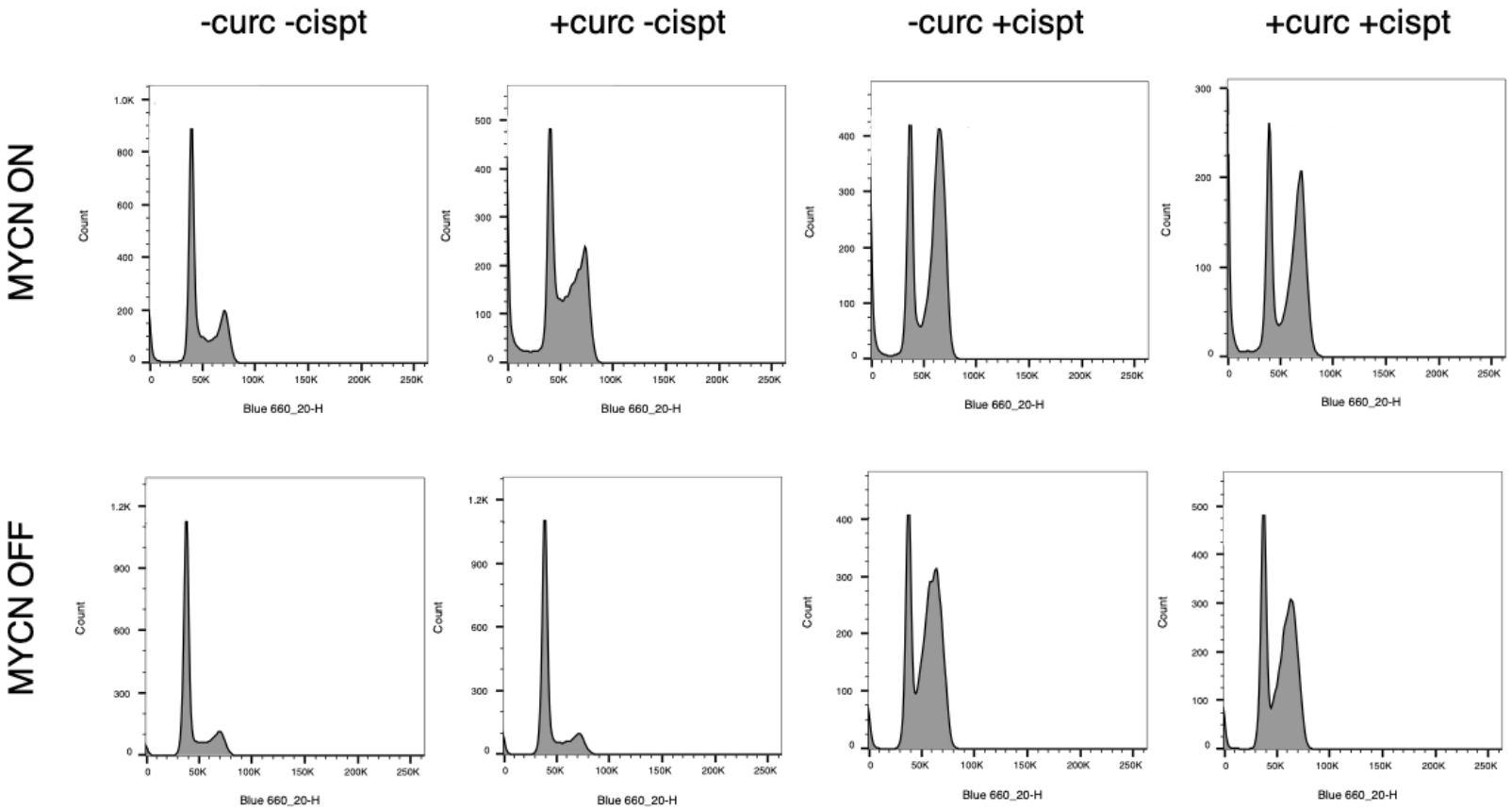

Figure A13. Curcumin has no substantial effect on the cell cycle distribution of SHEP-Tet21N MYCN ON and OFF cells (representative FACS cell cycle profiles).
SHEP-Tet21N MYCN ON and OFF cells were pre-treated with 0 μM or 5 μM curcumin for 16 hours before addition of 0 μM or 5 μM cisplatin for 24 hours. FACS cell cycle profiles were then determined with DNA content determined by propidium iodide staining (n=3). Representative FACS cell cycle profiles for each condition is displayed. Blue 660/20-H indicates PI fluorescence (DNA content). Count indicates cell count.

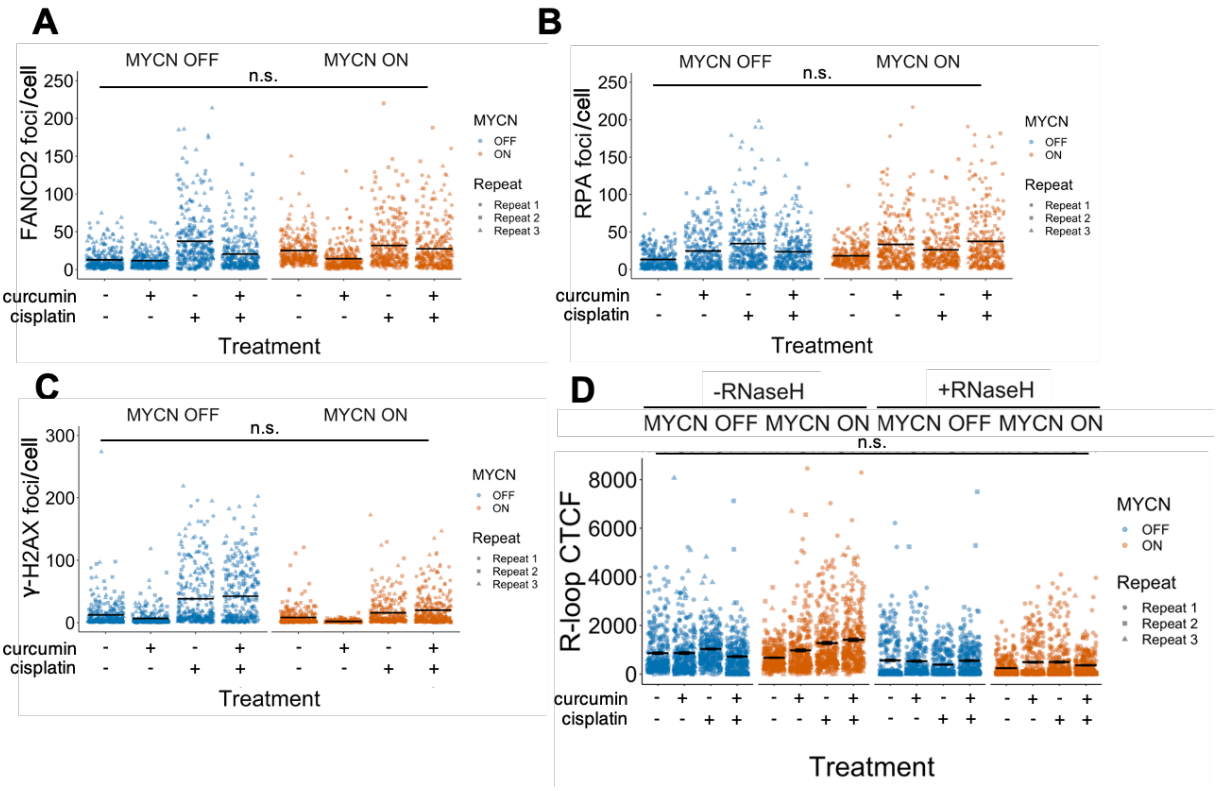

Appendix Figure A14. Curcumin inhibits FANCD2 foci formation, induces replication stress, exacerbates cisplatin-induced DNA damage, and induces accumulation of MYCN-induced R-loops in SHEP-Tet21N neuroblastoma cells (individual foci graphs).
SHEP-Tet21N MYCN ON and OFF cells were pre-treated with 0 μM or 5 μM curcumin for 16 hours before addition of 0 μM or 5 μM cisplatin for 24 hours. Cells were fixed and stained for immunofluorescence analysis of FANCD2 foci, pRPA foci, γ-H2AX foci and R-loops. Representative images and average point plots displayed in Figure 4.15 and 4.16. Number of **(A)** FANCD2 foci per cell, **(B)** pRPA foci per cell and **(C)** γ-H2AX foci per cell was quantified for each treatment condition. **(D)** R-loop corrected total cell fluorescence (CTCF) was quantified. To calculate R-loop CTCF, the R-loop intensity within each nucleus was quantified, the nucleoli R-loop intensity was deducted, and the nuclear R-loop intensity was normalised to the background intensity. Cells were incubated with RNase H for 24 hours before staining to digest R-loops as a negative control. For (A) - (D), 100 cells per repeat per treatment condition were quantified. The foci number and R-loop intensity in each cell across all repeats is presented (n=3). Statistical significance between treatments was determined by a two-way ANOVA using the means of each replicate where n.s. = not significant, *p<0.05, **p<0.01, ***p<0.001.

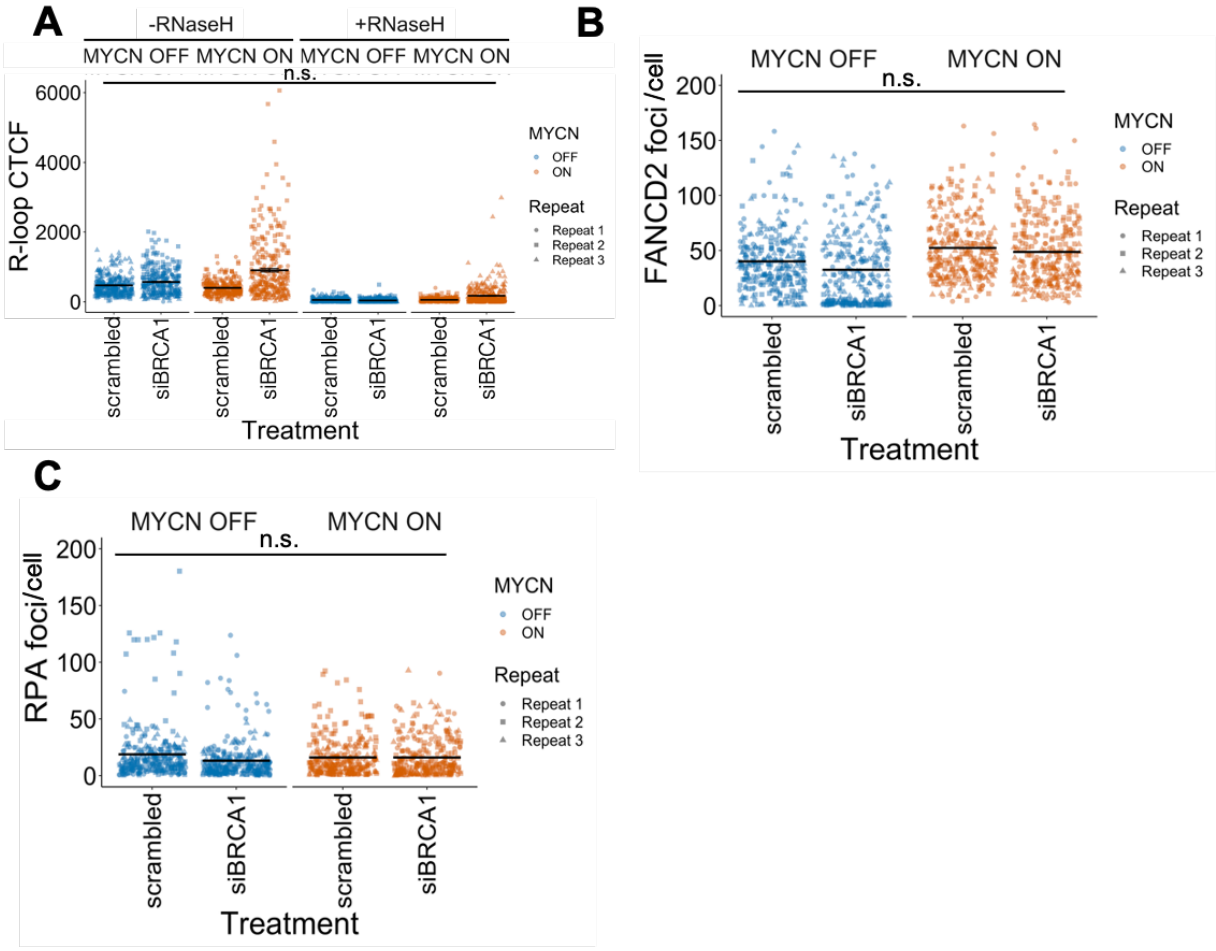

Appendix Figure A15. Depletion of BRCA1 induces R-loop accumulation in MYCN ON cells but does not alter FANCD2 or RPA foci formation (individual foci graphs).
SHEP-Tet21N MYCN ON and OFF cells were transfected with scrambled siRNA or BRCA1 siRNA using dharmafect-1 for 48 hours before cells were fixed and stained for immunofluorescence analysis of R-loops, FANCD2 foci and pRPA32/RPA2 foci. Representative images and average point plots displayed in Figure 4.17. **(A)** R-loop corrected total cell fluorescence (CTCF) was quantified. To calculate R-loop CTCF, the R-loop intensity within each nucleus was quantified, the nucleoli R-loop intensity was deducted, and the nuclear R-loop intensity was normalised to the background intensity. Cells were incubated with RNase H for 24 hours before staining to digest R-loops as a negative control. Number of **(B)** FANCD2 foci per cell and **(C)** pRPA foci per cell was quantified for each treatment condition. For (A) - (C), 100 cells per repeat per treatment condition were quantified. The foci number and R-loop intensity in each cell across all repeats is presented (n=3). Statistical significance between treatments was determined by a two-way ANOVA using the means of each replicate where n.s. = not significant, *p<0.05, **p<0.01, ***p<0.001.

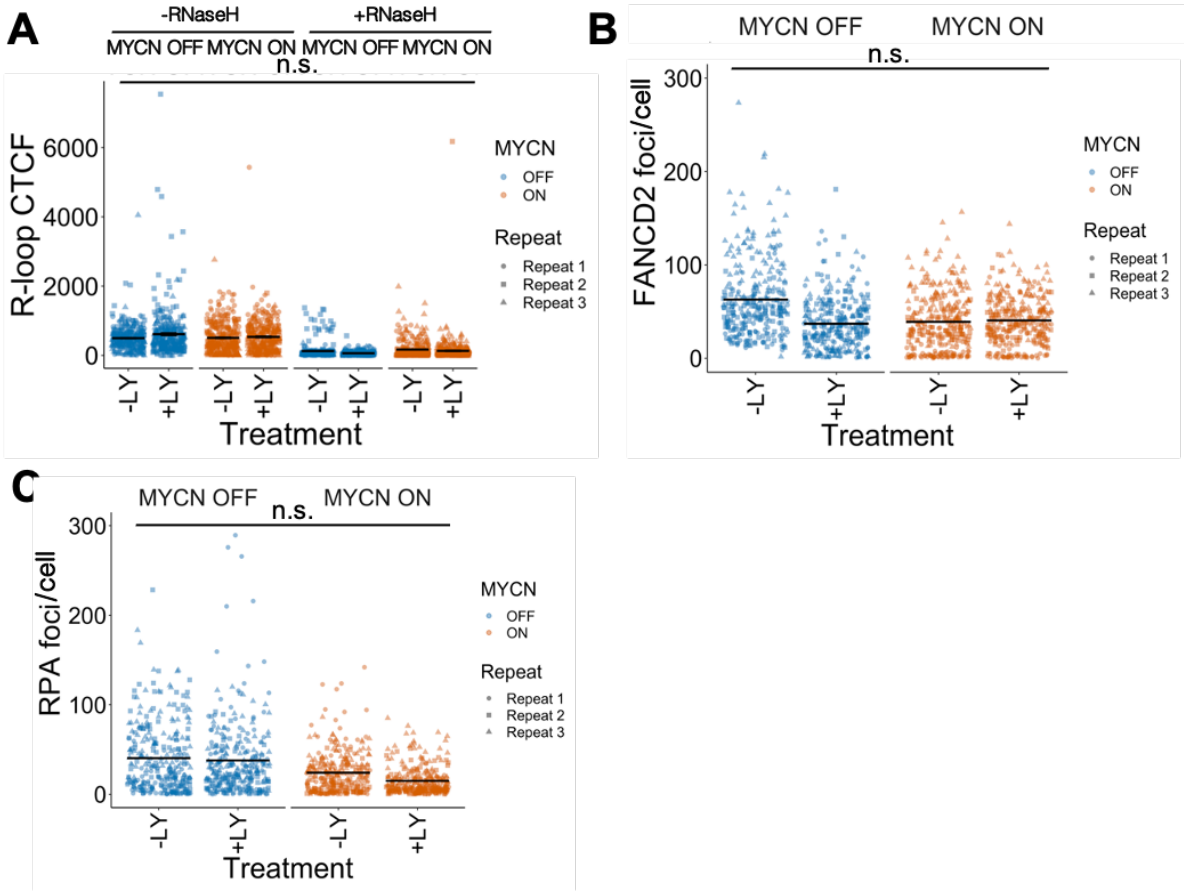

Appendix Figure A16. Treatment with AURKA inhibitor LY3295668 does not induce accumulation of R-loops, FANCD2 foci or RPA foci in SHEP-Tet21N MYCN ON and OFF cells (individual foci graphs).
SHEP-Tet21N MYCN ON and OFF cells were treated with 0 nM (-LY) or 50 nM (+LY) LY3295668, an AURKA inhibitor, for 2 hours. Cells were then fixed for immunofluorescence analysis of R-loops, FANCD2 foci and pRPA32/RPA2 foci. Representative images and average point plots displayed in Figure 4.18. **(A)** R-loop corrected total cell fluorescence (CTCF) was quantified. To calculate R-loop CTCF, the R-loop intensity within each nucleus was quantified, the nucleoli R-loop intensity was deducted, and the nuclear R-loop intensity was normalised to the background intensity. Cells were incubated with RNase H for 24 hours before staining to digest R-loops as a negative control. Number of **(B)** FANCD2 foci per cell and **(C)** pRPA foci per cell was quantified for each treatment condition. For (A) - (C), 100 cells per repeat per treatment condition were quantified. The foci number and R-loop intensity in each cell across all repeats is presented (n=3). Statistical significance between treatments was determined by a two-way ANOVA using the means of each replicate where n.s. = not significant, *p<0.05, **p<0.01, ***p<0.001.

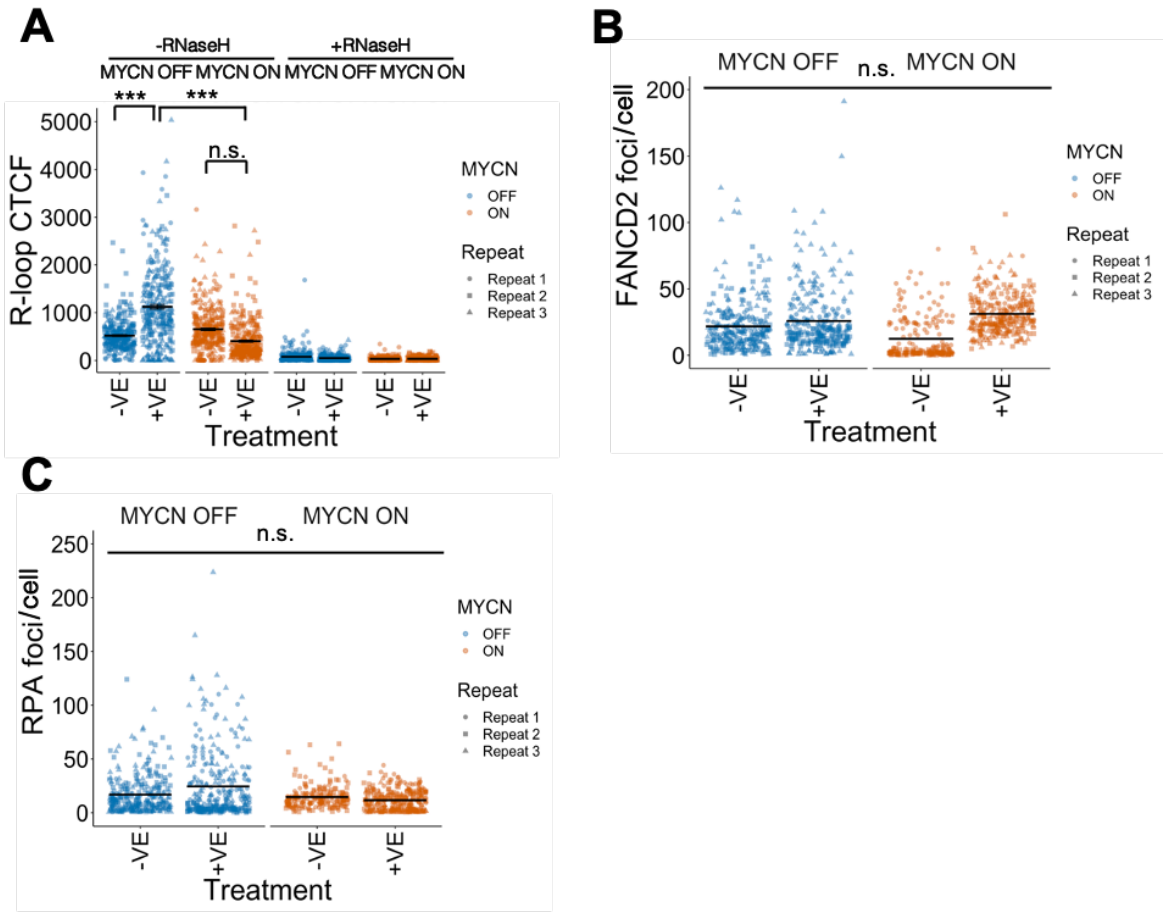

Appendix Figure A17. Treatment with ATR inhibitor VE-821 induces R-loop accumulation selectively in MYCN OFF cells but does not induce accumulation FANCD2 foci or RPA foci (individual foci graphs).
SHEP-Tet21N MYCN ON and OFF cells were treated with 0 μM (-VE) or 1 μM (+VE) VE-821 for 24 hours. Cells were then fixed for immunofluorescence analysis of R-loops, FANCD2 foci and pRPA32/RPA2 foci. Representative images and average point plots displayed in Figure 4.19. **(A)** R-loop corrected total cell fluorescence (CTCF) was quantified. To calculate R-loop CTCF, the R-loop intensity within each nucleus was quantified, the nucleoli R-loop intensity was deducted, and the nuclear R-loop intensity was normalised to the background intensity. Cells were incubated with RNase H for 24 hours before staining to digest R-loops as a negative control. Number of **(B)** FANCD2 foci per cell and **(C)** pRPA foci per cell was quantified for each treatment condition. For (A) - (C), 100 cells per repeat per treatment condition were quantified. The foci number and R-loop intensity in each cell across all repeats is presented (n=3). Statistical significance between treatments was determined by a two-way ANOVA using the means of each replicate where n.s. = not significant, *p<0.05, **p<0.01, ***p<0.001.

7.4 REDACTED

Figure A18. REDACTED

References

Ackermann S, Cartolano M, Hero B, Welte A, Kahlert Y, Roderwieser A, Bartenhagen C, Walter E, Gecht J, Kerschke L, et al.: **A mechanistic classification of clinical phenotypes in neuroblastoma**. *Science* 2018, **362**:1165.

Actis ML, Ambaye ND, Evison BJ, Shao Y, Vanarotti M, Inoue A, McDonald ET, Kikuchi S, Heath R, Hara K, et al.: **Identification of the first small-molecule inhibitor of the REV7 DNA repair protein interaction**. *Bioorg Med Chem* 2016, **24**:4339.

Adamo A, Collis SJ, Adelman CA, Silva N, Horejsi Z, Ward JD, Martinez-Perez E, Boulton SJ, La Volpe A: **Preventing Nonhomologous End Joining Suppresses DNA Repair Defects of Fanconi Anemia**. *Mol Cell* 2010, **39**:25–35.

Agarwal S, Milazzo G, Rajapakshe K, Bernardi R, Chen Z, Barbieri E, Koster J, Perini G, Coarfa C, Shohet JM: **MYCN acts as a direct co-regulator of p53 in MYCN amplified neuroblastoma.** *Oncotarget* 2018, **9**:20323–20338.

Ahler E, Sullivan WJ, Cass A, Braas D, York AG, Bensinger SJ, Graeber TG, Christofk HR: **Doxycycline Alters Metabolism and Proliferation of Human Cell Lines**. *PLoS One* 2013, **8**:64561.

Akkari YM, Bateman RL, Reifsteck CA, Olson SB, Grompe M: **DNA replication is required To elicit cellular responses to psoralen-induced DNA interstrand cross-links.** *Mol Cell Biol* 2000, **20**:8283–8289.

Alam G, Cui H, Shi H, Yang L, Ding J, Mao L, Maltese WA, Ding H-F: **MYCN Promotes the Expansion of Phox2B-Positive Neuronal Progenitors to Drive Neuroblastoma Development**. *Am J Pathol* 2009, **175**:856–866.

Alcón P, Shakeel S, Chen ZA, Rappsilber J, Patel KJ, Passmore LA: **FANCD2–FANCI is a clamp stabilized on DNA by monoubiquitination of FANCD2 during DNA repair**. *Nat Struct Mol Biol* 2020, **27**:240.

Alex R, Sözeri O, Meyer S, Dildrop R: **Determination of the DNA sequence recognized by the bHLH-zip domain of the N-Myc protein.** *Nucleic Acids Res* 1992, **20**:2257–2263.

Ali AM, Pradhan A, Singh TR, Du C, Li J, Wahengbam K, Grassman E, Auerbach AD, Pang Q, Meetei AR: **FAAP20: a novel ubiquitin-binding FA nuclear core-complex protein required for functional integrity of the FA-BRCA DNA repair pathway**. *Blood* 2012, **119**:3285–3294.

Allison DF, Wang GG: **R-loops: formation, function, and relevance to cell stress**. *Cell Stress* 2019, **3**:38–46.

Alonso MSM, Noordermeer SM: **Untangling the crosstalk between BRCA1 and R-loops during DNA repair**. *Nucleic Acids Res* 2021, **49**:4848.

Alter BP: **Fanconi's anemia and malignancies**. *Am J Hematol* 1996, **53**:99–110.

Amenábar JM, Torres-Pereira CC, Tang KD, Punyadeera C: **Two enemies, one fight: An update of oral cancer in patients with Fanconi anemia**. *Cancer* 2019, **125**:3936–3946.

Ameziane N, May P, Haitjema A, Van De Vrugt HJ, Van Rossum-Fikkert SE, Ristic D, Williams GJ, Balk J, Rockx D, Li H, et al.: **A novel Fanconi anaemia subtype associated with a dominant-negative mutation in RAD51**. *Nat Commun 2015 61* 2015, **6**:1–11.

Amiel J, Laudier B, Attié-Bitach T, Trang H, De Pontual L, Gener B, Trochet D, Etchevers H, Ray P, Simonneau M, et al.: **Polyalanine expansion and frameshift mutations of the paired-like homeobox gene PHOX2B in congenital central hypoventilation syndrome**. *Nat Genet* 2003, **33**:459–461.

Andreassen PR, D'Andrea AD, Taniguchi T: **ATR couples FANCD2 monoubiquitination to the DNA-damage response**. *Genes Dev* 2004, **18**:1958.

Applebaum MA, Henderson TO, Lee SM, Pinto N, Volchenboum SL, Cohn SL: **Second malignancies in patients with neuroblastoma: The effects of risk-based therapy**. *Pediatr Blood Cancer* 2015, **62**:128–133.

Aravindan N, Madhusoodhanan R, Ahmad S, Johnson D, Herman TS: **Curcumin inhibits NFkappaB mediated radioprotection and modulate apoptosis related genes in human neuroblastoma cells**. *Cancer Biol Ther* 2008, **7**:569–576.
Arkinson C, Chaugule VK, Toth R, Walden H: **Specificity for deubiquitination of monoubiquitinated FANCD2 is driven by the N-terminus of USP1**. *Life Sci alliance* 2018, **1**.
Armstrong C, Krystal W: **Isolation and Characterization for N-cym , a Gene Encoded Opposite to N-myc ' of Complementary by the DNA Strand DNA**. 1992, **3**:385–390.
Asgharzadeh S, Salo JA, Ji L, Oberthuer A, Fischer M, Berthold F, Hadjidaniel M, Liu CWY, Metelitsa LS, Pique-Regi R, et al.: **Clinical significance of tumor-associated inflammatory cells in metastatic neuroblastoma**. *J Clin Oncol* 2012, **30**:3525–3532.
Attiyeh EF, London WB, Mossé YP, Wang Q, Winter C, Khazi D, McGrady PW, Seeger RC, Look AT, Shimada H, et al.: **Chromosome 1p and 11q Deletions and Outcome in Neuroblastoma**. *N Engl J Med* 2005, **353**:2243–2253.
Auerbach AD: **A TEST FOR FANCONI'S ANEMIA**. *Blood* 1988, **72**:366.
Auerbach AD, Wolman SR: **Susceptibility of Fanconi's anaemia fibroblasts to chromosome damage by carcinogens**. *Nat 1976 2615560* 1976, **261**:494–496.
Bagatell R, London WB, Wagner LM, Voss SD, Stewart CF, Maris JM, Kretschmar C, Cohn SL: **Phase II study of irinotecan and temozolomide in children with relapsed or refractory neuroblastoma: a Children's Oncology Group study**. *J Clin Oncol* 2011, **29**:208–213.
Baker DL, Schmidt ML, Cohn SL, Maris JM, London WB, Buxton A, Stram D, Castleberry RP, Shimada H, Sandler A, et al.: **Outcome after Reduced Chemotherapy for Intermediate-Risk Neuroblastoma**. *N Engl J Med* 2010, **363**:1313–1323.
Ballo MT, Urman N, Lavy-Shahaf G, Grewal J, Bomzon Z, Toms S: **Correlation of Tumor Treating Fields Dosimetry to Survival Outcomes in Newly Diagnosed Glioblastoma: A Large-Scale Numerical Simulation-Based Analysis of Data from the Phase 3 EF-14 Randomized Trial**. *Int J Radiat Oncol* 2019, **104**:1106–1113.
Baluapuri A, Hofstetter J, Dudvarski Stankovic N, Endres T, Bhandare P, Vos SM, Adhikari B, Schwarz JD, Narain A, Vogt M, et al.: **MYC Recruits SPT5 to RNA Polymerase II to Promote Processive Transcription Elongation**. *Mol Cell* 2019, **74**:674.
Baluapuri A, Wolf E, Eilers M: **Target gene-independent functions of MYC oncoproteins**. *Nat Rev Mol Cell Biol* 2020, doi:10.1038/s41580-020-0215-2.
Barbieri E, Mehta P, Chen Z, Zhang L, Slack A, Berg S, Shohet JM: **MDM2 inhibition sensitizes neuroblastoma to chemotherapy-induced apoptotic cell death**. *Mol Cancer Ther* 2006, **5**:2358–2365.
Barone A, Casey D, McKee AE, Reaman G: **Cancer drugs approved for use in children: Impact of legislative initiatives and future opportunities**. *Pediatr Blood Cancer* 2019, **66**:e27809.
Barrilleaux BL, Cotterman R, Knoepfler PS: **Chromatin immunoprecipitation assays for Myc and N-Myc.** *Methods Mol Biol* 2013, **1012**:117–133.
Barroso S, Herrera-Moyano E, Muñoz S, García-Rubio M, Gómez-González B, Aguilera A: **The DNA damage response acts as a safeguard against harmful DNA–RNA hybrids of different origins**. *EMBO Rep* 2019, **20**.
Bartkova J, Hořejší Z, Koed K, Krämer A, Tort F, Zieger K, Guldberg P, Sehested M, Nesland JM, Lukas C, et al.: **DNA damage response as a candidate anti-cancer barrier in early human tumorigenesis**. *Nature* 2005, **434**:864–870.
Bartkova J, Rezaei N, Liontos M, Karakaidos P, Kletsas D, Issaeva N, Vassiliou L-VF, Kolettas E, Niforou K, Zoumpourlis VC, et al.: **Oncogene-induced senescence is part of the tumorigenesis barrier imposed by DNA damage checkpoints**. *Nature* 2006, **444**:633–637.
Bavisotto CC, Gammazza AM, Cascio FL, Mocciaro E, Vitale AM, Vergilio G, Pace A, Cappello F, Campanella C, Piccionello AP: **Curcumin Affects HSP60 Folding Activity and Levels in Neuroblastoma Cells**. *Int J Mol Sci* 2020, **21**.

Bell E, Lunec J, Tweddle D: **Cell Cycle Regulation Targets of MYCN Identified by Gene Expression Microarrays**. *Cell Cycle* 2007, **6**:1249–1256.
Bell E, Premkumar R, Carr J, Lu X, Lovat PE, Kees UR, Lunec J, Tweddle D: **The Role of MYCN in the Failure of MYCN Amplified Neuroblastoma Cell Lines to G1 Arrest After DNA Damage**. *Cell Cycle* 2006, **5**:2639–2647.
Benitez A, Liu W, Palovcak A, Wang G, Moon J, An K, Kim A, Zheng K, Zhang Y, Bai F, et al.: **FANCA promotes DNA double strand break repair by catalyzing single-strand annealing and strand exchange**. *Mol Cell* 2018, **71**:621.
Benitez A, Yuan F, Nakajima S, Wei L, Qian L, Myers R, Hu JJ, Lan L, Zhang Y: **Damage-dependent regulation of MUS81-EME1 by Fanconi anemia complementation group A protein**. *Nucleic Acids Res* 2014, **42**:1671.
Berg T, Cohen SB, Desharnais J, Sonderegger C, Maslyar DJ, Goldberg J, Boger DL, Vogt PK: **Small-molecule antagonists of Myc/Max dimerization inhibit Myc-induced transformation of chicken embryo fibroblasts**. *Proc Natl Acad Sci U S A* 2002, **99**:3830–3835.
Bernards R, Dessain SK, Weinberg RA: **N-myc amplification causes down-modulation of MHC class I antigen expression in neuroblastoma**. *Cell* 1986, **47**:667–674.
Berry T, Luther W, Bhatnagar N, Jamin Y, Poon E, Sanda T, Pei D, Sharma B, Vetharoy WR, Hallsworth A, et al.: **The ALK(F1174L) mutation potentiates the oncogenic activity of MYCN in neuroblastoma.** *Cancer Cell* 2012, **22**:117–130.
Berthold F, Boos J, Burdach S, Erttmann R, Henze G, Hermann J, Klingebiel T, Kremens B, Schilling FH, Schrappe M, et al.: **Myeloablative megatherapy with autologous stem-cell rescue versus oral maintenance chemotherapy as consolidation treatment in patients with high-risk neuroblastoma: a randomised controlled trial**. *Lancet Oncol* 2005, **6**:649–658.
Bester AC, Roniger M, Oren YS, Im MM, Sarni D, Chaoat M, Bensimon A, Zamir G, Shewach DS, Kerem B: **Nucleotide deficiency promotes genomic instability in early stages of cancer development.** *Cell* 2011, **145**:435–446.
Bhagwat N, Olsen AL, Wang AT, Hanada K, Stuckert P, Kanaar R, D'Andrea A, Niedernhofer LJ, McHugh PJ: **XPF-ERCC1 Participates in the Fanconi Anemia Pathway of Cross-Link Repair**. *Mol Cell Biol* 2009, **29**:6427.
Bhatia V, Barroso SI, García-Rubio ML, Tumini E, Herrera-Moyano E, Aguilera A: **BRCA2 prevents R-loop accumulation and associates with TREX-2 mRNA export factor PCID2**. *Nat 2014 5117509* 2014, **511**:362–365.
Bhatnagar SN, Sarin YK: **Neuroblastoma: A Review of Management and Outcome**. *Indian J Pediatr* 2012, **79**:787–792.
Biedler JL, Helson L, Spengler BA: **Morphology and growth, tumorigenicity, and cytogenetics of human neuroblastoma cells in continuous culture.** *Cancer Res* 1973, **33**:2643–2652.
Binz SK, Sheehan AM, Wold MS: **Replication Protein A phosphorylation and the cellular response to DNA damage**. *DNA Repair (Amst)* 2004, **3**:1015–1024.
Bissig H, Staehelin F, Tolnay M, Avoledo P, Richter J, Betts D, Bruder E, Kühne T: **Co-occurrence of neuroblastoma and nephroblastoma in an infant with Fanconi's anemia**. *Hum Pathol* 2002, **33**:1047–1051.
Bluteau D, Masliah-Planchon J, Clairmont C, Rousseau A, Ceccaldi R, D'Enghien CD, Bluteau O, Cuccuini W, Gachet S, De Latour RP, et al.: **Biallelic inactivation of REV7 is associated with Fanconi anemia**. *J Clin Invest* 2016, **126**:3580–3584.
Boeva V, Louis-Brennetot C, Peltier A, Durand S, Pierre-Eugène C, Raynal V, Etchevers HC, Thomas S, Lermine A, Daudigeos-Dubus E, et al.: **Heterogeneity of neuroblastoma cell identity defined by transcriptional circuitries**. *Nat Genet* 2017, **49**:1408–1413.
Bogliolo M, Bluteau D, Lespinasse J, Pujol R, Vasquez N, D'Enghien CD, Stoppa-Lyonnet D, Leblanc T, Soulier J, Surrallés J: **Biallelic truncating FANCM mutations cause early-onset cancer but not Fanconi anemia**. *Genet Med* 2018, **20**:458–463.

Bogliolo M, Lyakhovich A, Callén E, Castellà M, Cappelli E, Ramírez MJ, Creus A, Marcos R, Kalb R, Neveling K, et al.: **Histone H2AX and Fanconi anemia FANCD2 function in the same pathway to maintain chromosome stability**. *EMBO J* 2007, **26**:1340.
Bogliolo M, Schuster B, Stoepker C, Derkunt B, Su Y, Raams A, Trujillo JP, Minguillón J, Ramírez MJ, Pujol R, et al.: **Mutations in ERCC4, encoding the DNA-repair endonuclease XPF, cause Fanconi anemia**. *Am J Hum Genet* 2013, **92**:800–806.
Boon K, Caron HN, van Asperen R, Valentijn L, Hermus MC, van Sluis P, Roobeek I, Weis I, Voûte PA, Schwab M, et al.: **N-myc enhances the expression of a large set of genes functioning in ribosome biogenesis and protein synthesis.** *EMBO J* 2001, **20**:1383–1393.
Bordow SB, Norris MD, Haber PS, Marshall GM, Haber M: **Prognostic significance of MYCN oncogene expression in childhood neuroblastoma.** *J Clin Oncol* 1998, **16**:3286–3294.
Bosch PC, Segura-Bayona S, Koole W, Heteren JT van, Dewar JM, Tijsterman M, Knipscheer P: **FANCJ promotes DNA synthesis through G-quadruplex structures**. *EMBO J* 2014, **33**:2521–2533.
Bouchard C, Dittrich O, Kiermaier A, Dohmann K, Menkel A, Eilers M, Lüscher B: **Regulation of cyclin D2 gene expression by the Myc/Max/Mad network: Myc-dependent TRRAP recruitment and histone acetylation at the cyclin D2 promoter**. *Genes Dev* 2001, **15**:2042.
Bouchard C, Thieke K, Maier A, Saffrich R, Hanley-Hyde J, Ansorge W, Reed S, Sicinski P, Bartek J, Eilers M: **Direct induction of cyclin D2 by Myc contributes to cell cycle progression and sequestration of p27**. *EMBO J* 1999, **18**:5321–5333.
Bourseguin J, Bonet C, Renaud E, Pandiani C, Boncompagni M, Giuliano S, Pawlikowska P, Karmous-Benailly H, Ballotti R, Rosselli F, et al.: **FANCD2 functions as a critical factor downstream of MiTF to maintain the proliferation and survival of melanoma cells**. *Sci Rep* 2016, **6**.
Bouwman P, Aly A, Escandell JM, Pieterse M, Bartkova J, Van Der Gulden H, Hiddingh S, Thanasoula M, Kulkarni A, Yang Q, et al.: **53BP1 loss rescues BRCA1 deficiency and is associated with triple-negative and BRCA-mutated breast cancers**. *Nat Struct Mol Biol* 2010, **17**:688.
Bown N, Cotterill S, Łastowska M, O'Neill S, Pearson ADJ, Plantaz D, Meddeb M, Danglot G, Brinkschmidt C, Christiansen H, et al.: **Gain of Chromosome Arm 17q and Adverse Outcome in Patients with Neuroblastoma**. *N Engl J Med* 1999, **340**:1954–1961.
Bradford MM: **A rapid and sensitive method for the quantitation of microgram quantities of protein utilizing the principle of protein-dye binding**. *Anal Biochem* 1976, **72**:248–254.
Bradner JE, Hnisz D, Young RA: **Transcriptional Addiction in Cancer**. *Cell* 2017, **168**:629.
Branter J, Estevez-Cebrero M, Grundy R, Basu S, Smith S: **Abstract 4637: Tumor treating fields (TTFields) have antiproliferative effects on high-grade pediatric brain tumor cell lines**. *Cancer Res* 2018, **78**:4637.
Bravo-Navas S, Yáñez L, Romón Í, Pipaón C: **Elevated FANCA expression determines a worse prognosis in chronic lymphocytic leukemia and interferes with p53 function**. *FASEB J* 2019, **33**:10477–10489.
Breit S, Schwab M: **Suppression ofMYC by high expression ofNMYC in human neuroblastoma cells**. *J Neurosci Res* 1989, **24**:21–28.
Brenke JK, Popowicz GM, Schorpp K, Rothenaigner I, Roesner M, Meininger I, Kalinski C, Ringelstetter L, R'kyek O, Vincendeau M, et al.: **Targeting TRAF6 E3 ligase activity with a small-molecule inhibitor combats autoimmunity**. *J Biol Chem* 2018, **293**:13191.
Brenner C, Deplus R, Didelot C, Loriot A, Viré E, De Smet C, Gutierrez A, Danovi D, Bernard D, Boon T, et al.: **Myc represses transcription through recruitment of DNA methyltransferase corepressor.** *EMBO J* 2005, **24**:336–346.
Bretz AC, Gittler MP, Charles JP, Gremke N, Eckhardt I, Mernberger M, Mandic R, Thomale J, Nist A, Wanzel M, et al.: **ΔNp63 activates the Fanconi anemia DNA repair pathway**

and limits the efficacy of cisplatin treatment in squamous cell carcinoma. *Nucleic Acids Res* 2016, **44**:3204–3218.
Bridge WL, Vandenberg CJ, Franklin RJ, Hiom K: **The BRIP1 helicase functions independently of BRCA1 in the Fanconi anemia pathway for DNA crosslink repair**. *Nat Genet 2005 379* 2005, **37**:953–957.
Brockmann M, Poon E, Berry T, Carstensen A, Deubzer HE, Rycak L, Jamin Y, Thway K, Robinson SP, Roels F, et al.: **Small Molecule Inhibitors of Aurora-A Induce Proteasomal Degradation of N-Myc in Childhood Neuroblastoma**. *Cancer Cell* 2013, **24**:75.
Brodeur GM, Seeger RC, Schwab M, Varmus HE, Bishop JM: **Amplification of N-myc in untreated human neuroblastomas correlates with advanced disease stage.** *Science* 1984, **224**:1121–1124.
Bryant HE, Schultz N, Thomas HD, Parker KM, Flower D, Lopez E, Kyle S, Meuth M, Curtin NJ, Helleday T: **Specific killing of BRCA2-deficient tumours with inhibitors of poly(ADP-ribose) polymerase.** *Nature* 2005, **434**:913–917.
Büchel G, Carstensen A, Mak KY, Roeschert I, Leen E, Sumara O, Hofstetter J, Herold S, Kalb J, Baluapuri A, et al.: **Association with Aurora-A Controls N-MYC-Dependent Promoter Escape and Pause Release of RNA Polymerase II during the Cell Cycle**. *Cell Rep* 2017, **21**:3483.
Budke B, Logan HL, Kalin JH, Zelivianskaia AS, McGuire WC, Miller LL, Stark JM, Kozikowski AP, Bishop DK, Connell PP: **RI-1: a chemical inhibitor of RAD51 that disrupts homologous recombination in human cells**. *Nucleic Acids Res* 2012, **40**:7347.
Budzowska M, Graham TG, Sobeck A, Waga S, Walter JC: **Regulation of the Rev1–pol ζ complex during bypass of a DNA interstrand cross-link**. *EMBO J* 2015, **34**:1971.
Bunting SF, Callén E, Kozak ML, Kim JM, Wong N, López-Contreras AJ, Ludwig T, Baer R, Faryabi RB, Malhowski A, et al.: **BRCA1 functions independently of homologous recombination in DNA interstrand cross-link repair**. *Mol Cell* 2012, **46**:125.
Bunting SF, Callén E, Wong N, Chen HT, Polato F, Gunn A, Bothmer A, Feldhahn N, Fernandez-Capetillo O, Cao L, et al.: **53BP1 inhibits homologous recombination in Brca1-deficient cells by blocking resection of DNA breaks**. *Cell* 2010, **141**:243.
Burkhart CA, Cheng AJ, Madafiglio J, Kavallaris M, Mili M, Marshall GM, Weiss WA, Khachigian LM, Norris MD, Haber M: **Effects of MYCN antisense oligonucleotide administration on tumorigenesis in a murine model of neuroblastoma**. *J Natl Cancer Inst* 2003, **95**:1394–1403.
Burnette WN: **"Western Blotting": Electrophoretic transfer of proteins from sodium dodecyl sulfate-polyacrylamide gels to unmodified nitrocellulose and radiographic detection with antibody and radioiodinated protein A**. *Anal Biochem* 1981, **112**:195–203.
Cai MY, Dunn CE, Chen W, Kochupurakkal BS, Nguyen H, Moreau LA, Shapiro GI, Parmar K, Kozono D, D'Andrea AD: **Cooperation of the ATM and Fanconi Anemia/BRCA Pathways in Double-Strand Break End Resection**. *Cell Rep* 2020, **30**:2402.
Canete A, Gerrard M, Rubie H, Castel V, Di Cataldo A, Munzer C, Ladenstein R, Brichard B, Bermúdez JD, Couturier J, et al.: **Poor Survival for Infants With MYCN-Amplified Metastatic Neuroblastoma Despite Intensified Treatment: The International Society of Paediatric Oncology European Neuroblastoma Experience**. *J Clin Oncol* 2009, **27**:1014–1019.
Cantres-Velez JA, Blaize JL, Vierra DA, Boisvert RA, Garzon JL, Piraino B, Tan W, Deans AJ, Howlett NG: **Cyclin-Dependent Kinase-Mediated Phosphorylation of FANCD2 Promotes Mitotic Fidelity**. *Mol Cell Biol* 2021, **41**.
Cao L, Xu X, Bunting SF, Liu J, Wang RH, Cao LL, Wu JJ, Peng TN, Chen J, Nussenzweig A, et al.: **A selective requirement for 53BP1 in the biological response to genomic instability induced by Brca1 deficiency**. *Mol Cell* 2009, **35**:534.

Caporali S, Falcinelli S, Starace G, Russo MT, Bonmassar E, Jiricny J, D'Atri S: **DNA damage induced by temozolomide signals to both ATM and ATR: role of the mismatch repair system.** *Mol Pharmacol* 2004, **66**:478–491.
Carén H, Kryh H, Nethander M, Sjöberg RM, Träger C, Nilsson S, Abrahamsson J, Kogner P, Martinsson T: **High-risk neuroblastoma tumors with 11q-deletion display a poor prognostic, chromosome instability phenotype with later onset**. *Proc Natl Acad Sci U S A* 2010, **107**:4323–4328.
Carlsen NLT: **How frequent is spontaneous remission of neuroblastomas? Implications for screening**. *Br J Cancer* 1990, **61**:441–446.
Castella M, Taniguchi T, Hughes H: **The role of FAN1 nuclease in the Fanconi anemia pathway**. *Cell Cycle* 2010, **9**:4265–4266.
Catucci I, Osorio A, Arver B, Neidhardt G, Bogliolo M, Zanardi F, Riboni M, Minardi S, Pujol R, Azzollini J, et al.: **Individuals with FANCM biallelic mutations do not develop Fanconi anemia, but show risk for breast cancer, chemotherapy toxicity and may display chromosome fragility**. *Genet Med* 2018, **20**:452–457.
Cavalieri F, Goldfarb M: **N-myc proto-oncogene expression can induce DNA replication in Balb/c 3T3 fibroblasts.** *Oncogene* 1988, **2**:289–291.
Ceccaldi R, Parmar K, Mouly E, Delord M, Kim JM, Regairaz M, Pla M, Vasquez N, Zhang QS, Pondarre C, et al.: **Bone marrow failure in Fanconi anemia is triggered by an exacerbated p53/p21 DNA damage response that impairs hematopoietic stem and progenitor cells**. *Cell Stem Cell* 2012, **11**:36.
Ceccaldi R, Rondinelli B, D'Andrea AD: **Repair Pathway Choices and Consequences at the Double-Strand Break**. *Trends Cell Biol* 2016, **26**:52.
Ceresoli GL, Aerts JG, Dziadziuszko R, Ramlau R, Cedres S, van Meerbeeck JP, Mencoboni M, Planchard D, Chella A, Crinò L, et al.: **Tumour Treating Fields in combination with pemetrexed and cisplatin or carboplatin as first-line treatment for unresectable malignant pleural mesothelioma (STELLAR): a multicentre, single-arm phase 2 trial**. *Lancet Oncol* 2019, **20**:1702–1709.
Chan CH, Morrow JK, Li CF, Gao Y, Jin G, Moten A, Stagg LJ, Ladbury JE, Cai Z, Xu D, et al.: **Pharmacological inactivation of Skp2 SCF ubiquitin ligase restricts cancer stem cell traits and cancer progression**. *Cell* 2013, **154**.
Chan HS, Gallie BL, DeBoer G, Haddad G, Ikegaki N, Dimitroulakos J, Yeger H, Ling V: **MYCN protein expression as a predictor of neuroblastoma prognosis.** *Clin Cancer Res* 1997, **3**:1699–1706.
Chang CJ, Freeman DJ, Wu H: **PTEN regulates Mdm2 expression through the P1 promoter**. *J Biol Chem* 2004, **279**:29841–29848.
Chang E, Patel CB, Pohling C, Young C, Song J, Flores TA, Zeng Y, Joubert LM, Arami H, Natarajan A, et al.: **Tumor treating fields increases membrane permeability in glioblastoma cells**. *Cell Death Discov* 2018, **4**:113.
Chang EYC, Tsai S, Aristizabal MJ, Wells JP, Coulombe Y, Busatto FF, Chan YA, Kumar A, Dan Zhu Y, Wang AYH, et al.: **MRE11-RAD50-NBS1 promotes Fanconi Anemia R-loop suppression at transcription–replication conflicts**. *Nat Commun 2019 101* 2019, **10**:1–15.
Chang YM, Shih YL, Chen CP, Liu KL, Lee MH, Lee MZ, Hou HT, Huang HC, Lu HF, Peng SF, et al.: **Ouabain induces apoptotic cell death in human prostate DU 145 cancer cells through DNA damage and TRAIL pathways**. *Environ Toxicol* 2019, **34**:1329–1339.
Chanvorachote P, Pongrakhananon V, Wannachaiyasit S, Luanpitpong S, Rojanasakul Y, Nimmannit U: **Curcumin sensitizes lung cancer cells to cisplatin-induced apoptosis through superoxide anion-mediated Bcl-2 degradation**. *Cancer Invest* 2009, **27**:624–635.
Chapman TM, Wallace C, Gillen KJ, Bakrania P, Khurana P, Coombs PJ, Fox S, Bureau EA, Brownlees J, Melton DW, et al.: **N-Hydroxyimides and hydroxypyrimidinones as inhibitors of the DNA repair complex ERCC1-XPF**. *Bioorg Med Chem Lett* 2015, **25**:4104–4108.

Charron J, Malynn BA, Fisher P, Stewart V, Jeannotte L, Goff SP, Robertson EJ, Alt FW: **Embryonic lethality in mice homozygous for a targeted disruption of the N-myc gene.** *Genes Dev* 1992, **6**:2248–2257.
Chaudhry A, Benson L, Varshaver M, Farber O, Weinberg U, Kirson E, Palti Y: **NovoTTF™-100A System (Tumor Treating Fields) transducer array layout planning for glioblastoma: a NovoTAL™ system user study**. *World J Surg Oncol* 2015, **13**.
Chaudhury I, Sareen A, Raghunandan M, Sobeck A: **FANCD2 regulates BLM complex functions independently of FANCI to promote replication fork recovery**. *Nucleic Acids Res* 2013, **41**:6444.
Chayka O, D'Acunto CW, Middleton O, Arab M, Sala A: **Identification and Pharmacological Inactivation of the MYCN Gene Network as a Therapeutic Strategy for Neuroblastic Tumor Cells**. *J Biol Chem* 2015, **290**:2198.
Chen CC, Taniguchi T, D'Andrea A: **The Fanconi anemia (FA) pathway confers glioma resistance to DNA alkylating agents**. *J Mol Med* 2007, **85**:497–509.
Chen D, Cox J, Annam J, Weingart M, Essien G, Rathi KS, Rokita JL, Khurana P, Cuya SM, Bosse KR, et al.: **LIN28B promotes neuroblastoma metastasis and regulates PDZ binding kinase**. *Neoplasia* 2020, **22**:231.
Chen J, Guan Z: **Function of Oncogene Mycn in Adult Neurogenesis and Oligodendrogenesis**. *Mol Neurobiol* 2022, **59**:77.
Chen L, Iraci N, Gherardi S, Gamble LD, Wood KM, Perini G, Lunec J, Tweddle DA: **p53 is a direct transcriptional target of MYCN in neuroblastoma.** *Cancer Res* 2010, **70**:1377–1388.
Chen L, Pastorino F, Berry P, Bonner J, Kirk C, Wood KM, Thomas HD, Zhao Y, Daga A, Veal GJ, et al.: **Preclinical evaluation of the first intravenous small molecule MDM2 antagonist alone and in combination with temozolomide in neuroblastoma**. *Int J Cancer* 2019, **144**:3146–3159.
Chen L, Alexe G, Dharia NV, Ross L, Iniguez AB, Conway AS, Wang EJ, Veschi V, Lam N, Qi J, et al.: **CRISPR-Cas9 screen reveals a MYCN-amplified neuroblastoma dependency on EZH2**. *J Clin Invest* 2018, **128**:446.
Chen P, Li J, Chen YC, Qian H, Chen YJ, Su JY, Wu M, Lan T: **The functional status of DNA repair pathways determines the sensitization effect to cisplatin in non-small cell lung cancer cells**. *Cell Oncol (Dordr)* 2016, **39**:511–522.
Chen P, Li J, Jiang HG, Lan T, Chen YC: **Curcumin reverses cisplatin resistance in cisplatin-resistant lung caner cells by inhibiting FA/BRCA pathway**. *Tumour Biol* 2015, **36**:3591–3599.
Chen Q, Van Der Sluis PC, Boulware D, Hazlehurst LA, Dalton WS: **The FA/BRCA pathway is involved in melphalan-induced DNA interstrand cross-link repair and accounts for melphalan resistance in multiple myeloma cells**. *Blood* 2005, **106**:698.
Chen X, Wang J, Fu Z, Zhu B, Wang J, Guan S, Hua Z: **Curcumin activates DNA repair pathway in bone marrow to improve carboplatin-induced myelosuppression**. *Sci Reports 2017 71* 2017, **7**:1–11.
Chen Y, Li Z, Xu Z, Tang H, Guo W, Sun X, Zhang W, Zhang J, Wan X, Jiang Y, et al.: **Use of the XRCC2 promoter for in vivo cancer diagnosis and therapy**. *Cell Death Dis 2018 94* 2018, **9**:1–12.
Chen YH, Jones MJK, Yin Y, Crist SB, Colnaghi L, Sims RJ, Rothenberg E, Jallepalli PV, Huang TT: **ATR-mediated phosphorylation of FANCI regulates dormant origin firing in response to replication stress**. *Mol Cell* 2015, **58**:323.
Chen Z, Lin Y, Barbieri E, Burlingame S, Hicks J, Ludwig A, Shohet JM: **Mdm2 deficiency suppresses MYCN-Driven neuroblastoma tumorigenesis in vivo**. *Neoplasia* 2009, **11**:753–762.
Cheng AL, Hsu CH, Lin JK, Hsu MM, Ho YF, Shen TS, Ko JY, Lin JT, Lin BR, Ming-Shiang W, et al.: **Phase I clinical trial of curcumin, a chemopreventive agent, in patients with high-risk or pre-malignant lesions.** *Anticancer Res* 2001, **21**:2895–2900.
Cheung AY, Neyzari A: **Deep local hyperthermia for cancer therapy: external electromagnetic and ultrasound techniques.** *Cancer Res* 1984, **44**:4736s-4744s.

Cheung NK, Saarinen UM, Neely JE, Landmeier B, Donovan D, Coccia PF: **Monoclonal antibodies to a glycolipid antigen on human neuroblastoma cells.** *Cancer Res* 1985, **45**:2642–2649.
Cheung N-KV, Zhang J, Lu C, Parker M, Bahrami A, Tickoo SK, Heguy A, Pappo AS, Federico S, Dalton J, et al.: **Association of age at diagnosis and genetic mutations in patients with neuroblastoma.** *JAMA* 2012, **307**:1062–1071.
Chipumuro E, Marco E, Christensen CL, Kwiatkowski N, Zhang T, Hatheway CM, Abraham BJ, Sharma B, Yeung C, Altabef A, et al.: **CDK7 Inhibition Suppresses Super-Enhancer-Linked Oncogenic Transcription in MYCN-Driven Cancer**. *Cell* 2014, **159**:1126.
Chirnomas D, Toshiyasu T, de la Vega M, D'Andrea AD: **Chemosensitization to cisplatin by inhibitors of the Fanconi anemia/BRCA pathway**. *Mol Cancer Ther* 2006, **5**:952–961.
Ciccia A, Ling C, Coulthard R, Yan Z, Xue Y, Meetei AR, Laghmani EH, Joenje H, McDonald N, de Winter JP, et al.: **Identification of FAAP24, a Fanconi Anemia Core Complex Protein that Interacts with FANCM**. *Mol Cell* 2007, **25**:331–343.
Cimprich KA, Cortez D: **ATR: an essential regulator of genome integrity.** *Nat Rev Mol Cell Biol* 2008, **9**:616–627.
Clauson C, Schärer OD, Niedernhofer L: **Advances in understanding the complex mechanisms of DNA interstrand cross-link repair**. *Cold Spring Harb Perspect Biol* 2013, **5**.
Cobb JA, Schleker T, Rojas V, Bjergbaek L, Tercero JA, Gasser SM: **Replisome instability, fork collapse, and gross chromosomal rearrangements arise synergistically from Mec1 kinase and RecQ helicase mutations.** *Genes Dev* 2005, **19**:3055–3069.
Cognet M, Nougayrede A, Malan V, Callier P, Cretolle C, Faivre L, Genevieve D, Goldenberg A, Heron D, Mercier S, et al.: **Dissection of the MYCN locus in Feingold syndrome and isolated oesophageal atresia**. *Eur J Hum Genet 2011 195* 2011, **19**:602–606.
Cohen LE, Gordon JH, Popovsky EY, Gunawardene S, Duffey-Lind E, Lehmann LE, Diller LR: **Late effects in children treated with intensive multimodal therapy for high-risk neuroblastoma: high incidence of endocrine and growth problems**. *Bone Marrow Transplant* 2014, **49**:502–508.
Cohn SL, Pearson ADJ, London WB, Monclair T, Ambros PF, Brodeur GM, Faldum A, Hero B, Iehara T, Machin D, et al.: **The International Neuroblastoma Risk Group (INRG) classification system: An INRG task force report**. *J Clin Oncol* 2009, **27**:289–297.
Cole KA, Huggins J, Laquaglia M, Hulderman CE, Russell MR, Bosse K, Diskin SJ, Attiyeh EF, Sennett R, Norris G, et al.: **RNAi screen of the protein kinome identifies checkpoint kinase 1 (CHK1) as a therapeutic target in neuroblastoma.** *Proc Natl Acad Sci U S A* 2011, **108**:3336–3341.
Cole KA, Pal S, Kudgus RA, Ijaz H, Liu X, Minard CG, Pawel BR, Maris JM, Haas-Kogan DA, Voss SD, et al.: **Phase I Clinical Trial of the Wee1 inhibitor Adavosertib (AZD1775) with Irinotecan in Children with Relapsed Solid Tumors. A COG Phase 1 Consortium Report (ADVL1312)**. *Clin Cancer Res* 2020, **26**:1213.
Cole MD: **The MYC oncogene: its role in transformation and differentiation**. *https://doi.org/101146/annurev.ge20120186002045* 1986, **20**:361–384.
Cole WH, Everson TC: **Spontaneous regression of cancer: preliminary report.** *Ann Surg* 1956, **144**:366–383.
Colicchia V, Petroni M, Guarguaglini G, Sardina F, Sahún-Roncero M, Carbonari M, Ricci B, Heil C, Capalbo C, Belardinilli F, et al.: **PARP inhibitors enhance replication stress and cause mitotic catastrophe in MYCN-dependent neuroblastoma**. *Oncogene* 2017, **36**:4682–4691.
Collins NB, Wilson JB, Bush T, Thomashevski A, Roberts KJ, Jones NJ, Kupfer GM: **ATR-dependent phosphorylation of FANCA on serine 1449 after DNA damage is important for FA pathway function.** *Blood* 2009, **113**:2181–2190.
Collis SJ, Boulton SJ: **FANCM: fork pause, rewind and play**. *EMBO J* 2010, **29**:703.

Collis SJ, Ciccia A, Deans AJ, Hořejší Z, Martin JS, Maslen SL, Skehel JM, Elledge SJ, West SC, Boulton SJ: **FANCM and FAAP24 Function in ATR-Mediated Checkpoint Signaling Independently of the Fanconi Anemia Core Complex**. *Mol Cell* 2008, **32**:313–324.
Compostella A, Toffolutti T, Soloni P, Dall'Igna P, Carli M, Bisogno G: **Multiple synchronous tumors in a child with Fanconi anemia.** *J Pediatr Surg* 2010, **45**:e5-8.
Cornwell MJ, Thomson GJ, Coates J, Belotserkovskaya R, Waddell ID, Jackson SP, Galanty Y: **Small-Molecule Inhibition of UBE2T/FANCL-Mediated Ubiquitylation in the Fanconi Anemia Pathway**. *ACS Chem Biol* 2019, **14**:2148–2154.
Corvetta D, Chayka O, Gherardi S, D'Acunto CW, Cantilena S, Valli E, Piotrowska I, Perini G, Sala A: **Physical interaction between MYCN oncogene and polycomb repressive complex 2 (PRC2) in neuroblastoma: functional and therapeutic implications.** *J Biol Chem* 2013, **288**:8332–8341.
Cotterman R, Knoepfler PS: **N-Myc regulates expression of pluripotency genes in neuroblastoma including lif, klf2, klf4, and lin28b.** *PLoS One* 2009, **4**:e5799.
Cox D, Yuncken C, Spriggs A: **MINUTE CHROMATIN BODIES IN MALIGNANT TUMOURS OF CHILDHOOD**. *Lancet* 1965, **286**:55–58.
Cukras S, Lee E, Palumbo E, Benavidez P, Moldovan GL, Kee Y: **The USP1-UAF1 complex interacts with RAD51AP1 to promote homologous recombination repair**. *Cell Cycle* 2016, **15**:2636.
Cumming RC, Lightfoot J, Beard K, Youssoufian H, O'brien PJ, Buchwald M: **Fanconi anemia group C protein prevents apoptosis in hematopoietic cells through redox regulation of GSTP1**. *Nat Med 2001 77* 2001, **7**:814–820.
D'Aguanno S, D'Agnano I, De Canio M, Rossi C, Bernardini S, Federici G, Urbani A: **Shotgun proteomics and network analysis of neuroblastoma cell lines treated with curcumin**. *Mol Biosyst* 2012, **8**:1068–1077.
D'Alessandro G, Whelan DR, Howard SM, Vitelli V, Renaudin X, Adamowicz M, Iannelli F, Jones-Weinert CW, Lee MY, Matti V, et al.: **BRCA2 controls DNA:RNA hybrid level at DSBs by mediating RNase H2 recruitment**. *Nat Commun 2018 91* 2018, **9**:1–17.
D'Orazi G, Cecchinelli B, Bruno T, Manni I, Higashimoto Y, Saito S, Gostissa M, Coen S, Marchetti A, Del Sal G, et al.: **Homeodomain-interacting protein kinase-2 phosphorylates p53 at Ser 46 and mediates apoptosis**. *Nat Cell Biol 2001 41* 2001, **4**:11–19.
Dai C-H, Li J, Chen P, Jiang H-G, Wu M, Chen Y-C: **RNA interferences targeting the Fanconi anemia/BRCA pathway upstream genes reverse cisplatin resistance in drug-resistant lung cancer cells**. *J Biomed Sci* 2015, **22**:77.
Dai C-H, Wang Y, Chen P, Jiang Q, Lan T, Li M-Y, Su J-Y, Wu Y, Li J: **Suppression of the FA pathway combined with CHK1 inhibitor hypersensitize lung cancer cells to gemcitabine**. *Sci Rep* 2017, **7**:15031.
Dang CV: **MYC on the Path to Cancer**. *Cell* 2012, **149**:22.
Davidoff AM, Pence JC, Shorter NA, Iglehart JD, Marks JR: **Expression of p53 in human neuroblastoma- and neuroepithelioma-derived cell lines.** *Oncogene* 1992, **7**:127–133.
Davies SL, North PS, Hickson ID: **Role for BLM in replication-fork restart and suppression of origin firing after replicative stress**. *Nat Struct Mol Biol 2007 147* 2007, **14**:677–679.
Davis AC, Wims M, Spotts GD, Hann SR, Bradley A: **A null c-myc mutation causes lethality before 10.5 days of gestation in homozygotes and reduced fertility in heterozygous female mice.** *Genes Dev* 1993, **7**:671–682.
Daza-Martin M, Starowicz K, Jamshad M, Tye S, Ronson GE, MacKay HL, Chauhan AS, Walker AK, Stone HR, Beesley JFJ, et al.: **Isomerization of BRCA1–BARD1 promotes replication fork protection**. *Nature* 2019, doi:10.1038/s41586-019-1363-4.
De Brouwer S, De Preter K, Kumps C, Zabrocki P, Porcu M, Westerhout EM, Lakeman A, Vandesompele J, Hoebeeck J, Van Maerken T, et al.: **Meta-analysis of**

neuroblastomas reveals a skewed ALK mutation spectrum in tumors with MYCN amplification. *Clin Cancer Res* 2010, **16**:4353–4362.
De Oca RM, Andreassen PR, Margossian SP, Gregory RC, Taniguchi T, Wang XZ, Houghtaling S, Grompe M, D'Andrea AD: **Regulated interaction of the Fanconi anemia protein, FANCD2, with chromatin**. *Blood* 2005, **105**:1003–1009.
De Silva IU, McHugh PJ, Clingen PH, Hartley JA: **Defining the Roles of Nucleotide Excision Repair and Recombination in the Repair of DNA Interstrand Cross-Links in Mammalian Cells**. *Mol Cell Biol* 2000, **20**:7980.
De Winter JP, Léveillé F, Van Berkel CGM, Rooimans MA, Van Der Weel L, Steltenpool J, Demuth I, Morgan NV, Alon N, Bosnoyan-Collins L, et al.: **Isolation of a cDNA representing the Fanconi anemia complementation group E gene**. *Am J Hum Genet* 2000, **67**:1306–1308.
De Winter JP, Rooimans MA, Van Der Weel L, Van Berkel CGM, Alon N, Bosnoyan-Collins L, De Groot J, Zhi Y, Waisfisz Q, Pronk JC, et al.: **The Fanconi anaemia gene FANCF encodes a novel protein with homology to ROM**. *Nat Genet* 2000, **24**:15–16.
De Winter JP, Waisfisz Q, Rooimans MA, Van Berkel CGM, Bosnoyan-Collins L, Alon N, Carreau M, Bender O, Demuth I, Schindler D, et al.: **The Fanconi anaemia group G gene FANCG is identical with XRCC9**. *Nat Genet* 1998, **20**:281–283.
Deans AJ, West SC: **DNA interstrand crosslink repair and cancer.** *Nat Rev Cancer* 2011, **11**:467–480.
Deans AJ, West SC: **FANCM connects the genome instability disorders Bloom's Syndrome and Fanconi Anemia**. *Mol Cell* 2009, **36**:943–953.
Decaesteker B, Denecker G, Van Neste C, Dolman EM, Van Loocke W, Gartlgruber M, Nunes C, De Vloed F, Depuydt P, Verboom K, et al.: **TBX2 is a neuroblastoma core regulatory circuitry component enhancing MYCN/FOXM1 reactivation of DREAM targets.** *Nat Commun* 2018, **9**:4866.
Delehouzé C, Godl K, Loaëc N, Bruyère C, Desban N, Oumata N, Galons H, Roumeliotis TI, Giannopoulou EG, Grenet J, et al.: **CDK/CK1 inhibitors roscovitine and CR8 downregulate amplified MYCN in neuroblastoma cells**. *Oncogene 2014 3350* 2013, **33**:5675–5687.
Depuydt P, Boeva V, Hocking TD, Cannoodt R, Ambros IM, Ambros PF, Asgharzadeh S, Attiyeh EF, Combaret V, Defferrari R, et al.: **Genomic Amplifications and Distal 6q Loss: Novel Markers for Poor Survival in High-risk Neuroblastoma Patients**. *JNCI J Natl Cancer Inst* 2018, **110**:1084.
Di Giannatale A, Dias-Gastellier N, Devos A, Mc Hugh K, Boubaker A, Courbon F, Verschuur A, Ducassoul S, Malekzadeh K, Casanova M, et al.: **Phase II study of temozolomide in combination with topotecan (TOTEM) in relapsed or refractory neuroblastoma: a European Innovative Therapies for Children with Cancer-SIOP-European Neuroblastoma study**. *Eur J Cancer* 2014, **50**:170–177.
Di Giannatale A, Dias-Gastellier N, Devos A, Mc Hugh K, Boubaker A, Courbon F, Verschuur A, Ducassoul S, Malekzadeh K, Casanova M, et al.: **Phase II study of temozolomide in combination with topotecan (TOTEM) in relapsed or refractory neuroblastoma: A European Innovative Therapies for Children with Cancer-SIOP-European Neuroblastoma study**. *Eur J Cancer* 2014, **50**:170–177.
Di Micco R, Fumagalli M, Cicalese A, Piccinin S, Gasparini P, Luise C, Schurra C, Garre' M, Giovanni Nuciforo P, Bensimon A, et al.: **Oncogene-induced senescence is a DNA damage response triggered by DNA hyper-replication**. *Nature* 2006, **444**:638–642.
Domenech C, Maillard L, Rousseau A, Guidez F, Petit L, Pla M, Clay D, Guimiot F, Sanfilippo S, Jacques S, et al.: **Studies in an Early Development Window Unveils a Severe HSC Defect in both Murine and Human Fanconi Anemia**. *Stem Cell Reports* 2018, **11**:1075.
Dominguez-Sola D, Ying CY, Grandori C, Ruggiero L, Chen B, Li M, Galloway DA, Gu W, Gautier J, Dalla-Favera R: **Non-transcriptional control of DNA replication by c-Myc**. *Nature* 2007, **448**:445–451.

Dong R, Yang R, Zhan Y, Lai HD, Ye CJ, Yao XY, Luo WQ, Cheng XM, Miao JJ, Wang JF, et al.: **Single-Cell Characterization of Malignant Phenotypes and Developmental Trajectories of Adrenal Neuroblastoma**. *Cancer Cell* 2020, **38**:716-733.e6.

Dorsman JC, Levitus M, Rockx D, Rooimans MA, Oostra AB, Haitjema A, Bakker ST, Steltenpool J, Schuler D, Mohan S, et al.: **Identification of the Fanconi anemia complementation group I gene, FANCI**. *Cell Oncol* 2007, **29**:211–218.

Du J, Yan L, Torres R, Gong X, Bian H, Marugan C, Boehnke K, Baquero C, Hui YH, Chapman SC, et al.: **Aurora A–selective inhibitor LY3295668 leads to dominant mitotic arrest, apoptosis in cancer cells, and shows potent preclinical antitumor efficacy**. *Mol Cancer Ther* 2019, **18**:2207–2219.

Du J, Jiang L, Chen F, Hu H, Zhou M: **Cardiac Glycoside Ouabain Exerts Anticancer Activity via Downregulation of STAT3**. *Front Oncol* 2021, **11**:2565.

Du J, Shang J, Chen F, Zhang Y, Yin N, Xie T, Zhang H, Yu J, Liu F: **A CRISPR/Cas9-Based Screening for Non-Homologous End Joining Inhibitors Reveals Ouabain and Penfluridol as Radiosensitizers**. *Mol Cancer Ther* 2018, **17**:419–431.

Du W, Rani R, Sipple J, Schick J, Myers KC, Mehta P, Andreassen PR, Davies SM, Pang Q: **The FA pathway counteracts oxidative stress through selective protection of antioxidant defense gene promoters**. *Blood* 2012, **119**:4142.

DuBois SG, Kalika Y, Lukens JN, Brodeur GM, Seeger RC, Atkinson JB, Haase GM, Black CT, Perez C, Shimada H, et al.: **Metastatic sites in stage IV and IVS neuroblastoma correlate with age, tumor biology, and survival.** *J Pediatr Hematol Oncol* 1999, **21**:181–189.

DuBois SG, Geier E, Batra V, Yee SW, Neuhaus J, Segal M, Martinez D, Pawel B, Yanik G, Naranjo A, et al.: **Evaluation of Norepinephrine Transporter Expression and Metaiodobenzylguanidine Avidity in Neuroblastoma: A Report from the Children's Oncology Group**. *Int J Mol Imaging* 2012, **2012**:1–8.

DuBois SG, Kremer JD, De Wilde B, Jacobsen C, Aerts I, Mosse YP, Maris JM, Lithio A, Gosberg A, Banks CL, et al.: **A phase I study of Aurora kinase A inhibitor LY3295668 erbumine as a single agent and in combination in patients with relapsed/refractory neuroblastoma.** *J Clin Oncol* 2020, **38**:TPS10561–TPS10561.

DuBois SG, Mosse YP, Fox E, Kudgus RA, Reid JM, McGovern R, Groshen S, Bagatell R, Maris JM, Twist CJ, et al.: **Phase II trial of alisertib in combination with irinotecan and temozolomide for patients with relapsed or refractory neuroblastoma**. *Clin Cancer Res* 2018, **24**:6142–6149.

Dungwa JV, Uparkar U, May MT, Ramani P: **Angiogenin up-regulation correlates with adverse clinicopathological and biological factors, increased microvascular density and poor patient outcome in neuroblastomas**. *Histopathology* 2012, **60**:911–923.

Dunn J, Potter M, Rees A, Runger TM: **Activation of the Fanconi Anemia/BRCA Pathway and Recombination Repair in the Cellular Response to Solar Ultraviolet Light**. *Cancer Res* 2006, **66**:11140–11147.

Duquette ML, Zhu Q, Taylor ER, Tsay AJ, Shi LZ, Berns MW, McGowan CH: **CtIP Is Required to Initiate Replication-Dependent Interstrand Crosslink Repair**. *PLoS Genet* 2012, **8**:1003050.

Durbin AD, Wang T, Wimalasena VK, Zimmerman MW, Li D, Dharia NV, Mariani L, Shendy NAM, Nance S, Patel AG, et al.: **EP300 Selectively Controls the Enhancer Landscape of MYCN-Amplified Neuroblastoma**. *Cancer Discov* 2022, **12**:730–751.

Durbin AD, Zimmerman MW, Dharia NV, Abraham BJ, Iniguez AB, Weichert-Leahey N, He S, Krill-Burger JM, Root DE, Vazquez F, et al.: **Selective gene dependencies in MYCN-amplified neuroblastoma include the core transcriptional regulatory circuitry**. *Nat Genet* 2018, **50**:1240–1246.

Dzieran J, Rodriguez Garcia A, Westermark UK, Henley AB, Eyre Sánchez E, Träger C, Johansson HJ, Lehtiö J, Arsenian-Henriksson M: **MYCN-amplified neuroblastoma maintains an aggressive and undifferentiated phenotype by deregulation of estrogen and NGF signaling.** *Proc Natl Acad Sci U S A* 2018, **115**:E1229–E1238.

Eastman, A. (1986). **Reevaluation of Interaction of cis-Dichloro(ethylenediamine)platinum(II) with DNA.** *Biochemistry*, **25**:3912–3915.
Eccles LJ, Bell AC, Powell SN: **Inhibition of non-homologous end joining in Fanconi Anemia cells results in rescue of survival after interstrand crosslinks but sensitization to replication associated double-strand breaks**. *DNA Repair (Amst)* 2018, **64**:1.
Edwards SL, Brough R, Lord CJ, Natrajan R, Vatcheva R, Levine DA, Boyd J, Reis-Filho JS, Ashworth A: **Resistance to therapy caused by intragenic deletion in BRCA2**. *Nature* 2008, **451**:1111–1115.
Engeland K: **Cell cycle arrest through indirect transcriptional repression by p53: I have a DREAM**. *Cell Death Differ* 2018, **25**:114.
Fagerholm R, Sprott K, Heikkinen T, Bartkova J, Heikkilä P, Aittomäki K, Bartek J, Weaver D, Nevanlinna H, Blomqvist C: **Overabundant FANCD2, alone and combined with NQO1, is a sensitive marker of adverse prognosis in breast cancer**. *Ann Oncol Off J Eur Soc Med Oncol* 2013, **24**:2780–2785.
Fajardo NB, Taraviras S, Lygerou Z: **Fanconi anemia proteins and genome fragility: unraveling replication defects for cancer therapy**. *Trends in Cancer* 2022, **8**:467–481.
Fan Q, Zhang F, Barrett B, Ren K, Andreassen PR: **A role for monoubiquitinated FANCD2 at telomeres in ALT cells**. *Nucleic Acids Res* 2009, **37**:1740.
Farrell DP, Anishchenko I, Shakeel S, Lauko A, Passmore LA, Baker D, DiMaio F: **Deep learning enables the atomic structure determination of the Fanconi Anemia core complex from cryoEM**. *IUCrJ* 2020, **7**:881–892.
Federico SM, McCarville MB, Shulkin BL, Sondel PM, Hank JA, Hutson P, Meagher M, Shafer A, Ng CY, Leung W, et al.: **A Pilot Trial of Humanized Anti-GD2 Monoclonal Antibody (hu14.18K322A) with Chemotherapy and Natural Killer Cells in Children with Recurrent/Refractory Neuroblastoma**. *Clin Cancer Res* 2017, **23**:6441–6449.
Felsher DW, Bishop JM: **Transient excess of MYC activity can elicit genomic instability and tumorigenesis.** *Proc Natl Acad Sci U S A* 1999, **96**:3940–3944.
Feng L, Jin F: **Expression and prognostic significance of Fanconi anemia group D2 protein and breast cancer type 1 susceptibility protein in familial and sporadic breast cancer**. *Oncol Lett* 2019, **17**:3687.
Fernandes P, Miotto B, Saint-Ruf C, Said M, Barra V, Nähse V, Ravera S, Cappelli E, Naim V: **FANCD2 modulates the mitochondrial stress response to prevent common fragile site instability**. *Commun Biol* 2021, **4**.
Fiesco-Roa MO, Giri N, McReynolds LJ, Best AF, Alter BP: **Genotype-Phenotype Associations in Fanconi Anemia: A Literature Review**. *Blood Rev* 2019, **37**:100589.
Fletcher S, Prochownik EV: **Small-molecule inhibitors of the Myc oncoprotein**. *Biochim Biophys Acta* 2015, **1849**:525–543.
Fonseka P, Gangoda L, Pathan M, Angela DG, Mathivanan S: **Combinatorial treatment of curcumin or silibinin with doxorubicin sensitises high-risk neuroblastoma**. *J Cancer Metastasis Treat* 2020, **6**:7.
Foo TK, Xia B: **BRCA1-Dependent and Independent Recruitment of PALB2-BRCA2-RAD51 in the DNA Damage Response and Cancer**. *Cancer Res* 2022, **82**.
Foster JH, Voss SD, Hall DC, Minard CG, Balis FM, Wilner K, Berg SL, Fox E, Adamson PC, Blaney SM, et al.: **Activity of Crizotinib in Patients with ALK-aberrant Relapsed/Refractory Neuroblastoma: A Children's Oncology Group Study (ADVL0912)**. *Clin Cancer Res* 2021, **27**:3543.
Fredlund E, Ringnér M, Maris JM, Påhlman S: **High Myc pathway activity and low stage of neuronal differentiation associate with poor outcome in neuroblastoma**. *Proc Natl Acad Sci U S A* 2008, **105**:14094.
Freudlsperger C, Greten J, Schumacher U: **Curcumin Induces Apoptosis in Human Neuroblastoma Cells via Inhibition of NFκB**. *Anticancer Res* 2008, **28**:209–214.
Friedman DL, Kadan-Lottick NS, Whitton J, Mertens AC, Yasui Y, Liu Y, Meadows AT, Robison LL, Strong LC: **Increased Risk of Cancer among Siblings of Long-term**

Childhood Cancer Survivors: A Report from the Childhood Cancer Survivor Study. *Cancer Epidemiol Biomarkers Prev* 2005, **14**:1922–1927.
Friedman HS, Johnson SP, Dong Q, Schold SC, Rasheed BK, Bigner SH, Ali-Osman F, Dolan E, Colvin OM, Houghton P, et al.: **Methylator resistance mediated by mismatch repair deficiency in a glioblastoma multiforme xenograft.** *Cancer Res* 1997, **57**:2933–2936.
Fu D, Calvo JA, Samson LD: **Balancing repair and tolerance of DNA damage caused by alkylating agents**. *Nat Rev Cancer* 2012, **12**:104–120.
Fujita T, Igarashi J, Okawa ER, Gotoh T, Manne J, Kolla V, Kim J, Zhao H, Pawel BR, London WB, et al.: **CHD5, a Tumor Suppressor Gene Deleted From 1p36.31 in Neuroblastomas**. *JNCI J Natl Cancer Inst* 2008, **100**:940.
Fulda S, Lutz W, Schwab M, Debatin KM: **MycN sensitizes neuroblastoma cells for drug-induced apoptosis**. *Oncogene 1999 187* 1999, **18**:1479–1486.
Furlan A, Dyachuk V, Kastriti ME, Calvo-Enrique L, Abdo H, Hadjab S, Chontorotzea T, Akkuratova N, Usoskin D, Kamenev D, et al.: **Multipotent peripheral glial cells generate neuroendocrine cells of the adrenal medulla.** *Science* 2017, **357**.
Furman WL: **Monoclonal Antibody Therapies for High Risk Neuroblastoma**. *Biologics* 2021, **15**:205.
Furman WL, McCarville B, Shulkin BL, Davidoff A, Krasin M, Hsu CW, Pan H, Wu J, Brennan R, Bishop MW, et al.: **Improved Outcome in Children With Newly Diagnosed High-Risk Neuroblastoma Treated With Chemoimmunotherapy: Updated Results of a Phase II Study Using hu14.18K322A**. *J Clin Oncol* 2022, **40**:335–344.
Gallo S, Vanstone CA, Weiler HA: **Normative Data for Bone Mass in Healthy Term Infants from Birth to 1 Year of Age**. *J Osteoporos* 2012, **2012**.
Garaventa A, Poetschger U, Valteau-Couanet D, Luksch R, Castel V, Elliott M, Ash S, Chan GCF, Laureys G, Beck-Popovic M, et al.: **Randomized Trial of Two Induction Therapy Regimens for High-Risk Neuroblastoma: HR-NBL1.5 International Society of Pediatric Oncology European Neuroblastoma Group Study**. *J Clin Oncol* 2021, **39**:2552–2563.
Garaycoechea JI, Crossan GP, Langevin F, Daly M, Arends MJ, Patel KJ: **Genotoxic consequences of endogenous aldehydes on mouse haematopoietic stem cell function**. *Nature* 2012, **489**:571–575.
Garaycoechea JI, Crossan GP, Langevin F, Mulderrig L, Louzada S, Yang F, Guilbaud G, Park N, Roerink S, Nik-Zainal S, et al.: **Alcohol and endogenous aldehydes damage chromosomes and mutate stem cells**. *Nature* 2018, **553**:171.
Garaycoechea JI, Patel KJ: **Why does the bone marrow fail in Fanconi anemia?** *Blood* 2014, **123**:26–34.
Garcia-Higuera I, Taniguchi T, Ganesan S, Meyn MS, Timmers C, Hejna J, Grompe M, D'Andrea AD: **Interaction of the Fanconi anemia proteins and BRCA1 in a common pathway.** *Mol Cell* 2001, **7**:249–262.
García-Rubio ML, Pérez-Calero C, Barroso SI, Tumini E, Herrera-Moyano E, Rosado IV, Aguilera A: **The Fanconi Anemia Pathway Protects Genome Integrity from R-loops**. *PLOS Genet* 2015, **11**:e1005674.
Gari K, Décaillet C, Stasiak AZ, Stasiak A, Constantinou A: **The Fanconi Anemia Protein FANCM Can Promote Branch Migration of Holliday Junctions and Replication Forks**. *Mol Cell* 2008, **29**:141–148.
Gartlgruber M, Sharma AK, Quintero A, Dreidax D, Jansky S, Park YG, Kreth S, Meder J, Doncevic D, Saary P, et al.: **Super enhancers define regulatory subtypes and cell identity in neuroblastoma**. *Nat cancer* 2021, **2**:114–128.
Gatta G, Capocaccia R, Coleman MP, Gloeckler Ries LA, Berrino F: **Childhood cancer survival in Europe and the United States**. *Cancer* 2002, **95**:1767–1772.
Geoerger B, Bourdeaut F, DuBois SG, Fischer M, Geller JI, Gottardo NG, Marabelle A, Pearson ADJ, Modak S, Cash T, et al.: **A phase I study of the CDK4/6 inhibitor ribociclib (LEE011) in pediatric patients with malignant rhabdoid tumors, neuroblastoma, and other solid tumors**. *Clin Cancer Res* 2017, **23**:2433–2441.

George RE, London WB, Cohn SL, Maris JM, Kretschmar C, Diller L, Brodeur GM, Castleberry RP, Look AT: **Hyperdiploidy plus nonamplified MYCN confers a favorable prognosis in children 12 to 18 months old with disseminated neuroblastoma: A Pediatric Oncology Group study**. *J Clin Oncol* 2005, **23**:6466–6473.
George RE, Sanda T, Hanna M, Fröhling S, Luther W, Zhang J, Ahn Y, Zhou W, London WB, McGrady P, et al.: **Activating mutations in ALK provide a therapeutic target in neuroblastoma**. *Nature* 2008, **455**:975–978.
Gera N, Yang A, Holtzman TS, Lee SX, Wong ET, Swanson KD: **Tumor Treating Fields Perturb the Localization of Septins and Cause Aberrant Mitotic Exit**. *PLoS One* 2015, **10**.
German J, Schonberg S, Caskie S, Warburton D, Falk C, Ray J: **A Test for Fanconi's Anemia**. *Blood* 1987, **69**:1637–1641.
Gershon TR, Oppenheimer O, Chin SS, Gerald WL: **Temporally regulated neural crest transcription factors distinguish neuroectodermal tumors of varying malignancy and differentiation.** *Neoplasia* 2005, **7**:575–584.
Geurten C, Geurten M, Hoyoux C, Lebrethon MC: **Endocrine consequences of neuroblastoma treatment in children: 20 years' experience of a single center**. *J Pediatr Endocrinol Metab* 2019, **32**:347–354.
Ghasemi F, Shafiee M, Banikazemi Z, Pourhanifeh MH, Khanbabaei H, Shamshirian A, Amiri Moghadam S, ArefNezhad R, Sahebkar A, Avan A, et al.: **Curcumin inhibits NF-kB and Wnt/β-catenin pathways in cervical cancer cells**. *Pathol - Res Pract* 2019, **215**:152556.
Ghosh A, Maiti GP, Bandopadhyay MN, Chakraborty J, Biswas J, Roychoudhury S, Panda CK: **Inactivation of 9q22.3 tumor suppressor genes predict outcome for patients with head and neck squamous cell carcinoma.** *Anticancer Res* 2013, **33**:1215–1220.
Giladi M, Munster M, Schneiderman RS, Voloshin T, Porat Y, Blat R, Zielinska-Chomej K, Hååg P, Bomzon Z, Kirson ED, et al.: **Tumor treating fields (TTFields) delay DNA damage repair following radiation treatment of glioma cells**. *Radiat Oncol* 2017, **12**.
Giladi M, Schneiderman RS, Porat Y, Munster M, Itzhaki A, Mordechovich D, Cahal S, Kirson ED, Weinberg U, Palti Y: **Mitotic disruption and reduced clonogenicity of pancreatic cancer cells in vitro and in vivo by tumor treating fields**. *Pancreatology* 2014, **14**:54–63.
Giladi M, Schneiderman RS, Voloshin T, Porat Y, Munster M, Blat R, Sherbo S, Bomzon Z, Urman N, Itzhaki A, et al.: **Mitotic Spindle Disruption by Alternating Electric Fields Leads to Improper Chromosome Segregation and Mitotic Catastrophe in Cancer Cells**. *Sci Rep* 2015, **5**.
Giladi M, Weinberg U, Schneiderman RS, Porat Y, Munster M, Voloshin T, Blatt R, Cahal S, Itzhaki A, Onn A, et al.: **Alternating electric fields (tumor-treating fields therapy) can improve chemotherapy treatment efficacy in non-small cell lung cancer both in vitro and in vivo**. *Semin Oncol* 2014, **41 Suppl 6**:S35–S41.
Gogolin S, Ehemann V, Becker G, Brueckner LM, Dreidax D, Bannert S, Nolte I, Savelyeva L, Bell E, Westermann F: **CDK4 inhibition restores G(1)-S arrest in MYCN-amplified neuroblastoma cells in the context of doxorubicin-induced DNA damage.** *Cell Cycle* 2013, **12**:1091–1104.
Goldman SC, Chen CY, Lansing TJ, Gilmer TM, Kastan MB: **The p53 signal transduction pathway is intact in human neuroblastoma despite cytoplasmic localization.** *Am J Pathol* 1996, **148**:1381.
Goldman S, Margol A, Hwang EI, Tanaka K, Suchorska B, Crawford JR, Kesari S: **Safety of Tumor Treating Fields (TTFields) therapy in pediatric patients with malignant brain tumors: Post-marketing surveillance data**. *Front Oncol* 2022, **12**.
Gómez-Casares MT, García-Alegria E, López-Jorge CE, Ferrándiz N, Blanco R, Alvarez S, Vaqué JP, Bretones G, Caraballo JM, Sánchez-Bailón P, et al.: **MYC antagonizes the differentiation induced by imatinib in chronic myeloid leukemia cells through downregulation of p27KIP1**. *Oncogene* 2013, **32**:2239–2246.

Gomez-Roman N, Grandori C, Eisenman RN, White RJ: **Direct activation of RNA polymerase III transcription by c-Myc**. *Nat 2003 4216920* 2003, **421**:290–294.
Gorgoulis VG, Vassiliou L-VF, Karakaidos P, Zacharatos P, Kotsinas A, Liloglou T, Venere M, DiTullio RA, Kastrinakis NG, Levy B, et al.: **Activation of the DNA damage checkpoint and genomic instability in human precancerous lesions**. *Nature* 2005, **434**:907–913.
Gossen M, Freundlieb S, Bender G, Muller G, Hillen W, Bujard H: **Transcriptional activation by tetracyclines in mammalian cells**. *Science (80-)* 1995, **268**:1766–1769.
Gossen M, Bujard H: **Tight control of gene expression in mammalian cells by tetracycline-responsive promoters.** *Proc Natl Acad Sci* 1992, **89**:5547–5551.
Grandori C, Gomez-Roman N, Felton-Edkins ZA, Ngouenet C, Galloway DA, Eisenman RN, White RJ: **c-Myc binds to human ribosomal DNA and stimulates transcription of rRNA genes by RNA polymerase I**. *Nat Cell Biol 2005 73* 2005, **7**:311–318.
Green AL, Mulcahy Levy JM, Vibhakar R, Hemenway M, Madden J, Foreman N, Dorris K: **Tumor treating fields in pediatric high-grade glioma.** *Childs Nerv Syst* 2017, **33**:1043–1045.
Grossman R, Limon D, Bokstein F, Harosh CB, Ram Z: **Abstract CT203: Randomized Phase II trial of Tumor Treating Fields plus radiation therapy plus temozolamide compared to radiation therapy plus temozolomide in patients with newly diagnosed glioblastoma**. *Cancer Res* 2019, **79**:CT203–CT203.
Gu L, Zhang H, He J, Li J, Huang M, Zhou M: **MDM2 regulates MYCN mRNA stabilization and translation in human neuroblastoma cells.** *Oncogene* 2012, **31**:1342–1353.
Gu L, Chu P, Lingeman R, McDaniel H, Kechichian S, Hickey RJ, Liu Z, Yuan Y-C, Sandoval JA, Fields GB, et al.: **The Mechanism by Which MYCN Amplification Confers an Enhanced Sensitivity to a PCNA-Derived Cell Permeable Peptide in Neuroblastoma Cells.** *EBioMedicine* 2015, **2**:1923–1931.
Gu L, Smith S, Li C, Hickey RJ, Stark JM, Fields GB, Lang WH, Sandoval JA, Malkas LH: **A PCNA-Derived Cell Permeable Peptide Selectively Inhibits Neuroblastoma Cell Growth**. *PLoS One* 2014, **9**:94773.
Guerra L, Albihn A, Tronnersjö S, Yan Q, Guidi R, Stenerlöw B, Sterzenbach T, Josenhans C, Fox JG, Schauer DB, et al.: **Myc is required for activation of the ATM-dependent checkpoints in response to DNA damage.** *PLoS One* 2010, **5**:e8924.
Guglielmi L, Cinnella C, Nardella M, Maresca G, Valentini A, Mercanti D, Felsani A, D'Agnano I: **MYCN gene expression is required for the onset of the differentiation programme in neuroblastoma cells**. *Cell Death Dis* 2014, **5**:e1081.
Guo C, Sonoda E, Tang TS, Parker JL, Bielen AB, Takeda S, Ulrich HD, Friedberg EC: **REV1 protein interacts with PCNA: significance of the REV1 BRCT domain in vitro and in vivo**. *Mol Cell* 2006, **23**:265–271.
Guo C, White PS, Weiss MJ, Hogarty MD, Thompson PM, Stram DO, Gerbing R, Matthay KK, Seeger RC, Brodeur GM, et al.: **Allelic deletion at 11q23 is common in MYCN single copy neuroblastomas**. *Oncogene* 1999, **18**:4948–4957.
Gurney JG, Tersak JM, Ness KK, Landier W, Matthay KK, Schmidt ML: **Hearing loss, quality of life, and academic problems in long-term neuroblastoma survivors: a report from the Children's Oncology Group**. *Pediatrics* 2007, **120**.
Gustafson WC, Meyerowitz JG, Nekritz EA, Chen J, Benes C, Charron E, Simonds EF, Seeger R, Matthay KK, Hertz NT, et al.: **Drugging MYCN through an allosteric transition in Aurora Kinase A**. *Cancer Cell* 2014, **26**:414.
Haas-Kogan DA, Swift PS, Selch M, Haase GM, Seeger RC, Gerbing RB, Stram DO, Matthay KK: **Impact of radiotherapy for high-risk neuroblastoma: A Children's Cancer Group study**. *Int J Radiat Oncol Biol Phys* 2003, **56**:28–39.
Hackl H, Rommer A, Konrad TA, Nassimbeni C, Wieser R: **Tetracycline Regulator Expression Alters the Transcriptional Program of Mammalian Cells**. *PLoS One* 2010, **5**.

Hahn AD, Malkus A, Kammerman J, Higano N, Walkup L, Woods J, Fain SB: **"Characterization of R2* and Tissue Density in the Human Lung: Application to Neonatal Imaging in the Intensive Care Unit."** *Magn Reson Med* 2020, **84**:920.
Hallett RM, Seong ABK, Kaplan DR, Irwin MS: **Transcript signatures that predict outcome and identify targetable pathways in MYCN-amplified neuroblastoma.** *Mol Oncol* 2016, **10**:1461–1472.
Hamperl S, Bocek MJ, Saldivar JC, Swigut T, Cimprich KA: **Transcription-replication conflict orientation modulates R-loop levels and activates distinct DNA damage responses**. *Cell* 2017, **170**:774.
Hanada K, Budzowska M, Modesti M, Maas A, Wyman C, Essers J, Kanaar R: **The structure-specific endonuclease Mus81–Eme1 promotes conversion of interstrand DNA crosslinks into double-strands breaks**. *EMBO J* 2006, **25**:4921.
Hansford LM, Thomas WD, Keating JM, Burkhart CA, Peaston AE, Norris MD, Haber M, Armati PJ, Weiss WA, Marshall GM: **Mechanisms of embryonal tumor initiation: Distinct roles for MycN expression and MYCN amplification**. *Proc Natl Acad Sci U S A* 2004, **101**:12664.
Harenza JL, Diamond MA, Adams RN, Song MM, Davidson HL, Hart LS, Dent MH, Fortina P, Reynolds CP, Maris JM: **Transcriptomic profiling of 39 commonly-used neuroblastoma cell lines**. *Sci Data* 2017, **4**:170033.
Hasan MK, Nafady A, Takatori A, Kishida S, Ohira M, Suenaga Y, Hossain S, Akter J, Ogura A, Nakamura Y, et al.: **ALK is a MYCN target gene and regulates cell migration and invasion in neuroblastoma**. *Sci Rep* 2013, **3**:3450.
Hatchi E, Skourti-Stathaki K, Ventz S, Pinello L, Yen A, Kamieniarz-Gdula K, Dimitrov S, Pathania S, McKinney KM, Eaton ML, et al.: **BRCA1 Recruitment to Transcriptional Pause Sites Is Required for R-Loop-Driven DNA Damage Repair**. *Mol Cell* 2015, **57**:636.
Hatton BA, Knoepfler PS, Kenney AM, Rowitch DH, de Alborán IM, Olson JM, Eisenman RN: **N-myc Is an Essential Downstream Effector of Shh Signaling during both Normal and Neoplastic Cerebellar Growth**. *Cancer Res* 2006, **66**:8655–8661.
Hatzi E, Breit S, Zoephel A, Ashman K, Tontsch U, Ahorn H, Murphy C, Schweigerer L, Fotsis T: **MYCN oncogene and angiogenesis: down-regulation of endothelial growth inhibitors in human neuroblastoma cells. Purification, structural, and functional characterization.** *Adv Exp Med Biol* 2000, **476**:239–248.
Hatzi E, Murphy C, Zoephel A, Ahorn H, Tontsch U, Bamberger A-M, Yamauchi-Takihara K, Schweigerer L, Fotsis T: **N-myc oncogene overexpression down-regulates leukemia inhibitory factor in neuroblastoma.** *Eur J Biochem* 2002, **269**:3732–3741.
Hatzi E, Murphy C, Zoephel A, Rasmussen H, Morbidelli L, Ahorn H, Kunisada K, Tontsch U, Klenk M, Yamauchi-Takihara K, et al.: **N-myc oncogene overexpression down-regulates IL-6; evidence that IL-6 inhibits angiogenesis and suppresses neuroblastoma tumor growth**. *Oncogene* 2002, **21**:3552–3561.
He J, Gu L, Zhang H, Zhou M: **Crosstalk between MYCN and MDM2-p53 signal pathways regulates tumor cell growth and apoptosis in neuroblastoma**. *Cell Cycle* 2011, **10**:2994.
Helbling-Leclerc A, Dessarps-Freichey F, Evrard C, Rosselli F: **Fanconi anemia proteins counteract the implementation of the oncogene-induced senescence program**. *Sci Rep* 2019, **9**.
Helmsauer K, Valieva ME, Ali S, Chamorro González R, Schöpflin R, Röefzaad C, Bei Y, Dorado Garcia H, Rodriguez-Fos E, Puiggròs M, et al.: **Enhancer hijacking determines extrachromosomal circular MYCN amplicon architecture in neuroblastoma**. *Nat Commun 2020 111* 2020, **11**:1–12.
Henrich K-O, Schwab M, Westermann F: **p36 Tumor Suppression-A Matter of Dosage?** 2012, doi:10.1158/0008-5472.CAN-12-2230.
Henssen A, Althoff K, Odersky A, Beckers A, Koche R, Speleman F, Schäfers S, Bell E, Nortmeyer M, Westermann F, et al.: **Targeting MYCN-driven transcription by BET-bromodomain inhibition**. *Clin Cancer Res* 2016, **22**:2470–2781.

Hero B, Simon T, Spitz R, Ernestus K, Gnekow AK, Scheel-Walter H-G, Schwabe D, Schilling FH, Benz-Bohm G, Berthold F: **Localized Infant Neuroblastomas Often Show Spontaneous Regression: Results of the Prospective Trials NB95-S and NB97**. *J Clin Oncol* 2008, **26**:1504–1510.

Herold S, Kalb J, Büchel G, Ade CP, Baluapuri A, Xu J, Koster J, Solvie D, Carstensen A, Klotz C, et al.: **Recruitment of BRCA1 limits MYCN-driven accumulation of stalled RNA polymerase**. *Nature* 2019, **567**:545–549.

Heukamp LC, Thor T, Schramm A, De Preter K, Kumps C, De Wilde B, Odersky A, Peifer M, Lindner S, Spruessel A, et al.: **Targeted expression of mutated ALK induces neuroblastoma in transgenic mice**. *Sci Transl Med* 2012, **4**.

Higgins NP, Kato K, Strauss B: **A model for replication repair in mammalian cells**. *J Mol Biol* 1976, **101**:417–425.

Hira A, Yoshida K, Sato K, Okuno Y, Shiraishi Y, Chiba K, Tanaka H, Miyano S, Shimamoto A, Tahara H, et al.: **Mutations in the gene encoding the E2 conjugating enzyme UBE2T cause Fanconi anemia**. *Am J Hum Genet* 2015, **96**:1001–1007.

Hiyoshi H, Abdelhady S, Segerström L, Sveinbjörnsson B, Nuriya M, Lundgren TK, Desfrere L, Miyakawa A, Yasui M, Kogner P, et al.: **Quiescence and γH2AX in neuroblastoma are regulated by ouabain/Na,K-ATPase**. *Br J Cancer* 2012, **106**:1807.

Hodson C, Purkiss A, Miles JA, Walden H: **Structure of the Human FANCL RING-Ube2T Complex Reveals Determinants of Cognate E3-E2 Selection**. *Struct England1993)* 2014, **22**:337.

Hogarty MD, Norris MD, Davis K, Liu X, Evageliou NF, Hayes CS, Pawel B, Guo R, Zhao H, Sekyere E, et al.: **ODC1 is a critical determinant of MYCN oncogenesis and a therapeutic target in neuroblastoma**. *Cancer Res* 2008, **68**:9735–9745.

Holland PM, Abramson RD, Watson R, Gelfand DH: *Detection of specific polymerase chain reaction product by utilizing the 5'-> 3' exonuclease activity of Thermus aquaticus DNA polymerase*. 1991.

Hölzel M, van Diest PJ, Bier P, Wallisch M, Hoatlin ME, Joenje H, de Winter JP: **FANCD2 protein is expressed in proliferating cells of human tissues that are cancer-prone in Fanconi anaemia**. *J Pathol* 2003, **201**:198–203.

Hoskins EE, Gunawardena RW, Habash KB, Wise-Draper TM, Jansen M, Knudsen ES, Wells SI: **Coordinate regulation of Fanconi anemia gene expression occurs through the Rb/E2F pathway**. *Oncogene* 2008, **27**:4798–4808.

Hossain MS, Ozaki T, Wang H, Nakagawa A, Takenobu H, Ohira M, Kamijo T, Nakagawara A: **N-MYC promotes cell proliferation through a direct transactivation of neuronal leucine-rich repeat protein-1 (NLRR1) gene in neuroblastoma**. *Oncogene* 2008, **27**:6075–6082.

Houghtaling S, Timmers C, Noll M, Finegold MJ, Jones SN, Meyn MS, Grompe M: **Epithelial cancer in Fanconi anemia complementation group D2 (Fancd2) knockout mice.** *Genes Dev* 2003, **17**:2021–2035.

Howlett NG, Harney JA, Rego MA, Kolling IV FW, Glover TW: **Functional interaction between the fanconi anemia D2 protein and proliferating cell nuclear antigen (PCNA) via a conserved putative PCNA interaction motif**. *J Biol Chem* 2009, **284**:28935–28942.

Howlett NG, Taniguchi T, Durkin SG, D'Andrea AD, Glover TW: **The Fanconi anemia pathway is required for the DNA replication stress response and for the regulation of common fragile site stability**. *Hum Mol Genet* 2005, **14**:693–701.

Howlett NG, Taniguchi T, Olson S, Cox B, Waisfisz Q, De Die-Smulders C, Persky N, Grompe M, Joenje H, Pals G, et al.: **Biallelic inactivation of BRCA2 in Fanconi anemia**. *Science (80-)* 2002, **297**:606–609.

Hu A, Huang JJ, Zhang JF, Dai WJ, Li RL, Lu ZY, Duan JL, Li JP, Chen XP, Fan JP, et al.: **Curcumin induces G2/M cell cycle arrest and apoptosis of head and neck squamous cell carcinoma in vitro and in vivo through ATM/Chk2/p53-dependent pathway**. *Oncotarget* 2017, **8**:50747.

Hu H, Du L, Nagabayashi G, Seeger RC, Gatti RA: **ATM is down-regulated by N-Myc-regulated microRNA-421**. *Proc Natl Acad Sci* 2010, **107**:1506–1511.
Huang F, Motlekar NA, Burgwin CM, Napper AD, Diamond SL, Mazin AV: **Identification of specific inhibitors of human RAD51 recombinase using high-throughput screening**. *ACS Chem Biol* 2011, **6**:628.
Huang L, He X, Zuo X: **The Effect and Mechanism of Curcumin Combined with Carboplatin Chemotherapy Promoting on Apoptosis of Lung Cancer HCC827 Cells**. *J Immunol Res* 2022, **2022**.
Huang M, Weiss WA: **Neuroblastoma and MYCN.** *Cold Spring Harb Perspect Med* 2013, **3**:a014415.
Huang R, Cheung N-KV, Vider J, Cheung IY, Gerald WL, Tickoo SK, Holland EC, Blasberg RG: **MYCN and MYC regulate tumor proliferation and tumorigenesis directly through BMI1 in human neuroblastomas**. *FASEB J* 2011, **25**:4138.
Huang Y, Leung JWC, Lowery M, Matsushita N, Wang Y, Shen X, Huong D, Takata M, Chen J, Li L: **Modularized Functions of the Fanconi Anemia Core Complex**. *Cell Rep* 2014, **7**:1849.
Infarinato NR, Park JH, Krytska K, Ryles HT, Sano R, Szigety KM, Li Y, Zou HY, Lee NV, Smeal T, et al.: **The ALK/ROS1 Inhibitor PF-06463922 Overcomes Primary Resistance to Crizotinib in ALK-Driven Neuroblastoma**. *Cancer Discov* 2016, **6**:96–107.
Irwin MS, Naranjo A, Zhang FF, Cohn SL, London WB, Gastier-Foster JM, Ramirez NC, Pfau R, Reshmi S, Wagner E, et al.: **Revised Neuroblastoma Risk Classification System: A Report From the Children's Oncology Group**. *J Clin Oncol* 2021, **39**:3229–3241.
Isaacs JS, Hardman R, Carman TA, Barrett JC, Weissman BE: **Differential subcellular p53 localization and function in N- and S-type neuroblastoma cell lines.** *Cell Growth Differ* 1998, **9**:545–555.
Ishiai M, Kitao H, Smogorzewska A, Tomida J, Kinomura A, Uchida E, Saberi A, Kinoshita E, Kinoshita-Kikuta E, Koike T, et al.: **FANCI phosphorylation functions as a molecular switch to turn on the Fanconi anemia pathway**. *Nat Struct Mol Biol* 2008, **15**:1138–1146.
Izumi H, Kaneko Y: **Evidence of asymmetric cell division and centrosome inheritance in human neuroblastoma cells.** *Proc Natl Acad Sci U S A* 2012, **109**:18048–18053.
Jaber S, Toufektchan E, Lejour V, Bardot B, Toledo F: **p53 downregulates the Fanconi anaemia DNA repair pathway**. *Nat Commun* 2016, **7**:11091.
Jacquemont C, Simon JA, D'Andrea AD, Taniguchi T: **Non-specific chemical inhibition of the Fanconi anemia pathway sensitizes cancer cells to cisplatin**. *Mol Cancer* 2012, **11**:26.
Jain M, Arvanitis C, Chu K, Dewey W, Leonhardt E, Trinh M, Sundberg CD, Bishop JM, Felsher DW: **Sustained loss of a neoplastic phenotype by brief inactivation of MYC**. *Science (80-)* 2002, **297**:102–104.
Jakobovits A, Schwab M, Bishop JM, Martin GR: **Expression of N-myc in teratocarcinoma stem cells and mouse embryos**. *Nat 1985 3186042* 1985, **318**:188–191.
Janoueix-Lerosey I, Schleiermacher G, Michels E, Mosseri V, Ribeiro A, Lequin D, Vermeulen J, Couturier J, Peuchmaur M, Valent A, et al.: **Overall genomic pattern is a predictor of outcome in neuroblastoma**. *J Clin Oncol* 2009, **27**:1026–1033.
Jansky S, Sharma AK, Körber V, Quintero A, Toprak UH, Wecht EM, Gartlgruber M, Greco A, Chomsky E, Grünewald TGP, et al.: **Single-cell transcriptomic analyses provide insights into the developmental origins of neuroblastoma**. *Nat Genet 2021 535* 2021, **53**:683–693.
Jeison M, Ash S, Halevy-Berko G, Mardoukh J, Luria D, Avigad S, Feinberg-Gorenshtein G, Goshen Y, Hertzel G, Kapelushnik J, et al.: **2p24 Gain region harboring MYCN gene compared with MYCN amplified and nonamplified neuroblastoma: biological and clinical characteristics**. *Am J Pathol* 2010, **176**:2616–2625.

Jo Y, Kim EH, Sai S, Kim JS, Cho JM, Kim H, Baek JH, Kim JY, Hwang SG, Yoon M: **Functional Biological Activity of Sorafenib as a Tumor-Treating Field Sensitizer for Glioblastoma Therapy**. *Int J Mol Sci* 2018, **19**.
Johnson RD, Liu N, Jasin M: **Mammalian XRCC2 promotes the repair of DNA double-strand breaks by homologous recombination**. *Nat 1999 4016751* 1999, **401**:397–399.
Jones RM, Mortusewicz O, Afzal I, Lorvellec M, García P, Helleday T, Petermann E: **Increased replication initiation and conflicts with transcription underlie Cyclin E-induced replication stress**. *Oncogene 2013 3232* 2012, **32**:3744–3753.
Joo W, Xu G, Persky NS, Smogorzewska A, Rudge DG, Buzovetsky O, Elledge SJ, Pavletich NP: **Structure of the FANCI-FANCD2 Complex: Insights into the Fanconi Anemia DNA Repair Pathway**. *Science* 2011, **333**:312.
Jun DW, Hwang M, Kim HJ, Hwang SK, Kim S, Lee C-H: **Ouabain, a Cardiac Glycoside, Inhibits the Fanconi Anemia/BRCA Pathway Activated by DNA Interstrand Cross-Linking Agents**. *PLoS One* 2013, **8**:e75905.
Jung M, Ramanagoudr-Bhojappa R, van Twest S, Rosti RO, Murphy V, Tan W, Donovan FX, Lach FP, Kimble DC, Jiang CS, et al.: **Association of clinical severity with FANCB variant type in Fanconi anemia**. *Blood* 2020, **135**:1588–1602.
Kai, Y., Li, B. E., Zhu, M., Li, G. Y., Chen, F., Han, Y., Cha, H. J., Orkin, S. H., Cai, W., Huang, J., & Yuan, G. C. (2021). **Mapping the evolving landscape of super-enhancers during cell differentiation.** *Genome Biology*, **22**:1–21.
Kais Z, Rondinelli B, Holmes A, O'Leary C, Kozono D, D'Andrea AD, Ceccaldi R: **FANCD2 maintains fork stability in BRCA1/2-deficient tumors and promotes alternative end-joining DNA repair**. *Cell Rep* 2016, **15**:2488.
Kalashnikova I, Mazar J, Neal CJ, Rosado AL, Das S, Westmoreland TJ, Seal S: **Nanoparticle delivery of curcumin induces cellular hypoxia and ROS-mediated apoptosis via modulation of Bcl-2/Bax in human neuroblastoma**. *Nanoscale* 2017, **9**:10375–10387.
Kameneva P, Artemov AV, Kastriti ME, Faure L, Olsen TK, Otte J, Erickson A, Semsch B, Andersson ER, Ratz M, et al.: **Single-cell transcriptomics of human embryos identifies multiple sympathoblast lineages with potential implications for neuroblastoma origin**. *Nat Genet* 2021, **53**:694.
Kang J, Rychahou PG, Ishola TA, Mourot JM, Evers BM, Chung DH: **N-MYC IS A NOVEL REGULATOR OF PI3K–MEDIATED VEGF EXPRESSION IN NEUROBLASTOMA**. *Oncogene* 2008, **27**:3999.
Kang JH, Kang HS, Kim IK, Lee HY, Ha JH, Yeo CD, Kang HH, Moon HS, Lee SH: **Curcumin sensitizes human lung cancer cells to apoptosis and metastasis synergistically combined with carboplatin**. *Exp Biol Med* 2015, **240**:1416.
Kang J-H, Rychahou PG, Ishola TA, Qiao J, Evers BM, Chung DH: **MYCN silencing induces differentiation and apoptosis in human neuroblastoma cells.** *Biochem Biophys Res Commun* 2006, **351**:192–197.
Kanner AA, Wong ET, Villano JL, Ram Z: **Post Hoc Analyses of Intention-to-Treat Population in Phase III Comparison of NovoTTF-100A™ System Versus Best Physician's Choice Chemotherapy**. *Semin Oncol* 2014, **41**:S25–S34.
Kao WH, Riker AI, Kushwaha DS, Ng K, Enkemann SA, Jove R, Buettner R, Zinn PO, Sánchez NP, Villa JL, et al.: **Upregulation of Fanconi anemia DNA repair genes in melanoma compared with non-melanoma skin cancer.** *J Invest Dermatol* 2011, **131**:2139–2142.
Kapeli K, Hurlin PJ: **Differential regulation of N-Myc and c-Myc synthesis, degradation, and transcriptional activity by the Ras/mitogen-activated protein kinase pathway.** *J Biol Chem* 2011, **286**:38498–38508.
Karanam NK, Ding L, Aroumougame A, Story MD: **Tumor treating fields cause replication stress and interfere with DNA replication fork maintenance: Implications for cancer therapy**. *Transl Res* 2020, **217**:33–46.
Karanam NK, Srinivasan K, Ding L, Sishc B, Saha D, Story MD: **Tumor-treating fields elicit a conditional vulnerability to ionizing radiation via the downregulation of**

BRCA1 signaling and reduced DNA double-strand break repair capacity in non-small cell lung cancer cell lines. *Cell Death Dis* 2017, **8**:e2711.
Kasinski AL, Du Y, Thomas SL, Zhao J, Sun SY, Khuri FR, Wang CY, Shoji M, Sun A, Snyder JP, et al.: **Inhibition of IκB Kinase-Nuclear Factor-κB Signaling Pathway by 3,5-Bis(2-flurobenzylidene)piperidin-4-one (EF24), a Novel Monoketone Analog of Curcumin**. *Mol Pharmacol* 2008, **74**:654.
Kastan MB, Bartek J: **Cell-cycle checkpoints and cancer**. *Nature* 2004, **432**:316–323.
Ke XX, Zhang D, Zhao H, Hu R, Dong Z, Yang R, Zhu S, Xia Q, Ding HF, Cui H: **Phox2B correlates with MYCN and is a prognostic marker for neuroblastoma development**. *Oncol Lett* 2015, **9**:2507–2514.
Kenney AM, Cole MD, Rowitch DH: **Nmyc upregulation by sonic hedgehog signaling promotes proliferation in developing cerebellar granule neuron precursors.** *Development* 2003, **130**:15–28.
Kerosuo L, Neppala P, Hsin J, Mohlin S, Vieceli FM, Török Z, Laine A, Westermarck J, Bronner ME: **Enhanced expression of MycN/CIP2A drives neural crest toward a neural stem cell-like fate: Implications for priming of neuroblastoma.** *Proc Natl Acad Sci U S A* 2018, **115**:E7351–E7360.
Kessler AF, Frömbling GE, Gross F, Hahn M, Dzokou W, Ernestus RI, Löhr M, Hagemann C: **Effects of tumor treating fields (TTFields) on glioblastoma cells are augmented by mitotic checkpoint inhibition**. *Cell Death Discov 2018 41* 2018, **4**:1–10.
Khanal S, Galloway DA: **High-risk human papillomavirus oncogenes disrupt the Fanconi anemia DNA repair pathway by impairing localization and de-ubiquitination of FancD2**. *PLoS Pathog* 2019, **15**.
Kildisiute G, Kholosy WM, Young MD, Roberts K, Elmentaite R, van Hooff SR, Pacyna CN, Khabirova E, Piapi A, Thevanesan C, et al.: **Tumor to normal single-cell mRNA comparisons reveal a pan-neuroblastoma cancer cell**. *Sci Adv* 2021, **7**.
Kim EH, Jo Y, Sai S, Park MJ, Kim JY, Kim JS, Lee YJ, Cho JM, Kwak SY, Baek JH, et al.: **Tumor-treating fields induce autophagy by blocking the Akt2/miR29b axis in glioblastoma cells**. *Oncogene* 2019, **38**:6630–6646.
Kim EH, Song HS, Yoo SH, Yoon M: **Tumor treating fields inhibit glioblastoma cell migration, invasion and angiogenesis**. *Oncotarget* 2016, **7**:65125.
Kim H, D'Andrea AD: **Regulation of DNA cross-link repair by the Fanconi anemia/BRCA pathway**. *Genes Dev* 2012, **26**:1393–1408.
Kim H, Yang K, Dejsuphong D, D'Andrea AD: **Regulation of Rev1 by the Fanconi Anemia Core Complex**. *Nat Struct Mol Biol* 2012, **19**:164.
Kim Y, Lach FP, Desetty R, Hanenberg H, Auerbach AD, Smogorzewska A: **Mutations of the SLX4 gene in Fanconi anemia**. *Nat Genet* 2011, **43**:142–146.
Kim Y, Spitz GS, Veturi U, Lach FP, Auerbach AD, Smogorzewska A: **Regulation of multiple DNA repair pathways by the Fanconi anemia protein SLX4**. *Blood* 2013, **121**:54.
King D, Li XD, Almeida GS, Kwok C, Gravells P, Harrison D, Burke S, Hallsworth A, Jamin Y, George S, et al.: **MYCN expression induces replication stress and sensitivity to PARP inhibition in neuroblastoma**. *Oncotarget* 2020, **11**:2141–2159.
King D, Southgate HED, Roetschke S, Gravells P, Fields L, Watson JB, Chen L, Chapman D, Harrison D, Yeomanson D, et al.: **Increased Replication Stress Determines ATR Inhibitor Sensitivity in Neuroblastoma Cells**. *Cancers (Basel)* 2021, **13**.
Kirson ED, Dbalý V, Tovaryš F, Vymazal J, Soustiel JF, Itzhaki A, Mordechovich D, Steinberg-Shapira S, Gurvich Z, Schneiderman R, et al.: **Alternating electric fields arrest cell proliferation in animal tumor models and human brain tumors**. *Proc Natl Acad Sci U S A* 2007, **104**:10152.
Kirson ED, Giladi M, Gurvich Z, Itzhaki A, Mordechovich D, Schneiderman RS, Wasserman Y, Ryffel B, Goldsher D, Palti Y: **Alternating electric fields (TTFields) inhibit metastatic spread of solid tumors to the lungs**. *Clin Exp Metastasis* 2009, **26**:633.

Kirson ED, Gurvich Z, Schneiderman R, Dekel E, Itzhaki A, Wasserman Y, Schatzberger R, Palti Y: **Disruption of cancer cell replication by alternating electric fields**. *Cancer Res* 2004, **64**:3288–3295.
Klein Douwel D, Boonen RACM, Long DT, Szypowska AA, Räschle M, Walter JC, Knipscheer P: **XPF-ERCC1 acts in unhooking DNA interstrand crosslinks in cooperation with FANCD2 and FANCP/SLX4**. *Mol Cell* 2014, **54**:460.
Knies K, Inano S, Ramírez MJ, Ishiai M, Surrallés J, Takata M, Schindler D: **Biallelic mutations in the ubiquitin ligase RFWD3 cause Fanconi anemia**. *J Clin Invest* 2017, **127**:3013–3027.
Knipscheer P, Räschle M, Smogorzewska A, Enoiu M, Ho TV, Schärer OD, Elledge SJ, Walter JC: **The Fanconi anemia pathway promotes replication-dependent DNA interstrand crosslink repair**. *Science* 2009, **326**:1698.
Knoepfler PS, Zhang X, Cheng PF, Gafken PR, McMahon SB, Eisenman RN: **Myc influences global chromatin structure.** *EMBO J* 2006, **25**:2723–2734.
Knoepfler PS, Cheng PF, Eisenman RN: **N-myc is essential during neurogenesis for the rapid expansion of progenitor cell populations and the inhibition of neuronal differentiation**. *Genes Dev* 2002, **16**:2699–2712.
Knudson AG, Strong LC: **Mutation and Cancer: Neuroblastoma and Pheochromocytoma**. *Amer J Hum Genet* 1972, **24**:514–532.
Kohl NE, Kanda N, Schreck RR, Bruns G, Latt SA, Gilbert F, Alt FW: **Transposition and amplification of oncogene-related sequences in human neuroblastomas**. *Cell* 1983, **35**:359–367.
Kohl NE, Legouy E, DePinho RA, Nisen PD, Smith RK, Gee CE, Alt FW: **Human N-myc is closely related in organization and nucleotide sequence to c-myc**. *Nature* 1986, **319**:73–77.
Komatsu H, Masuda T, Iguchi T, Nambara S, Sato K, Hu Q, Hirata H, Ito S, Eguchi H, Sugimachi K, et al.: **Clinical Significance of FANCD2 Gene Expression and its Association with Tumor Progression in Hepatocellular Carcinoma**. *Anticancer Res* 2017, **37**:1083–1090.
Komuro H, Hayashi Y, Kawamura M, Hayashi K, Kaneko Y, Kamoshita S, Hanada R, Yamamoto K, Hongo T, Yamada M: **Mutations of the p53 gene are involved in Ewing's sarcomas but not in neuroblastomas.** *Cancer Res* 1993, **53**:5284–5288.
Kondo N, Takahashi A, Ono K, Ohnishi T: **DNA Damage Induced by Alkylating Agents and Repair Pathways**. *J Nucleic Acids* 2010, **2010**.
Koppen A, Ait-Aissa R, Hopman S, Koster J, Haneveld F, Versteeg R, Valentijn LJ: **Dickkopf-1 is down-regulated by MYCN and inhibits neuroblastoma cell proliferation**. *Cancer Lett* 2007, **256**:218–228.
Koppen A, Ait-Aissa R, Koster J, van Sluis PG, Øra I, Caron HN, Volckmann R, Versteeg R, Valentijn LJ: **Direct regulation of the minichromosome maintenance complex by MYCN in neuroblastoma**. *Eur J Cancer* 2007, **43**:2413–2422.
Kotsantis P, Petermann E, Boulton SJ: **Mechanisms of Oncogene-Induced Replication Stress: Jigsaw Falling into Place.** *Cancer Discov* 2018, **8**:537–555.
Kotsantis P, Silva LM, Irmscher S, Jones RM, Folkes L, Gromak N, Petermann E: **Increased global transcription activity as a mechanism of replication stress in cancer.** *Nat Commun* 2016, **7**:13087.
Kottemann MC, Smogorzewska A: **Fanconi anemia and the repair of Watson and Crick crosslinks**. *Nature* 2013, **493**:356.
Kramer M, Ribeiro D, Arsenian-Henriksson M, Deller T, Rohrer H: **Proliferation and Survival of Embryonic Sympathetic Neuroblasts by MYCN and Activated ALK Signaling**. *J Neurosci* 2016, **36**:10425.
Kratz K, Schöpf B, Kaden S, Sendoel A, Eberhard R, Lademann C, Cannavó E, Sartori AA, Hengartner MO, Jiricny J: **Deficiency of FANCD2-associated nuclease KIAA1018/FAN1 sensitizes cells to interstrand crosslinking agents**. *Cell* 2010, **142**:77–88.

Krueger C, Pfleiderer K, Hillen W, Berens C: **Tetracycline derivatives: alternative effectors for Tet transregulators**. *Biotechniques* 2004, **37**:546–550.
Kuchenbaecker KB, Hopper JL, Barnes DR, Phillips K-A, Mooij TM, Roos-Blom M-J, Jervis S, Leeuwen FE van, Milne RL, Andrieu N, et al.: **Risks of Breast, Ovarian, and Contralateral Breast Cancer for BRCA1 and BRCA2 Mutation Carriers**. *JAMA* 2017, **317**:2402–2416.
Kulikov A, Eva A, Kirch U, Boldyrev A, Scheiner-Bobis G: **Ouabain activates signaling pathways associated with cell death in human neuroblastoma**. *Biochim Biophys Acta* 2007, **1768**:1691–1702.
Kumari U, Ya Jun W, Huat Bay B, Lyakhovich A: **Evidence of mitochondrial dysfunction and impaired ROS detoxifying machinery in Fanconi Anemia cells**. *Oncogene 2014 332* 2013, **33**:165–172.
Kumps C, Fieuw A, Mestdagh P, Menten B, Lefever S, Pattyn F, De Brouwer S, Sante T, Schulte JH, Schramm A, et al.: **Focal DNA copy number changes in neuroblastoma target MYCN regulated genes.** *PLoS One* 2013, **8**:e52321.
Kunnumakkara AB, Guha S, Krishnan S, Diagaradjane P, Gelovani J, Aggarwal BB: **Curcumin potentiates antitumor activity of gemcitabine in an orthotopic model of pancreatic cancer through suppression of proliferation, angiogenesis, and inhibition of nuclear factor-kappaB-regulated gene products**. *Cancer Res* 2007, **67**:3853–3861.
Kuraoka I, Kobertz WR, Ariza RR, Biggerstaff M, Essigmann JM, Wood RD: **Repair of an interstrand DNA cross-link initiated by ERCC1-XPF repair/recombination nuclease**. *J Biol Chem* 2000, **275**:26632–26636.
Kushner BH, Budnick A, Kramer K, Modak S, Cheung NKV: **Ototoxicity from high-dose use of platinum compounds in patients with neuroblastoma**. *Cancer* 2006, **107**:417–422.
Labib K, Hodgson B: **Replication fork barriers: pausing for a break or stalling for time?** *EMBO Rep* 2007, **8**:346–353.
Lachaud C, Castor D, Hain K, Muñoz I, Wilson J, MacArtney TJ, Schindler D, Rouse J: **Distinct functional roles for the two SLX4 ubiquitin-binding UBZ domains mutated in Fanconi anemia**. *J Cell Sci* 2014, **127**:2811–2817.
Lachaud C, Moreno A, Marchesi F, Toth R, Blow JJ, Rouse J: **Ubiquitinated Fancd2 recruits Fan1 to stalled replication forks to prevent genome instability**. *Science* 2016, **351**:846–849.
Lacouture ME, Elizabeth Davis M, Elzinga G, Butowski N, Tran D, Villano JL, Dimeglio L, Davies AM, Wong ET: **Characterization and Management of Dermatologic Adverse Events With the NovoTTF-100A System, a Novel Anti-mitotic Electric Field Device for the Treatment of Recurrent Glioblastoma**. *Semin Oncol* 2014, **41**:S1–S14.
Ladenstein R, Pötschger U, Pearson ADJ, Brock P, Luksch R, Castel V, Yaniv I, Papadakis V, Laureys G, Malis J, et al.: **Busulfan and melphalan versus carboplatin, etoposide, and melphalan as high-dose chemotherapy for high-risk neuroblastoma (HR-NBL1/SIOPEN): an international, randomised, multi-arm, open-label, phase 3 trial**. *Lancet Oncol* 2017, **18**:500–514.
Ladenstein R, Pötschger U, Valteau-Couanet D, Luksch R, Castel V, Yaniv I, Laureys G, Brock P, Michon JM, Owens C, et al.: **Interleukin 2 with anti-GD2 antibody ch14.18/CHO (dinutuximab beta) in patients with high-risk neuroblastoma (HR-NBL1/SIOPEN): a multicentre, randomised, phase 3 trial**. *Lancet Oncol* 2018, **19**:1617–1629.
Landais I, Hiddingh S, McCarroll M, Yang C, Sun A, Turker MS, Snyder JP, Hoatlin ME: **Monoketone analogs of curcumin, a new class of Fanconi anemia pathway inhibitors.** *Mol Cancer* 2009, **8**:133.
Landais I, Sobeck A, Stone S, LaChapelle A, Hoatlin ME: **A novel cell-free screen identifies a potent inhibitor of the Fanconi anemia pathway**. *Int J Cancer* 2009, **124**:783–792.

Langevin F, Crossan GP, Rosado IV, Arends MJ, Patel KJ: **Fancd2 counteracts the toxic effects of naturally produced aldehydes in mice**. *Nature* 2011, **475**:53–58.
Lasorella A, Boldrini R, Dominici C, Donfrancesco A, Yokota Y, Inserra A, Iavarone A: **Id2 is critical for cellular proliferation and is the oncogenic effector of N-myc in human neuroblastoma.** *Cancer Res* 2002, **62**:301–306.
Lasorella A, Noseda M, Beyna M, Iavarone A, Iavarone A: **Id2 is a retinoblastoma protein target and mediates signalling by Myc oncoproteins**. *Nature* 2000, **407**:592–598.
Laverdiére C, Liu Q, Yasui Y, Nathan PC, Gurney JG, Stovall M, Diller LR, Cheung NK, Wolden S, Robison LL, et al.: **Long-term outcomes in survivors of neuroblastoma: a report from the Childhood Cancer Survivor Study**. *J Natl Cancer Inst* 2009, **101**:1131–1140.
Le Grand M, Kimpton K, Gana CC, Valli E, Fletcher JI, Kavallaris M: **Targeting Functional Activity of AKT Has Efficacy against Aggressive Neuroblastoma**. *ACS Pharmacol Transl Sci* 2020, **3**:148–160.
Leathers TA, Rogers CD: **Time to go: neural crest cell epithelial-to-mesenchymal transition**. *Development* 2022, **149**.
Lee YJ, Seo HW, Baek JH, Lim SH, Hwang SG, Kim EH: **Gene expression profiling of glioblastoma cell lines depending on TP53 status after tumor-treating fields (TTFields) treatment**. *Sci Reports 2020 101* 2020, **10**:1–14.
Lemée F, Bavoux C, Pillaire MJ, Bieth A, Machado CR, Pena SD, Guimbaud R, Selves J, Hoffmann JS, Cazaux C: **Characterization of promoter regulatory elements involved in downexpression of the DNA polymerase κ in colorectal cancer**. *Oncogene 2007 2623* 2006, **26**:3387–3394.
Lempiäinen H, Halazonetis TD: **Emerging common themes in regulation of PIKKs and PI3Ks.** *EMBO J* 2009, **28**:3067–3073.
Levitus M, Waisfisz Q, Godthelp BC, De Vries Y, Hussain S, Wiegant WW, Elghalbzouri-Maghrani E, Steltenpool J, Rooimans MA, Pals G, et al.: **The DNA helicase BRIP1 is defective in Fanconi anemia complementation group J**. *Nat Genet* 2005, **37**:934–935.
Li J, Du W, Maynard S, Andreassen PR, Pang Q: **Oxidative stress–specific interaction between FANCD2 and FOXO3a**. *Blood* 2010, **115**:1545.
Li T, Shukla G, Peng C, Lockamy V, Liu H, Shi W: **Dosimetric Impact of a Tumor Treating Fields Device for Glioblastoma Patients Undergoing Simultaneous Radiation Therapy**. *Front Oncol* 2018, **8**:51.
Liang CC, Li Z, Lopez-Martinez D, Nicholson WV, Vénien-Bryan C, Cohn MA: **The FANCD2–FANCI complex is recruited to DNA interstrand crosslinks before monoubiquitination of FANCD2**. *Nat Commun* 2016, **7**.
Liang CC, Zhan B, Yoshikawa Y, Haas W, Gygi SP, Cohn MA: **UHRF1 is a sensor for DNA interstrand crosslinks and recruits FANCD2 to initiate the Fanconi anemia pathway**. *Cell Rep* 2015, **10**:1947–1956.
Liang F, Miller AS, Longerich S, Tang C, Maranon D, Williamson EA, Hromas R, Wiese C, Kupfer GM, Sung P: **DNA requirement in FANCD2 deubiquitination by USP1-UAF1-RAD51AP1 in the Fanconi anemia DNA damage response**. *Nat Commun* 2019, **10**.
Liang Z, Liang F, Teng Y, Chen X, Liu J, Longerich S, Rao T, Green AM, Collins NB, Xiong Y, et al.: **Binding of FANCI-FANCD2 Complex to RNA and R-Loops Stimulates Robust FANCD2 Monoubiquitination**. *Cell Rep* 2019, **26**:564.
Liebetrau W, Rünger TM, Mehling BE, Poot M, Hoehn H: **Mutagenic activity of ambient oxygen and mitomycin C in Fanconi's anaemia cells**. *Mutagenesis* 1997, **12**:69–77.
Lin CY, Lovén J, Rahl PB, Paranal RM, Burge CB, Bradner JE, Lee TI, Young RA: **Transcriptional Amplification in Tumor Cells with Elevated c-Myc**. *Cell* 2012, **151**:56.
Ling C, Huang J, Yan Z, Li Y, Ohzeki M, Ishiai M, Xu D, Takata M, Seidman M, Wang W: **Bloom syndrome complex promotes FANCM recruitment to stalled replication forks and facilitates both repair and traverse of DNA interstrand crosslinks**. *Cell Discov* 2016, **2**:16047.

Ling C, Ishiai M, Ali AM, Medhurst AL, Neveling K, Kalb R, Yan Z, Xue Y, Oostra AB, Auerbach AD, et al.: **FAAP100 is essential for activation of the Fanconi anemia-associated DNA damage response pathway**. *EMBO J* 2007, **26**:2104–2114.
Liontas A, Yeger H: **Curcumin and resveratrol induce apoptosis and nuclear translocation and activation of p53 in human neuroblastoma.** *Anticancer Res* 2004, **24**:987–998.
Liu L, Xu F, Chang CK, He Q, Wu LY, Zhang Z, Li X: **MYCN contributes to the malignant characteristics of erythroleukemia through EZH2-mediated epigenetic repression of p21**. *Cell Death Dis 2017 810* 2017, **8**:e3126–e3126.
Liu L, Gerson SL: **Targeted modulation of MGMT: clinical implications**. *Clin Cancer Res* 2006, **12**:328–331.
Liu P, Ying Q, Liu H, Yu SQ, Bu LP, Shao L, Li XY: **Curcumin enhances anti-cancer efficacy of either gemcitabine or docetaxel on pancreatic cancer cells**. *Oncol Rep* 2020, **44**:1393.
Liu T, Ghosal G, Yuan J, Chen J, Huang J: **FAN1 acts with FANCI-FANCD2 to promote DNA interstrand cross-link repair**. *Science (80-)* 2010, **329**:693–696.
Liu W, Palovcak A, Li F, Zafar A, Yuan F, Zhang Y: **Fanconi anemia pathway as a prospective target for cancer intervention**. *Cell Biosci* 2020, **10**.
Liu Y, Liu D, Wan W: **MYCN-induced E2F5 promotes neuroblastoma cell proliferation through regulating cell cycle progression**. *Biochem Biophys Res Commun* 2019, **511**:35–40.
Liu Z, Chen SS, Clarke S, Veschi V, Thiele CJ: **Targeting MYCN in Pediatric and Adult Cancers**. *Front Oncol* 2021, **10**:3252.
Livak KJ, Schmittgen TD: **Analysis of Relative Gene Expression Data Using Real-Time Quantitative PCR and the 2−ΔΔCT Method**. *Methods* 2001, **25**:402–408.
Lo Ten Foe JR, Rooimans MA, Bosnoyan-Collins L, Alon N, Wijker M, Parker L, Lightfoot J, Carreau M, Callen DF, Savoia A, et al.: **Expression cloning of a cDNA for the major Fanconi anaemia gene, FAA**. *Nat Genet 1996 143* 1996, **14**:320–323.
Loizidou MA, Hadjisavvas A, Tanteles GA, Spanou-Aristidou E, Kyriacou K, Christophidou-Anastasiadou V: **Fanconi anemia-D1 due to homozygosity for the BRCA2 gene Cypriot founder mutation: A case report**. *Oncol Lett* 2016, **11**:471–473.
London WB, Castleberry RP, Matthay KK, Look AT, Seeger RC, Shimada H, Thorner P, Brodeur G, Maris JM, Reynolds CP, et al.: **Evidence for an Age Cutoff Greater Than 365 Days for Neuroblastoma Risk Group Stratification in the Children's Oncology Group**. *J Clin Oncol* 2005, **23**:6459–6465.
London WB, Castel V, Monclair T, Ambros PF, Pearson ADJ, Cohn SL, Berthold F, Nakagawara A, Ladenstein RL, Iehara T, et al.: **Clinical and biologic features predictive of survival after relapse of neuroblastoma: a report from the International Neuroblastoma Risk Group project**. *J Clin Oncol* 2011, **29**:3286–3292.
Long DT, Raschle M, Joukov V, Walter JC: **Mechanism of RAD51-Dependent DNA Interstrand Cross-Link Repair**. *Science (80-)* 2011, **333**:84–87.
Long DT, Joukov V, Budzowska M, Walter JC: **BRCA1 promotes unloading of the CMG helicase from a stalled DNA replication fork**. *Mol Cell* 2014, **56**:174.
Lossaint G, Larroque M, Ribeyre C, Bec N, Larroque C, Décaillet C, Gari K, Constantinou A: **FANCD2 Binds MCM Proteins and Controls Replisome Function upon Activation of S Phase Checkpoint Signaling**. *Mol Cell* 2013, **51**:678–690.
Loven J, Zinin N, Wahlstrom T, Muller I, Brodin P, Fredlund E, Ribacke U, Pivarcsi A, Pahlman S, Henriksson M: **MYCN-regulated microRNAs repress estrogen receptor- (ESR1) expression and neuronal differentiation in human neuroblastoma**. *Proc Natl Acad Sci* 2010, **107**:1553–1558.
Lu R, O'Rourke JJ, Sobinoff AP, Allen JAM, Nelson CB, Tomlinson CG, Lee M, Reddel RR, Deans AJ, Pickett HA: **The FANCM-BLM-TOP3A-RMI complex suppresses alternative lengthening of telomeres (ALT)**. *Nat Commun* 2019, **10**.

Lu W-T, Lemonidis K, Drayton RM, Nouspikel T: **The Fanconi anemia pathway is downregulated upon macrophage differentiation through two distinct mechanisms**. *Cell Cycle* 2011, **10**:3300–3310.
Lu X, Tweddle DA, Pearson ADJ, Lunec J: **Comparison between MYCN status as a determinant of in vitro cellular chemosensitivity and clinical response to chemotherapy in human neuroblastoma**. *Cancer Res* 2005, **65**:691.
Luttikhuis MEMO, Powell JE, Rees SA, Genus T, Chughtai S, Ramani P, Mann JR, McConville CM: **Neuroblastomas with chromosome 11q loss and single copy MYCN comprise a biologically distinct group of tumours with adverse prognosis**. *Br J Cancer* 2001, **85**:531–537.
Lutz W, Stöhr M, Schürmann J, Wenzel A, Löhr A, Schwab M: **Conditional expression of N-myc in human neuroblastoma cells increases expression of alpha-prothymosin and ornithine decarboxylase and accelerates progression into S-phase early after mitogenic stimulation of quiescent cells.** *Oncogene* 1996, **13**:803–812.
Lyakhovich A, Surralles J: **FANCD2 depletion sensitizes cancer cells repopulation ability in vitro**. *Cancer Lett* 2007, **256**:186–195.
Ma L, Young J, Prabhala H, Pan E, Mestdagh P, Muth D, Teruya-Feldstein J, Reinhardt F, Onder TT, Valastyan S, et al.: **miR-9, a MYC/MYCN-activated microRNA, regulates E-cadherin and cancer metastasis.** *Nat Cell Biol* 2010, **12**:247–256.
MacKay C, Déclais AC, Lundin C, Agostinho A, Deans AJ, MacArtney TJ, Hofmann K, Gartner A, West SC, Helleday T, et al.: **Identification of KIAA1018/FAN1, a DNA Repair Nuclease Recruited to DNA Damage by Monoubiquitinated FANCD2**. *Cell* 2010, **142**:65.
Madireddy A, Kosiyatrakul ST, Boisvert RA, Herrera-Moyano E, García-Rubio ML, Gerhardt J, Vuono EA, Owen N, Yan Z, Olson S, et al.: **FANCD2 facilitates replication through common fragile sites**. *Mol Cell* 2016, **64**:388.
Mah LJ, El-Osta A, Karagiannis TC: **γH2AX: a sensitive molecular marker of DNA damage and repair**. *Leuk 2010 244* 2010, **24**:679–686.
Malynn BA, de Alboran IM, O'Hagan RC, Bronson R, Davidson L, DePinho RA, Alt FW: **N-myc can functionally replace c-myc in murine development, cellular growth, and differentiation.** *Genes Dev* 2000, **14**:1390–1399.
Mandriota SJ, Valentijn LJ, Lesne L, Betts DR, Marino D, Boudal-Khoshbeen M, London WB, Rougemont A-L, Attiyeh EF, Maris JM, et al.: **Ataxia-telangiectasia mutated (ATM) silencing promotes neuroblastoma progression through a MYCN independent mechanism.** *Oncotarget* 2015, **6**:18558–18576.
Maréchal A, Zou L: **DNA damage sensing by the ATM and ATR kinases.** *Cold Spring Harb Perspect Biol* 2013, **5**.
Maréchal A, Zou L: **RPA-coated single-stranded DNA as a platform for post-translational modifications in the DNA damage response**. *Cell Res* 2015, **25**:9.
Maris JM, Guo C, Blake D, White PS, Hogarty MD, Thompson PM, Rajalingam V, Gerbing R, Stram DO, Matthay KK, et al.: **Comprehensive analysis of chromosome 1p deletions in neuroblastoma.** *Med Pediatr Oncol* 2001, **36**:32–36.
Maris JM, Weiss MJ, Guo C, Gerbing RB, Stram DO, White PS, Hogarty MD, Sulman EP, Thompson PM, Lukens JN, et al.: **Loss of heterozygosity at 1p36 independently predicts for disease progression but not decreased overall survival probability in neuroblastoma patients: a Children's Cancer Group study.** *J Clin Oncol* 2000, **18**:1888–1899.
Maris JM: **Recent Advances in Neuroblastoma**. *N Engl J Med* 2010, **362**:2202–2211.
Marshall GM, Liu PY, Gherardi S, Scarlett CJ, Bedalov A, Xu N, Iraci N, Valli E, Ling D, Thomas W, et al.: **SIRT1 promotes N-Myc oncogenesis through a positive feedback loop involving the effects of MKP3 and ERK on N-Myc protein stability.** *PLoS Genet* 2011, **7**:e1002135.
Marshall GM, Carter DR, Cheung BB, Liu T, Mateos MK, Meyerowitz JG, Weiss WA: **The prenatal origins of cancer**. *Nat Rev Cancer* 2014, **14**:277.

Martínez-Castillo M, Villegas-Sepúlveda N, Meraz-Rios MA, Hernández-Zavala A, Berumen J, Coleman MA, Orozco L, Cordova EJ: **Curcumin differentially affects cell cycle and cell death in acute and chronic myeloid leukemia cells**. *Oncol Lett* 2018, **15**:6777.
Mason JM, Chan YL, Weichselbaum RW, Bishop DK: **Non-enzymatic roles of human RAD51 at stalled replication forks**. *Nat Commun* 2019, **10**.
Masutani C, Kusumoto R, Yamada A, Dohmae N, Yokol M, Yuasa M, Araki M, Iwai S, Takio K, Hanaoka F: **The XPV (xeroderma pigmentosum variant) gene encodes human DNA polymerase η**. *Nat 1999 3996737* 1999, **399**:700–704.
Matos DA, Zhang J-M, Ouyang J, Nguyen HD, Genois M-M, Zou L: **ATR Protects the Genome against R Loops through a MUS81-Triggered Feedback Loop**. *Mol Cell* 2020, **77**:514-527.e4.
Matthay KK, Maris JM, Schleiermacher G, Nakagawara A, Mackall CL, Diller L, Weiss WA: **Neuroblastoma**. *Nat Rev Dis Prim* 2016, **2**:16078.
Matthay KK, Perez C, Seeger RC, Brodeur GM, Shimada H, Atkinson JB, Black CT, Gerbing R, Haase GM, Stram DO, et al.: **Successful treatment of stage III neuroblastoma based on prospective biologic staging: a Children's Cancer Group study**. *J Clin Oncol* 1998, **16**:1256–1264.
Matthay KK, Reynolds CP, Seeger RC, Shimada H, Adkins ES, Haas-Kogan D, Gerbing RB, London WB, Villablanca JG: **Long-term results for children with high-risk neuroblastoma treated on a randomized trial of myeloablative therapy followed by 13-cis-retinoic acid: a children's oncology group study**. *J Clin Oncol* 2009, **27**:1007–1013.
Matthay KK, Villablanca JG, Seeger RC, Stram DO, Harris RE, Ramsay NK, Swift P, Shimada H, Black CT, Brodeur GM, et al.: **Treatment of High-Risk Neuroblastoma with Intensive Chemotherapy, Radiotherapy, Autologous Bone Marrow Transplantation, and 13-cis-Retinoic Acid**. *N Engl J Med* 1999, **341**:1165–1173.
Mayo LD, Dixon JE, Durden DL, Tonks NK, Donner DB: **PTEN protects p53 from Mdm2 and sensitizes cancer cells to chemotherapy**. *J Biol Chem* 2002, **277**:5484–5489.
McKenzie PP, Guichard SM, Middlemas DS, Ashmun RA, Danks MK, Harris LC: **Wild-type p53 can induce p21 and apoptosis in neuroblastoma cells but the DNA damage-induced G1 checkpoint function is attenuated.** *Clin Cancer Res* 1999, **5**:4199–4207.
McNeil EM, Astell KR, Ritchie AM, Shave S, Houston DR, Bakrania P, Jones HM, Khurana P, Wallace C, Chapman T, et al.: **Inhibition of the ERCC1-XPF structure-specific endonuclease to overcome cancer chemoresistance**. *DNA Repair (Amst)* 2015, **31**:19–28.
Meetei AR, De Winter JP, Medhurst AL, Wallisch M, Waisfisz Q, Van de Vrugt HJ, Oostra AB, Yan Z, Ling C, Bishop CE, et al.: **A novel ubiquitin ligase is deficient in Fanconi anemia**. *Nat Genet 2003 352* 2003, **35**:165–170.
Meetei AR, Levitus M, Xue Y, Medhurst AL, Zwaan M, Ling C, Rooimans MA, Bier P, Hoatlin M, Pals G, et al.: **X-linked inheritance of Fanconi anemia complementation group B**. *Nat Genet 2004 3611* 2004, **36**:1219–1224.
Meetei AR, Medhurst AL, Ling C, Xue Y, Singh TR, Bier P, Steltenpool J, Stone S, Dokal I, Mathew CG, et al.: **A human ortholog of archaeal DNA repair protein Hef is defective in Fanconi anemia complementation group M**. *Nat Genet* 2005, **37**:958–963.
Megison ML, Stewart JE, Nabers HC, Gillory LA, Beierle EA: **FAK inhibition decreases cell invasion, migration and metastasis in MYCN amplified neuroblastoma.** *Clin Exp Metastasis* 2013, **30**:555–568.
Mehmet D, Unal S, Gumruk F, Akarsu NA: **A Homozygous Germ Line Nonsense Mutation in BRCA1 Leading Fanconi Anemia and Neuroblastoma**. *Blood* 2016, **128**.
Meitar D, Crawford SE, Rademaker AW, Cohn SL: **Tumor angiogenesis correlates with metastatic disease, N-myc amplification, and poor outcome in human neuroblastoma.** *J Clin Oncol* 1996, **14**:405–414.
Melaiu O, Mina M, Chierici M, Boldrini R, Jurman G, Romania P, D'Alicandro V, Benedetti MC, Castellano A, Liu T, et al.: **PD-L1 Is a Therapeutic Target of the Bromodomain**

Inhibitor JQ1 and, Combined with HLA Class I, a Promising Prognostic Biomarker in Neuroblastoma. *Clin Cancer Res* 2017, **23**:4462–4472.
Merajver SD, Frank TS, Xu J, Pham TM, Calzone KA, Bennett-Baker P, Chamberlain J, Boyd J, Garber JE, Collins FS: **Germline BRCA1 mutations and loss of the wild-type allele in tumors from families with early onset breast and ovarian cancer.** *Clin Cancer Res* 1995, **1**:539–544.
Meyer N, Penn LZ: **Reflecting on 25 years with MYC**. *Nat Rev Cancer 2008 812* 2008, **8**:976–990.
Mina M, Boldrini R, Citti A, Romania P, D'Alicandro V, Ioris MD, Castellano A, Furlanello C, Locatelli F, Fruci D: **Tumor-infiltrating T lymphocytes improve clinical outcome of therapy-resistant neuroblastoma**. *Oncoimmunology* 2015, **4**:1–14.
Miranda PC, Mekonnen A, Salvador R, Basser PJ: **Predicting the Electric Field Distribution in the Brain for the Treatment of Glioblastoma**. *Phys Med Biol* 2014, **59**:4137.
Mirchandani KD, McCaffrey RM, D'Andrea AD: **The Fanconi anemia core complex is required for efficient point mutagenesis and Rev1 foci assembly**. *DNA Repair (Amst)* 2008, **7**:902–911.
Mitxelena J, Apraiz A, Vallejo-Rodríguez J, García-Santisteban I, Fullaondo A, Alvarez-Fernández M, Malumbres M, Zubiaga AM: **An E2F7-dependent transcriptional program modulates DNA damage repair and genomic stability.** *Nucleic Acids Res* 2018, **46**:4546–4559.
Mlakar V, Jurkovic Mlakar S, Lopez G, Maris JM, Ansari M, Gumy-Pause F: **11q deletion in neuroblastoma: a review of biological and clinical implications.** *Mol Cancer* 2017, **16**:114.
Mo F, Xiao Y, Zeng H, Fan D, Song J, Liu X, Luo M, Ma X: **Curcumin-Induced Global Profiling of Transcriptomes in Small Cell Lung Cancer Cells**. *Front Cell Dev Biol* 2021, **8**:588299.
Mody R, Naranjo A, Van Ryn C, Yu AL, London WB, Shulkin BL, Parisi MT, Servaes SEN, Diccianni MB, Sondel PM, et al.: **Irinotecan-temozolomide with temsirolimus or dinutuximab in children with refractory or relapsed neuroblastoma (COG ANBL1221): an open-label, randomised, phase 2 trial**. *Lancet Oncol* 2017, **18**:946–957.
Mody R, Yu AL, Naranjo A, Zhang FF, London WB, Shulkin BL, Parisi MT, Servaes SEN, Diccianni MB, Hank JA, et al.: **Irinotecan, Temozolomide, and Dinutuximab With GM-CSF in Children With Refractory or Relapsed Neuroblastoma: A Report From the Children's Oncology Group**. *J Clin Oncol* 2020, **38**:2160–2169.
Moghadam MK, Firoozabadi SM, Janahmadi M: **50 Hz alternating extremely low frequency magnetic fields affect excitability, firing and action potential shape through interaction with ionic channels in snail neurones**. *Environmentalist* 2008, **28**:341–347.
Moldovan G-L, D'Andrea AD: **How the Fanconi Anemia pathway guards the genome**. *Annu Rev Genet* 2009, **43**:223–249.
Molenaar JJ, Ebus ME, Geerts D, Koster J, Lamers F, Valentijn LJ, Westerhout EM, Versteeg R, Caron HN: **Inactivation of CDK2 is synthetically lethal to MYCN over-expressing cancer cells**. *Proc Natl Acad Sci U S A* 2009, **106**:12968.
Molenaar JJ, Koster J, Zwijnenburg DA, van Sluis P, Valentijn LJ, van der Ploeg I, Hamdi M, van Nes J, Westerman BA, van Arkel J, et al.: **Sequencing of neuroblastoma identifies chromothripsis and defects in neuritogenesis genes**. *Nature* 2012, **483**:589–593.
Moll UM, Ostermeyer AG, Haladay R, Winkfield B, Frazier M, Zambetti G, Moll M, LaQuaglia M, Benard J, Riou G: **Cytoplasmic sequestration of wild-type p53 protein impairs the G1 checkpoint after DNA damage.** *Mol Cell Biol* 1996, **16**:1126.
Montecucco, A., Zanetta, F., & Biamonti, G. (2015). **Molecular mechanisms of etoposide.** *EXCLI Journal*, **14**:95.
Moreau LA, McGrady P, London WB, Shimada H, Cohn SL, Maris JM, Diller L, Look AT, George RE: **Does MYCN amplification manifested as homogeneously staining**

regions at diagnosis predict a worse outcome in children with neuroblastoma? A Children's Oncology Group study. *Clin Cancer Res* 2006, **12**:5693–5697.
Morreale FE, Bortoluzzi A, Chaugule VK, Arkinson C, Walden H, Ciulli A: **Allosteric Targeting of the Fanconi Anemia Ubiquitin-Conjugating Enzyme Ube2T by Fragment Screening**. *J Med Chem* 2017, **60**:4093–4098.
Mossé YP, Laudenslager M, Longo L, Cole KA, Wood A, Attiyeh EF, Laquaglia MJ, Sennett R, Lynch JE, Perri P, et al.: **Identification of ALK as a major familial neuroblastoma predisposition gene.** *Nature* 2008, **455**:930–935.
Mosse YP, Balis FM, Lim MS, Laliberte J, Voss SD, Fox E, Bagatell R, Weigel B, Adamson PC, Ingle AM, et al.: **Efficacy of crizotinib in children with relapsed/refractory ALK-driven tumors including anaplastic large cell lymphoma and neuroblastoma: A Children's Oncology Group phase I consortium study**. *J Clin Oncol* 2017, **30**.
Mosse YP, Laudenslager M, Khazi D, Carlisle AJ, Winter CL, Rappaport E, Maris JM: **Germline PHOX2B Mutation in Hereditary Neuroblastoma**. *Am J Hum Genet* 2004, **75**:727.
Mossé YP, Voss SD, Lim MS, Rolland D, Minard CG, Fox E, Adamson P, Wilner K, Blaney SM, Weigel BJ: **Targeting ALK With Crizotinib in Pediatric Anaplastic Large Cell Lymphoma and Inflammatory Myofibroblastic Tumor: A Children's Oncology Group Study**. *J Clin Oncol* 2017, **35**:3215–3221.
Mrugala MM, Engelhard HH, Dinh Tran D, Kew Y, Cavaliere R, Villano JL, Annenelie Bota D, Rudnick J, Love Sumrall A, Zhu JJ, et al.: **Clinical practice experience with NovoTTF-100A™ system for glioblastoma: The Patient Registry Dataset (PRiDe)**. *Semin Oncol* 2014, **41 Suppl 6**:S4–S13.
Mullis KB, Faloona FA: **Specific synthesis of DNA in vitro via a polymerase-catalyzed chain reaction**. *Methods Enzymol* 1987, **155**:335–350.
Mulpuru SK, Madhavan M, McLeod CJ, Cha YM, Friedman PA: **Cardiac Pacemakers: Function, Troubleshooting, and Management: Part 1 of a 2-Part Series**. *J Am Coll Cardiol* 2017, **69**:189–210.
Mumblat H, Martinez-Conde A, Braten O, Munster M, Dor-On E, Schneiderman RS, Porat Y, Voloshin T, Davidi S, Blatt R, et al.: **Tumor Treating Fields (TTFields) downregulate the Fanconi Anemia-BRCA pathway and increase the efficacy of chemotherapy in malignant pleural mesothelioma preclinical models**. *Lung Cancer* 2021, **160**:99–110.
Murga M, Campaner S, Lopez-Contreras AJ, Toledo LI, Soria R, Montaña MF, D'Artista L, Schleker T, Guerra C, Garcia E, et al.: **Exploiting oncogene-induced replicative stress for the selective killing of Myc-driven tumors**. *Nat Struct Mol Biol* 2011, **18**:1331–1335.
Murina O, von Aesch C, Karakus U, Ferretti LP, Bolck HA, Hänggi K, Sartori AA: **FANCD2 and CtIP cooperate to repair DNA interstrand crosslinks**. *Cell Rep* 2014, **7**:1030–1038.
Murphy AK, Fitzgerald M, Ro T, Kim JH, Rabinowitsch AI, Chowdhury D, Schildkraut CL, Borowiec JA: **Phosphorylated RPA recruits PALB2 to stalled DNA replication forks to facilitate fork recovery**. *J Cell Biol* 2014, **206**:493.
Murphy DM, Buckley PG, Bryan K, Das S, Alcock L, Foley NH, Prenter S, Bray I, Watters KM, Higgins D, et al.: **Global MYCN Transcription Factor Binding Analysis in Neuroblastoma Reveals Association with Distinct E-Box Motifs and Regions of DNA Hypermethylation**. *PLoS One* 2009, **4**:e8154.
Myers, A. L., Kawedia, J. D., Champlin, R. E., Kramer, M. A., Nieto, Y., Ghose, R., & Andersson, B. S. (2017). **Clarifying Busulfan Metabolism and Drug Interactions to Support New Therapeutic Drug Monitoring Strategies: A Comprehensive Review.** *Expert Opinion on Drug Metabolism & Toxicology*, **13**:901.
Nagel ZD, Kitange GJ, Gupta SK, Joughin BA, Chaim IA, Mazzucato P, Lauffenburger DA, Sarkaria JN, Samson LD: **DNA Repair Capacity in Multiple Pathways Predicts Chemoresistance in Glioblastoma Multiforme**. *Cancer Res* 2017, **77**:198.

Nagy A, Moens C, Ivanyi E, Pawling J, Gertsenstein M, Hadjantonakis AK, Pirity M, Rossant J: **Dissecting the role of N-myc in development using a single targeting vector to generate a series of alleles**. *Curr Biol* 1998, **8**:661–666.
Naifeh J, Varacallo M: *Biochemistry, Aerobic Glycolysis*. StatPearls Publishing; 2018.
Nakanishi K, Yang YG, Pierce AJ, Taniguchi T, Digweed M, D'Andréa AD, Wang ZQ, Jasin M: **Human Fanconi anemia monoubiquitination pathway promotes homologous DNA repair**. *Proc Natl Acad Sci U S A* 2005, **102**:1110.
Nakanishi R, Kitao H, Fujinaka Y, Yamashita N, Iimori M, Tokunaga E, Yamashita N, Morita M, Kakeji Y, Maehara Y: **FANCJ expression predicts the response to 5-fluorouracil-based chemotherapy in MLH1-proficient colorectal cancer**. *Ann Surg Oncol* 2012, **19**:3627–3635.
Nalepa G, Clapp DW: **Fanconi anaemia and cancer: An intricate relationship**. *Nat Rev Cancer* 2018, **18**:168–185.
Namkaew J, Jaroonwitchawan T, Rujanapun N, Saelee J, Noisa P: **Combined effects of curcumin and doxorubicin on cell death and cell migration of SH-SY5Y human neuroblastoma cells**. *In Vitro Cell Dev Biol Anim* 2018, **54**:629–639.
Nara K, Kusafuka T, Yoneda A, Oue T, Sangkhathat S, Fukuzawa M: **Silencing of MYCN by RNA interference induces growth inhibition, apoptotic activity and cell differentiation in a neuroblastoma cell line with MYCN amplification.** *Int J Oncol* 2007, **30**:1189–1196.
Nazareth D, Jones MJK, Gabrielli B: **Everything in Moderation: Lessons Learned by Exploiting Moderate Replication Stress in Cancer**. *Cancers (Basel)* 2019, **11**.
Negroni A, Scarpa S, Romeo A, Ferrari S, Modesti A, Raschellà G: **Decrease of proliferation rate and induction of differentiation by a MYCN antisense DNA oligomer in a human neuroblastoma cell line.** *Cell Growth Differ* 1991, **2**:511–518.
Newman EA, Chukkapalli S, Bashllari D, Thomas TT, Van Noord RA, Lawlor ER, Hoenerhoff MJ, Opipari AW, Opipari VP: **Alternative NHEJ pathway proteins as components of MYCN oncogenic activity in human neural crest stem cell differentiation: implications for neuroblastoma initiation.** *Cell Death Dis* 2017, **8**:3208.
Newman EA, Lu F, Bashllari D, Wang L, Opipari AW, Castle VP: **Alternative NHEJ Pathway Components Are Therapeutic Targets in High-Risk Neuroblastoma.** *Mol Cancer Res* 2015, **13**:470–482.
Nie Z, Hu G, Wei G, Cui K, Yamane A, Resch W, Wang R, Green DR, Tessarollo L, Casellas R, et al.: **c-Myc is a universal amplifier of expressed genes in lymphocytes and embryonic stem cells**. *Cell* 2012, **151**:68.
Niedernhofer LJ, Lalai AS, Hoeijmakers JHJ: **Fanconi anemia (cross)linked to DNA repair**. *Cell* 2005, **123**:1191–1198.
Niedernhofer LJ, Odijk H, Budzowska M, Drunen E van, Maas A, Theil AF, Wit J de, Jaspers NGJ, Beverloo HB, Hoeijmakers JHJ, et al.: **The Structure-Specific Endonuclease Ercc1-Xpf Is Required To Resolve DNA Interstrand Cross-Link-Induced Double-Strand Breaks**. *Mol Cell Biol* 2004, **24**:5776.
Niedzwiedz W, Mosedale G, Johnson M, Ong CY, Pace P, Patel KJ: **The Fanconi Anaemia Gene FANCC Promotes Homologous Recombination and Error-Prone DNA Repair**. *Mol Cell* 2004, **15**:607–620.
Nijman SMB, Huang TT, Dirac AMG, Brummelkamp TR, Kerkhoven RM, D'Andrea AD, Bernards R: **The deubiquitinating enzyme USP1 regulates the fanconi anemia pathway**. *Mol Cell* 2005, **17**:331–339.
Niraj J, Färkkilä A, D'Andrea AD: **The Fanconi Anemia Pathway in Cancer**. *Annu Rev cancer Biol* 2019, **3**:457–478.
Nojima K, Hochegger H, Saberi A, Fukushima T, Kikuchi K, Yoshimura M, Orelli BJ, Bishop DK, Hirano S, Ohzeki M, et al.: **Multiple repair pathways mediate tolerance to chemotherapeutic cross-linking agents in vertebrate cells**. *Cancer Res* 2005, **65**:11704–11711.
Norsker FN, Rechnitzer C, Andersen EW, Linnet KM, Kenborg L, Holmqvist AS, Tryggvadottir L, Madanat-Harjuoja LM, Øra I, Thorarinsdottir HK, et al.: **Neurologic**

disorders in long-term survivors of neuroblastoma - a population-based cohort study within the Adult Life after Childhood Cancer in Scandinavia (ALiCCS) research program. *Acta Oncol* 2020, **59**:134–140.
Noujaim D, van Golen CM, van Golen KL, Grauman A, Feldman EL: **N-Myc and Bcl-2 coexpression induces MMP-2 secretion and activation in human neuroblastoma cells**. *Oncogene* 2002, **21**:4549–4557.
Nuchtern JG, London WB, Barnewolt CE, Naranjo A, McGrady PW, Geiger JD, Diller L, Schmidt ML, Maris JM, Cohn SL, et al.: **A Prospective Study of Expectant Observation as Primary Therapy for Neuroblastoma in Young Infants**. *Ann Surg* 2012, **256**:573–580.
Nuss JE, Patrick SM, Oakley GG, Alter GM, Robison JG, Dixon K, Turchi JJ: **DNA Damage Induced Hyperphosphorylation of Replication Protein A. 1. Identification of Novel Sites of Phosphorylation in Response to DNA Damage**. *Biochemistry* 2005, **44**:8428.
O'Connell D, Shen V, Loudon W, Bota DA: **First report of tumor treating fields use in combination with bevacizumab in a pediatric patient: a case report**. *CNS Oncol* 2017, **6**:11.
Ochiai H, Takenobu H, Nakagawa A, Yamaguchi Y, Kimura M, Ohira M, Okimoto Y, Fujimura Y, Koseki H, Kohno Y, et al.: **Bmi1 is a MYCN target gene that regulates tumorigenesis through repression of KIF1Bβ and TSLC1 in neuroblastoma**. *Oncogene* 2010, **29**:2681–2690.
Okamoto Y, Abe M, Itaya A, Tomida J, Ishiai M, Takaori-Kondo A, Taoka M, Isobe T, Takata M: **FANCD2 protects genome stability by recruiting RNA processing enzymes to resolve R-loops during mild replication stress**. *FEBS J* 2019, **286**:139–150.
Okamoto Y, Abe M, Itaya A, Tomida J, Takaori-Kondo A, Taoka M, Isobe T, Takata M: **hnRNP U and DDX47 Are Novel FANCD2 Interactors That May Help to Resolve R-Loops during Mild Replication Stress**. *Blood* 2018, **132**:1301.
Okamoto Y, Iwasaki WM, Kugou K, Takahashi KK, Oda A, Sato K, Kobayashi W, Kawai H, Sakasai R, Takaori-Kondo A, et al.: **Replication stress induces accumulation of FANCD2 at central region of large fragile genes**. *Nucleic Acids Res* 2018, **46**:2932–2944.
Okawa ER, Gotoh T, Manne J, Igarashi J, Fujita T, Silverman KA, Xhao H, Mosse YP, White PS, Brodeur GM: **Expression and sequence analysis of candidates for the 1p36.31 tumor suppressor gene deleted in neuroblastomas**. *Oncogene* 2008, **27**:803–810.
Oliynyk G, Ruiz-Pérez MV, Sainero-Alcolado L, Dzieran J, Zirath H, Gallart-Ayala H, Wheelock C, Johansson HJ, Nilsson R, Lehtiö J, et al.: **MYCN-enhanced Oxidative and Glycolytic Metabolism Reveals Vulnerabilities for Targeting Neuroblastoma**. *iScience* 2019, **21**:188.
Olsen RR, Otero JH, García-López J, Wallace K, Finkelstein D, Rehg JE, Yin Z, Wang YD, Freeman KW: **MYCN induces neuroblastoma in primary neural crest cells**. *Oncogene* 2017, **36**:5075.
Osborne, M. R., & Lawley, P. D. (1993). **Alkylation of DNA by melphalan with special reference to adenine derivatives and adenine-guanine cross-linking.** *Chemico-Biological Interactions*, **89**:49–60.
Otsuki T, Young DB, Sasaki DT, Pando MP, Li J, Manning A, Hoekstra M, Hoatlin ME, Mercurio F, Liu JM: **Fanconi anemia protein complex is a novel target of the IKK signalsome**. *J Cell Biochem* 2002, **86**:613–623.
Otte J, Dyberg C, Pepich A, Johnsen JI: **MYCN Function in Neuroblastoma Development**. *Front Oncol* 2021, **10**:3210.
Otto T, Horn S, Brockmann M, Eilers U, Schüttrumpf L, Popov N, Kenney AM, Schulte JH, Beijersbergen R, Christiansen H, et al.: **Stabilization of N-Myc is a critical function of Aurora A in human neuroblastoma.** *Cancer Cell* 2009, **15**:67–78.
Ozawa H, Iwatsuki M, Mimori K, Sato T, Johansson F, Toh H, Watanabe M, Mori M: **FANCD2 mRNA overexpression is a bona fide indicator of lymph node metastasis in human colorectal cancer**. *Ann Surg Oncol* 2010, **17**:2341–2348.

Ozer E, Altungoz O, Unlu M, Aygun N, Tumer S, Olgun N: **Association of MYCN amplification and 1p deletion in neuroblastomas with high tumor vascularity**. *Appl Immunohistochem Mol Morphol* 2007, **15**:181–186.
Pace P, Mosedale G, Hodskinson MR, Rosado IV, Sivasubramaniam M, Patel KJ: **Ku70 corrupts DNA repair in the absence of the fanconi anemia pathway**. *Science (80-)* 2010, **329**:219–223.
Palovcak A, Liu W, Yuan F, Zhang Y: **Maintenance of genome stability by Fanconi anemia proteins**. *Cell Biosci* 2017, **7**.
Pan Q, Fang Y, Xu Y, Zhang K, Hu X: **Down-regulation of DNA polymerases κ, η, ι, and ζ in human lung, stomach, and colorectal cancers**. *Cancer Lett* 2005, **217**:139–147.
Pan X, Chen Y, Biju B, Ahmed N, Kong J, Goldenberg M, Huang J, Mohan N, Klosek S, Parsa K, et al.: **FANCM suppresses DNA replication stress at ALT telomeres by disrupting TERRA R-loops**. *Sci Rep* 2019, **9**.
Pan X, Drosopoulos WC, Sethi L, Madireddy A, Schildkraut CL, Zhang D: **FANCM, BRCA1, and BLM cooperatively resolve the replication stress at the ALT telomeres**. *Proc Natl Acad Sci U S A* 2017, **114**:E5940–E5949.
Park JI, Song KH, Jung SY, Ahn J, Hwang SG, Kim J, Kim EH, Song JY: **Tumor-Treating Fields Induce RAW264.7 Macrophage Activation Via NK-κB/MAPK Signaling Pathways**. *Technol Cancer Res Treat* 2019, **18**.
Park JR, Bagatell R, London WB, Maris JM, Cohn SL, Mattay KM, Hogarty M: **Children's Oncology Group's 2013 blueprint for research: Neuroblastoma**. *Pediatr Blood Cancer* 2013, **60**:985–993.
Park JR, Kreissman SG, London WB, Naranjo A, Cohn SL, Hogarty MD, Tenney SC, Haas-Kogan D, Shaw PJ, Kraveka JM, et al.: **Effect of Tandem Autologous Stem Cell Transplant vs Single Transplant on Event-Free Survival in Patients With High-Risk Neuroblastoma: A Randomized Clinical Trial**. *JAMA* 2019, **322**:746–755.
Park JY, Virts EL, Jankowska A, Wiek C, Othman M, Chakraborty SC, Vance GH, Alkuraya FS, Hanenberg H, Andreassen PR: **Complementation of hypersensitivity to DNA interstrand crosslinking agents demonstrates that XRCC2 is a Fanconi anaemia gene**. *J Med Genet* 2016, **53**:672–680.
Patil AA, Sayal P, Depondt M-L, Beveridge RD, Roylance A, Kriplani DH, Myers KN, Cox A, Jellinek D, Fernando M, et al.: **FANCD2 re-expression is associated with glioma grade and chemical inhibition of the Fanconi Anaemia pathway sensitises gliomas to chemotherapeutic agents**. *Oncotarget* 2014, **5**:6414.
Pearl LH, Schierz AC, Ward SE, Al-Lazikani B, Pearl FMG: **Therapeutic opportunities within the DNA damage response**. *Nat Rev Cancer* 2015, **15**:166–180.
Peifer M, Hertwig F, Roels F, Dreidax D, Gartlgruber M, Menon R, Krämer A, Roncaioli JL, Sand F, Heuckmann JM, et al.: **Telomerase activation by genomic rearrangements in high-risk neuroblastoma**. *Nature* 2015, **526**:700.
Peirce SK, Findley H: **High level MycN expression in non-MYCN amplified neuroblastoma is induced by the combination treatment nutlin-3 and doxorubicin and enhances chemosensitivity**. *Oncol Rep* 2009, **22**:1443–1449.
Pejovic T, Yates JE, Liu HY, Hays LE, Akkari Y, Torimaru Y, Keeble W, Rathbun RK, Rodgers WH, Bale AE, et al.: **Cytogenetic Instability in Ovarian Epithelial Cells from Women at Risk of Ovarian Cancer**. *Cancer Res* 2006, **66**:9017–9025.
Perez CA, Matthay KK, Atkinson JB, Seeger RC, Shimada H, Haase GM, Stram DO, Gerbing RB, Lukens JN: **Biologic Variables in the Outcome of Stages I and II Neuroblastoma Treated With Surgery as Primary Therapy: A Children's Cancer Group Study**. *J Clin Oncol* 2000, **18**:18.
Perini G, Diolaiti D, Porro A, Della Valle G: **In vivo transcriptional regulation of N-Myc target genes is controlled by E-box methylation**. *Proc Natl Acad Sci* 2005, **102**:12117–12122.
Perry P, Evans HJ: **Cytological detection of mutagen–carcinogen exposure by sister chromatid exchange**. *Nat 1975 2585531* 1975, **258**:121–125.

Petermann E, Helleday T: **Pathways of mammalian replication fork restart**. *Nat Rev Mol Cell Biol* 2010, **11**:683–687.
Petermann E, Lan L, Zou L: **Sources, resolution and physiological relevance of R-loops and RNA–DNA hybrids**. *Nat Rev Mol Cell Biol 2022 238* 2022, **23**:521–540.
Petroni M, Sardina F, Heil C, Sahún-Roncero M, Colicchia V, Veschi V, Albini S, Fruci D, Ricci B, Soriani A, et al.: **The MRN complex is transcriptionally regulated by MYCN during neural cell proliferation to control replication stress**. *Cell Death Differ* 2016, **23**:197.
Petroni M, Sardina F, Infante P, Bartolazzi A, Locatelli E, Fabretti F, Di Giulio S, Capalbo C, Cardinali B, Coppa A, et al.: **MRE11 inhibition highlights a replication stress-dependent vulnerability of MYCN-driven tumors**. *Cell Death Dis* 2018, **9**:895.
Petroni M, Veschi V, Gulino A, Giannini G: **Molecular mechanisms of MYCN-dependent apoptosis and the MDM2–p53 pathway: an Achille's heel to be exploited for the therapy of MYCN-amplified neuroblastoma**. *Front Oncol* 2012, **2**:141.
Petroni M, Veschi V, Prodosmo A, Rinaldo C, Massimi I, Carbonari M, Dominici C, McDowell HP, Rinaldi C, Screpanti I, et al.: **MYCN sensitizes human neuroblastoma to apoptosis by HIPK2 activation through a DNA damage response.** *Mol Cancer Res* 2011, **9**:67–77.
Pickering MT, Stadler BM, Kowalik TF: **miR-17 and miR-20a temper an E2F1-induced G1 checkpoint to regulate cell cycle progression**. *Oncogene* 2009, **28**:140–145.
Picone P, Nuzzo D, Caruana L, Messina E, Scafidi V, Carlo MD: **Curcumin induces apoptosis in human neuroblastoma cells via inhibition of AKT and Foxo3a nuclear translocation**. *http://dx.doi.org/103109/107157622014960410* 2014, doi:10.3109/10715762.2014.960410.
Pierantoni GM, Rinaldo C, Mottolese M, Benedetto AD, Esposito F, Soddu S, Fusco A: **High-mobility group A1 inhibits p53 by cytoplasmic relocalization of its proapoptotic activator HIPK2**. *J Clin Invest* 2007, **117**:693.
Pilch DR, Sedelnikova OA, Redon C, Celeste A, Nussenzweig A, Bonner WM: **Characteristics of gamma-H2AX foci at DNA double-strand breaks sites**. *Biochem Cell Biol* 2003, **81**:123–129.
Pinto N, Naranjo A, Hibbitts E, Kreissman SG, Granger MM, Irwin MS, Bagatell R, London WB, Greengard EG, Park JR, et al.: **Predictors of differential response to induction therapy in high-risk neuroblastoma: A report from the Children's Oncology Group (COG)**. *Eur J Cancer* 2019, **112**:66–79.
Pisano M, Pagnan G, Dettori MA, Cossu S, Caffa I, Sassu I, Emionite L, Fabbri D, Cilli M, Pastorino F, et al.: **Enhanced anti-tumor activity of a new curcumin-related compound against melanoma and neuroblastoma cells**. *Mol Cancer* 2010, **9**:137.
Pladevall-Morera D, Munk S, Ingham A, Garribba L, Albers E, Liu Y, Olsen JV, Lopez-Contreras AJ: **Proteomic characterization of chromosomal common fragile site (CFS)-associated proteins uncovers ATRX as a regulator of CFS stability**. *Nucleic Acids Res* 2019, doi:10.1093/nar/gkz510.
Plantaz D, Vandesompele J, Roy NV, Łastowska M, Bown N, Combaret V, Favrot MC, Delattre O, Michon J, Bénard J, et al.: **COMPARATIVE GENOMIC HYBRIDIZATION (CGH) ANALYSIS OF STAGE 4 NEUROBLASTOMA REVEALS HIGH FREQUENCY OF 11Q DELETION IN TUMORS LACKING MYCN AMPLIFICATION**. *Int J Cancer* 2001, **91**:680–686.
Polk C: **Bioelectromagnetic Dosimetry**. 1995, doi:10.1021/BA-1995-0250.CH004.
Pontel LB, Rosado IV, Burgos-Barragan G, Garaycoechea JI, Yu R, Arends MJ, Chandrasekaran G, Broecker V, Wei W, Liu L, et al.: **Endogenous Formaldehyde Is a Hematopoietic Stem Cell Genotoxin and Metabolic Carcinogen**. *Mol Cell* 2015, **60**:177–188.
Ponzoni M, Bachetti T, Corrias MV, Brignole C, Pastorino F, Calarco E, Bensa V, Giusto E, Ceccherini I, Perri P: **Recent advances in the developmental origin of neuroblastoma: an overview**. *J Exp Clin Cancer Res* 2022, **41**.

Postow L, Ullsperger C, Keller RW, Bustamante C, Vologodskii AV, Cozzarelli NR: **Positive Torsional Strain Causes the Formation of a Four-way Junction at Replication Forks**. *J Biol Chem* 2001, **276**:2790–2796.
Prakash R, Satory D, Dray E, Papusha A, Scheller J, Kramer W, Krejci L, Klein H, Haber JE, Sung P, et al.: **Yeast Mph1 helicase dissociates Rad51-made D-loops: implications for crossover control in mitotic recombination**. *Genes Dev* 2009, **23**:67.
Pritchard J, Cotterill SJ, Germond SM, Imeson J, de Kraker J, Jones DR: **High dose melphalan in the treatment of advanced neuroblastoma: Results of a randomised trial (ENSG-1) by the European Neuroblastoma Study Group**. *Pediatr Blood Cancer* 2005, **44**:348–357.
Pugh TJ, Morozova O, Attiyeh EF, Asgharzadeh S, Wei JS, Auclair D, Carter SL, Cibulskis K, Hanna M, Kiezun A, et al.: **The genetic landscape of high-risk neuroblastoma**. *Nat Genet* 2013, **45**:279–284.
Pugh TJ, Weeraratne SD, Archer TC, Pomeranz Krummel DA, Auclair D, Bochicchio J, Carneiro MO, Carter SL, Cibulskis K, Erlich RL, et al.: **Medulloblastoma exome sequencing uncovers subtype-specific somatic mutations**. *Nature* 2012, **488**:106–110.
Puissant A, Frumm SM, Alexe G, Bassil CF, Qi J, Chanthery YH, Nekritz EA, Zeid R, Gustafson WC, Greninger P, et al.: **Targeting MYCN in Neuroblastoma by BET Bromodomain Inhibition**. *Cancer Discov* 2013, **3**:308–323.
Qiao F, Mi J, Wilson JB, Zhi G, Bucheimer NR, Jones NJ, Kupfer GM: **Phosphorylation of fanconi anemia (FA) complementation group G protein, FANCG, at serine 7 is important for function of the FA pathway**. *J Biol Chem* 2004, **279**:46035–46045.
Qiu B, Matthay KK: **Advancing therapy for neuroblastoma**. *Nat Rev Clin Oncol 2022 198* 2022, **19**:515–533.
Raabe EH, Laudenslager M, Winter C, Wasserman N, Cole K, Laquaglia M, Maris DJ, Mosse YP, Maris JM: **Prevalence and functional consequence of PHOX2B mutations in neuroblastoma**. *Oncogene 2008 274* 2007, **27**:469–476.
Rader J, Russell MR, Hart LS, Nakazawa MS, Belcastro LT, Martinez D, Li Y, Carpenter EL, Attiyeh EF, Diskin SJ, et al.: **Dual CDK4/CDK6 Inhibition Induces Cell Cycle Arrest and Senescence in Neuroblastoma**. *Clin Cancer Res* 2013, **19**:6173–6182.
Raetz EA, Kim MKH, Moos P, Carlson M, Bruggers C, Hooper DK, Foot L, Liu T, Seeger R, Carroll WL: **Identification of Genes that Are Regulated Transcriptionally by Myc in Childhood Tumors**. 2003, doi:10.1002/cncr.11584.
Raffaghello L, Prigione I, Airoldi I, Camoriano M, Levreri I, Gambini C, Pende D, Steinte A, Ferrone S, Pistoia V: **Downregulation and/or release of NKG2D ligands as immune evasion strategy of human neuroblastoma**. *Neoplasia* 2004, **6**:558–568.
Raghunandan M, Chaudhury I, Kelich SL, Hanenberg H, Sobeck A: **FANCD2, FANCJ and BRCA2 cooperate to promote replication fork recovery independently of the Fanconi Anemia core complex**. *Cell Cycle* 2015, **14**:342–353.
Raghunandan M, Yeo JE, Walter R, Saito K, Harvey AJ, Ittershagen S, Lee EA, Yang J, Hoatlin ME, Bielinsky AK, et al.: **Functional cross talk between the Fanconi anemia and ATRX/DAXX histone chaperone pathways promotes replication fork recovery**. *Hum Mol Genet* 2020, **29**:1083.
Rajendra E, Oestergaard VH, Langevin F, Wang M, Dornan GL, Patel KJ, Passmore LA: **The genetic and biochemical basis of FANCD2 monoubiquitination.** *Mol Cell* 2014, **54**:858–869.
Rak S, Čimbora-Zovko T, Gajski G, Dubravčić K, Domijan AM, DelaŠ I, Garaj-Vrhovac V, Batinić D, Sorić J, Osmak M: **Carboplatin resistant human laryngeal carcinoma cells are cross resistant to curcumin due to reduced curcumin accumulation**. *Toxicol In Vitro* 2013, **27**:523–532.
Räschle M, Knipsheer P, Enoiu M, Angelov T, Sun J, Griffith JD, Ellenberger TE, Schärer OD, Walter JC: **Mechanism of Replication-Coupled DNA Interstrand Crosslink Repair**. *Cell* 2008, **134**:969–980.

Ray S, Atkuri KR, Deb-Basu D, Adler AS, Chang HY, Herzenberg LA, Felsher DW: **MYC Can Induce DNA Breaks In vivo and In vitro Independent of Reactive Oxygen Species**. *Cancer Res* 2006, **66**:6598–6605.
Raya Á, Rodríguez-Piz I, Guenechea G, Vassena R, Navarro S, Barrero MJ, Consiglio A, Castell M, Río P, Sleep E, et al.: **Disease-corrected haematopoietic progenitors from Fanconi anaemia induced pluripotent stem cells**. *Nature* 2009, **460**:53.
Reid S, Schindler D, Hanenberg H, Barker K, Hanks S, Kalb R, Neveling K, Kelly P, Seal S, Freund M, et al.: **Biallelic mutations in PALB2 cause Fanconi anemia subtype FA-N and predispose to childhood cancer**. *Nat Genet* 2007, **39**:162–164.
Reimann M, Loddenkemper C, Rudolph C, Schildhauer I, Teichmann B, Stein H, Schlegelberger B, Dörken B, Schmitt CA: **The Myc-evoked DNA damage response accounts for treatment resistance in primary lymphomas in vivo.** *Blood* 2007, **110**:2996–3004.
Renaudin X, Guervilly JH, Aoufouchi S, Rosselli F: **Proteomic analysis reveals a FANCA-modulated neddylation pathway involved in CXCR5 membrane targeting and cell mobility**. *J Cell Sci* 2014, **127**:3546–3554.
Ribatti D, Raffaghello L, Pastorino F, Nico B, Brignole C, Vacca A, Ponzoni M: **In vivo angiogenic activity of neuroblastoma correlates with MYCN oncogene overexpression**. *Int J Cancer* 2002, **102**:351–354.
Rickman DS, Schulte JH, Eilers M: **The Expanding World of N-MYC-Driven Tumors.** *Cancer Discov* 2018, **8**:150–163.
Rickman KA, Lach FP, Abhyankar A, Donovan FX, Sanborn EM, Kennedy JA, Sougnez C, Gabriel SB, Elemento O, Chandrasekharappa SC, et al.: **Deficiency of UBE2T, the E2 Ubiquitin Ligase Necessary for FANCD2 and FANCI Ubiquitination, Causes FA-T Subtype of Fanconi Anemia**. *Cell Rep* 2015, **12**:35–41.
Ridpath JR, Nakamura A, Tano K, Luke AM, Sonoda E, Arakawa H, Buerstedde J-M, Gillespie DAF, Sale JE, Yamazoe M, et al.: **Cells Deficient in the FANC/BRCA Pathway Are Hypersensitive to Plasma Levels of Formaldehyde**. *Cancer Res* 2007, **67**:11117–11122.
Robinson K, Asawachaicharn N, Galloway DA, Grandori C: **c-Myc Accelerates S-Phase and Requires WRN to Avoid Replication Stress**. *PLoS One* 2009, **4**:e5951.
Roderwieser A, Sand F, Walter E, Fischer J, Gecht J, Bartenhagen C, Ackermann S, Otte F, Welte A, Kahlert Y, et al.: **Telomerase Is a Prognostic Marker of Poor Outcome and a Therapeutic Target in Neuroblastoma**. *https://doi.org/101200/PO1900072* 2019, doi:10.1200/PO.19.00072.
Rodríguez A, D'Andrea A: **Fanconi anemia pathway**. *Curr Biol* 2017, **27**:R986–R988.
Rodríguez A, Yang C, Furutani E, García de Teresa B, Velázquez M, Filiatrault J, Sambel LA, Phan T, Flores-Guzmán P, Sánchez S, et al.: **Inhibition of TGFβ1 and TGFβ3 promotes hematopoiesis in Fanconi anemia**. *Exp Hematol* 2021, **93**:70-84.e4.
Rodríguez A, Zhang K, Färkkilä A, Filiatrault J, Yang C, Velázquez M, Furutani E, Goldman DC, García de Teresa B, Garza-Mayén G, et al.: **MYC Promotes Bone Marrow Stem Cell Dysfunction in Fanconi Anemia**. *Cell Stem Cell* 2021, **28**:33.
Roeschert I, Poon E, Henssen AG, Dorado Garcia H, Gatti M, Giansanti C, Jamin Y, Ade CP, Gallant P, Schülein-Völk C, et al.: **Combined inhibition of Aurora-A and ATR kinase results in regression of MYCN-amplified neuroblastoma**. *Nat cancer* 2021, **2**:312.
Rominiyi O, Vanderlinden A, Clenton SJ, Bridgewater C, Al-Tamimi Y, Collis SJ: **Tumour treating fields therapy for glioblastoma: current advances and future directions**. *Br J Cancer 2020 1244* 2020, **124**:697–709.
Root H, Larsen A, Komosa M, Al-Azri F, Li R, Bazett-Jones DP, Meyn MS: **FANCD2 limits BLM-dependent telomere instability in the alternative lengthening of telomeres pathway**. *Hum Mol Genet* 2016, **25**:3255–3268.
Rosado IV, Langevin F, Crossan GP, Takata M, Patel KJ: **Formaldehyde catabolism is essential in cells deficient for the Fanconi anemia DNA-repair pathway**. *Nat Struct Mol Biol* 2011, **18**:1432–1434.

Rosenbaum H, Webb E, Adams JM, Cory S, Harris AW: **N-myc transgene promotes B lymphoid proliferation, elicits lymphomas and reveals cross-regulation with c-myc.** *EMBO J* 1989, **8**:749–755.
Rosenberg PS, Tamary H, Alter BP: **How high are carrier frequencies of rare recessive syndromes? Contemporary estimates for Fanconi Anemia in the United States and Israel**. *Am J Med Genet Part A* 2011, **155**:1877–1883.
Roy U, Schärer OD: **Involvement of Translesion Synthesis DNA Polymerases in DNA Interstrand Crosslink Repair**. *DNA Repair (Amst)* 2016, **44**:33.
Rubie H, De Bernardi B, Gerrard M, Canete A, Ladenstein R, Couturier J, Ambros P, Munzer C, Pearson ADJ, Garaventa A, et al.: **Excellent outcome with reduced treatment in infants with nonmetastatic and unresectable neuroblastoma without MYCN amplification: Results of the prospective INES 99.1**. *J Clin Oncol* 2011, **29**:449–455.
Rudland PS, Platt-Higgins AM, Davies LM, Rudland SDS, Wilson JB, Aladwani A, Winstanley JHR, Barraclough DL, Barraclough R, West CR, et al.: **Significance of the Fanconi anemia FANCD2 protein in sporadic and metastatic human breast cancer**. *Am J Pathol* 2010, **176**:2935–2947.
Rueden CT, Schindelin J, Hiner MC, DeZonia BE, Walter AE, Arena ET, Eliceiri KW: **ImageJ2: ImageJ for the next generation of scientific image data**. *BMC Bioinformatics* 2017, **18**:529.
Sabò A, Kress TR, Pelizzola M, De Pretis S, Gorski MM, Tesi A, Morelli MJ, Bora P, Doni M, Verrecchia A, et al.: **Selective transcriptional regulation by Myc in cellular growth control and lymphomagenesis**. *Nature* 2014, **511**:488.
Sackton KL, Dimova N, Zeng X, Tian W, Zhang M, Sackton TB, Meaders J, Pfaff KL, Sigoillot F, Yu H, et al.: **Synergistic Blockade of Mitotic Exit by Two Chemical Inhibitors of the APC/C**. *Nature* 2014, **514**:646.
Sakai W, Swisher EM, Karlan BY, Agarwal MK, Higgins J, Friedman C, Villegas E, Jacquemont C, Farrugia DJ, Couch FJ, et al.: **Secondary mutations as a mechanism of cisplatin resistance in BRCA2-mutated cancers**. *Nature* 2008, **451**:1116–1120.
Sanmartín E, Mu~ Noz L, Piqueras M, Sirerol JA, Berlanga P, Ca~ Nete A, Castel V, Font De Mora J: **Deletion of 11q in Neuroblastomas Drives Sensitivity to PARP Inhibition**. *Clin Cancer Res* 2017, **23**.
Sanmartín E, Mu~ Noz L, Piqueras M, Sirerol JA, Berlanga P, Ca~ Nete A, Castel V, Font De Mora J: **Personalized Medicine and Imaging Deletion of 11q in Neuroblastomas Drives Sensitivity to PARP Inhibition**. *Clin Cancer Res* 2017, **23**.
Santos-Pereira JM, Aguilera A: **R loops: new modulators of genome dynamics and function**. *Nat Rev Genet 2015 1610* 2015, **16**:583–597.
Sareen A, Chaudhury I, Adams N, Sobeck A: **Fanconi anemia proteins FANCD2 and FANCI exhibit different DNA damage responses during S-phase**. *Nucleic Acids Res* 2012, **40**:8425–8439.
Sarkar S, Davies AA, Ulrich HD, McHugh PJ: **DNA interstrand crosslink repair during G1 involves nucleotide excision repair and DNA polymerase ζ**. *EMBO J* 2006, **25**:1285.
Sarkaria JN, Kitange GJ, James CD, Plummer R, Calvert H, Weller M, Wick W: **Mechanisms of Chemoresistance in Malignant Glioma**. *Clin Cancer Res* 2008, **14**:2900.
Sasaki MS: **Is Fanconi's anaemia defective in a process essential to the repair of DNA cross links?** *Nat 1975 2575526* 1975, **257**:501–503.
Sausen M, Leary RJ, Jones S, Wu J, Reynolds CP, Liu X, Blackford A, Parmigiani G, Diaz LA, Papadopoulos N, et al.: **Integrated genomic analyses identify ARID1A and ARID1B alterations in the childhood cancer neuroblastoma**. *Nat Genet* 2013, **45**:12.
Sawai S, Shimono A, Wakamatsu Y, Palmes C, Hanaoka K, Kondoh H: **Defects of embryonic organogenesis resulting from targeted disruption of the N-myc gene in the mouse.** *Development* 1993, **117**:1445–1455.

Sawyer SL, Tian L, Kähkönen M, Schwartzentruber J, Kircher M, Majewski J, Dyment DA, Innes AM, Boycott KM, Moreau LA, et al.: **Biallelic mutations in BRCA1 cause a new Fanconi anemia subtype**. *Cancer Discov* 2015, **5**:135–142.
Schärer OD: **DNA Interstrand Crosslinks: Natural and Drug-Induced DNA Adducts that Induce Unique Cellular Responses**. *ChemBioChem* 2005, **6**:27–32.
Schaub FX, Dhankani V, Berger AC, Trivedi M, Richardson AB, Shaw R, Zhao W, Zhang X, Ventura A, Liu Y, et al.: **Pan-cancer Alterations of the MYC Oncogene and Its Proximal Network across the Cancer Genome Atlas**. *Cell Syst* 2018, **6**:282-300.e2.
Schindelin J, Arganda-Carreras I, Frise E, Kaynig V, Longair M, Pietzsch T, Preibisch S, Rueden C, Saalfeld S, Schmid B, et al.: **Fiji: an open-source platform for biological-image analysis**. *Nat Methods* 2012, **9**:676–682.
Schindler D, Hoehn H: **Fanconi anemia mutation causes cellular susceptibility to ambient oxygen.** *Am J Hum Genet* 1988, **43**:429.
Schlacher K, Christ N, Siaud N, Egashira A, Wu H, Jasin M: **Double-Strand Break Repair Independent Role For BRCA2 In Blocking Stalled Replication Fork Degradation By MRE11**. *Cell* 2011, **145**:529.
Schlacher K, Wu H, Jasin M: **A distinct replication fork protection pathway connects Fanconi anemia tumor suppressors to RAD51-BRCA1/2.** *Cancer Cell* 2012, **22**:106–116.
Schleiermacher G, Janoueix-Lerosey I, Ribeiro A, Klijanienko J, Couturier J, Pierron G, Mosseri V, Valent A, Auger N, Plantaz D, et al.: **Accumulation of Segmental Alterations Determines Progression in Neuroblastoma**. *J Clin Oncol* 2010, **28**:3122–3130.
Schmittgen TD, Zakrajsek BA, Mills AG, Gorn V, Singer MJ, Reed MW: **Quantitative Reverse Transcription–Polymerase Chain Reaction to Study mRNA Decay: Comparison of Endpoint and Real-Time Methods**. *Anal Biochem* 2000, **285**:194–204.
Schneiderman RS, Voloshin T, Giladi M, Porat Y, Munster M, Blat R, Sherbo S, Kirson ED, Weinberg U, Palti Y: **ATPS-25p53 STATUS DEPENDENCE OF TUMOR TREATING FIELDS (TTFIELDS) EFFICACY AGAINST GLIOMA CANCER CELLS**. *Neuro Oncol* 2015, **17**:v23–v23.
Schnepp RW, Khurana P, Attiyeh EF, Raman P, Chodosh SE, Oldridge DA, Gagliardi ME, Conkrite KL, Asgharzadeh S, Seeger RC, et al.: **A LIN28B-RAN-AURKA Signaling Network Promotes Neuroblastoma Tumorigenesis**. *Cancer Cell* 2015, **28**:599.
Schönherr C, Ruuth K, Kamaraj S, Wang C-L, Yang H-L, Combaret V, Djos A, Martinsson T, Christensen JG, Palmer RH, et al.: **Anaplastic Lymphoma Kinase (ALK) regulates initiation of transcription of MYCN in neuroblastoma cells**. *Oncogene* 2012, **31**:5193–5200.
Schoppy DW, Ragland RL, Gilad O, Shastri N, Peters AA, Murga M, Fernandez-Capetillo O, Diehl JA, Brown EJ: **Oncogenic stress sensitizes murine cancers to hypomorphic suppression of ATR**. *J Clin Invest* 2012, **122**:241.
Schramm A, Köster J, Marschall T, Martin M, Schwermer M, Fielitz K, Büchel G, Barann M, Esser D, Rosenstiel P, et al.: **Next-generation RNA sequencing reveals differential expression of MYCN target genes and suggests the mTOR pathway as a promising therapy target in MYCN-amplified neuroblastoma**. *Int J Cancer* 2013, **132**:E106–E115.
Schulte JH, Lindner S, Bohrer A, Maurer J, De Preter K, Lefever S, Heukamp L, Schulte S, Molenaar J, Versteeg R, et al.: **MYCN and ALKF1174L are sufficient to drive neuroblastoma development from neural crest progenitor cells**. *Oncogene* 2013, **32**:1059–1065.
Schulte JH, Eggert A: **ALK Inhibitors in Neuroblastoma: A Sprint from Bench to Bedside**. *Clin Cancer Res* 2021, **27**:3507–3509.
Schwab M, Varmus HE, Bishop JM: **Human N-myc gene contributes to neoplastic transformation of mammalian cells in culture.** *Nature* 1985, **316**:160–162.
Schwab M: **Oncogene amplification in solid tumors**. *Semin Cancer Biol* 1999, **9**:319–325.
Schwab M: **Amplification of the MYCN oncogene and deletion of putative tumour suppressor gene in human neuroblastomas**. *Brain Pathol* 1990, **1**:41–46.

Schwab M, Alitalo K, Klempnauer K-H, Varmus HE, Bishop JM, Gilbert F, Brodeur G, Goldstein M, Trent J: **Amplified DNA with limited homology to myc cellular oncogene is shared by human neuroblastoma cell lines and a neuroblastoma tumour**. *Nature* 1983, **305**:245–248.
Schwab M, Varmus HE, Bishop JM, Grzeschik K-H, Naylor SL, Sakaguchi AY, Brodeur G, Trent J: **Chromosome localization in normal human cells and neuroblastomas of a gene related to c-myc**. *Nature* 1984, **308**:288–291.
Schwab RA, Blackford AN, Niedzwiedz W: **ATR activation and replication fork restart are defective in FANCM-deficient cells.** *EMBO J* 2010, **29**:806–818.
Schwab RA, Nieminuszczy J, Shah F, Langton J, Lopez Martinez D, Liang C-C, Cohn MA, Gibbons RJ, Deans AJ, Niedzwiedz W: **The Fanconi Anemia Pathway Maintains Genome Stability by Coordinating Replication and Transcription.** *Mol Cell* 2015, **60**:351–361.
Seeger RC, Brodeur GM, Sather H, Dalton A, Siegel SE, Wong KY, Hammond D: **Association of Multiple Copies of the N- *myc* Oncogene with Rapid Progression of Neuroblastomas**. *N Engl J Med* 1985, **313**:1111–1116.
Serra A, Eirich K, Winkler AK, Mrasek K, Göhring G, Barbi G, Cario H, Schlegelberger B, Pokora B, Liehr T, et al.: **Shared Copy Number Variation in Simultaneous Nephroblastoma and Neuroblastoma due to Fanconi Anemia**. *Mol Syndr* 2012, **3**:120–130.
Shah DR, Green S, Elliot A, McGahan JP, Khatri VP: **Current oncologic applications of radiofrequency ablation therapies**. *World J Gastrointest Oncol* 2013, **5**:71.
Shahaf GL, Giladi M, Schneiderman R, Kinzel A, Weinberg U, Kirson E, Palti Y: **P04.17 Cancer cell lines response to tumor treating fields: results of a meta-analysis**. *Neuro Oncol* 2018, **20**:iii282.
Shakeel S, Rajendra E, Alcón P, O'Reilly F, Chorev DS, Maslen S, Degliesposti G, Russo CJ, He S, Hill CH, et al.: **Structure of the Fanconi anaemia monoubiquitin ligase complex**. *Nature* 2019, **575**:234–237.
Shakeel S, Rajendra E, Alcón P, O'Reilly F, Chorev DS, Maslen S, Degliesposti G, Russo CJ, He S, Hill CH, et al.: **Structure of the Fanconi anaemia monoubiquitin ligase complex**. *Nature* 2019, **575**:234–237.
Shang HS, Chang CH, Chou YR, Yeh MY, Au MK, Lu HF, Chu YL, Chou HM, Chou HC, Shih YL, et al.: **Curcumin causes DNA damage and affects associated protein expression in HeLa human cervical cancer cells**. *Oncol Rep* 2016, **36**:2207–2215.
Shang X, Burlingame SM, Okcu MF, Ge N, Russell HV, Egler RA, David RD, Vasudevan SA, Yang J, Nuchtern JG: **Aurora A is a negative prognostic factor and a new therapeutic target in human neuroblastoma**. *Mol Cancer Ther* 2009, **8**:2461.
Sharp MF, Bythell-Douglas R, Deans AJ, Crismani W: **The Fanconi anemia ubiquitin E3 ligase complex as an anti-cancer target**. *Mol Cell* 2021, **81**:2278–2289.
Sharp MF, Murphy VJ, Twest SV, Tan W, Lui J, Simpson KJ, Deans AJ, Crismani W: **Methodology for the identification of small molecule inhibitors of the Fanconi Anaemia ubiquitin E3 ligase complex**. *Sci Reports 2020 101* 2020, **10**:1–11.
Shi H, Tao T, Abraham BJ, Durbin AD, Zimmerman MW, Kadoch C, Thomas Look A: **ARID1A loss in neuroblastoma promotes the adrenergic-to-mesenchymal transition by regulating enhancer-mediated gene expression**. *Sci Adv* 2020, **6**.
Shimada H, Stram DO, Chatten J, Joshi VV, Hachitanda Y, Brodeur GM, Lukens JN, Matthay KK, Seeger RC: **Identification of subsets of neuroblastomas by combined histopathologic and N-myc analysis.** *J Natl Cancer Inst* 1995, **87**:1470–1476.
Sholler GLS, Ferguson W, Bergendahl G, Bond JP, Neville K, Eslin D, Brown V, Roberts W, Wada RK, Oesterheld J, et al.: **Maintenance DFMO Increases Survival in High Risk Neuroblastoma**. *Sci Rep* 2018, **8**.
Shreeram S, Hee WK, Demidov ON, Kek C, Yamaguchi H, Fornace AJ, Anderson CW, Appella E, Bulavin DV, Bulavin DV: **Regulation of ATM/p53-dependent suppression of myc-induced lymphomas by Wip1 phosphatase.** *J Exp Med* 2006, **203**:2793–2799.

Shteingauz A, Porat Y, Voloshin T, Schneiderman RS, Munster M, Zeevi E, Kaynan N, Gotlib K, Giladi M, Kirson ED, et al.: **AMPK-dependent autophagy upregulation serves as a survival mechanism in response to Tumor Treating Fields (TTFields)**. *Cell Death Dis* 2018, **9**.
Sidhar H, Giri RK: **Induction of Bex genes by curcumin is associated with apoptosis and activation of p53 in N2a neuroblastoma cells**. *Sci Rep* 2017, **7**.
Silginer M, Weller M, Stupp R, Roth P: **Biological activity of tumor-treating fields in preclinical glioma models**. *Cell Death Dis* 2017, **8**:e2753.
Silva B, Pentz R, Figueira AM, Arora R, Lee YW, Hodson C, Wischnewski H, Deans AJ, Azzalin CM: **FANCM limits ALT activity by restricting telomeric replication stress induced by deregulated BLM and R-loops**. *Nat Commun* 2019, **10**:2253.
Simon T, Hero B, Faldum A, Handgretinger R, Schrappe M, Niethammer D, Berthold F: **Consolidation treatment with chimeric anti-GD2-antibody ch14.18 in children older than 1 year with metastatic neuroblastoma.** *J Clin Oncol* 2004, **22**:3549–3557.
Sims AE, Spiteri E, Sims RJ, Arita AG, Lach FP, Landers T, Wurm M, Freund M, Neveling K, Hanenberg H, et al.: **FANCI is a second monoubiquitinated member of the Fanconi anemia pathway**. *Nat Struct Mol Biol* 2007, **14**:564–567.
Singh TR, Ali AM, Paramasivam M, Pradhan A, Wahengbam K, Seidman MM, Meetei AR: **ATR-Dependent Phosphorylation of FANCM at Serine 1045 is Essential for FANCM Functions**. *Cancer Res* 2013, **73**:4300.
Singh TR, Bakker ST, Agarwal S, Jansen M, Grassman E, Godthelp BC, Ali AM, Du CH, Rooimans MA, Fan Q, et al.: **Impaired FANCD2 monoubiquitination and hypersensitivity to camptothecin uniquely characterize Fanconi anemia complementation group M**. *Blood* 2009, **114**:174–180.
Sinha S, Singh RK, Alam N, Roy A, Roychoudhury S, Panda CK: **Alterations in candidate genes PHF2, FANCC, PTCH1 and XPA at chromosomal 9q22.3 region: Pathological significance in early- and late-onset breast carcinoma**. *Mol Cancer* 2008, **7**:84.
Škubník, J., Pavlíčková, V. S., Ruml, T., & Rimpelová, S. (2021). **Vincristine in Combination Therapy of Cancer: Emerging Trends in Clinics.** *Biology*, **10**.
Slack A, Chen Z, Tonelli R, Pule M, Hunt L, Pession A, Shohet JM: **The p53 regulatory gene MDM2 is a direct transcriptional target of MYCN in neuroblastoma.** *Proc Natl Acad Sci U S A* 2005, **102**:731–736.
Smith V, Foster J: **High-Risk Neuroblastoma Treatment Review**. *Children* 2018, **5**:114.
Smogorzewska A, Desetty R, Saito TT, Schlabach M, Lach FP, Sowa ME, Clark AB, Kunkel TA, Harper JW, Colaiácovo MP, et al.: **A genetic screen identifies FAN1, a Fanconi anemia-associated nuclease necessary for DNA interstrand crosslink repair**. *Mol Cell* 2010, **39**:36–47.
Smogorzewska A, Matsuoka S, Vinciguerra P, McDonald ER, Hurov KE, Luo J, Ballif BA, Gygi SP, Hofmann K, D'Andrea AD, et al.: **Identification of the FANCI protein, a monoubiquitinated FANCD2 paralog required for DNA repair**. *Cell* 2007, **129**:289–301.
Sobeck A, Stone S, Costanzo V, Graaf B de, Reuter T, Winter J de, Wallisch M, Akkari Y, Olson S, Wang W, et al.: **Fanconi Anemia Proteins Are Required To Prevent Accumulation of Replication-Associated DNA Double-Strand Breaks**. *Mol Cell Biol* 2006, **26**:425.
Somyajit K, Subramanya S, Nagaraju G: **RAD51C: a novel cancer susceptibility gene is linked to Fanconi anemia and breast cancer**. *Carcinogenesis* 2010, **31**:2031.
Southgate HED, Chen L, Tweddle DA, Curtin NJ: **ATR Inhibition Potentiates PARP Inhibitor Cytotoxicity in High Risk Neuroblastoma Cell Lines by Multiple Mechanisms**. *Cancers (Basel)* 2020, **12**:1095.
Spitz R, Hero B, Ernestus K, Berthold F: **Clinical Cancer Research**. *Clin Cancer Res* 2003, **9**:52–58.
Sreenivasan S, Ravichandran S, Vetrivel U, Krishnakumar S: **Modulation of multidrug resistance 1 expression and function in retinoblastoma cells by curcumin**. *J Pharmacol Pharmacother* 2013, **4**:103.

Srinivasan SV, Dominguez-Sola D, Wang LC, Hyrien O, Gautier J: **Cdc45 Is a Critical Effector of Myc-Dependent DNA Replication Stress**. *Cell Rep* 2013, **3**:1629–1639.
Stanton BR, Perkins AS, Tessarollo L, Sassoon DA, Parada LF: **Loss of N-myc function results in embryonic lethality and failure of the epithelial component of the embryo to develop.** *Genes Dev* 1992, **6**:2235–2247.
Steinberg-Shemer O, Goldberg TA, Yacobovich J, Levin C, Koren A, Revel-Vilk S, Ben-Ami T, Kuperman AA, Zemer VS, Toren A, et al.: **Characterization and genotype-phenotype correlation of patients with Fanconi anemia in a multi-ethnic population**. *Haematologica* 2020, **105**:1825.
Stoepker C, Hain K, Schuster B, Hilhorst-Hofstee Y, Rooimans MA, Steltenpool J, Oostra AB, Eirich K, Korthof ET, Nieuwint AWM, et al.: **SLX4, a coordinator of structure-specific endonucleases, is mutated in a new Fanconi anemia subtype**. *Nat Genet* 2011, **43**:138–141.
Strathdee CA, Gavish H, Shannon WR, Buchwald M: **Cloning of cDNAs for Fanconi's anaemia by functional complementation**. *Nature* 1992, **358**:434.
Strober W: **Trypan Blue Exclusion Test of Cell Viability**. *Curr Protoc Immunol* 2001, **21**:A.3B.1-A.3B.2.
Strother DR, London WB, Schmidt ML, Brodeur GM, Shimada H, Thorner P, Collins MH, Tagge E, Adkins S, Reynolds CP, et al.: **Outcome After Surgery Alone or With Restricted Use of Chemotherapy for Patients With Low-Risk Neuroblastoma: Results of Children's Oncology Group Study P9641**. *J Clin Oncol* 2012, **30**:1842–1848.
Stupp R, Taillibert S, Kanner A, Read W, Steinberg DM, Lhermitte B, Toms S, Idbaih A, Ahluwalia MS, Fink K, et al.: **Effect of Tumor-Treating Fields Plus Maintenance Temozolomide vs Maintenance Temozolomide Alone on Survival in Patients With Glioblastoma: A Randomized Clinical Trial**. *JAMA* 2017, **318**:2306.
Stupp R, Taillibert S, Kanner AA, Kesari S, Steinberg DM, Toms SA, Taylor LP, Lieberman F, Silvani A, Fink KL, et al.: **Maintenance Therapy With Tumor-Treating Fields Plus Temozolomide vs Temozolomide Alone for Glioblastoma: A Randomized Clinical Trial**. *JAMA* 2015, **314**:2535–2543.
Stupp R, Wong ET, Kanner AA, Steinberg D, Engelhard H, Heidecke V, Kirson ED, Taillibert S, Liebermann F, Dbalý V, et al.: **NovoTTF-100A versus physician's choice chemotherapy in recurrent glioblastoma: a randomised phase III trial of a novel treatment modality**. *Eur J Cancer* 2012, **48**:2192–2202.
Suenaga Y, Islam SMR, Alagu J, Kaneko Y, Kato M, Tanaka Y, Kawana H, Hossain S, Matsumoto D, Yamamoto M, et al.: **NCYM, a Cis-Antisense Gene of MYCN, Encodes a De Novo Evolved Protein That Inhibits GSK3β Resulting in the Stabilization of MYCN in Human Neuroblastomas**. *PLoS Genet* 2014, **10**:e1003996.
Sukumari-Ramesh S, Bentley JN, Laird MD, Singh N, Vender JR, Dhandapani KM: **DIETARY PHYTOCHEMICALS INDUCE p53- AND CASPASE-INDEPENDENT CELL DEATH IN HUMAN NEUROBLASTOMA CELLS**. *Int J Dev Neurosci* 2011, **29**:701–710.
Sumpter R, Levine B: **Emerging functions of the Fanconi anemia pathway at a glance**. *J Cell Sci* 2017, **130**:2657.
Sun W, Nandi S, Osman F, Ahn JS, Jakovleska J, Lorenz A, Whitby MC: **The FANCM Ortholog Fml1 Promotes Recombination at Stalled Replication Forks and Limits Crossing Over during DNA Double-Strand Break Repair**. *Mol Cell* 2008, **32**:118.
Surade S, Blundell TL: **Structural Biology and Drug Discovery of Difficult Targets: The Limits of Ligandability**. *Chem Biol* 2012, **19**:42–50.
Swarbrick A, Woods SL, Shaw A, Balakrishnan A, Phua Y, Nguyen A, Chanthery Y, Lim L, Ashton LJ, Judson RL, et al.: **miR-380-5p represses p53 to control cellular survival and is associated with poor outcome in MYCN-amplified neuroblastoma.** *Nat Med* 2010, **16**:1134–1140.
Swarts DRA, Van Neste L, Henfling MER, Eijkenboom I, Eijk PP, van Velthuysen ML, Vink A, Volante M, Ylstra B, Van Criekinge W, et al.: **An exploration of pathways involved in**

lung carcinoid progression using gene expression profiling. *Carcinogenesis* 2013, **34**:2726–2737.
Swisher EM, Gonzalez RM, Taniguchi T, Garcia RL, Walsh T, Goff BA, Welcsh P: **Methylation and protein expression of DNA repair genes: association with chemotherapy exposure and survival in sporadic ovarian and peritoneal carcinomas**. *Mol Cancer* 2009, **8**:48.
Swuec P, Renault L, Borg A, Shah F, Murphy VJ, van Twest S, Snijders AP, Deans AJ, Costa A: **The FA Core Complex Contains a Homo-dimeric Catalytic Module for the Symmetric Mono-ubiquitination of FANCI-FANCD2**. *Cell Rep* 2017, **18**:611–623.
Takagi M, Ogawa C, Iehara T, Aoki-Nogami Y, Ishibashi E, Imai M, Kimura T, Nagata M, Yasuhara M, Masutani M, et al.: **First phase 1 clinical study of olaparib in pediatric patients with refractory solid tumors**. *Cancer* 2022, **128**:2949–2957.
Takagi M, Sato M, Piao J, Miyamoto S, Isoda T, Kitagawa M, Honda H, Mizutani S: **ATM-dependent DNA damage-response pathway as a determinant in chronic myelogenous leukemia**. *DNA Repair (Amst)* 2013, **12**:500–507.
Takagi M, Yoshida M, Nemoto Y, Tamaichi H, Tsuchida R, Seki M, Uryu K, Nishii R, Miyamoto S, Saito M, et al.: **Loss of DNA Damage Response in Neuroblastoma and Utility of a PARP Inhibitor**. *J Natl Cancer Inst* 2017, **109**:1–12.
Takaku M, Kainuma T, Ishida-Takaku T, Ishigami S, Suzuki H, Tashiro S, van Soest RWM, Nakao Y, Kurumizaka H: **Halenaquinone, a chemical compound that specifically inhibits the secondary DNA binding of RAD51**. *Genes Cells* 2011, **16**:427–436.
Takata M, Sasaki MS, Tachiiri S, Fukushima T, Sonoda E, Schild D, Thompson LH, Takeda S: **Chromosome Instability and Defective Recombinational Repair in Knockout Mutants of the Five Rad51 Paralogs**. *Mol Cell Biol* 2001, **21**:2858.
Tanaka N, Fukuzawa M: **MYCN downregulates integrin alpha1 to promote invasion of human neuroblastoma cells.** *Int J Oncol* 2008, **33**:815–821.
Taniguchi T, Garcia-Higuera I, Andreassen PR, Gregory RC, Grompe M, D'Andrea AD: **S-phase-specific interaction of the Fanconi anemia protein, FANCD2, with BRCA1 and RAD51**. *Blood* 2002, **100**:2414–2420.
Taniguchi T, Garcia-Higuera I, Xu B, Andreassen PR, Gregory RC, Kim S-T, Lane WS, Kastan MB, D'Andrea AD: **Convergence of the fanconi anemia and ataxia telangiectasia signaling pathways.** *Cell* 2002, **109**:459–472.
Taniguchi T, Tischkowitz M, Ameziane N, Hodgson SV, Mathew CG, Joenje H, Mok SC, D'Andrea AD: **Disruption of the Fanconi anemia–BRCA pathway in cisplatin-sensitive ovarian tumors**. *Nat Med* 2003, **9**:568–574.
Tao L, Mohammad MA, Milazzo G, Moreno-Smith M, Patel TD, Zorman B, Badachhape A, Hernandez BE, Wolf AB, Zeng Z, et al.: **MYCN-driven fatty acid uptake is a metabolic vulnerability in neuroblastoma**. *Nat Commun 2022 131* 2022, **13**:1–17.
Taylor SJ, Arends MJ, Langdon SP: **Inhibitors of the Fanconi anaemia pathway as potential antitumour agents for ovarian cancer**. *Explor Target Anti-tumor Ther* 2020, **1**:26.
ten Berge D, Brugmann SA, Helms JA, Nusse R, Kurimoto K, Saitou M, Matsuzaki F: **Wnt and FGF signals interact to coordinate growth with cell fate specification during limb development**. *Development* 2008, **135**:3247–3257.
Theruvath J, Menard M, Smith BAH, Linde MH, Coles GL, Dalton GN, Wu W, Kiru L, Delaidelli A, Sotillo E, et al.: **Anti-GD2 synergizes with CD47 blockade to mediate tumor eradication**. *Nat Med* 2022, **28**:333–344.
Thiele CJ, Reynolds CP, Israel MA: **Decreased expression of N-myc precedes retinoic acid-induced morphological differentiation of human neuroblastoma.** *Nature* 1985, **313**:404–406.
Thompson D, Vo KT, London WB, Fischer M, Ambros PF, Nakagawara A, Brodeur GM, Matthay KK, DuBois SG: **Identification of patient subgroups with markedly disparate rates of MYCN amplification in neuroblastoma: A report from the International Neuroblastoma Risk Group project**. *Cancer* 2016, **122**:935–945.

Thompson EL, Yeo JE, Lee EA, Kan Y, Raghunandan M, Wiek C, Hanenberg H, Schärer OD, Hendrickson EA, Sobeck A: **FANCI and FANCD2 have common as well as independent functions during the cellular replication stress response**. *Nucleic Acids Res* 2017, **45**:11837.

Timmers C, Taniguchi T, Hejna J, Reifsteck C, Lucas L, Bruun D, Thayer M, Cox B, Olson S, D'Andrea AD, et al.: **Positional cloning of a novel Fanconi anemia gene, FANCD2**. *Mol Cell* 2001, **7**:241–248.

Timmons JJ, Preto J, Tuszynski JA, Wong ET: **Tubulin's response to external electric fields by molecular dynamics simulations**. *PLoS One* 2018, **13**:e0202141.

Tisato V, Voltan R, Gonelli A, Secchiero P, Zauli G: **MDM2/X inhibitors under clinical evaluation: perspectives for the management of hematological malignancies and pediatric cancer**. *J Hematol Oncol* 2017, **10**.

Toledo LI, Murga M, Zur R, Soria R, Rodriguez A, Martinez S, Oyarzabal J, Pastor J, Bischoff JR, Fernandez-Capetillo O: **A cell-based screen identifies ATR inhibitors with synthetic lethal properties for cancer-associated mutations**. *Nat Struct Mol Biol* 2011, **18**:721–727.

Toms SA, Kim CY, Nicholas G, Ram Z: **Increased compliance with tumor treating fields therapy is prognostic for improved survival in the treatment of glioblastoma: a subgroup analysis of the EF-14 phase III trial**. *J Neurooncol* 2019, **141**:467–473.

Tonelli R, Purgato S, Camerin C, Fronza R, Bologna F, Alboresi S, Franzoni M, Corradini R, Sforza S, Faccini A, et al.: **Anti-gene peptide nucleic acid specifically inhibits MYCN expression in human neuroblastoma cells leading to cell growth inhibition and apoptosis**. *Mol Cancer Ther* 2005, **4**:779–786.

Tonini GP, Mazzocco K, Scaruffi P: **Oncogenes and suppressor genes in the genesis and progression of solid tumors in children**. *Pediatr Med Chir* 1994, **16**:203–209.

Torres R, Schreiber-Agus N, Morgenbesser SD, DePinho RA: **Myc and Max: a putative transcriptional complex in search of a cellular target.** *Curr Opin Cell Biol* 1992, **4**:468–474.

Towbin H, Staehelin T, Gordon J: **Electrophoretic transfer of proteins from polyacrylamide gels to nitrocellulose sheets: procedure and some applications.** *Proc Natl Acad Sci U S A* 1979, **76**:4350–4354.

Trivedi RN, Almeida KH, Fornsaglio JL, Schamus S, Sobol RW: **The Role of Base Excision Repair in the Sensitivity and Resistance to Temozolomide-Mediated Cell Death**. *Cancer Res* 2005, **65**:6394–6400.

Trochet D, Bourdeaut F, Janoueix-Lerosey I, Deville A, De Pontual L, Schleiermacher G, Coze C, Philip N, Frébourg T, Munnich A, et al.: **Germline mutations of the paired-like homeobox 2B (PHOX2B) gene in neuroblastoma**. *Am J Hum Genet* 2004, **74**:761–764.

Tsubota S, Kadomatsu K: **Origin and mechanism of neuroblastoma.** *Oncoscience* 2017, **4**:70–72.

Tsubota S, Kishida S, Shimamura T, Ohira M, Yamashita S, Cao D, Kiyonari S, Ushijima T, Kadomatsu K: **PRC2-mediated transcriptomic alterations at the embryonic stage govern tumorigenesis and clinical outcome in MYCN-driven neuroblastoma**. 2018, doi:10.1158/0008-5472.CAN-16-3144.

Tumilowicz JJ, Nichols WW, Cholon JJ, Greene Departments AE, Biology C: **Definition of a Continuous Human Cell Line Derived from Neuroblastoma**. *CANCER Res* 1970, **30**:2110–2118.

Turinetto V, Giachino C: **Multiple facets of histone variant H2AX: a DNA double-strand-break marker with several biological functions**. *Nucleic Acids Res* 2015, **43**:2489.

Valentijn LJ, Koster J, Haneveld F, Aissa RA, van Sluis P, Broekmans MEC, Molenaar JJ, van Nes J, Versteeg R: **Functional MYCN signature predicts outcome of neuroblastoma irrespective of MYCN amplification.** *Proc Natl Acad Sci U S A* 2012, **109**:19190–19195.

Valentijn LJ, Koster J, Zwijnenburg DA, Hasselt NE, Van Sluis P, Volckmann R, Van Noesel MM, George RE, Tytgat GAM, Molenaar JJ, et al.: **TERT rearrangements are frequent**

in neuroblastoma and identify aggressive tumors. *Nat Genet 2015 4712* 2015, **47**:1411–1414.
Valli E, Trazzi S, Fuchs C, Erriquez D, Bartesaghi R, Perini G, Ciani E: **CDKL5, a novel MYCN-repressed gene, blocks cell cycle and promotes differentiation of neuronal cells**. *Biochim Biophys Acta - Gene Regul Mech* 2012, **1819**:1173–1185.
Valovka T, Schönfeld M, Raffeiner P, Breuker K, Dunzendorfer-Matt T, Hartl M, Bister K: **Transcriptional control of DNA replication licensing by Myc**. *Sci Rep* 2013, **3**.
Van Der Groep P, Hoelzel M, Buerger H, Joenje H, De Winter JP, Van Diest PJ: **Loss of expression of FANCD2 protein in sporadic and hereditary breast cancer**. *Breast Cancer Res Treat* 2008, **107**:41.
Van Der Heijden MS, Brody JR, Dezentje DA, Gallmeier E, Cunningham SC, Swartz MJ, DeMarzo AM, Offerhaus GJA, Isacoff WH, Hruban RH, et al.: **In vivo therapeutic responses contingent on Fanconi anemia/BRCA2 status of the tumor**. *Clin Cancer Res* 2005, **11**:7508–7515.
Van Goethem A, Yigit N, Moreno-Smith M, Vasudevan SA, Barbieri E, Speleman F, Shohet J, Vandesompele J, Van Maerken T: **Dual targeting of MDM2 and BCL2 as a therapeutic strategy in neuroblastoma**. *Oncotarget* 2017, **8**:57047.
van Golen CM, Soules ME, Grauman AR, Feldman EL: **N-Myc overexpression leads to decreased β1 integrin expression and increased apoptosis in human neuroblastoma cells**. *Oncogene* 2003, **22**:2664–2673.
van Groningen T, Akogul N, Westerhout EM, Chan A, Hasselt NE, Zwijnenburg DA, Broekmans M, Stroeken P, Haneveld F, Hooijer GKJ, et al.: **A NOTCH feed-forward loop drives reprogramming from adrenergic to mesenchymal state in neuroblastoma**. *Nat Commun* 2019, **10**:1530.
van Groningen T, Koster J, Valentijn LJ, Zwijnenburg DA, Akogul N, Hasselt NE, Broekmans M, Haneveld F, Nowakowska NE, Bras J, et al.: **Neuroblastoma is composed of two super-enhancer-associated differentiation states**. *Nat Genet* 2017, **49**:1261–1266.
Van Twest S, Murphy VJ, Hodson C, Rg Heierhorst J, Crismani W, Deans Correspondence AJ, Tan W, Swuec P, O'rourke JJ, Deans AJ: **Mechanism of Ubiquitination and Deubiquitination in the Fanconi Anemia Pathway Article Mechanism of Ubiquitination and Deubiquitination in the Fanconi Anemia Pathway**. *Mol Cell* 2017, **65**:247–259.
Varlakhanova NV, Cotterman RF, deVries WN, Morgan J, Donahue LR, Murray S, Knowles BB, Knoepfler PS: **myc maintains embryonic stem cell pluripotency and self-renewal.** *Differentiation* 2010, **80**:9–19.
Vassin VM, Anantha RW, Sokolova E, Kanner S, Borowiec JA: **Human RPA phosphorylation by ATR stimulates DNA synthesis and prevents ssDNA accumulation during DNA-replication stress**. *J Cell Sci* 2009, **122**:4070.
Vaughan L, Clarke PA, Barker K, Chanthery Y, Gustafson CW, Tucker E, Renshaw J, Raynaud F, Li X, Burke R, et al.: **Inhibition of mTOR-kinase destabilizes MYCN and is a potential therapy for MYCN-dependent tumors**. *Oncotarget* 2016, **7**:57525.
Vaughn JP, Cirisano FD, Huper G, Berchuck A, Futreal PA, Marks JR, Iglehart JD: **Cell cycle control of BRCA2.** *Cancer Res* 1996, **56**:4590–4594.
Vaz F, Hanenberg H, Schuster B, Barker K, Wiek C, Erven V, Neveling K, Endt D, Kesterton I, Autore F, et al.: **Mutation of the RAD51C gene in a Fanconi anemia-like disorder**. *Nat Genet* 2010, **42**:406–409.
Velleuer E, Carlberg C: **Impact of Epigenetics on Complications of Fanconi Anemia: The Role of Vitamin D-Modulated Immunity**. *Nutr 2020, Vol 12, Page 1355* 2020, **12**:1355.
Veschi V, Petroni M, Cardinali B, Dominici C, Screpanti I, Frati L, Bartolazzi A, Gulino A, Giannini G: **Galectin-3 Impairment of MYCN-Dependent Apoptosis-Sensitive Phenotype Is Antagonized by Nutlin-3 in Neuroblastoma Cells**. *PLoS One* 2012, **7**:e49139.
Virts EL, Jankowska A, Mackay C, Glaas MF, Wiek C, Kelich SL, Lottmann N, Kennedy FM, Marchal C, Lehnert E, et al.: **AluY-mediated germline deletion, duplication and**

somatic stem cell reversion in UBE2T defines a new subtype of Fanconi anemia. *Hum Mol Genet* 2015, **24**:5093–5108.
Vo KT, Matthay KK, Neuhaus J, London WB, Hero B, Ambros PF, Nakagawara A, Miniati D, Wheeler K, Pearson ADJ, et al.: **Clinical, Biologic, and Prognostic Differences on the Basis of Primary Tumor Site in Neuroblastoma: A Report From the International Neuroblastoma Risk Group Project**. *J Clin Oncol* 2014, **32**:3169.
Voeller, J., & Sondel, P. M. (2019). **Advances in Anti-GD2 Immunotherapy for Treatment of High-Risk Neuroblastoma.** *Journal of Pediatric Hematology/Oncology*, **41**:163.
Vogel C, Marcotte EM: **Insights into the regulation of protein abundance from proteomic and transcriptomic analyses**. *Nat Rev Genet* 2012, **13**:227.
Vogelzang NJ, Rusthoven JJ, Symanowski J, Denham C, Kaukel E, Ruffie P, Gatzemeier U, Boyer M, Emri S, Manegold C, et al.: **Phase III study of pemetrexed in combination with cisplatin versus cisplatin alone in patients with malignant pleural mesothelioma**. *J Clin Oncol* 2003, **21**:2636–2644.
Voloshin T, Kaynan N, Davidi S, Porat Y, Shteingauz A, Schneiderman RS, Zeevi E, Munster M, Blat R, Tempel Brami C, et al.: **Tumor-treating fields (TTFields) induce immunogenic cell death resulting in enhanced antitumor efficacy when combined with anti-PD-1 therapy**. *Cancer Immunol Immunother* 2020, **69**:1191–1204.
Voloshin T, Munster M, Blatt R, Shteingauz A, Roberts PC, Schmelz EM, Giladi M, Schneiderman RS, Zeevi E, Porat Y, et al.: **Alternating electric fields (TTFields) in combination with paclitaxel are therapeutically effective against ovarian cancer cells in vitro and in vivo**. *Int J Cancer* 2016, **139**:2850.
Voter AF, Manthei KA, Keck JL: **A High-Throughput Screening Strategy to Identify Protein-Protein Interaction Inhibitors That Block the Fanconi Anemia DNA Repair Pathway**. *J Biomol Screen* 2016, **21**:626–633.
Wakamatsu Y, Watanabe Y, Nakamura H, Kondoh H: **Regulation of the neural crest cell fate by N-myc: promotion of ventral migration and neuronal differentiation.** *Development* 1997, **124**:1953–1962.
Walter D, Lier A, Geiselhart A, Thalheimer FB, Huntscha S, Sobotta MC, Moehrle B, Brocks D, Bayindir I, Kaschutnig P, et al.: **Exit from dormancy provokes DNA-damage-induced attrition in haematopoietic stem cells**. *Nat 2015 5207548* 2015, **520**:549–552.
Walz S, Lorenzin F, Morton J, Wiese KE, Von Eyss B, Herold S, Rycak L, Dumay-Odelot H, Karim S, Bartkuhn M, et al.: **Activation and repression by oncogenic MYC shape tumour-specific gene expression profiles**. *Nature* 2014, **511**:483–487.
Wang AT, Smogorzewska A: **SnapShot: Fanconi Anemia and Associated Proteins**. 2015, doi:10.1016/j.cell.2014.12.031.
Wang AT, Kim T, Wagner JE, Conti BA, Lach FP, Huang AL, Molina H, Sanborn EM, Zierhut H, Cornes BK, et al.: **A Dominant Mutation in Human RAD51 Reveals Its Function in DNA Interstrand Crosslink Repair Independent of Homologous Recombination**. *Mol Cell* 2015, **59**:478–490.
Wang G, Duan P, Wei Z, Liu F: **Curcumin sensitizes carboplatin treatment in triple negative breast cancer through reactive oxygen species induced DNA repair pathway**. *Mol Biol Rep* 2022, **49**:3259–3270.
Wang HQ, Halilovic E, Li X, Liang J, Cao Y, Rakiec DP, Ruddy DA, Jeay S, Wuerthner JU, Timple N, et al.: **Combined ALK and MDM2 inhibition increases antitumor activity and overcomes resistance in human ALK mutant neuroblastoma cell lines and xenograft models**. *Elife* 2017, **6**.
Wang JYJ, Edelmann W: **Mismatch repair proteins as sensors of alkylation DNA damage**. *Cancer Cell* 2006, **9**:417–418.
Wang L, Hu R, Dai A: **Curcumin Increased the Sensitivity of Non-Small-Cell Lung Cancer to Cisplatin through the Endoplasmic Reticulum Stress Pathway**. *Evid Based Complement Alternat Med* 2022, **2022**.
Wang L, Tan TK, Durbin AD, Zimmerman MW, Abraham BJ, Tan SH, Ngoc PCT, Weichert-Leahey N, Akahane K, Lawton LN, et al.: **ASCL1 is a MYCN- and LMO1-dependent**

member of the adrenergic neuroblastoma core regulatory circuitry. *Nat Commun* 2019, **10**.
Wang R, Wang S, Dhar A, Peralta C, Pavletich NP: **DNA clamp function of the monoubiquitinated Fanconi anaemia ID complex**. *Nature* 2020, **580**:278–282.
Wang S, Wang R, Peralta C, Yaseen A, Pavletich NP: **Structure of the FA core ubiquitin ligase closing the ID clamp on DNA**. *Nat Struct Mol Biol* 2021, **28**:300–309.
Wang T, Liu L, Chen X, Shen Y, Lian G, Shah N, Davidoff AM, Yang J, Wang R: **MYCN drives glutaminolysis in neuroblastoma and confers sensitivity to an ROS augmenting agent**. *Cell Death Dis* 2018, **9**:220.
Wang X, Kennedy RD, Ray K, Stuckert P, Ellenberger T, D'Andrea AD: **Chk1-mediated phosphorylation of FANCE is required for the Fanconi anemia/BRCA pathway.** *Mol Cell Biol* 2007, **27**:3098–3108.
Wang Y, Pandey M, Ballo MT: **Integration of Tumor-Treating Fields into the Multidisciplinary Management of Patients with Solid Malignancies**. *Oncologist* 2019, **24**:e1426.
Waters LS, Minesinger BK, Wiltrout ME, D'Souza S, Woodruff RV, Walker GC: **Eukaryotic Translesion Polymerases and Their Roles and Regulation in DNA Damage Tolerance**. *Microbiol Mol Biol Rev* 2009, **73**:134.
Weinstein IB: **Cancer: Addiction to oncogenes - The Achilles heal of cancer**. *Science (80-)* 2002, **297**:63–64.
Weir NM, Selvendiran K, Kutala VK, Tong L, Vishwanath S, Rajaram M, Tridandapani S, Anant S, Kuppusamy P: **Curcumin Induces G2/M Arrest and Apoptosis in Cisplatin-Resistant Human Ovarian Cancer Cells by Modulating Akt and p38 MAPK**. *Cancer Biol Ther* 2007, **6**:178.
Weiss WA, Aldape K, Mohapatra G, Feuerstein BG, Michael Bishop J: *Targeted expression of MYCN causes neuroblastoma in transgenic mice*. 1997.
Wells JCK, Williams JE, Chomtho S, Darch T, Grijalva-Eternod C, Kennedy K, Haroun D, Wilson C, Cole TJ, Fewtrell MS: **Pediatric reference data for lean tissue properties: density and hydration from age 5 to 20 y**. *Am J Clin Nutr* 2010, **91**:610–618.
Wenger C, Giladi M, Bomzon Z, Salvador R, Basser PJ, Miranda PC: **Modeling Tumor Treating Fields (TTFields) application in single cells during metaphase and telophase**. *Annu Int Conf IEEE Eng Med Biol Soc IEEE Eng Med Biol Soc Annu Int Conf* 2015, **2015**:6892–6895.
Wenger C, Salvador R, Basser PJ, Miranda PC: **The electric field distribution in the brain during TTFields therapy and its dependence on tissue dielectric properties and anatomy: a computational study**. *Phys Med Biol* 2015, **60**:7339–7357.
Westerhout EM, Hamdi M, Stroeken P, Nowakowska NE, Lakeman A, Van Arkel J, Hasselt NE, Bleijlevens B, Akogul N, Haneveld F, et al.: **Mesenchymal-Type Neuroblastoma Cells Escape ALK Inhibitors**. *Cancer Res* 2022, **82**:484–496.
Westermann F, Muth D, Benner A, Bauer T, Henrich K-O, Oberthuer A, Brors B, Beissbarth T, Vandesompele J, Pattyn F, et al.: **Distinct transcriptional MYCN/c-MYC activities are associated with spontaneous regression or malignant progression in neuroblastomas.** *Genome Biol* 2008, **9**:R150.
White PS, Thompson PM, Gotoh T, Okawa ER, Igarashi J, Kok M, Winter C, Gregory SG, Hogarty MD, Maris JM, et al.: **Definition and characterization of a region of 1p36.3 consistently deleted in neuroblastoma**. *Oncogene* 2005, **24**:2684–2694.
Whitfield JR, Beaulieu ME, Soucek L: **Strategies to inhibit Myc and their clinical applicability**. *Front Cell Dev Biol* 2017, **5**:10.
Wick W: **TTFields: where does all the skepticism come from?** *Neuro Oncol* 2016, **18**:303.
Wilson JB, Yamamoto K, Marriott AS, Hussain S, Sung P, Hoatlin ME, Mathew CG, Takata M, Thompson LH, Kupfer GM, et al.: **FANCG promotes formation of a newly identified protein complex containing BRCA2, FANCD2 and XRCC3**. *Oncogene* 2008, **27**:3641–3652.

Winer J, Jung CKS, Shackel I, Williams PM: **Development and Validation of Real-Time Quantitative Reverse Transcriptase–Polymerase Chain Reaction for Monitoring Gene Expression in Cardiac Myocytesin Vitro**. *Anal Biochem* 1999, **270**:41–49.
Wölfl M, Jungbluth AA, Garrido F, Cabrera T, Meyen-Southard S, Spitz R, Ernestus K, Berthold F: **Expression of MHC class I, MHC class II, and cancer germline antigens in neuroblastoma**. *Cancer Immunol Immunother* 2005, **54**:400–406.
Woo CW, Tan F, Cassano H, Lee JH, Kwang CL, Thiele CJ: **Use of RNA interference to elucidate the effect of MYCN on cell cycle in neuroblastoma**. *Pediatr Blood Cancer* 2008, **50**:208–212.
Wreesmann VB, Estilo C, Eisele DW, Singh B, Wang SJ: **Downregulation of Fanconi Anemia Genes in Sporadic Head and Neck Squamous Cell Carcinoma**. *ORL* 2007, **69**:218–225.
Wu X, Shell SM, Zou Y: **Interaction and co-localization of Rad9/Rad1/HUS1 checkpoint complex with replication protein A in human cells**. *Oncogene* 2005, **24**:4728.
Wysham WZ, Mhawech-Fauceglia P, Li H, Hays L, Syriac S, Skrepnik T, Wright J, Pande N, Hoatlin M, Pejovic T: **BRCAness Profile of Sporadic Ovarian Cancer Predicts Disease Recurrence**. *PLoS One* 2012, **7**.
Xia Y, Ye B, Ding J, Yu Y, Alptekin A, Thangaraju M, Prasad PD, Ding ZC, Park EJ, Choi JH, et al.: **Metabolic reprogramming by MYCN confers dependence on the serine-glycine-one-carbon biosynthetic pathway**. *Cancer Res* 2019, **79**:3837.
Xu M, Qin J, Wang L, Lee HJ, Kao CY, Liu D, Songyang Z, Chen J, Tsai MJ, Tsai SY: **Nuclear receptors regulate alternative lengthening of telomeres through a novel noncanonical FANCD2 pathway**. *Sci Adv* 2019, **5**.
Xue X, Sung P, Zhao X: **Functions and regulation of the multitasking FANCM family of DNA motor proteins**. *Genes Dev* 2015, **29**:1777.
Xue Y, Li Y, Guo R, Ling C, Wang W: **FANCM of the Fanconi anemia core complex is required for both monoubiquitination and DNA repair**. *Hum Mol Genet* 2008, **17**:1641.
Yaari S, Jacob-Hirsch J, Amariglio N, Haklai R, Rechavi G, Kloog Y: **Disruption of Cooperation Between Ras and MycN in Human Neuroblastoma Cells Promotes Growth Arrest**. *Clin Cancer Res* 2005, **11**:4321–4330.
Yallapu MM, Maher DM, Sundram V, Bell MC, Jaggi M, Chauhan SC: **Curcumin induces chemo/radio-sensitization in ovarian cancer cells and curcumin nanoparticles inhibit ovarian cancer cell growth**. *J Ovarian Res* 2010, **3**.
Yamamoto K, Hirano S, Ishiai M, Morishima K, Kitao H, Namikoshi K, Kimura M, Matsushita N, Arakawa H, Buerstedde J-M, et al.: **Fanconi anemia protein FANCD2 promotes immunoglobulin gene conversion and DNA repair through a mechanism related to homologous recombination**. *Mol Cell Biol* 2005, **25**:34–43.
Yamamoto KN, Kobayashi S, Tsuda M, Kurumizaka H, Takata M, Kono K, Jiricny J, Takeda S, Hirota K: **Involvement of SLX4 in interstrand cross-link repair is regulated by the Fanconi anemia pathway**. *Proc Natl Acad Sci U S A* 2011, **108**:6492–6496.
Yancopoulos GD, Nisen PD, Tesfaye A, Kohl NE, Goldfarb MP, Alt FW: **N-myc can cooperate with ras to transform normal cells in culture.** *Proc Natl Acad Sci U S A* 1985, **82**:5455.
YANG JL, YANG MEID, CHEN JAWC, LU KW, HUANG YIP, PENG SHUF, CHUEH FUS, LIU KUOC, LIN TZUS, CHEN POY, et al.: **Ouabain Induces DNA Damage in Human Osteosarcoma U-2 OS Cells and Alters the Expression of DNA Damage and DNA Repair–associated Proteins**. *In Vivo (Brooklyn)* 2021, **35**:2687.
Yang Y, Liu Z, Wang F, Temviriyanukul P, Ma X, Tu Y, Lv L, Lin YF, Huang M, Zhang T, et al.: **FANCD2 and REV1 cooperate in the protection of nascent DNA strands in response to replication stress**. *Nucleic Acids Res* 2015, **43**:8325.
Yarde DN, Oliveira V, Mathews L, Wang X, Villagra A, Boulware D, Shain KH, Hazlehurst LA, Alsina M, Chen DT, et al.: **Targeting the Fanconi Anemia/BRCA Pathway Circumvents Drug Resistance in Multiple Myeloma**. *Cancer Res* 2009, **69**:9367.

Ye Z, Chen D, Zheng R, Chen H, Xu T, Wang C, Zhu S, Gao X, Zhang J, Li D, et al.: **Curcumin induced G2/M cycle arrest in SK-N-SH neuroblastoma cells through the ROS-mediated p53 signaling pathway**. *J Food Biochem* 2021, **45**:e13888.
Yeo JE, Lee EH, Hendrickson EA, Sobeck A: **CtIP mediates replication fork recovery in a FANCD2-regulated manner**. *Hum Mol Genet* 2014, **23**:3695.
Yin Y, Xu L, Chang Y, Zeng T, Chen X, Wang A, Groth J, Foo WC, Liang C, Hu H, et al.: **N-Myc promotes therapeutic resistance development of neuroendocrine prostate cancer by differentially regulating miR-421/ATM pathway**. *Mol Cancer* 2019, **18**.
Yoshida GJ: **Beyond the Warburg Effect: N-Myc Contributes to Metabolic Reprogramming in Cancer Cells**. *Front Oncol* 2020, **10**:791.
Yoshida K, Toden S, Ravindranathan P, Han H, Goel A: **Curcumin sensitizes pancreatic cancer cells to gemcitabine by attenuating PRC2 subunit EZH2, and the lncRNA PVT1 expression**. *Carcinogenesis* 2017, **38**:1036.
Yoshikiyo K, Kratz K, Hirota K, Nishihara K, Takata M, Kurumizaka H, Horimoto S, Takeda S, Jiricny J: **KIAA1018/FAN1 nuclease protects cells against genomic instability induced by interstrand cross-linking agents**. *Proc Natl Acad Sci U S A* 2010, **107**:21553–21557.
Yu AL, Gilman AL, Ozkaynak MF, London WB, Kreissman SG, Chen HX, Smith M, Anderson B, Villablanca JG, Matthay KK, et al.: **Anti-GD2 Antibody with GM-CSF, Interleukin-2, and Isotretinoin for Neuroblastoma**. *N Engl J Med* 2010, **363**:1324–1334.
Yu AL, Gilman AL, Ozkaynak MF, Naranjo A, Diccianni MB, Gan J, Hank JA, Batova A, London WB, Tenney SC, et al.: **Long-Term Follow-up of a Phase III Study of ch14.18 (Dinutuximab) + Cytokine Immunotherapy in Children with High-Risk Neuroblastoma: COG Study ANBL0032**. *Clin Cancer Res* 2021, **27**:2179–2189.
Yuan F, Qian L, Zhao X, Liu JY, Song L, D'Urso G, Jain C, Zhang Y: **Fanconi Anemia Complementation Group A (FANCA) Protein Has Intrinsic Affinity for Nucleic Acids with Preference for Single-stranded Forms**. *J Biol Chem* 2012, **287**:4800.
Yuan J, Yankner BA: **Apoptosis in the nervous system**. *Nat 2000 4076805* 2000, **407**:802–809.
Yustein JT, Liu YC, Gao P, Jie C, Le A, Vuica-Ross M, Chng WJ, Eberhart CG, Bergsagel PL, Dang CV: **Induction of ectopic Myc target gene JAG2 augments hypoxic growth and tumorigenesis in a human B-cell model**. *Proc Natl Acad Sci U S A* 2010, **107**:3534.
Zafar MK, Eoff RL: **Translesion DNA Synthesis in Cancer: Molecular Mechanisms and Therapeutic Opportunities**. *Chem Res Toxicol* 2017, **30**:1942.
Zaizen Y, Taniguchi S, Noguchi S, Suita S: **The effect of N-myc amplification and expression on invasiveness of neuroblastoma cells.** *J Pediatr Surg* 1993, **28**:766–769.
Zeid R, Lawlor MA, Poon E, Reyes JM, Fulciniti M, Lopez MA, Scott TG, Nabet B, Erb MA, Winter GE, et al.: **Enhancer invasion shapes MYCN-dependent transcriptional amplification in neuroblastoma**. *Nat Genet* 2018, **50**:515–523.
Zellweger R, Dalcher D, Mutreja K, Berti M, Schmid JA, Herrador R, Vindigni A, Lopes M: **Rad51-mediated replication fork reversal is a global response to genotoxic treatments in human cells**. *J Cell Biol* 2015, **208**:563.
Zeng X, Sigoillot F, Gaur S, Choi S, Pfaff KL, Oh DC, Hathaway N, Dimova N, Cuny GD, King RW: **Pharmacologic Inhibition of the Anaphase-Promoting Complex Induces A Spindle Checkpoint-Dependent Mitotic Arrest in the Absence of Spindle Damage**. *Cancer Cell* 2010, **18**:382.
Zhai K, Brockmüller A, Kubatka P, Shakibaei M, Büsselberg D: **Curcumin's Beneficial Effects on Neuroblastoma: Mechanisms, Challenges, and Potential Solutions**. *Biomol 2020, Vol 10, Page 1469* 2020, **10**:1469.
Zhang B, Chen R, Lu J, Shi Q, Zhang X, Chen J: **Expression of FANCD2 in sporadic breast cancer and clinicopathological analysis**. *J Huazhong Univ Sci Technol [Medical Sci 2010 303* 2010, **30**:322–325.

Zhang C, Yan Z, Painter CL, Zhang Q, Chen E, Arango ME, Kuszpit K, Zasadny K, Hallin M, Hallin J, et al.: **PF-00477736 mediates checkpoint kinase 1 signaling pathway and potentiates docetaxel-induced efficacy in xenografts**. *Clin Cancer Res* 2009, **15**:4630–4640.
Zhang H, Kozono DE, O'Connor KW, Vidal-Cardenas S, Rousseau A, Hamilton A, Moreau L, Gaudiano EF, Greenberger J, Bagby G, et al.: **TGF-β Inhibition Rescues Hematopoietic Stem Cell Defects and Bone Marrow Failure in Fanconi Anemia**. *Cell Stem Cell* 2016, **18**:668–681.
Zhang H, Yu T, Wen L, Wang H, Fei D, Jin C: **Curcumin enhances the effectiveness of cisplatin by suppressing CD133+ cancer stem cells in laryngeal carcinoma treatment**. *Exp Ther Med* 2013, **6**:1317.
Zhang H, Chen Z, Ye Y, Ye Z, Cao D, Xiong Y, Srivastava M, Feng X, Tang M, Wang C, et al.: **SLX4IP acts with SLX4 and XPF–ERCC1 to promote interstrand crosslink repair**. *Nucleic Acids Res* 2019, **47**:10181–10201.
Zhang J, Walter JC: **Mechanism and regulation of incisions during DNA interstrand cross-link repair**. *DNA Repair (Amst)* 2014, **19**:135.
Zhang Q-S, Eaton L, Snyder ER, Houghtaling S, Mitchell JB, Finegold M, Van Waes C, Grompe M: **Tempol Protects against Oxidative Damage and Delays Epithelial Tumor Onset in Fanconi Anemia Mice**. *Cancer Res* 2008, **68**:1601–1608.
Zhang W, Liu B, Wu W, Li L, Broom BM, Basourakos SP, Korentzelos D, Luan Y, Wang J, Yang G, et al.: **Targeting the MYCN-PARP-DNA Damage Response Pathway in Neuroendocrine Prostate Cancer.** *Clin Cancer Res* 2018, **24**:696–707.
Zhang X, Chiang HC, Wang Y, Zhang C, Smith S, Zhao X, Nair SJ, Michalek J, Jatoi I, Lautner M, et al.: **Attenuation of RNA polymerase II pausing mitigates BRCA1-associated R-loop accumulation and tumorigenesis**. *Nat Commun 2017 81* 2017, **8**:1–12.
Zhao L, Li Y, He M, Song Z, Lin S, Yu Z, Bai X, Wang N, Wei M: **The Fanconi anemia pathway sensitizes to DNA alkylating agents by inducing JNK-p53-dependent mitochondrial apoptosis in breast cancer cells**. *Int J Oncol* 2014, **45**:129–138.
Zhao W, Duan W, Leon ME, Chen AP, Sofletea G, Thurmond J, Ramaswamy B, O'Malley D, Bekaii-Saab TS, Calero MAV-: **Targeting fanconi anemia (FA) repair pathway deficiency for treatment with PARP inhibitors.** *https://doi.org/101200/jco20102815_suppl.tps168* 2010, **28**:TPS168–TPS168.
Zhao X, D'Arca D, Lim WK, Brahmachary M, Carro MS, Ludwig T, Cardo CC, Guillemot F, Aldape K, Califano A, et al.: **The N-Myc-DLL3 Cascade Is Suppressed by the Ubiquitin Ligase Huwe1 to Inhibit Proliferation and Promote Neurogenesis in the Developing Brain**. *Dev Cell* 2009, **17**:210–221.
Zheng DJ, Krull KR, Chen Y, Diller L, Yasui Y, Leisenring W, Brouwers P, Howell R, Lai JS, Balsamo L, et al.: **Long-term psychological and educational outcomes for survivors of neuroblastoma: A report from the Childhood Cancer Survivor Study**. *Cancer* 2018, **124**:3220–3230.
Zhou X, Vink M, Klaver B, Berkhout B, Das AT: **Optimization of the Tet-On system for regulated gene expression through viral evolution**. *Gene Ther* 2006, **13**:1382–1390.
Zhu JJ, Demireva P, Kanner AA, Pannullo S, Mehdorn M, Avgeropoulos N, Salmaggi A, Silvani A, Goldlust S, David C, et al.: **Health-related quality of life, cognitive screening, and functional status in a randomized phase III trial (EF-14) of tumor treating fields with temozolomide compared to temozolomide alone in newly diagnosed glioblastoma**. *J Neurooncol* 2017, **135**:545–552.
Zhu J, Zhou L, Wu G, Konig H, Lin X, Li G, Qiu XL, Chen CF, Hu CM, Goldblatt E, et al.: **A novel small molecule RAD51 inactivator overcomes imatinib-resistance in chronic myeloid leukaemia**. *EMBO Mol Med* 2013, **5**:353.
Zhu S, Lee JS, Guo F, Shin J, Perez-Atayde AR, Kutok JL, Rodig SJ, Neuberg DS, Helman D, Feng H, et al.: **Activated ALK collaborates with MYCN in neuroblastoma pathogenesis**. *Cancer Cell* 2012, **21**:362–373.

Zimmerman KA, Yancopoulos GD, Collum RG, Smith RK, Kohl NE, Denis KA, Nau MM, Witte ON, Toran-Allerand D, Gee CE, et al.: **Differential expression of myc family genes during murine development**. *Nature* 1986, **319**:780–783.
Zou J, Zhu L, Jiang X, Wang Y, Wang Y, Wang X, Chen B: **Curcumin increases breast cancer cell sensitivity to cisplatin by decreasing FEN1 expression**. *Oncotarget* 2018, **9**:11268.